Reducing Shipping Carbon Emissions under Real Operative Conditions: A Study of Alternative Marine Waste Heat Recovery Systems based on the Organic Rankine Cycle

---

Santiago Suárez de la Fuente

A Thesis submitted to UCL for the degree of Doctor of Philosophy

Department of Mechanical Engineering

UCL

Torrington Place, London

WC1E 7JE, UK

June 2016

(Page left intentionally blank)

I, Santiago Suárez de la Fuente confirm that the work presented in this thesis is my own. Where information has been derived from other sources, I confirm that this has been indicated in the thesis.

Signature

Date: 28/June/2016

ABSTRACT

The biggest source of energy loss in shipping is found in the propulsion system. This study focuses on analysing, and working with, the concept of heat management for waste heat energy from the exhaust gas and scavenge air. Using waste heat recovery systems (WHRS) to make shipping more efficient represent a good area of opportunity. On board ships, a water-based Rankine cycle (RC) is typically installed; this has the task of providing steam and power. This work explores alternative waste heat technologies to assess the development and suitability, but also to find better solutions to the traditional RC.

Different models coupled with advance optimisation processes were created to understand the marine WHRS. The results show that WHRS are sensitive to environmental and operational factors which must be considered at design stage. While water offers the possibility of producing both steam and power; organic Rankine cycles (ORC) produce larger power outputs at temperatures between 90˚C and 230˚C which translate to lower CO_2 emissions.

Organic WHRS will play an important role in the future as regulations push for tighter emission controls, and waste energy availability for power production reduces due to an increase in prime mover efficiency and waste heat utilisation for other processes (e.g. ballast treatment). The ORC technology can be applied to any kind of vessel type and size, keeping in mind that the ORC benefits depend on the waste heat temperature and availability, the ship's heat requirements and operational profile. It is also then important to bear in mind some of the drawbacks, such as larger mass flow rates and flammability of some of the organic fluids studied which will introduce additional safety equipment and costs.

ACKNOWLEDGEMENTS

I would like to thank my supervisor Dr Greig for his support and guidance during this research project. Thank you for your comments, ideas and discussions which propel my research. My thanks also for the opportunities to teach and help with conferences which have strengthened my academic and professional skills. My PhD would have been impossible without your interest and work. My deepest appreciation to Dr Balachandran for his support and time in polishing my research.

I would like to express my gratitude to Dr Calleya, Dr Pawling, Dr Schaumeier, Dr Smith and Dr Suen for their support in marine engineering, naval architecture, routing, thermodynamics, data analysis and useful insights during my research. With regard to Arctic knowledge, I wish to thank Mihailo Pavic and Ema Muk-Pavic for all their help and support.

I express my warm thanks to my colleagues, but also friends, Dr Larsen and Dr Pierobon for sharing with me their knowledge, opinions and comments on marine engineering, thermodynamics and everything in between. I would also want to thank Dr Kærn for his insights and comments on air-cooled designs. I owe gratitude to Professor Haglind for allowing me to join his team in the summer of 2014 to explore the implications of navigating in the Arctic. Hopefully, more collaborative work can be undertaken in the near future.

Thanks too for the financial aid provided by the Mexican Council of Science and Technology (CONACYT), but also for the many organised events and conferences during my PhD which allowed me to link my research and expertise to Mexico.

I am truly grateful to the Institute of Marine Engineering, Science and Technology (IMarEST) for its support via the Stanley Gray fellowship. In the same line, my PhD would have never been begun nor continued without the help of both Low Carbon Shipping and Shipping in Changing Climates projects funding, many thanks.

On a personal note, the first in the list is my wife Sofia. Thank you so much for encouraging me into this great adventure that has been my Masters and PhD, I still remember the day we decided to embark on this journey back in that winter of 2008. Thank you so much for all your patience and understanding in the dark days; for the laughs and good memories; for listening to my crazy ideas about thermodynamics. Without you, this new path in our life would have never happened. Thank you.

To my dad, Toño; my brother, Sebastian; and my sister, Laurracarrana; for being always there and listening to our adventures, you are always my examples of how to enjoy life. To my awesome political family for never forgetting us by visiting us, you were always close and your support permanently strong.

To my British family – Patricia, Katie and Carl – many thanks for the great diner nights and travels to the North, you have made feel Mexico really close. To my friends who are like my second family, thank you for letting me being part of your road.

LIST OF PUBLICATIONS

PEER-REVIEWED JOURNAL ARTICLES

Suárez de la Fuente, S. & Greig, A., 2015. Making shipping greener: comparative study between organic fluids and water for Rankine cycle waste heat recovery. *Journal of Marine Engineering & Technology*, 14(2), pp.70–84.

Suárez de la Fuente, S., Roberge, D. & Greig, A.R., 2015. Safety and CO_2 emissions: Implications of using organic fluids in a ship's waste heat recovery system (in press). *Marine Policy*, p.21. doi:10.1016/j.marpol.2016.02.008.

OTHER PUBLICATIONS

Suárez de la Fuente, S., 2016. Marine Waste Heat Recovery Systems (in press). *Encyclopedia of Marine and Offshore Engineering*, ed. Carlton, Jukes & Choo. (C) John Wiley & Sons, Ltd.

CONFERENCE PROCEEDINGS

Suárez de la Fuente, S. & Greig, A., 2013. Making shipping greener: ORC modelling under realistic operative conditions. In *Low Carbon Shipping Conference*. London, p.18.

Raucci, C., Calleya, J., Suárez de la Fuente, S. & Pawling, R., 2015. Hydrogen on board ship: a first analysis of key parameters and implications. In International Conference on Shipping in Changing Climates. Glasgow, p.11.

NOMENCLATURE

Greek Symbol	Name	Units
α	Area footprint	m^2
β	Volume footprint	m^3
Δ	Displacement	t
Δ	Difference/Delta	-
ε	Inverse of the Vapour saturated slope	J/kg-K^2
η	Efficiency	%
κ	Thermal conductivity	W/m-K
μ	Dynamic viscosity	Pa-s
ρ	Density	Kg/m^3
σ	Electrical conductivity	S/m

Symbol	Name	Units
A	Area	m^2
A_c	Admiralty coefficient	-
CE	Carbon dioxide emission	t/h
C_F	Carbon factor	t CO_2/t Fuel
C_p	Specific heat at constant pressure	J/kg-K
CL	Cargo level indicator	-
CS	Carbon emission savings	t/h
d	Diameter	m
E	Energy	J
$\dot{E}$	Energy flow	W
$EEDI$	Energy Efficiency Design Index	g CO_2/t-nm
$efficiency$	Efficiency performance indicator	-
f	Correction factor	-
F	Flow ratio	-

Symbol	Name	Units
FC	Fuel consumption	t/h
f_h	Fin height	mm
f_p	Fin pitch	mm
FP	Fuel price	£/t
FS	Fuel savings	t/h
f_t	Fin thickness	mm
F_t	Counter flow temperature correction factor	-
g	Gravitational acceleration	m/s^2
h	Specific enthalpy	J/kg
h^*	Convective heat transfer coefficient	W/m^2-K
H	Enthalpy	J
i	Discount rate	%
I	Current	A
j_f	Friction correction factor	-
j_{th}	Heat transfer correction factor	-
l	Length	m
$\dot{m}$	Mass flow	kg/s
M	Mass flow rate ratio	-
MS	Profit	£/h
N	Rotational speed	rpm
N_f	Number of fins per tube	-
N_t	Number of tubes	-
N_{tpr}	Number of tubes per row	-
N_{tr}	Number of tube rows	-
NI	Year indicator	-
NPV	Net present value	£
Nu	Nusselt number	-
OS	Operative segments indicator	-

Nomenclature

Symbol	Name	Units
OT	Time observations	-
P	Pitch	mm
P	Pressure	Pa
PB	Payback time	years
$Power$	Power performance indicator	-
Pr	Prandtl number	-
PV	Present value	£
Q	Specific heat	J/kg
Q	Heat	J
$\dot{Q}$	Heat flow	W
q_{LCV}	Low Calorific Value Specific heat	J/kg
R	Electrical resistance	Ω
R	Resistance	N
Re	Reynolds number	-
RST	Route segments indicator	-
S	Specific entropy	J/kg
S	Entropy	J
S	Seebeck coefficient	V/K
$Score$	Total performance indicator	-
$size$	Size performance indicator	-
$SFOC$	Specific fuel oil consumption	g/kWh
ST	Single trips	-
T	Time	s (h)
T	Temperature	K (˚C)
T	Thrust	N
ΔT_{lm}	Log temperature difference	K (˚C)
TW	Transport work	t-nm/h
U	Internal energy	J
U	Overall heat transfer coefficient	W/m^2-K
v	Speed	m/s (kn)
V	Voltage	V
V	Volume	m^3
$\dot{V}$	Volumetric flow rate	m^3/s
w	Weight factors	-
W	Work	J
$\dot{W}$	Power	W
x	Wetness factor	%
Y	Operational life	years
ZT	Figure-of-merit	-

Subscripts	Name
a	Air
AE	Auxiliary engine
amb	Ambient
ap	Approach
b	Baffle
B	Tube Bundle
c	Cubic capacity
C	Cold
cl	Clearance
co	Condenser/cooler
cr	Critical
cs	Cross-sectional
d	Design
ds	Desuperheater
e	Electric
E	Expander
eff	Availability
eg	Exhaust gas
ev	Evaporator
f	Fins
fr	Frictional
$fuel$	Fuel
gen	Generator set
GT	Green technology
H	Hot
ht	Heat transfer
i	In/Inlet/Inside
if	Inside fouling
l	Liquid
L	Load
ME	Main engine

Symbol	Name	Units
Min	Minimum	
NI	Year indicator	
O	Out/Outlet/Outside	
Of	Outside fouling	
Off	Off-design	
ORC	Organic Rankine cycle	
P	Pump	
Pgp	Power generating plant	
Pp	Pinch point	
PTI	Shaft motor/generator	
R	Reduced	
RC	Rankine cycle	
Rec	Recuperator	
Ref	Reference	
Reg	Regulatory/Technical	
Rs	Residual	
rsat	Reduced saturated conditions	
S	Shell	
S	Coolant (e.g. seawater)	
Sat	Saturated condition	
Sc	Subcooler	
Sh	Superheater	
Sw	Shell wall	
SW	Seawater	
T	Tube	
T	Total	
Th	Thermal	
To	Thermal oil	
Tw	Tube wall	
V	Vapour	
Vap	Vaporisation	
W	Weather	
W	Power	
Wf	Working fluid	
WH	Waste heat source	
WHB	Waste heat boiler	
WHRS	Waste heat recovery system	

Contents

FIGURES

TABLES

1

Introduction and motivation: Shipping's Carbon Dioxide And Greenhouse Gases Emissions

This dissertation explores the availability of alternative waste heat recovery systems to reuse the low/medium quality waste heat found in the exhaust and scavenge air system on board ships. It seeks to determine, from those technologies available, what are the conditions of operation that favour one kind of technology over others and the best one to implement. This is with the objective of finding an alternative and viable way to contribute to the reduction of carbon and other greenhouse gases (GHG) emissions by increasing the vessel's propulsive system fuel efficiency.

Since the beginning of the industrial revolution, around 1750, man began to use carbon and hydrogen storage systems, such as coal and wood, to power new machines and processes to increase productivity and progress. Over the years more energy was required, new machines built and different types of fuels used. The legacy of this industrial era is an ever rising demand for energy supply mainly by fossil fuels. For example, CO_2 concentration has seen an increase of around 40% in a period of 260 years [Environmental Protection Agency 2012], reaching in 2006 $2.72x10^4$ Mt which was only derived from burning fossil fuels [America's Climate Choices 2010]. To keep this in perspective, it is noted that volcanos emit around 300 Mt of CO_2 per year [Hards 2005].

This chapter provides the motivation for the research by showing the importance and magnitude of the relevant of greenhouse gases in climate change. Next, it shows how shipping contributes to global emissions, the environmental regulations implemented within the industry and explains why it is an important actor in mitigating noxious emissions. Finally, the end of this chapter shows different possible improvements inside ships to conclude that the prime mover is an important and relevant area of opportunity in the increase of fuel efficiency in shipping.

From chapter 2 to chapter 4, different alternative waste heat recovery systems are studied with the aim of understanding their advantages and disadvantages. Chapter 5 presents the chosen waste heat recovery systems and the state of the literature regarding their marine application. Chapter 6 gives an overview of the methodology used in each empirical chapters. Chapter 7 offers a sensitivity study for a container vessel; chapter 8 uses a multi-objective optimisation approach to understand the benefits of a waste heat recovery system on board a tanker; and chapter 9 explores the possibility of using air-cooled waste heat recovery systems when navigating in extremely cold weathers. Final conclusions and future work are presented in the last chapter.

1.1 GREENHOUSE GASES

The Earth's atmosphere plays an important role in sustaining and protecting nature and living organisms by filtering dangerous Sun radiation, controlling temperature, transporting heat and water and being a reservoir of oxygen, carbon and nitrogen which are important for life. The atmosphere is composed of various gases: nitrogen (N), oxygen (O), inert gases (e.g. argon), carbon dioxide (CO_2), and methane (CH_4) among others. Each gas behaves as a filter for the different types of radiations emitted by the Sun. For example, ozone allows visible light to pass through but absorbs ultraviolet radiation.

Some of the Sun's radiation, around 66%, arrives to Earth's surface and warms it. The excess heat is returned via infrared radiation to the atmosphere [UNEP/GRID-Arendal 2005]. Part of the reverted radiation is absorbed by CO_2 and other gases affecting Earth's temperature, while the rest escapes to space. The absorption of infrared radiation and its change in temperature by atmospheric gases is known as the greenhouse effect [Stix 2006], and the gases responsible are known as greenhouse gases (GHG). There are six direct GHG: CO_2, CH_4, hydrofluorocarbons (HFC), nitro oxide (N_2O), perfluorocarbons (PFC) and sulphur hexafluoride (SF_6); and four indirect GHG: nitrogen oxides (NO_x), carbon monoxide (CO), sulphur dioxide (SO_2) and non-methane volatile organic compounds. The difference between direct and indirect GHG is that direct GHG are responsible for the radiation absorption, hence a temperature change, coming from Earth's surface, while indirect GHG force a temperature change due to an increment in atmospheric ozone concentration [Forster et al. 2007].

As the presence of GHG increases in the atmosphere due to human activities, so does the global anthropogenic radiative forcing, warming Earth and augmenting changes on climate systems around the globe [Intergovermental Panel on Climate Change 2014]. Anthropogenic radiative forcing is on average more than 12 times larger than solar irradiance arriving to Earth's surface [America's Climate Choices 2010]. The Intergovernmental Panel on Climate Change (IPCC) created scenarios to predict future GHG emissions and climate change [Nakicenovic & Swart 2000]. The predictions of CO_2 concentrations and other GHG gases emissions for the next century are presented in Table 1. Even though there are scenarios which predict a drastic reduction in GHG emissions, the IPCC models indicate that there could be an increase in Earth's temperature within a range of 0.5°C[1] to 2.5°C by 2050 and from 1.25°C to 5.5°C by 2100 when compared to the average temperature seen in the year 2000. This prediction behaviour is caused by the longevity of some of the compounds which are active over a long period after being deposited in the atmosphere. For example, CH_4 has a lifetime in the atmosphere of 12 years, while R236fa can reach up to 240 years [Forster et al. 2007].

Table 1: Averaged predicted emissions for different compounds on the atmosphere from the 26 IPCC scenarios. The table also shows the compound's emissions in the year 1990.

Compound	GHG type	1990 (Mt/year)	2050 (Mt/year)	2100 (Mt/year)
CO_2 ‡	Direct	7,100	11,000 – 23,900	4,200 – 28,200
CFC/HFC/HCFC ϑ,∂	Direct	1,672	312 – 566	64 – 614
CO	Indirect	879	471 – 2,159	363 – 2,570
CH_4	Direct	310	359 – 630	236 – 889
SO_2	Indirect	71	40 – 105	20 – 60
NO_x	Indirect	31	39 – 95	19 – 110

‡ Considering both fossil fuel and land use CO_2 emissions.

ϑ Using carbon equivalent emission factors (see [Nakicenovic & Swart 2000]).

∂ CFC stands for chlorofluorocarbon and HCFC for hydrochlorofluorocarbons.

[1] The temperature units used in this document will be degree centigrade (°C) for an easier understanding for the reader. For modelling, coding and thermodynamic demonstrations Kelvin (K) will be used.

The bulk of anthropogenic GHG emissions come from CO_2 (see Table 1) which is heavily dependent on the use of fossil fuels and deforestation. Economic development and population growth has been linked to CO_2 emissions but recently a decoupling between global economic growth and emissions has been seen [International Energy Agency 2014; Harvey 2015]. This could be the first sign of the positive effects offered by green technologies, policies and alternative fuels for the environment without losing economic momentum. Carbon monoxide follows a similar growth pattern than CO_2 because it also depends on the same causes [Dentener et al. 2001].

After CO, the compounds CFC, HFC and HCFC most affected the atmosphere thermal equilibrium in 1990. The amount of emissions for these compounds, seen in Table 1, is calculated using carbon equivalencies based on their contribution in warming the atmosphere. To explain this, first it is important to introduce the concept of global warming potential (GWP). GWP is defined by Nakicenovic and Swart [2000] as *"a measurement technique to define the relative contribution of each GHG to atmospheric warming"* [2]. The GWP uses as a reference the CO_2 GWP to compare the influence of the different gases in warming the atmosphere. Returning to the three different types of fluorocarbons, their GWP tend to be much larger than CO_2, for example R236fa – a hydrofluorocarbon – has a GWP, over a timeframe of 100 years, of around 9,800 [Forster et al. 2007]. When the emissions shown in Table 1 are calculated, the GWP of the most used fluids containing these compounds are considered.

The decrement of the influence of these compounds in the atmosphere is caused by efforts from policymakers to ban the use of fluids, in the majority refrigerants which contain HFC, CFC or HCFC. Industry and academia have researched and created fluids that have low GWP but that still offer the same level of performance as the phased out, or soon to be phased out, fluids that contain these noxious compounds [Calm 2008].

The main activities that cause anthropogenic CH_4 are found in agriculture, natural gas exploitation and usage, and landfills [Nakicenovic & Swart 2000; Forster et al. 2007; Mønster et al. 2015]. Methane has a GWP of 30 and a relatively short life in the atmosphere of 12 years [Myhre et al. 2013]. While the study of other GHG is relevant, these will not be discussed since their contribution to global warming is overshadowed by the warming effect that CO_2 has on the atmosphere.

As shown earlier, CO_2 emissions have the largest impact on global warming due to their abundance in the atmosphere, and it is important to consider its distribution according to human activity: Electricity and heating production are the highest at 35%, followed by transportation with 27%, industry with 22.8% and the rest in other types of energy uses [Buhaug et al. 2009]. This study will focus on the international shipping and fishing sector which represents around an average of 3.1% of the global carbon emissions between the years 2007 and 2012 [Smith et al. 2014].

[2] For a more detailed explanation on GWP please refer to Appendix I – Environmental and health characteristics of a working fluid.

1.2 SHIPPING'S EMISSIONS

At first sight, CO_2 emissions might seem irrelevant due to shipping totalling a small contribution of total emissions but, still, in order to mitigate the effects of climate change due to anthropogenic activities, the efforts of all energetic sectors are required. If nothing was done in the maritime sector and the economic and population growth were to keep increasing, the CO_2 emissions in 2050 could triple the levels seen in 2012 [Smith et al. 2014]. Interestingly, there was a reduction of around 17.1% in the participation of global CO_2 emissions by shipping: from 3.5% in 2007 – 1,100 Mt of CO_2 – to 2.7% – around 949 Mt of CO_2 – by the end of 2012. The shipping emission drop represented 32.3% of the UK total CO_2 emissions in the year 2013 [Department of Energy and Climate Change 2015]. The percentual decline is mainly caused by a constant rise in global CO_2 emissions, except for the year 2009. For the maritime industry these annual CO_2 emissions fluctuate considerably, however, overall it is clear that shipping is reducing its carbon emissions from the levels seen in 2007 (see Table 2).

Table 2: Global CO_2 emissions, its growth – both per year and compared to 2007 and including the average annual growth for the six years – are compared to those produced by shipping. The table also presents the proportion of marine CO_2 to the global annual emissions of CO_2 [Smith et al. 2014]**.**

Year	Global CO_2 emissions (10^6 t)	Global annual CO_2 emissions growth (%)	Global CO_2 emissions growth to the year 2007 (%)	Shipping CO_2 emissions (10^6 t)	Shipping annual CO_2 emissions growth (%)	Shipping CO_2 emissions growth to the year 2007 (%)
2007	31,409	-	-	1,100	-	-
2008	32,204	2.5	2.5	1,135	3.2	3.2
2009	32,047	-0.5	2.0	978	-13.8	-11.1
2010	33,612	4.9	7.0	915	-6.4	-16.8
2011	34,723	3.3	10.6	1,022	11.7	-7.1
2012	35,640	2.6	13.5	949	-7.1	-13.7
Average annual growth		2.6			-2.5	

Another important cause for the CO_2 emissions reduction in shipping is known as slow steaming. It is an operative strategy where vessels navigate at slower speeds than the speed for which the vessel was designed. The basic idea of slow steaming is to reduce the total average speed of the voyage, which will reduce the engine's power requirement and fuel consumption, hence a reduction in CO_2 emissions. Smith et al. [2014] found that the average ratio between navigational speed and design speed changed from 0.85 in 2007 to 0.75 at the end of 2012.

The number of vessels entering service between 2007 and 2011 increased the global fleet by around 7.0%, from 97,504 ships to 104,304 [Maritime Knowledge Centre 2009; Maritime Knowledge Centre 2012]. The global fleet CO_2 emissions could not be only explained by the size of the fleet and average fleet speed, but also because shipping emissions depend on the

fleet's age and is probably more important as stated by Smith et al. [2014], to the increasing need for shipping (i.e. fleet and capacity growth).

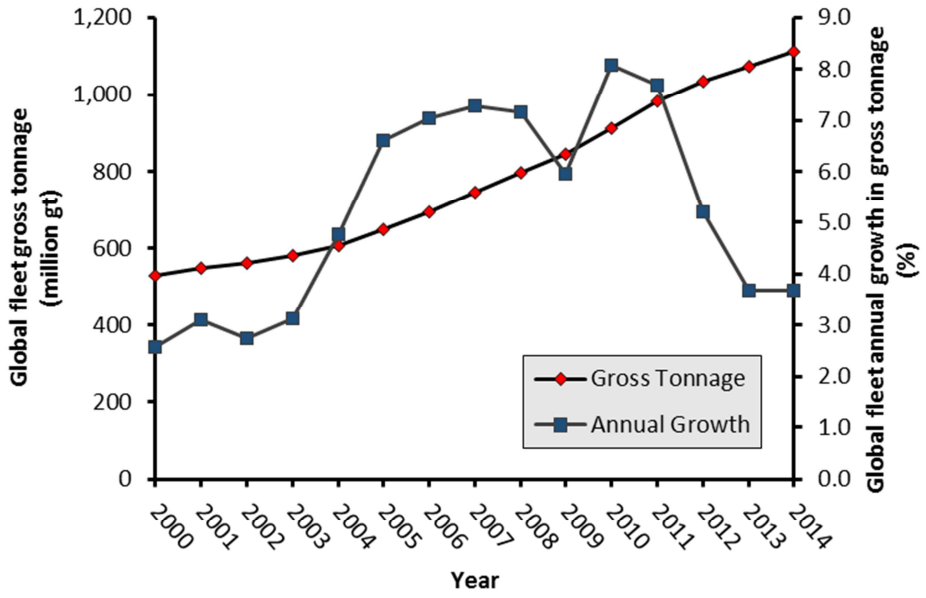

Figure 1: Total gross tonnage and annual growth in gross tonnage of world's fleet registered trading vessels of 100 gt and over from 2000 to 2014 [Department of Transport 2015]**. Between 2000 and 2008, the data recorded was at the end of June, while after 2009 it was at the end of December. The author took the average between years that were recorded at the end of June in order to predict the Gross tonnage and its annual growth at the end of each year.**

Gross tonnage (GT) is a dimensionless index which measures the ship's internal cargo spaces and is used to calculate port duties and regulation fees among others. In terms of GT, it is seen in Figure 1 that by the end of 2011 there was a growth of around 32.1% from the levels in 2007, but having had a considerable dip in 2008 due to the economic crisis. For the same years, the global fleet GT per vessel changed from 7,600 gross tonnes (gt) per vessel in 2007 to 9,500 gt per vessel at the end of 2011 [Maritime Knowledge Centre 2009; Maritime Knowledge Centre 2012; Department of Transport 2015]. The annual growth in GT has been in a downward trend since 2010 which can be explained by the vessels' GT entering and exiting service between the year 2011 and 2013[3]. From Figure 2, it is seen that the net GT per year reduces, almost in a linear trend, by around 17.0 million gt. The year 2012 is the highest year during which gross tonnage was scraped at around 36.3 million gt, representing around 3.5% of the global fleet GT of that year [United Nations Conference on Trade and Development 2014; Department of Transport 2015]. Buhaug et al. [2009] forecasted that by the end of 2050 the fleet growth, expressed in gross tonnage, could be around an average of 215% when compared to the levels seen in 2007.

With regard to carrying capacity, shipping uses the concept of deadweight tonnage (DWT) which is a measure that gives the difference in mass between the light – no cargo – and loaded

[3] Data for the analysis was only available from the United Nations Conference on Trade and Development (UNCTAD) for the years mentioned (i.e. [United Nations Conference on Trade and Development 2013; United Nations Conference on Trade and Development 2014; United Nations Conference on Trade and Development 2015]). While it is not the same database used for the global fleet gross tonnage, it helps to understand the causes of the negative trend for the annual growth in gross tonnage between 2011 and 2013.

displacement – cargo, crew and fluids etc. – representing the total mass that the ship can carry. By the end of 2011, the global fleet increased around 35.0% from the levels in the year 2007 (see Figure 3) [Department of Transport 2015]. The average deadweight per vessel increased from 11,200 t in 2006 to 14,000 t in 2011 which indicates that newer vessels tend to have larger capacities [United Nations Conference on Trade and Development 2013]. Similar to the gross tonnage, the DWT growth has been slowing since 2010 at an average pace of 16.0 million t per year [Department of Transport 2015]. Smith et al. [2014] predicted that by the year 2050 the majority of the vessel capacity distribution will stay the same except for the case of container ships, liquefied gas carriers and dry bulk carriers where the majority of their DWT will be shifting to larger ships augmenting even more the deadweight per vessel.

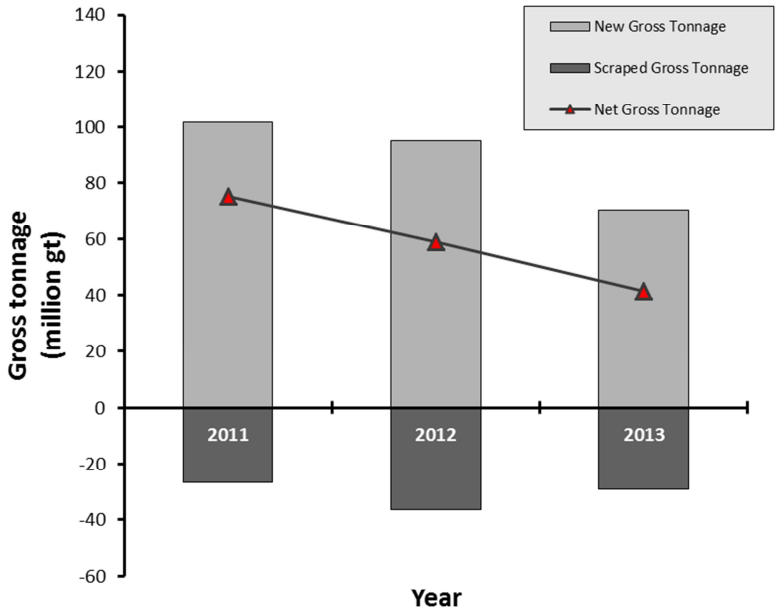

Figure 2: Representation of new and demolished vessels represented in gross tonnage between 2011 and 2013. The gross tonnage balance is represented by the line series which shows a reduction of around 22% in gross tonnage per year [United Nations Conference on Trade and Development 2013; United Nations Conference on Trade and Development 2014; United Nations Conference on Trade and Development 2015].

Larger capacities per vessel require larger installed power on board. On average, the global fleet in 2012 saw an increment in installed power, depending on the ship's category, between 15% and 30% from the year 2007 [Smith et al. 2014]. For example, bulk carriers with more than 200,000 dwt changed from an average of 18.9 MW in 2007 to 22.2 MW in 2012, an increment of 17.4%.

Shipping is one of the transportation modes with more growth in energy demand in the past two decades (i.e. 1990-2006). In countries belonging to the Organization for Economic Co-operation and Development (OECD), the shipping energy demand increased by 2.0% whilst compared to non-members, it reached 7.3%. Just to give a comparative point of view, aviation in the same period, grew only 3.4% and 2.1% in the above mentioned groups [International Energy Agency

2009]. By 2007, the seaborne trade had crossed the barrier of 40 billion t-nm [4], six years later it reached 50 billion t-nm a growth of 23.7% [United Nations Conference on Trade and Development 2015]. The International Maritime Organization (IMO), using the IPCC scenarios, predicted an average growth limit for shipping in t-nm of around 147% to 302% for 2050 [Buhaug et al. 2009]. These calculations are strongly linked with GDP, population, market, fuel price and route growth.

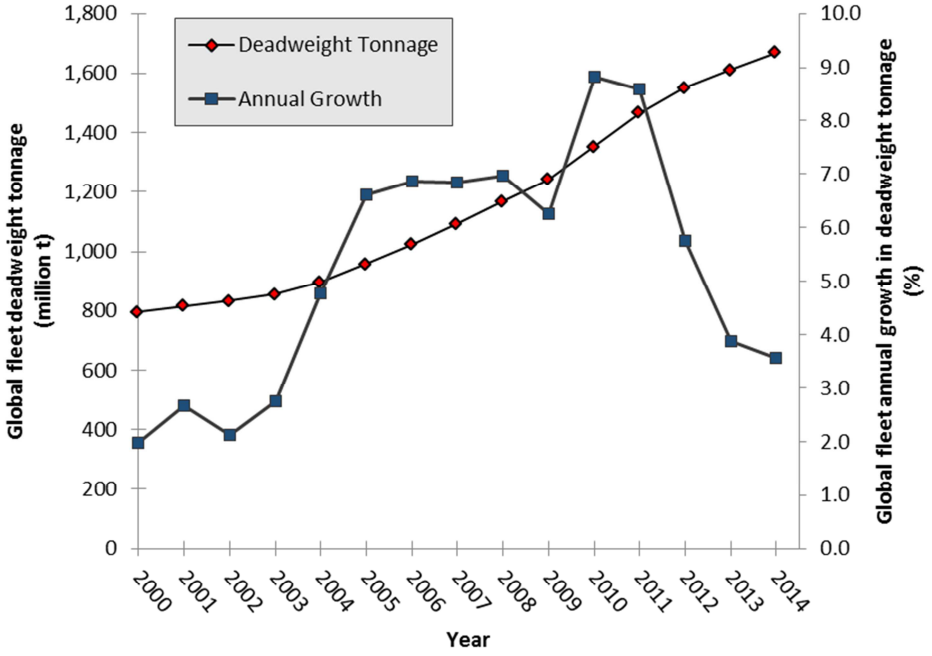

Figure 3: Total DWT and annual growth of world's fleet registered trading vessels of 100 gt and over from 2000 to 2014 [Department of Transport 2015]**. Between the years 2000 and 2008 the data recorded was at the end of June, while after 2009 it was at the end of December. The author took the average between years that were recorded at the end of June in order to predict the DWT and annual growth at the end of each year.**

By translating the future energy demand for shipping to CO_2 emissions, it was found that if no other policy is implemented, and the patterns of social and economic behaviour do not change by 2050, the CO_2 emissions would grow by 350% from the 2012 level (i.e. 810 million t of CO_2). More optimistic prospects expect a reduction in emissions of around 1.0% by the year 2050, assuming an economy that will depend more on local markets, population growth rate stagnation and whether there is a large take-up of liquefied natural gas (LNG) in the marine industry [Smith et al. 2014]. Thus, shipping compared with other modes of transportation represents an opportune sector to target, with a higher probability of significant impact, the long term reduction of GHG emissions.

1.2.1.1 Energy Efficiency Design Index

Growing environmental concerns drove the IMO, through Emission Control Areas (ECA) to enforce a number of measures aimed at regulating emissions, particularly SO_x and NO_x. More

[4] The t-nm unit measures the activity of the shipping industry. This unit combines demand, routes, fleet (their capacities) and growth, and can be translated into energy requirements and CO_2 emissions. Tonne is used here as a metric ton, 1 tonne = 1,000 kg. The nm stands for nautical mile, where 1 nm = 1,852 m [Thompson 2008].

recently for CO_2 the Internal Convention for the Prevention of Pollution from Ships (MARPOL) adopted the Energy Efficiency Design Index (EEDI). The EEDI only applies to newly built ships and is determined by different ship characteristics such as rated power, fuel consumption and capacity, among others. The index units are given in g CO_2/t-nm, meaning that it measures the ship's carbon footprint per unit of transport work (*TW*) [International Maritime Organization 2009a]. A generic and simple way of presenting the EEDI formula is shown below[5]:

$$EEDI = \frac{\Sigma CE_{ME} + \Sigma CE_{AE} + \Sigma CE_{PTI} - \Sigma CE_{GT}}{TW} \quad [1]$$

Where the CE_{ME} refers to the main engine CO_2 emission per hour, CE_{AE} to the auxiliary engine CO_2 emission per hour, CE_{PTI} to the CO_2 emission produced by the shaft motor per hour, CE_{GT} reflects the CO_2 emission mitigated by the use of different energy efficient technologies on board per hour, and *TW* is given by the capacity of the vessel multiplied by its reference speed – in kn per hour – in deep and calm waters. It is important to keep in mind that the EEDI formula is calculated at the 75% rated installed power – 75% Maximum Continuous Rating (MCR) – of the main engine and shaft motor. For the auxiliary engines, the power output is calculated at 100% MCR only considering the power required for propulsion machinery, and accommodation.

The EEDI formula uses conversion factors to calculate the CO_2 emitted by vessels when using a particular type of fuel; these are called carbon factors (C_F) and are shown in Table 3. Inside the EEDI formula, there are correction factors that account for the different vessel' design elements (e.g. Ice class or levels of redundancy), weather conditions (e.g. wave height), regulation limitations on capacity, green technology availability (e.g. sails), among others.

Table 3: Values of carbon content and carbon factors for different marine fuels used in the industry [International Maritime Organization 2012]**.**

Fuel		Carbon Content (m/m)	C_F (t CO_2/t Fuel)
Diesel/Gas Oil (MDO/MGO)		0.8744	3.206
Light Fuel Oil (LFO)		0.8594	3.151
Heavy Fuel Oil (HFO)		0.8493	3.114
Liquefied Petroleum Gas (LPG)	Propane	0.8182	3.000
	Butane	0.8264	3.030
Liquefied Natural Gas (LNG)		0.7500	2.750

The EEDI became compulsory at the beginning of 2013; the limits imposed that year became the reference line for the following stages of the index. The reference lines are specific for each type of vessel (i.e. tankers, containers, etc.) and were based on the EEDI from existing vessel data [Lloyd's Register 2012a]. The EEDI reference curve is of the form $\alpha\beta^{-\gamma}$, where α and γ are parameters that apply to the type of ship given in International Maritime Organization [2011a], and β is the ship's DWT. With the passage of the years, the EEDI becomes more stringent (see

[5] For the complete formula with all variables and factors, please refer to Appendix II – Energy Efficiency Design Index and for how the formula works refer to the following reference: [International Maritime Organization 2012].

Table 4 and Figure 4) forcing the shipping industry to create new solutions for which can reduce effectively its global participation on CO_2 emissions.

Table 4: EEDI reduction percentage for the different stages established by IMO [Lloyd's Register 2012a].

Stage	Starting Year	EEDI Reduction from reference line (%)
1	2013	0
2	2015	10
3	2020	15-20 [3]
4	2025	30

[3] For general cargo vessels above 15,000 dwt the limit is 15%, for other type of vessels is 20%.

The EEDI is an incentive to realise the subject of this research because it provides the industry with a clear indicator of the impact of applying green technologies to ships. Theotokatos and Livanos [2012] achieved an EEDI reduction of around 1.8% by converting the available waste energy from a bulk carrier's two-stroke diesel engine to steam, by using a waste heat recovery boiler, but also to produce electricity via a thermodynamic cycle. The reduction achieved by installing the energy efficient technologies allowed the vessel to have an EEDI of 5.02 g CO_2/t-nm, below the 2013 EEDI requirement of 5.11 g CO_2/t-nm. Using LNG instead of HFO produces a drop of around 26.9% in the EEDI, from 32.4 g CO_2/t-nm to 23.7 g CO_2/t-nm, on the EEDI of a RoRo ship [Livanos et al. 2014].

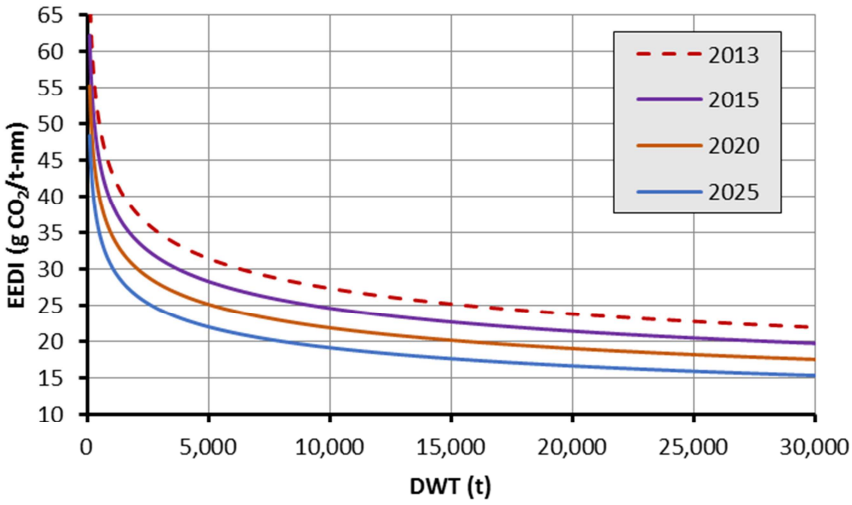

Figure 4: Container ships' EEDI curves for different deadweight at the four initial stages of this index. The dash line is known as the EEDI reference line.

Calleya et al. [2015] found that there is a considerable drop in CO_2 emissions when using LNG for a Panamax container but argue that by considering the loss of cargo space due to the larger fuel volume – when compared to HFO or MDO – the EEDI would be higher. In this case the EEDI of the baseline design is found at 43.0 g CO_2/t-nm, and when considering the LNG volume requirement the index increases to 53.4 g CO_2/t-nm. Suárez de la Fuente et al. [2015] found

that a simple waste heat recovery system (WHRS) using the available waste heat from the exhaust gas could reduce the EEDI of a Aframax tanker by a maximum of 1.9%. It is important to remember that this index is under development and there are areas of improvement which can help to achieve greener shipping.

1.2.1.2 SULPHUR REGULATION

The sulphur contained in any fuel during combustion reacts with the oxygen available in the scavenge air and produces sulphur oxides (SO_x) such as SO_2 [Pan 2011]. Sulphur oxides are harmful to the environment since the acidification potential of the surrounding atmosphere is increased meaning that with the air's humidity the formation of sulphuric acid is possible [Gilbert 2014]. For example, SO_2 is classified by the Hazardous Materials Identification System (HMIS) from the National Paint and Coatings Association [2002] as a toxic substance level 3 – out of a maximum of four – and a physical hazard level of 2 – where the maximum is three. A higher presence of SO_x has a negative impact on human health principally in the respiratory system, such as difficulty in breathing and inflammation of the airways [Pan 2011].

In order to mitigate the SO_x emissions caused by the marine industry, the IMO established Regulation 14 which delimits the amount of sulphur content by mass for a marine fuel [International Maritime Organization 2013a]. Also, the IMO recognises a number of target areas considered particularly sensible to marine emissions designated ECA (e.g. the Baltic Sea), and are subject to stricter emission regulations. Inside ECAs the sulphur content is limited to 0.1%, or less in mass, while outside ECAs the content should be equal or less than 3.5% (see Figure 5). The number of ECAs is expected to increase in the near future, requiring ship owners to comply with more stringent regulations to continue shipping globally [International Maritime Organization 2014a].

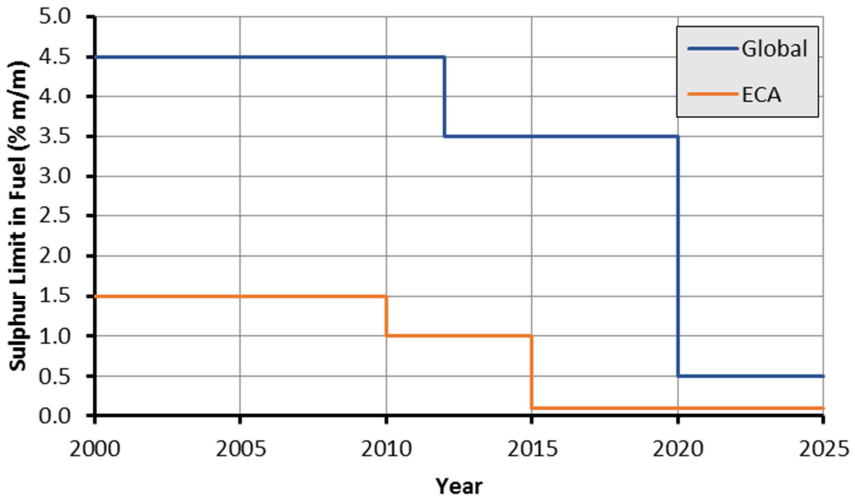

Figure 5: IMO regulation 14 fuel sulphur limits.

Ship operators have different approaches to comply with the sulphur regulations. The first option is to switch to a fuel that contains less sulphur, such as LNG or MGO. If the vessel is navigating in and out of ECAs, then dual fuel engines are required. A second option is to continue using the same high sulphur content marine fuel inside ECAs and then remove the SO_x from the exhaust gas, via a scrubber, before the exhaust gas escapes into the atmosphere.

An alternative option is given by Nielsen et al. [2014] where the exhaust gas temperature is lowered below the SO_x dew point (i.e. 165°C for high sulphur fuels) which allows it to absorb more waste heat from the exhaust gas in order to produce power via a WHRS. The lower temperature causes the condensation of the SO_x to then be captured inside a special heat exchanger.

In this thesis, the study of the formation and quantification of SO_x reduced by increasing the vessel's fuel efficiency will not be undertaken. The regulations in place for marine fuels regarding sulphur content will be considered. This will play an important role since depending on the vessel's route, the fuel to be used will change. The selection of different fuels presents a large range of outcomes such as, for example, MDO which is around 60% more expensive than HFO[6] [Bunker Index 2015]. This means that if a fuel efficient technology is used on board it could be assumed, a priori, that when using MDO the payback time will be shorter.

1.2.1.3 NITROGEN REGULATION

The scavenge air in its majority is composed by nitrogen (N_2) (i.e. around 78% by volume) and oxygen (O_2) (i.e. around 21% by volume) which react chemically to form nitrogen oxides (NO_x). But NO_x can be also formed when the fuel's N_2 is oxidised in the combustion chambers, for example, HFO contains 0.46% of N_2 by mass while MGO is below 0.05% by mass [Winnes & Fridell 2009; Kristensen 2012]. Nitrogen oxides emissions in a combustive process are dependent on the engine's temperature, where higher temperatures produce more NO_x [Woodyard 2009; Winnes & Fridell 2009]. The primary NO_x compound found after combustion is nitric oxide (NO), of which a maximum of 10% will be reacting with more O_2 to form nitrogen dioxide (NO_2) and a small proportion of nitrous oxide (N_2O) is formed at the same time [Kristensen 2012].

Nitrogen oxides have important negative effects in humans, nature and the environment. The different compounds produce breathing problems, help in acid deposition, are believed to be carcinogenic, contribute to photochemical smog; but also – in conjunction with volatile organic compounds – increase the tropospheric ozone[7] [Woodyard 2009; Kristensen 2012].

For these reasons, the IMO created Regulation 13 which limits the NO_x emission both in ECA and non-ECA [International Maritime Organization 2013b]. As per Figure 6, any ship built in 2015 should comply with Tier II limits which bring a reduction of between 15% and 22% on NO_x emissions – depending on the engine's speed – from the levels imposed by Tier I.

Tier III levels represent a drop in NO_x emissions of around 80% from Tier I, and this will only apply for vessels constructed after the end of 2015 which are navigating in ECA. For non-ECA ships, Tier II levels will be used. As stated by MAN Diesel & Turbo [2012a], Tier III levels will be possible by the use of different technologies. Ladommatos et al. [1998] show that it is possible

[6] Average prices were taken between November 2014 and May 2015 for MDO and HFO with a viscosity of 380 cSt.

[7] Please refer to Appendix I – Environmental and health characteristics of a working fluid for more about ozone depletion.

to reduce diesel engine NO_x emissions via an exhaust gas recirculation (EGR) which adds a small part of the exhaust gas into the scavenge air.

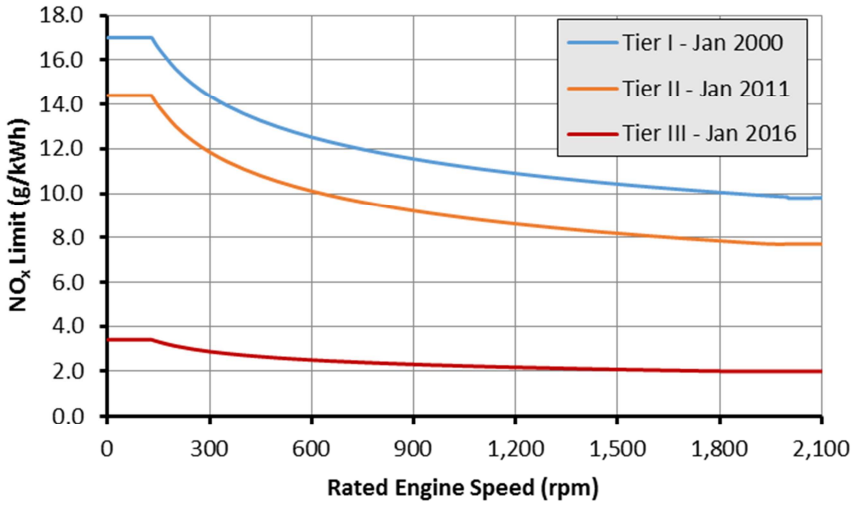

Figure 6: IMO's NOx caps for ships depending on the year of construction and engine's speed [International Maritime Organization 2013b].

As was the case with SO_x emissions, the study of NO_x and its reduction is out of the scope of this study but the regulations will be considered with regard to engine selection and the ECA status of the sea area navigated.

1.2.1.4 METHANE AND LIQUEFIED NATURAL GAS

Liquefied natural gas is composed of more than 85% of its volume by methane (CH_4), and is basically natural gas but stored at extremely low temperatures (i.e. around -162˚C) at which it becomes liquid and suffers a considerable reduction in volume (i.e. 600 times less than its gaseous state) which facilitates its transportation and usage [Strategic Center for Natural Gas 2004]. An important environmental advantage of using LNG on board is that SO_x emissions are almost eliminated; but there is also a reduction of around 25% in CO_2 and a maximum reduction of 90% for NO_x emissions when compared to traditional marine fuel oils [Woodyard 2009; Afon & Ervin 2012; Burel et al. 2013]. On the economic side, the vessel operator could be saving around 35% in operational cost when switching to LNG [Burel et al. 2013]. Furthermore, with the revolution on shale gas extraction, gas availability has increased which helps reducing the logistical obstacles of supplying LNG to ports and ships [Royal Academy of Engineering 2013].

The concept of methane slip attempts to quantify the CH_4 that goes unburnt during combustion. The importance of this is that CH_4, as previously mentioned, has a GWP of 30 [Myhre et al. 2013] meaning that any percentage of it escaping into the atmosphere will have a greater impact than CO_2. For old Otto cycle gas engines the CH_4 escaping could be as high as 15.0 g/kWh which represents around 9.0% of the specific fuel consumption [Corbett et al. 2015]. Rolls-Royce has been working on the concept of lean-burn in order to achieve a lower CH_4 slip claiming around 3 g/kWh of gas excaping the Otto engine [Pospiech 2014]. New two-stroke dual fuel diesel engines achieve a CH_4 slip of less than 0.2 g/kWh, representing less than 0.2% of the specific fuel consumption [Juliussen et al. 2011].

It has been projected that the usage of LNG as a fuel by the marine industry will increase in the coming years, causing an increment in CH_4 emission of up to 7,900% for 2020 and it will rise 42,000% in 2050 when compared to the levels seen in 2012 (i.e. close to 288,000 t) [Smith et al. 2014]. Because of this, CH_4 emissions will play an important role in the global warming mitigation strategy for the shipping industry. For now there is no regulation limiting CH_4 emissions, but it is the opinion of the author that as LNG begins to play a bigger role in the maritime world, and transport in general, it will be of high priority to cap and control CH_4 emissions. In this work, the study of CH_4 emissions and its reduction is out of scope.

1.3 AREAS TO MITIGATE THE SHIP' CARBON DIOXIDE

The projections of CO_2 and other GHG emissions stress the importance of beginning to generate intelligent environmental-friendly solutions today, based on new strategies and technologies, which will help to follow a green agenda.

According to Alvik et al. [2010], the three most efficient options to reduce the maritime CO_2 footprint are: using LNG to power the ship, speed reduction (i.e. slow steaming) and the use of WHRS.

The use of LNG in the maritime industry along with some of its advantages and disadvantages, as well as its future role in GHG emissions, was discussed in the previous subsection. The second option mentioned, slow steaming – briefly covered in section 1.2 – is a practice that is becoming common in the shipping industry which reduces fuel consumption, hence a reduction in the CO_2 footprint. The engine power requirement changes by the vessel's speed as shown in the following formula [Taylor 1996; Woud & Stapersma 2012]:

$$\dot{W} \approx 0.073 \frac{\Delta^{2/3} v^n}{A_c} \qquad [\,2\,]$$

Where $\dot{W}$ is the power required to move the ship in kW, Δ is the ship displacement in kg [8], v is the ship speed in m/s and Ac is the Admiralty coefficient which is dimensionless, constant and depends on the hull shape, and n is the speed's power normally assumed between 3.0 and 4.0 [MAN Diesel & Turbo 2011]. The cubic value of the ship's speed is a common approximation but MAN Diesel & Turbo [Ibid.] recommends a value between 3.2 and 4.0 – depending on the type of vessel.

Figure 7 is the representation of the power demand of a 4,100 twenty-foot unit (TEU) container vessel using equation [2] – assuming a cubic power speed relationship – and the data available from MAN Diesel & Turbo [2015a] and Container-Info [2014]. From this figure, it is seen that the power requirement will change drastically with small changes in the ship's speed while the specific fuel oil consumption (SFOC) is more dependent on the engine's tuning. In this particular case, the tuning was set for operations between 60% and 70% MCR.

[8] Normally in this formula the Δ is expressed in tonnes and v in knots. To use tonnes and knots only remove the coefficient 0.073.

The positive effect of slow steaming is a reduction in CO_2 emission – via fuel savings – without the necessity of installing new and complicated equipment. Jorgensen [2011] states that there was a reduction of around 4,000 t in bunker oil for large container ships on the same route when changing their navigation speed from 24 kn to 12 kn. The fuel savings are attractive enough for ship owners and operators to implement this strategy in their fleets. In 2012, MAN PrimeServ [2012] performed a survey about the common practices regarding slow steaming. The survey showed that 15.4% of container fleet operators who responded said that more than half of their fleet is using slow steaming; for bulk carriers it was above 26.2%.

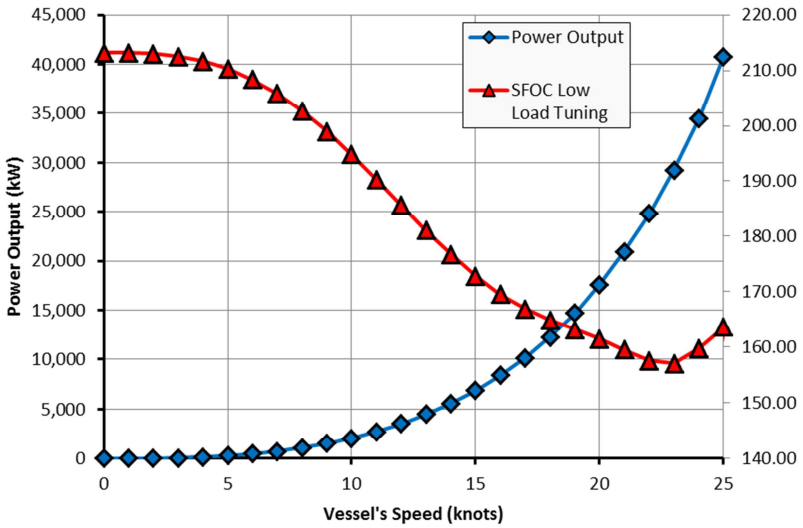

Figure 7: 4,100 TEU container ship mechanical power demand – calculated using a cubic relationship between vessel speed and power output – and fuel consumption for its operative speeds. The engine has a tuning suitable for an engine loading between 60% and 70% MCR. The data is obtained using an ambient temperature of 25˚C [Containership-Info 2014; MAN Diesel & Turbo 2015a]**.**

Maersk's slow steaming procedure among its fleet dictates that the engine load should be set to 40% MCR, instead of the usual 70% - 85% MCR [Wiesmann 2010]. But this strategy requires optimising cargo utilisation, time on port and scheduling in order to avoid penalties for late arrivals and disruptions [American Bureau of Shipping 2013]. Wiesmann [2010] shows some slow steaming side effects which are relevant to ship operation: A) it can deliver a low fuel efficiency even though CO_2 and fuel consumption is lower; and B) there will be a requirement to buy more ships in order to cover the demand lost by reducing voyage speed. Furthermore, with slow steaming there is the possibility of engine fouling, excessive lubrication oil consumption, and increased heat load on engine components, among others. These side effects can be lessened with the engine's modifications to cope with low load, change to the ship's propellers, and other strategies are implemented, such as increasing the engine loading occasionally to blow soot [American Bureau of Shipping 2013].

The last option discussed in this chapter is WHRS that has been discarded in the past due to poor effectiveness in generating useful power, costs, space required, and mass among others [Alvik et al. 2010]. Nowadays, with new greenhouse gas emission restrictions and increases in fuel prices, the maritime industry has begun to revisit the feasibility of WHRS. The IMO has

predicted that WHRS could reduce, by the year 2050, CO_2 emissions by around 2%-6% depending on the ship type [Bazari & Longva 2011]. MAN Diesel & Turbo forecasted, by using the BIMCO EEDI calculator, that the use of WHRS would result in a drop in the EEDI of around 9.2% for an 11,000 TEU container ship [MAN Diesel & Turbo 2012b].

Furthermore, Buhaug et al. [2009] calculated the percentage of energy loss found in the different shipping systems operating in a range of ship types and cruising conditions (e.g. calm seas). For all the different ship configurations, only around 30% of the energy used ends as useful thrust. The losses arise from the hull's friction with the sea, heat escaping from the prime mover's surface due to the combustion process or transmission losses. Areas of great loss are found inside the prime mover system (e.g. heat from the gas exhaust) and propulsion (e.g. propeller losses) which amounts to an average of 52% and 17% of the total fuel energy respectively. This gives a good overview of areas for opportunities to reduce ship energy losses, but above all shows the importance of improving the prime mover's performance.

1.3.1 SHIP'S PRIME MOVER

The prime mover is responsible for performing the combustion process where the fuel chemical energy is converted to mechanical work. Common combustion engines found in ships are slow (90-130 rpm), medium (400-600 rpm) and high speed (1000-1800 rpm) diesel, gas and steam turbines [Molland et al. 2011]. Steam and gas turbines represent the lowest thermal efficiency (η_{th}) at around 32% with it highest example – an intercooled recuperated gas turbine – at around 42% [Woodyard 2009]; while the large low-speed diesels have their highest thermal efficient example at around 53% [Buhaug et al. 2009].

Gas turbines present interesting characteristics for vessels such as high power-to-weight/volume ratios, low NO_x and SO_x emissions when compared to diesel engines, fast start-ups and shut downs and low operational and maintenance costs. Diesel engines are typically the prime mover of choice for high efficiency shipping vessels. From the more than 100,000 commercial ships above 100 dwt navigating the oceans, only around 3% are not powered by diesel primer movers, making them the main polluters in the shipping sector [Smil 2010; Smith et al. 2014]. Furthermore, using the projections of Smith et al. [2014], it is appreciated that the consumption of HFO and MDO from the maritime industry for the year 2050 could represent between 75% and 92% of the bunker market, with a growing demand for LNG which will represent the rest of the market. The work of the Royal Academy of Engineering [2013] does not project any considerable growth in the future for other alternative fuels such as biofuels. This does not mean that they will not play an important role in the future of the maritime world, but rather that their development and technical requirements are still under development. Good examples are the *Stena Germanica* using methanol [Browne 2015] and *Maersk Kalmar* using algae-based biodiesel [The Maritime Executive LLC. 2011].

Two-stroke diesel engines operating at slow speed are the most powerful diesel prime movers, having examples that can deliver an excess of 80 MW such as the MAN B&W ME-series [Woodyard 2009] or Wärtsilä RT-flex series [Wärtsilä Corporation 2012]. These powerful engines are typically seen in large vessels such as container ships and bulk carriers [Smil 2010;

Shu et al. 2013]. These engines are preferred over their four-stroke counterparts because of their robustness, the fact that they require no gearbox between the engine and propeller, and the possibility to burn HFO efficiently [Woodyard 2009; Smil 2010]. On the other hand, it is common to see four-stroke medium and high speed diesel engines as prime movers for small size ships such as tugs, but also as auxiliary engines on board vessels to generate electricity where electrical power outputs are well above 5.0 MW_e [Smil 2010; Wärtsilä Corporation 2012].

Diesel engine thermal efficiency has plateaued in recent years [Woodyard 2009], but there are efforts to include more efficient designs that can satisfy current regulations while still being profitable for the vessel operator. For example, tuning an engine is a standard procedure of ship maintenance and will guarantee that the ship engine will run correctly. Since there are several variables that can directly affect the engine performance of a ship such as weather, wear, operating conditions and fuel properties, that will require better tuning than that set at the design conditions. To solve this and deliver the best performance from the engine, disregarding the external variables, an auto-tuning system can be installed. Benefits coming from auto-tuning are around 1%-3% in fuel savings with a payback period of a maximum of 20 months [Gary 2009]. Another example is the designing of engine elements, such as pistons and bearings, with lower friction levels helping to reduce energy loss. Jensen [2009] was able to reduce engine friction losses by 20% by improving only the guide shoe bearings.

Looking into the exhaust gas, it is common in marine engines to harvest energy through the usage of turbochargers which convert the high pressure and high velocity gas flow into rotation via an expansion turbine. The mechanical power generated compresses incoming air which makes the fluid denser but also increases its temperature. Before entering the combustion chamber, the air must be cooled down. This will guarantee a better combustion process that allows burning fuel more efficiently inside the engine's cylinders than in a natural aspirated engine [Shu et al. 2013]. These factors produce a more powerful and environmentally-friendly engine with the same displacement; or it is common to have smaller engines that produce the same amount of power output as a natural aspirated marine power plant [Shu et al. 2013]. Nowadays, turbochargers can reach efficiencies of up to 70% [Woodyard 2009]; Baines et al. [2010] give an approximate map of the turbocharger's heat losses where 70% go to the surroundings via conduction, convection and radiation, while 25% escape to the cooling system and 5% is transferred to the compressor side.

Another technology that uses the wasted energy from the exhaust gas is the power turbine – also known as turbo-compound – which works in a similar way to a turbocharger but instead of the expander's shaft being connected to a compressor, it can be connected to the vessel's shaft or to an electrical generator. Weerasinghe et al. [2010] found that a turbo-compound system installed in a small diesel engine could reduce the fuel consumption by 2%, and MAN Diesel & Turbo [2012b] predicts that this technology could return between 3.3% and 5.5% of the engine's power output[9] depending on the vessel's operating conditions and engine's loading.

[9] The return power was calculated using the electrical power return predicted by MAN Diesel & Turbo and assuming an electrical efficiency of 90%.

As mentioned before, heat is how the majority of the energy not used on board is transported out of the diesel engine. Focusing on the energy map of large two-stroke slow speed diesel engines, a maximum of 53% – depending on load and operative conditions – of the fuel's energy used manages to produce useful mechanical work. The rest of the fuel's energy can be found in the heat removed from the engine by the cooling system (20%-30%), heat escaping from the engine surface due to convection or radiation (1%-5%) and finally a significant proportion through the exhaust gases (25%-45%) [Woodyard 2009; Balaji & Yaakob 2012; Tchanche et al. 2014]. Figure 8 shows an example of an energy map for a large marine diesel engine which produces a maximum of 70 MW and has a thermal efficiency of around 49% which means that more than 50% of the fuel's energy is wasted.

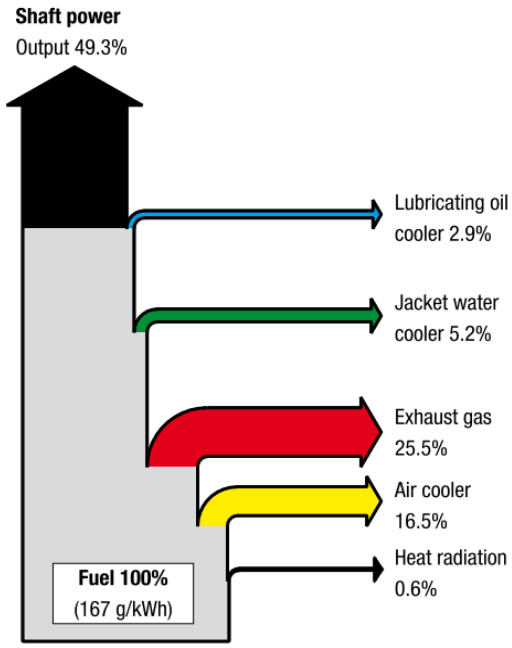

Figure 8: Sankey diagram representing the energy map of a large two-stroke diesel engine manufactured by MAN Diesel & Turbo at is maximum load and an ambient temperature of 25°C [MAN Diesel & Turbo 2012b].

While the waste heat coming from auxiliary engines is another area of opportunity on board a ship to reduce CO_2 emissions, this work will focus only on the prime mover, in particular for two-stroke diesel engines. As previously shown, this source of waste heat is an area of great potential for enhancing the ship's overall efficiency, with a final result of fewer emissions. There are various ingenious approaches to solve the problem of how this waste energy can be obtained and reused.

1.4 RESEARCH QUESTIONS

This thesis has the main objective of answering the following research questions:

1. Can other power waste heat recovery technologies reuse the low/medium quality waste heat available from the ship's prime mover more efficiently than the water-based Rankine cycle?

2. How does a waste heat recovery system behave under different WHRS plant layouts, environmental temperatures and the ship's operating conditions?
3. How does an alternative waste heat recovery system using the available waste heat from the ship's prime mover compare to a traditional water-based Rankine cycle in terms of the ship's CO_2 emission reductions?

These questions are answered with three different empirical strategies. First, a sensitivity analysis which will bring about an understanding of the probable operating conditions that a vessel will face during its useful life (chapter 7). In the second stage, three parameters are established which define the optimum WHRS on board and compare the performance of the alternative WHRS in a hypothetical case study in the Baltic (chapter 8). Finally, the implications and areas of opportunity for a marine WHRS when navigating in extreme cold weathers are explored via a case study near the Arctic Circle in chapter 9. Further details on the empirical strategy are presented in chapter 6.

(Page left intentionally blank)

2

Reusing The Ship's Prime Mover Waste Heat: Available Approaches And Technologies

Based on Suárez de la Fuente, S., 2016. Marine Waste Heat Recovery Systems (in press). *Encyclopedia of Marine and Offshore Engineering*, ed. Carlton, Jukes & Choo. (C) John Wiley & Sons, Ltd.

The engine's waste heat is an area of potential for enhancing the ship's overall efficiency, with the final result being fewer emissions. Some examples of how this waste energy can be reused are in the production of drinkable water or preheating the engine's intake air [Al-Rabghi et al. 1993]. There have been some projects where these concepts were applied with good results: a collaborative work between three different companies – Air Pressure Vessel (APV), DESMI A/S and LR-Marine – achieved a reduction of 20% in CO_2, NO_x and SO_x emissions by channelling the waste heat from the water system of a tanker in order to keep warm the vessel's cargo [Gary 2009].

A more technically-complicated waste heat usage occurs when it is used to generate mechanical power to assist in the vessel's propulsion or when used to generate electricity to cover part of the electrical demand inside the ship, but it is also possible to use the waste heat in the production of cooling power which supports the HVAC system (i.e. heating, ventilation and air conditioning). The aim of this chapter is to distinguish the most suitable technology for the prime mover's available waste heat with the purpose of reducing fuel consumption on board and hence a reduction in CO_2 emissions.

2.1 WASTE HEAT QUALITY AND INFLUENCE OF THE HEAT SINK

Before going through some of the waste heat recovery technologies, it is important to classify the waste heat by the temperature at which it is found. The higher the waste heat temperature, the more effectively it can be used, hence better quality. With this in mind, the waste heat will be classified in this work as follows [Dharmalingam et al. 2004; Utlu 2015]:

a) **High Temperature or high quality:** This is the waste heat that comes from a variety of processes with temperatures from 650°C and higher. These temperatures are commonly seen in furnaces, incinerators and cement kilns.
b) **Medium Temperature or medium quality:** The temperature range is around 230°C to 650°C. Common processes in this temperature range include the flue gases from reciprocating engines, turbines and boilers, as well as some furnaces and ovens. For example, efficient diesel engines present exhaust gas temperatures between 280°C and 360°C [Woodyard 2009].
c) **Low Temperature or low quality:** From around 30°C to 230°C. The heat waste arises from bearings, injection machines, internal combustion engines, pumps and air compressors, among others. This field presents the most challenging scenario for waste recovery systems because it is more difficult to extract energy when the temperature gradient between the source and the sink is smaller; it also tends to be less cost effective. In this classification also the internal combustion engines are found [Dharmalingam et al. 2004], it is not uncommon to see temperatures as low as 75°C coming out of a marine diesel engine cooling system [MAN Diesel & Turbo 2013a].

The extraction of available energy from any waste heat is limited by the temperature gradient between the waste heat source and the heat sink [Cengel & Boles 2007]. As per Carnot's

theorem, and only when using absolute temperatures (i.e. Kelvin), the reversible thermal efficiency – also known as Carnot thermal efficiency – can be expressed as follows[10]:

$$\eta_{th,reversible} = 1 - \frac{T_C}{T_H} \qquad [\,3\,]$$

Where T_H is waste heat source temperature and T_C is the sink temperature. For example, in an ideal thermodynamic cycle which uses a given type of waste heat quality (e.g. medium) to generate mechanical power, the only possible way that the cycle will be capable of exploiting all the energy potential – assuming a perfect system which does not suffer loss – is by lowering the sink temperature to -273.15°C (see Figure 9). This is an improbable scenario on board a ship due to material and equipment limitations, but there is also the fact that it has not been possible to reach the absolute zero [de Podesta 2013].

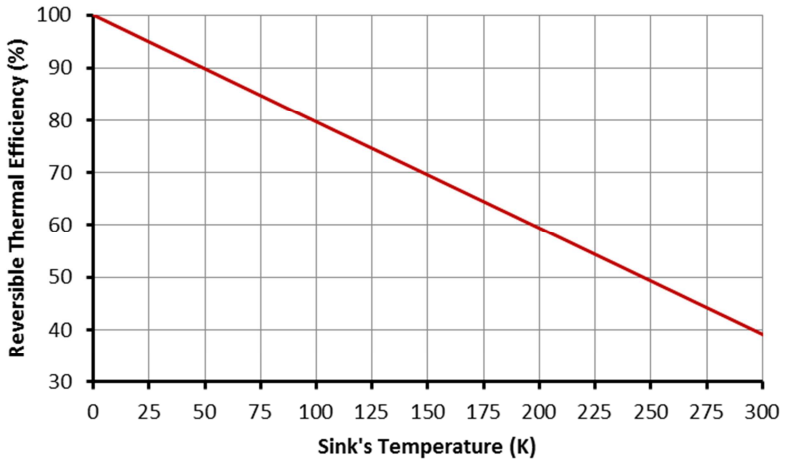

Figure 9: Thermal efficiency as defined in equation [3] of an idealised thermodynamic cycle which extracts the available waste heat from a ship's exhaust gas at a temperature of 220°C.

Even with high quality waste heat and absolute zero temperatures at the heat sink, it is not possible to utilise all the energy available as waste heat due to energy changes (e.g. from heat energy to kinetic energy) and imperfections found in the heat recovery system equipment (e.g. heat transfer losses from heat exchangers) among others [Energy Efficiency Guide for Industry in Asia 2006].

Seawater is the preferred fluid in marine WHRS due to its high specific heat and density, requiring low pump power consumption and compact condensers, but also due to its easy availability [Quoilin et al. 2013]. The sea surface temperature (SST) average annual minimum and maximum is between -0.6°C and 31.9°C respectively [US Department et al. 1998; Climate Change Division US EPA 2012]. On the other hand, seawater is highly corrosive and allows bio-organisms to settle inside the heat exchangers. These shortcomings require use of specialised materials to resist corrosion, constant monitoring and cleaning to reduce the negative effects of fouling – can represent up to 40% of the thermal resistance experience in a heat exchanger

[10] Please refer to Cengel & Boles [2007] for Carnot's theorem and the demonstration of equation .

[Cristiani & Giancola 2000]. These solutions will have an important repercussion in initial, operational and maintenance costs. Air can see temperatures as low as -50˚C at the polar latitudes while temperatures above 35˚C are not uncommon near the Equator [Jones et al. 1999; Jones et al. 2012]. The air's temperature is an area of opportunity not fully explored for improving the performance of marine WHRS.

2.2 STEAM DEMAND

It is common nowadays inside a vessel to have a waste heat boiler (WHB) to generate steam [McGeorge 2002; Tien et al. 2007]. Steam is needed to cover part of the ship's thermal demand which is built by the thermal requirement for living spaces or when cold-starting the engine, warming the fuel in order to have the viscosity as recommended by the engine's manufacturers – especially for HFO – or to operate different ship equipment.

The steam demand varies with the environment's temperature, and the type and size of the vessel. This is demonstrated by MAN Diesel & Turbo [2005] where a 6,000 TEU at an ambient temperature of 25˚C requires around 2,400 kg/h of steam, while at a temperature of 45˚C the demand reduces to 1,600 kg/h. It is also shown that a very large crude carrier (VLCC) requires around 20% less steam than a 4,500 TEU container ship at an ambient temperature of 25˚C. Benvenuto et al. [2014] considered a steam consumption of around 1,400 kg/h only for thermal services on board a 158,000 dwt crude tanker. Burel et al. [2013] give a detailed thermal demand analysis where the majority of the thermal energy is used to warm the cargo carried to a stable temperature of 65˚C; the rest of the available steam was used to produce mechanical work via a thermodynamic WHRS. Going further, Gymnopoulos [2013] calculated the heating demand for the living spaces of a 45,170 dwt bulk carrier navigating through the Arctic waters – assuming a temperature of -10˚C – the heat analysis was performed room by room and considered the heat input of the crew. Gymnopoulos found that 846 kW of thermal power was required to keep warm the vessel. Soffiato et al. [2015] studied the production of steam using a WHB and auxiliary boilers – when the waste heat sources were not enough – but the work failed to outline the steam demand of the LNG carrier.

The importance of steam production and thermal management is highlighted by these works and it is important for this thesis to consider a balance between the production of thermal and power from the different ship waste heat sources. A suitable approach involves sharing the waste heat between steam and power plants, giving priority to cover the ship's heating demand.

2.3 POWER WASTE HEAT RECOVERY TECHNOLOGIES

There are many applications, technologies and systems that can use the vessel's available waste heat sources, opening many possibilities. It is the author's opinion that using low/medium waste heat to generate cooling power is as effective as producing mechanical or electrical power to reduce fuel consumption and carbon emissions as demonstrated in Little and Garimella [2011] and Shu et al. [2013]. However, the multiple uses and needs on board for mechanical and electrical power results in this thesis focusing on the use of shipping waste heat

to generate mechanical and electrical power. Figure 10 shows a simplified representation of a thermal machine where high quality waste heat enters the system and generates mechanical or electrical work, rejecting the energy not used in a heat sink.

Also, it is important to mention that WHRS are not intended to substitute the actual power production – of both prime mover and auxiliary engines – or cooling/heating systems; they are installed to play a supporting role inside the ship since the availability of waste recovery systems depend on the ship's operating task (e.g. manoeuvring, alongside, at anchor) and operating conditions, and thus there may not always be sufficient waste heat to operate the vital ship systems. From the costing point of view, WHRS tend to be more expensive than diesel engines when used as the main and auxiliary sources of power on board. Figure 11 shows the specific cost of new four-stroke diesel engines used either for propulsion or electric power generation but also the specific cost of different WHRS technologies. From this figure it can be seen that the WHRS specific cost is at least one order more expensive than diesel engines. Benvenuto et al. [2011] gives a cost of around £13.2 million for a large two-stroke diesel engine capable of producing more than 87 MW [MAN Diesel & Turbo 2013b] which gives an specific cost of around £160/kW. The costs found for this comparison come from different sources, markets and dates creating a difficult exact comparison. However, they are useful for highlighting the cost gap between the typical marine and auxiliary engines and WHRS technologies.

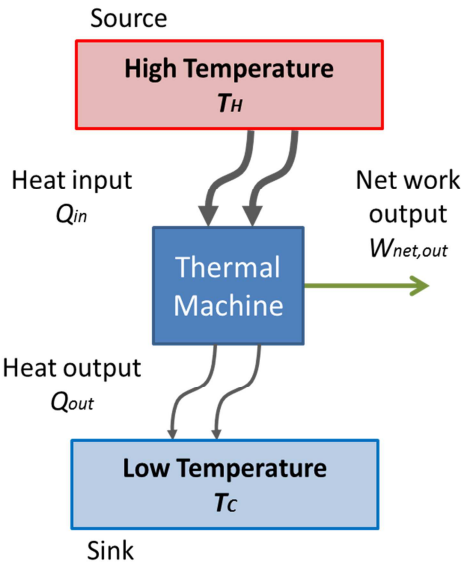

Figure 10: Thermal machine which produces work by using a waste heat source at T_H and a sink at a temperature of T_C.

In conjunction with environmental regulations and technological progress on marine systems, it could be expected that the waste heat availability and quality will be lower with time, making it harder and more expensive for the WHRS to convert the waste heat to useful power on board [McGeorge 2002]. For example, the use of wet scrubbers that spray water onto the exhaust gas in order to capture SO_X reduces the waste heat quality of the exhaust gas [Lloyd's Register 2012b]. This scenario should not be detrimental for the use of waste heat, but more as a chance to look into more advanced technologies and strategies which can work effectively with lower temperature gradients.

In order to take some benefit from energy in its heat form, apart from heating, it is necessary to have a device that through the means of different processes can produce work. Such devices are known as thermal machines in which WHRS are found. All thermal machines receive heat from the highest temperature available while producing work. The excess heat not used by the machine is rejected to a lower temperature sink which, depending on the waste heat quality,

could be used in another thermal machine. Each type of machine will have different mechanisms to operate and will return different power outputs when using the same heat source and sink. The difference in performance comes from the machine's own inefficiencies, such as friction, electrical and heat transfer losses, and pressure drops among others. As in diesel engines, the most common form that the energy losses take is as heat.

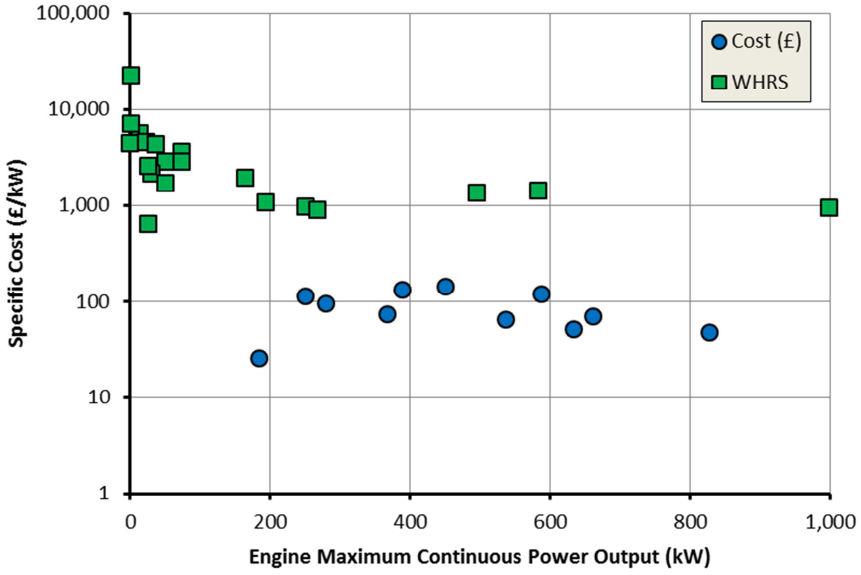

Figure 11: Specific cost for different WHRS technologies and marine diesel engines taken from different commercial and scientific sources. [Majeski 2002; Quoilin et al. 2013; Alibaba.com 2016; Dieselenginetrader.com 2016; Boatsandoutboards.co.uk 2016]**.**

In these following subsections, two different thermal machines that fall into the waste heat technology category will be briefly examined: thermoelectric generators (TEG) and thermodynamic cycles. The aim of this subsection is to detect from the literature available which of the two technologies offer a better proposal for the use of waste heat on board with the purpose of generating mechanical or electrical power.

2.3.1 THERMOELECTRIC GENERATOR

A thermoelectric generator (TEG) is a device which directly transforms heat energy into electricity. The generation process is based on the Seebeck effect where temperature gradient drives electrons from the metal's hot side to the cold one, generating a voltage [Terasaki 2011; Zhang & Zhao 2015]. This can be represented by the following equation:

$$V = S\Delta T \qquad [4]$$

Where V is voltage, T is temperature and S is the Seebeck coefficient which measures the thermoelectric power given in V/K [11]. When connecting a load to the TEG, the electrical power generated could be defined as follows:

[11] For more about how the Seebeck coefficient is found and developed, please refer to the work of Terasaki [2011].

$$\dot{W}_e = I^2 R_L = \frac{S^2(T_H - T_C)}{R}\left(\frac{{R_L}/{R}}{\left({R_L}/{R} + 1\right)^2}\right) \quad [5]$$

Where I is the electrical current, R and R_L are the internal TEG electrical resistances and the load electrical resistance respectively. The temperature subscripts C and H refer to the sink and heat source respectively.

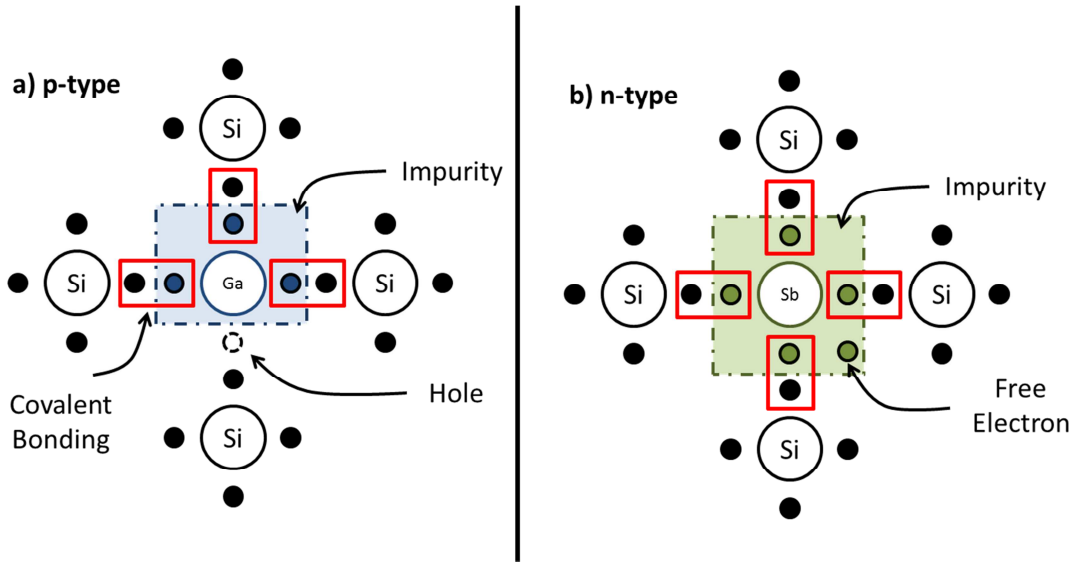

Figure 12: a) representation of a p-type semiconductor which has as impurity gallium in a silicon lattice. It can be seen in the diagram that the lower silicon atom is missing an electron to form a covalent bonding, this missing atom is called a hole. b) Shows an n-type semiconductor based in silicon and with antimony as impurity; here the antimony atom is missing an electron, making the antimony electron a free electron.

Thermoelectric generators use semiconductors in order to produce the Seebeck effect when a temperature gradient is present. Semiconductors are formed when a small percentage of impurities, such as aluminium or arsenic, are added to a silicon or geranium crystal lattice, changing considerably their electrical properties (e.g. conductivity) [Eto & Kamimura 2011]. Thermoelectric generators are normally formed with two different types of electrically-conducting materials, known as n-type and p-type semiconductors. P-type semiconductors have deficiencies of valence of electrons called “holes” caused by adding trivalent elements (i.e. a valence of three) – boron, aluminium and gallium – to the crystal lattice (see Figure 12). The holes are created when one silicon atom is missing its covalent bond[12] which causes the lattice to have, in its majority, positive charge ions and increases in silicon or geranium conductivity [Williams 2006a]. On the other hand, n-type semiconductors have pentavalent impurities (i.e. a valance of five) which satisfy all the silicon covalent bonding, but in this case the impure atom misses one covalent bonding. The extra electron from the impure atom is weakly attached to the crystal lattice and is called a “free” electron, this causes the semiconductor to have a negative charge [Williams 2006b]. Common impurities for n-type semiconductors are antimony, arsenic and phosphorous.

[12] This bond happens when a pair of shared electrons from different atoms holds both atoms together.

In order to evaluate the performance of n-type and p-type semiconductors a concept called figure-of-merit (*ZT*) must be introduced [Zheng et al. 2014]:

$$ZT = \frac{\sigma S^2}{\kappa} T \qquad [6]$$

Where σ is the electrical conductivity (S/m) and κ is the thermal conductivity (W/m-K), *ZT* is dimensionless and as this number grows the better the performance of the material will be. With the *ZT* is possible to define the thermal efficiency of a TEG as follows [Zheng et al. 2014]:

$$\eta_{th} = \left(\frac{T_H - T_C}{T_H}\right)\left(\frac{\sqrt{1+ZT}-1}{\sqrt{1+ZT}+{T_C}/{T_H}}\right) \qquad [7]$$

From the previous equation, it is clear that in order to improve the TEG's thermal efficiency it is possible to do so by increasing the temperature gradient between the heat source and the sink, and by increasing the *ZT* which in turn can be improved by increasing the electrical conductivity of semiconductors and the Seebeck number, or by reducing the thermal conductivity. Zhang and Zhao [2015] show that there have been three different stages in the development of higher *ZT*: the first leads up to 1990 where the maximum *ZT* achieved is 1.0; this is followed by 20 years of development which saw an increase of up to 1.7 thanks to the introduction of nanotechnology; and a third stage with advances in materials which so far have been able to achieve a *ZT* value of 1.8. Zhao et al. [2014] demonstrated that it is possible to achieve a *ZT* value of 2.6 at a temperature of 650°C thanks to a low thermal conductivity of 0.23 W/m-K. However, Zheng et al. [2014] argue that high *ZT* values are difficult to replicate due to incorrect measurements in the different variables from equation [6], the manufacture of materials that suit only specific equipment, or by the extrapolation errors of other physical characteristics (e.g. density). Furthermore, high *ZT* values are achieved only where the heat source is of high quality; as it reduces its temperature, so does the TEG's *ZT*.

As mentioned before, TEG are formed in a combination of arrays of n-type and p-type semiconductors connected electrically in series by a metal plate and thermally in parallel (see Figure 13) [DiSalvo 1999]. When a TEG is subjected to a temperature difference, the free electrons in the n-type semiconductor and the holes in the p-type semiconductor move away from the heat source, generating a direct electrical current delivering an electrical power output; but also the semiconductors move the heat energy to the sink [Riffat & Ma 2003; Zheng et al. 2014].

It was not until 1960s that TEG had any real application in the supply of electrical power to spacecraft where the use of hydrocarbons as fuel is not possible due to the lack of oxygen in outer space [Date et al. 2014]. Other initial applications are found for pipelines and sea buoys where costs are less relevant than operability and reliability in remote areas [Riffat & Ma 2003]. Due to a growing interest in the Seebeck effect there has been important progress in the area of materials which has produced an improvement in TEG's energy conversion [Date et al. 2014; Liu et al. 2015]. Crane et al. [2012] successfully tested an automotive TEG which was able to

produce an electrical power output of 700 W in a test bench and 600 W – around 30% of the electrical power required – on a passenger vehicle test where the TEG used the available waste heat coming from the vehicle's exhaust gas. The source temperature was set about 650°C at a mass flow rate of 0.045 kg/s while the sink was cold water at 25°C and a mass flow rate of 0.33 kg/s. This translates to a fuel saving of around 1.2% at an average vehicle speed of 110 km/h. Smith and Thornton [2009] found that assuming the TEG had a thermal efficiency of 5.0%, it could bring fuel savings in the range of 2.0% to 3.0% for a heavy diesel truck. Espinosa et al. [2010] modelled a TEG using the available waste heat from a diesel engine exhaust gas at a temperature between 300°C and 330°C. Their model shows that it is possible to generate around 1.2 kW_e thanks to an optimisation in the number of semiconductors and the configuration of the TEG module.

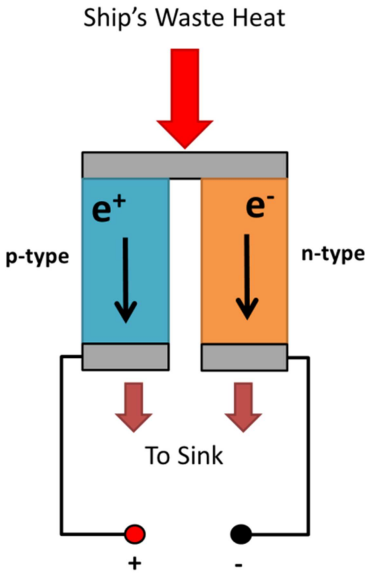

Figure 13: Depiction of TEG using two different materials (i.e. p- and n-type) joined by a metal, represented by black boxes. The temperature difference between the heat source and sink produces a voltage difference at the end of both electrodes.

Looking into the marine applications, TEG offer some valuable advantages over other thermal machines [Riffat & Ma 2003; Quoilin et al. 2013]:

- Lower mass.
- There are no moving parts, reducing maintenance costs and enabling silent operation.
- Long life, which has been shown to go beyond the 100,000 operational hours.
- Scales linearly, can be applied to small heat sources.
- Direct DC electric output.
- No need for fluids to be operated or cooled down.

Kristiansen and Nielsen [2010] studied the possibility of using TEG to generate electricity from the different sources of waste heat from a 52,000 dwt bulk carrier with a 7.8 MW diesel engine. They found out that a maximum power output of around 45 kW_e was achieved when using the scavenge air or exhaust gas waste heat, representing around 0.6% of the vessel's installed

power. Khalykov [2014] performed tests on a TEG prototype for a marine environment for the exhaust gas system changing the source temperature from 200°C to 500°C and a constant sink temperature of 5°C. The prototype achieved 7 W with a voltage of 55 V at the highest temperature and a mass flow rate of 4 g/s, It is important to bear in mind that while the power output seems low, so does the exhaust gas mass flow rate. Shu et al. [2013] analysed the feasibility of using TEG on board vessels and concluded that while the cost per kW_e is still high, it is recommended to use TEG in conjunction with other waste heat technologies.

TEG have some setbacks for marine application: a) costs tend to be high due to the specialised materials, heat exchangers, and processes required by semiconductors; b) thermal efficiencies that for now are low for low/medium waste heat quality [Riffat & Ma 2003; Crane et al. 2012; Yee et al. 2013; Zheng et al. 2014]. As an example of TEG's cost, Yee et al. [2013] analysed numerically the optimum cost per kW generated for a Bismuth telluride (Bi_2Te_3) TEG by modifying the TEG's electrical resistance ratio between the module and the load, and the concentration of semiconductors. They found out that the cost of generating electricity – without considering the heat exchanger cost – was around £5,160 per kW_e [13]. TECTEG MFR [2015], offers modules that range from £8,220 to £14,000 per kW_e. Kristiansen et al. [2012] modelled a marine TEG that absorbed the available energy from the waste incinerator flue gases. It produced 58kW_e at a cost of £4,310 per kW_e; by reducing the power output to 25 kW_e, it was possible to achieve a cost as low as £1,630 per kW_e. This lower cost, when compared to the previous works discussed is caused mainly to a *ZT* equal to 1 and source temperature above 1100˚C. In the area of thermal efficiency, Zheng et al. [2014] show that an n-type semiconductor based on $CoSB_3$ reduces its *ZT* value from 1.2 at a temperature above 530°C down to 0.4 at 230°C. Using equation [7] this will represent a drop in the maximum theoretical thermal efficiency – assuming a constant sink temperature of 5˚C – from 17.3% at 530°C to 4.7% at 230°C. The latter temperature is representative of the temperature seen in diesel engine exhaust gas, while lower temperatures are seen for waste heat coming from the scavenge air and engine's cooling system.

This subsection has shown that TEG systems have interesting characteristics and capabilities to offer to the shipping industry, but it is their low energetic conversion from low/medium quality waste heat to electrical power and its high cost that makes this technology unfeasible, for now, for marine application. Kristiansen et al. [2012] shows that the cost of this technology can be lowered thanks to the waste incinerator heat quality, but also it is true that the operational time of a waste incinerator is much lower than the main or auxiliary engines, taking longer to payback the initial investment. Zhang et al. [2015] used a simple thermodynamic WHRS, using as a working fluid R123 coupled with a TEG. The exhaust gas of a small diesel engine passed first through the TEG to later enter the thermodynamic WHRS boiler which absorbed more of the waste heat. This configuration was capable of producing at the highest loading position around 23.0 kW_e, of which only 3.7 kW_e come from the TEG. Furthermore, the same authors performed the same simulations for two different thermodynamic WHRS which were capable of

[13] An exchange rate of $1.53 to £1 was used throughout this work [Board of Governors of the Federal Reserve System 2015].

producing more than 30.0 kW_e at the highest loading conditions, a difference of 30%. The work of Zhang et al. [2015] highlights the possibilities of TEG on board a vessel, but more importantly it shows that a thermodynamic WHRS is a more attractive solution for the ship's waste heat, fuel consumption and noxious emissions.

2.3.2 THERMODYNAMIC CYCLES

In the previous subsection it was shown that thermodynamic cycles can bring a much larger power output than TEG which will be more relevant for the ship scenario. The use of this type of thermodynamic WHRS in land-based systems has been well covered: in cement processes [Bronicki 2000; Cunningham 2002], solar [Tchanche et al. 2011; Vélez et al. 2012], geothermal [Mlcak 2004; DiPippo 2004; Bronicki 2010; Öhman & Lundqvist 2013] and, land-based vehicles using internal combustion engines [Dinanno et al. 1983; Feng et al. 2010; Weerasinghe et al. 2010; Dolz et al. 2012].

A thermodynamic WHRS absorbs part of the waste heat available from the vessel to evaporate a working fluid (e.g. water, benzene, R245fa). Next, the fluid expands (e.g. inside a turbine or scroll expander), and converts part of the heat energy into mechanical work or electrical work with the assistance of an electrical generator.

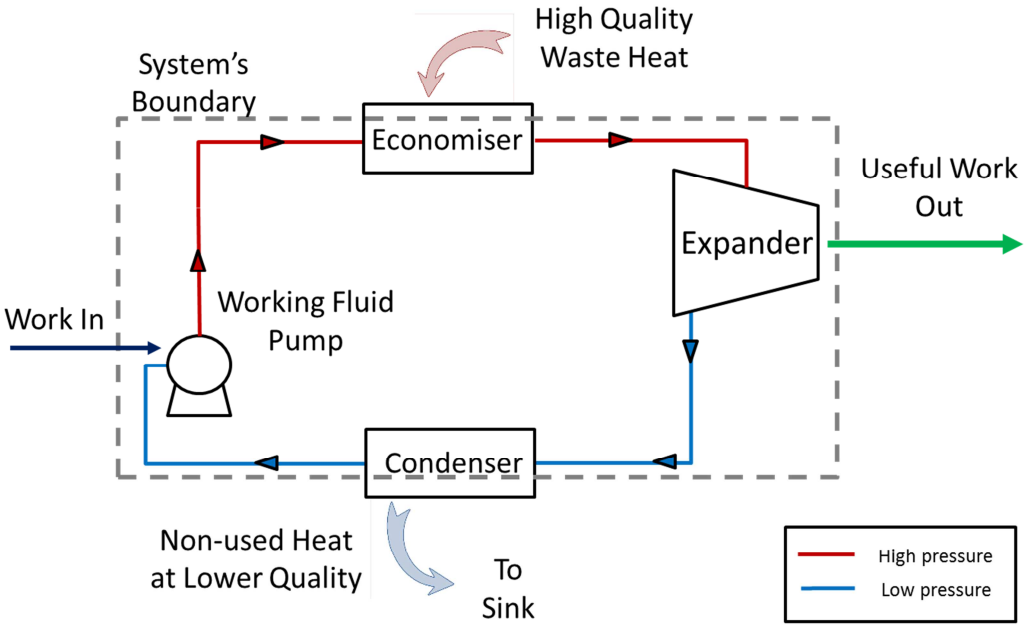

Figure 14: Representation of a basic thermodynamic WHRS with two pressure levels which shows the different heat and work transfers. The arrows indicate the direction of the working fluid inside the system, while the dashed square represents the limits of the closed system.

The basic components for a thermodynamic WHRS are: a) the heat exchangers, of which one is connected to the heat source and boils the working fluid (i.e. boiler, but also known as economiser which will be used onwards to describe the WHRS boiler), and another one in contact with the heat sink responsible for condensing the working fluid (i.e. condenser); b) a pump which increases the thermodynamic cycle pressure after the condensing process; c) an expander responsible for generating the mechanical work from the working fluid at the expense of a pressure drop; and d) the working fluid which is the energetic transport system inside the

WHRS. Depending on the complexity, conditions, regulations, requirements and budget, other equipment can be added to the WHRS (thermal oil circuit, recuperator, etc.). This study only considers the thermodynamic cycle as a mass closed boundary, meaning that there is no mass entering or leaving the system, although it accepts heat and work transfer. The closed boundary is represented in Figure 14 by the dashed line, which leaves out the mass flow rates from the source and sink, but not the heat flow happening inside the heat exchangers.

The first law of thermodynamics (FLT) talks about the conservation of energy. It looks into power output and requirements, heat addition and rejection, mass flow rates and thermal efficiency of the thermodynamic cycles. The general equation for the FLT is given as [Cengel & Boles 2007]:

$$\Delta Q - \Delta W = \Delta E \qquad [\ 8\ ]$$

Where ΔQ is the net heat input, ΔW is net work output and ΔE is the system's energy change. The variable E is formed by the potential, kinetic and internal energy (U). In the close boundary system, the changes in potential and kinetic energy are negligible. The internal energy refers to all forms of microscopic energies related to the molecular structure and activity [Cengel & Boles 2007]. But for a closed system with no mass transfer across its boundaries – assuming that there are no losses along the path – the internal energy, hence the total energy change is equal to zero. Equation [8] can be modified as follows:

$$\Delta Q = \Delta W \qquad [\ 9\ ]$$

This means that the net work output obtained from a waste heat source is equal to the system's net heat input. The thermal efficiency (η_{th}) then can be defined as follows:

$$\eta_{th} = \frac{\Delta Q}{Q_i} = \frac{Q_i - Q_o}{Q_i} \qquad [\ 10\ ]$$

Where Q_i is the heat entering the system and Q_o is the heat rejected to the sink. For the purpose of this section the theoretical development is sufficient, but it will be covered in more detailed in the following sections, especially in the Methodology chapter.

Thermal efficiencies for thermodynamic WHRS will depend on the sink and source temperature, system equipment and pressure levels; thus, it is difficult to determine the typical value for a thermodynamic WHRS. The work of Suárez de la Fuente and Greig [2013] explored how the thermal efficiency of different working fluids behave under different WHRS high pressures in a marine scenario (see Figure 15). Nguyen et al. [2014] used a split Kalina cycle as a WHRS for a diesel engine, using the waste heat from the engine's exhaust gas. The thermodynamic cycle achieved a thermal efficiency of 25.7% with a source temperature of 346˚C and a sink of 25˚C. Sala and Invernizzi [2014] modelled a Stirling cycle using a heat source at 300˚C, achieving a maximum thermal efficiency of 18.7% at 2,000 kPa, using ethane as a working fluid, and a minimum thermal efficiency of 8.7% when using hydrogen at 2,000 kPa. Gu et al. [2009] performed a series of experiments to understand the behaviour of thermal efficiencies under different high and low pressure and saturation temperatures. They found that a maximum

thermal efficiency of 5.0% is possible when the source temperature is 100˚C and a high pressure of 1,000 kPa; the sink temperature was set to 12˚C and a low pressure of 450 kPa when using the refrigerant R600a. This seems similar to TEG's thermal efficiency but the source temperature is of low quality and the temperature difference between source and sink is smaller.

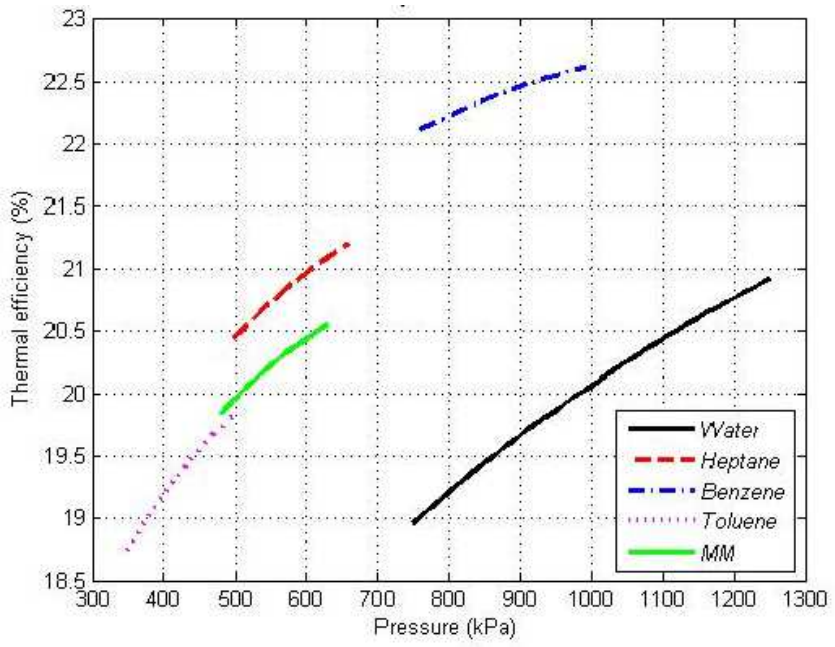

Figure 15: A comparison of different working fluids and their thermal efficiencies when the high pressure of a thermodynamic WHRS changes. The WHRS uses the exhaust gas waste heat from a large container vessel at its 75% MCR [Suárez de la Fuente & Greig 2013].

In the field of costs, the range is quite broad due to extensive thermodynamic technology. Analysing the data available from academic and industrial literature for some of the typical thermodynamic cycles (i.e. Rankine, Kalina and Stirling cycles) a cost range between £620 and £22,500 per kW_e is seen [Majeski 2002; BCS Incorporated 2008; Saavedra et al. 2010; Rodriguez Garcia 2010; Tchanche et al. 2011; Eymel et al. 2012; Quoilin et al. 2013]. The highest price is for Stirling engines [Majeski 2002], followed by a 20kW_e WHRS Rankine cycle which is around £5,600 per kW_e[14] [Quoilin et al. 2013]. While the costs of some of these thermodynamic cycles may seem similar to TEG's, the cost per kW_e generated reduces drastically as the WHRS power output increases, for example, a 1,000 kW_e has a cost of £910 per kW_e.

Another interesting advantage of a thermodynamic WHRS on board a ship over TEG is the power output. MAN Diesel & Turbo manufacture a marine Rankine cycle based on water which is capable of producing up to 2,500 kW [MAN Diesel & Turbo 2012b], assuming that an electric generator – with an electrical efficiency of 90% – is connected to the expander's shaft, this system is capable of producing 2,250 kW_e at the engine's 70% MCR. Saavedra et al. [2010] showed that it was possible to get from different Rankine cycles a power output of more than 1,200 kW_e or 1,080 kW_e – using the same assumption as before regarding the generator

[14] An exchange rate of €1.37 to £1 was used throughout this work [European Central Bank 2013].

efficiency – for a waste heat source of 320˚C and a sink temperature of 35˚C. Larsen, Haglind et al. [2013], using a marine two-stroke diesel engine exhaust gas waste heat, demonstrated that three different thermodynamic cycles were capable of producing more than 800 kW with a maximum of 1,160 kW when using the refrigerant R245ca in a Rankine cycle. In the case of a container ship with 6,800 TEU a trilateral cycle using a sink a second thermodynamic cycle was design by Choi and Kim [2013] to generate more than 2,000 kW when the source temperature was set at 237˚C.

2.4 CLOSING REMARKS

This chapter discussed the options available in using the prime mover's available waste heat to determine which of the available technologies offer reasonable power outputs and efficiencies at affordable costs which could represent a viable option for the shipping industry in its effort to reduce CO_2 emissions. Within the multiple WHRS options available, this work focused on systems that can generate mechanical or electrical power, without forgetting the importance of thermal demand on board. Thermodynamic cycles and TEGs – which only produce electricity – were compared in this chapter and it was seen from the literature review that a thermodynamic power WHRS is a better option than TEG since they offer a larger power output at a lower cost per kW_e, but also operate at higher thermal efficiencies. These three performances overcome the TEG's benefits as a technology with no moving parts, silent operation and high reliability.

From this evidence, the thesis will focus on the study of power thermodynamic WHRS producing mechanical or electrical power using the prime mover's waste heat.

3

An Overview Of Power Thermodynamic Waste Heat Recovery Systems

This chapter will cover the available literature for four different thermodynamic cycles: Rankine cycle (RC) – also known as the steam cycle –, organic Rankine cycle (ORC), Kalina cycle (KC) and Stirling cycle (SC). It gives a general overview of the different cycles focusing on different WHRS applications and their thermodynamic processes with the aim of distinguishing the cycles' strengths and weaknesses. The WHRS applications shown here are more land-based than marine since the literature covers the general aspects of the cycles in more detail. Still, chapter 5 is solely dedicated for marine WHRS and their difference with land-based systems.

3.1 RANKINE CYCLE

Steam power engines and systems have been available since before the appearance of thermodynamic laws and the full understanding of the phenomena happening inside the thermodynamic process [Parsons 1925]. The use of steam as a means to produce work was realised as early as 150BC. In later centuries, steam pumps were used to help miners move water from mines. The early steam engines where too inefficient due to moving cylinders, technological limitation in manufacturing processes and a lack of thermodynamic expertise [Spear 2008]. James Watt not only improved the performance of the steam engine by allowing the cylinder to be warm at all times and providing an external condenser, but also managed to advance the study of steam as a working fluid. Watt's work attracted the attention of different important physicists of that era. One such physicist was John Macquorn Rankine who, in his work, describes the thermodynamic process for adiabatic cylinder engines [Rankine 1881]. With the development of the steam turbine many of the inefficiencies of the steam engine were reduced and nowadays the Rankine cycle (RC) is used as the idealised cycle to understand the behaviour of steam power plants. The RC is the preferable thermodynamic cycle for heat sources found at temperatures above 500°C, but also it exhibits acceptable performances for lower heat qualities [Feng et al. 2010; Wang et al. 2011; Quoilin et al. 2013; Cheang et al. 2015]. In 2011, steam power plants (i.e. thermal and nuclear) produced around 80% of the total electricity generated for the European Union [Eurostat 2012].

3.1.1 IDEAL AND REAL RANKINE CYCLE

The ideal RC without superheating is similar to the Carnot vapour cycle (see Appendix III – Some important concepts for a thermal machine). The main difference between them is the heat addition: for the RC, it is assumed at constant pressure while for the Carnot cycle it is isothermal. This difference makes the Carnot cycle a more efficient thermodynamic process but also brings some impracticalities such as formation of droplets at the expansion process and high power required at compression [Cengel & Boles 2007; Nag 2010; Balmer 2011]. The RC overcomes or limits these difficulties by superheating the steam and condensing it completely. The superheated RC has the following steps, as seen in Figure 16:

1-2: Isentropic expansion (i.e. same entropy before and after expansion)
2-3: Constant pressure heat rejection
3-4: Isentropic compression

4-1: Constant pressure heat addition

The superheated vapour enters the turbine (1) and expands isentropically giving up its energy when rotating the shaft which generates power. Having superheated steam inside the turbine reduces the possibility of water droplets as the fluid loses its temperature and pressure (2), but still the turbine needs to have several stages that can deal effectively with the vapour expansion. The condenser (2-3) then condenses the steam at constant pressure by rejecting heat to a cooler medium (i.e. sink), having at the end of the process a sub-cooled or saturated liquid. Condensing the exhaust wet vapour (2-3) will eliminate the difficulty of pumping wet vapour into the economiser and the necessity of controlling the steam quality[15] [Balmer 2011]. At point 3, the saturated liquid is pumped isentropically and sent to the economiser (4). Inside the economiser (4-1) the working fluid absorbs the available waste heat to increase the saturated liquid's temperature until it becomes a superheated steam, closing the cycle.

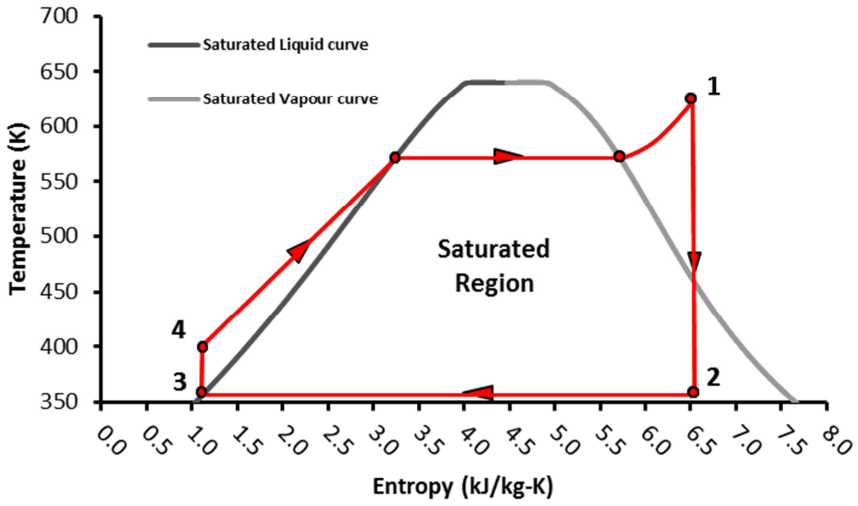

Figure 16: Ideal superheated RC (1-2-3-4) in a temperature-entropy diagram.

In reality, the applied RC must deal with different losses such as fluid friction and pressure drops that will affect the cycle's performance. Considering these losses, it is seen in Figure 17 that the enclosed area in a temperature (*T*) - entropy (*s*) diagram is modified for the real cycle (1R-2R-3-4R). In the real RC, the heat addition and rejection do not happen at the same pressure. This translates into a larger pressure increase for the pump and a shorter pressure drop for the expander, affecting directly the RC's net power output and thermal efficiency. Another source of deviation comes from the fact that the expansion and compression processes are not isentropic due to irreversibilities, such as heat loss and fast expansion and compression. Typical values seen in different RC works put the pump and expander isentropic efficiency around 80% at design point [Veres 1994; Cengel & Boles 2007]. The differences seen between

[15] Quality here refers to the percentage of the fluid that is completely a vapour. Quality is also known as wetness factor which measures the mass of liquid inside the total mass of the working fluid or in other words gives the proportion of liquid inside the fluid. A dryness factor, on the other hand, measures the fluid's vapour proportion [Cengel & Boles 2007]. Any fluid inside the saturated region will have a part of itself that it is fully evaporated coexisting with the rest that is fully condensed.

ideal and real RC are also present in other thermodynamic cycles but will not be discussed in further sections.

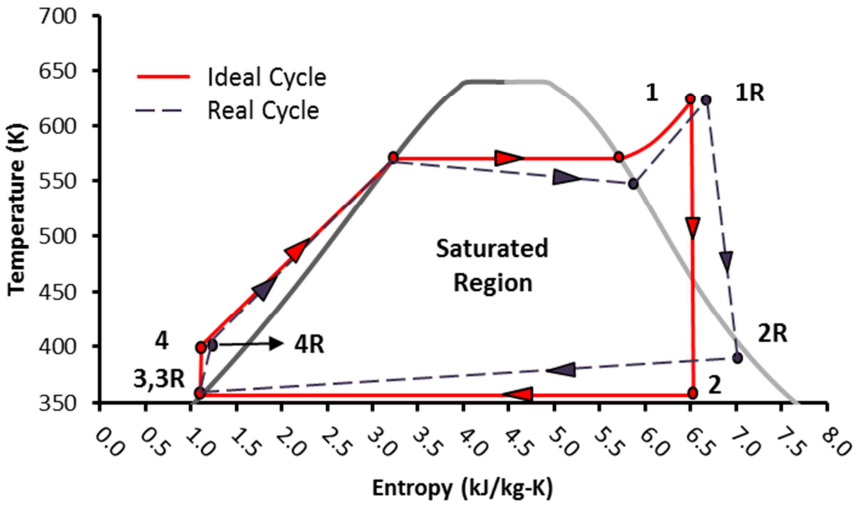

Figure 17: Comparison of an ideal and a real superheated RC. The positions that end with R represent the real cycle. It is assumed for both cycles the same starting point (i.e. point 3).

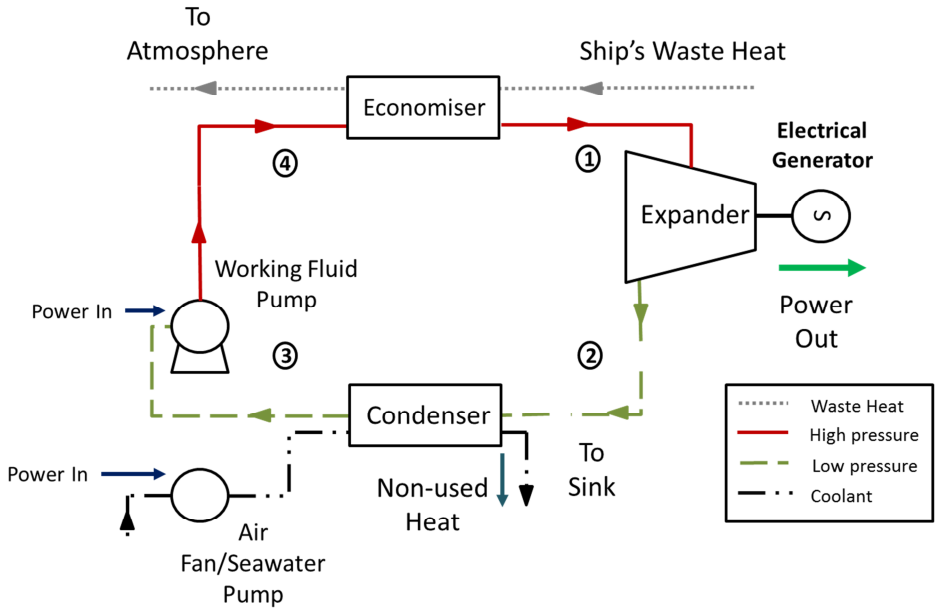

Figure 18: A simple ship based RC with its different components. Extra equipment shown: electrical generator connected to the expander and seawater pump or air fan.

As with any thermodynamic cycle using the expansion process to convert the heat energy into mechanical work, the higher the enthalpy drop – assuming constant mass flow rate – the larger the work output will be. This can be achieved by increasing the working fluid's pressure or temperature at point 1 in Figure 18. High pressure systems will require thicker pipes, stronger heat exchangers and more powerful pumps. In the case of increasing the temperature, the limitations depend on the type of material used (e.g. aluminium, steel or titanium). The ship's exhaust gas and other waste heat sources retain temperature that will be quite low to consider any thermal effect on the different WHRS equipment. Other strategies are reheating the steam

after a partial expansion by reintroducing it to the heat source; or use, when possible, the superheated steam after expansion to pre-heat the high-pressure liquid which also increases the RC performance [Parsons 1925; Cengel & Boles 2007]. A typical external improvement for the water WHRS, and also possible for other cycles, is the use of a power turbine working in parallel with the RC to increase the net WHRS power output [Poullikkas 2005; Benvenuto et al. 2014]. This study will only work with a simple thermodynamic layout due to its plant simplicity and size. For readers interested in the different RC's plant configurations, the following references are recommended: the British Electricity International [1991] and Cengel and Boles [2007].

3.1.2 WATER AS WORKING FLUID

The RC normally employs water as the working fluid, but can also use other fluids that do not contain carbon, such as ammonia. Water being a non-toxic and non-flammable fluid is an ideal candidate for WHRS in confined spaces such as the case of the ship. Other positive characteristics of water are its low cost and viscosity, it has high chemical stability at high temperatures, negligible global warming and ozone depletion potential and is easily found around the globe [Tchanche et al. 2011; Quoilin et al. 2013]. Also, it is the fluid that has the largest latent heat of vaporisation – assuming the same pressure – which enables it to absorb and store energy in the smallest mass possible. This will cause smaller mass flow rates, a more compact plant layout and a lower pump power consumption in the thermodynamic cycle [Maizza & Maizza 1996; Chen et al. 2010; Boretti 2012a].

Before going further with water as a working fluid, it is important to define the fluids per their saturated vapour curve in a *T-s* diagram. The classification is useful since it will tell if the thermodynamic cycle requires superheating before expansion (point 1 in Figure 18) or after going through the expander (process 1-2 in Figure 18), if it will be a superheated vapour or a mixture of liquid and vapour. This will have an important impact on fluid applicability, WHRS efficiency and plant design and operation [Mago et al. 2008].

The working fluids can be classified as wet, isentropic and dry. The "wet" adjective comes from the fact that after the expansion process (1-2), the working fluid state will be inside the saturated region. A dry fluid after expansion will be found in a superheated state. For an isentropic fluid, its condition could be found as a saturated or superheated vapour depending on the fluid's conditions and assumptions taken before the expansion process (isentropic expansion, superheated, etc.). Some examples of these working fluids with their saturation curves in *T-s* diagram are shown in Figure 19.

Liu et al. [2004] developed a formula useful for classifying working fluids. This formula is an approximation that holds for a fluid at its normal boiling point [Chen et al. 2010]:

$$\varepsilon = \frac{C_p}{T_{sat}} - \frac{\left[\left(\frac{nT_{rsat}}{1-T_{rsat}}\right)\right]+1}{T_{sat}^2}\Delta H_{vap} \qquad [11]$$

Where ε is the inverse of the saturated vapour curve's slope, n is taken as 0.375 which is commonly used in the Watson relation [Reid et al. 2001], ΔH_{vap} is the enthalpy of vaporisation, T_{rsat} is the reduced saturated temperatures (i.e. $T_{rsat}= T_{sat}/T_{cr}$), T_{sat} is the temperature of saturation, also known as vaporisation, and T_{cr} is the fluid's critical temperature. Depending on the value of ε the working fluid can be classified as follows [Liu et al. 2004; Chen et al. 2010]:

i) If $\varepsilon > 0$, the fluid is dry.
ii) If $\varepsilon < 0$, the fluid is wet.
iii) If $\varepsilon \approx 0$, the fluid is isentropic.

Water is classified as a wet fluid per its negative slope in the saturated vapour curve. Chen et al. [2010] found that water had the largest negative ε – a value of -17.78 J/kg-K^2 – among a large catalogue of inorganic and organic fluids, followed by ammonia and ethane with values of -10.48 J/kg-K^2 and -8.28 J/kg-K^2 respectively.

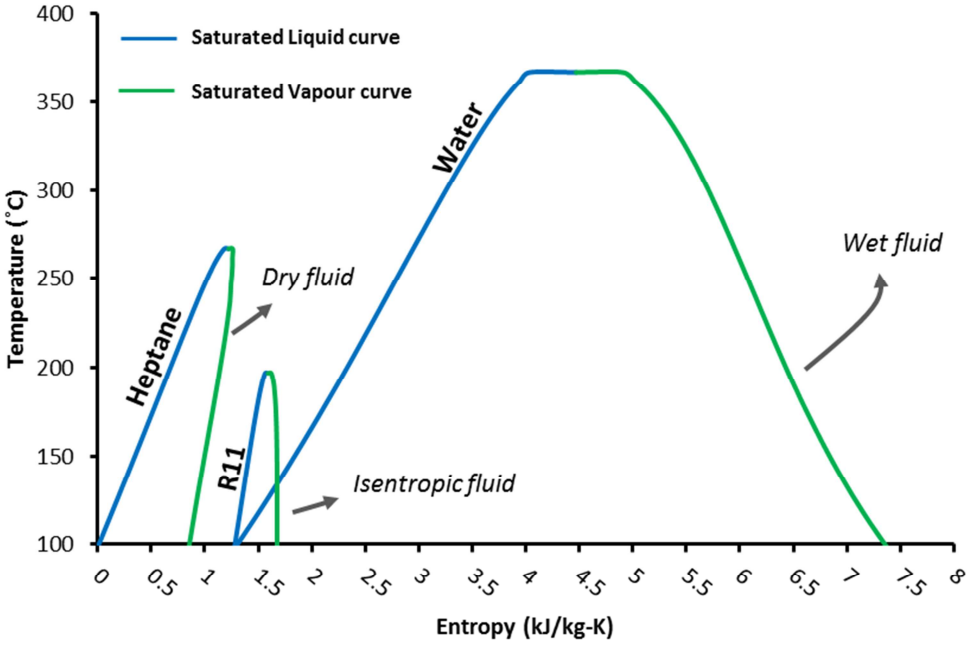

Figure 19: Representation in a *T-s* diagram of the three different types of working fluids: wet, dry and isentropic. Data taken from Refrprop 9.0 [Lemmon et al. 2010]**.**

The main issue with wet working fluids occurs during the expansion process where condensation, in the form of droplets, begins inside the expander. Droplets in conjunction with the expander's rotational speed erode the expander's blades which will have an impact on the maintenance cost. To reduce the effect of erosion the RC can, apart from superheating the steam, increase the high pressure or bleed the expander at different sections to capture the liquid [Cengel & Boles 2007; Stoppato et al. 2012; Quoilin et al. 2013]. Water has a relatively high freezing temperature (i.e. 0°C at ambient pressure) which can be an issue in extremely cold weathers. Finally, the water used inside the RC has to be chemically treated and degassed to minimise equipment damage. This treatment is around twice the cost of raw water [Towler & Sinnott 2013; Quoilin et al. 2013] and will require and on-site water plant treatment or a large tank in order to compensate for any water top-up in the system.

3.1.3 RANKINE CYCLE APPLICATIONS

3.1.3.1 AS TOPPING CYCLE

The RC cycle is commonly employed as topping cycle (see Appenidx III) such as large power stations and processes where the heat source has high temperatures [Tchanche et al. 2011; Peng et al. 2014; Cheang et al. 2015]. Steam turbines were common as the prime movers back in vessels in the 20th century, with examples found in the *Turbina* and *H.M.S. Hood* [Parsons 1925], and inside nuclear powered ships such as the NS *Savannah* and *Otto Hahn* [Carlton et al. 2011]. Nowadays, the RC is used on nuclear power submarines.

Rankine Cycle power plants, due to the size of the steam turbine, normally work at stable conditions over time in order to preserve the life of the equipment by reducing the thermal and mechanical fatigue and stresses [Bachmann et al. 1999; Stoppato et al. 2012], meaning that they do not see variations in their operating conditions. The variations that may arise through time can be dealt with by modifying or replacing equipment, and normally there is enough time to plan modifications.

3.1.3.2 AS BOTTOMING CYCLE

The RC has been applied to recover waste heat at low/medium temperatures generated by internal combustion engines [Endo et al. 2007; Feng et al. 2010; Weerasinghe et al. 2010; Dolz et al. 2012; Boretti 2012a; Domingues et al. 2013], cement processes [Cunningham 2002; Karellas et al. 2013], and coal plants [Martelli et al. 2013], among others.

Vanslambrouck et al. [2011] tried different RC high pressures for a heat source of 350˚C. They found that the higher the water's superheating temperature and the system's high pressure were, the larger the RC's thermal efficiency was. On the other hand, the RC's maximum power output is seen at high superheating temperatures and low high-pressure (i.e. around 790 kPa). Similar behaviour was seen in Suárez de la Fuente and Greig [2013] while keeping constant the superheating temperature. They argue that at large RC high-pressures the WHRS absorb less waste heat through equation [10] while holding constant the heat rejection, so the thermal efficiency increases. The thermal efficiency gradient reduces as the high-pressure increases since the low heat absorption produces lower mass flow rates and power outputs (see Figure 15). For the shipping point of view, one of the most important WHRS deliverables is the power generated and not the thermal efficiency, since it is related to fuel savings and payback times.

Of particular interest for the vessel case is the use of the RC as the car or truck WHRS, where the topping cycle's load changes constantly. Dolz et al. [2012] applied various configurations of WHRS to a heavy duty truck, focusing on increasing its power output. They found that the RC could generate 31 kW of extra power and 35 kW with higher quality heat sources. Feng et al. [2010] studied WHRS for an internal combustion engine where different pressures at different source temperatures were changed. Similar to previous works described in this section, they found that the overall system thermal efficiency increases with a higher source temperature. The WHRS' high-pressure had almost no effect on the power output, having

slightly higher power output at higher pressures. Horst et al. [2014], using a typical car operating profile on a road, showed that the fuel consumption savings could be as high as 3.4% when installing a RC, the study considered the energy losses due to mass increment, cooling air and back pressure on the main engine. The RC WHRS is capable of delivering around 2 kW of electrical power which covers entirely the car's electric demand. BMW developed the Turbosteamer, a water-based RC, for its 3 Series car, improving the fuel consumption by up to 15% [Obieglo et al. 2009; Freymann et al. 2012].

3.1.4 Is the Rankine Cycle the best option for low/medium quality heat?

As the EEDI pushes for low CO_2 emission vessels, the increasing preference of the shipping industry for slow speed steaming combined with the rise of diesel engine thermal efficiency and other GHG reduction technologies using part of the available waste heat (e.g. exhaust gas scrubbers), it is expected that the waste heat quality will be reduced. These reasons make it harder for the marine RC to reduce CO_2 emissions and payback times.

In the following subsections, it will be shown that from the academic literature there are other alternative thermodynamic cycles which can match or even outperform the RC when having low/medium waste heat temperatures. This opens the door to new WHRS candidates for the use of on board waste heat which could produce improved fuel savings and, hence, a larger CO_2 reduction from a typical water-based RC.

3.2 Organic Rankine cycle

The organic Rankine cycle (ORC) uses the same cycle proposed by Rankine for the water-based RC. The main difference between RC and ORC is the working fluid used which will basically affect the thermodynamic behaviour of the system, plant layout and equipment required. The ORC uses organic fluids which must contain any carbon compound, whether it has a biological origin or not such as in the case of benzene or R123 [Balmer 2011]. One of the strongest points of an ORC is its large working fluid catalogue which is formed from pure fluids or a mixture thereof. The ample range of organic fluids permits the creation of tailored thermodynamic designs to match any heat source. Furthermore, the creation of new organic fluids, due to stringent environmental, economic and safety regulations, is constant. As an example, DuPont™ DR-2 – also known as R1336mzz-Z – and R1233zd(E) are refrigerants that have low GWP and are classified as non-flammable [Molés et al. 2014].

The ORC, depending on the working fluid utilised, can use the same plant layouts as with the RC, such as a reheated process [Tchanche et al. 2014]. With enough plant complexity most of the working fluids will reach similar levels of performance, but this complexity will increase costs and the potential for losses [Calm & Didion 1998; Calm 2008].

A recuperative[16] ORC (see Figure 20) is a common plant layout for dry and isentropic fluids which uses the available heat after expansion to increase the working fluid's temperature on the

[16] Refers to the use of a recuperator which is a heat exchanger that transfers heat from the working fluid's hot side to the cold one without having mass transfer.

cold side [Branchini et al. 2013]. After the expansion process (1-2) the working fluid enters the recuperator (2) where it gives part of its heat to the cold stream exiting of the pump (4). After the recuperator, the hot stream (2r) goes to the condenser to reject the unused waste heat at low temperatures, while the warmer cold stream (4r) enters the economiser. The recuperator is used when the temperature at point 2 is warm enough to transfer heat to the cold stream at point 4.

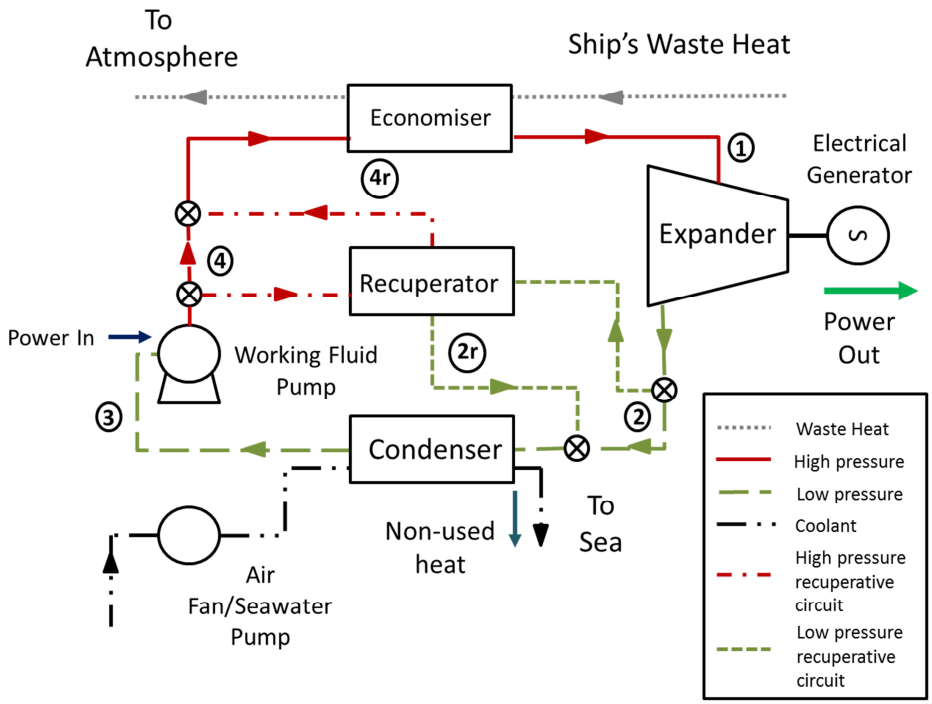

Figure 20: Recuperative WHRS using the available waste heat from the engine's exhaust gas and rejecting heat to the ocean.

The purpose of a recuperator is to increase the ORC power output and thermal efficiency. Branchini et al. [2013] performed simulations to different types of organic fluids under different plant configurations in order to visualise which plant layout offered the best performance. A recuperative plus regenerative[17] configuration with superheating brings the highest thermal efficiency, but the highest power output is obtained by a superheated recuperative plant layout. Since a recuperative ORC can bring larger power outputs, in addition to the regenerative ORC's more complex configuration, it is decided that only the recuperative layout will be explored for any ORC. Bahaa et al. [2007] compared a large catalogue of organic fluids to understand the benefit of a recuperator. From their results it is seen that the recuperator increases the system's thermal efficiency when the working fluid is not classified as a wet fluid. Larsen, Pierobon et al. [2013] observed that aromatic and alkane fluids (i.e. toluene and pentene respectively) performed better in a recuperative plant layout than in a simple one due to the high temperature of the fluids after expansion. The positive effects of using a recuperator are neutralised at low waste heat source temperatures. At these temperatures the best option is to use a simple configuration with superheating. Papers that use low quality heat sources, such as geothermal

[17] Refers to the use of a regenerator which is a heat exchanger that transfers heat by mixing together the hot stream coming out of the expander (2) and the cold stream exiting of the pump (4). The mixture then passes through another pump before entering the economiser. For more detail please refer to Mago et al. [2008].

plants, agree with these findings and use a simple ORC [Tchanche et al. 2009; Wang, Yan, Wang, Ma, et al. 2013; Kalikatzarakis & Frangopoulos 2014].

The work of Pierobon et al. [2014] allowed the WHRS to have a certain amount of superheating – chosen by the optimisation methodology – but did not quantify the benefit of superheating the organic fluids. Similarly, Imran et al. [2014] allowed the optimisation to choose the degree of superheating, and it is seen from their results that for a simple ORC WHRS, a superheating of maximum 3°C can offer the best thermal efficiency. Superheating seems to have a positive influence on the system's specific work output with some cases where the thermal efficiency reduces due to an increase in the heat absorbed by the ORC [Branchini et al. 2013]. Yang and Yeh [2015] demonstrated that it is better to superheat the organic fluids in order to have a shorter payback time. However, it was seen that the degree of superheating must be maintained low for best results, this is also appreciated in the work of Fernández et al. [2011] and Molés et al. [2014]. Calise et al. [2014] recommends the use of a superheater in a recuperative WHRS since it brings an improvement in power-generation. This argument is backed-up by Delgado-Torres and García-Rodríguez [2012] where they show that there is an increment in the recuperative ORC's thermal efficiency of around 1.2 percentual points when the superheating temperature increases by almost 105°C.

On the other hand, Calise et al. [2014] also argue that the use of a superheater is not required when using dry fluids in a simple configuration, such as that seen in Figure 19, since the benefit is minimal. Additionally, a superheater increases considerably the capital cost of a WHRS due to the low overall heat transfer coefficient (*U*) when the fluid becomes vapour, leading to large heat transfer areas. Delgado-Torres and García-Rodríguez [2012] demonstrated that the thermal efficiency of a simple ORC plant reduces from 11.1% to 10.2% when raising the superheating temperature from 15°C to 105°C. Chen et al. [2010] and Vanslambrouck et al. [2012] did not recommend the use of superheating on ORC since the fluids used, dry and isentropic, will not condensate inside the expander. Yamamoto et al. [2001] found that superheating the ORC's working fluid reduces its power output by around 5% when the superheating temperature is 30°C larger than the saturation temperature. Mago et al. [2007] found out that while superheating did not affect the thermal efficiency of the ORC it did add irreversibility, hence their recommendation to just heat the working fluid up to its saturated vapour condition before expansion. In the work of Hung et al. [1997] it is seen that the efficiency of the fluids is closely related to the evaporative latent heat at low pressures. Non-wet organic fluids present a reduction in efficiency as the temperature in the expander's inlet increases from its saturated vapour temperature.

Imran et al. [2014] performed an analysis of more complex configuration for ORC plants. It was found that bleeding and using regenerators did produce a higher thermal efficiency – between 1 to 1.5 percentual points – than the simplest ORC plant. But the down-side is an increment in installation cost that could be as high as £194 per kW when compared to the basic cycle. For other ORC plant layouts, please refer to the work of Branchini et al. [2013] and Quoilin et al. [2013].

3.2.1 THE STUDY OF ORGANIC FLUIDS

The ORC, when compared to the traditional water-based RC, has an extra degree of freedom at design point: the working fluid. The study of organic fluids (i.e. that contain carbon compounds in their structure) has being extensively covered from critical temperature and pressures to their impact on the environment in the form of their Global Warming Potential (GWP) and Ozone Depletion potential (ODP)[18]. It is recommended that the interested reader survey the following references [Hung et al. 1997; Chen et al. 2010; Bao & Zhao 2013; Tchanche et al. 2014] in order to gain a concise review of organic working fluids and their properties, as well as equipment and installation costs and preferred applications.

Using equation [11] from section 3.1.2 for organic fluids, it is possible to find wet, dry and isentropic fluids (i.e. $\varepsilon > 0$ and $\varepsilon \approx 0$ respectively) [Liu et al. 2004]. Some wet organic fluids include CO_2 and ethanol, while heptane and pentane are dry organic fluids, and R1234yf and R134a are examples of isentropic organic fluids. Figure 19 presents the three different types of fluids in which the difference in saturated vapour slopes can be seen.

Dry and isentropic fluids can overcome some of the drawbacks found in water and are recommended for ORC WHRS [Wang et al. 2012]. Some of the advantages of these fluids when compared to water have been studied [Larjola 1995; Hung et al. 1997; Liu et al. 2004; Saavedra et al. 2010; Chen et al. 2010; Bao & Zhao 2013; Quoilin et al. 2013][19]:

a) the lower vaporisation heat allows a better match for the waste heat at low temperatures;
b) lower relative enthalpy drops during expansion which enables the use of turbines with less pressure stages, and due to a larger vapour density than water, the size of the expander can be reduced;
c) also, due to the low enthalpy drop, the expander rotational speed is lower which will require smaller gearboxes between the electrical generator and the expander;
d) lower evaporative pressures;
e) there will not be formation of droplets inside the expander;
f) no water treatment plant and deaerator required;
g) lower freezing temperatures than water; and
h) large catalogue of fluids that facilitates the creation of a tailored WHRS for the heat source.

However, using organic fluids has some disadvantages to water. Chemical decomposition due to high temperature and pressure limits the operating life of the organic fluid [Hung et al. 1997]. Organic fluids have lower latent heat of vaporisation than water, which means larger mass flow rates, pump losses and equipment. Yamamoto et al. [2001] found out that an ORC mass flow rate required more than 10 times what was needed by RC to produce a the same power output. Suárez de la Fuente et al. [2015] found that an R245fa ORC required more than seven times more mass flow rate than a water-based RC using the available waste heat from an Aframax

[18] More about ODP in Appendix I – Environmental and health characteristics of a working fluid.
[19] The impact of the benefits must be determined on a fluid by fluid basis.

tanker. The cost of the working fluid is another disadvantage for the organic fluids but when compared to other WHRS costs, like the expander or heat exchangers, its influence is minimal [Chacartegui et al. 2009]. Organic fluids can be flammable and toxic, but could also be a major hazard for the environment. These risks can be mitigated by the use of an intermediary fluid which can decouple the waste heat source from the ORC plant [Vanslambrouck et al. 2012]. Even though this solution will reduce the working fluid's mass going through the plant it will also increase heat losses, cost and complexity. Some of the disadvantages shown here could be mitigated by selecting the correct fluid for the specific process [Sarbu 2014].

Saavedra et al. [2010] compared different organic fluids to detect which working fluid was the best option for heat recovery from a medium grade source in order to generate electricity. The results show that on average an organic working fluid can deliver more power and hence is more thermally efficient than water. In Saavedra et al.'s work, benzene and cyclohexane are organic fluids that offer the greatest power output. When comparing thermal efficiency, only n-pentene shows a lower efficiency than water; while Decamethytetrasiloxane (MD2M) is the most efficient fluid. Branchini et al. [2013] found out that benzene and toluene returned high power outputs for temperature sources of 200˚C and 400˚C without requiring large heat transfer areas. On the other hand, the thermal efficiencies for these fluids were lower when compared to the refrigerant R245fa at 200˚C. These comparisons highlight the importance of choosing the correct working fluid for the heat source and sink.

Taking into account the thermodynamics, flammability and toxicity levels of the different organic fluids, Larsen, Pierobon et al. [2013] show how the selection of the optimum organic working fluid changed for a marine application. The focus of the previous work was the WHRS' thermal efficiency and they used the Hazardous Materials Identification System (HMIS)[20] to categorise per hazard each of the different organic fluids. If there were no hazard restrictions on board, the best working fluid is I-hexane with a thermal efficiency of 25.9%, increasing the hazard level to two showed that the best working fluid was R245ca at a thermal efficiency of 24.5%. While this work did not consider the environmental effect as an optimisation constraint, they do highlight the fact that R245ca has a high GWP. A similar methodology was used by Pierobon et al. [2013] but in an application for a woodchips gasification plant.

While water is not harmful to the environment if there is a spill, the same cannot be said of some of the carbon compounds used in the ORC WHRS. Global Warming Potential, ODP and toxicity are important characteristics when choosing the fluid since these have a profound impact on the environment. For example, cryogens, such as R11, have a high content of chlorofluorocarbons (CFC) which play a significant role in ozone depletion [Hung et al. 1997; Calm 2008] because of which now they have now been phased out of production. But even their substitutes can contribute to environmental harm if the fluid is not supervised properly when handling and using them. This is the case of R134a which substitutes R12, having a GWP of 1,600 and a life in the atmosphere of around 14 years [Sarbu 2014]. Having harmful fluids in a

[20] Please refer to the following reference to read more about hazard levels and how they are categorised [National Paint and Coatings Association 2002].

WHRS is not desirable but that does not mean that they cannot be used if the benefits brought by the ORC – CO_2 emissions, payback time, etc. – are considerable. Different options to mitigate the fluid's hazards are discussed in various studies [Granryd 2001; Roberge 2014; Suárez de la Fuente et al. 2016]. It is suggested that the use of advance monitoring, detection, containment and firefighting systems on board vessels could considerably reduce the risk for the crew, vessel and environment.

3.2.2 THERMAL FLUID

In ORC WHRS, there is a need to protect the organic fluid from decay when the waste heat source temperature is higher than the fluid's decomposition temperature. While a straightforward solution in the design process would be to choose another working fluid, the use of a thermal fluid could offer another option when the availability of the design working fluid is scarce. Thermal fluid circuits are tasked with transporting the waste heat from source (exhaust gas, solar collectors, etc.) to the working fluid at lower temperatures; effectively decoupling the physical position of the WHRS with the waste heat source. This ability is attractive for applications in which the decomposition of the working fluid is not relevant, although it is from the safety point of view. For example, having flammable fluids close to hot surface areas or where sparks are likely is a dangerous combination because the chances of igniting the organic fluid increase, hence, a requirement to separate them.

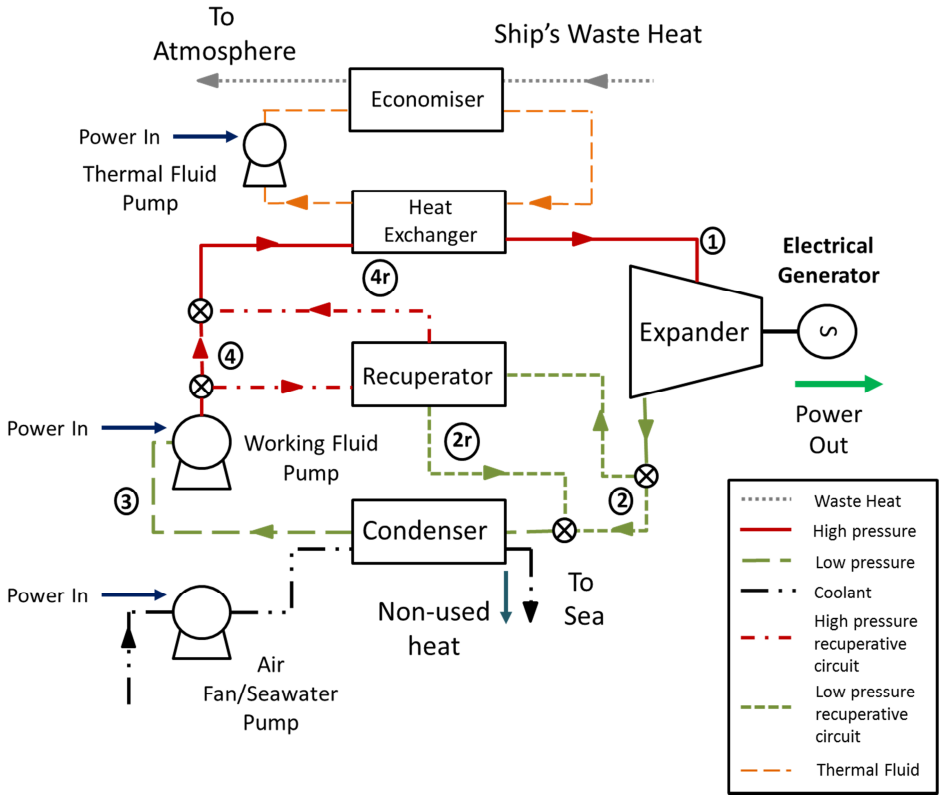

Figure 21: Simplified diagram of a recuperative ORC using a thermal oil circuit.

This is a critical point in the marine environment where fluids that have flash points lower than 60°C cannot be kept inside the machine room [International Maritime Organization 2009b]. For the marine scenario, a thermal fluid, provided sufficient care was taken in the design of the

system, enables the use of low flashpoint organic fluids on board. Another advantage that the intermediate circuit offers is that it acts like a thermal buffer which mitigates variations on the heat source, allowing a smoother thermodynamic operation [Quoilin et al. 2013].

Common heat transfer fluids are mineral oils or special chemical compounds, such as Downtherm or Therminol VP-1, that offer high levels of thermal and chemical stability [Solutia Inc. 1999; Towler & Sinnott 2013].

Adding extra heat and mass transfer processes, as in the case of the thermal fluid circuit, will increase the WHRS losses (i.e. pressure and temperature drops), costs and complexity. Also, using the Carnot cycle efficiency, it is seen that lowering the source temperature will represent a reduction in the power potential of the thermal machine (see Appendix III – Some important concepts for a thermal machine section 3.5). Form the industrial side, Quoilin et al. [2013] claim that ORC manufacturers do provide an intermediate thermal loop which highlights the importance of adding this fluid into the study of WHRS when the working fluid requires it.

There are only a few examples in the ORC WHRS literature where thermal fluid is used. Kane et al. [2003] use water as the thermal fluid in the prototype stage of a small solar collector which powers an ORC. Bini et al. [2010] use a thermal oil to give a biomass ORC plant more operational flexibility and lower WHRS high-pressures. In the same vein, Fernández et al. [2011] use a thermal oil circuit in between exhaust gases and the ORC which lowers the operational pressure but also avoids the heating organic fluids beyond their decomposition temperature. Pierobon, Rokni et al. [2013] use a Downtherm Q fluid to protect the working fluid in a gasified solid oxide fuel cell plant but also to reduce the risk of an explosion due to leakages of the organic fluid inside the burner. Öhman and Lundqvist [2013] give a comprehensive list of actual ORC plants using thermal oils to split the waste heat source and working fluid. The work of Roberge [2014] found that there was a reduction of more than 2,000 kg in toluene when a thermal oil was required. This was noted by Vanslambrouck et al. [2012] but not demonstrated. To broaden more into the subject – the use of thermal fluids is common on power stations based on the RC – Towler and Sinnott [2013] state that the initial cost of using a thermal circuit are small but it is important to consider the energetic requirement of pumping the thermal fluid around the circuit.

3.2.3 DESIRABLE CHARACTERISTICS

Upon reviewing the available literature regarding organic fluids, it is difficult to pin-point which is the best fluid since there are too many variables that can influence the decision. But in general a good organic fluid should have some of the following characteristics [Maizza & Maizza 1996; Andersen & Bruno 2005; Chen et al. 2010; Sarbu 2014][21]:

- High liquid specific heat, latent heat of vaporisation and density which enable the fluid to absorb large amounts of energy without needing large mass flow rates. But also, low viscosity which reduces the pumping power requirement.

[21] It is important to highlight that the list shown is also applicable to any thermodynamic cycle, but since the ORC has the largest option of fluids it was convenient to show it here.

- Fluids that have an ε that equal or are larger than zero (i.e. isentropic or dry) which guarantees that during the expansion process the formation of droplets does not happen, increasing the expander's blade life expectancy and costs. This also requires simpler ORC systems which do not need a multi-stage expander and reheating to avoid internal condensation. Different ORC can reach similar thermal efficiencies by adding components to the plant layout, so it will be preferable to have working fluids which return high performance with the simplest configuration possible [Domanski et al. 1994; Calm 2008].
- High chemical stability at operating temperatures. This will guarantee that the properties of the working fluid will not be affected during operation and that the initial investment on the working fluid is not lost.
- Low freezing point in order to be able to work even under the harshest weathers like that seen close to the Arctic where the temperature can reach as low as -37˚C [Jones et al. 1999; Jones et al. 2012].
- Ideally, the organic fluid should be non-flammable and non-toxic in order to avoid risks to the crew and ship, but also to have lower installation costs on safety systems. Classifications of organic fluid hazard levels are found in publications by National Paint and Coatings Association [2002] and American Society of Heating Refrigerating and Air-Conditioning Engineers [2007]. The use of highly-flammable organic fluids will require the use of thermal oils which will reduce the ORC overall efficiency and power production[22].
- Low GWP and ODP values so in case of a leak the working fluid do not harm the environment.
- Low cost and high availability, this will help the marine ORC WHRS to be attractive to vessels' owners and operators, while easy to find them near ports or along the route. Advanced refrigerants are expensive and difficult to find, becoming an important cost factor, but increasing the demand could bring costs down and availability up [Dinanno et al. 1983; Calm 2008]. Another option is the use of hydrocarbons (e.g. pentene or toluene) as the working fluid since these are common and have lower prices [Douglas et al. 1999].
- Non-Corrosiveness affects the type of materials that can be used on the WHRS and impact the cost of the plant. It is important to mention that the corrosive nature of a working fluid can change with temperature and pressure, and if thermal or chemical decomposition start to happen then some of the new products could be corrosive [Andersen & Bruno 2005].

Calm and Didion [1998] point out that there is no organic fluid which could comply with the list of desirable characteristics. For example, hydrocarbons, such as toluene, have low GWP and ODP but are highly flammable. On the other hand, some refrigerants have low levels of flammability as is the case of R245fa but have high GWP or ODP, substitute fluids such as

[22] For further details on fluids flammability and toxicity please refer to Appendix I – Environmental and health characteristics of a working fluid.

R1234yf, but then again the cost and availability is low. From Saavedra et al. [2010], it is shown that there is no working fluid which can perform as the best fluid in all scenarios. For the shipping case, where the scenarios can change depending on the load or sea temperature, it is necessary to choose a fluid that can deliver an overall good performance in the full scope of the ship's environment, especially in the most frequent circumstances. That means that the WHRS designer has to deal with the different trade-off and implications when choosing a working fluid. Still, as mentioned before, the search of better organic fluids is ongoing as shown in the work of Calm [2008].

3.2.4 ORGANIC RANKINE CYCLE WASTE HEAT APPLICATIONS

Organic-based WHRS applications are similar to those seen for RC, but ORC systems can work better for low/medium heat sources opening a new range of applications where normally the system's waste energy will have to be dumped into the environment. Tartière [2016] calculated, from 19 ORC vendors, that there are more than 560 ORC land-based power plants with a total power installed of 2.75 TW_e of which 12.7% are soley coming from waste heat applications.

Land-based ORC plants can reach power outputs as high as 125 MW [Kaplan 2007a; Bronicki 2008] with thermal and exergetic efficiencies that can reach to 53.9% [Kaplan 2007b; Saavedra et al. 2010]. Boronicki [2000] studied the use of an ORC as a waste recovery system for a cement plant. Cement plants waste heat losses represent on average 30% at a temperature range between 275°C and 350°C, used in some cases to dry raw materials. By not using the waste heat, there is a loss of around £915k per year. The ORC WHRS discussed is installed as a bottoming cycle capable of producing 1.3 MW and saving annually around $6.35x10^3$ t CO_2[23].

For compressor stations, the losses are even greater than those seen in cement plants reaching levels of around 65%-75% mainly due to compressor thermal inefficiencies [Popov 2004]. Saavedra et al. [2010] optimised an ORC WHRS to use the low/medium waste heat from a compressor plant. The results show that an ORC can achieve a thermal efficiency of around 28.0% and power outputs close to 1,220 kW when the source temperature is at 405°C and the sink temperature is 35°C. For the same operational scenarios, a typical RC has a thermal efficiency of around 24.3% and a power output of 1,032 kW. This paper highlights the importance of optimising the ORC design by the selection of a suitable working fluid for the waste heat scenario.

An interesting application for the ORC is its use in a floating Ocean Thermal Energy Conversion (OTEC) plant. This source of energy could provide around 10 TW of power produced by small temperature differences (i.e. around 20-25°C) between the surface and bottom of the ocean [Pelc & Fujita 2002]. Due to the small gradient demanded by OTEC plants for large equipment (e.g. heat exchangers and pumps), it is possible to extract enough energy [Yang & Yeh 2014]. This means that the initial investment and the necessary area and volume footprint are considerably large, while the cooling source pump will play an important role in the OTEC net power output – due to its large power requirement. All these factors elevate the cost of

[23] Original unit of case study is in tons, known as short tons. 1 ton = 0.91 tonne [Thompson 2008].

producing electricity to higher levels than when using fossil fuels [Pelc & Fujita 2002; Syamsuddin et al. 2015]. For this kind of application ORC are ideal due to low temperature boiling fluids such as R134a or R152a. Yang and Yeh [2014] found that an OTEC based on isobutene could deliver a better power output at a higher thermal efficiency than ammonia but with a larger requirement for heat transfer area.

The use of ORC as bottoming cycles for gas turbines is studied by Chacartegui et al. [2009] who discovered that a recuperative gas turbine coupled with a recuperative toluene ORC could increase by around 3% the combined thermal efficiencies than when using water as working fluid. Also, steam was found to be the most sensitive working fluid for the turbine inlet temperature, followed by toluene. Another important finding shows that the combined cycle using ORC is financially attractive when the ORC cost is below £2,190/kW_e for gas turbine temperatures of around 1,300°C, and below £1,460/kW_e for temperatures of 1000°C. Nowadays, the prices for ORC WHRS are inside the cost range given by Chacartegui et al. [Quoilin et al. 2013; Shu et al. 2013]. Pierobon et al. [2013] also found that an ORC plant is the preferable thermodynamic WHRS for a natural gas turbine operating in an offshore platform. The downside of the finding is that in order to have a substantially better performance than a RC, the total heat transfer area will have to be larger; this also increases the initial cost due to the use of a recuperator and larger economiser.

The ORC WHRS applications are not only evident in large size plants, but also in compact and portable efficient power generators. The trucking and automotive sector has analysed its use for exhaust and cooling waste heat. Dinanno et al. [1983] proposed an ORC in order to reduce the fuel consumption of a heavy duty truck. The study focused on four different engine configurations with different performances. The maximum improvement achieved by this study was a 24% increase in the maximum power output and a 19% reduction in fuel consumption, which was obtained by the least efficient engine. Inefficient engines will have higher cooling demands and temperatures at the exhaust gas which will increase the WHRS thermal efficiency and power output [Chacartegui et al. 2009]. This same pattern is seen when the engine loading changes [Hossain & Bari 2013], for example, marine propulsive plants have different tunings which allow a more efficient operation at the designed point. The work of Suárez de la Fuente and Greig [2013] shows that thermal efficiency seems to be more sensible to the waste heat quality, while the power output responds more strongly to heat availability.

Boretti [2012] simulated an ORC system installed in an 1.8 litre hybrid non-supercharged passenger car. He studied two different waste heat sources from which the ORC system could work: the exhaust gas system and cooling system. The author simulates different real scenarios of a hybrid car (i.e. different loads and weather conditions) by changing different variables in the system like the exhaust flow rate, temperature of exhaust gases, and turbine and pump speeds. The electric power output from the ORC system charges the car's batteries, enabling faster charging times and longer distances covered with the same amount of fuel. The R245fa ORC system achieves its best overall performance when combining together the exhaust gas and cooling system. The car's total plant efficiency increases from its base line of 34.8% to 40.5%

with the combined WHRS. Similar improvements (i.e. power increment, fuel consumption and thermal efficiency) on internal combustion engines are found in the works of Katsanos et al. [2012] for a truck's diesel engine using a R245ca ORC with the maximum fuel saving of 10.2% at lower loads. Yang et al. [2014] use an R245fa ORC for a six cylinder diesel engine, having a maximum combined power output of 309 kW of which the ORC provides 29 kW. In the same field of internal combustion engines, Hossain and Bari [2013] achieved a power increase of 3.4% from a 40 kW diesel generator which meant a reduction of around 3.3% in its fuel consumption.

Experience with land-based ORC systems show that these systems are realiable. Bronicki [1995] shows that ORC power plants have recorded a maximum of 3.7 million hours while Dinanno et al. [1983] achieved more than 2,000 operating hours – representing a distance of 55,000 miles on board a truck – for their ORC WHRS prototype. Obernberger et al. [2001] installed an ORC biomass cogenerative plant and found out that only for a few days the plant was off-line due to maintenance while operating successfully over more than 10,000 hours.

For more on ORC WHRS applications and manufacturers, please see the following references: [Tchanche et al. 2011; Bianchi & De Pascale 2011; Vélez et al. 2012; Campana et al. 2013; Quoilin et al. 2013; Sprouse & Depcik 2013].

3.3 KALINA CYCLE

The Kalina cycle (KC) was designed and introduced by Alexander Kalina in the 1980's [Kalina 1982]. The KC cycle is a hybrid system between the RC and an absorption cycle commonly used in refrigeration processes [Kalina & Leibowitz 1987], taking from each cycle components to operate. From the RC, uses an economiser, turbine – similar to a steam turbine [Tchanche et al. 2014] – and condenser; from the absorption cycle, it uses an absorber or distillator, and a binary working fluid. Figure 22 shows a broad idea of the KC structure.

The KC manages to improve the RC heat transfer at the economiser and condenser thanks to the usage of a binary working fluid which, because of its changing mix ratio, will have a variable boiling and condensing point, enabling the fluid to have a better match for the heat source and sink, thus effectively reducing the cycle's irreversibilities.

The KC has different configurations which are used in order to achieve the best cycle possible for different types of heat sources (e.g. solar energy or exhaust gas from a gas turbine); some of the differences are the location of the distiller, and the amount and location of condensers among others. Kalina [1989] showed various KC configurations for different requirements, it named the systems with the initials KCS (Kalina Cycle System) and numbers from 1 to 12, some are still at design stage while the first to be constructed was a KCS 1 with the purpose of demonstrating the technology [Bliem 1988]. Each of the initial configurations have a specific application, for example, KCS11 was designed for low temperature geothermal heat sources [Mlcak 2004; Akbari et al. 2014]. Other systems configurations, using the same nomenclature, have appeared all this time such as KCS 34 and KCS 34g [Zhang et al. 2012].

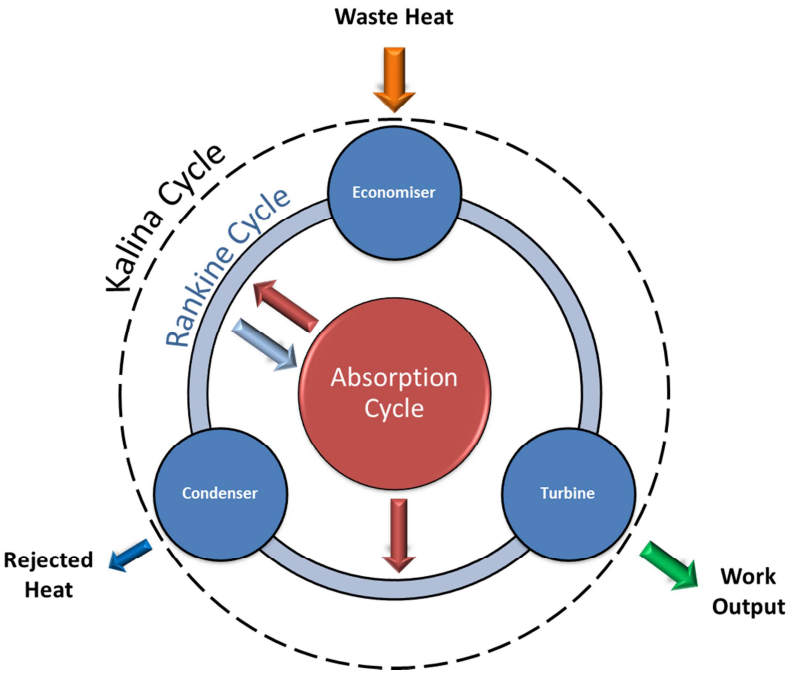

Figure 22: KC illustration. The colour blue represents a RC and red represents an absorption cycle.

A spin-off of the KC is the Uehara Cycle – named after its inventor Haruro Uehara – which operates under the same KC principle but has two expanders, two regenerators, two mixing units, a diffuser and the condenser is followed by an after condenser [Uehara et al. 1998]. The cycle was designed for low grade heat (around 30˚C) specifically for OTEC plants, where it improved the OTEC thermal efficiency by around 10% from a typical KC [Uehara et al. 1997]. Further study of the Uehara Cycle will not be carried out in this thesis.

3.3.1 KALINA CYCLE OPERATION AND STUDIES

To explain how the KC works, the single stage distillation KC proposed by Zhang et al. [2008] will be used (Figure 23). Starting at the economiser's entrance, the working fluid (9) absorbs heat from the waste heat until it is superheated (10). It then enters the turbine and produces work where its pressure is reduced as it exits the expander (11), the low pressure vapour is used to heat the basic solution in a recuperator. At (14) the solution is mixed with a lean liquid (7) to form a basic solution (13), this has the purpose of having a greater content of water, making the new solution a completely saturated liquid at the low-pressure condenser's exit (15). The saturated liquid pressure is increased by the low pressure pump (1) and it then moves into two different routes: (2) and (3). The basic solution (2) is heated in the recuperator (5) and enters the distillator where it is again divided into an enriched vapour (6) and the lean liquid (7). The basic solution (3) is mixed with the enriched vapour (6) to form the working solution (4) which is then cooled in the high-pressure condenser to ensure that it is a saturated liquid (8). Finally, the solution is again pumped to increase its pressure (9) before entering the economiser and start the cycle again.

From the *T-s* diagram for a single stage distillation KC in Figure 24, it can be distinguished the following thermodynamic processes [Zhang et al. 2008]:

1. Heat absorbing at constant pressure (points 9-10).

2. Work produced adiabatically and isentropically (points 10-11s).
3. Distillation (points 5-6 and 5-7).
4. Condensation at constant low pressure (points 13-15).
5. Adiabatic compression at low pressure (points 15-1).
6. Condensation at constant high pressure (points 4-8).
7. Adiabatic compression at high pressure (points 8-9).

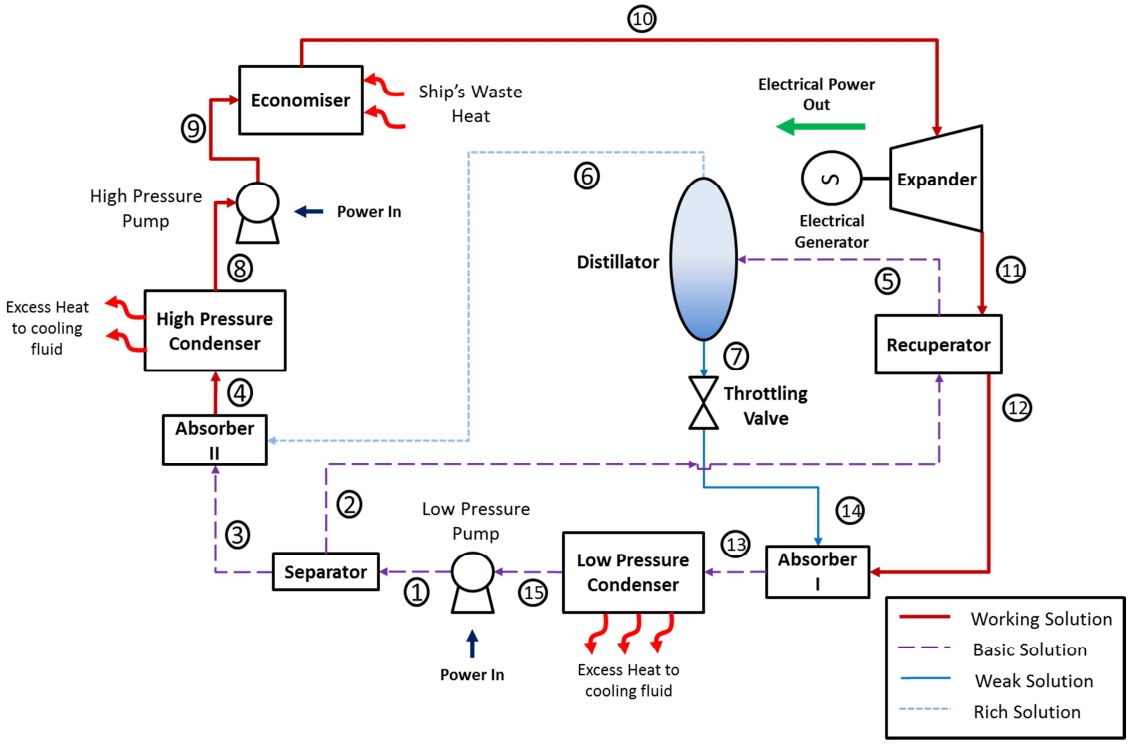

Figure 23: Basic KC configuration of a single stage distillation unit.

The KC *T-s* diagram is composed of various saturated liquid and vapour lines, which represent the different behaviours of the working fluid compositions along the process. Due to the working fluid variable mix, the KC has an extra degree of freedom when compared with a traditional RC [Zhang et al. 2012] which enables, as previously outlined, a better match in the heat transfer processes.

Looking in detail, the binary working fluid will start boiling when absorbing heat from the heat source due to the presence of a low boiling temperature fluid in the mixture, named here as fluid A. As the working fluid goes through the economiser and absorbs more heat the higher boiling temperature fluid in the mixture, called fluid B, will start to boil while fluid A increases its temperature and becomes a superheated vapour [Mlcak 2004]. This temperature increase by fluid A allows the working fluid to follow more closely the temperature profile from the waste heat (Figure 25). When analysing the boiling process of each fluid, it is seen that it is done isothermally as in the RC, but because it is a mixture it will have a variable boiling process.

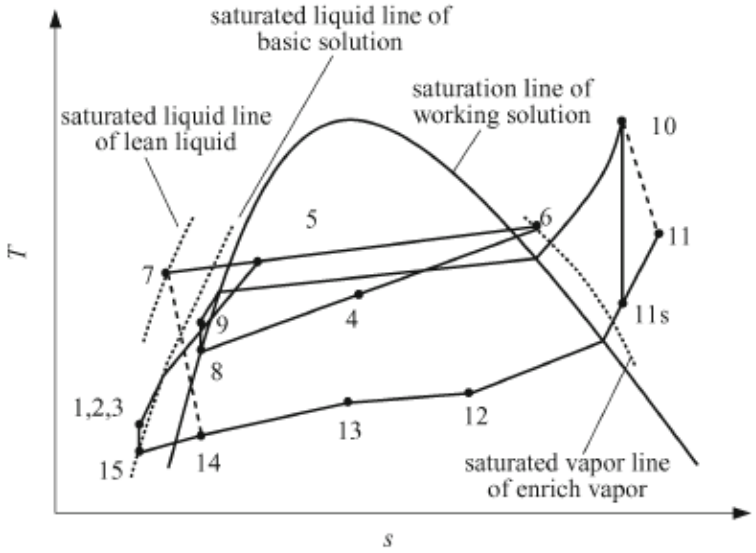

Figure 24: The *T–s* diagram for a single stage distillation KC [Zhang et al. 2008]**.**

The same variability happens at condensation point in the condensers. Here (point 13 of Figure 24) the fluid concentration is changed to a higher proportion of fluid B, which is closer to its dew point. In other words, it has a higher condensing temperature. This helps to improve the heat transfer with the cooling media and reducing the exergy losses – loss in the energy potential to transform into other forms of energy such as work – when compared to a single fluid RC [Mlcak 2004].

Most of the KC literature focuses on low quality heat sources. Leibowitz and Micak [1999] studied the use of a 1.7 MW_e KC using the available heat from a geothermal well at 121˚C, while Coskun et al. [2014] looked into geothermal sources from 92˚C to 162˚C and Eymel et al. [2012] produced power from a Brazilian geothermal heat source found at a temperature between 90˚C and 140˚C. For a heat source of 90˚C, Madhawa Hettiarachchi et al. [2007] used a KCS11 while Arslan [2011] used a KCS34 for a heat source of 148˚C. In the field of solar power, Lolos and Rogdakis [2009] simulated a KC which extracted from the solar collectors heat at a temperature of 130˚C. Zare and Mahmoudi [2015] used a KC to use the waste heat coming at 200˚C from a helium reactor. Recently, there has been an increase in KC studies for medium and high quality waste heat. Nguyen et al. [2014] designed a KC using a genetic algorithm for a heat source of 346˚C. He et al. [2014] modified a KCS11 to use a heat source of 400˚C which brought a thermal efficiency increase of 27% – from 10.2% to

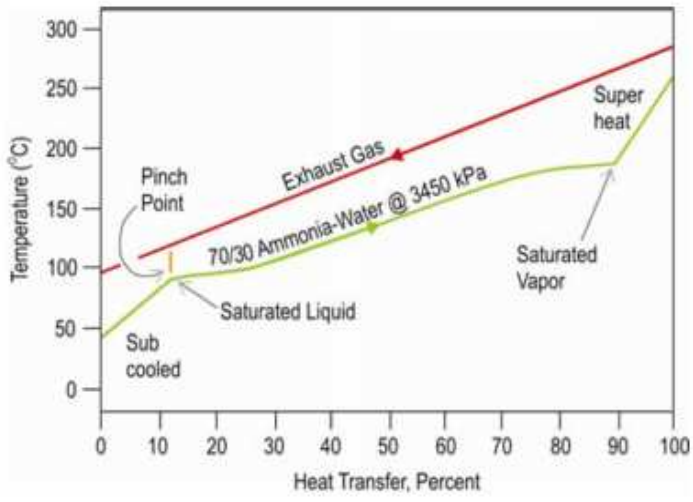

Figure 25: Heat transfer process with an ammonia-water solution at 3,450 kPa [Mlcak 2004]**.**

13.0% – when compared to the KCS11. Modi and Haglind [2015] compared different KC configurations for a heat source coming from solar collectors at a temperature above 500˚C and found that a KCS1234 achieves its highest efficiency at 31.5%. Yue et al. [2015] tested a WHRS based in the KC for a range of temperatures that went from 440˚C to 146˚C, with the highest power output at 217 kW.

When KC is compared with basic RC or ORC there are mixed results as to which systems are better. Valdimarsson [2003] showed that for a geothermal plant with temperatures ranging from 100˚C to 150˚C, the KC brought larger power outputs at lower costs than two different ORC. Wang et al. [2009] demonstrated that a KC could deliver 10.7 MW from using the available waste heat from a cement plant while a RC achieved 10.1 MW and an ORC 8.9 MW. Li and Dai [2014] performed a comparison of a KC with a supercritical[24] CO_2 ORC, finding that the KC produced 220 kW more – around 122% – from the same heat source. Coskun et al. [2014] showed that a KC could deliver around 6.1 MW from a geothermal source while an RC reached 3.9 MW. On the other hand, the results do not always go in favour of the KC, as discovered by Bombarda et al. [2010] who found that a KC would deliver the same power output than ORC, but the complexity of the KC plant will require a more advance control and monitor system leaning the balance to the ORC. Larsen, Haglind et al. [2013] showed that a marine WHRS using an ORC could return a power of 1.16 MW, while a water-based RC produced 0.86 MW and a KC 0.83 MW. Zare and Mahmoudi [2015] showed that a pentane ORC could produce 46.7 MW while a KC produced 34.8 MW from a modular helium reactor. Yue et al. [2015] found that an ORC using decane achieved 146 kW more than the KC.

It is important to note that KC WHRS tend to operate at higher pressures than their counterparts, which can translate to cost increments for the KC. Bombarda et al. [2010] found that a 10.0 MPa KC would deliver a similar power output to a 1.0 MPa ORC. Wang et al. [2009] discovered that the optimum KC operated between 6.0 MPa and 18.0 MPa while an ORC has its maximum pressure between 2.0 MPa and 3.5 MPa. The optimum marine WHRS designed by Larsen, Haglind et al. [2013] showed that a typical water-based RC operated at a pressure of 1.0 MPa, while an ORC at 3.7 MPa and the KC reached 8.7 MPa.

From these comparative studies, it is seen that the results depend greatly on the heat source, KC complexity level (number of equipment required) and optimisation methodology.

3.3.2 WORKING FLUID

Kalina [1982; 1983; 1984] recommended as a working fluid a mixture of ammonia and water (NH_3-H_2O). The KC working fluid is in theory not limited to this mixture, but no reference to another combination of pure fluids that can be used as a KC working fluid can be found in the scientific or commercial literature. The NH_3-H_2O mixture will have a different set of properties than the individual composing fluids; and the new properties will depend on the concentration of each fluid in the mixture [Peng & Robinson 1976]. The basic idea is to create a working fluid

[24] For more about subcritical and supercritical systems please refer to Appendix III – Some important concepts for a thermal machine.

which will produce a heat transfer enhancement for the required process when it is compared to the pure fluids that compose it.

The NH_3-H_2O offers a low boiling point but, at the same time, a high condensing point that can be mixed together without becoming dangerous or unstable. Both fluids have a similar molecular weight – water 18.02 g/mol and ammonia 17.03 g/mol – which enables the use of equipment normally used for pure fluids [Zhang et al. 2012]. Additionally, the pure fluids are abundant and compatible with standard materials (i.e. carbon steels or aluminium), reducing installation and running costs. Finally, both are environmentally friendly since they have negligible Global Warming Potential (GWP) and Ozone Depletion Potential (ODP) [Calm & Hourahan 2001]. However, the American Society of Heating, Refrigerating, and Air-Conditioning Engineers (ASHRAE) has given it a classification of B2 to NH_3 [Doerr et al. 2007], meaning that has low flammability but high toxicity. In the shipping scenario, this is viewed as hazardous since leakage will demand a more complex system of monitoring, prevention and contention that can control and minimise the hazard. On the other hand, NH_3 is easy to detect and vent, and when diluted with water becomes less harmful [Mlcak 2004].

Figure 26: Húsavík KC [Global Geothermal 2013a].

It is important to be critical when trying to find the best composition for the KC mixture of NH_3-H_2O which depends greatly on the conditions set by the heat and cooling sources. For example, Mounir and Kovach [1993] found that the thermal efficiency increases as the concentration of NH_3 is reduced, while Zhang et al. [2008] found the contrary. In both cases, this would not be entirely true since at the extremes of these statements, the KC will be using a pure working fluid, eliminating its uniqueness. Nag and Gupta [1998] discovered an optimum NH_3 concentration point where increasing or reducing the NH_3 concentration will produce a reduction in the exergy efficiency value. Li and Dai [2014] showed that the optimum mixture of NH_3-H_2O mix was close to 95% for a geothermal source at a temperature of 91˚C. Coskun et al. [2014] found that for a low temperature heat source, the optimum concentration was at 70% achieving a power output of 6.1 MW. A common value for the concentration of NH_3 is around 70% [Kalina & Leibowitz 1987; Wall et al. 1989; Leibowitz & Micak 1999]. Equally important for the mixture concentration are the installation and running costs [Arslan 2010]. An overview of studies that

have analysed ammonia concentration give, as an optimum, a concentration between 58% and 90% in the mixture depending on the application and operating conditions.

3.3.3 KALINA CYCLE WASTE HEAT APPLICATIONS

The majority of KC installations found today fall under land-based installation for power generation as the top cycle (i.e. low grade heat from a geothermal source) or as a bottoming cycle (i.e. WHRS in cement or oil refineries). In some cases, the information available is scarce and only part of the KC plant characteristics are available.

Table 5: Other KC plants built for different waste heat sources. The table presents the waste heat temperature, plant's power output, and operating hours as reported in the available literature and, finally, the year where the plants were commissioned. The sink temperature was not reported in any of the references.

Location	Type of plant	Source temperature (°C)	Power output (kW_e)	Operating hours	Date commissioned
Canoga Park, USA [Leibowitz & Mirolli 1997; Mirolli 2012]	WHRS for nuclear reactor	543	3,050	10,000+	1992
Fukuoka, Japan [Mirolli 2012]	Waste incinerator	900	4,500	N/A	1998
Kashima, Japan [Yanagisawa, Muraoka, Sasaki & Sugita 2012; Global Geothermal 2013b]	WHRS for steel plant	98	3,450	10,000+	1999
Húsavík, Iceland [Mlcak et al. 2002; Mirolli 2012]	Geothermal	121	1,700	10,000+	2000
Fuji Oil, Japan [Ogriseck 2009; Mirolli 2012]	WHRS for hydrocarbons and steam	118	4,000	N/A	2005
Bruchsal, Germany [Wasabi Energy Limited 2015]	Geothermal	550	120	N/A	2009
Shanghai Expo, China [Wasabi Energy Limited & Global Geothermal Limited 2010; Mirolli 2012]	Solar thermal	90-95	50	N/A	2010
Matsunoyama Onsen, Japan [Yanagisawa, Muraoka, Sasaki, Sugita, et al. 2012]	Geothermal	100	50	N/A	2013

The Húsavík geothermal plant was the first commercial KC application, seen in Figure 26 [Global Geothermal 2013a]. The geothermal fluid enters at 121°C and has a sink temperature of 5°C. The KC plant produces 1.7 MW_e at a thermal efficiency of around 10.2% and exergetic efficiency of around 23.1% [DiPippo 2004]. The working fluid concentration is set at 96% NH_3 before entering the expander [Hjartarson & Gullev 2003; Whittaker 2009]. The plant had several issues of corrosion inside the turbine while in operation [Whittaker 2009; Mirolli 2012]. Another geothermal plant using KC technology is in Unterhaching, Germany. It produces 3.4 MW_e with efficiencies from 10% to 13%. This geothermal plant has an annual CO_2 savings of around $2.25x10^4$ t [Milles 2001].

There are other KC plants that have been built to show the capabilities of the cycle under different conditions, and different waste heat sources (see Table 5).

Further projects that are under construction are the 4.0 MW_e Hainan plant in China [Wasabi Energy Limited 2012]; the cement plant WHRS in Khairpur, Pakistan with an estimated power output of around 8.0 MW_e [Mirolli 2012]; and Taufkirchen's geothermal plant in Germany with a capacity of 3.4 MW_e [Wasabi Energy Limited 2011].

3.4 Stirling Cycle

The Stirling Cycle (SC) was developed by Robert Stirling who he patented, in 1816, a closed-cycle regenerative engine called the Stirling engine. The engine did not require valves or ports, introduced a regenerator to store the heat available and, being a closed cycle, allowed the increase of pressure to have a better engine efficiency [Urieli & Berchowitz 1984]. Xu et al. [2015] recently proposed a new Stirling engine design that works as an open-closed cycle. This modification of the cycle will not be covered by this thesis since its application is only for atmospheric temperatures and requires cryogenic temperatures as sink (i.e. temperatures below -150˚C).

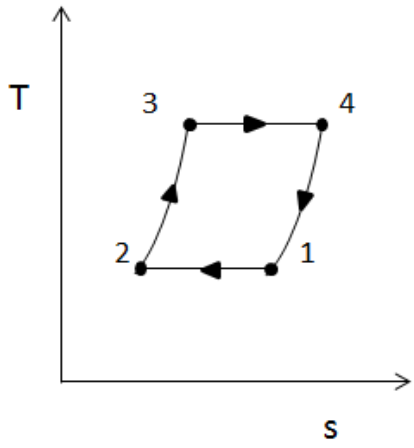

Figure 27: SC *T-s* diagram.

The ideal SC, seen in Figure 27, is composed by two isothermal processes (i.e. compression and expansion) and two isochoric processes (i.e. heat addition and rejection) [Walker 1980; Urieli & Berchowitz 1984]:

1. Isothermal compression (points 1-2).
2. Isochoric heat absorption (points 2-3).
3. Isothermal expansion (points 3-4).
4. Isochoric heat rejection (points 4-1).

The ideal SC assumes that there is only heat absorption at the cycle maximum temperature and its rejection at its minimum, resulting in an identical performance as that found in the Carnot cycle. One main difference to the Carnot Cycle is that the SC can be replicated in reality because it replaces the two isentropic processes, found in the Carnot cycle, with two isochoric processes [Walker 1980].

As seen in Figure 28, the components of an engine using an ideal SC can be divided in three different regions [Urieli & Berchowitz 1984]:

1. A compression volume, located in the cold side at the minimum temperature.
2. A regenerator which is in charge of the heat transfer between the cold and hot zones.
3. An expansion volume, located in the hot side at the maximum temperature of the system.

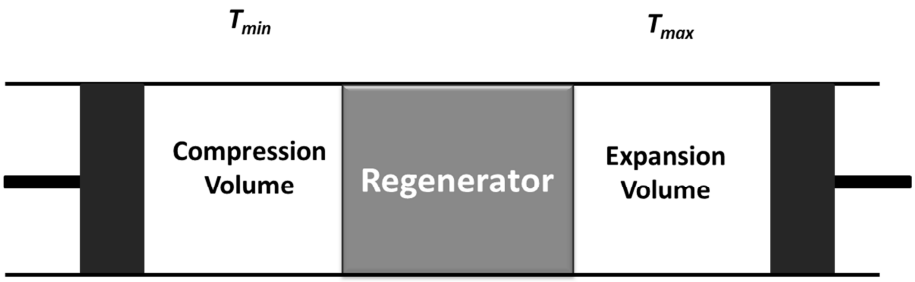

Figure 28: Ideal SC components.

3.4.1 STIRLING ENGINES: THE REAL STIRLING CYCLE

Stirling engines are external combustion engines capable of using any fuel or waste heat as their heat source [Vieira da Rosa 2009]; and they are the practical application of the SC. The Stirling engine delivers less power than its ideal cycle because [Walker 1980; Kongtragool & Wongwises 2006; Puech & Tishkova 2011]:

- In order to have an isothermal compression and expansion (points 1-2 and 3-4 from Figure 27), it is required that there is perfect heat transfer between the engine's volumes and fluid. In reality, these processes tend to be more adiabatic which means they are an almost zero heat transfer process. The addition of heat exchangers in Stirling engines is required in order to increase the heat transfer, but they also introduce pressure losses and increase the size and mass of the engine.
- Regenerators have a thermal efficiency that can reach up to 98% depending on the operating conditions [GmbH 2003; Epcon Industrial Systems LP 2010; Yildirim & Guo 2012].
- Friction losses.
- Working fluid flow losses.
- Continuous sinusoidal pistons movement, when in the ideal case the compression and expansion volumes should have a discontinuous movement.
- Introduction of volumes that are not swept by the pistons known as dead volumes. These volumes are part of heat exchangers and piping; and are normally 58% of the total engine volume [Martin 1978].

Stirling engine manufacturers put the thermal efficiency of their engine as high as 30%, but take into account the engine's waste heat as being utilised for other uses which increases considerably its thermal efficiency. Also, in some cases, the manufacturer uses extreme temperatures for the source and sink in order to improve engine efficiency, even when these temperature may damage the engine's integrity [Majeski 2002].

Researchers have investigated the effects of operating conditions, dead spaces, heat and friction losses in order to have a better picture of a real SC thermal efficiency. Wu et al. [1998] found that the Stirling engine's power output was reduced, almost in a linear way, by an increase in the regenerative inefficiency. Kongtragool and Wongwises [2006], in a more comprehensive study, analysed the effect of dead space and imperfect regeneration in Stirling engines. They performed simulations, modifying the amount of dead space (i.e. from 0% to 66%

of the total volume), and the regenerator efficiency (i.e. from 0% to 100%) which mapped the Stirling engine. From the results of this study, it can be seen that with dead volumes around 60% and with a regenerator efficiency set at 80% it is possible to have thermal efficiencies not higher than 10%. Meijer [1970] in his work presented a theoretical four cylinders 660 kW Stirling engine using as a working fluid hydrogen. He changed the engine speed, temperature and maximum pressure and found that by increasing the source temperature from 700°C to 800°C and keeping the pressure constant at 21.6 MPa, the maximum thermal efficiency of the engine grew around four percentage points, from 58% to 62%. However, when the pressure of the engine changed from 10.8 MPa to 21.6 MPa at a temperature of 700°C, there is a lower increase in the maximum thermal efficiency, from 57% to 58%.

Tailor et al. [1988] used a Stirling cycle as a cooling engine. They tested SC engines with helium, nitrogen and hydrogen and performed a parametric study of different variables such as compression and temperature ratio, regenerator efficiency and dead volume. The results showed that as the dead volume increases, the Coefficient of Performance (*COP*)[25] and thermal efficiency of the engine will drop. The same happened with the regeneration efficiency which appeared to be more sensible, since a drop of 4% in the regenerator efficiency can result in a thermal efficiency equal to zero. It was shown that the thermal efficiency of a Stirling engine is highly sensitive to temperature changes and inefficiencies in the heat exchangers; this is to bear in mind when having constant change in the operation conditions, such as in the vessel case.

Throughout the middle and late part of the 20th century, thanks to large investment in research and development, Stirling engines were capable of producing larger power outputs. There are three examples of engines reaching above 250 kW [Walker 1980]:

1. The 4-1400 DA Stirling engine. Designed and constructed by Koninklijke Philips Electronic and Ford motor company, it had four cylinders and used hydrogen with a heat source of 700°C and a sink of 70°C. It reached a thermal efficiency of around 40% with a power output of 295 kW.
2. The 8-500 DA Stirling engine. Similar to its brother, the 4-1400 DA, but uses eight cylinders.
3. The 4-S1210 Stirling engine. Designed and constructed by General Motors, it was composed by four 65 kW Philips Stirling engines reaching 265 kW power output. It used hydrogen as its working fluid.

Kockums maritime solutions offers kinematic Stirling submarine propulsion units using as a working fluid helium. The engine produces 75 kW_e at a source temperature between 700°C and 750°C by burning liquid oxygen with a reported thermal efficiency of around 39% [Majeski 2002; Kockums AB 2009]. Another marine engine but developed by Philips is shown in Figure 29 it had a thermal efficiency of 41% producing 85 kW.

[25] *COP* is used for cooling or heating cycles and measures the amount of cooling/heating effect that the cycle can produce with an energy input. *COP* is a number without units, instead of a percentage used by η_{Th}, and this number can be bigger than the unit. For a more in depth *COP* explanation, please refer to Cengel and Boles [2007].

The majority of the research carried out reports power outputs from a few Watts to around 300 kW per unit. Hsu et al. [2003] showed that a SC engine was capable of producing 160 kW from an incinerator at a temperature of 1,427°C. A low temperature difference Stirling engine was modelled by Kongtragool and Wongwises [2007] and capable of producing around 12 W as a heat source, providing 2.4 kW. An advanced SC was tested by Aksoy and Cinar [2013], finding that it was capable of producing up to 270 kW if the heat transfer coefficients were improved to 400 W/m^2-K from the experimental value obtained of 104 W/m^2-K. Sala and Invernizzi [2014] used a wide variety of working fluids inside a SC engine finding that the maximum power output was achieved by CO_2 at 6.5 kW from a source of 300°C.

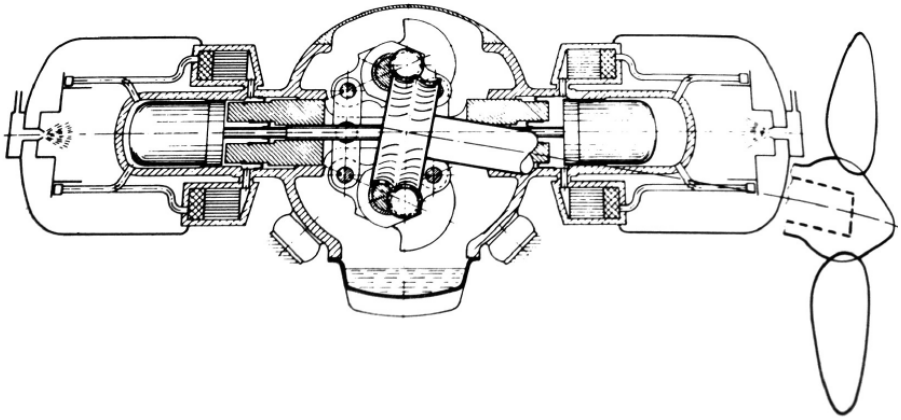

Figure 29: Philips 4-235 Stirling engine for marine propulsion capable of producing 85 kW, this engine was never installed [Walker 1980]**.**

One of the most interesting characteristics from a Stirling engine is its modularisation capacity which helps overcome the lower power outputs at low/medium waste heat when compared to the more traditional RC. Mancini et al. [2003] proposed to assemble solar-powered plants using modular dish Stirling units which in total could produce up to 10 MW_e. The same concept was taken by Abbas et al. [2011] where by using 25 kW_e dish Stirling modules, it was possible to design a 100 MW_e plant using the solar energy available in Africa's northern region. The plant reaches a solar efficiency to grid of around 23% which is eight percentual points lower than the highest solar efficiency to grid ever achieved for a solar plant [Taggart 2008]. In 2010, Stirling Energy Systems Inc. put into operation for a full year a 1.5 MW_e solar plant for demonstration running at an efficiency of around 26% [Alliance for Sustainable Energy LLC 2013; Stirling Energy Systems Inc. 2015]. While modularisation can bring the Stirling engine's power output up, increase the level of redundancy and – if sufficiently large quantities of module are installed – reduce the initial cost it will also imply a busier maintenance schedule, a large stock of replacement parts, and complex control and monitoring systems which will affect the operation costs, and will probably require large cargo spaces.

For a description and applications of the different types of Stirling engine please refer to Stirling engines in detail on Appendix IV – Further on thermodynamic cycles.

3.4.1.1 STIRLING ENGINE WORKING FLUID

Any gas available which will not condense inside the engine under the operating conditions can be used as the SC working fluid. But to define a good SC working fluid it is important to observe its thermodynamic and physical properties since, as previously observed, the fluid will determine in some scale the performance and physical characteristics of system. Flow friction and heat transfer losses are amongst the highest inefficiencies found in a SC. The working fluid properties play an important role in these two areas. Air, helium and hydrogen are the preferable working fluids for a SC. Helium and hydrogen are a better choice due to their thermodynamic properties which allows a high heat transfer and moderates pressure losses. On the other hand, a major problem is the fluid leakage through the engine seals due to the lower molecular size. Furthermore, hydrogen exposure can cause embrittlement and diffusion which can increase the probability of fracturing the engine block [Klell 2010]. Air is a better option for slow engines that demand a simple design [Meijer 1970; Walker 1980; Invernizzi 2010].

Meijer [1970] performed simulations to a 165 kW Stirling engine using as a working fluid air, helium and hydrogen. The temperatures of the simulations where set at 700°C and the sink temperature at 25°C. The results show that as the engine volume increases, the effect of using different working fluids is reduced. The fastest engine used hydrogen, delivering around 51.5 W/cm^3 with a thermal efficiency of around 32% at a speed of 1,500 rpm. From the previous values it can be inferred that a compact and powerful Stirling engine, which are attractive characteristics inside a ship, can be achieved by using hydrogen. Due to hydrogen being a highly flammable gas, odourless and colourless, it is required to install strong safety control systems that can prevent or contain any possible hazard inside a confined space, such as the shipping environment [Klell 2010]. With this in mind, a better option for shipping is helium which delivers high power output in compact designs at high efficiencies and is an inert non-toxic gas.

Invernizzi [2010] performed simulations inside an ideal and real Stirling engine in order to assess how different working fluids affected the engine performance. The study compared CO_2, nitrogen, argon, R23, and R125 among others. The results in the ideal case show that as the compression pressure increases the power output for nitrogen, argon, hydrogen and helium stays the same, while CO_2, ethane, R23 and R125 do increase the power output. In the case of the real engine, where the effect of imperfect heat exchangers and pressure losses are accounted for, it is seen in all cases that the cycle efficiency increased as the cycle pressure does. Ethane achieved the highest efficiency of all working fluids at around 23% – down from around 45% in the ideal case – while the lowest is found when using nitrogen at a maximum efficiency of around 2%. It is important to notice how introducing some real conditions into the model decreases in great measure the efficiency of the cycle. Even though Invernizzi's paper did not specify the operating temperature, it could be assumed that the Stirling engine's thermal efficiency could be increased by having a higher operational pressure when the source temperature is lower, especially for the refrigerants R23 and R125. Higher pressures will translate into more robust engine blocks – affecting the system mass – better seals and more frequent maintenance.

There are some studies performed with compound fluids, especially with water-air combination, which were compiled in Walker [1980]. The theoretical results indicated that the power output will be increased when using a compound working fluid. The idea was that by adding a working fluid that changes phase inside the Stirling engine will produce an increase in the compression ratio without having to raise the system's maximum pressure. The liquid would help to reduce the sealing problem and also with the lubrication of moving parts. The high idealisation of the behaviour of the compound working fluid and its applicability into real engines meant that the few experiments done had unsatisfactory results which reduced the interest in the subject.

3.5 CLOSING REMARKS

The water-based RC has been successfully applied as a bottoming cycle to different waste heat sources, such as exhaust gases from cement plants or internal combustion engines. This thermodynamic cycle shows great qualities thanks to its working fluid, water. Among water's advantages are that is abundant, has high chemical and thermal stability, high latent heat of vaporisation and does not represent a risk to the environment. On the other hand, water is a wet fluid which means that special precautions and turbine design must be in place in order to minimise erosion and corrosion happening inside the steam turbine. Another important consideration is that water must have a high purity in order to be used in the RC.

As the ship's waste heat availability and quality reduces due to improvements in diesel engine thermal efficiency and other green technologies require more of the available waste heat, the RC will struggle to deliver strong benefits to shipping. From the academic literature, it was detected that there are other alternative power thermodynamic cycles which could offer a better performance with low/medium waste heats in regard to power output and thermal efficiency and could translate into better fuel savings and larger CO_2 emission reductions.

Starting with the ORC, it uses identical equipment, layout and design as the RC. The difference is due to the working fluids which contain carbon compounds in their structure. ORC achieve a better performance at low/medium temperatures than a RC, becoming a common option for geothermal and waste heat recovery. The adaptability to different low/medium waste heat has been demonstrated when used as a WHRS in cars and trucks where the changes in engine load are frequent and sometimes fluctuate from either extreme. For shipping, the flexibility between the load and temperature range are important and desirable characteristics. The WHRS flexibility can be achieved by understanding the characteristics of the working fluid and equipment.

Special care must be taken when selecting the fluid since its characteristics and availability can dictate the cost, safety and complexity of the entire system. In the maritime application, the level of toxicity and flammability should be low – or else the use of a thermal oil and advance safety system is required – but it must also be common enough to be easily available. However, the large carbon-based fluid catalogue allows the ORC to adapt to any type of scenario and deliver good efficiency and power outputs.

The KC uses a NH_3-H_2O as a working fluid that gives two different evaporation and condensation points to improve the match between the heat source/sink. This allows for a reduction in the system irreversibilities compared to Rankine systems. Another important benefit is that KC uses the same equipment as RC, since the molecular masses between ammonia and water are similar, thus helping to reduce the cost of turbines and pumps. The cost will also benefit due to water and ammonia low cost and high availability. The use of a binary working fluid adds an extra degree of freedom which allows for improved operational flexibility. On the other hand, the KC has large operating pressures and complex plant layouts.

The KC is a young thermodynamic cycle that is nowadays a viable option for waste heat recovery. In academic papers and studies, it is among the strongest candidates for low/medium heat sources but lacks practical examples on board cars, trucks or ships. However, as seen in this section there are few examples of land-based practical KC plants working, and not actual KC design was discovered in use in movable plants (e.g. lorries).

From the review undertaken on Stirling engines, hence SC, there are characteristics attractive for shipping WHRS such as its low operating sound and vibrations and the capabilities of using multiple heat sources. Due to the different engine configurations it is possible to find a suitable design for different heat sources.

The majority of modern SC applications are focused on small power plants, but it is thanks to the engine's modularity that it can reach larger power outputs [Taggart 2008; Abbas et al. 2011], while increasing the levels of redundancy which is an attractive characteristic for the marine environment. On the other hand, some disadvantages are the high sensitivity to operating conditions, lower thermal efficiencies for low/medium heat quality – due to friction and flow losses among other reasons – and large installation surface areas.

Thus, a consensus emerges from the literature that water may not be the best option when working with low/medium waste heat. In the following chapter, the alternative thermodynamic cycles will be assessed for their potential to offer a better method for recovering waste heat arising from the ship's engine compared to the traditional RC.

(Page left intentionally blank)

4

QUALITATIVE ASSESSMENT BETWEEN THERMODYNAMIC WASTE HEAT RECOVERY SYSTEMS

The qualitative assessment presents a comparison based on the information obtained from academic and industrial literature between the cycles studied in the previous chapter. It shows the relative performance of the relevant characteristics that each cycle should have – compared to the water-based RC – to be fitted on board a vessel. With the qualitative model it will be possible to:

1. Synthesise the information from multiple sources of information for WHRS operating in the low/medium heat quality spectrum.
2. Suggest which of the three alternative thermodynamic cycles investigated has the best probabilities to be used in a shipping environment with the aim of reducing carbon emissions by increasing the ship's fuel efficiency.
3. Highlight the benefits of each type of thermodynamic cycle, but also to understand the cycles' caveats.

4.1 COMPARATIVE ANALYSIS

To perform the analysis between the thermodynamic cycles, a group of WHRS characteristics relevant for a vessel were selected:

- **Initial** and **operational and maintenance (O&M) costs.** This will be measuring the affordability of the plants and how expensive it is to operate each of the power cycles.
- **Area footprint per kW_e (α_{fp}).** This looks into how much floor area on board is required per the power produced by the WHRS.
- **Volume footprint per kW_e (β_{fp}).** Different to the previous characteristic since it will measure the thermodynamic cycle impact on cargo volume. Systems can have a small α_{fp} but when analysing the volume they can occupy a considerable space on board. This characteristic and α_{fp} are crucial for cruise ships, warships and small vessels, but it is less critical for mass-driven designs such as bulk carriers.
- **Start-up time.** This characteristic determines how long it will take the WHRS to be "alive" and begin to recover the waste heat.
- **Applicability.** This characteristic will measure the feasibility of installing a thermodynamic WHRS inside a ship from examples found in other industries which promote compactness, portability and suitability for marine applications.
- **Flexibility.** This refers to the capacity of the WHRS to adapt to different operating conditions. The degrees of freedom of each cycle which increase the operational flexibility are counted.
- **Maximum power output.** This characteristic will determine if there are limitations in the thermodynamic WHRS power output. Small power outputs will mean that to extract all the available energy from the source will require several WHRS. This will impact maintenance, installation and costs.

- **Thermal efficiency**. The intention of this variable is to understand how well the alternative WHRS will take advantage of the ship's waste heat source at low/medium temperatures.
- **Flammability and toxicity.** The classification for this category is taken from the ASHRAE [American Society of Heating Refrigerating and Air-Conditioning Engineers 2007] where A1 refers to a non-flammable and non-toxic working fluid and B3 is the most extreme case of flammability and toxicity.

The RC WHRS will be used as a reference case in this comparison since it has already been applied successfully as a ship WHRS. The characteristics of the RC will be set as datum point in order to have an accurate comparison. The other thermodynamic cycles' values will be assessed as follow:

- **Positive:** Characteristics and performances that offer an improvement over the RC case.
- **Zero:** Characteristics and performances similar to the RC.
- **Negative:** Characteristics and performances that deliver a worse result than the RC.

The value of the analysed characteristic can be presented in different forms:

1. **Sole value:** When the data available is only one value. This is the case of the maximum power developed by a thermodynamic cycle.
2. **Range of values:** Where minimum and maximum values are found, such as the case of WHRS thermal efficiency. In these cases the arithmetic average value between the extremes will be used.
3. **Ordinal value:** The interval between values is not interpretable in this scale. The value will change according to the number of events identified; an example of this is the degree of flexibility.

In general, the values of this analysis can face the following circumstances:

1. When the water-based RC value is the upper or lower extreme value. For example, when comparing flammability; water is a non-flammable fluid. In this case, the other cycles will be located between zero and the negative extreme value, since it is considered that having a flammable fluid on board is a drawback.
2. When the values oscillate between the extremes of each characteristic. In this case the characteristic of the water-based RC will be set to zero and the values found by the alternative WHRS will be scaled to fit the criteria.

There are characteristics that weigh more for the ship than others, such as cost when compared to examples of applicability. It was decided that the most important characteristics will have a range of $\pm$ 5, while the less important will have $\pm$ 2. By using these ranges, it will be possible to reduce the weight of less important characteristics over the final result.

Table 6: The WHRS characteristic table defines for each type of characteristics its type, RC score – which is used as reference, the range of scores possible and the minimum and maximum extremes which are used for the analysis of the other thermodynamic cycles.

Characteristic	Type of value	RC value	Range of scores	RC Score	Extremes	
					Min.	Max.
Initial cost (£/kW_e)	Range	782	± 5	0	0.00	22,500
O&M cost (£ x10^{-2}/kW_e-h)	Range	0.78	± 5	0	0.00	8.60
α_{fp} (x10^{-2} m^2/kW_e)	Sole	3.40	± 5	0	0.00	7.20
β_{fp} (x10^{-1} m^3/kW_e)	Range	1.60	± 5	0	0.00	3.20
Start-up time (minutes)	Range	145	0 to 2	0	0.00	145
Applicability (-)	Ordinal	3.00	-2 to 0	0	-2.00	0.00
Flexibility (-)	Ordinal	0.00	0 to 2	0	0.00	2.00
Max. Power output (kW)	Sole	2,500	-5 to 0	0	0.00	2,500
Thermal Efficiency (%)	Range	6.50	± 5	0	0.00	19.5
Flammability and Toxicity	Ordinal	0.00	-5 to 0	0	A1	B3

The mean and extreme values are defined for each field using the data available from the different thermodynamic cycles. Table 6 contains the characteristics, with their possible ranges and scores, used for the qualitative comparison. The water-based RC's final score will be zero since it is used as the reference case. For the other thermodynamic cycles, their final score will be obtained by adding up the marks of each characteristic analysed.

4.2 COMPARISON RESULTS

After performing the procedure explained in the previous subsection for each characteristic measured, the final qualitative scores were obtained and are shown in Table 7. Positive scores mean that the thermodynamic cycle performed better than the RC[26].

Please refer to Appendix V – Qualitative analysis for a brief explanation regarding the selection of the extreme values and scales, but also for the specific values of each cycle's characteristic.

[26] Please refer to Appendix V – Qualitative analysis Table 49 which shows the academic and industrial references used in the comparison.

Table 7: Final results from the qualitative analysis when compared to the RC. Cycles' characteristics that outperformed the RC are highlighted in grey.

Characteristic	ORC Score	KC Score	SC Score
Initial cost	-2.00	-2.00	-5.00
O&M cost	0.00	1.38	1.67
α_{fp}	-2.11	-5.00	-5.00
β_{fp}	3.17	-5.00	0.88
Start-up time	1.69	1.69	1.69
Applicability	0.00	-2.00	0.00
Flexibility	2.50	5.00	2.50
Max. Power output	0.00	0.00	-1.76
Thermal Efficiency	0.40	0.75	-4.73
Flammability and Toxicity	-1.09	-3.00	-1.33
Total	2.56	-8.18	-11.08

4.2.1 Initial Cost

It is seen from Table 7 that there is no thermodynamic cycle that can beat the typical RC WHRS averaged initial cost, even when the KC offers the cheapest WHRS per kW_e (see Figure 30). Some of the reasons include the RC's maturity; a common and highly available working fluid (i.e. water); and a high demand on the market for these systems.

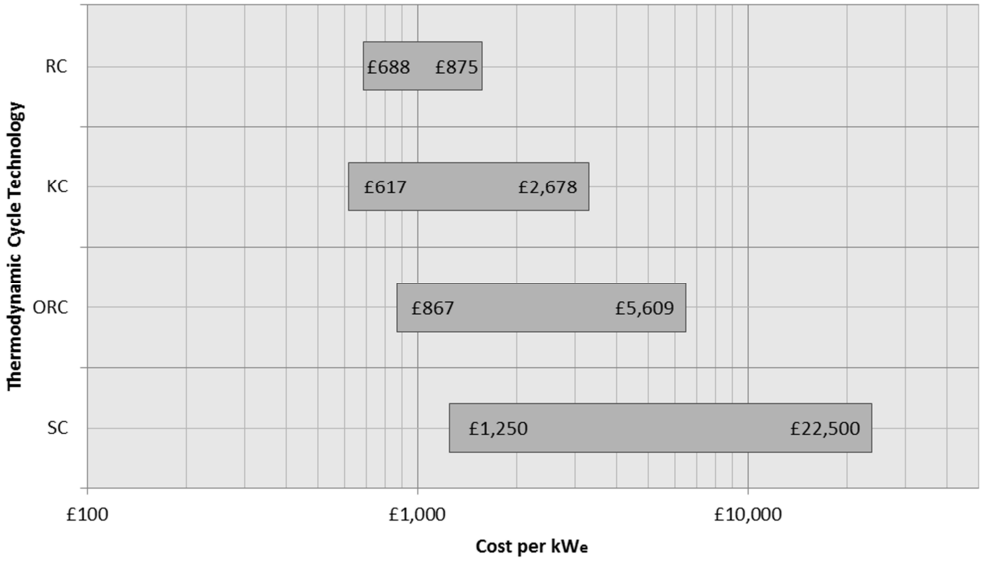

Figure 30: Range of costs per kW_e generated for each thermodynamic cycle shown in a logarithm scale found from the available literature.

Tied in the second position are found the KC and the ORC with -2 points. From Figure 30 and the averages in Tables 45 and 47 in Appendix V – Qualitative analysis, show that the KC is a better option than the ORC in this field even though the KC, by design will have more heat exchangers which can draw the reader to the conclusion that it will be more expensive than the ORC [Eymel et al. 2012]. Having components that are identical to those used in a RC improves greatly the KC's initial cost, while the ORC requires specialised modifications to cope with the larger volume flow rates and large catalogue of working fluids [Yamamoto et al. 2001].

In the last place is the SC which obtains the maximum negative value possible, this is caused by two reasons: the low power output and an almost non-existent demand in the market.

4.2.2 Operation and maintenance cost

The SC shows the lowest operating and maintenance cost caused by its simple mechanical construction and few moving parts [Majeski 2002; Sunpower Inc. 2011]. Also, the SC's low maintenance requirement makes it an ideal cycle for remote equipment [Kockums AB 2009; Vieira da Rosa 2009; Sugden & Drury 2012].The average SC O&M cost is around 30% cheaper than for the RC.

The KC cycle offers an improvement in the average O&M cost over the water-based RC by around 25%; this result is interesting since the KC equipment is similar to the RC but has a larger heat transfer area. A probable reason is that the maintenance increases as the plant ages. Since the KC is still a young WHRS with few operational hours, it is possible that the reported operational and maintenance costs are underestimated. Early O&M costs could include the change of seals, cleaning and the working fluid's top-up which can be classified as inexpensive cost. As the operating hours increase, damage to the expander and heat exchangers could be expected thanks to the presence of a corrosive fluid [Whittaker 2009], such as ammonia, which will have a major detrimental impact on the O&M cost.

The RC and ORC have approximately the same averaged O&M cost, which is around £7.90x10^{-3}/kW_e-h. This means that there is no significant difference in O&M cost when working with higher volume flows, assuming that the equipment is sized correctly for each cycle.

4.2.3 Area footprint

The KC and SC had the largest area footprint (α_{fp}), exceeding the maximum value set. This will affect drastically the selection of these technologies since space is a vital characteristic for the vessel's environment. While the ORC includes examples of system compactness [Dinanno et al. 1983; Infinity Turbine LLC 2012], the KC cycle has not yet been developed to efficiently reduce its size since its main application is for land-based systems where size and mass of plant are considerably less important. Moreover, recent research tends to increase the use of heat exchangers in the quest of further improving its thermal efficiency and power output [Larsen et al. 2014; Modi & Haglind 2015].

For the case of the SC, its major problem is again its low power output per area; its maximum is found at 0.78 m^2/kW_e [UWE Moch 2010], if the gamma engine configurations were removed

from the analysis, the average will fall to 0.072 m^2/kW_e [Majeski 2002] which is the maximum value of the comparison (see Table 6). The large area footprint per power produced required by gamma engines is due to the fact that only one small vendor was found (i.e. UWE Moch) whose model produced a modest 500 W power output [UWE Moch 2010].

The ORC is the thermodynamic cycle that performed best in this characteristic, without counting the RC. When compared in its simplest configuration to the KC, the ORC will require fewer heat exchangers and will not need a separator, reducing considerably its area footprint. Still, its footprint is around 47% larger than a RC caused mainly by the larger volume flow rate required by the ORC and the use of a regenerator [Yamamoto et al. 2001; Wang et al. 2009].

4.2.4 VOLUME FOOTPRINT

With respect to the volume footprint (β_{fp}), the ORC has the best result being smaller than the RC by around 63%. The drastic change between the area and volume is due to the compactness and stacking capabilities shown by the ORC plant example (i.e. Infinity Turbine LLC [2012]). By being able to stack up equipment it greatly reduces the effect of having a large footprint area. These qualities are desirable in ship design, since ORC manages to save space. The same approach could be easily implemented for a RC but it was not possible to find in the industrial literature an example of such compactness.

In second place, with 0.88 points, is the SC. While it has a large area footprint, its volume footprint is drastically reduced, mainly because of the Stirling engine low height. The Stirling engine modularity, as explained in section 3, gives the cycle the chance to increase its plant power output but, equally important in the vessel's scenario, it can help to reduce the footprint. The SC's modularity enables the WHRS designer to pile the engines in order to mitigate the effect of its large area footprint.

The KC also suffers from its volume footprint, achieving again the maximum negative points available. The lack of compactness can be due to the amount of heat exchangers required and that the principal usage of the KC is for land-based systems, which show little interest in finding ways of reducing its volume footprint. The low performance in this area makes the decision of using a WHRS based on KC difficult in ships where the volume is a vital part of the business, especially if retrofitting.

4.2.5 START-UP TIME

The ORC has a start-up time, where all the components are warm-up, of around 20 to 25 minutes which is an improvement of 85% when compared to the RC. The water-based RC, having a more complex expander with different stages to deal with moisture and droplets, requires more time. The start-up time for marine diesel engines depends on the engine's size and ambient temperature. MAN Diesel & Turbo [2009a] recommends that it is necessary to give 30 minutes in order to reach engine speeds above 90% of the MCR. Further on this, if it is a cold start, first it has to be guaranteed that the engine temperature is at least 50˚C before the load can be increased, requiring larger periods of time. Yau et al. [2012] show that a container ship navigating near Honk Kong will take around 20 to 40 minutes to reach its operational

speed, enough time to have the ORC WHRS up and running. Still, 20 minutes can be seen as a long waiting time when compared to the start-up times of small diesel engines. For example, a 7 MW marine diesel generator at 25°C and in stand-by mode can reach nominal speed in a range of 50 to 70 seconds after ignition [Wärtsilä Engines 2012].

For the case of the KC and SC, the data available is descriptive and not numerical, and state only that the start-up times are fast or that they are better than the RC's time. Because of this, it was decided that both cycles will received the same amount of points as the ORC.

4.2.6 APPLICABILITY

The ORC and SC are tied with the RC, which include examples in all the areas analysed. The degree of development and research performed into these cycles is one of the main reasons for having a vast list of applications. Having examples in a wide range of applications assures that it will be possible to use one of those cycles as the ship's WHRS.

Not having WHRS examples for land-based systems or movable waste heat sources such as trains or trucks does not mean that it is impossible to have a ship WHRS based on that cycle. This is the case of the KC which does not have any clear example detected except for large land-based plants. The lack of examples may be caused by the cycle's maturity and patented protected nature. To solve this requires investment, development and more research into KC applications.

4.2.7 FLEXIBILITY

The cycle that presented the maximum positive result is the KC. Having a binary working fluid allows the KC to reduce the system's irreversibilities inside the heat transfer processes, offering greater work availability than other cycles. Also, being a binary working fluid, the proportions of the two fluids can be changed to adapt to different operating conditions.

In second place are located the ORC and SC, because of the large working fluid catalogue that enable an optimum setting for low/medium heat sources. But on the other hand, as soon as the fluid is selected, the thermodynamic cycle will not be able to adapt itself to achieve the best performance possible under off-design conditions.

4.2.8 MAXIMUM POWER OUTPUT

The maximum power output will define if the thermodynamic cycle is capable of extracting the energy available from the source with a single plant. Here the SC performed badly since the larger plants studied achieved a maximum power output of 295 kW [Walker 1980] when the goal was set to 2,500 kW (see Appendix V – Qualitative analysis). Assuming that the SC could extract the 2,500 kW from the ship's exhaust gas, the SC WHRS will require around nine engines working simultaneously. Having more plants will cause more work for the engineers and maintenance crew than supervising only one WHRS.

The RC, ORC and KC have active examples, mainly in land-based power plants that can reach power outputs larger than 2.5 MW. With these examples it is possible to assure that the WHRS based on these thermodynamic cycles will be capable of producing 2.5 MW with a single plant.

4.2.9 THERMAL EFFICIENCY AT LOW/MEDIUM TEMPERATURES

This field was difficult to assess since there are a wide range of conditions, plant layouts and simulations that affect the WHRS outcomes and performances. The most thermal efficient cycle assessed was the KC which showed a 30% increase from the RC in a low/medium heat source. This is caused by the ability of the KC working fluid to adapt itself to achieve the maximum efficiency possible with the heat conditions available [Tchanche et al. 2011; Global Geothermal 2013b].

The ORC also performed better than the RC at similar conditions with an efficiency of 7.5%, representing an 18.0% improvement. The reason why the ORC is better also comes from the working fluid. Having a large set of working fluids allows the designer to tailor the ORC WHRS to the heat source and shipping operating conditions.

The SC offers the lowest performance for this range of temperatures. From the literature it is seen that a SC requires large temperature differences between the heat source and sink to operate. The temperature difference in the shipping case is much smaller than that normally seen in high-efficient SC engines. In order to solve these issues, a burner can be added after the main engine exhaust exit in order to increase the temperature difference [Zmudzki 1999], but by doing this the WHRS becomes more complex and there will be extra fuel consumption, meaning an increment in CO_2 emissions.

4.2.10 FLAMMABILITY AND TOXICITY

The importance of measuring these characteristics is high since the safety of the crew and the vessel's integrity could be in danger by transporting a hazardous fluid on board without the proper risk assessment and safety equipment installed.

The RC is the WHRS that has the safest score at zero since water is a non-flammable and non-toxic fluid. Next comes the ORC WHRS with a score of -1.09, this score is the average of all the organic fluids classified by the American Society of Heating Refrigerating and Air-Conditioning Engineers (ASHRAE). That said, there are non-toxic and non-flammable organic fluids in the ORC large catalogue of working fluids that mitigates the presence of the most noxious and dangerous fluids. In third place comes the SC with a score of -1.33, the value is achieved by averaging the ASHRAE classification of its three most common fluids: air, helium and hydrogen.

Finally, the KC system achieves the lowest score at -3 since the binary fluid delivers a better thermodynamic performance when the concentration of ammonia is high. This means that the ASHRAE value was taken as that given to ammonia.

4.2.11 TOTAL SCORE AND POINT DISTRIBUTION

As seen in Figure 31 the ORC came first and was a better option than the RC, with a total score of 2.56. These results are similar to those obtained by Yamamoto et al. [2001] and

Vankeirsbilck et al. [2011] and, as noted by Quoilin et al. [2013], the ORC retains attractive characteristics for lower temperature waste heat. The results show that this thermodynamic cycle is a strong candidate to help solve the problem of how to reduce CO_2 emissions in shipping.

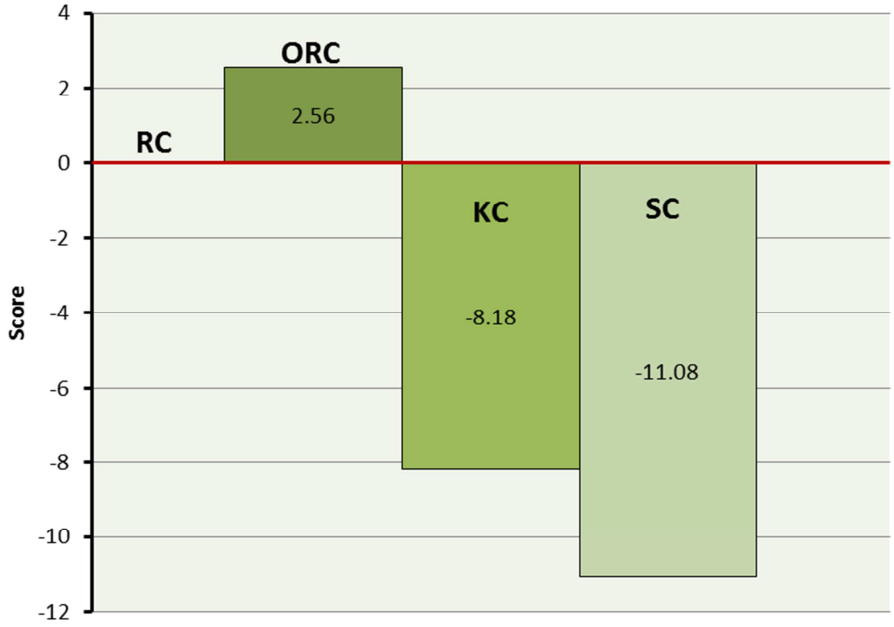

Figure 31: Final score obtained from the qualitative analysis relative to RC which is represented with a red line at the zero value.

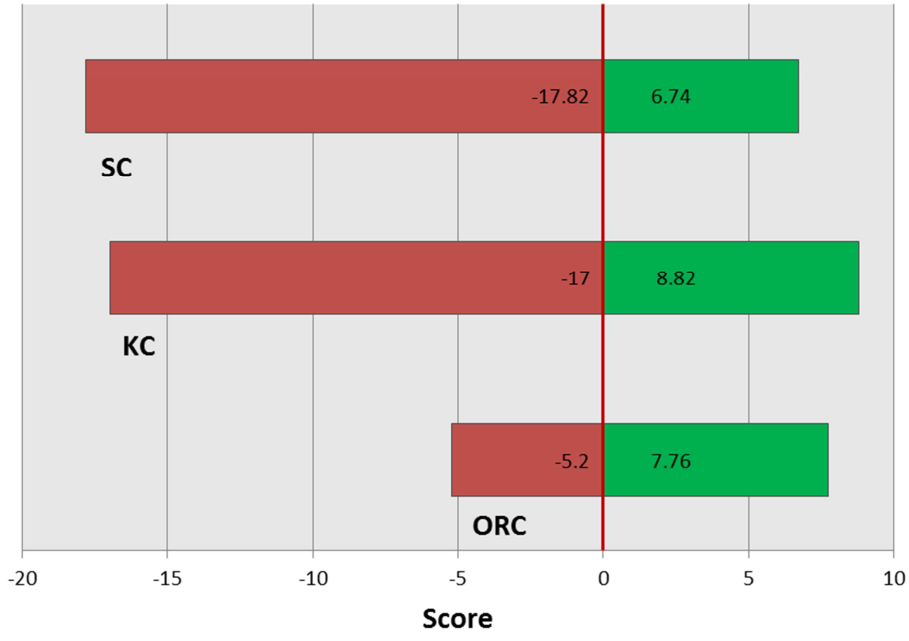

Figure 32: Positive/negative point distribution per thermodynamic cycle compared to the water-based RC.

In second place, if the RC is not considered, is the KC with a total score of -8.18. From Figure 32 it is seen that the KC offers a relatively higher benefit than the ORC (i.e. O&M cost, flexibility and higher thermal efficiency). However, the disadvantages of this cycle eliminate the positive

impact that shown in this analysis. The main reason for this lack of performance is found in the size of the plant which exceeds the maximum values set in this analysis. Similar findings were outlined by DiPippo [2004] when comparing ORC and KC plants at the same operating conditions. DiPippo concluded that the KC advantages over the ORC are reduced due to larger heat exchanger areas, high pressures and the requirement of non-corrosive materials due to the presence of ammonia.

Even though the SC performs better than the other thermodynamic cycles in maintenance cost, the high initial cost overshadows its own benefits. The SC achieved -11.08 of which its negative points add to -17.82 which was caused, apart from its high initial cost, by its large surface area footprint, and low power output and thermal efficiencies.

4.2.12 Result precision

The qualitative analysis performed above shows the results of using the available data from different academic and industrial sources. Its precision is difficult to assess since there are too many factors that affect the scores of different WHRS based on a thermodynamic power cycle: diverse measuring tools, methodologies, scenarios and software. Additionally different vendors try to promote their technology, giving performances that are only possible under the most ideal conditions. For these reasons, it was necessary to restrict the full scope of data analysed in order to make sense of the information and give the fairest comparison possible between the different WHRS. If not, every thermodynamic cycle will be the best and the worst for the same characteristic analysed.

The limitations established were set bearing in mind the ship application requirements and desirable characteristics that should be provided by a WHRS. It will be expected that the results from this analysis will change if the restrictions imposed by this study are removed or modified.

4.3 Closing remarks

The qualitative analysis performed in this study tries to assess the advantages and disadvantages of an ORC, KC and SC WHRS from the shipping point of view when compared to a traditional RC by establishing scenario restrictions and scaling the results obtained. The results from the qualitative methodology show that:

1. The best option in using the shipping waste heat at low/medium quality available from the exhaust gas and cooling system is the ORC because of the system's compactness, good level of flexibility for source temperatures, lower start-up times, and better thermal efficiencies for low/medium heat sources. Also it has negative aspects, such as the surface footprint and initial cost, but these have a low negative impact on the analysis.
2. The KC offers a great degree of flexibility, low O&M cost and higher thermal efficiencies at low temperatures than the other cycles. That said, the KC achieves a negative result from this analysis, making it a less effective solution than the RC when being used as a vessel WHRS. The lack of compactness makes it difficult to implement in ships since volume is a vital part of the business.

3. The SC arrives in the last position being the worst performing cycle because the negative performances are much greater than the benefits offered. Some of the negative characteristics include high initial – probably scaring investors – large surface area, and the fact that it produces low power outputs at low efficiencies when using a low medium heat source.

Because of the performance shown by the ORC in the analysis, it will be used as the main thermodynamic cycle where the WHRS will be based. This positive result is backed up by the area of opportunity detected from the literature review where the ORC is viewed as a strong candidate to recover waste heat from the ship's low/medium waste heat sources.

It was decided that the KC and SC thermodynamic cycles will not form part of the following research stages because of the negative performances of both cycles. This decision will simplify the coding required, allowing the author to focus on the other WHRS thermodynamic cycles (i.e. the RC and ORC) that represent better opportunities.

Summarising, the analysis performed in this section shows that the ORC is a strong candidate to improve the CO_2 emission reduction achieved by the RC thanks to its advantages and low impact disadvantages. The KC appears to be a worse candidate than the RC due mainly to its size; while an interesting quality from this cycle is its ability to adapt, via its working fluid, to different heat sources. But it has to be kept in mind that this thermodynamic cycle is still under development while the others are more mature technologies. Finally, the SC is overshadowed by its high impact disadvantages, being the worst option to be used as a WHRS inside shipping vessels.

5

THERMODYNAMIC WASTE HEAT RECOVERY SYSTEMS FOR THEIR USAGE ON BOARD SHIPS

This chapter begins with relevant differences between land-based WHRS and marine, highlighting the challenges of being on board. After that it gives an in-depth analysis of the state of the art literature regarding marine WHRS based in the water RC and ORC thermodynamic cycles. The purpose of this chapter is to detect the challenges of power WHRS on board, but also the available literature shortcomings which will dictate the area of opportunities for this thesis.

While the decision has been made regarding which cycles are to be investigated in this work (i.e. RC and ORC), a brief coverage of the research undertaken for marine KC and SC WHRS is found in Appendix IV – Further on thermodynamic cycles.

5.1 Differences between marine and a land-based Waste Heat Recovery System: The challenge

The thermodynamics of a land-based and marine WHRS are basically the same: the available waste heat (e.g. exhaust gas or scavenge air) is absorbed via a heat exchanger process (e.g. economiser), which evaporates a working fluid. The fluid is then expanded (e.g. inside a turbine) and converted into mechanical or electrical power. The remaining energy after expansion is rejected to a heat sink, to finally have an increase in pressure via a pump before entering again to the economiser. But the similarities end here due to the complexity of the vessel's environment and operating conditions.

5.1.1 Weather

At sea, the ship has a low probability of encountering its design conditions all the time, these are normally assumed to be calm waters and between 75% and 85% of its MCR. For example, when facing high seas the vessel resistance, due to waves, will increase requiring larger power to maintain the design speed [Wit 1990].

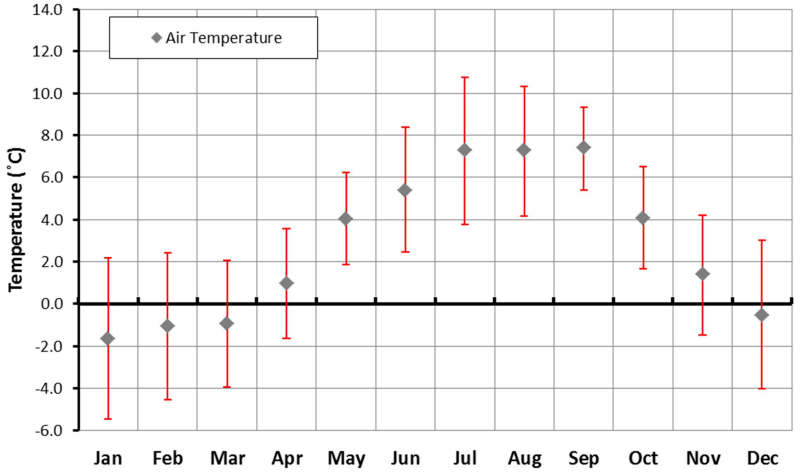

Figure 33: Average air's temperatures near the ocean surface, including anomalies. The region shown has a latitude that goes from 62.5˚N to 67.5˚N and longitude from -22.5˚E to 12.5˚E and. The bars on both figures represent the temperatures' standard deviation.

The ship's movements on board – pitch, roll, yaw, heave, surge and sway – will add extra stresses to the marine WHRS which will impact on the system reliability and maintenance cost. No reference, commercial or academic, was found in relation to marine WHRS reliability. This is possibly due to the low penetration into the market of these systems. However, due to land-based systems' reliability record it could be implied that marine WHRS could be also reliable but more expensive to maintain.

For land-based systems, typically, the weather has little effect on the behaviour of waste heat sources except for the case of solar plants which depend on the sun availability and inclination, and cloud coverage [Cheang et al. 2015].

In the case of the air's temperature, the annual average temperature goes from -35˚C to 28˚C, while using the monthly average temperatures the range changes from -46˚C to 35˚C, found near the polar and equatorial coasts respectively [Jones et al. 2012]. Figure 33 shows the seasonal air temperature change in the northern waters.

The ambient temperature has an influence in the engine's fuel consumption, exhaust gas and scavenge air temperature, and mass flow rate. It will impact the ship's heat and cooling demand which will play an important role in energy production and waste heat availability.

5.1.2 HEAT SINK

Normally, land-based plants have a fixed sink temperature which delimits the size and thermal efficiency of the WHRS. Land-based plants can use water, air or other fluids to absorb the rejected heat from the thermodynamic cycles. If there are changes in the sink temperature, normally they come gradually as the seasons go by or the condenser's system can control the sink temperature as happens in cooling towers. From the work of Saavedra et al. [2010], it is seen how the sink temperature fluctuation affects the cycle's performance, an increase of 15˚C in the sink temperature reduces the water's thermal efficiency in 0.8 percentual points while losing around 9% of the power output.

For the case of the ship, the seawater is used as a cooling medium due to its availably and low cost. As the ship navigates across the globe, the temperature of the seawater changes as seen in Figure 34, but also the temperature change happens throughout the year [Rayner et al. 2006]. Depending on the ship's route it could experience drastic changes in the sink temperature in a matter of just a few weeks (e.g. navigating from the north of Norway to Greece). Using annual averaged temperatures, seawater can be found as low as -1.8˚C in the polar oceans to 30˚C close to the Equator. With the monthly averaged data the low temperature would not be found at cooler temperature than that found in the annual average since it will become ice, but near the Equator the temperatures can reach up to 36˚C in the summer months [Rayner 2003; Rayner et al. 2006]. These temperature fluctuations will delimit the WHRS' power production (i.e. the pressure drop at the expansion process) since the working fluid's saturation temperature cannot be below the seawater in order to reject the WHRS excess heat. On top of that, seawater is highly corrosive which will require corrosion resistance materials, such as

stainless steel or titanium, for the condensers. These materials, when compared with carbon steel, tend to be more expensive.

Latitude (˚N) \ Longitude (˚E)	-7.5	-2.5	2.5	7.5	12.5	17.5	22.5
77.5	-0.61	0.23	1.59	3.77	3.10	1.85	0.23
72.5	1.54	2.78	4.15	5.28	6.09	5.78	5.33
67.5	4.55	6.36	7.69	8.16	7.83	7.13	5.45
62.5	8.23	8.63	9.17	8.93	8.28	6.25	6.51
57.5	10.61	9.55	9.67	9.63	9.03	8.09	7.90
52.5	11.90	11.45	10.67	10.22	9.19	9.05	
47.5	13.88	13.71	12.26		16.86		
42.5	15.40	15.67	17.47	17.54	18.21	18.38	18.47
37.5	17.93	18.48	18.86	18.92	19.24	19.63	19.48
32.5	19.21				20.48	21.02	20.53
27.5							
22.5							
17.5							

Figure 34: Annual averaged near the surface seawater's temperature distribution in degrees Celsius including anomalies for a sector of the northern hemisphere. The darker cells without numbers represent sectors covered in its majority by land.

A second option to cool down the working fluid, which is seen in land-based systems, is by forcing air into the condensers. The ship can redirect outside air into the condensers, creating a flow with the forward motion of the ship. When the voyage air flow is insufficient, fans installed in the condenser can cover the heat rejection demand. The advantage of this option is that there is a reduction in condenser corrosion. On the other hand, it is easier to remove heat via conduction, as in the seawater option, than via convection, as in the cooling system based on air. Also, the air heat transfer coefficient at natural convection fluctuates between 2 W/m^2-˚C to 15 W/m^2-˚C, much lower than water's which is between 200 W/m^2-˚C and 1,000 W/m^2-˚C [Palm 2002]. This means that air coolers will require larger heat transfer areas and coolant mass flow rates and thus a larger power requirement. This option has not been seen to be applied to marine WHRS.

Another option available to the heat sink is the cold LNG that requires warming from its storage temperature of -162°C to the conditions required by the engine [Algell et al. 2012; Harperscheidt n.d.]. This has been explored using a Kalina cycle by Wang, Yan, Wang and Dai [2013] who found that they could produce 390 kW at a thermal efficiency of around 15%. But the low temperature and high pressure of the LNG requires the use of compact heat exchangers which will have an important impact on installation costs [Li et al. 2011; Meggitt PLC 2015].

5.1.3 Operating profile

Thermodynamic cycles are sensitive to changes in their operating profile, as seen in the work of Rovira et al. [2011] and Peng et al. [2014]. For this reason, land-based WHRS tend to force a constant operating profile that delivers the highest benefit overall. Still, off-design operations in some cases are unavoidable and in this case the plant designers use the modularisation of the

power generating units, while in drastic cases they shut down the WHRS [Rovira et al. 2011; Abbas et al. 2011; Cheang et al. 2015].

Due to optimised weather routing and scheduling, focusing on cost reduction, safety, comfort or a combination of these characteristics [e.g. Kosmas & Vlachos 2012] create a varied operational profile which requires a wider range of power demands, affecting the waste heat quality and availability from the ship's different heat sources [Livanos et al. 2014].

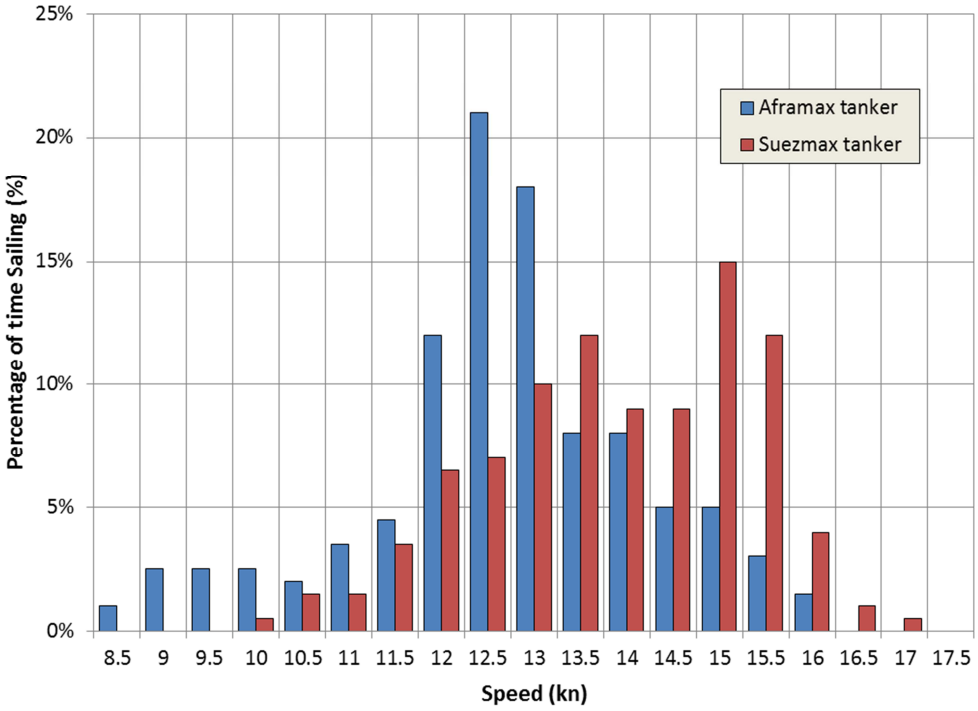

Figure 35: An example of two different types of tankers and their representative operating profile based on voyage speed [Banks et al. 2013].

In addition, the vessel's cargo level has an important impact. For example, an Aframax[27] tanker navigating on the Baltic Sea will spend half of the navigational time being fully loaded while the other half will be at ballast [Banks et al. 2013]. Assuming the same ship's speed for the ballast and fully loaded voyages – this means that there are two different resistance curves, the engine's power requirement, using the usual cubic power-speed approximation, will be increased by around 26.1% from ballast to fully loaded. Furthermore, the vessel will see a power requirement increment of around 180% when going from 65% to 95% of the design speed when the vessel is fully loaded (see Table 8).

Fouling also plays an important role in the ship's power consumption. As living organisms, such as barnacles and mussels, attach to the submerged hull the vessel's resistance increases gradually. Values around 10% and 15% increment on the ship's overall resistance are commonly assumed for six months in operation [Brown 1976; Calleya et al. 2015].

[27] An Aframax tanker is a type of liquid carrier vessel with a DWT between 80,000 to 120,000 t [Molland 2008].

Table 8: Power required by a 107,000 dwt Aframax tanker, assuming that the power requirement is related to the cube of the vessel's speed, the same speeds are maintained between fully loaded and ballast voyages and there is no fouling on the hull.

Normalised Speed (%)	Power required fully loaded (MW)	Power required ballast (MW)
<20	0.2	0.1
65	5.9	4.8
90	16.4	13.0

In the marine literature, the operating profiles tend to have a general and simple approach. Sasaki et al. [2002] use three speeds for the general operating profile of a tanker, in the case of the presence of ice and the month of the year some of the speeds in the general profile are modified. Choi and Kim [2013], even though they have a large data set, decided to pick only two broad operating speeds to represent the performance of a marine trilateral cycle coupled to a ORC WHRS bottoming cycle. Livanos et al. [2014] consider an average speed of 20 kn throughout the voyage of a ferry which will take 57 hours to complete, but also adds 30 minutes for the time spent at port in the ferry's operating profile. The same approach is taken for a bulk carrier which has to cover a distance of 5,243 nm (i.e. 9,716 km) at a speed of 14.8 kn in Theotokatos and Livanos [2012]. MAN Diesel & Turbo [2012b] give a more detailed operating profile which covers from 15% MCR to 100% MCR. As stated, the consideration of the operating profile variations into the study of marine WHRS, especially in regards to ORC, is almost non-existent.

5.1.4 FUEL'S SULPHUR CONTENT

Another limitation with which the marine WHRS must cope is the fuel's sulphur content. Vessel regulations permit the use of high sulphur content fuels (i.e. below 1 and 35 grams of sulphur per kilogram of fuel for Emission Control Areas (ECA) and non-ECA respectively) when compared to that required for cars and land machinery (just 0.01 grams of sulphur per kilogram of fuel) [Council of the European Union & European Parliament 2009; International Maritime Organization 2013a]. This limits the amount of absorbed exhaust heat due to sulphuric acid corrosion [Huijbregts & Leferink 2004]. For example, an exhaust gas that contains $1x10^5$ parts per million of SO_2 will have a dew point around 160°C, having exhaust gas temperatures below this point will affect the lifespan of the heat exchanger and could be dangerous for the ship's crew [Ibid.]. Achieving low temperatures on the exhaust gas is possible if the engine load is low, such as in the case of slow steaming, or if the marine WHRS heat exchangers are larger than those required by the process [MAN Diesel & Turbo 2009b; MAN Diesel & Turbo 2012b]. These issues disappear or are mitigated when the ship is using LNG, low sulphur MDO/MGO and low sulphur biodiesel, since the fuel's sulphur content is minimal.

5.1.5 NATIONAL AND INTERNATIONAL REGULATIONS

While the vessel is navigating the globe, depending on the route, it could enter several different national waters which will make it subject to a variety of safety, operational, economic and environmental regulations. On top of that, when navigating in international waters the ship will have to comply with IMO regulations. To fulfil these requirements a ship will contain several

technologies or operational strategies working together which can have a direct effect on the waste heat quality, availability and how this energy could be harvested [Calleya et al. 2015].

A good example is found when vessels are navigating through ECA which requires reduced SO_x emissions. In this case the vessel operator, depending on the equipment on board, could use exhaust gas wet or dry scrubbers, or switch to lower sulphur fuels such as LNG [Gary 2009; Lockley & Jarabo-Martin 2011; Gilbert 2014].

Changing the fuel burnt due to sailing in an ECA would alter the temperature profile of the exhaust gas. In order to demonstrate this, since the author could not find literature that discusses this matter, some assumptions had to be made for a comparison between high-sulphur HFO and low-sulphur MDO:

- The data from the engine vendor is always given with a Low Calorific Value (*LCV*) of 42,700 kJ/kg which is for MDO and used here as reference.
- The energy demand at the chosen MCR is the same independently of the fuel used.
- The same amount of waste heat at the exhaust gas system is available for any of the fuels used.
- All fuels have the same concentration in mass of sulphur.
- The air to fuel ratio is the same for different fuels.
- The change in the exhaust gas mass flow rate will be the same as the change in fuel consumption.
- The exhaust gas for any fuel used will have the same specific heat (C_p).

The first step is to find the amount of fuel ($\dot{m}_{fuel}$) and energy required ($\dot{E}_{fuel}$) to power the ship using the specific fuel oil consumption (*SFOC*) and ship power ($\dot{W}_{engine}$):

$$\dot{m}_{fuel} = \frac{SFOC\ \dot{W}_{engine}}{1{,}000} \quad [\ 12\ ]$$

$$\dot{E}_{fuel} = \frac{q_{LCV}\ \dot{m}_{fuel}}{3{,}600} \quad [\ 13\ ]$$

Where $\dot{E}_{fuel}$ is given in kW and q_{LCV} is the fuel's Low Calorific Value (LCV) in kJ/kg. Clearing the fuel's mass flow rate from equation [13] gives on average a 4.6% larger mass flow rate when using HFO. The next step is to find the exhaust gas temperature after the turbochargers. To find this, a hypothetical WHRS or WHB is installed at the exit of the turbochargers which absorbs the exhaust gas heat until it is cooled to 160˚C.

Using the assumptions mentioned before it is possible to find the exhaust gas temperature (T_i):

$$\dot{Q}_{eg,MDO} = \dot{m}_{eg,MDO} C_{p,eg,MDO}\left(T_{i,MDO} - T_o\right) = \dot{m}_{eg,HFO} C_{p,eg,HFO}\left(T_{i,HFO} - 160\right) \quad [\ 14\ ]$$

$$T_{i,HFO} = 160 + \frac{\dot{Q}_{eg,MDO}}{\dot{m}_{eg,HFO} * C_{p,eg,HFO}} \quad [\ 15\ ]$$

Where T_o is the outlet temperature of the exhaust gas from the WHRS or WHB. Figure 35 shows that consuming MDO increases the exhaust gas temperature after the turbocharger by an average of 1.2%[28] when compared to HFO.

While the uncertainty of this calculation is high, it does show that there is a difference in the exhaust gas temperature when using different fuels which could have an effect in the marine WHRS capabilities of extracting the waste heat and producing useful power on board. Another important consideration that should be kept in mind when switching fuels is that with lower sulphur content it is possible to cool even further the exhaust gas, harvesting more waste heat [Nielsen & Schack 2012; Dimopoulos et al. 2012].

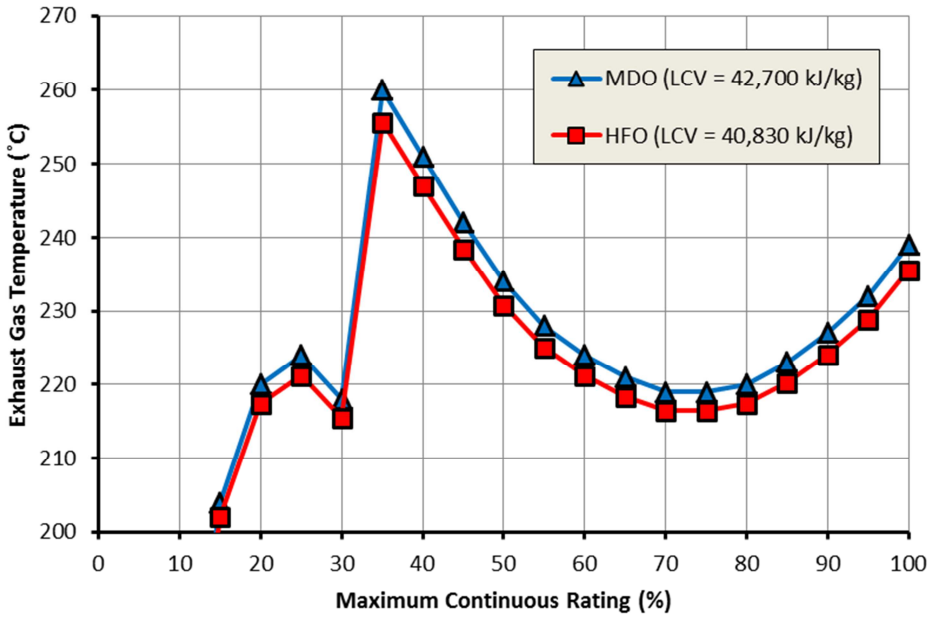

Figure 36: Exhaust gas temperatures for two different fuels using the same marine engine at ISO conditions [Kontoulis et al. 2013; MAN Diesel & Turbo 2015b].

Normally, scrubbers are installed before any WHRS which will have an important influence over the vessel's WHRS performance every time the scrubber is operating [Lloyd's Register 2012b]. In the case of wet scrubbers, the exhaust gas is washed in order to remove the SO_x cooling down the exhaust gas and reducing the waste heat quality. In the case of dry scrubbers, the chemical reaction happening is exothermic which means that there will be a heat release that will be absorbed by the exhaust gas. This change in temperature will have a knock-off effect on the waste heat quality.

5.1.6 Waste Heat Recovery System mass and size

On board ships, the WHRS's mass and size (i.e. volume and surface area) can translate into business loss and energy expenditure, but can also impact on stability. If, for example, the WHRS plant volume is similar to one or two TEU it will mean that for every trip that the vessel does there is a loss in cargo space equal to the WHRS volume. This kind of discussion is not required for a land-based systems since WHRS plants are stationary, having only as constraint the land size on which they are built. The volume requirement and optimal space between

[28] This was calculated using degree Celsius and must be corrected when using Kelvins.

components, for ease of installation and maintenance supervision, will be stated in the early stages of the land-based plant design. The mass will only be important in a land-based system again in the design process and when installing or maintaining the WHRS. In the case that there is an increment in the WHRS's capacity requiring larger surface areas and volumes, a building expansion can be undertaken or more land could be used. Of course this will translate into a larger initial investment, but on the other hand this will be a more challenging scenario for the ship.

5.2 State of the art research on Marine Thermodynamic Waste Heat Recovery Systems

5.2.1 Rankine cycle

The preferred thermodynamic exhaust gas WHRS used inside ships is the water-based RC coupled to an electric generator [Hatchman 1991; Tien et al. 2007; Theotokatos & Livanos 2012; Livanos et al. 2014; Sakalis & Frangopoulos 2014; Benvenuto et al. 2014] and the WHRS are available for the marine industry [Schmid 2004; MAN Diesel & Turbo 2012b]. The marine RC WHRS, in its most integrated form, uses other vessels' low/medium grade waste heat such as in the case of scavenge air system or the engine's cooling water system to pre-heat the subcooled water as seen in Figure 37.

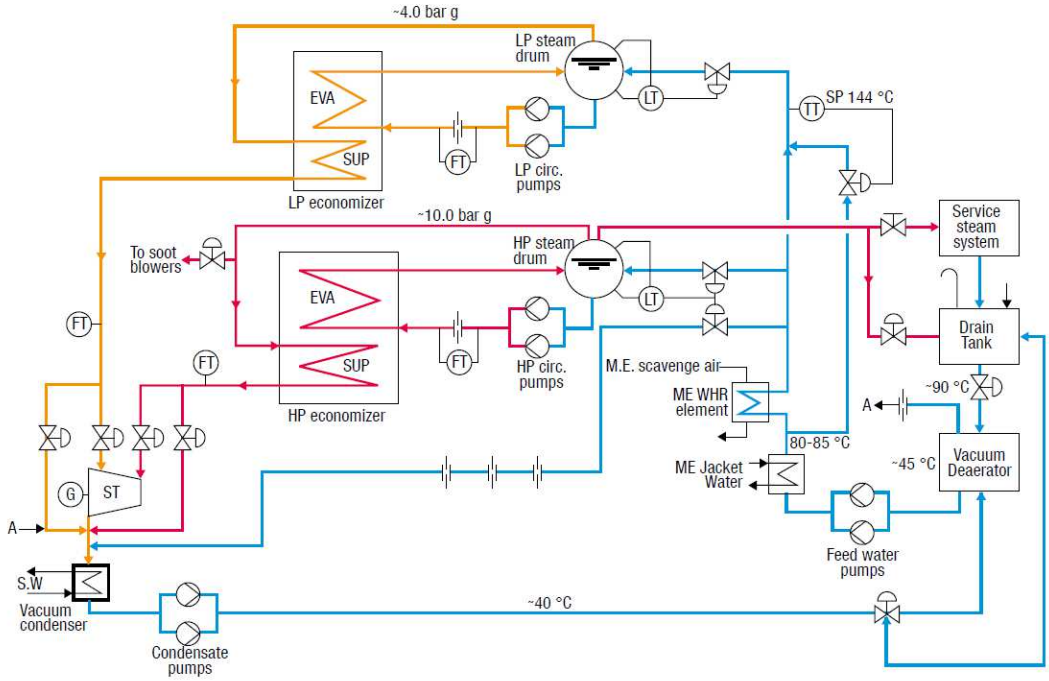

Figure 37: A MAN Diesel & Turbo double pressure WHRS which also covers the steam demand on board a vessel [MAN Diesel & Turbo 2012b].

Water has been a reliable candidate as the WHRS working fluid on board due to its strong performance using the medium heat coming from the exhaust gas, but also water – in its steam form – is used to heat different ship systems and spaces. This combined heat and power capability gives the ship operator a great deal of flexibility [Tien et al. 2007]. The integration would not be possible for other thermodynamic cycles requiring an independent steam waste

heat boiler (WHB) to cover the heating demand. Other advantages of water, as explained in 3.1.2, are that it is non-flammable, non-toxic, and has negligible impact on the environment and crew.

Hatchman [1991] simulated two different RC plants – single and dual pressure – inside a ship which recovered heat from a 50.5% efficient diesel engine. The objective was to observe the effects on performance at different loading scenarios (i.e. from 60% to 100% MCR). The RC plants were optimised to work at 300°C. Seawater is used as the sink with a temperature of 25°C. At the rated MCR and source temperature of 310°C, a power output of 300 kW_e with a thermal efficiency of around 6.5% was achieved, thus giving a system total plant efficiency of around 53.5%. The double pressure system results, under the same conditions, yielded a power output of around 325kW_e with a thermal efficiency of around 7.5% and a final total plant efficiency of around 54.5%. But keeping in mind that these conditions are at the engine's maximum power output – which in today's shipping behaviour will not be realistic (see section 5.1.3) – such WHRS power outputs and efficiencies will be achieved only for short periods of time. A more realistic operating load would be at 85% of MCR, which drops the power output of the double-pressure RC to around 280 kW_e and the total plant efficiency to levels lower than the ones seen with the single pressure at the same MCR. Still, with slow steaming, those values will decline such that this option may have marginal saving versus the cost of investment.

The operating conditions around vessels are varied, Tien et al. [2007] studied the effects of changing the engine loading – via variations in the exhaust gas and sink temperatures, and mass flow rates – and WHRS' characteristics – working fluids mass flow rates and heat exchangers areas. An interesting finding is the fact that the three sections inside the economiser (i.e. subcooler, evaporator and superheater) change in size as the exhaust gas temperature and, to a lesser degree, the WHRS mass flow rate change. The less sensitive area is the subcooler which barely increases as the exhaust gas temperature does.

A RC WHRS for a cruise ship was studied by Dimopoulos et al. [2008] under different fuel price scenarios. They discovered that as the price of fuel increased, the more viable became the use on board of more powerful and complex RC. With low fuel costs, it is better just to have a WHB while with the highest cost assumed of £0.65/kg, a double pressure RC WHRS producing electricity and steam was the best option since the payback time will be shorter and the profits larger. This work focused mainly in the economic side since it was completed before the upcoming EEDI.

The introduction of the EEDI brings a new dimension to shipping which Theotokatos and Livanos [2012] explored by performing a thermodynamic analysis for a RC WHRS on board a handymax bulk carrier. Two different types of engines were used – a two-stroke and four-stroke marine diesel engine – to understand how the RC affected the WHRS' payback time and the vessel's EEDI. Interestingly, for the case of the two-stroke engine, the RC WHRS installed had a low electric output and was discarded as a viable option, instead it was proposed that a WHB took advantage of the waste heat giving a plant improvement between 1.8% and 3.0% depending on the engine load. The reason behind this is that the exhaust gas temperature was

in the 250˚C region, while for the four-stroke engine the exhaust gas temperature was between 340˚C and 400˚C, depending on the engine loading. These results highlight the area of opportunity for alternative thermodynamic cycles on board ships which can use low temperature waste heat. Similar analysis was performed by Livanos et al. [2014] but in this case, the operational profile of a RoRo ship was used. They compared the performance of a RC WHRS coupled to a two-stroke diesel engine and for a dual fuel engine using LNG as fuel. The results show that the most effective option to reduce the EEDI is by using an LNG-fuelled engine with the RC as the bottoming cycle, achieving an EEDI reduction of around 35%. Furthermore, it is seen that the RC WHRS positive influence is stronger on the LNG engine which produces a drop of around 2.5 g CO_2/t-nm while for the diesel engine with only a reduction of around 1.5 g CO_2/t-nm. This difference is caused again by a higher exhaust gas temperature on the LNG engine at the design point.

The use of a water-based RC as the WHRS for different marine propulsive engines (i.e. gas turbine, slow speed diesel engine and a dual fuel engine) is investigated by Sakalis and Frangopoulos [2014]. Even though the three engines had different power outputs it is seen that when the exhaust gas waste heat is used solely for the RC, the power returned is higher than when producing steam and power. This seems attractive but it is not the most effective way to use the vessel's waste heat. The work of Benvenuto et al. [2014] compared four different waste heat RC plant layouts and their economic and environmental benefit for a 158,000 dwt tanker. But different to Livanos et al. [2014], they changed the components of the cogeneration plant such as the power turbine and the electrical motor attached to the engine's shaft. The cogeneration systems are prioritised to first cover the steam demand followed by the electric demand and finally, if there is still more power available, it will be used to increase the tanker's power output. The best options seen are those that use the power turbine in conjunction with the steam turbine, achieving at least £111k per year more in fuel savings and 2.2 percentual points lower than the reference EEDI. It also shows the importance of having a flexible electrical system, able to use the extra electric power output to increase the vessel's efficiency. The electric motor is able to reduce the fuel consumption of at least £63k per year; interestingly the EEDI is not affected much by the engine's shaft assistance having a drop of only 1.3 percentual points.

The majority of the papers previously mentioned integrate the vessel's operating conditions and profile in order to understand how the RC behaves. The work of Dimopoulos et al. [2014] integrates the behaviour not only of the engine coupled with the WHRS but also the behaviour of the generator, auxiliary engines and control systems. They also analyse the transient behaviour of all these systems working together during the voyage which gives the vessel's operator a good and realistic quantification of the benefits of a combined RC. The optimal solution for a large bulk carrier was a single pressure WHRS covering also the steam demand and coupled to a power turbine. The total efficiency of the ship increased by 9.5% and had a payback time of eight years. The steam turbine was able to produce at 80% MCR 1,051 kW for the loaded trip and 781 kW for the ballast condition while it was turned off manoeuvring at port. The combined cycle was available for the 40% MCR upwards and had its maximum power

output at around 1,400 kW. The degree of specialisation found in this work is high, although it does not mention the optimisation methodologies used nor the time taken to perform a single case study. A further look into the evolution of Dimopoulos et al.'s [2014] system integration can be found in the following works [Frangopoulos & Dimopoulos 2004; Dimopoulos et al. 2008; Dimopoulos & Frangopoulos 2008].

On the industrial front, Schmid [2004], from the Wärtsilä ship power division, presented an improved WHRS based on a dual pressure RC. The plant uses an auxiliary power turbine which helps the RC operate between 55% and 100% of the MCR. This WHRS, when working with a 68 MW Wärtsilä engine, can improve the power output by 12% at the 85% MCR and increases the engine's thermal efficiency in the range of 49.3% to 54.9%. MAN Diesel & Turbo [2012] also offers similar solutions to Wärtsilä, but gives some configuration options. They recommend that engines above 25 MW should use the RC – single or double pressure – in combination with a power turbine; engines between 15 MW and 25 MW should use one of the two options stated before (i.e. the WHRS or the power turbine); while for a power lower than 15 MW, an ORC is indicated. MAN Diesel & Turbo state that it is possible to increase the power output by around 8% to 11% for the RC with a power turbine; from 4% to 7% when using the single pressure; and from 5% to 8% with the double pressure RC. These power output estimates are dependent on engine load and voyage conditions. The operability of these systems is between 50% and 100% of the MCR. The *Emma Mærsk* is powered by an 80 MW diesel engine using a RC WHRS achieving, in 2006, a reduction of 10% in GHG emissions and a total plant efficiency of around 55%. This represents an increase from its standard efficiency of 49.3% [Hultqvist 2008].

From this analysis it is clearly seen that the RC is a proven technology that can reduce GHG emissions effectively by providing extra electrical power to the ship's power plant and also supplying the vessel's steam demand. On the other hand, with engine modifications to meet more stringent emission regulations, higher marine engine thermal efficiencies, and speed reduction strategies, it can be expected that the waste heat quality and availability will be reduced. This produces an important decrement in power production and thermal efficiency for the RC. Furthermore, while the global economy is still recovering, the competition between ship companies to transport goods is fierce. For these reasons, fuel efficient technologies that can reduce operational costs even further and improve the vessel's performance when compared to traditional technologies are welcomed by the industry, opening the door to ORC WHRS.

5.2.2 Organic Rankine Cycle

As seen in section 3.2.4, ORC WHRS is a mature technology in land-based plants having a total capacity of more than 1,600 MW_e installed [Vélez et al. 2012; Quoilin et al. 2013], and the systems are starting to gain momentum in the marine industry for low grade waste heat (i.e. up to a temperatures of 160˚C) such as in the vessel's excess steam [e.g. Opcon Energy Systems AB 2012a]. Before 2012, the application of marine ORC on board was only mentioned – not simulated – by both industry and academia, as a possible alternative to harvest the vessel's waste heat [Hua et al. 2008; Levander 2009]. Since 2012, there has been an increase of

interest in academia on marine ORC WHRS using one or several of the engine's waste heat sources to produce power (see Figure 38).

Using the exhaust gas waste heat of a large marine engine, Larsen, Haglind et al. [2013] undertook a comparison between an ORC WHRS using R245ca, RC and a Kalina cycle (KC). They found that under the same conditions the marine ORC outperformed the water-based RC and KC. In order to assess the different characteristics and performance of different organic WHRS coupled to a low speed two-stroke marine diesel engine, Larsen, Pierobon et al. [2013] used a multi-objective optimisation with the genetic algorithm (MOGA). They found that when taking into consideration the fluids' flammability, the best working fluids for a vessel, regarding its thermal efficiency, were R245fa and R236ea. Burel et al. [2013] explored different options to improve an LNG-powered vessel; they found the highest total vessel efficiency at 72.2% – with a reduction of almost 22% in CO_2 emissions – when installing an ORC WHRS which uses the exhuast gas and jacket water waste heat. To achieve this performance, the ORC, after the expander, has a high temperarture which is used to heat the cargo. This paper highlights the importance of heat management inside ships, where heat is a valuable resource.

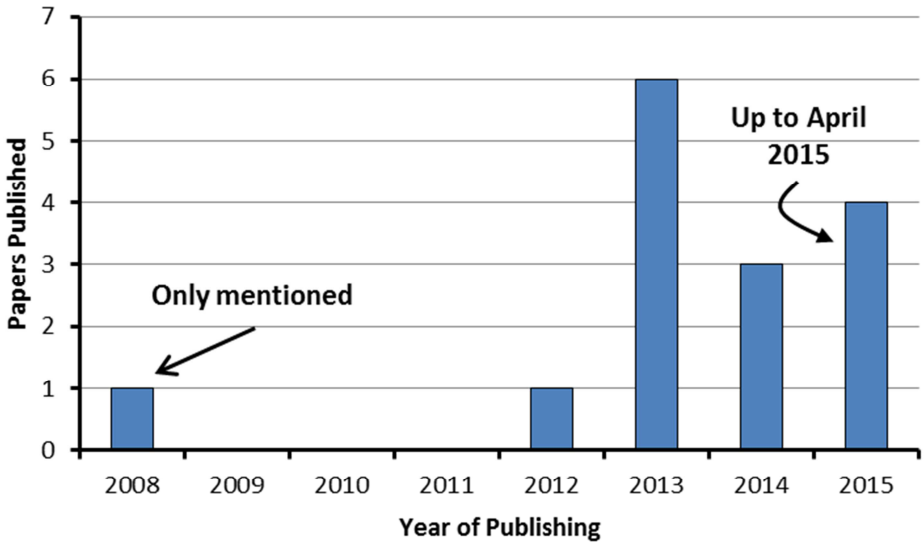

Figure 38: Academic papers from 2008 to 2015 recorded by the author, to the best of his knowledge and excluding supercritical systems, which talk about marine ORC WHRS with the purpose of producing power.

Nielsen et al. [2014] use MOGA in order to find optimum settings for a unique marine ORC WHRS design that can reduce CO_2 emissions, but at the same time could reduce considerably SO_x emissions. Their plant layout is coupled with a traditional marine RC and uses the available exhaust gas and scavenge air waste heat. The organic fluid is preheated by the scavenge air and evaporated by the exhaust gas after the RC WHRS until the exhaust gas temperature reaches 84°C. They assume that the sulphur in the exhaust gas will condense and be captured on board. This configuration could allow the ship to operate using HFO inside ECA since the SO_x reduction is at around 98%.

Yue et al. [2012] studied the possibility of using an isopentane WHRS to take advantage of the waste heat coming from the jacket cooling water and exhaust gas system of a marine diesel engine. The main focus of the paper was the design of the ORC expander which shows that the organic fluid is at supersonic speeds at the end of expansion process. The results show that after one year of operation (i.e. 220 days a year), the fuel savings would be around 275 ton (250 t) of HFO[29].

Using a less powerful engine (i.e. close to 1 MW), Song et al. [2015] studied different configurations for the same engine's waste heat sources (i.e. jacket water and exhaust gas). When they integrated the two waste heat sources into one WHRS, which is capable of returning around 100 kW, the recommended organic fluid was cyclohexane. The waste heat integration approach is an optimal option since the cost and space requirement is lower and the system's management would be easier. When having independent WHRS for each waste heat source, they recommended the use of R245fa with a thermal efficiency of 5.2% and a power output of around 10 kW for the jacket water; the thermal efficiency is similar to that used for a car engine ORC WHRS using the same organic fluid [Boretti 2012a]. Benzene with a thermal efficiency of 21.3% and a power output of around 91 kW is recommended for the exhaust gas system; this organic fluid is also suggested by Suárez de la Fuente and Greig [2013] where their ORC achieved a thermal efficiency of around 22.0% at design point. Apart from the engine's size, there is an important difference between these two works which is related to the exhaust gas temperature lower limit. The latter study used as the exhaust gas temperature limit a temperature of 165˚C due to the MDO used, where Song et al. used a temperature of around 100˚C and did not specify which type of fuel is being used. As per Huijbregts and Leferink [2004] equation, it would mean that the sulphur content is low and, with this low temperature on the exhaust gas, it is important to consider the condensation of other exhaust gas components such as nitrogen and water [Pla Perujo 2004]. Furthermore, the use of flammable fluids – in this case benzene – inside the engine room is restricted by Safety Of Life At Sea (SOLAS) [International Maritime Organization 2009b], hence it is required the use of a thermal oil, not used in Song et al., or the working fluid would have to be changed for another non-flammable fluid.

As shown with low quality waste heats, it is better to integrate all waste heat sources into one WHRS. Yang and Yeh [2015] use the exhaust gas and jacket water waste heat to operate an ORC and show how the operational conditions change the performance of the WHRS. They recommend the use of R1234yf due to improved power returned per money invested. The study of how the sink temperature affects the performance of the WHRS is constantly overlooked but in Yang and Yeh work is shown how the thermal efficiency and economic benefit is reduced as the sink temperature increases due to an increment in the working fluid condensing temperature, hence a smaller drop in enthalpy in the expansion process. The work of Yang and Yeh presents a similar issue to that in Song et al. [2015], albeit to a lesser degree, with the exhaust gas minimum temperature allowed which in this case is set at 140°C. While it is

[29] Conversion factor used 1 ton = 0.91 tonne [Thompson 2008].

possible to extract heat up to this temperature, the paper does not specify what type of fuel is used which opens two possibilities: 1) The diesel engine uses HFO. With this low exhaust gas temperature there will be sulphuric condensation which will require special tanks and heat exchanger designs to store the acidic substance as mentioned in the work of Nielsen et al. [2014]; 2) It could be using MGO with low sulphur content which is compliant with ECA regulations in 2015 [International Maritime Organization 2013a]. Using the methodology of Bahadori [2011], the sulphur dew point of an ECA's MGO, assuming 10% excess in air for the fuel-air mixture that enters the combustion chamber, is around 127˚C. Another point that Yang and Yeh did not clarify is why they assumed that the exhaust gas temperature at the entrance of the WHRS is set at 170˚C; normally large marine diesel engines show higher temperatures at loadings above 25% MCR [e.g. MAN Diesel & Turbo 2014a]. The probable cause, in the author's consideration, is that they used the exhaust gas after the WHB which could mean that there are two WHRS technologies on board the studied vessel: one, a RC for the higher temperatures in the exhaust gas; and two, for the lower temperature an ORC WHRS, but this is not stated in the paper.

In a more complex marine waste heat thermal machine, Choi and Kim [2013] explore the use of R1234yf for a low heat grade system. The ORC uses the rejection heat from a trilateral cycle – which absorbs part of the waste heat from the exhaust gas system – but also takes advantage of more of the heat available in the exhaust gas (i.e. takes the exhaust gas from 171˚C to 63˚C). They discovered that the incorporation of an ORC as the bottoming cycle of the marine trilateral cycle increased by 16% the net WHRS power output when compared to the case where just a trilateral cycle was used. However, it is acknowledged that this configuration will require higher temperature after the trilateral expansion so the ORC can return a better power output. As mentioned in previous paragraphs, this work also suffers from a lack of consideration regarding the sulphur content and its dew point in the exhaust gas. The researchers used HFO to power the vessel which produced an exhaust gas with a sulphuric dew point at around 160˚C.

Kalikatzarakis and Frangopoulos [2014] recommended that a double stage marine ORC is used on board when the engine's loading is around or above 85% MCR. The high temperature ORC uses the waste heat in the scavenge air cooler, while the lower temperature ORC uses the heat rejected by the first WHRS, lubrication and engine's cooling water. The double ORC achieves an increment on power output of around 650 kW to the most efficient and simple ORC. The use of two expanders for the ORC WHRS is also explored by Soffiato et al. [2015] who analysed the waste heat harvesting of a LNG carrier power generation plant. Using the jacket water, lubricating oil and scavenge air waste heat, they propose a two-stage ORC WHRS. The best operating fluid is R227ea, in both supercritical and subcritical forms. It achieves the highest power output of any plant configurations at 587 kW but the lowest thermal efficiency at 7.7%, similar behaviour is seen in Kalikatzarakis and Frangopoulos [2014]. The results are around 30% to 40% better than what was achieved with a simple non-regenerative ORC.

Opcon Marine manufactures RC and ORC waste heat recovery plants specially made for shipping. Its ORC plant is made for low grade source temperature spectra (90°C-160°C), in

particular for the cooling system's water, oil systems, scavenging air and excess steam not used inside the vessel. The plant produces around 500 kW; it has a mass of 37 t, an area footprint of 36.2 m^2 and a volume of approximately 134.0 m^3 [Opcon Energy Systems AB 2012b]. Opcon's waste heat recovery plants are installed in *MV Figaro* with a reported saving in fuel consumption of around 5% [Opcon Energy Systems AB 2012a]. Wärstila studied the use of an ORC as the vessel WHRS as seen in the article published by Levander [2009] which claimed that the WHRS could offer a return of 8% of the main engine power. By 2010, Wärstila and Turboden had created an association to work on the development of a marine ORC WHRS with the aim of having the system ready for the year 2011, but as yet it is not offered in the Wärstila marine catalogue [Wärtsilä 2010]. Samsung Heavy Industries [Lee & Lee 2013] saw that the ideal waste heat for a marine ORC comes from the engine's jacket water and scavenge air. Their results show that the two-stage ORC could cover around 73% of the electric demand of a Suezmax tanker. Another manufacturer to note a big area of opportunity for an ORC WHRS on board a vessel is Calentix in its partnership with Mitsubishi Heavy Industries. They offer an ORC which uses the waste heat from the engine's jacket water to produce electricity. The system is capable of producing 125 kW [Marine Engineers Review 2014]. Recently MAN Diesel & Turbo included on its web page a marine ORC WHRS for four-stroke engines with thermal oil as an option, but there are no technical details regarding the power output, working fluid and size [2015c].

Other ship applications in the industrial literature are scarce and few examples were found. One is an article in *Green magazine* promoting a Mols-Linien ferry using an ORC power plant for waste recovery system which it claims increases ship efficiency up to 35% [Gary 2009] compared with one without the system installed. Infinity Turbine offers compact ORC modules for heat recovery and can fit to almost any heat source which is capable of generating electricity of up to 900 W [Infinity Turbine LLC 2012]. The majority of the examples from big engine manufacturers use a RC [Schmid 2004; Hultqvist 2008; MAN Diesel & Turbo 2012b], meaning that there is a good area of opportunity in the market to take advantage of high and medium quality temperature heat sources, such as in the exhaust system.

5.3 CLOSING REMARKS

As seen in the previous discussion, there are important differences between land-based and shipping WHRS which require a different approach. While the steady state thermodynamic study will be the same for both cases (i.e. equations and thermodynamic assumptions), the changes in the operating conditions and restrictions in the marine scenario must be integrated into the study [e.g. Dimopoulos et al. 2014]. Normally in land-based systems, as previously explained; stable operation conditions are assumed to simplify the operational profile with the thermodynamic performance of different systems. In the vessel's case, it is clearly seen that more often than not, the operation conditions will fall outside the WHRS' design operation point. This will require the analysis of larger combinations of operating conditions in order to understand, in a more realistic way, the advantages and challenges of installing a WHRS on board a ship.

The majority of works focus solely on water or organic fluids but are seldom tested in direct competition. When providing an alternative to a well-established technology, such as the case of the RC, it is important to compare them in order to have a better understanding of advantages, weaknesses, requirements and side effects. The work of Larsen, Haglind et al. [2013] does compare advanced thermal machines for waste heat recovery but falls short in analysing their performance on the full operative scope of the vessel. Suárez de la Fuente and Greig [2015] compare a RC and ORC in a simpler approach but considering a ship-based operating scenario throughout the year which gives an idea of how the engine conditions affect the benefit of using a WHRS.

The vessel's route is only considered as an important performance factor for a marine WHRS in a few academic works [e.g. Dimopoulos et al. 2014]. When navigating in different waters at different times of the year, it is expected that the seawater – the most common sink for a marine WHRS – would change. A seawater temperature variation of 25°C or more is not untypical from North Europe to Singapore or Hong Kong via the Suez Canal. There are thermodynamic, heat transfer and operative considerations that affect the WHRS performance due to the change in sink temperature [Yang & Yeh 2015]. Therefore, it is important to recognise these changes and incorporate them into the marine WHRS operating scenario.

One of the most common arguments for not installing an ORC in a vessel is the flammability of the organic fluid, which in the case of hydrocarbons, completely exiles them from the marine environment. As seen in the works of Suárez de la Fuente and Greig [2013], Larsen, Pierobon et al. [2013] and Song et al. [2015], the use of hydrocarbons achieves high power outputs with high thermal efficiencies. This discussion has recently been taken by Suárez de la Fuente et al. [2015] arguing that the ORC with flammable fluids could use the same technology seen inside the vessel when using LNG or methanol as the main fuel. A thermal oil could be the piece that enables the use of organic fluids on board a vessel.

On board a vessel, steam provides heat to the different rooms, cargo and services such as fuel heating; and it is common to use the exhaust gas and other engine waste heat sources to complement the steam production. The works analysed in this chapter, except for the case of Burel et al. [2013] and Soffiato et al. [2015], do not study the fact that using the engine's waste heat to produce only power reduces or totally eliminates the vessel's alternative steam production. These works do not consider the implications – economically and environmentally – of producing steam using a fired boiler or sharing the waste heat with the power WHRS.

Therefore, while good quality technical work has been undertaken in the area of marine WHRS, and there are plant configurations ready to be installed on board, there is still a need to cover a more integrated view between vessel operation and the WHRS, especially in case of the ORC systems. In particular three caveats in the literature have been identified:

a. lack of direct comparison between the RC and ORC under the vessel's operating conditions, particularly in part load operation;

b. missing the integration of the route's temperature, operating conditions, fuel type and sulphur content affects ORC performance; and
c. existing research has omitted the side effects of installing ORC systems on board from the vessel's thermal and safety management point of view.

This research fills some of the shortcomings identified in the literature by:

A) Creating a unique code based in Matlab® language which will enable the author to design and optimise a catalogue of marine WHRS under real ship operation.
B) Performing an in-depth direct comparison between a marine WHRS based on the simple water-based RC and different ORC which will measure among other performance variables: power output, thermal efficiency, CO_2 emissions and fuel consumption reductions, mass flow rates and coolant requirement.
C) Building from known data sources and methodologies a temperature map of seawater and air temperature which will enable the exploration of sink temperature on WHRS performance.
D) Modelling of the ship's operating profile, capturing the marine WHRS capabilities during voyage.
E) Using a sensitivity analysis which will emulate the fluctuations seen in the vessel's engine waste heat sources due to changing operative conditions. This also will show the advantages and disadvantages of superheating and using a recuperator which were not conclusive from the literature review.
F) Integrating into the WHRS methodology the operative profile, type of fuel, engine performance, safety and regional regulations, vessel's heat demand and sink temperature.
G) Case studies that will bring a deeper understanding of how different alternative WHRS can benefit vessels in a highly regulated industry and challenging economic environment.

6

METHODOLOGY

This chapter will cover the methodology used in this work which defines the main equations used and the scope of the calculations, as well the software and packages used to define the thermodynamic WHRS on board a vessel.

The model can be divided into three groups: external, internal and environmental/financial performance. The external group consists of everything that does not directly affect the WHRS and its performance such route, type of vessel, fuels, regulations, vessel's profile, among others. This group is responsible of feeding with relevant data and imposing the boundary conditions to the internal group so that simulations can be performed. The internal group is formed by the thermodynamic WHRS, exhaust gas or scavenge air system, thermal oil and the fan/pump for the cooling fluid. The last group is responsible for quantifying the benefits – CO_2 emissions and fuel consumption reductions, and payback times – when installing a marine WHRS; also it is in this group that the EEDI is calculated.

This work covers three different optimisation strategies: single variable (while the other variables are fixed) which is suitable for a sensitivity analysis over a broad range of operating profiles and conditions; a multi-objective optimisation using the genetic algorithm which allows for the study of optimal WHRS designs considering power output, thermal and volume efficiency; a two-step method approach using a particle swarm and pattern search suitable to find a wide range of optimal designs to suit the vessel and its operating profile. The optimisation strategies will be discussed in detail in each of the different result chapters (i.e. chapters 7, 8 and 9), while the generalities shared will be discussed here.

6.1 SOFTWARE USED

The thermodynamic WHRS, vessel's heat management and operating profile are modelled using Matlab®. From the beginning of this research project it was decided to generate an original code to simulate the WHRS on board at different operating conditions, such as temperature and engine loading. The drawback of this direction is that it takes a longer period to generate useful results, but at the same time gives a great amount of flexibility regarding the approach of the problem and the addition of different areas of study. On the other hand, coding gives a more profound understanding and familiarisation of the thermodynamic WHRS and the different optimisation strategies.

Additionally, tools from NIST Refprop 9.0 [Lemmon et al. 2010] and CoolProp [Bell et al. 2014] are used for the thermodynamic properties of the working fluids, coolants and thermal oil. The code developed by Sharqawy et al. [2010] is used to find the seawater properties when the condenser requires it. The total ship resistance, hence the power output at any given speed, is calculated by a Matlab® code developed by Calleya [2014].

6.2 HEAT SOURCE AND SINK

The heat source data – exhaust gas and scavenge air – is taken from the engine's manufacturer data, which gives enough detail to be able to integrate the WHRS economiser to the waste heat. The required data are the exhaust gas temperature after the turbocharger or the

scavenge air temperature after the compressor; and their mass flow rates. Figure 39 shows an example of the data used as heat source when utilising the energy available at the exhaust gas.

The thesis will focus only on the use of HFO and MDO (when navigating through ECA) to power the ship. The use of different fuels to power the vessel has two important effects when studying the available heat from the exhaust gas: minimum temperature to extract the waste heat and exhaust gas temperature. Subsection 5.1.4 and 5.1.5 highlighted how the fuel's sulphur content could limit the exhaust gas minimum temperature without having sulphuric acid condensation. The exhaust gas dew point is calculated using the method proposed by Bahadori [2011] which only requires the fuels' carbon and sulphur concentration, and excess air to fuel ratio.

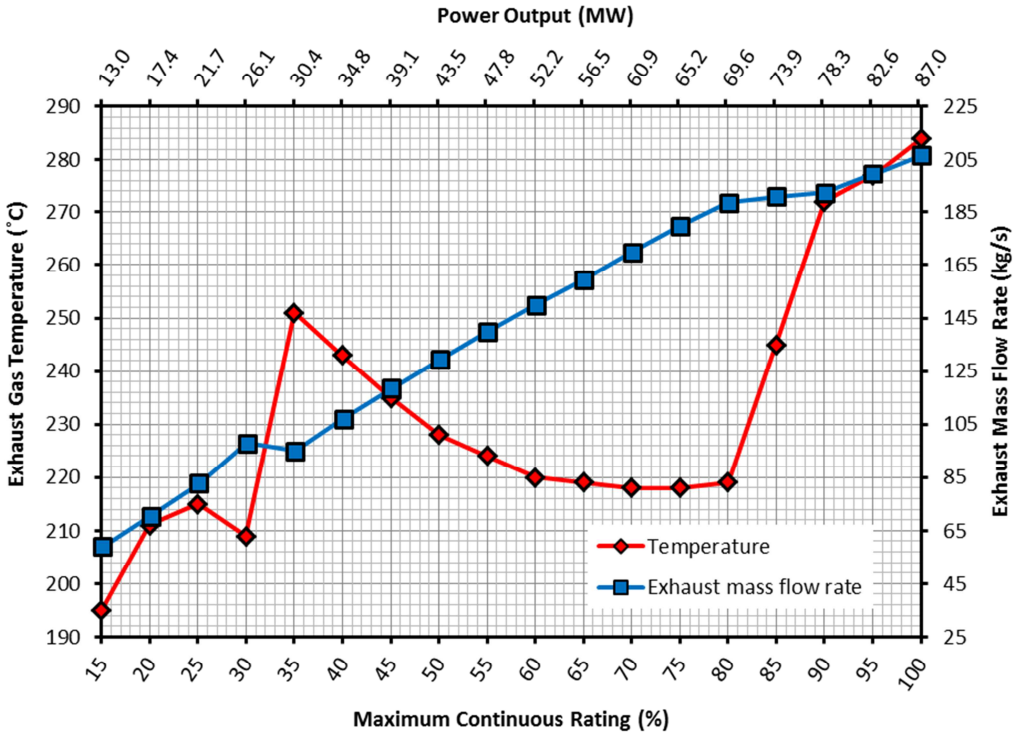

Figure 39: Two-stroke diesel engine capable of producing more than 87 MW. The plot depicts the temperature profile and the mass flow rate of the engine's exhaust gas [MAN Diesel & Turbo 2013b].

As seen in Table 9, there is an important difference in the sulphuric dew point between both fuels studied. The more than 30˚C temperature difference between low-sulphur MDO and high-sulphur HFO (i.e. 2.7% in mass) will allow the WHRS connected to the exhaust gas system to extract more heat when using MDO than HFO.

As discussed in 5.1.5, the fuel used to power the ship will have an effect on the exhaust gas temperature profile. It is shown that MDO exhaust gas is around 1.2% warmer than when using HFO, but the exhaust mass flow rate is around 4.6% larger. Normally, engine manufacturers use MDO's energy content to calculate the exhaust gas temperature [MAN Diesel & Turbo 2013b]. So when using HFO, the exhaust gas temperature given by the engine vendor will be lowered by 1.2% across all MCR, while increasing the mass flow rate by 4.6%.

Table 9: Carbon and sulphur composition of the fuels used in this study. The excess air to fuel ratio was assumed for both fuels at 10%. The last column shows the temperature when sulphuric condensation occurs [International Maritime Organization 2010]**.**

Fuel	Carbon Concentration (kg of C/kg of fuel)	Sulphur Concentration (kg of S/kg of fuel)	Excess Air Ratio (%)	Sulphuric Dew Point (˚C)
HFO 380 [a]	0.825	0.027	10	158.6
MDO [b]	0.842	0.001	10	126.3

[a] The sulphur content was assumed as the minimum sulphur content for a high-sulphur content fuel defined in International Maritime Organization [2010].

[b] The sulphur content was taken as the minimum acceptable by IMO's regulation 14 for fuels that can be used in ECA [International Maritime Organization 2013a]. The sulphur concentration for MDO in International Maritime Organization [2010] is 0.8%, so it was assumed that the carbon concertation remained the same for MDO with a sulphur concentration of 0.1%.

Another important consideration for the waste heat source is the air's temperature along the voyage. Table 10 presents the three different ambient reference conditions – known as winter, ISO and tropical – which engine manufacturers use for their designs; the engine's performance is normally given at these three conditions (see MAN Diesel & Turbo [2015a]). When ambient temperatures are different to those given by the three reference conditions, a performance correction must be made in order to have the real engine waste heat behaviour. MAN Diesel & Turbo [2014d] stipulates that the exhaust gas temperature after the turbochargers will decrease by 1.6˚C for each 1˚C from the intake air temperature, if a by-pass is used then each degree reduced at the air intake will lower the exhaust gas temperature by 0.3˚C. For fuel consumption and exhaust gas mass flow rate, the effect of ambient temperature changes from engine to engine and this must be assessed per each case studied.

Table 10: Reference ambient conditions used for the design of marine engines [MAN Diesel & Turbo 2014b]**.**

Variables	Winter	ISO	Tropical
Turbocharger air intake temperature (˚C)	10	25	45
Air/Seawater coolant temperature (˚C)	10	25	32
Pressure (kPa)	100	100	100

The temperatures vary with the globe's latitude and longitude, but also according to the time of the year. For example, the maximum sea surface temperature (SST) can be found in the Indian Ocean in the summer while the coldest is found in the polar seas. The temperature variations geographically and throughout the year demand a flexible model that can represent adequately voyage's temperature.

Air and seawater temperature are measured all over the world by different equipment and systems (e.g. buoys for the oceans). Due to the large catalogue of equipment, techniques to

measure temperature and non-homogeneous distribution of stations throughout the regions there is an intrinsic uncertainty in temperature measurement. The SST and air temperature data is normally found only for the changes to the long-term average temperature – known as anomalies – for each region that has been studied; in doing so, the temperature's uncertainty is reduced and data can be compared between different regions [National Centers for Environmental Information 2015]. The temperature model for SST was constructed using the HadSST2 dataset formed by two different datasets [Rayner et al. 2006]: 1) temperature anomalies since January 1850 to December 2013; and 2) long-term average temperature for the oceans from 1960 to 1990. For the air case the datasets used were: 1) HadCRUT4 for the anomalies from 1850 to December 2013 [Morice et al. 2012]; and 2) the Absolute dataset for the air's long-term average temperature between the years 1960 and 1990 [Jones et al. 1999]. The HadCRUT4's anomalies are taken from air when the region is over land and from seawater when it is over the sea, thus in order to complete the model it was assumed that the same seawater's temperature anomalies were seen for air over the ocean.

The final result of the temperature model is an excel file which shows and compares – monthly and annually – the temperatures of air and seawater over 5,184 different regions of 5° by 5° (i.e. latitude and longitude) which cover the full globe (see Figure 40). The usefulness of this model is that when modelling a ship's voyage between two points, it is possible to know the air or seawater temperature along the route and the month of the year, enhancing the relevance of the WHRS model.

	-47.5	-42.5	-37.5	-32.5	-27.5	-22.5	-17.5	-12.5	-7.5	-2.5	2.5	7.5
77.50							-12.07	-10.67	-10.48	-10.47	-10.74	-12.10
72.50						-9.44	-7.84	-6.90	-6.23	-7.31	-7.84	-8.69
67.50			-14.95	-9.52	-6.72	-4.59	-4.55	-3.83	-4.58	-5.94	-6.02	-4.85
62.50	-7.54	-8.23	-5.65	-6.72	-5.25	-4.16	-4.83	-3.71	-2.74	-3.03	-2.50	-5.05
57.50	-1.97	-2.20	-2.49	-2.75	-2.26	-2.30	-2.18	-1.89	-1.77	-1.69	-0.87	-2.51

Figure 40 : Temperature difference between air and water annual average temperature between -47.5°E and 7.5°E, and a latitude between 57.5°N and 77.5°N. As the cells become more orange, the larger the temperature difference between air and water is. Data shows annual average temperature difference, significant seasonal variations can be expected especially in the higher latitudes. The brown cells represent land and temperature data which is not represented since it is irrelevant for a ship.

Regarding the WHRS sink there are different processes, such as another WHRS or heating water connected, that can absorb the marine WHRS unused heat [e.g. Choi & Kim 2013]. This work will only focus on rejecting the unused energy to a cooling fluid. Chapter 9 will test two different and widely available – in the marine environment – sink fluids: seawater and air.

6.3 ROUTE

The vessel's route information is difficult to obtain: a) the data is private and not meant to be shared; b) the data can be shared and used but does not contain some of the relevant information (e.g. normalised data) which force the user to make assumptions, that might be wrong, in order to make use of the route; c) the web sites that do share it, such as marinetraffic.com, allow the storage of the ship's speed and location but do not grant permission

to use the data in publishable works. The route approach taken by the author changed during the research period and this is reflected in the different result chapters.

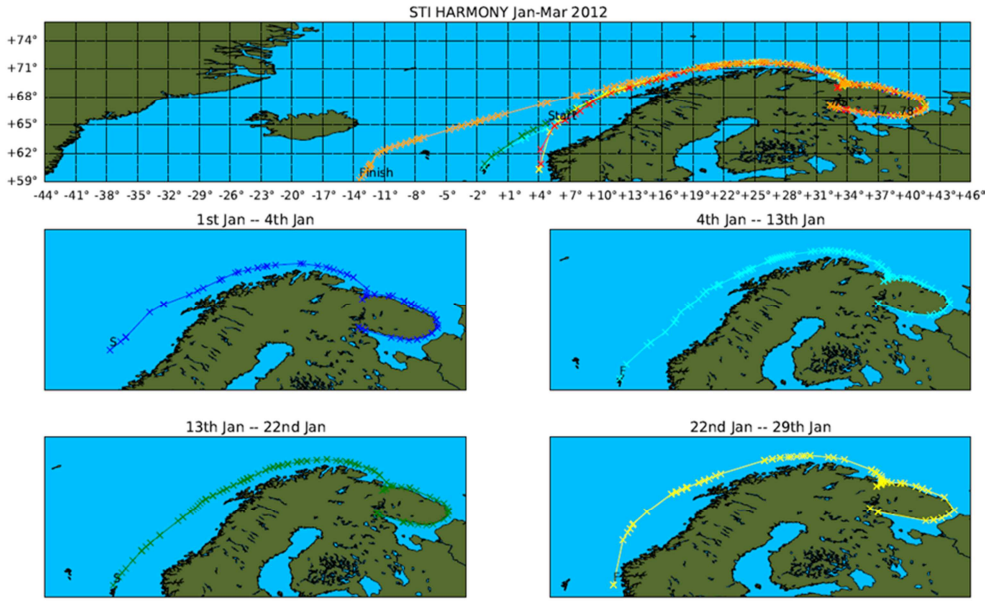

Figure 41: Different routes taken by the tanker ship *STI Harmony* during the month of January in the year 2012. The vessel was tracked by AIS satellites. The "S" stands for starting point, while "F" is the finishing point of the route. The top image represents all the routes taken during the observed months, while the four bottom images represent individually the four voyages taken by the ship.

As a first approach in chapter 7, only the operating profile data was available [MAN Diesel & Turbo 2012b] and the route was assumed not to be relevant since the study is focused more on the WHRS sensitivity. For chapter 8, the route is taken from the work of Sasaki et al. [2002] and is segmented in 11 different sections of which the vessel speed is given as normalised to the design speed. Chapter 9 uses data from the Automatic Identification System (AIS) for vessel traffic services between the months of January and March 2012, the data was provided by University College London (UCL) Energy Institute with the sensitive data removed.

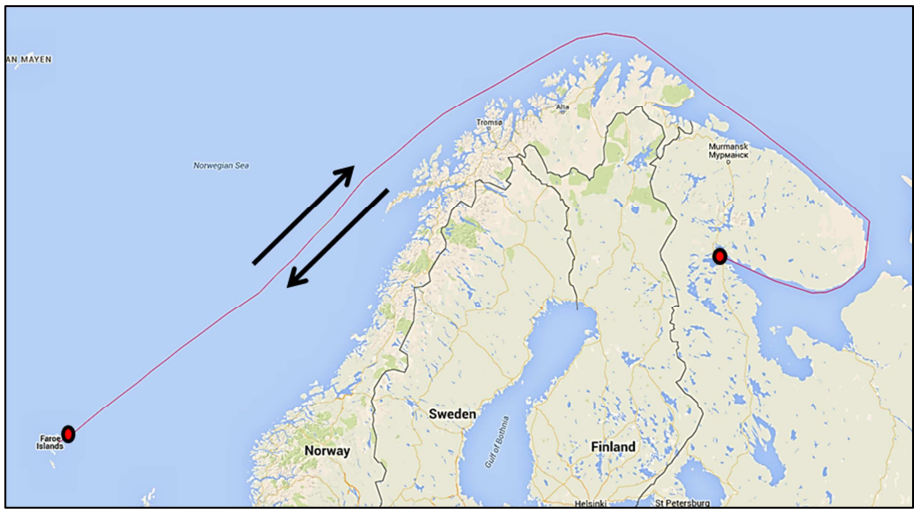

Figure 42: Average annual route for a tanker navigating in the northern part of the Atlantic Ocean. The red dots are the starting/end ports. The route will be the same back and forth [Google & GeoBasis-De/BKG 2015]**.**

While the route approach will be discussed in more detail in the relevant result chapters, Figure 41 offers a good representation of how the AIS data was provided. In the particular case of Figure 41 there were four different routes during January 2012. Since the author's purpose is to use a route that can depict in broader terms the ship's movement to determine its operating profile, it is the opinion of the author that a high definition route is not required. An average route is created using the high definition route data which covers the same ports with a similar distance. This average route function is used as the vessel's constant annual route throughout the simulation/optimisation process (see Figure 42).

The manner in which the annual route is created uncouples position and speed – ship's resistance and power consumption – which helps the simulation process by reducing the complexity and computer power requirement.

6.4 OPERATING PROFILE

What is relevant about the operating profile to the marine WHRS is the exhaust gas and scavenge air temperature, and mass flow rate. These values are dependent on the ship's engine operation which in turn depends on the ship's speed and hull's characteristics (e.g. displacement or prismatic coefficient). The model used in this research needs only the power requirement by the ship and the percentage of time in one year spent on that engine loading in order to begin the WHRS simulations (see Table 11).

Table 11: A sample of the operating profile of a 14,000 TEU container vessel required to perform the WHRS simulations. The table only shows the higher engine loading representing only 26% of the operational time. In this case, the vessel is assumed to be operating 6,480 hours per year [MAN Diesel & Turbo 2012b]**.**

Maximum Continuous Rating (%)	Power (kW)	Operational Time (% of one year)	Time (h)
100	57,823	1	65
90	52,040	5	324
80	46,258	20	1,296

The simplest approach, used in chapter 7, to have an operating profile which relates engine power output and percentage of time is to find one that already exists; this is the case of the example given by that MAN Diesel & Turbo [2012b]. Here the amount of hours spent at each engine speed is given during a full year of operation, making quite straight forward the integration of the operating profile with the annual WHRS performance and CO_2 emission reductions. The downside is that there is no flexibility in the data since the vessel's type, size and engine are fixed, it is not accurate to extrapolate the profile behaviour to other vessels. For example, a container ship such as that shown by MAN Diesel & Turbo [2012b] operates normally fully loaded around 66% of the year while a tanker rates at around 44%. The average speed of a Post Panamax container ship is around 19 kn, while for a Suezmax tanker it is 14 kn [Banks et al. 2013]. Furthermore, if the data provider is not clear enough then assumptions,

such as time distribution for ballast condition and fully loaded operation, need to be taken. This increases the uncertainty of the final results.

A second approach which gives more flexibility is to study a particular type of vessel speed profile over a period of time. Chapter 8 uses data from Sasaki et al. [2002] on a similar Aframax tanker – which assumes that there is no ice on any of the voyages – to analyse the performance of a marine WHRS.

In chapter 9, the data given by UCL's Energy Institute is in the form of the ship's speed observations. The first step taken to achieve a generic speed profile was to divide the observed speed by the ship's design speed, and create speed groups defined by its normalised speed. The speed group sizes are defined by the fidelity required: high fidelity or small speed groups will require longer simulation times and could return similar results than when using broader – or larger – speed groups. The second step was to find the proportion of observations in each speed group to the total number of observations (see Table 12). From the normalised observations in Table 12, it is assumed that they can be translated to the annual sailing time spent at different ship's speeds. Vessel speeds that were zero knots were not counted in the speed profile since it is assumed that the vessel was waiting for the port or oil platform call.

The data sources for chapters 8 and 9 do not record fully the zero speed time spent during the observation period. In order to have a better certainty over the full annual operating profile of a given vessel, the time percentage at port and manoeuvring, as well as the percentage of time sailing per type of vessel is taken from Banks et al. [2013].

Table 12: Normalised data which will be used as the ship's operating profile. The data is from AIS satellites tracking the *STI Harmony* tanker in the first months of 2012. The last column represents the sailing time spent at the different speed groups which conforms to the tanker's speed profile.

Normalised Design Speed (%)	Number of Observations	Normalised Observations (%)	Sailing Time (h)
<50	25	3.8	202
50-60	9	1.4	73
60-70	54	8.2	437
70-80	133	20.1	1,075
80-90	143	21.6	1,156
90-100	142	21.5	1,148
100-110	137	20.7	1,108
110-120	18	2.7	146
Total	661	100.0	5,340

Figure 43 is a representation of the *STI Harmony* speed profile including the time spent at port and manoeuvring during a year of operation. This profile is used to assess the marine WHRS capabilities and limitations.

A resistance model is required to translate the ship's speed to its power requirement. Equation [2] in section 1.3 gives an estimate between the power required and vessel speed which is good for gaining a quick approximation as to the ship's power requirement without the need of model experiments [Stroke 2003]. In this thesis the approach recommended in Holtrop and Mennen [1982] and Holtrop [1984] is used and is implemented to Matlab® by Calleya [2014]. Being a model based on regression analysis it is limited to ships that corresponds to the same ship type and that are inside the boundaries of Holtrop and Mennen [1982] and Holtrop [1984] database. The interested reader can find more detail about the resistance model and its limitations in Appendix VI.

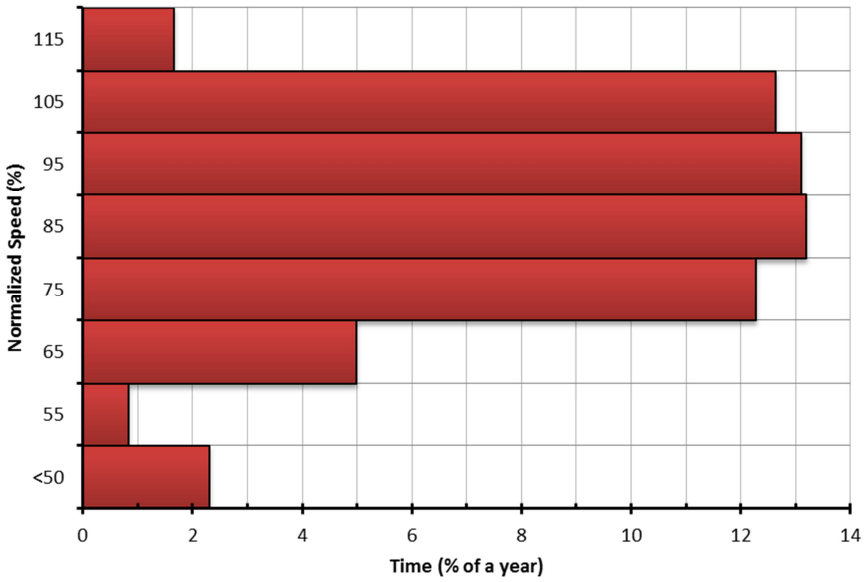

Figure 43: Speed operating profile during a full year in operation for the *STI Harmony*. The tanker's speed is normalised to its design speed which is 15 kn. The percentage of time shown is given with respect to 8,760 hours (i.e. year).

6.5 WORKING FLUID SELECTION

There are some important characteristics that must be pondered on board a vessel when using a working fluid for a low/medium quality waste heat: safety (e.g. flammability and auto-ignition temperature), environmental (e.g. GWP and ODP), and performance (e.g. power output). These three characteristics can be represented in a similar way to the scope triangle used in project management where cost, quality and time can be substituted by the three desired working fluid characteristics discussed before.

While cost and availability are other important characteristics when choosing a working fluid, they are not considered in this thesis. The working fluid's cost data is not easy to obtain from the different vendors and normally change from region to region. For the case of availability it is difficult to know if ports will have in storage the working fluids that are under study, so it can be assumed that in case a top-up is required from the vessel's WHRS, the working fluid vendor will find the means to send the working fluid to the port where the vessel is located.

Figure 44 represents what would look like an ideal working fluid as described in section 3.2.1 non-flammable, deliver high performance at low/medium quality waste heat and will have a GWP and ODP equal to zero. While there is only one possible fluid for the water RC WHRS, there are plenty of fluids and mixtures that can find their way into an ORC WHRS. In order to begin choosing organic fluids that can bring the best performance and CO_2 reduction on board a vessel, the author used the results from other works to identify them.

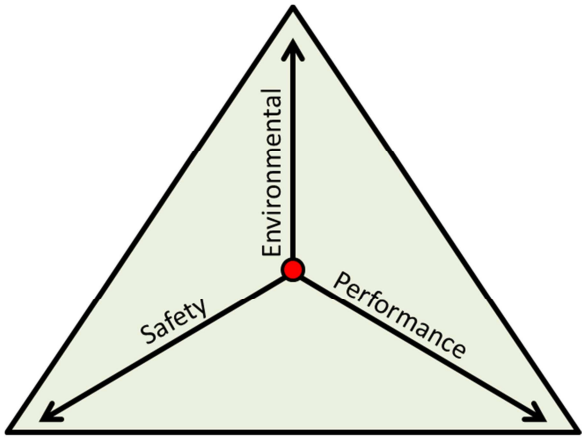

Figure 44: The ideal working fluid represented by a triangle whose vertices represent the maximum value possible for each of the desirable characteristics on board a ship.

Three hydrocarbons – benzene, toluene and heptane – and one siloxane – hexamethyldisiloxane (MM) – were selected due to their performance over water according to Saavedra et al. [2010]. Safety Of Life At Sea prescribes a flash point of no less than 60˚C inside the engine room without specific Administration approval [International Maritime Organization 2009b], this regulation dates back to 1974 and was written having in mind the technology of that time. Since then it has been seen a change in shipping requirments, practices and priorities but also technology and proceses have improved. Furthermore, The use of a thermal oil permits the separation between the organic fluid and the heat source; double walled pipes allows a complete separation from the machinery room; limited amount of working fluid required for the system, and today's leak detection and firefighting technology allow for the risks associated with such fluids to be adequately monitored, handled and reduced. In light of this, a regulation revision based on the requirements from the International Code of Safety for Ships using Gases or other Low Flashpoint Fuels draft code [International Maritime Organization 2014b] and the DNV GL Tentative Regulation for Low Flashpoint Liquid (LFL) Fuelled Ships [Det Norske Veritas AS 2013a] would be desired so ship can extract the maximum from ORC WHRS. On a final note regarding hydrocarbon and in particular to benzene, this organic fluid is deemed as carcinogen and it is related to some types of leukaemia. The World Health Organisation (WHO) recommends a maximum of air exposure of 5 ppb (17 $\mu g/m^3$) for long period of time [World Health Organization 2010]. In the UK, the limit for any 8 hour exposure period has to be not larger than 1 ppm [Chilcott 2011]. It is important to have in mind this highly health risk for the crew but it is thought, as mentioned previously, that this risk can be monitored and mitigated to safety levels with the technology available today.

Table 13: Working fluids selected with their global warming potential value in a time interval of 100 years; ozone depletion potential; auto-ignition, and decomposition temperatures; flash points, flammability classification; and critical temperature and pressure. This table will be used as the limiting factor for the applicability of working fluids in the different case studies.

Working Fluid	GWP_{100} [a]	ODP [b]	Auto-ignition Temperature (˚C)[c]	Flash Point (˚C)[d]	Decomposition Temperature (˚C)[e]	Flammability [f]	T_{cr} (˚C)[g]	P_{cr} (MPa)[g]
Water	N/A	N/A	-	-	2,000	0	374	22.06
Benzene	N/A	0.0	562	-11	760	3	289	4.91
Toluene	2.7	0.0	536	4	399	3	318	4.13
Heptane	3.0	0.0	223	-4	550	3	267	2.74
Hexamethyldisiloxane (MM)	<10	N/A	341	-2	300	3	246	1.94
R1233zd(E)	<5	0.0	380	N/A *	175	0	167	3.62
R236ea	1,596	0.0	N/A*	N/A *	N/A	0	139	3.50
R236fa	8,060	0.0	N/A*	N/A *	400	0	125	3.20
R245fa	950	0.0	412	N/A *	250	0	154	3.65

[a] Toluene: [Forster et al. 2007]; heptane: [Environmental Protection Agency 2013]; MM: [Environment Agency 2011]; R1233zdE: [Hulse et al. 2012]; R236ea and R236fa: [Myhre et al. 2013]; R245fa:[Rusch et al. 2004].
[b] Benzene and toluene: [Anastas et al. 2009]; heptane: [Loctite UK limited 1998]; R1233zdE: [Hulse et al. 2012]; R236ea: [Rui et al. 2013]; R236fa: [Calm & Hourahan 2001]; R245fa: [Honeywell 2001].
[c] Taken from [Yaws 1997]; R1233zdE: [Honeywell 2014]; R245fa:[Honeywell 2001].
[d] Taken from [Yaws 1997]; R1233zdE: [Honeywell 2014]; R245fa:[Honeywell 2001].
[e] The flammability classification used is based on the Hazardous Materials Identification System (HMIS). Water: [Bilgen et al. 1977], benzene: [Brioukov et al. 1999], toluene: [Hnat et al. 1982], heptane:[Appleby et al. 1947] , MM: [Heberle et al. 2013]; R1233zd(E): [Kontomaris 2014]; R236fa: [Angelino & Invernizzi 2003]; R245fa: [Honeywell 2001].
[f] Water, benzene, toluene and heptane: [National Paint and Coatings Association 2002]; MM: [Sarchem Laboratories Inc. 2010]; R1233zdE: [Honeywell 2014]; R236ea and R245fa: [Larsen, Pierobon, et al. 2013]; R236fa: [Airgas USA LLC 2015].
[g] Taken from [Lemmon et al. 2010].
* Auto-ignition and flash point tests are not applicable for these fluids since the vendors consider them as gases, hence ISO 2719 and ASTM D1310 does not apply.

R245fa, R236fa and R236ea were taken from Larsen, Pierobon et al. [2013] these fluids are not flammable and have low hazard levels. R1233zd(E) was selected due to its high efficiency at medium waste heat temperatures and was selected by Lecompte et al. [2015] due to its environmental friendliness and good thermodynamic performance for a WHRS [Datla & Brasz 2014].

Table 13 shows some of the important characteristics from the working fluids selected such as GWP and flammability. The table has missing data from some of the organic fluids; this is due to two main reasons in the author's opinion: 1) the data has not been measured due to technicalities in the standards (e.g. ISO); and 2) The data has not been measured or published, being impossible to find. For the first reason the majority has to do with the limitation of the standards used by vendors to test the working fluids. ISO 2719 and ASTM D1310 (flash point test), and ASTM E659 (auto-ignition temperature test) only cover liquids while vendors sell their organic fluids as gases and so are not required to perform these tests [International Organization for Standardization 2002; ASTM International 2014a; ASTM International 2014b].

In terms of the second reason, the academic literature does not cover all organic fluids due to the extent of the catalogue but also because there are many different ways to perform the tests which at the same time are limited to temperature, pressure, test length, decomposition materials produced and application of the working fluid. For example, the chemical stability for R1233zd(E) and R1336mzz-Z was tested by Kontomaris [2014]. He raised the temperature from 175˚C to 250˚C with a mid-step at 200˚C. The results show that between 175˚C and 200˚C R1233zd(E) decomposes but since the aim was to show the thermal stability of R1336mzz-Z, the R1233zd(E) decomposition temperature is not truly assessed. The ORC WHRS literature recognises the importance of the organic fluids' flash points, auto-ignition temperatures and thermal and chemical stability since these guarantees a long-lasting and safe operation [Andersen & Bruno 2005; Kontomaris 2014].

In order to limit the application of the working fluids that are missing data, there were a set of assumptions taken to complete Table 13:

- Water and hexamethyldisiloxane ODP. Water is known for its environmental friendliness so it is assumed that water's ODP is zero. Hexamethyldisiloxane's ODP should follow the trend of benzene, heptane and toluene which is a negligible ODP.
- Auto-ignition temperature: R236ea and R236fa are assumed to have a similar auto-ignition temperature to other refrigerants used in this study, even though their chemical structures are different.
- All refrigerants' flash points: It is assumed that this information is not relevant since the hazard classification regarding flammability is given as zero.
- R236ea decomposition temperature: It will be assumed to be similar to that found for R236fa since both organic fluids contain the same molecules but are differently structured.

It is important to mention again that these assumptions could be incorrect due to the author's lack of chemistry knowledge and any related hazardous characteristics. Accordingly, the author highlights the importance of covering this literature gap regarding organic fluid's hazards characteristics and physical properties which will bring about a better understanding of the limits and applicability of the organic working fluids. A good example of an advance work on computing some of the characteristics shown in Table 13 is the work of Kazakov et al. [2012]. In this research, a catalogue of 56,000 compounds was used to predict their suitability and depending on the GWP_{100}, critical temperature (T_{cr}), chemical stability, flammability (i.e. the lower flame level) and toxicity, these compounds are eliminated, finishing with around 1,234 compounds at the end of the process, of which the biggest group are halogenated compounds (i.e. that contain fluorine, chlorine, bromine, iodine or astatine). However, Kazakov et al.'s [2012] work focuses only on a refrigeration process and not power generation, this affects the fluid selection since one of the filters is the T_{cr} which was set to be below 127°C in order to overcome refrigeration equipment limitations. Furthermore, the study, in terms of chemical stability, does not calculate the decomposition temperature; it only eliminates compounds that contain certain type of functional molecule groups (e.g. peroxide) that are related to stability problems. This approach, as efficient as it is, still leaves the question open: up to what temperature can the compound be used before it is starts to decompose on a thermodynamic WHRS? This is an important question that has been partially answered depending on the organic fluids used, as seen in Table 13.

The values in Table 13 limit the working fluids' applicability under the vessel's operating conditions, but also dictate the system configuration required for the marine ORC WHRS.

6.6 THERMODYNAMICS AND HEAT TRANSFER

The thermodynamic and heat transfer modelling is regarded as the backbone of this work. While the previous sections described in this chapter and the different optimisation strategies bring a more accurate operating conditions and effective WHRS designs, it is the thermodynamic and heat transfer processes which allow the use of waste heat as a means of reducing the ship's CO_2 emissions.

Here, the application of the First Law of Thermodynamics (FLT) into the ship's waste heat problem is studied with the assistance of heat transfer's basic concepts to generate a model which is capable of utilising the available ship's waste heat to produce steam – to cover the thermal demand on board – and produce power which will effectively reduce the ship's fuel consumption. Thermodynamic modelling will allow the author to understand the energetic processes happening inside and outside the WHRS. Heat transfer models would be used for the energy transfer across the closed boundaries of the WHRS and the heat source and sink.

The WHRS thermodynamic and heat transfer models can be visualised as modules where the energy and mass transfers occur and are balanced (see Figure 45). The module that must always be present in the WHRS problem is the simple plant. The heat source and sink blocks contain the relevant conditions regarding the ship's waste heat and cooling medium. To the

simple plant module depending on the operating conditions, working fluid selected and analysis detail the other four modules – thermal oil, steam, recuperator and seawater pump/air fan – can be incorporated.

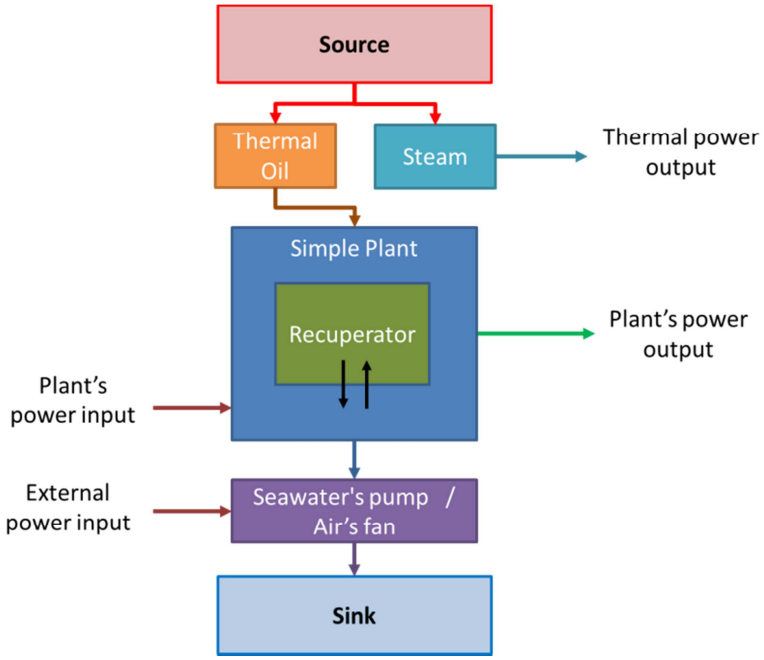

Figure 45: Module representation of the thermodynamic and heat transfer model. Each module can be a plug-in to the heat source. The arrows represent the energy transfer in between modules and outside the WHRS model.

The marine WHRS layouts studied are the simple plant (see Figure 18) – simple plant module in Figure 45 – and the recuperative plant (see Figure 20) which is represented by the simple plant and recuperator modules in Figure 45. First the simple plant layout will be discussed; next the equations will be modified to reflect the presence of a recuperator; the last steps are a general overview of the thermal oil, steam and coolant modules.

6.6.1 Setting the ground for the model

The vessel's waste heat problem is treated as a steady flow at steady state conditions. Thermal inertia and instant electrical power production are important phenomena occurring on a marine WHRS. A dynamic analysis can give a more detailed energy map on board a ship, giving the plant designer a better understanding about the operation and limitation of a marine WHRS, and allows for the creation of efficient controller systems that manage the WHRS safe operation. While these aspects are important in the implementation on board a vessel, the author believes that the study of alternative marine WHRS assuming steady state conditions is sufficient as a starting point.

In regards to thermodynamics, this work will use only the FLT. The real strength of the Second Law of Thermodynamics lies in its capacity to tell where there are areas of improvement in plant design. The author recognises the importance and relevance of using the Second Law for the study of marine WHRS, but it is regarded as sufficient to use only the FLT as this is a

comparative study between relatively simple plants where the benefit/cost of using the extra information from the Second Law of Thermodynamics could be low.

It is assumed that there are no pressure drops inside the WHRS and that there is a uniform pressure distribution at the different WHRS sections. The WHRS is a perfectly insulated system with no leaks and there are no dead volumes. The isentropic efficiencies of the expander and pumps will be assumed to be constant, except in chapter 9 where the isentropic efficiency change due to off-design conditions is considered.

The thesis will focus only on subcritical systems (i.e. the WHRS evaporating condition cannot go simultaneously beyond T_{cr} and P_{cr} values shown in Table 13) that are treated as a closed boundary and are meant to produce useful work – electrical or mechanical – for the ship.

When using the available waste heat from the exhaust gas, the exhaust gas will be treated as air. The specific heat (C_p) – for both exhaust gas or scavenge air – will be assumed as the averaged C_p between the inlet temperature and minimum outlet temperature. Seawater will be assumed to have a salinity of 35,000 ppm which is between the oceans extremes of 31,000 ppm and 39,000 ppm [Abe & Ebuchi 2014]. While this value can fluctuate throughout the voyage, the resulting changes in mass flow rate due to variations in the seawater's specific heat are of the order of 0.5% when the salinity changes from 31,000 ppm to 39,000ppm at a temperature of 9˚C. Since this work will consider the power requirement to move the cooling medium to the WHRS, it was assumed that a minimum pressure of 200 kPa was required for the seawater pump in order to overcome head losses. For the case of air, in chapter 9, a maximum pressure of 106 kPa was set since small changes in air pressure produce large changes in the fluid's energy system, becoming in some instances unfeasible.

This work will not focus on high-detail heat exchanger design (except for the final results chapter). All heat exchangers used for the simulations, except for the heat exchanger in contact with the exhaust gas or scavenge air, are assumed to be counter flow. Counter flow heat exchangers are preferred in this study over parallel flow heat exchangers due to the following reasons [Engineers Edge 2013]:

- There is a more uniform temperature difference, minimising thermal stresses.
- There is a superior heat transfer throughout the heat exchangers.
- The cold fluid outlet temperature can reach the maximum temperature possible within the heat transfer process.

A once-through economiser will be considered for the heat exchanger between the heat source and the working fluid or thermal oil. While this heat exchanger is not designed in this work, it is its performance and flexibility with changing loads that makes it suitable for the absorption of the exhaust gas and scavenge air waste heat [Godbole 1990].

The sign convention used will be a positive sign for the heat coming into the cycle, and negative when leaving it. For the work, it will be positive when it is generated by the cycle, while work coming in will be negative.

6.6.2 SIMPLE PLANT

The simple plant module layout with its temperature (*T*) – entropy (*s*) diagram is represented by Figure 46. For the sake of completeness, the processes happening inside the simple plant layout will be written again. First, the WHRS receives the waste heat from the vessel at the economiser and is absorbed at high pressure by a working fluid which in turn is expanded inside the expander to produce work. The unused energy is rejected to a cooling fluid until the working fluid is cooled to a desired temperature at low pressure. The pump is in charge of increasing the working fluid pressure to close the WHRS circuit and start again.

6.6.2.1 ECONOMISER

Starting with the waste heat addition (q_i) to the thermodynamic plant occurring in the economiser (i.e. between points 4 and 1):

$$q_i = h_1 - h_4 \qquad [\ 16\ ]$$

Where h_1 and h_4 are the high pressure specific enthalpies after and before the heat addition respectively. The minimum temperature allowed for $T_{WH,o}$ is set by the sulphur content in the exhaust gas (see Table 9), while for the scavenge air, the temperature will be limited to 50°C since lower temperatures will bring negligible benefits with a large cost in the heat transfer area. Before calculating the working fluid's mass flow rate ($\dot{m}_{wf}$) it is important first to study in more detail the economiser.

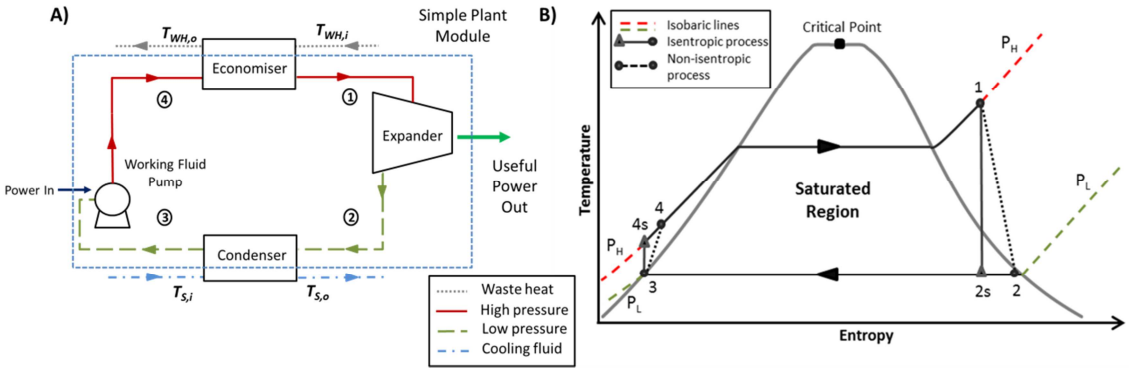

Figure 46: A) The main components from the simple plant module delimited by the dashed light blue line. The blue dashed line represents the module. B) The simple plant *T-s* diagram is shown. In this graph the isentropic and non-isentropic processes are represented.

The economiser is divided into three different sections (see Figure 47) to accurately measure the energy transfer between the processes, state changes (i.e. from liquid to vapour) happening inside it and calculate the total heat transfer area when the analysis requires using temperature instead of enthalpy:

- Subcooler: In this section of the economiser, the high pressure working fluid is subcooled, this means that it has a lower temperature than its boiling temperature at the given pressure. In here the working fluid starts to absorb the waste heat from the exhaust gas or scavenge air until it reaches its saturated liquid state.
- Evaporator: The working fluid moves from its saturated liquid state to its saturated vapour state. Here, both liquid and vapour coexist.

Superheater: The last part of the economiser is responsible for raising the temperature of the working fluid after its saturated vapour state. As discussed in section 3.2.1, sometimes the superheater does not bring a substantial benefit to the WHRS performance, hence the model must be flexible to be able to remove or add this section.

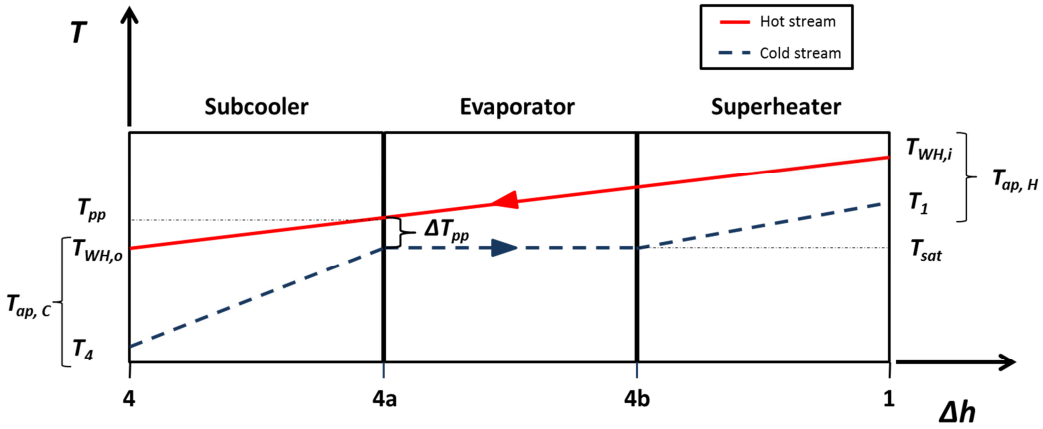

Figure 47: Representation of the economiser and its three subsections in a *T-Δh* plot. Different temperature values are also defined, such as approach temperature (T_{ap}) and pinch point temperature (T_{pp}) among others.

Analysing the temperature versus change of specific enthalpy (Δh) graph in Figure 47, the hot stream is defined by the red line and moves from right to left, in other words, becomes colder. The area below the red line represents the available energy in the heat exchange process. The blue line represents the working fluid moving in the opposite direction of the red line, meaning that it becomes hotter. Between points 4a and 4b the temperature stays constant due to the working fluid's change of phase. The area below the blue line is the energy absorbed by the process.

The approach temperature (T_{ap}) is defined as the temperature difference between the hot and cold streams at the counter flow heat exchanger's inlets and outlets:

$$T_{ap,C} = T_{WH,o} - T_4 \quad [17]$$

$$T_{ap,H} = T_{WH,i} - T_1 \quad [18]$$

Where *H* and *C* subscripts stand for the hot and cold approach temperature respectively, *WH* subscript refers to the waste heat (i.e. hot stream), and *i* and *o* mean the waste heat's inlet and outlet respectively. The pinch point temperature difference (ΔT_{pp}) is the temperature difference between the working fluid's saturated temperature (T_{sat}) and the waste heat temperature at that point (T_{pp}) [Mago & Srinivasan 2010], and is the minimum temperature difference found in a heat exchanger:

$$\Delta T_{pp} = T_{pp} - T_{sat} \quad [19]$$

The study of the pinch point and temperature approach permits an understanding of the maximum heat transfer possible between a system's hot and cold flow streams [Quoilin 2008;

Marechal 2010]. Going back to Figure 47, the area between the hot and cold streams is the process irreversibility – energy that is not absorbed by the working fluid – meaning that as ΔT_{pp} or any of the approach temperature increase, the less useful is the work that can be produced from the same waste heat quality and availability by the WHRS [Butcher & Reddy 2007; Quoilin 2008].

Ideally, the best option possible will be that ΔT_{pp} and T_{ap} are equal to zero so the irreversibilities can be reduced to the minimum possible, but there are some drawbacks in sizing and cost. To understand the implications of modifying ΔT_{pp} and T_{ap}, it is first necessary to analyse the heat transfer phenomena inside a counter-flow heat exchanger. The analysis will focus on the subcooler region and then in a broader analysis it will cover the evaporator and superheater together since the evaporator temperature difference (i.e. $T_{4b} - T_{4a}$) is zero due to the working fluid change of phase.

The heat found in the hot and cold stream inside a counter flow heat exchanger can be defined as follows [Incropera et al. 2007; Marechal 2010]:

$$\dot{Q}_{WH,sc} = \dot{m}_{WH} c_{p\,WH} \left(T_{pp} - T_{WH,o}\right) \quad [\ 20\ ]$$

$$\dot{Q}_{wf,sc} = \dot{m}_{wf} c_{p\,wf} (T_{4a} - T_4) \quad [\ 21\ ]$$

Where $\dot{Q}$ is the heat flux, $\dot{m}$ is the mass flow rate of each stream, c_p is the specific heat capacity, the subscript *wf* denotes the working fluid stream (i.e. inside the WHRS), and the subscript *sc* is for the subcooler region of the economiser. The variable T_{4a} is the same as T_{sat}, and it will be used onwards in the following calculations. Assuming there are no heat transfer losses inside the heat exchanger, the heat gained by the cold stream is equal to that lost by the hot stream. The variable T_{pp} is an unknown in the thermodynamic problem, hence it will be substituted by clearing it from equation [19]:

$$T_{pp} = T_{sat} + \Delta T_{pp} \quad [\ 22\ ]$$

Another definition to calculate the heat transferred inside the counter flow subcooler is given by Incropera et al. [2007]:

$$\dot{Q}_{WH,sc} = U_{sc} A_{ht,sc} \Delta T_{lm,sc} \quad [\ 23\ ]$$

Where U is the overall heat transfer coefficient and its calculation will be explained in the different result chapters where the heat exchanger area is required to be known. The variable A_{ht} is the heat transfer area and ΔT_{lm} is the logarithm temperature difference for a counter flow heat exchanger and is given as the following expression:

$$\Delta T_{lm,sc} = \frac{\left(T_{pp} - T_{sat}\right) - \left(T_{WH,o} - T_4\right)}{ln\left[\left(T_{pp} - T_{sat}\right)/\left(T_{WH,o} - T_4\right)\right]} \quad [\ 24\ ]$$

Using equations [17] and [22], ΔT_{lm} can be written as follows:

$$\Delta T_{lm,sc} = \frac{\Delta T_{pp} - T_{ap,C}}{ln\left(\Delta T_{pp}/T_{ap,C}\right)} \quad [25]$$

To know the required A_{ht} then it is necessary to clear A_{ht} from equation [23]:

$$A_{ht,sc} = \frac{\dot{Q}_{WH,sc}}{U_{sc}\,\Delta T_{lm,sc}} \quad [26]$$

Using equation [25], and substituting them into equation [26] then:

$$A_{ht,sc} = \frac{\dot{Q}_{WH}\; ln\left(\Delta T_{pp}/T_{ap,C}\right)}{U_{sc}\left(\Delta T_{pp} - T_{ap,C}\right)} \quad [27]$$

This means that when keeping everything constant except ΔT_{pp}, the subcooler area is reduced when ΔT_{pp} increases, while as ΔT_{pp} tends to zero the area will tend to infinity (see Figure 48). Leaving everything constant and modifying $T_{ap,C}$ it is seen that the behaviour is identical to that seen for ΔT_{pp}. The $A_{ht,sc}$ will also increase when the heat flux increases, while an increment in U_{sc} – which has to do with the physical properties and construction of the heat exchanger, and the thermodynamic properties of the working fluid – will reduce the area. It is possible to say from this analysis that the cost of reducing the irreversibilities in the economiser's subcooler region will be larger heat transfer areas which in turn will impact the WHRS' initial cost and the vessel's available space. These findings are discussed by MAN Diesel & Turbo [2009] for a waste heat boiler.

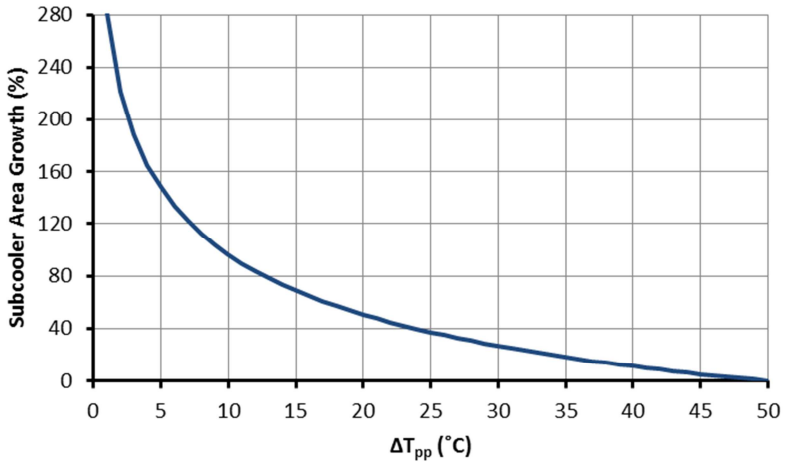

Figure 48: Representation of the requirement increase in heat transfer area when the pinch point temperature difference is reduced. The graph assumes as a starting point the area required when the pinch point temperautre difference is 50˚C.

The mass flow rate can be found from the economiser's subcooled region using equations [20] and [22]; and the assumption that the heat coming in to the working fluid is equal to that removed from the source:

$$\dot{Q}_{WH,sc} = \dot{m}_{WH} c_{p\,WH}\left(T_{sat} + \Delta T_{pp} - T_{WH,o}\right) \quad [28]$$

$$\dot{Q}_{wf,sc} = \dot{m}_{wf}(h_{4a} - h_4) \quad [29]$$

$$\dot{Q}_{wf,sc} = \dot{Q}_{WH,sc} \quad [30]$$

$$\dot{m}_{wf} = \frac{\dot{m}_{WH} c_{p\,WH}\left(T_{sat} + \Delta T_{pp} - T_{WH,o}\right)}{(h_{4a} - h_4)} \quad [31]$$

Continuing with the heat available between the evaporator and superheater:

$$\dot{Q}_{WH,ev-sh} = \dot{m}_{WH} c_{p\,WH}\left[T_{WH,i} - T_{pp}\right] \quad [32]$$

$$\dot{Q}_{wf,ev-sh} = \dot{m}_{wf} c_{p\,wf}(T_1 - T_{4a}) \quad [33]$$

Where the subscript *ev-sh* refers to the evaporator and superheater sections of the economiser. The logarithm temperature difference for these regions is given by:

$$\Delta T_{lm,ev-sh} = \frac{\left(T_{WH,i} - T_1\right) - \left(T_{pp} - T_{sat}\right)}{ln\left[\left(T_{WH,i} - T_1\right)/\left(T_{pp} - T_{sat}\right)\right]} = \frac{T_{ap,H} - \Delta T_{pp}}{ln\left(T_{ap,H}/\Delta T_{pp}\right)} \quad [34]$$

This equation can be used for the calculation of the heat transfer area from the evaporator and superheater:

$$A_{ht,ev-sh} = \frac{\dot{Q}_{WH,ev-sh}}{U_{ev-sh}\,\Delta T_{lm,ev-sh}} = \frac{\dot{Q}_{WH,ev-sh}\,ln\left(T_{ap,H}/\Delta T_{pp}\right)}{U_{ev-sh}\left(T_{ap,H} - \Delta T_{pp}\right)} \quad [35]$$

The behaviour of this equation is identical to that seen in Figure 48. The WHRS model is able to modify both approach temperatures and pinch point differences in order to improve the WHRS efficiency and cost. From Figure 48, it is seen that when the approach temperature or pinch point temperature differences are below 5°C the change in area is large. On the other hand, the impact on heat transfer area savings when having large temperature differences is reduced while the irreversibilities increase. For these reasons, it was a temperature difference for both pinch point and an approach of between 5°C and 40°C that were chosen for the simulations performed in the result chapters.

The total heat flux absorbed by the WHRS economiser can be written as follows:

$$\dot{Q}_i = \dot{Q}_{sc} + \dot{Q}_{ev} + \dot{Q}_{sh} = \dot{m}_{wf}[(h_{4a} - h_4) + (h_{4b} - h_{4a}) + (h_1 - h_{4b})] = \dot{m}_{wf}(h_1 - h_4) \quad [36]$$

6.6.2.2 EXPANDER

The next stage is the working fluid's expansion (i.e. between points 1 and 2) where the power output $(\dot{W}_o)$ is given by the following equation:

$$\dot{W}_o = \dot{m}_{wf}(h_1 - h_{2s})\eta_E \quad [37]$$

Where h_1 is the specific enthalpy of the working fluid before entering the expander, h_{2s} is the isentropic specific enthalpy (i.e. that the entropy at point 2 (s_2) is equal to s_1) at low pressure after the expansion process, and η_E is the isentropic efficiency of the expander. A constant value of 80% will be used throughout all calculations for η_E, this value is normally used for different types of expanders. For example, a Euler turbine developed for WHRS can generate isentropic efficiencies above 80% [Welch & Boyle 2009]. Bao and Zhao [2013] present a list of expander prototypes which can reach in some cases efficiencies of 85%. The real enthalpy after expansion can be found as follows:

$$h_2 = h_1 + \eta_E(h_1 - h_{2s}) \quad [38]$$

Depending on the type of working fluid (e.g. wet) and the pressure drop in the expander, the working fluid could end inside the saturated region. To calculate the wetness factor (x), the following equation is used:

$$x = \frac{h_2 - h_l}{h_v - h_l} \quad [39]$$

Where h_l is the saturated liquid enthalpy and h_v is the saturated vapour enthalpy at the same pressure.

6.6.2.3 CONDENSER

For ease of explanation in this subsection, the condenser (i.e. the whole heat exchanger) will be named cooler and the cooler's two-phase region where the working fluid condensates will be named condenser. Beyond this subsection, except in chapter 9, condenser will refer solely to the heat exchanger.

After the expansion process, the working fluid enters the cooler where it rejects heat to the cooling fluid. As with the economiser, the cooler is subdivided in order to study the heat transfer phenomena (see Figure 49). In the case of the cooler, it was divided into only two regions – desuperheater and condenser – because it is assumed that the working fluid will always exit the cooler as a saturated liquid instead of a subcooled one. This assumption has the purpose of rejecting the minimum energy possible to the cooling medium. From Figure 49 the hot working fluid enters the cooler as a superheated vapour and starts to cool down until it reaches its saturation temperature, after that point the working fluid rejects its energy by condensing until it reaches its saturated liquid state at point 3. The cooling fluid increases its temperature at a constant rate due to the energy received from the working fluid. An important point to bear in mind is that the cooling fluid temperature is not controlled by the code and is a fixed boundary condition. This means that the saturation temperature, thus the WHRS low pressure, must adapt to the cooling medium temperature in order to be able to operate.

Using the same methodology as in the economiser, the heat transfer area for the desuperheater and condenser is found as follows:

$$A_{ht,ds} = \frac{\dot{Q}_{wf,ds}}{U_{ds}\,\Delta T_{lm,ds}} = \frac{\dot{Q}_{wf,ds}\,ln\left(T_{ap,H}/\Delta T_{pp}\right)}{U_{ds}\left(T_{ap,H} - \Delta T_{pp}\right)} \quad [40]$$

$$A_{ht,co} = \frac{\dot{Q}_{wf,co}}{U_{scd}\,\Delta T_{lm,co}} = \frac{\dot{Q}_{wf,co}\,ln(\Delta T_{pp}/T_{ap,C})}{U_{co}\,(\Delta T_{pp} - T_{ap,C})} \quad [41]$$

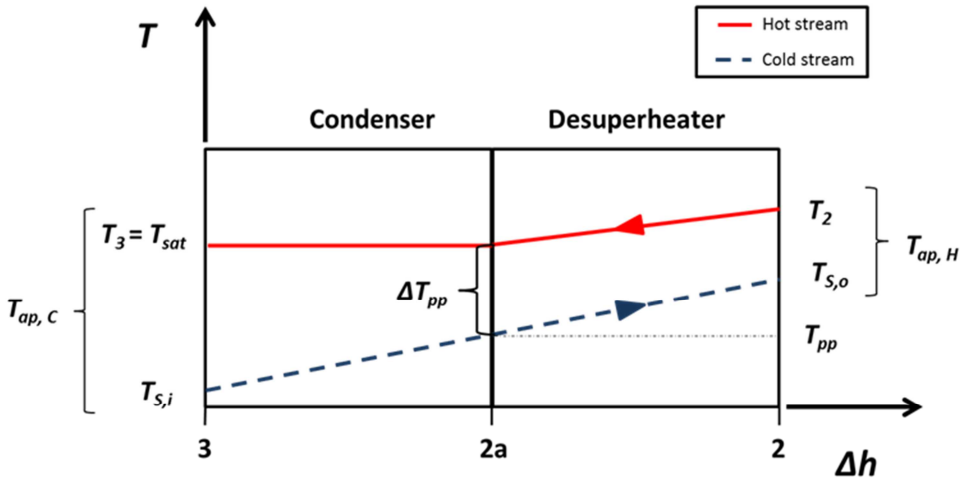

Figure 49: Representation of the cooler and its two subsections in a *T-Δh* plot.

Where the subscripts *ds* and *co* are for the desuperheating and condenser regions respectively. The desuperheater will not be used when the wetness factor is less than one since the working fluid is already at its saturated temperature. The analysis of the condenser's pinch point and the approach temperatures shows identical behaviour as that seen for the economiser in Figure 48, and for the same reasons the limitation for these temperature differences is between 5˚C and 40˚C. The total heat rejected to the cooling fluid is given by the following:

$$\dot{Q}_o = \dot{Q}_{ds} + \dot{Q}_{co} = \dot{m}_{wf}(h_3 - h_2) \quad [42]$$

Where h_3 is the specific enthalpy at the exit of the cooler and h_2 at the entrance.

6.6.2.4 PUMP

For the pumping process (i.e. between points 3 and 4), the working fluid enters the pump as a saturated liquid and the pump increases its pressure, becoming a subcooled liquid. The pumping process also allows the working fluid to circulate inside the system. The power required to operate the pump at the specified pressure difference and mass flow rate is given by:

$$\dot{W}_i = \frac{\dot{m}_{wf}(h_3 - h_{4s})}{\eta_p} \quad [43]$$

Where h_{4s} is the specific enthalpy at the outlet of the compression stage assuming the process is isentropic, and η_p is the isentropic efficiency of the pump. For the pump's isentropic values, Nielsen et al. [2014] use a value of 80% for a marine ORC WHRS and a value of 82% for the steam generator feed water system. In other applications the same value is used for the pump: Walraven et al. [2015] studied the differences of air and water as cooling fluids in a solar power plant; and Chen et al. [2006] compared a subcritical and supercritical approach to take advantage of a low quality waste heat. A value of 80% will be used for the pump's isentropic efficiency.

The real enthalpy after the pumping process is given by the following:

$$h_4 = h_3 + {(h_{4s} - h_3)}/{\eta_p} \quad [44]$$

6.6.2.5 WASTE HEAT RECOVERY SYSTEM OVERALL PERFORMANCE

The net power output ($\dot{W}_T$) is given by adding the power output and input:

$$\dot{W}_T = \dot{W}_o + \dot{W}_i \quad [45]$$

The definition of the thermal efficiency (η_{th}) from equation [10] can be expressed in terms of power and heat flux and enthalpies:

$$\eta_{th} = \frac{\dot{W}_T}{\dot{Q}_i} = \frac{\dot{W}_o + \dot{W}_i}{\dot{Q}_i} = \frac{(h_1 - h_{2s})\eta_E + {(h_3 - h_{4s})}/{\eta_p}}{h_1 - h_4} \quad [46]$$

6.6.3 RECUPERATOR

The recuperator module is in charge of the heat exchange process that can happen between the WHRS' low pressure/high temperature stream coming from the expander and the high pressure/low temperature when exiting the pump. The use of the recuperator will depend on the working fluid's temperature difference between the exit of the pump (point 4 from Figure 50) and that of the expander (2). The hot stream's temperature must be at least 10°C warmer than the cold stream in order to avoid large heat transfer areas and make it worth the investment of adding an extra heat exchanger.

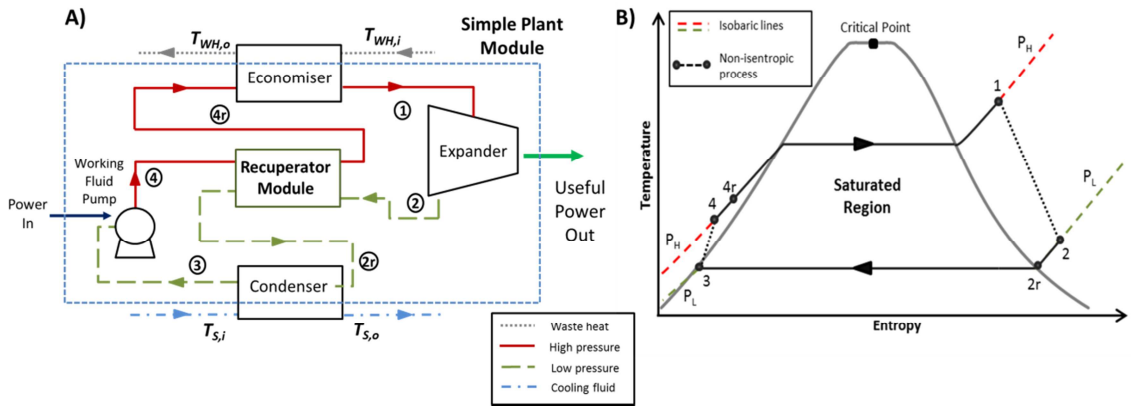

Figure 50: Representation of a recuperative WHRS. A) The recuperator module is added to the simple plant module. New streams are added in order for the working fluid to enter the recuperator. B) The recuperative plant *T-s* diagram is displayed assuming a non-isentropic expansion and pumping.

As seen in Figure 50, there are four different analysis points for the recuperator – 2, 2r, 4 and 4r – which must be balanced in order to follow the First Law and heat transfer phenomena. Following the simple plant module calculations, there are two known points, 2 and 4, which are the streams coming into the recuperator and two unknowns, 2r and 4r, being the streams exiting the recuperator. To find the important information from the recuperator's exits some assumptions and limitations must be used:

- While there is no mass transfer inside this heat exchanger, it is important to balance the energy without having a temperature crossover.
- No working fluid phase change in either stream.
- The minimum approach temperature in both sides of the recuperator is 5°C. In order to have flexibility in the simulations there is no upper boundary limit for the recuperator's approach temperature.
- The energy available in the hot stream can be transferred in its totality to the cold stream.

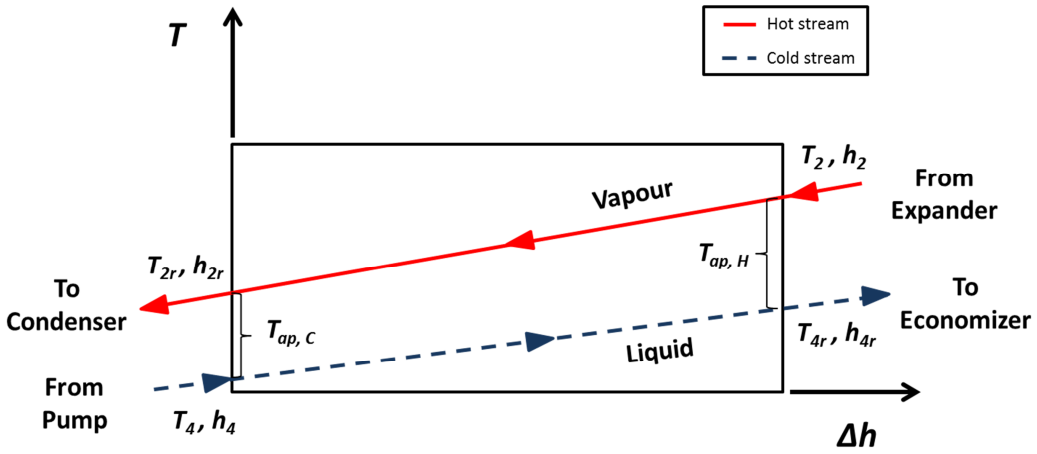

Figure 51: The image shows the hot and cold stream of the same working fluid with its relevant temperatures and enthalpies for the recuperator.

However, there is not enough information to find the recuperator's stream exit data. Saavedra et al. [2010] proposed the use of the recuperator efficiency concept, using the stream temperatures to solve the energy balance. The problem with this approach is that it must be assumed that the working fluid's specific heat at constant pressure (c_p) is the same for both streams which introduces a considerable degree of error. For example, at atmospheric pressure, subcooled water at 25°C has a c_p of 4.18 kJ/kg-K, while being a vapour at a temperature of 177°C, the c_p is around 1.93 kJ/kg-K, a difference of around 117%.

To balance the recuperator's energy transfer, an iterative process using enthalpies and temperatures of both streams is used. Using Figure 51 and the restrictions stated earlier, first the code guesses T_{2r} using the lower limit established for T_{ap}:

$$T_{2r} = T_4 + T_{ap,min} = T_4 + 5 \qquad [47]$$

The enthalpy h_{2r} at low pressure is found to then make an energy balance to find h_{4r}:

$$h_{4r} = h_4 + (h_2 - h_{2r}) \qquad [48]$$

With the value of h_{4r} it is possible to find T_{4r}. The next step is to verify that the recuperator's hot side does not have a temperature cross-over or falls below the limits imposed for T_{ap}. In the case that this occurs, then T_{4r} is defined as follows:

$$T_{4r} = T_2 - T_{ap,min} = T_2 - 5 \quad [49]$$

The energy balance is carried out again to find the new h_{2r} and T_{2r}.

Equations [31] and [36] must be modified to reflect the usage of a recuperator by using h_{4r} instead of h_4. At the condenser, equation [42] changes from h_2 to h_{2r} to find the total heat rejected to the sink. From these equations, assuming that the conditions stay the same, it can be deduced that a recuperative cycle will have a larger mass flow rate than a simple WHRS which allows it to absorb the available waste heat. Larger mass flow rates mean larger power output at the expander but also lager power inputs in the pump. At the other end of the heat transfer phenomena, the working fluid will arrive at cooler temperatures and a lower energy level to the condenser, reducing the power input from the cooling fluid.

The recuperator's heat transfer area ($A_{ht,rec}$) can be found as in equation [26] having a logarithmic temperature difference ($\Delta T_{lm,rec}$) as follows:

$$\Delta T_{lm,rec} = \frac{(T_2 - T_{4r}) - (T_{2r} - T_4)}{ln[(T_2 - T_{4r})/(T_{2r} - T_4)]} \quad [50]$$

6.6.4 THERMAL OIL

As mentioned in section 3.2.2 the purpose of the thermal oil is to decouple the waste heat source from the WHRS with the purpose of protecting the integrity of the vessel and personnel, but also to take care of the working fluid. The thermal fluid circuit provides flexibility in the plant layout which is particularly useful for retrofits, but also reduces the amount of working fluid on board the ship [Roberge 2014]. Therminol VP-1 is used in this work due to its suitable temperature operating range and its low viscosity at the WHRS operational conditions (see Table 14).

Table 14: Some properties for the thermal oil Therminol VP-1 [Solutia Inc. 1999].

Flash Point (˚C)	124
Auto-ignition Temperature (˚C)	621
Kinematic Viscosity at 40˚C (cSt)	2.48
Density at 25˚C (kg/m^3)	1,060
Maximum Operating Temperature (˚C)	400

The code will automatically add a thermal oil module:

- When working with flammable fluids (i.e. a flash point below 60˚C).
- If at any point of the operating profile the exhaust gas or scavenge air temperature is higher than:
  - Auto-ignition temperature.
  - Decomposition temperature.

In order to study this module, the simple plant layout will be used and is represented by Figure 52. It is important to keep in mind that the purpose of this work is not to study in detail this

module, but that the study is enough to capture the main thermodynamic effects of using a thermal oil circuit. Some assumptions that are made for the thermal oil are that all the heat energy available from the waste heat is absorbed by the thermal oil, this is assumed also by the work of Fernández et al. [2011] and Pierobon, Rokni et al. [2013]; the heat exchangers' temperature approach has a minimum of 5°C while the maximum is not limited, following the demonstration in Figure 48 to avoid large heat transfer areas; and the thermal oil was treated as an incompressible fluid with thermodynamic properties calculated by Coolprop [Bell et al. 2014].

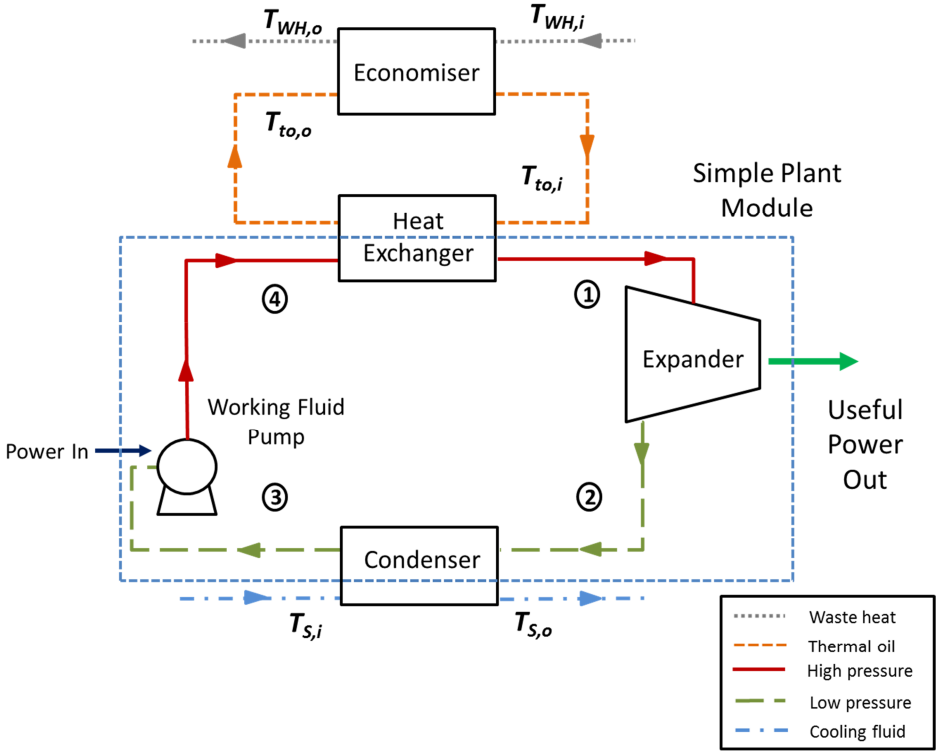

Figure 52: Plant representation of a simple WHRS coupled with a thermal oil circuit which absorbs the available waste heat from the vessel. The different approach temperatures related to the thermal oil circuit are shown in this diagram.

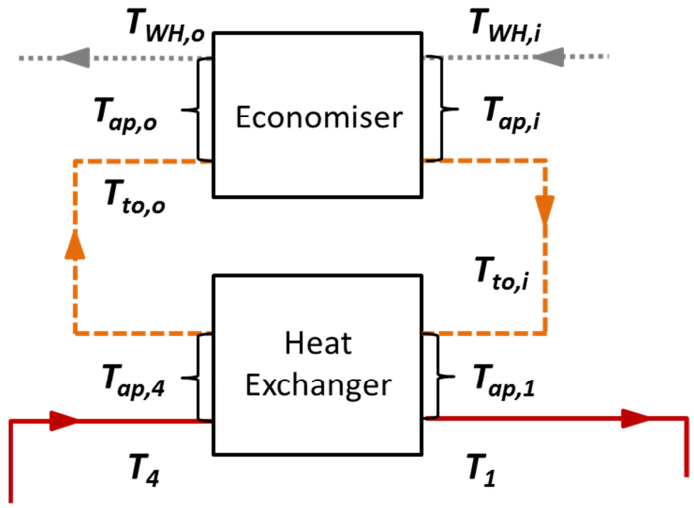

Figure 53: Diagram that shows the different relevant temperatures when a thermal oil is used between the waste heat source and a simple WHRS.

The critical side of the thermal circuit, from the working fluid's point of view, is given by temperature $T_{to,i}$ which is the highest temperature seen in the circuit. The code will adapt to avoid higher temperatures than the working fluid's auto-ignition and decomposition temperature plus a safety margin of 2.5˚C. So, for example, R245fa has a decomposition temperature of 250.0˚C, then $T_{to,i}$ cannot be higher than 247.5˚C.

The thermal oil mass flow rate ($\dot{m}_{to}$) can be found as follows:

$$\dot{m}_{to} = \frac{\dot{m}_{WH} c_{p,WH} \left(T_{WH,i} - T_{WH,o}\right)}{c_{p,to} \left(T_{to,i} - T_{to,o}\right)} \quad [\ 51\ ]$$

The equations will not be developed for the processes happening inside the heat exchanger between the working fluid and thermal oil since they are identical to that developed for the economiser without thermal oil. The reader can follow the development from equation [17] to equation [36] and changing $T_{WH,i}$, $T_{WH,o}$, $T_{ap,i}$ and $T_{ap,o}$ for $T_{to,i}$, $T_{to,o}$, $T_{ap,1}$ and $T_{ap,4}$.

6.6.5 STEAM

Since the study of steam demand is complex and there is not much information available to perform an analysis such as that undertaken by Gymnopoulos [2013], the data provided by MAN Diesel & Turbo [2005] will be used. Some assumptions were taken in order to be able to have a working model that depicts the thermal demand on board a ship:

- The steam demand is related to engine power.
- The container ship's case can be extrapolated to any ship type.
- The ambient temperature affects the steam demand linearly.

Since the aim of this work is not the study of steam demand but the application of alternative WHRS on board a vessel, the assumptions are deemed acceptable for a first approach to the ship's heat management and WHRS performance in a more realistic approach. A two-step process is required to find the steam demand for any given power output and temperature. First, the steam demand – or steam mass flow rate – in kg/h for the vessel's power at design point ($\dot{m}_{steam,power}$) is found at an ambient temperature of 25˚C with the following linear relationship:

$$\dot{m}_{steam,power} = 0.0437 \dot{W}_{vessel} + 14.03 \quad [\ 52\ ]$$

Where $\dot{W}_{vessel}$ is the engine's power output given in kW. The second step takes the average effect from the six observations given by MAN Diesel & Turbo [2005] and centres it to the reference temperature which is 25˚C:

$$\dot{m}_{steam,amb} = -40 T_{amb} + 1000 \quad [\ 53\ ]$$

Where $\dot{m}_{steam,amb}$ is the corrected steam demand to T_{amb} which is the ambient temperature in degrees Celsius. What equation [53] does is to correct the steam demand by the deviation of the voyage's ambient temperature to the reference ambient temperature. Then, the steam demand ($\dot{m}_{steam}$) is found as follows:

$$\dot{m}_{steam} = \dot{m}_{steam,power} + \dot{m}_{steam,amb} \quad [54]$$

The steam requirement will be assumed to be constant irrespective of the engine's loading condition but will change due to the ambient temperature. The steam demand will be covered partially or totally – in the case of navigating in extremely cold weather where the demand is higher [Lloyd's Register 2012c] – by the exhaust gas, unless it is specified to be the contrary in any of the results chapters. The exhaust gas temperature at the waste heat boiler (WHB) inlet is the temperature after the turbocharger and is normally given by the engine's manufacturers (see Figure 39).

Extracting energy from the exhaust gas before entering the power cycle will affect the waste heat quality and this must be considered. To find the exhaust gas temperature before first entering the WHRS, it is necessary to calculate the energy taken by the WHB. The WHB can be treated as the economiser with its three different sections (see Figure 54). It is assumed that feed water enters the WHB subcooler at a temperature of 50°C and ΔT_{pp} is set to 20°C [MAN Diesel & Turbo 2005], and exits the superheater at a maximum temperature of 270°C and constant pressure of 700 kPa [MAN Diesel & Turbo 2005]. In the case that the exhaust gas temperature is lower than 270°C, an approach temperature ($T_{ap,H}$) of 5°C will be used.

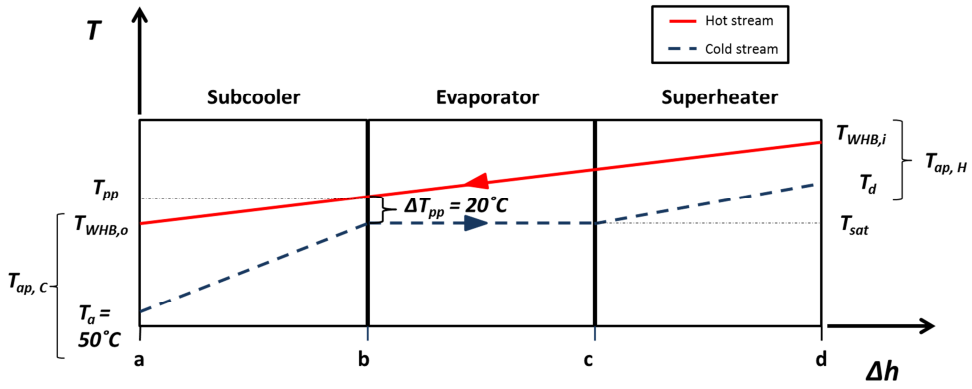

Figure 54: WHB with its three different sections and relevant temperatures for the study of the ship's steam production.

It is possible to find the heat required to change from water to steam using water's enthalpy change:

$$q_{steam} = h_{WHB,o} - h_{WHB,i} \quad [55]$$

Where the subscript *WHB* represents the exhaust gas variables (see Figure 54). Then it is possible to find the heat flux ($\dot{Q}_{WHB}$) in kW required from the exhaust gas using the steam's mass flow rate:

$$\dot{Q}_{WHB} = {}^{\dot{m}_{steam} q_{steam}}/_{3{,}600\eta_{WHB}} \quad [56]$$

Auxiliary boilers and WHB manufacturers give a range for the thermal efficiency (η_{WHB}) between 79% and 90% depending on the design, fuel used and operating conditions [SCI-Pak 2010; Cleaver-Brooks Inc 2011a; Cleaver-Brooks Inc 2011b]. In this work, the boiler's thermal

efficiency is assumed to be a constant 85%. The exhaust gas exit temperature from the WHB is calculated as follows:

$$T_{WHB,o} = T_{WHB,i} + \frac{\dot{Q}_{WHB}}{\dot{m}_{WHB} c_{p,WHB}} \quad [57]$$

Where $T_{WHB,o}$ will become $T_{WH,i}$ when the exhaust gas enters one of the different WHRS plant layouts or the thermal oil module.

In the case where the steam is not produced by using the available waste heat, then it is covered by an auxiliary fired boiler. The boiler will utilise the same fuel used by the vessel to produce the steam required on board as calculated in this subsection.

6.6.6 COOLING FLUID POWER REQUIREMENT

The unused heat by the WHRS must be rejected to the sink via a cooling fluid – in the case of this work either air or seawater are considered – until the cold working fluid at point 3 reaches its saturated liquid condition (see Figure 55).

Using Figure 49's terminology and equation [42], the mass flow rate required from the cooling fluid ($\dot{m}_S$) so it can absorb the energy from the expander's exit can be calculated as follows:

$$\dot{m}_S = \frac{\dot{Q}_{co}}{c_{p,S}\left(T_{pp,S} - T_{S,i}\right)} = \frac{\dot{Q}_{co}}{c_{p,S}\left(T_{sat,wf} - \Delta T_{pp,S} - T_{S,i}\right)} = \frac{\dot{m}_{wf}(h_{2a} - h_3)}{c_{p,S}\left(T_3 - \Delta T_{pp,S} - T_{S,i}\right)} \quad [58]$$

Where $\dot{Q}_{co}$ is the heat flux rejected from the condenser, $T_{sat,wf}$ is the working fluid saturation temperature which is the same as T_3. Still, from equation [58] $T_{S,i}$ is unknown since the temperature changes when the pump/fan increase the cooling fluid pressure from atmospheric pressure. To find $T_{S,i}$ first the specific enthalpy at the condenser entrance must be found ($h_{S,i}$), using the cooling fluid's ambient conditions.

The temperature (T_{amb}) is given by the weather model explained in section 6.2, and it is assumed that before the pumping process the coolant is at atmospheric pressure. With this data, it is possible to find the cooling fluid's specific enthalpy (h_{amb}) and entropy (s_{amb}) at ambient conditions. Assuming an isentropic compression then $h_{S,i}$ can be found as follows:

$$h_{S,i} = h_{amb} + \left(h_{S,isentropic} - h_{amb}\right)\Big/\eta_S \quad [59]$$

Where η_S is the pump/fan isentropic efficiency which is set to 80% when using a seawater pump. A value of 60% will be used as the fan's isentropic efficiency as mentioned in the work of Walraven et al. [2015], other references stating the value of this variable have not been found.

The fan/pump power input is given as follows:

$$\dot{W}_S = \dot{m}_S\left(h_{amb} - h_{S,i}\right) \quad [60]$$

Finally, the cooling fluid's temperature ($T_{S,o}$) at the condenser outlet is given by:

$$T_{S,o} = T_{S,i} - \frac{\dot{Q}_o}{\dot{m}_S C_{p,S}} = T_{S,i} - \frac{\dot{m}_{wf}(h_3 - h_2)}{\dot{m}_S C_{p,S}} \quad [61]$$

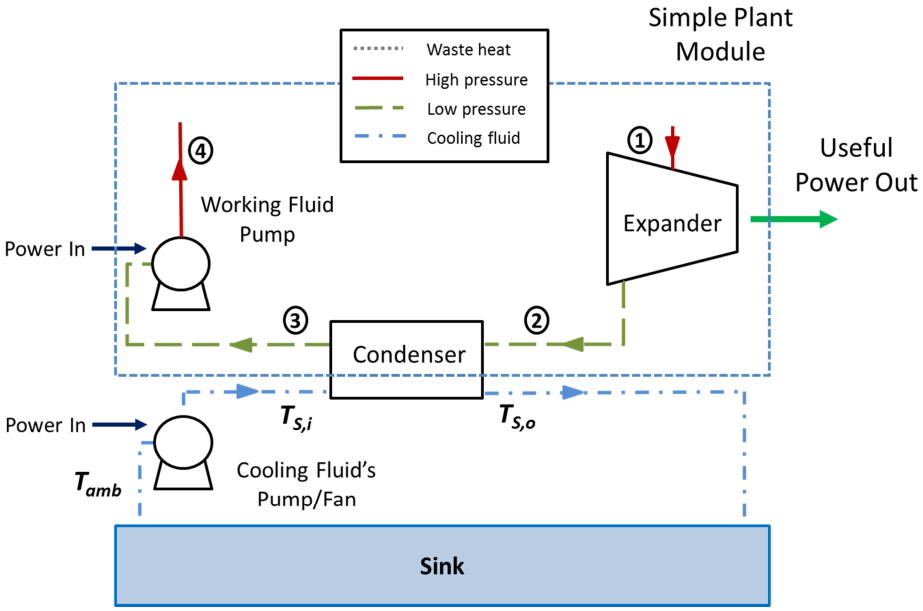

Figure 55: Illustration of the cooling fluid module. The figure shows the lower section of the simple plant module which is connected at the condenser to the marine WHRS sink via the cooling fluid which could be seawater or air.

Here, it was considered all the heat flux rejected ($\dot{Q}_o$) from the WHRS to the sink, but that the same results will be obtained if only the desuperheater was used.

6.7 Off-design conditions

Since the WHRS will not always operate at its optimal point due to the nature of the operating conditions of the vessel, it is necessary to assess the cost in performance of operating under different conditions. Pinch points, approach temperatures, WHRS' pressures, and mass flow rates change constantly to adapt to the changing waste heat source and sink.

Two pieces of WHRS equipment will be considered for the off-design performance: pumps and heat exchangers. The functions for pumps will be explained in this chapter, while the heat exchangers will be discussed in chapter 9 since the off-design Matlab® functions are developed by the Technical University of Denmark (DTU).

The working fluid pump is normally used to control the working fluid mass flow rate, hence its volumetric flow rate ($\dot{V}$), and the WHRS' high pressure [Quoilin et al. 2013]. In chapter 8, the affinity laws, in conjunction with the assumption that all the waste heat available at the different conditions can be absorbed by the economiser, are used for finding the off-design WHRS high pressure:

$$\frac{\dot{V}_d}{\dot{V}_{off}} = \frac{N_d}{N_{off}} = \left(\frac{P_d}{P_{off}}\right)^2 \quad [62]$$

Where *N* is the pump's rotational speed and *P* is the pressure at the exit of the pump. The subscripts *d* and *off* refer to the design and off-design condition respectively. When the pump

changes its rotational speed – and hence its pressure levels – the efficiency changes must be considered. Veres [1994] proposed an empirical correlation to determine the hydraulic efficiency at off-design conditions; in this work it is assumed that the correlation also describes the changes in the pump's isentropic efficiency (η_p):

$$\eta_{p,off} = \eta_{p,d}(0.86387 + 0.3096F - 0.14086F^2 - 0.029265F^3) \quad [\,63\,]$$

Remembering that the density of an incompressible fluid after a pressure change is negigible, it can be assumed that the working fluid's density in its liquid saturated state will be the same in any WHRS operating condition. This will mean that equation [62] can be equated to $\dot{m}_d/\dot{m}_{off}$. So, *F* is defined as follows:

$$F = \frac{\left(\dot{V}/_N\right)_{off}}{\left(\dot{V}/_N\right)_d} = \frac{\left(\dot{m}/_{P^2}\right)_{off}}{\left(\dot{m}/_{P^2}\right)_d} \quad [\,64\,]$$

A representation of equation [63] is given in Figure 56 in which it is possible to see the change in the proportion between the isentropic efficiency at off-design and design condition. Interestingly, the largest isentropic efficiency is found at an *F* value of 85% which is 0.4% larger than at design point (i.e. *F* equal to one). This discrepancy is not discussed by Veres [1994] but may be due to curve fitting and experimental measurement tolerances.

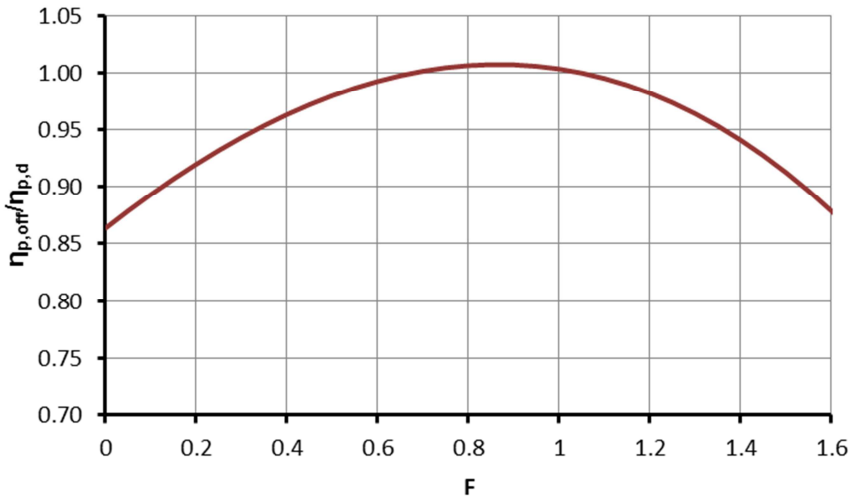

Figure 56: Change in the isentropic efficiency ratio due to a change in the *F* factor which represents different operating conditions as shown in equation [64].

The off-design isentropic efficiency is used in equations [43] and [59]. When using a fan to cool the working fluid, the isentropic efficiency will stay the same at 60%; the author of this work was not able to locate literature that describes the relation between the fan's off-design operation and isentropic efficiency.

6.8 OTHER CALCULATIONS

It is important to remember that the overall efficiency of the system should consider the auxiliary elements that are outside the thermodynamic cycle, such as the pumping requirement for the

sink water system. By adding these expenditures to the WHRS net work ($\dot{W}_{WHRS}$), it is possible to have a more realistic picture of the operation of a marine WHRS:

$$\dot{W}_{WHRS} = \dot{W}_0 + \dot{W}_i + \dot{W}_S \quad [65]$$

6.9 PRODUCING ELECTRICITY

Up to this section, the WHRS power output has been treated as mechanical power which can be used to assist in the shaft rotation, reducing the amount of power delivered by the two-stroke marine diesel engine. In order to transform from mechanical power to electrical power an electrical generator is connected to the expander's shaft:

$$\dot{W}_{e,o} = \dot{W}_0 \eta_e \quad [66]$$

Where $\dot{W}_{e,o}$ is the electrical power output produced by the WHRS given in kW_e; and η_e is the generator efficiency which is assumed to be 97%. A value between 95% and 99% is normally used in the literature for the generator's electrical efficiency [O´Brien 1988; Wang et al. 2011; Nielsen et al. 2014]. This same electrical efficiency can be assumed for pumps and fans:

$$\dot{W}_{e,i} = \dot{W}_i/\eta_e \quad [67]$$

$$\dot{W}_{e,S} = \dot{W}_S/\eta_e \quad [68]$$

The net electrical power output for the thermodynamic cycle and for the whole WHRS system can be described as follows:

$$\dot{W}_{e,T} = \dot{W}_{e,o} + \dot{W}_{e,i} = \dot{W}_o \eta_e + \dot{W}_i/\eta_e \quad [69]$$

$$\dot{W}_{e,WHRS} = \dot{W}_{e,o} + \dot{W}_{e,i} + \dot{W}_{e,S} = \dot{W}_o \eta_e + \left(\dot{W}_i + \dot{W}_S\right)/\eta_e \quad [70]$$

6.10 FUEL, CARBON DIOXIDE EMISSIONS AND COST

This section covers the methodology to translate the net power – mechanical or electrical – output produced by the marine WHRS to fuel consumption reduction, CO_2 emissions and money savings.

6.10.1 FUEL SAVINGS

As previously mentioned, the power output of a marine WHRS could be mechanical or electrical, these options will have an important effect on fuel savings and how they are calculated. When the WHRS is installed to produce mechanical power, which assists the engine's shaft, the fuel savings (FS_{WHRS}) in tonnes per hour are given by:

$$FS_{WHRS} = \frac{\dot{W}_T SFOC_{engine}}{10^6} \quad [71]$$

Where $SFOC_{engine}$ is the specific fuel oil consumption at the engine's MCR at which the operating point was calculated. This data is provided by the engine manufacturer, for example, the reader can access MAN Diesel & Turbo [2015d] to observe the fuel consumption along

different MCR, fuel types, engine sizes and temperatures. The units given regarding the engine's fuel consumption are set in g/kW-h, where kW-h is a unit of energy flux ($\dot{E}$):

$$\dot{E} = \dot{W}_{engine} t \quad [72]$$

Where *t* is time and $\dot{W}_{engine}$ is the engine's power output at the respective MCR.. The issue with *t* and the engine's fuel consumption data is that the engine's manufacturers do not specify the time period used – how many hours taken – to measure $\dot{E}$. For the thesis it was assumed that this period was one hour, hence it is possible to quantify the fuel savings as tonnes per hour. The fuel savings produced when a WHRS generates electricity can be found as follows:

$$FS_{WHRS} = \frac{\dot{W}_{e,T} SFOC_{gen}}{10^6} \quad [73]$$

Where $SOFC_{engine}$ is the specific fuel consumption of a marine genset (i.e. generation set), normally they operate at a constant load and thus tend to have a constant fuel consumption. In each case study analysed where the aim of the WHRS is to produce electricity, a suitable genset will be selected.

When using an auxiliary boiler to cover the vessel's steam demand, marine fuel must be burnt and should be considered in the calculation of the overall WHRS *FS*. The fuel consumption of an auxiliary boiler can be calculated using the information obtained from equation [56]:

$$FS_{boiler} = \frac{3.60 \dot{Q}_{steam}}{q_{LCV} \eta_{boiler}} \quad [74]$$

Where FS_{boiler} is the fuel consumption required by the boiler given in t/h; q_{LCV} is the fuel's Low Calorific Value (LCV)[30]; and η_{boiler} is the boiler's thermal efficiency assumed to be 85% [Towler & Sinnott 2013]. Using the same equation [74], the fuel savings achieved by the WHB (FS_{WHB}) can be found by changing $\dot{Q}_{steam}$ for $\dot{Q}_{WHB}$. The overall WHRS fuel saving per hour (FS_T) is given as:

$$FS_T = FS_{WHRS} + FS_{WHB} - FS_{boiler} \quad [75]$$

In the case where there is no auxiliary boiler or WHB installed on board to cover the steam demand, FS_{boiler} and FS_{WHB} should be considered as zero.

The engine's fuel consumption (FC_{engine}) can be found:

$$FC_{engine} = \frac{\dot{W}_{engine} SFOC_{engine}}{10^6} \quad [76]$$

6.10.2 Carbon dioxide emission reduction

The fuel savings can be translated to CO_2 emission reduction by using the Carbon factors (C_F) shown in Table 3. Using equations [71] or [73] and [74], it is possible to find the total CO_2

[30] See Figure 36 for the values used for HFO and MDO in this thesis.

emission reductions (CS_T) caused by the marine WHRS when returning mechanical or electrical power:

$$CS_T = FS_{WHRS}C_{F,pgp} + (FS_{WHB} - FS_{boiler})C_{F,boiler} = CS_{WHRS} + CS_{WHB} - CS_{boiler} \quad [\ 77\ ]$$

Where $C_{F,pgp}$ is the carbon factor from the fuel used by the ship's engine or the genset depending on what type of power is delivered by the WHRS. The variable $C_{F,boiler}$ comes from the fuel used in the auxiliary boiler; CS_{WHRS} and CS_{WHB} are the CO_2 reductions caused by the marine WHRS and WHB respectively; and CS_{boiler} is the increment on CO_2 caused by using an auxiliary boiler to cover the vessel's steam demand. The units for all terms are in tonnes of CO_2 per hour.

The ship's main engine CO_2 emission (*CE*) can be found by:

$$CE_{engine} = FC_{engine}C_{F,engine} \quad [\ 78\ ]$$

Since this work does not consider the study of auxiliary engines or shaft generators on board, then equations [77] and [78] can be used in equation [1] to find the ship's *EEDI* at the design condition:

$$EEDI = \frac{10^6\left(CE_{engine,design} - CS_{WHRS,design}\right)}{TW} \quad [\ 79\ ]$$

Where *TW* represents the vessel's transport work. The 10^6 factor is used to correct the units from tonne to gram required by the *EEDI* formula (see equation [114]). It is important to have in mind that the *EEDI* is measured using the mechanical power returned by the WHRS.

6.10.3 Annual performance

The results obtained in the previous two subsections are given per hour which is convenient when integrating them with the vessel's operating profile (see section 6.4). The following model development will be only for marine WHRS that produce mechanical power, for electrical power output the same steps can be followed. The Matlab® code adds together the hourly fuel savings and CO_2 emissions per operative bracket (e.g. Table 12), cargo level, single trips, observation time, and route segments:

$$FS_{annual} = \sum_{i=0}^{OT}\sum_{j=0}^{ST}\sum_{k=0}^{CL}\sum_{m=0}^{OS}\sum_{n=0}^{RST} FS_{WHRS_{i,j,k,m,n}}t_{i,j,k,m,n} \quad [\ 80\ ]$$

Where *t* is the time spent at each condition of the operating profile given in hours; *OT* is the observation time which could be monthly (i.e. *OT*=12) or annually (i.e. *OT*=1); *ST* are the number of single trips performed at the given operating condition; *CL* is the vessel's cargo level condition – fully loaded or ballast; *OS* is the number of the vessel's operative segments; and *RST* refers to the amount of segments used to describe the ship's route. Both *OS* and *RST* depend on the data available and analysis definition (i.e. coarse or fine). Equation [80] contains inside the FS_T term respective to the fuel used in each segment of the route – or in the case of not having a segment, the full route – which gives enough flexibility to consider any

change of fuel required by the stricter SO_X rules of the Emission Control Areas (ECA). The annual CO_2 emission reduction can be calculated as follows:

$$CS_{annual} = \sum_{i=0}^{OT}\sum_{j=0}^{ST}\sum_{k=0}^{CL}\sum_{m=0}^{OS}\sum_{n=0}^{RST} FS_{WHRS_{i,j,k,m,n}} C_{F_{i,j,k,m,n}} t_{i,j,k,m,n} \quad [81]$$

With the data obtained by equations [80] and [81] it is possible to analyse the financial aspect of a marine WHRS.

6.10.4 Cost and payback period

In order to determine if the use of the technology is feasible on board a commercial vessel, an economic analysis of the different marine WHRS is required. This model will have the task of calculating the WHRS total investment, annual financial savings and payback period. The initial investment uses the data collected by Quoilin et al. [2013] shown in Figure 57 for the specific cost of an ORC WHRS (SC_{ORC}) and from Cunningham [2002] – which gives a linear relationship for the specific cost (SC_{RC}) – to estimate the cost of the water-based RC on board a vessel:

$$SC_{ORC} = 8{,}700\dot{W}^{-0.301} \quad [82]$$

$$SC_{RC} = 915\dot{W} \quad [83]$$

It is important to bear in mind that $\dot{W}$ is given in kW. If the case study is working with electrical power output then it must be divided by the generator's electrical efficiency in order to be used in equations [82] and [83]. The cost of the electrical generator is taken from Lian et al. [2010]. Operation, maintenance and installation – including special WHRS safety systems costs – as well as tax reductions due to CO_2 and other GHG emissions are not considered.

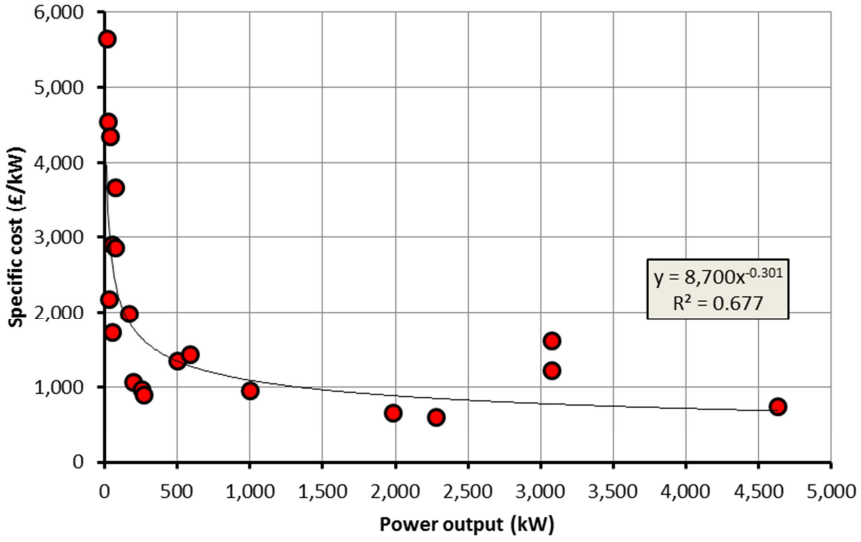

Figure 57: Different specific cost for different ORC WHRS manufacturers given in £ and kW. A power curve is fitted to the data given by Quoilin et al. [2013] in order to be able to approximate the cost of the different marine ORC plants.

The fuel savings – equations [71], [73] and [74] – can be multiplied by the fuel price used on board the ship in order to find the savings per hour (MS_T):

$$MS_T = FS_{WHRS} * FP \quad [\ 84\ ]$$

Where *FP* is the fuel price given in the currency selected for each case study and the data has been collected from Bunker Index [2015] between July 2013 and July 2015 for both MDO and HFO (see Figure 58 for MDO).

The data is recorded in four observation groups per month which contain five daily average fuel prices. The fuel price can be assumed as the overall price of all the data set or it could be selected for a particular point in time which is useful for a sensitivity analysis. The fuel price is also assumed to stay constant during the vessel's lifetime, since future fuel prices are impossible to predict as recent volatility has shown (see Figure 58).

The annual financial savings (MS_{annual}) when using a marine WHRS on board can be developed using equations [80] and [84], and using the respective fuel price for each operating condition:

$$MS_{annual} = \sum_{i=0}^{OT}\sum_{j=0}^{ST}\sum_{k=0}^{CL}\sum_{m=0}^{OS}\sum_{n=0}^{RST} FS_{WHRS_{i,j,k,m,n}} FP_{i,j,k,m,n} t_{i,j,k,m,n} \quad [\ 85\ ]$$

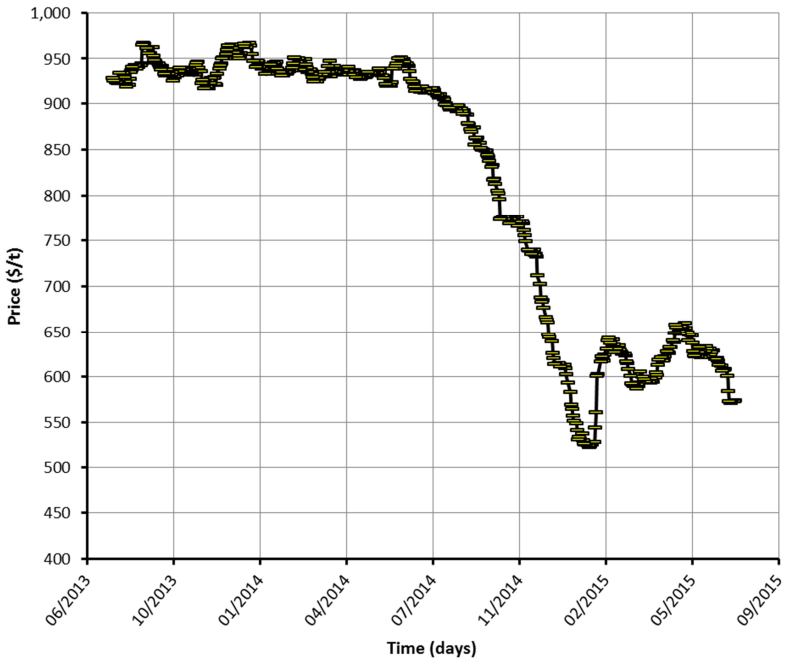

Figure 58: Price variation of MDO during July 2013 to July 2015 given in American dollars per tonne of fuel.

To calculate the present value (*PV*) of the cash inflow – MS_{annual} – at any given time of the vessel's operative life, the following formula is used:

$$PV = \frac{MS_{annual}}{(1+i)^t} \quad [\ 86\ ]$$

Where *t* is the time given in years and *i* is the discount rate. Theotokatos and Livanos [2012] explained that equation [86] is sensible to the discount rate and it must be selected according

to the risk in MS_{annual}, proposing a value for the discount rate between 4.0% and 4.5%. Walraven et al. [2015] used a value of 4.0% when comparing two different approaches to cool down an ORC solar power plant; while Pierobon et al. [2014] proposed a value of 6.0% when using WHRS on an offshore platform. A value of 5.0% will be used in this work which is in line with the literature.

The next step is to calculate the net present value (*NPV*) of the WHRS investment – MS_{annual} and *ME*– which explains the depreciation of the technology benefit – strictly financial and not environmental – through the operational life of the vessel:

$$NPV = ME_{WHRS} + \sum_{t=1}^{Y} \frac{MS_{annual}}{(1+i)^t} \quad [\ 87\ ]$$

Where ME_{WHRS} is the investment made by the vessel's owner on any of the WHRS an shown in equations [82] or [83]; *Y* is the ship's years in operation, assumed in this work to be 20 years.

The *NPV* also helps to find the payback time (*PB*) – or the time it takes to break even – of the marine WHRS investment. This work uses the concept of discounted payback time which considers the effects of *NPV*:

$$PB = NI + \frac{PV_{NI}}{NPV_{NI}} \quad [\ 88\ ]$$

Where *NI* represents the years (integer) with a negative *NPV;* PV_{NI+1} represents the *PV* one year after *NI* and NPV_{NI} is the *NPV* for the same year as the *NI*.

6.11 RESEARCH LIMITATIONS

There have been different approaches made to use the energy available from the engine's waste heat, each has its own advantages and disadvantages, which must be assessed in turn to select the best system. The intended ships' WHRS to be studied will be operating within the heat available from the exhaust gas after it has gone through the turbochargers (i.e. medium quality heat source) or scavenge air after the compression process (i.e. low/medium quality heat source), being the two largest source of waste heat on the vessel (see Figure 8 as an example).

Several papers have highlighted the advantages of cogeneration or even trigeneration [Ziegler & Riesch 1993; Saavedra et al. 2010] with good levels of efficiency. In chapter 7, the focus is on cogeneration with priority for energy usage for steam generation followed by electrical power production by a thermodynamic WHRS when the waste heat energy is coming from the exhaust gas. In chapter 8, the exhaust gas is used only for electrical power production, while in chapter 9 the power production comes from the waste heat available in the scavenge air, and steam demand is covered fully by the exhaust gas waste heat.

The thermodynamic WHRS is studied without any other emission reduction or energy efficient technology on board, such as scrubbers or power turbines. The WHRS plant layout will be simple or recuperative (see Figure 18 and Figure 20) depending on the heat quality, operating

conditions and working fluid. While other more complex thermodynamic layouts (e.g. multi-pressure or more than one expander in cascade layout) can improve the WHRS power output, their overall difference compared to a simple/recuperative plant will be minimal when counting the additional plant's size, cost and complexity. Taking this decision saves simulation and programming time, plus it gives flexibility to be easily applied to other different waste heat sources. However, the author recognises that complex plants integrated to other technologies, such as a power turbine, should be explored as future research.

A detailed design of the heat exchanger has been excluded from this chapter since the focus is mainly on the thermodynamic behaviour of the WHRS and its broader implications on board a vessel. Still, in chapter 8, some basic assumptions are made to quantify better the off-design performance and requirements of the waste heat plant. In chapter 9, since the centre of attention is the study of the WHRS' bottoming section the code from Pierobon et al. [2014] will be used to design the shell and tube condensers, and the code from Kærn et al. [2013] for finned tube coolers.

The detailed study of the thermal oil circuit, such as pressure drops and power requirements to move thermal fluid, was out of the scope of this thesis. The research will only take into consideration that by using, when required, a thermal oil in between the waste heat and WHRS, there will be a reduction in waste heat quality due to the approach temperature restrictions established in section 6.6.4.

The cost analysis is limited to the average of what was found by Quoilin et al. [2013] and Cunningham [2002] whose data probably came from land-based systems rather than marine. The costs used in this thesis are estimates, which are based on different assumptions over the years. The volatility of marine fuel prices makes difficult to predict profits along the vessel operational life. Payback periods depend on how the marine WHRS is operated which is highly uncertain. However, under the same assumptions, the relative values when comparing the financial performance of the different WHRS bring a suitable comparison. A more detailed cost study is seen in Astolfi et al. [2014] or in the work of Bejan et al. [1995] who include installation costs and other ancillary expenditures as important financial considerations. This approach was deemed beyond the scope of this comparative work, but it is important to assess all aspects of a marine WHRS.

7

SENSITIVITY ANALYSIS FOR DIFFERENT WASTE HEAT RECOVERY SYSTEMS ON BOARD A VESSEL

Based on Suárez de la Fuente, S. & Greig, A., 2015. Making shipping greener: comparative study between organic fluids and water for Rankine cycle waste heat recovery. *Journal of Marine Engineering & Technology*, 14(2), pp.70–84.

When a ship is navigating a route during different times of the year, the operative conditions change. Weather, regulation constraints and crew can have an important effect over the ship's power requirement which in turn will impact the waste heat quality and availability. This will have a knock-on effect on the marine WHRS and the benefits that the system can deliver to the ship's operator and environment. As seen in the work of Tien et al. [2007], changes in the exhaust gas temperature and mass flow rate have an important effect on the design and performance of marine WHRS.

This chapter will assess the performance and sensitivity of a marine WHRS on board a large container ship – 14,770 TEU – at its 75% Maximum Continuous Rating (MCR), which is assumed to be its design point. The study will modify the WHRS structure (e.g. recuperator) and operating conditions (e.g. high pressure and superheating temperature), but also the type of fuel used on board. These changes emulate what a ship designer may face when analysing the use of available waste heat and the cost in performance for each decision taken. The base WHRS design and its operating conditions will be first defined in order to then modify them as follows:

- Change in the WHRS high pressure.
- Change in seawater and air temperature.
- Change of fuel.
- Expander's inlet temperature.
- Change of plant layouts for the marine WHRS ORC (i.e. recuperator and thermal oil circuit).

The main focus will be the net electrical power output coming from the marine WHRS, while examining other important parameters, such as the thermal efficiency and mass flow rates. The costs will not be assessed in this chapter since the analysis will be made only at the design point. At the end of the chapter, the change in the vessel's fuel, CO_2 emissions and EEDI reductions will be discussed.

7.1 DIESEL ENGINE AND EXHAUST GAS

The engine used for this case study is an 82.4 MW 12 cylinder two-stroke slow speed diesel manufactured by MAN Diesel & Turbo. The engine's model is G95ME-C9.5-TII with four turbochargers [MAN Diesel & Turbo 2014a]. It is capable of working with both HFO and MDO. It is assumed that the vessel is designed for ISO conditions which means that the ambient – air – temperature is set to 25°C. The vessel's steam demand at ISO conditions is found by using equations [52] to [54] and give around 2,716 kg/h. The seawater temperature is assumed to be 5°C above the air temperature per the annualised temperature difference between air and the seawater around the oceans [Rayner 2003; Rayner et al. 2006; Jones et al. 2012]. The container ship has a size of 156,907 dwt and achieves at design point (i.e. at 75% MCR and a speed of 24.0 kn) an EEDI of 12.569 g CO_2/t-nm, when not considering its auxiliary power and no fuel saving technology on board [The Baltic and International Maritime Council 2013].

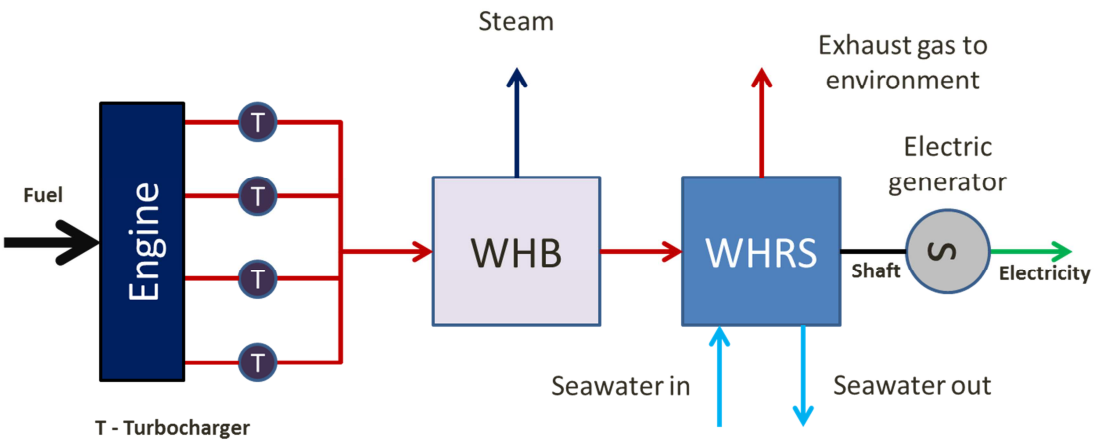

Figure 59: Overview of the WHRS on board the container ship.

In its base design as shown in Figure 59, the marine WHRS uses the waste heat available from the exhaust gas after it has passed the turbochargers and the waste heat boiler (WHB). Since the fuel has sulphur in its composition it is expected that the exhaust gas will contain SO_x. To avoid sulphuric acid condensation, the exhaust gas cannot be lower than the temperatures shown in Table 9, but in the case study – and also in the following result chapters – a safety margin of 5˚C will be added, allowing for any temperature fluctuation in the economiser. This will mean that the WHRS economiser will be able to extract energy until the exhaust gas reaches a temperature of 164°C when using HFO or 132°C when the vessel uses low-sulphur MDO.

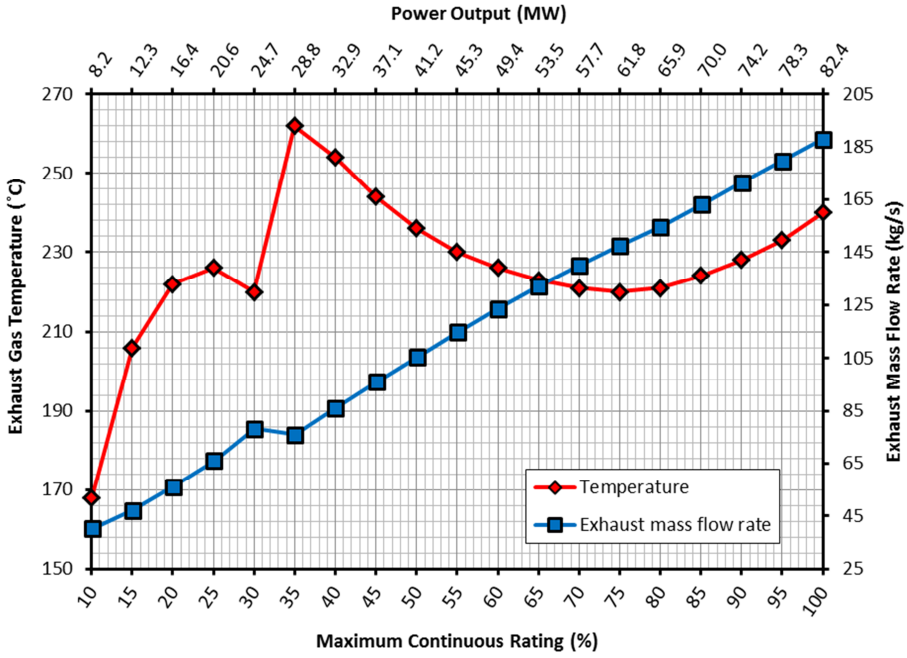

Figure 60: Engine performance and exhaust gas behaviour when using MDO on board the container ship. Taken at ISO ambient reference conditions [MAN Diesel & Turbo 2014a].

Figure 60 represents the engine's loading conditions that extend from 15% to 100% MCR in steps of 5%. At 75% MCR the exhaust gas temperature when using MDO is 218°C and a mass flow rate of 180 kg/s – or 215°C and 188 kg/s when using HFO per the calculations performed in section 5.1.5.

7.2 WEATHER CONSIDERATIONS

In this sensitivity analysis, the air temperature is modified in order to understand the change in the marine WHRS performance and design parameters. The relevant WHRS areas affected by a change in the air temperature are: A) the steam demand which is covered by equations [52] to [54]; B) exhaust gas temperature handled by the linear relationship recommended by MAN Diesel & Turbo [2014d] which is a decrease of 1.6°C in the exhaust gas for each 1°C from the intake air temperature; and C) the exhaust mass flow rate which is adapted via a linear relationship taken from the data of the engine's manufacturer (see Figure 61).

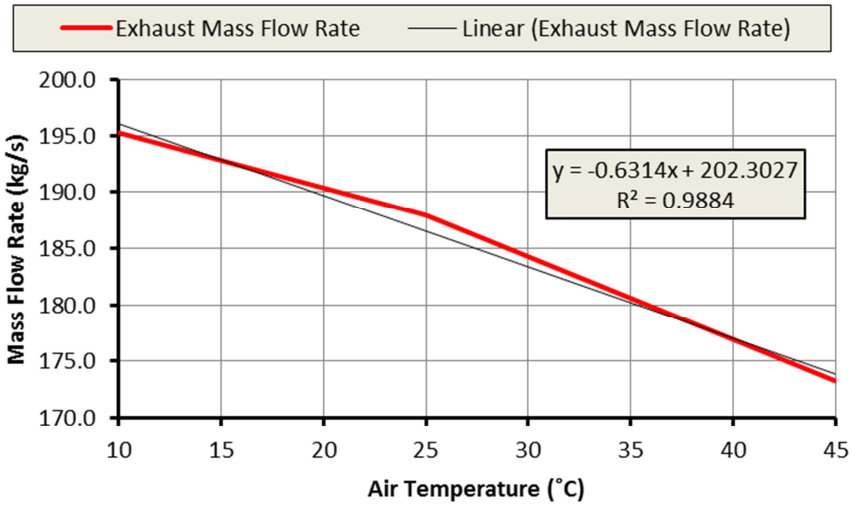

Figure 61: Change of the ship's exhaust gas mass flow rate with the variation of the air temperature using MAN Diesel & Turbo data [2014a].

7.3 WORKING FLUIDS

The working fluids selected were water, heptane, benzene, toluene and hexamethyldisiloxane (MM) due to their performance as identified by Saavedra et al. [2010] and their low global warming potential (GWP).

Due to the nature of the organic fluids a thermal oil between the waste heat source and the WHRS is used.

7.4 WASTE HEAT RECOVERY SYSTEM

The study will cover the simple and recuperative plant layout with or without thermal oil. The WHRS expander will be connected to an electrical generator which will produce part of the electrical demand on board the container ship.

Figure 62 represents all the equipment examined, which will be turned on or off in the code depending on the working fluid or by the author in order to be able to see the variables' relevance on the WHRS power production. The terminology and numbering shown in Figure 62 will be used throughout the chapter, while the equations used were developed in the Methodology chapter.

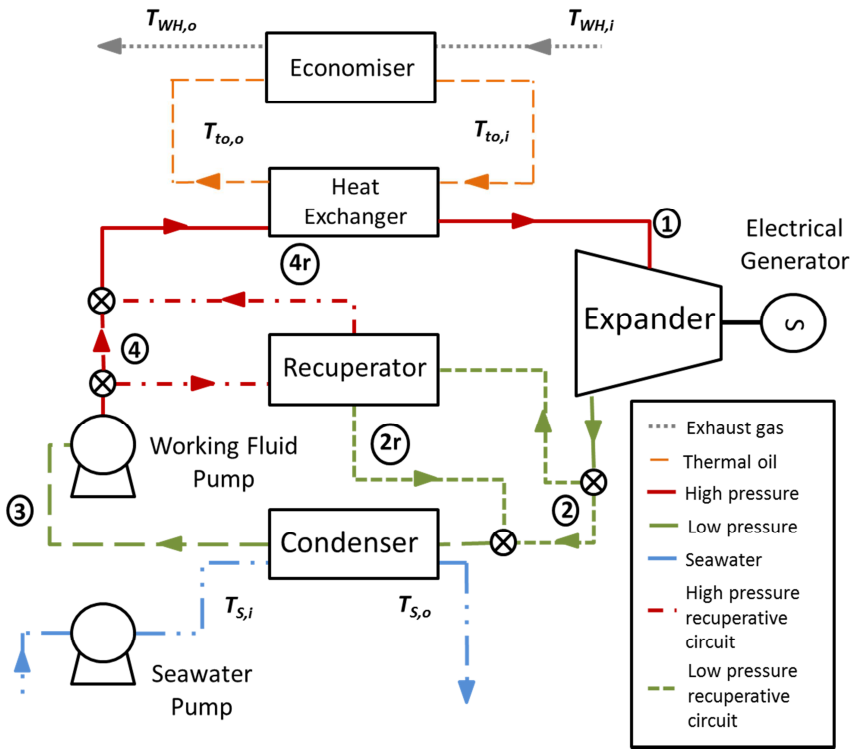

Figure 62: WHRS layout including recuperator and thermal oil circuit.

Table 15: Operating parameters for the reference case. These parameters will be varied to investigate their impact on the WHRS power output.

Equipment	*Variable*	*Value*
Expander		
	Inlet temperature, T_1 (°C)	$T_{WH,i} - 5$ *or* $T_{to,i} - 5$
	Min. exit pressure, (kPa)	20
Condenser		
	T_{ap} (°C)	≥ 5
	$\Delta T_{pp,C}$ (°C)	5
	Inlet Sink Temperature, $T_{S,i}$ (°C)	30 – Variable, depending on subsection
Pump		
	Inlet temperature, T_3 (°C)	Liquid saturation temperature at low pressure
Heat Exchanger/Economizer		
	T_{ap} (°C)	≥ 5
	$\Delta T_{pp,H}$ (°C)	5
	Inlet Source Temperature, $T_{WH,i}$ (°C)	Per Figure 60 and adapted for HFO
	HFO (MDO) minimum exit Source Temperature, T_{WH,o_min} (°C)	164 (132)
Recuperator		
	T_{ap} (°C)	≥ 5
Steam		
	T_{in}(°C)	50
	T_{out}(°C)	$T_{H,i}$ -5
	P_{steam} (kPa)	700

The reference design will include the thermal oil – if required – and a recuperator – if the conditions from 6.6.3 are met. Table 15 shows the different constraints and conditions imposed on the different parts of the WHRS and WHB model. All WHRS isentropic efficiencies were

assumed to be constant at 80%; the generator had an efficiency of 97% while for the WHB the thermal efficiency is set at a constant 85%. Also, it was assumed that there are no pressure changes except for the expander and pump; no heat losses, no leakages and the problem is solved as a steady-state operation.

7.5 OPTIMISATION APPROACH

The model iterated the high pressure level in steps of 10 kPa up to the critical pressure (P_{cr}) of each working fluid keeping all other variables constant. The iterative process stopped when the critical pressure was reached or when the working fluid saturation temperature was higher than the value set for the expander's inlet temperature (T_1) in Table 15. The purpose of the iterative process was to find the WHRS maximum net electrical power output for a given engine load. This simple optimisation strategy allows for an understanding of the effects of gradual changes in the design, making it easier to explain what is happening inside the WHRS.

Equation [31] finds the working fluids' mass flow rates ($\dot{m}_{wf}$) using the heat available in the economiser/heat exchanger subcooler region (i.e. between points 4 and 4a in Figure 47), the optimisation algorithm also has the function of finding at what pressure the WHRS design is viable. The working fluid mass flow rate is set as the maximum mass flow rate possible which falls inside the restrictions set by the pinch point temperature and exhaust gas exit temperature. Since the algorithm will be changing the WHRS high pressure to find the most powerful system, the calculated working fluid mass flow rate would be different and not follow the restrictions imposed in Table 15. A lower mass flow rate than that set by $\dot{m}_{wf}$ will not be able to absorb all the energy available at the subcooler region but it will still be inside the restriction limits. On the other hand, a larger mass flow rate could cause a temperature cross over at the hot side of the economiser or an exhaust temperature below the limits imposed. In order to check how the mass flow rate behaves at different pressures, an "alternative" mass flow rate is calculated using the waste heat available in the evaporator and superheater (i.e. points 4a and 1 in Figure 47):

$$\dot{m}_{wf,ev-sh} = \frac{\dot{Q}_{WH} - \dot{Q}_{WH,sc}}{(h_1 - h_{4a})} \qquad [\ 89\ ]$$

Where $\dot{m}_{wf,ev-sh}$ is the mass flow rate required to absorb all the energy available in the evaporator and superheater. The logic of the algorithm will eliminate WHRS designs that do not comply with the restriction shown in equation [90], which guarantees that there is no temperature crossover inside the heat exchanger:

$$\dot{m}_{wf} \geq \dot{m}_{wf,ev-sh} \qquad [\ 90\ ]$$

With the mass flow rate established, the other WHRS variables can be found.

7.6 OPERATING HOURS

It was assumed that the WHRS would be installed in a ship that is in operation for 6,480 hours

per year (i.e. it is in use around 75% of the time). The operating profile, shown in Figure 63, is similar to that found for a 14,000 TEU ship [MAN Diesel & Turbo 2012b].

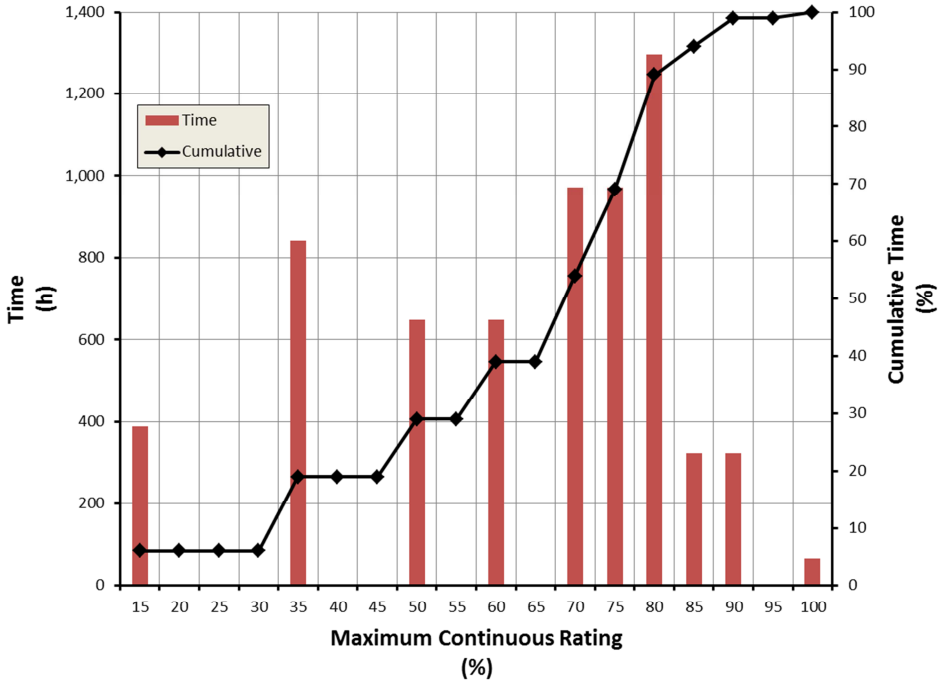

Figure 63: Ship's annual operating profile while at sea in percentage and hours per year.

7.7 Model Validation

The code was validated against results presented by Butcher and Reddy [2007] and Saavedra et al. [2010]. The validation process indicated that the WHRS model had an agreement to within 1.4% of the results given by Butcher and Reddy [2007]. This difference is caused mainly due to visual measurement errors when reading the mass flow rates and pinch point temperature graphs from the paper, data tables were not available. When the model is compared against the work of Saavedra et al. [2010] the difference was 0.95%, a small difference due to the different approaches used to calculate the thermodynamic properties of the working fluids. Saavedra et al. integrated the Peng-Robison Stryek Vera equation of state, while in this work the data was extracted from NIST Refprop 9.0 [Lemmon et al. 2010].

7.8 Results and Discussion

7.8.1 Effect of the High Pressure

In the first subsection, the different WHRS performances were found for different pressure levels at the expander's entrance (P_1) as stated in section 7.5. The WHB leaves available more than 8,400 kW from the exhaust gas at a temperature of 202˚C when the vessel consumes HFO.

As per the constraints given in section 7.4, T_1 and $T_{pp,H}$ are fixed throughout all the simulations, so as P_1 increases, the latent heat and h_1 are reduced which also decreases the mass flow rate and power output. This behaviour can be seen Figure 64 where the maximum electrical power output is seen at the lowest possible P_1. Benzene is the working fluid that produces the largest

electrical power but is also the most thermal efficient system as can be seen in Table 16. On the other hand, this WHRS along with the water-based RC have a higher high-pressure – almost double in all cases – than the other three organic fluids. This would mean that they may require thicker pipes and better seals throughout the systems circuit which will increase the installation cost for the WHRS. However, the maximum pressure for the benzene WHRS (i.e. 761 kPa) is below any pressure limit for any seamless pipe size – diameter and wall thickness – meaning that the same pipes can be used for any marine WHRS [The American Society of Mechanical Engineers 2014; ASTM International 2015].

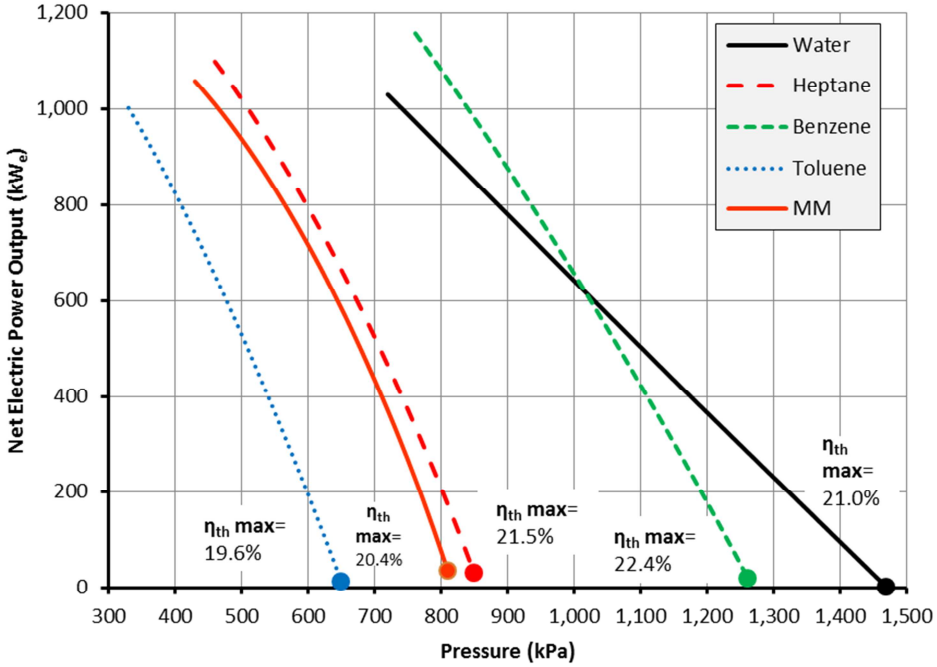

Figure 64: WHRS electrical net power output at 75% MCR including the power requirement from the seawater pump at different P_1. The plot also shows where the WHRS' maximum thermal efficiencies occur.

As the pressure increases, so does the working fluids' saturation temperature, reducing the heat absorbed by the cycles. So even though the thermal efficiency increases, the total power output declines as seen in Figure 64. At low pressures, the saturation point is reached at lower temperatures, allowing the working fluid to absorb more heat from the waste heat source. The power demand from the pumps begins to dominate as the pressure increases, causing a reduction in the thermal efficiency gradient (see Figure 65). All working fluids increased their thermal efficiency as the high pressure increased. This behaviour is caused by equation [46] which measures thermal efficiency with respect to the heat absorbed, and not by the total heat available at the exhaust gas.

The behaviour of the WHRS thermal efficiency, as measured in this work, is also discussed by Liu et al. [2004] but instead of using the pressure as independent variable they use the saturation temperature. In their study benzene delivered a maximum thermal efficiency of 21.6% while toluene achieved the lowest at 19.2%.

Table 16: Maximum net electric power output achieved by the different working fluids. The first column shows the electrical power output not including the power demand from the seawater pump, while in the second column this is considered. The final two columns give the high pressure and thermal efficiencies when the maximum net electrical power output is achieved.

Working Fluids	$\dot{W}_{e,T}$ (kW_e)	$\dot{W}_{e,WHRS}$ (kW_e)	P_1 (kPa)	η_{th} (%)
Water	1,035	1,029	720	17.8
Heptane	1,107	1,098	460	19.1
Benzene	1,228	1,157	761	21.3
Toluene	1,007	1,001	330	17.2
MM	1,065	1,058	430	18.5

As previously explained, as P_1 increases, the heat absorption is diminished which causes a lower mass flow rate for any of the working fluids, this pattern is similar to that seen for the electrical power output. The difference seen in Figure 66 between water and the organic fluids is mainly to do with water having the highest specific heat of all the working fluids tested which means that if they are carrying the same amount of energy, the mass flow rate will be lower. Hexamethyldisiloxane's mass flow rate is the largest at 20.8 kg/s at the highest electrical power production, while water exhibits the lowest at 2.3 kg/s. Hexamethyldisiloxane is also the most sensitive to a change in high pressure with a slope of -5.2×10^{-2} kg/kPa-s, while water is -3.1×10^{-3} kg/kPa-s.

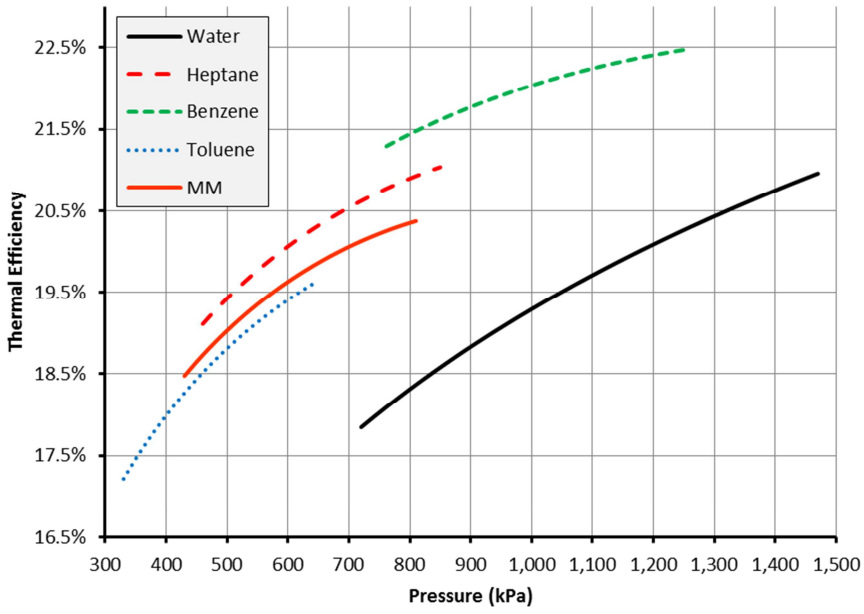

Figure 65: Thermal efficiency achieved by the working fluids at 75% MCR.

At higher pressures the heat absorption and the WHRS' electrical power output are greater, but so is the heat rejection to seawater since not only is there more heat in the system but the WHRS is also less efficient, as seen in Figure 65. This causes the seawater mass flow rate to reduce as the WHRS P_1 increases. At larger WHRS pressures the seawater mass flow rate

reduces considerably and since its pressure increase is only 200 kPa, the power inputs for both seawater and working fluid pumps are similar (see Figure 67). It is seen from the same figure that the seawater pump requires more power, especially at higher WHRS pressures, than the working fluid pump, except in the case of MM where the working fluid mass flow rate is considerably higher (see Figure 66).

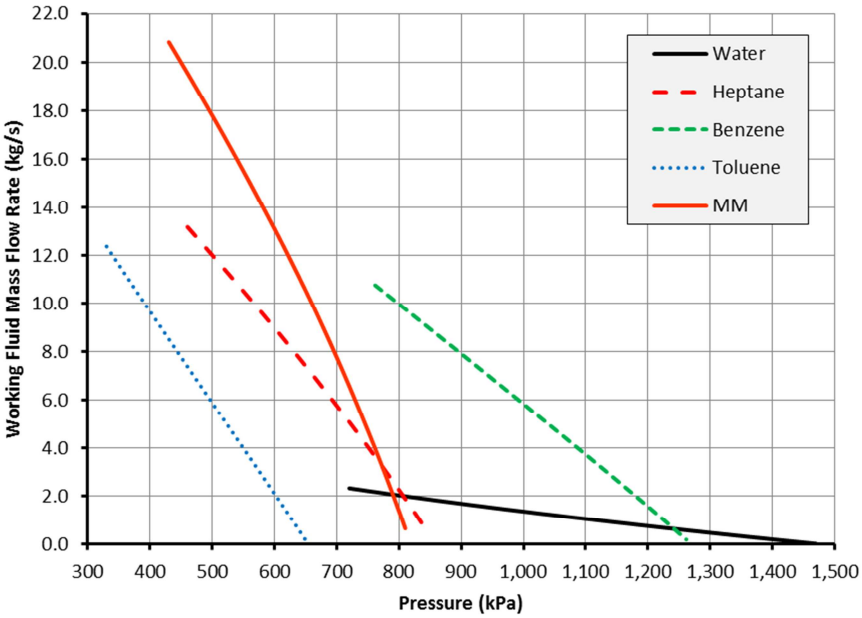

Figure 66: Working fluid mass flow rate for the different operating high pressures in the WHRS.

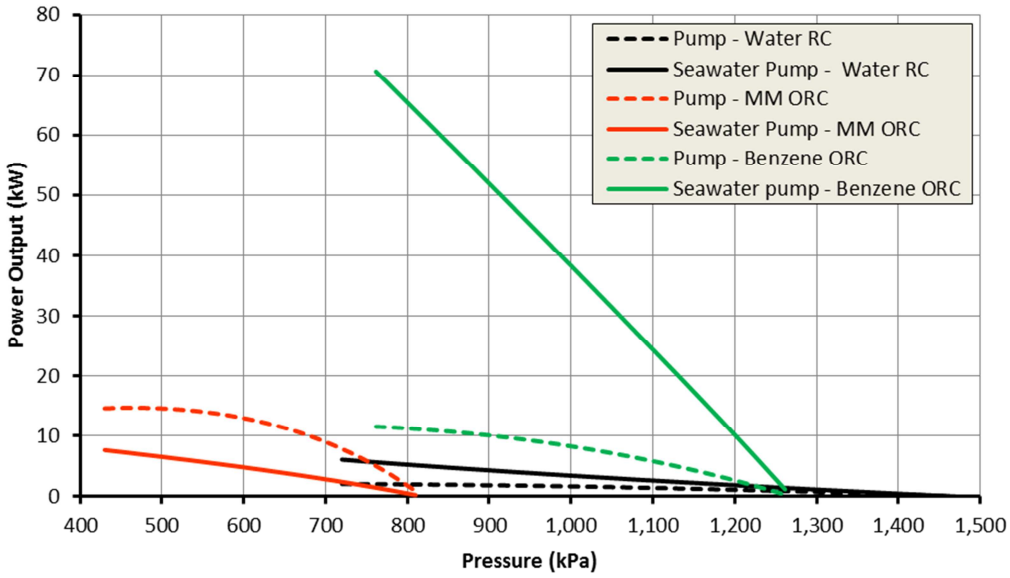

Figure 67: Power input requirement from some of the working fluids tested. Seawater pump power input is represented by a solid line, while the working fluid pump power requirement uses a dashed line.

The high power requirement for benzene's seawater pump – the net electrical power output reduces by around 71 kW_e due to this pump (see Table 16) – is due to the pinch point constraint (i.e. 5°C), the small temperature difference between the saturated point at 22 kPa (i.e. 38°C) and the seawater inlet temperature (i.e. 30°C), having only 3°C available for the seawater

temperature to rise. This means that in order to effectively remove the excess heat in the working fluid, the pump will be required to move large volumes of seawater hence larger power inputs (see Figure 67). By increasing the low pressure of the system to 27 kPa – an increment in the saturation temperature of around 5°C – the seawater mass flow rate is reduced from 570 kg/s to around 155 kg/s, losing 3.5% of the expander's power output (i.e. from 1,280 kW to 1,235 kW). However, due to a lower power input requirement from the seawater pump, the net electric power output reaches 1,167 kW_e – an improvement of around 10 kW_e. The other systems do not benefit from this rise in the WHRS lower pressure side, since the power cost to the expander is much higher than the reduction in the seawater power input.

7.8.2 Effect of the seawater and air temperature

For the analysis of the effect levied by air temperature – hence also the seawater temperature – on the WHRS power output, the air temperature will be changed in steps of 5°C from -5°C to 30°C as per the discussion in sections 5.1.1 and 5.1.2. This will have a direct effect on the heat availability and quality which will be adjusted as per section 7.2.

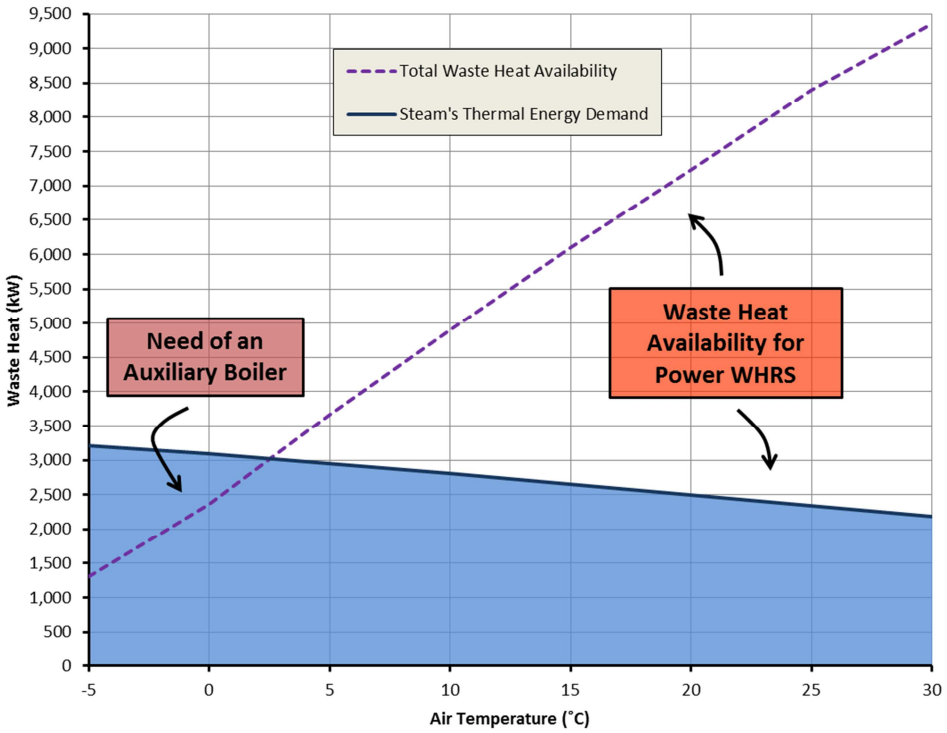

Figure 68: Representation of the total waste heat availability for both the steam and power generation on board the ship at the 75% MCR. The available waste heat for power production is delimited by the steam's energy demand and the total waste heat available.

The first important thing to analyse is how the weather conditions affect the waste heat availability and quality on board the vessel. As the air temperature reduces, the larger the heating demand on board becomes, as described by equation [53], and shown in Figure 68. Also important: the exhaust gas temperature is lower at colder air temperatures, as explained in MAN Diesel & Turbo [2013a], leaving the WHB with a shorter operating temperature range – being the lower limit of the exhaust gas dew point – and not being able to cover fully the steam demand with the waste heat available. This can be improved, as recommended by MAN Diesel

& Turbo [2013a], through bypassing the turbochargers but also by complementing the steam generation with other waste heat sources such as the scavenge air. In the case study presented in this chapter these recommendations are not explored.

For the container vessel there is the need to use an auxiliary boiler to cover the heat requirements on board when the air temperature is below 3˚C. As the temperature increases, so too does the waste heat availability, but also the heat demand of the vessel reduces from 3,876 kg/h at -5˚C to around 2,500 kg/h at 30˚C.

Between an air temperature of 3˚C and 8˚C, it is possible to start using the exhaust gas waste heat to produce power, but the benefit will be minimal due to low waste heat availability and exhaust gas temperature (see Figure 69). The WHRS will be operative up to an air temperature above 8˚C while navigating at 75% MCR, since it is until this temperature that considerable heat availability and quality is found from the exhaust gas after the WHB.

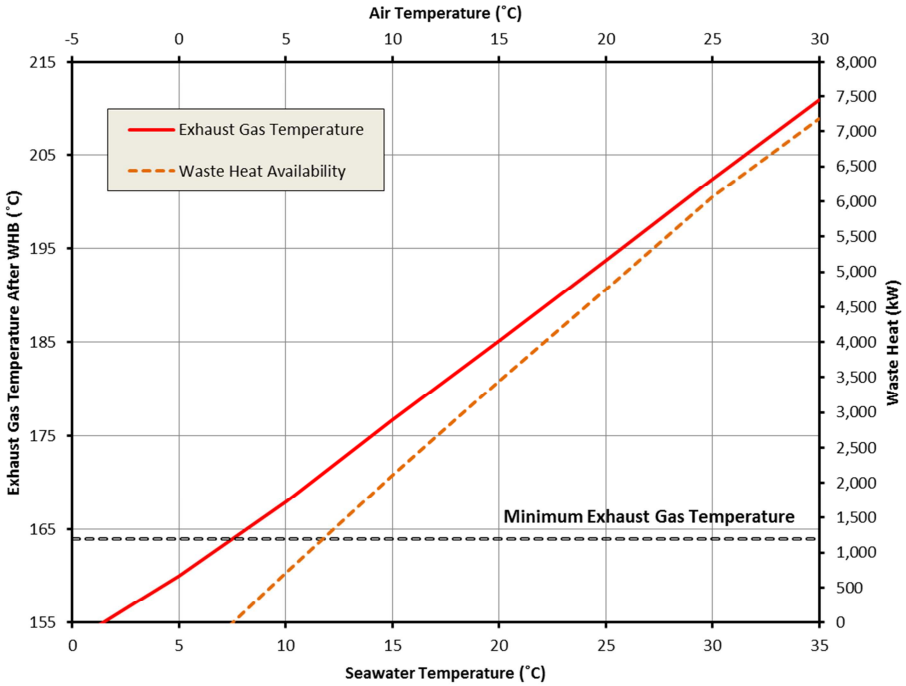

Figure 69: Waste heat availability for its use to assist in the vessel's power production. The solid line represents the exhaust gas temperature after the WHB for the different ambient conditions. The dark dashed line represents the minimum temperature of 164˚C for the exhaust gas.

The electrical power production for the different WHRS follows a linear trend with the air temperature which has to do with the waste heat availability after the WHB. The benzene ORC is the WHRS that produces the most electrical power, having more than 75 kW_e between an air temperature of 15˚C and 20˚C than the second best fluid. This difference reduces considerably at 30˚C since the seawater's pump power consumption increases – due to more waste heat entering the WHRS – to 87 kW_e which represents 6.4% of the net electrical power production. All WHRS show an important power drop as the air temperature reduces, of which the most affected is heptane with a drop of more than 980 kW_e while toluene is the least affected at

876 kW_e. At the lowest air temperatures in which the WHRS can still operate, the difference between working fluids is negligible and the preferable fluid is water due to its simplicity and safety (see Figure 70).

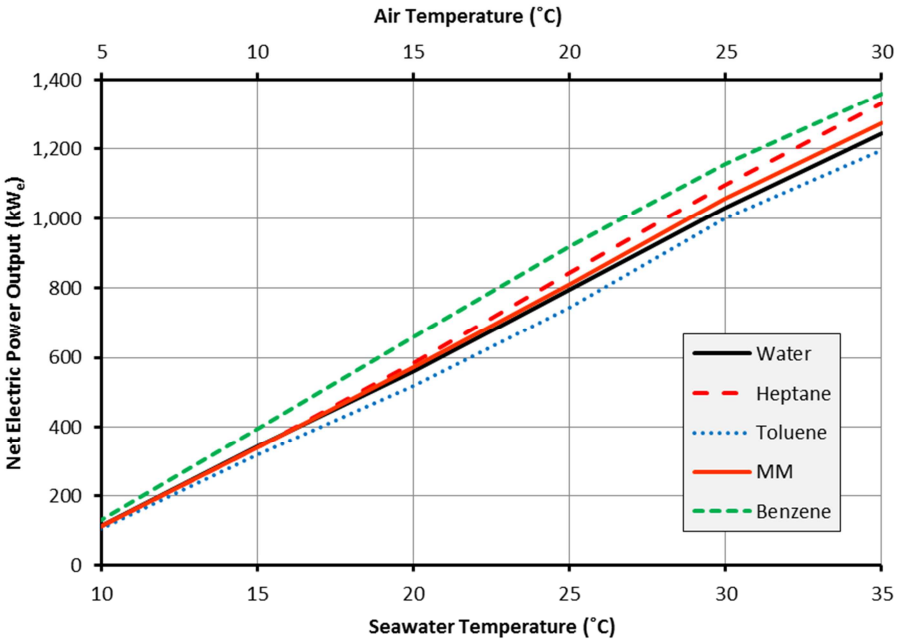

Figure 70: WHRS net electric power output for different air and seawater temperatures.

Saavedra et al. [2010] studied the effects of changing the sink temperature while keeping constant the inlet temperature and waste heat mass flow rate. They found that by changing the sink temperature from 35°C to 90°C there was a 35% drop in power output when using n-heptane, 37% for water and 39% for toluene. For this study, an increase in temperature produces an increase in power output. The different behaviour to the study of Saavedra et al. [2010] is caused by the increase in waste heat availability due to a lower steam demand which shadows the loss of power as a result of a higher saturation temperature at point 3 in Figure 62. There is a power increase of 74% for heptane, 72% for water and 73% for toluene when the seawater temperature changes from 10˚C to 35˚C. It is probable that the WHRS power production will drop if the sink temperature increases above 35°C, which is only possible if the sink has changed from the ocean to another ship system on board that requires the waste heat coming from the WHRS. An example of this is seen in the work of Choi and Kim [2013] where the waste heat from a trilateral cycle is used to power a secondary ORC.

7.8.3 Effect of fuel

In this subsection, the effect of changing fuel on the marine WHRS electrical power production is measured under ISO conditions. The most important aspect of such a fuel change is due to the lowest temperature exhaust gas that is allowed before reaching the sulphuric dew point. For the same engine at 75% MCR the waste heat available when using HFO is around 8,400 kW and for a low-sulphur MDO is 13,300 kW – a difference of more than 55%.

The lower exhaust temperature limit due to the use of MDO (i.e. 132˚C) forces, in order to absorb the most energy possible from the waste heat source, a lower P_1 than that required for

HFO. This has a knock-on effect over the degree of superheating (i.e. the difference between the saturation temperature and T_1) and the working fluid's mass flow rate. Reducing P_1 will effectively, in this model, increase the degree of superheating and thus the enthalpy difference between the liquid saturation point and h_1. It is important to note that when speaking of enthalpy in this chapter and onwards it is referring to the specific enthalpy. The system that takes the most of the advantage of this increment of waste heat availability is benzene which increases its mass flow rate by around 88% while only losing around 16% in the enthalpy drop between points 1 and 2 (see Table 17). The power output for the benzene ORC changes from 1,157 kW_e to 1,812 kW_e as seen in Figure 71.

Table 17: System operational parameters under different fuels when the vessel is operated at its 75% MCR and under ISO conditions.

Working Fluids	Superheating Temperature (°C)		Mass Flow Rate (kg/s)		Waste Heat Absorbed (%)		Enthalpy Drop (kJ/kg)	
	HFO	MDO	HFO	MDO	HFO	MDO	HFO	MDO
Water	31.3	62.6	2.3	4.1	98.7	98.7	462.3	374.8
Heptane	32.6	63.7	13.2	20.5	98.6	82.3	87.5	72.0
Benzene	28.8	66.5	10.7	20.2	98.3	99.0	119.1	99.8
Toluene	34.2	64.6	12.4	20.0	99.5	86.0	84.5	67.0
MM	33.5	60.0	20.8	29.3	98.1	77.4	53.5	45.4

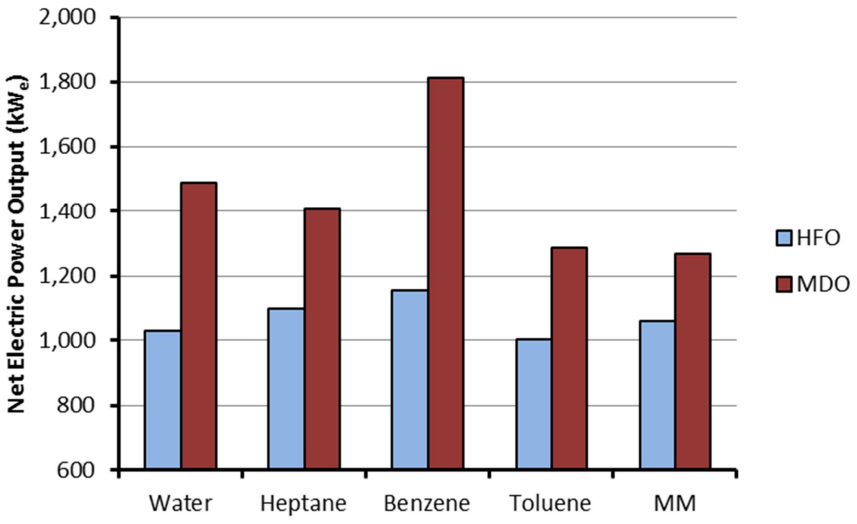

Figure 71: Change of electric power output when the fuel is switched.

Heptane, toluene and MM achieve comparatively lower power output increments when using MDO. Referring to equations [89] and [90], a larger enthalpy difference between the different economiser sections will cause smaller mass flow rate limits. Equally important, P_1 – pressure before the expander entrance – can be lowered until it is operationally unfeasible and in the case of heptane, toluene and MM this limit has been reached. This limitation has an effect on the amount of waste heat absorbed. As seen in Table 17, all working fluids absorb almost all the waste heat available after the WHB when using HFO, but when switching to MDO this falls

below 90% for the three ORC. The lower waste heat absorption will mean that proportionally these three organic fluids will require smaller mass flow rates than the other two working fluids, thus producing lower power outputs. The smallest increments in mass flow rates when switching from HFO to MDO are found as 55%, 61% and 41% for heptane, toluene and MM respectively.

The lower mass flow rates explain part of the reason of the organic WHRS diminishing performance when compared to benzene and water upon switching to MDO. The other part has to do again with a lower P_1 but now in the expansion process. With a lower P_1, and remembering that T_1 is constant, there is an enthalpy drop reduction at the expander (i.e. between h_1 and h_2) for which the degree of superheating cannot compensate entirely. This effectively has an adverse effect on the electric power generation of all WHRS of which the largest enthalpy drop when switching from HFO to MDO is seen for toluene ORC at around 20.7%, followed by water at 18.9%.

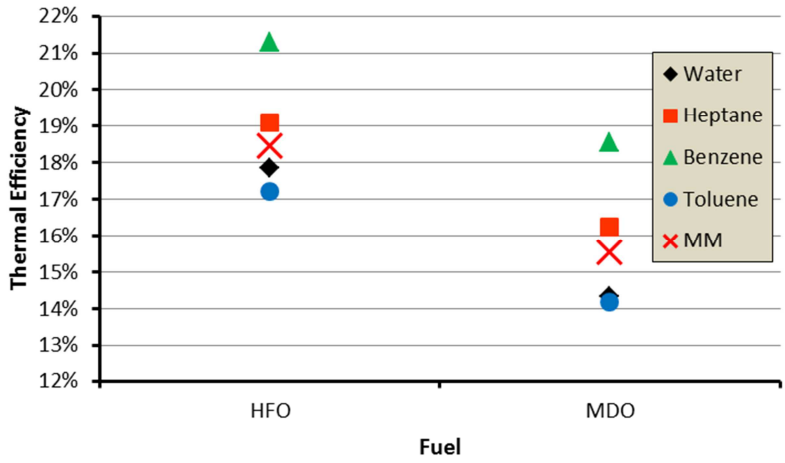

Figure 72: Thermal efficiency change due to variation in the marine fuel used on board for the different WHRS.

The enthalpy drop reduction has an important impact on the WHRS thermal efficiency, as seen in Figure 72. All the working fluids suffer a lower thermal efficiency, but the largest drop in enthalpy difference is seen for water and toluene with 3.5 and 3.0 percentual points respectively.

7.8.4 Effect of superheating

From the literature review in section 3.2, it was shown that the benefit of superheating is not clear and must be tested on a case by case basis. In this subsection, the different marine WHRS will be subjected to different T_1 temperatures, hence different superheating temperatures (i.e. the temperature difference between the saturation temperature and T_1) in order to understand its benefits. The vessel will be using HFO at ISO conditions and the superheating temperatures will range from 0°C (i.e. the saturation temperature) to 30°C in steps of 5°C. The exhaust gas exits the WHB at a temperature of 202°C which limits T_1 to 197°C for water and 192°C for the organic fluids due to the thermal oil.

Benzene has a maximum power output increase due to superheating of 55 kW_e; followed by toluene, MM and heptane with 29 kW_e, 26 kW_e and 17 kW_e respectively (see Table 18). The results in this subsection are in line with what was found by Fernández et al. [2011], Molés et al. [2014] and Calise et al. [2014] where the use of a superheater brings about an improvement in the WHRS power generation when using organic fluids. Water does not benefit from an increase in the superheating temperature with regard to power generation, but a higher superheating degree increases the RC WHRS dryness factor. After expansion, the dryness factor changes from 87.6% to 90.0% with a superheating temperature change of 30°C which reduces the formation of droplets inside the expander, hence the erosion inside the expander can be reduced.

Table 18: Maximum power output found for the different WHRS when changing its superheating temperature.

Working Fluids	$\dot{W}_{e,WHRS}$ no superheating (kW_e)	Maximum $\dot{W}_{e,WHRS}$ (kW_e)	*Superheating Temperature* (˚C)	P_1 (kPa)
Water	1,029	1,029	All	720
Heptane	1,075	1,091	15	500
Benzene	1,109	1,164	25	761
Toluene	965	994	25	340
MM	1,045	1,071	25	450

Benzene reaches the minimum approach temperature of 5˚C after under a superheating temperature of 25˚C where it is not possible to go higher since its temperature would have been close to or above the thermal oil temperature. The same would have happened to the other working fluids if the superheating temperature were to reach 35˚C.

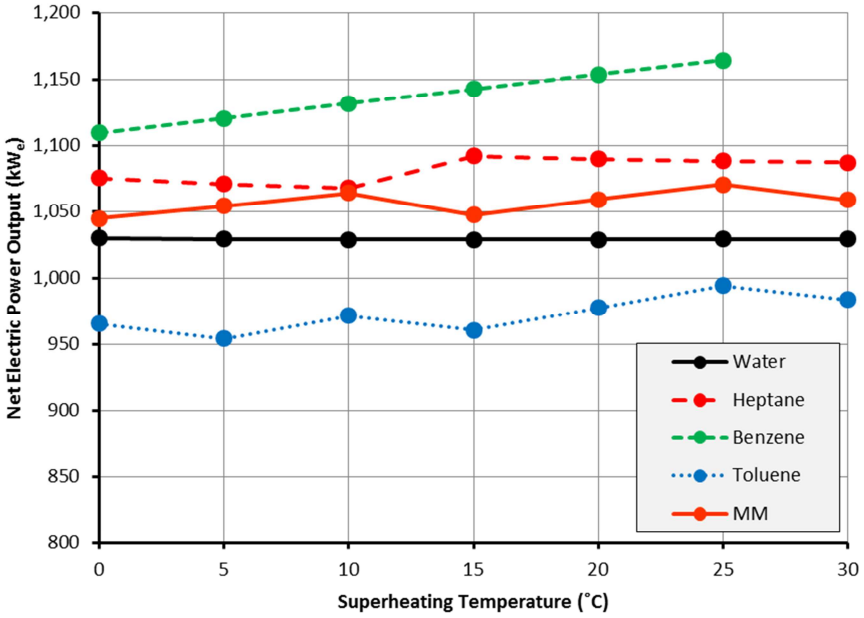

Figure 73: Net electric power generation by the different working fluids at various superheating temperatures.

From Figure 73 it is appreciated that there is not a clear pattern which could define the behaviour of all working fluids analysed with the change of superheating temperature. The next parts of this subsection explain in a clear way what happens with the marine WHRS electric power output. To achieve this, the working fluids are divided into three groups: A) benzene – isentropic organic fluid; B) water – wet inorganic fluid and; C) heptane, toluene and MM – dry organic fluids.

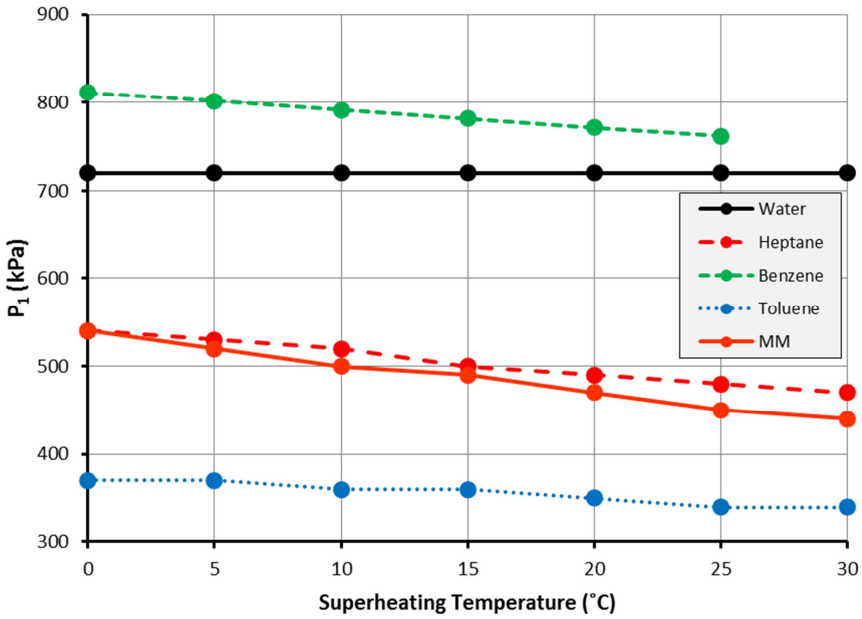

Figure 74: Change in pressure when the superheating temperature is increased.

As the superheating temperature of the WHRS increases, the high pressure of the system reduces (see Figure 74). As per equation [89] the incorporation of the economiser's superheater changes the working fluid's mass flow rate minimum limit at which the WHRS can begin absorbing the waste heat from the exhaust gas. This lower limit allows the WHRS to operate at lower P_1, which – as it was demonstrated in subsection 7.8.1 – as P_1 is reduced, the larger the electrical power output will be if the superheating temperature is held constant.

For benzene ORC there is a reduction in P_1 of around 50 kPa when the superheating temperature is increased by 25°C, caused by the system trying to absorb the most from the heat source. As the superheater temperature increases and the high pressure drops, the heat absorption at the subcooler reduces while increasing at the superheater. Adding the waste heat absorption at these two sections of the economiser shows a constant heat input of around 2,515 kW no matter what the superheating temperature is. From Figure 75, the small losses in waste heat absorption by the benzene ORC – around 7 kW from 0°C to 25°C – come from the evaporator, due principally to a lower mass flow rate which cannot be compensated by a larger enthalpy difference between the liquid and vapour saturated states.

The case for water is different to the other organic fluids since its P_1 stays constant for all superheating temperatures. The increase of superheating temperature at constant pressure causes a reduction of waste heat absorption at the subcooler of around 37 kW, the largest losses are seen at the evaporator at around 164 kW, while the superheater achieves an

increase of 165 kW. The net effect is a waste heat absorption reduction as the superheater temperature increases.

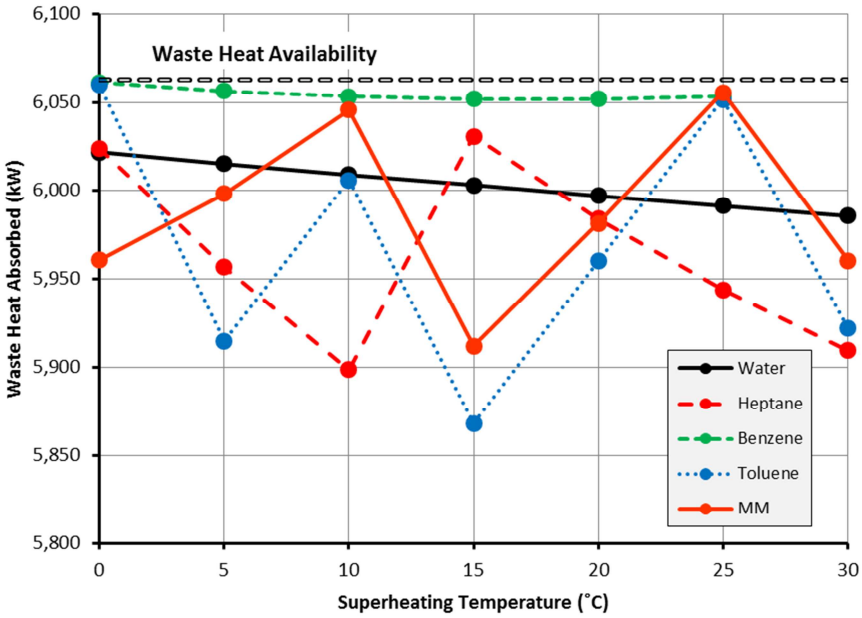

Figure 75: Exhaust waste heat available after exiting the WHB. It also displays how much waste heat is taken by the different WHRS at different superheating temperatures.

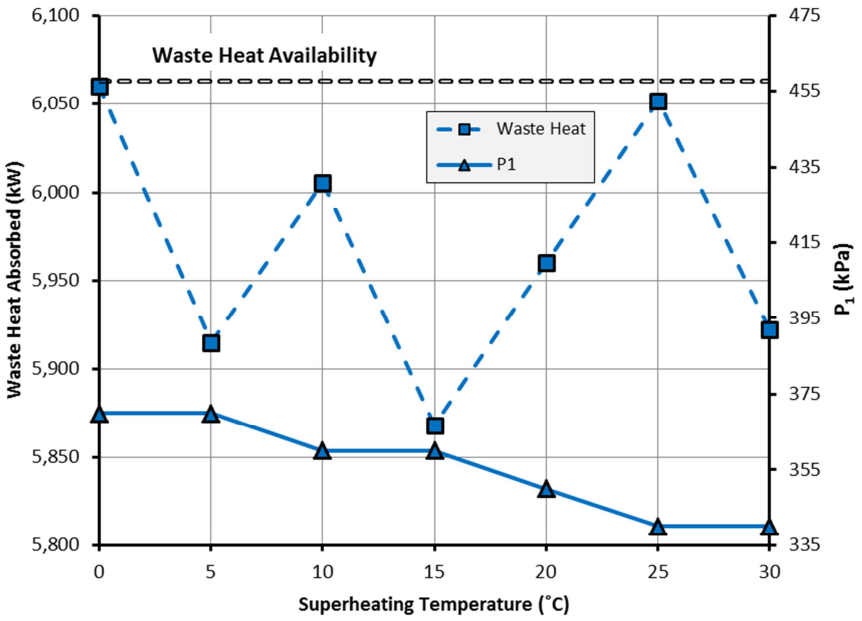

Figure 76: Toluene's high pressure and waste heat absorption for different superheating temperatures.

For the three other organic fluids, P_1 in general reduces as the superheating increases but there are also periods of similar pressure levels at different P_1 step changes. When retaining the same pressure but increasing the superheating temperature, the waste heat absorption reduces. Figure 76 shows this effect in the toluene WHRS, at the step where the pressure reduces, the waste heat absorption increases. This allows toluene and MM to match the waste heat absorption of benzene at different superheating temperatures. Heptane, on the other hand,

drops its absorption capabilities at a less steep rate but requires higher superheating temperature to reach its minimum points, while the contrary happens when achieving its maximum waste heat absorption.

The last piece of the puzzle in understanding how superheating affects the net electric power output of the marine WHRS has to do with the change in the enthalpy at the expander. Reducing the high pressure of a system, keeping the same temperature T_1, will reduce the enthalpy at the expander entrance (i.e. h_1). Keeping the same high pressure but increasing T_1 – superheating – would increase h_1. So, when the optimisation process looks for the most powerful WHRS possible for each working fluid at different superheating temperatures, there is a net effect in the enthalpy drop at the expander shown in Figure 77.

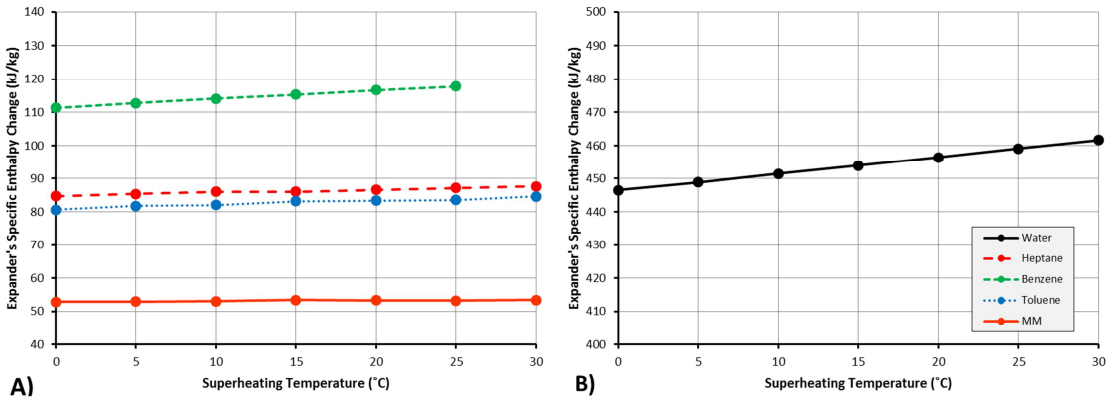

Figure 77: Enthalpy change during the expansion process (i.e. between points 1 and 2). Figure A) shows all the organic fluids while B) shows only the water-based RC.

When changing the superheating temperature from 0˚C to 25˚C, the benzene ORC enthalpy drop increases by 5.8% at expansion which counteracts its mass flow rate reduction of 1.4%. This explains why there is a power increase of around 5.0% when having a superheating temperature of 25˚C.

Water has a negligible reduction in mass flow rate (i.e. less than 0.5%) when increasing the superheating temperature, but overcomes its lower waste heat absorption at higher superheating temperatures by increasing its h_1 by 15.1 kJ/kg. The reduction in waste heat entering the system and the h_1 linear increase explain why the optimisation process found the RC net electric power to be the same at any superheating temperature. For the rest of the organic fluids, their change in enthalpy at the expansion process is almost static with the change in superheating, leaving the waste heat absorption as the main driver of the ORC WHRS power output.

While in this chapter the heat exchanger sizing is not considered, an important note must be highlighted when requiring a superheater section inside the economiser. The overall heat transfer coefficient (U) between two gases is much lower than one when having a heat transfer between a liquid and a gas. For example, a heat transfer between steam and the exhaust gas has an overall heat transfer between 30 W/m^2-˚C and 100 W/m^2-˚C, while water with the

exhaust gas is between 100 W/m^2-°C and 250 W/m^2-°C [Sinnott 2005]. Looking into equation [26] it is seen that as the *U* reduces, so the area required will increase.

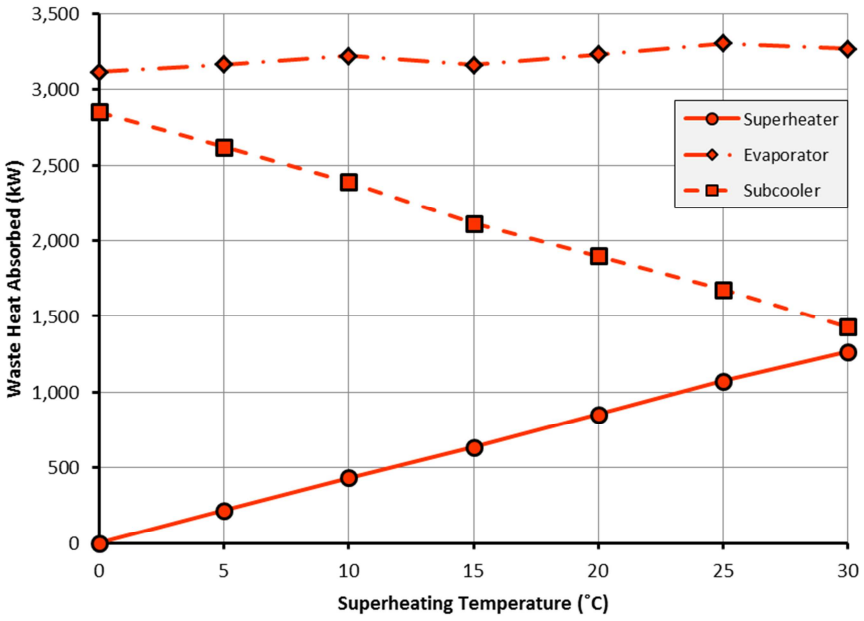

Figure 78: Waste heat absorption at the different economiser's sections for a MM WHRS at different superheating temperatures.

Also, as the heat entering the superheater increases, the area requirement will also grow. Figure 78 shows the heat absorption of the economiser's sections when analysing MM: as the superheating increases, the subcooler region take less heat from the exhaust gas; this will effectively reduce its size. The size reduction in the subcooler will be smaller than the size increment in the superheater due to a lower *U* in this section. Overall, it can be deducted that the total heat exchanger area could be larger on a superheated system than that which only has a subcooler and evaporator. Finally, the marine WHRS designer will have to balance costs and size against the performance achieved by superheating.

7.8.5 Effect of the recuperator

This section presents a comparison between a simple and recuperative cycle in order to understand its benefits for a WHRS. The study will cover only organic fluids, since water after expansion is always inside the saturation bell and it is, therefore, not possible to use a recuperator. The results shown are at the maximum electric net power output, using HFO and at ISO conditions.

When removing the recuperator from an ORC WHRS the working fluid will enter the economiser at a cooler temperature requiring a larger amount of energy to reach its liquid saturation state, assuming P_1 has stayed the same. Due to the pinch point restriction of 5°C and the lower T_4, P_1 must increase. Table 19 shows the change of P_1 between a simple and a recuperative plant layout which causes a larger enthalpy difference between h_4 and h_{4a}. In theory, as per equation [31], could reduce the working fluid mass flow rate. The other reason as to why the mass flow rate reduces is because of the fact that the waste heat availability after the economiser's

subcooler is reduced allowing for a lower limit imposed by equations [89] and [90]. In Table 19, it is also seen that MM loses around 47% of the waste heat availability, with benzene losing around 12% when removing the recuperator. Hexamethyldisiloxane and heptane reduce their mass flow rate the most with a reduction of around 35% and 27% respectively.

On the other hand, an increase in P_1 would have a larger enthalpy drop at the expander, but the relatively small change in high pressure brings an even smaller change in h_1. The largest h_1 change is seen for MM at around 7.9%, while the lowest is for benzene at 1.2%.

Table 19: Parameters for a recuperative and simple ORC WHRS. REC refers to a recuperative plant layout while SIM to a simple WHRS.

Working Fluids	P_1 (kPa)		Enthalpy Increase at Subcooler (kJ/kg)		Waste Heat after Subcooler (kW)		Mass Flow Rate (kg/s)	
	REC	SIM	REC	SIM	REC	SIM	REC	SIM
Heptane	460	580	114.7	325.9	4,551	2,941	13.2	9.6
Benzene	762	812	190.3	258.9	4,018	3,547	10.7	9.7
Toluene	330	380	103.5	211.5	4,784	3,861	12.4	10.4
MM	430	590	66.1	263.9	4,687	2,479	20.8	13.6

The reduction in mass flow rate overcomes the increase in h_1 causing a reduction in the net electric power output of the different simple marine ORC WHRS. Benzene and toluene are the least affected with a power reduction of around 100 kW_e and 125 kW_e respectively, while heptane looses 255 kW_e and MM 315 kW_e. This leaves the RC as the second best marine WHRS just 30 kW_e behind benzene.

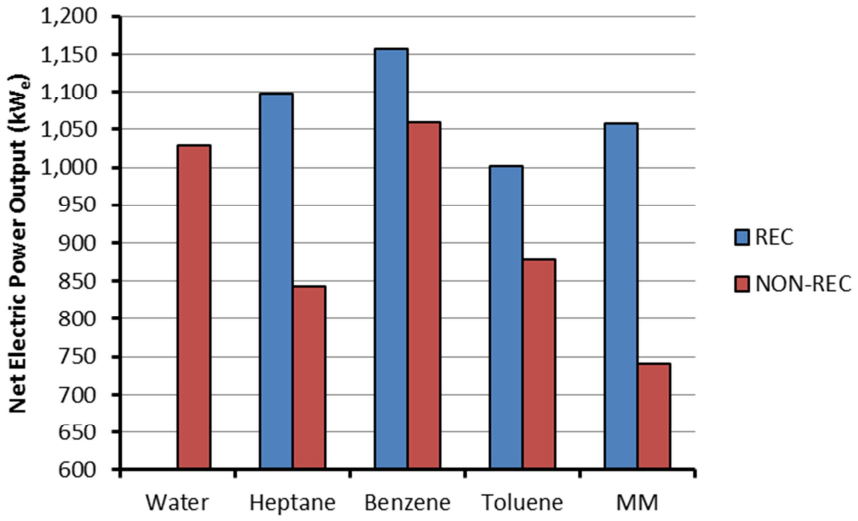

Figure 79: Maximum net electric power output for the different working fluid comparing a recuperative –except for the RC system – and a simple plant layout.

The seawater mass flow rate is larger when having a recuperator caused by larger waste heat absorption in the heat exchanger, hence a larger working fluid mass flow rate. The largest

coolant mass flow rate increase when adding the recuperator is for benzene with 55 kg/s which represents 10% of its seawater mass flow rate without the recuperator. The least affected is toluene with an increment of 7 kg/s, representing 16% of its coolant mass flow rate without a recuperator.

As seen in this subsection, there is a large impact in the net power production of an ORC WHRS when using a recuperator. Power increases of more than 30% are seen while increasing the amount of waste heat absorbed from the exhaust gas of a vessel. The seawater mass flow rate did not increase when analysing a simple layout due to the fact that the recuperative cycle recovers at least 10% more heat.

7.9 Energy Efficiency Design Index Reduction

This last section will show how the WHRS can reduce the EEDI of the container vessel. Without any green technology installed, the vessel's EEDI stands at 12.569 g CO_2/t-nm. In this section, the WHRS per working fluid that achieved the maximum net electrical power output throughout all the previous subsections will be used. The ISO conditions are assumed and the vessel consumes HFO at a rate of 168.4 g/kW-h [31] [MAN Diesel & Turbo 2014a]. It is important to consider that the fuel required by the boiler in order to cover the vessel's steam demand is not considered by the EDDI; hence the usage of a WHB will be ignored for the EDDI calculation. Still, it is important to quantify the amount of CO_2 saved by installing a WHB. At the established conditions for this subsection, the WHB supplies more than 2,700 kg/h of steam which represents 2,345 kW-h of thermal power.

Table 20: WHRS systems that achieved the largest power output found during this chapter where the high pressure, superheating temperature and the WHRS layout was changed.

Working Fluids	$\dot{W}_{e,WHRS}$ (kW_e)	Plant Layout	Superheating Temperature (°C)	P_1 (kPa)	P_3 (kPa)
Water	1,029	SIM	31.3	720	20
Heptane	1,098	REC	32.6	460	20
Benzene	1,167	REC	39.8	747	27
Toluene	1,001	REC	34.2	330	20
MM	1,070	REC	25.0	450	20

To measure the EDDI effect first, the power gains achieved by the WHRS must be translated into CO_2 emission reductions using the main engine fuel consumption and the HFO carbon factor (*CF*) – 3.114 tonnes of CO_2 per tonne of fuel. However, the net electrical power output must be converted into mechanical power by using the generator's electrical efficiency of 97%. Finally, the EDDI reduction due to the use of the WHRS is calculated by equation [79].

[31] The Specific Fuel Oil Consumption is corrected to HFO using the 4.6% increase in fuel consumption from MDO to HFO discussed in section 5.1.5.

The impact of the WHRS on the EDDI is low for either option; the primary reason being that the EEDI is dominated by the main engine's power at design point which is more than 60,000 kW. This power, in comparison to the mechanical power output from the different WHRS, is large. This should not be detrimental to the usages of marine WHRS but as a realisation of the importance of combining technologies and strategies to achieve lower emissions in the most efficient way. As seen in Table 21, benzene brings the largest reduction in the EDDI with 0.171 g CO_2/t-nm leaving the container vessel EEDI at 12.398 g CO_2/t-nm, a reduction of around 1.36%. The lowest reduction comes from Toluene WHRS with 1.17%. Theotokatos and Livanos [2012] used a marine RC WHRS to measure its impact on the EEDI of a bulk carrier and found that it was possible to reduce the EDDI by around 1.80% when using a two-stroke engine. The EEDI value reduction achieved for the RC in this chapter is 1.20%.

Table 21: Impact on the vessel's EEDI due to the use of an exhaust gas WHRS.

Working Fluids	CO_2 Savings (t/h)	EEDI Reduction (g CO_2/t-nm)	Attained EEDI (g CO_2/t-nm)	EEDI Reduction (%)
Baseline	0.00	0.000	12.569	0.00
Water	0.56	0.151	12.418	1.20
Heptane	0.59	0.161	12.408	1.28
Benzene	0.63	0.171	12.398	1.36
Toluene	0.54	0.147	12.422	1.17
MM	0.58	0.157	12.412	1.25

The EEDI of the container vessel before the WHRS installation is already below the 2015 required EEDI of 14.158 g CO_2/t-nm. However, if the ship were to be built in the year 2020, the limit is set at 12.500 g CO_2/t-nm. In this case, installing any of the marine WHRS would bring the EEDI inside compliance.

Using equations [71] and [74], it is possible to quantify the amount of CO_2 saved per hour when the WHB and WHRS work together. The CO_2 saved by the WHB boiler is a constant reduction of 0.76 t CO_2/h. Such are larger than that achieved by any of the WHRS due to the large amount of thermal energy required by the ship, but also because of the assumed thermal efficiency of the auxiliary boiler (i.e. 85%) which is replaced by the WHB. Combining the savings from both waste heat systems it is possible to save at least more than 1.2 t CO_2/h which represents around 4% of what the main engine is producing (i.e. approximately 32 t CO_2/h).

7.10 Conclusions

This chapter compared the performance of a marine WHRS using five different working fluids – water and four organic fluids – with the aim of achieving the highest CO_2 emission reduction by generating electricity for the container vessel needs while also supplying steam with a WHB. The aim of this chapter was to understand the performance behaviour of a marine WHRS when changing its operating conditions and plant layouts. Different fuels, air and seawater temperature changes are common on board a vessel and have an important effect on the ship's waste heat quality and availability which it is important to quantify. The WHRS, in order to adapt

to these changes, can modify its high pressure and superheating temperature, but the WHRS designer could also alter its plant layout.

By changing the high pressure level of different WHRS for the vessel's slow speed diesel main engine, it was possible to distinguish that an ORC WHRS – except for the case of Toluene – could offer a larger electrical power output at higher thermal efficiency than a water-based RC WHRS. The results also showed that the maximum power output did not occur when the WHRS was operating at its maximum thermal efficiency. Further, it was demonstrated that a certain degree of superheating temperature is beneficial for all organic fluids since it gives them more flexibility to match the waste heat source. In the case of the RC, there is no real benefit in superheating other than having a dryer expansion. On the other hand, is important to keep in mind that a superheater section in the WHRS economiser means a larger heat exchanger area due to the lower *U* value. This will have an important effect on the WHRS cost and size which must be considered when deciding the marine WHRS operating parameters.

The use of a recuperator on any ORC gives the opportunity to make a better use of the waste heat. Hexamethyldisiloxane WHRS takes more advantage of the recuperator, increasing its net electric power output from 741 kW_e to 1,058 kW_e, while benzene increases by just 100 kW_e. These gains must be balanced against an increase in plant size and system complexity.

With a change of ambient – air and seawater – conditions it was shown that at temperatures below 8˚C it is not possible to operate the power WHRS due to an increased demand on steam – lower heat availability – and a lower waste heat quality. For the same reasons, at warmer temperatures the net electric power production of all the marine WHRS increased. Still, under all ambient temperatures where the vessel's WHRS was able to operate, the benzene ORC achieved the maximum net electrical power output while the lowest was for toluene. When changing fuels from a high-sulphur HFO to a low-sulphur MDO, the waste heat availability increases. This is possible since the exhaust gas minimum temperature changes from 164°C with high-sulphur to 132°C with low-sulphur, meaning that the net electric power was increased substantially. Benzene and water took the most out of the extra waste heat, increasing its power output by 655 kW_e and 461 kW_e respectively.

The seawater pump plays an important role in the WHRS net electric power, especially when the working fluid saturation temperature in the low pressure side is close to the seawater temperature. The benzene WHRS increased the electric power production by increasing the low pressure side of the system which caused a lower seawater mass flow rate demand. It was also found that by adding a recuperator the seawater mass flow rate increased, contrary to what is shown in the academic literature. This is caused by a greater waste heat absorption by the ORC, increasing the condenser's heat duty. In the literature where the coolant side is studied, it is normally assumed that the waste heat absorption stays constant between a simple and recuperative plant layout.

Using all the results from this chapter, it was found that the benzene WHRS achieved the maximum power output at 1,167 kW_e – a difference of 13.4% to the best RC. This ORC system

achieves a reduction of 0.168 g CO_2/t-nm which represents 1.3% of the container ship EEDI. The combination of a WHB with a WHRS can achieve a maximum reduction of 1.39 t CO_2/h, of which 0.76 t CO_2/h are delivered by the waste heat boiler and 0.63 t CO_2/h by the benzene WHRS.

Finally, the sensitivity study has shown the relevance of analysing the behaviour of the marine WHRS under different vessel's operating conditions and scenarios. While a single variable optimisation enables the understanding of the marine WHRS behaviour causalities, the visibility and ease with which to find the optimum design is low. In the following chapters, multivariable optimisations will be used in order to increase the on board benefit of using a power WHRS.

(Page left intentionally blank)

8

ANALYSIS OF MARINE WASTE HEAT RECOVERY SYSTEMS ON BOARD AN AFRAMAX TANKER USING A MULTI-OBJECTIVE OPTIMISATION

Based on Suárez de la Fuente, S., Roberge, D. & Greig, A.R., 2015. Safety and CO_2 emissions: Implications of using organic fluids in a ship's waste heat recovery system (forthcoming). *Marine Policy*, p.21. doi:10.1016/j.marpol.2016.02.008

This chapter studies the case of an Aframax tanker navigating the North and Baltic Sea using a slow speed two-stroke diesel engine. A code with a multi-objective optimisation approach generated explicitly for this purpose produces different optimal WHRS designs for the vessel's operating profile. The different optimal designs are compared with a RC WHRS to show the strengths and weaknesses of using an ORC WHRS on board.

8.1 OPERATIONAL CONDITIONS

A platform located in the North Sea extracts oil from deep waters to supply the energy demand in Finland. The distance between the platform and the sea port in Naantali (Figure 80) is 2,235 km. This route is inside Europe's North Sea and Baltic Sea ECA [International Maritime Organization 2014a] hence the requirement to use a low-sulphur fuel. Throughout the year it will be assumed that the route is free of ice with a yearly average seawater temperature of 5˚C [Rayner 2003].

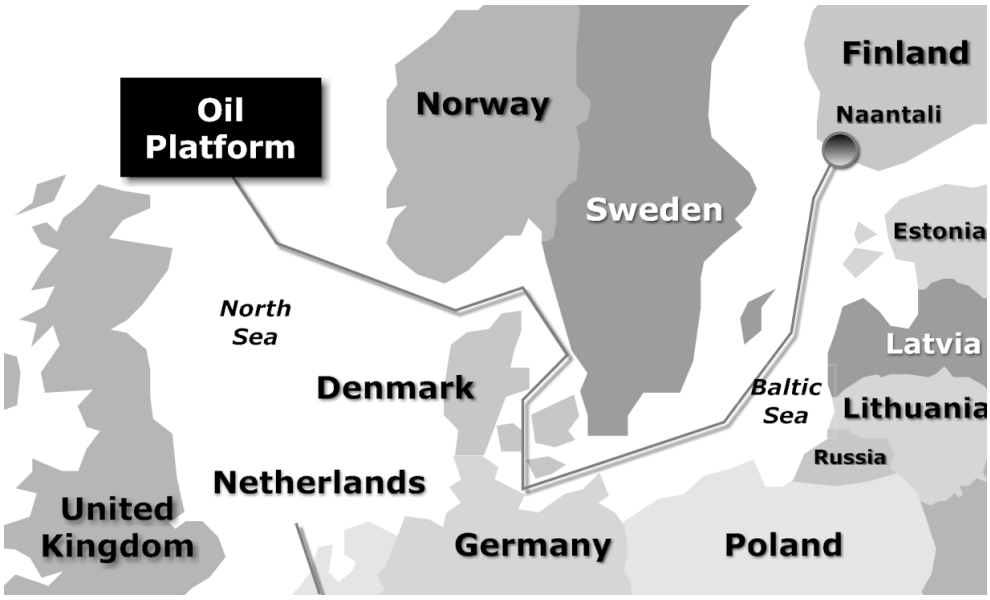

Figure 80: Route covered by the Aframax tanker [Sasaki et al. 2002]**.**

An Aframax tanker, with the characteristics shown in Table 22, is commissioned to transport oil between the platform and port. The tanker's design speed is 14.3 kn requiring 10.0 MW of power, and it has a maximum speed of 15.6 kn which requires an engine capable of delivering 13.3 MW.

Table 22: Some of the Aframax tanker characteristics [Nippon Kaiji Kyokai 2014]**.**

Deadweight **(t)**	**Overall Length (m)**	**Beam (m)**	**Summer Draught (m)**
107,113	247	42	15

The duration of a single voyage is about 92 hours using the operating profile shown in Figure 81. Assuming that the vessel will operate for 58% of the year (i.e. around 5,100 hours) it will complete 55 single voyages [Banks et al. 2013]. Of these, half will be fully loaded and the other half in ballast conditions. It is also assumed that the vessel will be in operation for 20 years.

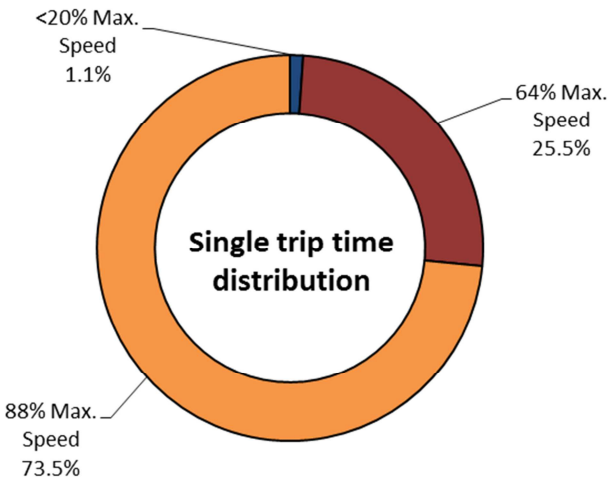

Figure 81: Aframax tanker percentage of time spent at the different speeds in a single trip [Sasaki et al. 2002]**.**

The engine conditions at the design speed (calm sea and clean hull) and fully loaded will be used as the reference point for this study. It is assumed that the ballast speed profile will be the same as in the fully loaded condition, changing only the ship's power requirement due to a draught reduction (see Table 23).

Table 23: Power required by the Aframax tanker calculated as shown in section 6.4.

Normalised Speed (% of maximum speed)	Power required fully loaded (MW)	Power required ballast (MW)
<20	0.1	0.1
65	3.3	2.8
90	10.0	8.3

8.2 Engine on board the Aframax tanker

The vessel has an installed power output of 13.3 MW delivered by MAN 5S65ME-C8.5. The engine uses low-sulphur MDO [MAN Diesel & Turbo 2015e] with a price of £586 per tonne which is the average price seen between the months of July and October 2014 [Bunker Index 2015; European Central Bank 2015].

The exhaust gas temperature at its mass flow rate shown in Figure 82 has been corrected to an ambient temperature of 5˚C by MAN Diesel & Turbo [2015d].

8.3 Waste Heat Recovery System

The WHRS uses the heat available from the exhaust gas after it has passed the turbochargers (see Figure 83). With this layout it is assumed that the ship's steam demand will be covered by an auxiliary boiler, the impact of this assumption is out of the scope of this chapter.

Since marine fuel contains sulphur, the minimum exhaust gas temperature at the outtakes is assumed to be 132˚C – including a safety margin of 5˚C – in order to avoid soot and acid corrosion [Schmid 2004; MAN Diesel & Turbo 2009b].

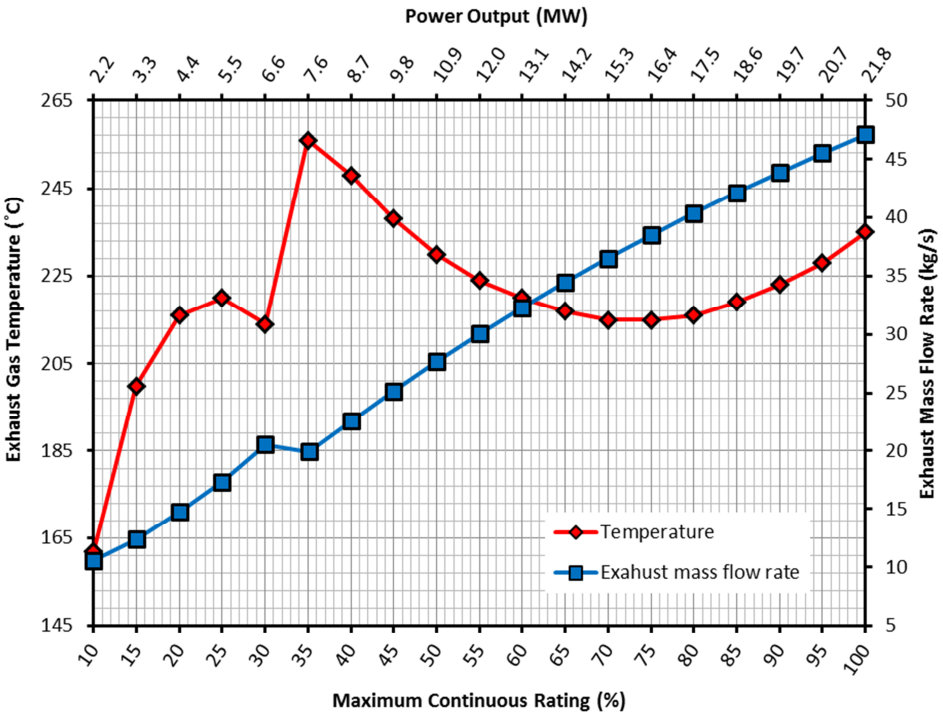

Figure 82: Engine's power output, exhaust gas temperature after the turbocharger and mass flow rate for different loadings [MAN Diesel & Turbo 2015e].

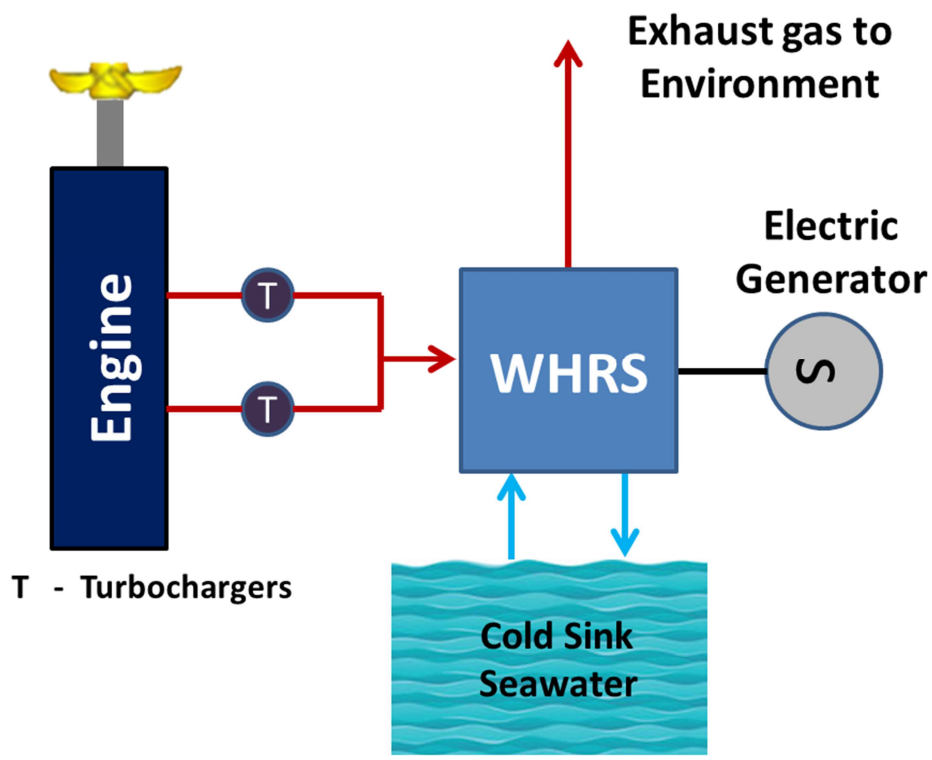

Figure 83: WHRS location in the exhaust gas system.

When the vessel is fully loaded and navigating at design speed – which was set at 75% MCR for the simulation – and using an exhaust gas' C_p of 1.02 kJ/kg-K – taken as the average between the air's C_p at $T_{H,i}$ (i.e. 200˚C) and $T_{H,o}$ (i.e. 132˚C) – allowing for approximately 1.8 MW of available waste heat.

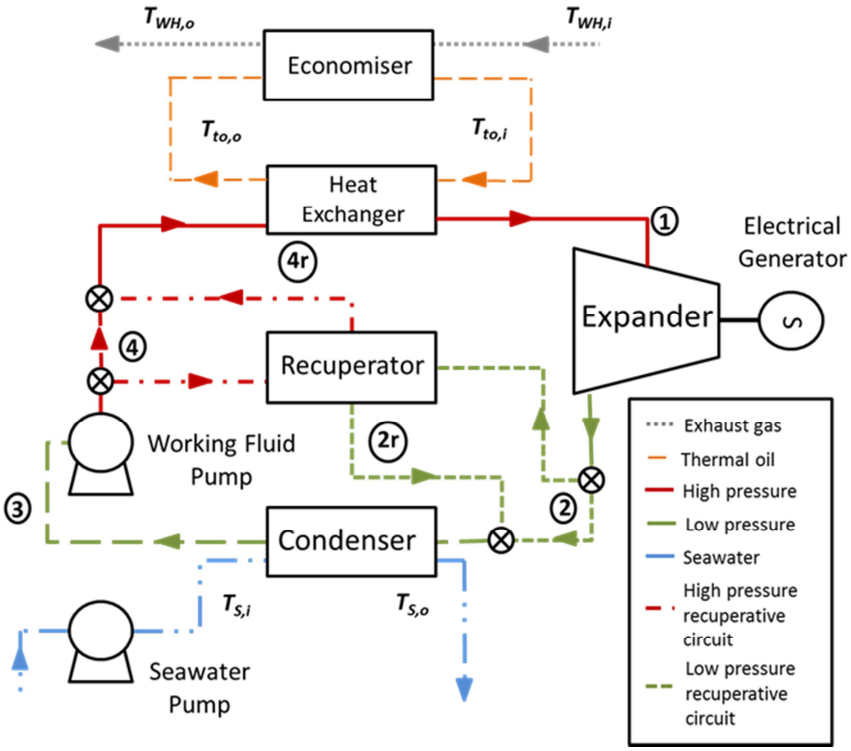

Figure 84: WHRS layout including recuperator and thermal oil circuit.

The general thermodynamic system layout (Figure 84) is the same as that used in the previous chapter represented in Figure 62; it is added again here for the reader's convenience.

8.4 Working fluids

The working fluids selected are water, heptane, benzene, toluene, hexamethyldisiloxane and R245fa. R245fa is a refrigerant selected because it is not flammable, it has low hazard levels and performed well in Larsen, Pierobon et al. [2013]. On the other hand, the global warming potential (GWP) of R245fa is 950.

While SOLAS prescribes a flash point of no less than 60˚C inside the engine room [International Maritime Organization 2009b], the limited amount of working fluid required for the system and today's leak detection and firefighting technology allow for the risks associated with such fluids to be adequately reduced. Therminol VP-1 is chosen as the thermal oil in this case study which enables the heat transfer between the heat source and organic working fluid.

8.5 Theory and calculations

In this chapter, the WHRS will be designed thermodynamically per sections 6.6.2 to 6.6.4. The development not shown in the previous sections will be described in the following subsections.

8.5.1 Marine diesel generator

Equation [73] is used to quantify the fuel savings achieved by installing a marine WHRS which produces electricity. It is assumed that the WHRS will be covering part of the electrical demand inside the vessel. The generator model uses data from a Wärtsilä 6L20 diesel generator which has an MDO specific fuel consumption ($SOFC_g$) of 187 g/kW$_e$-h – assumed constant and per

hour – and delivers around 1.1 MW_e of electrical power at an electrical efficiency of 97% [Wärtsilä Corporation 2012].

For CO_2 savings, equation [78] can be used with a carbon conversion factor (C_F) of 3.206 tonnes of CO_2 per tonne of MDO (see Table 3).

8.5.2 HEAT EXCHANGERS

The heat exchangers are assumed to be of the type shell and tube and counter-flow. A recuperator is used for all organic fluids in order to take advantage of the excess temperature at the exit of the expander.

Table 24: The overall heat transfer coefficient (*U*) values for shell and tube heat exchanger. Each row represents a different heat exchange process happening at different heat transfer equipment along the WHRS [Sinnott 2005].

Hot Fluid	Cold Fluid	Heat transfer equipment	*U* (kW/m^2-K)
Exhaust gas	Water	Economiser	0.075
Exhaust gas	Thermal oil	Economiser	0.120
Thermal oil	Organic fluid	Heat Exchanger	0.760
Organic fluid	Organic fluid	Recuperator	0.200
Water	Seawater	Condenser	0.800
Organic fluid	Seawater	Condenser	0.600

The area of the counter-flow heat exchanger is calculated from equations [27], [35], [40] and [41]. Overall heat transfer coefficients were obtained from Sinnott [2005] and are displayed in Table 24. These values were assumed constant throughout the simulations.

8.5.3 OFF-DESIGN CONDITIONS

The design condition for the Aframax tanker is set as fully loaded and navigating at 14.3 kn (i.e. 88% of the maximum speed). From Table 23 it can be seen that there would be five different off-design conditions (i.e. 2 fully loaded and 3 at ballast). At very low speeds (<20% the maximum speed) the WHRS will be off-line.

While the heat transfer area for all heat exchangers and design constraints from the system's low pressure side are kept constant, the WHRS is set to absorb all the heat available. The Matlab® model modifies the working fluid's mass flow rate and WHRS high pressure with the affinity laws shown in equation [62]. It is assumed that no pressure or heat transfer losses are present; there are no leakages; constant efficiencies for the expander, pump and heat exchangers; and it is solved as a steady-state problem.

8.5.4 MULTI-OBJECTIVE OPTIMISATION

When designing a vessel's WHRS, it is important to consider several aspects of the problem such as WHRS thermal efficiency and sizing (e.g. piping and heat exchangers). The "best" solution will not always be the one with the highest thermal efficiency or most compact unit; it will be a trade-off between the "ideal" properties of each characteristic considered. A

multi-objective optimisation (MO) enables the researcher to find different optimal[32] solutions with different trade-offs between the desired characteristics.

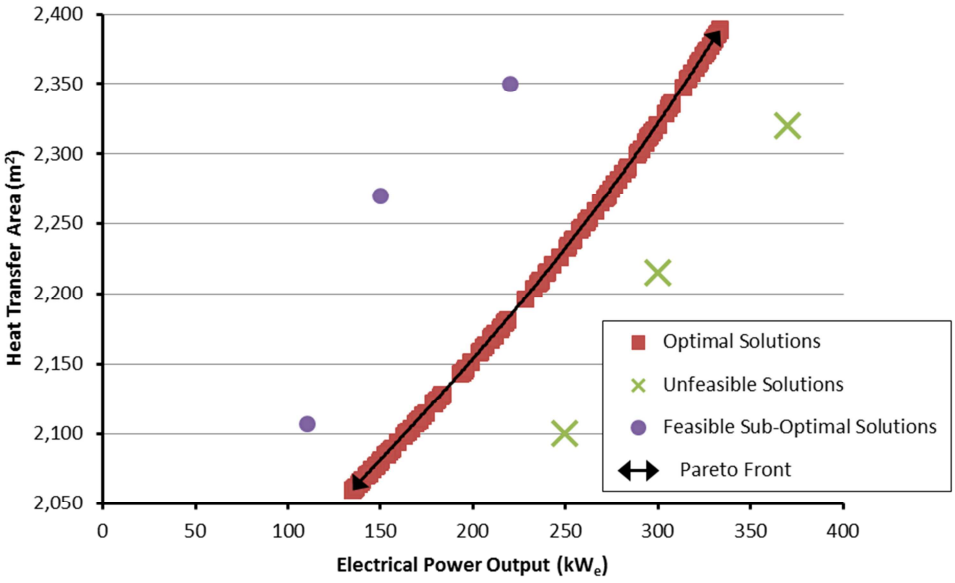

Figure 85: Representation of the pareto front which is formed by the different optimal solutions (represented by squares). Feasible but sub-optimal solutions (dots) are found behind the pareto front, while unrealistic solutions (crosses) are ahead of the pareto front.

These characteristics are known as objectives and the multi-objective process uses them to search for an optimal solution. The set of optimal solutions is known as the pareto front (see Figure 85) and it indicates that no other solution can be better than that found with a specific trade-off [Deb 2011]. The MO is coupled with an evolutionary optimisation, in this case the genetic algorithm (GA), which allows for more than one solution – known as population – per iteration (i.e. generation) and creates a new population based on the previous generation [Mezura-Montes et al. 2008; Deb 2011]. The GA uses gradients or derivatives to guide the population into regions of the search space that offer better trade-offs between the desired objectives.

The GA emulates evolutionary concepts seen in nature, such as mutation and crossover, with the intention of having a more diverse population which will enhance the possibility of finding the most optimal marine WHRS. These terms also play an important role in helping MO to unstick itself from any apparent optimum solution also known as local maxima.

The objectives selected for the optimisation are the electrical power output of the marine WHRS (related to CO_2 emission), working fluid mass flow rate (piping and pump sizing), and heat exchanger area. The multi-objective optimisation with the genetic algorithm (MOGA) has four independent variables: high pressure (P_1), low pressure (P_3), boiler pinch point temperature difference ($\Delta T_{pp,H}$), and condenser pinch point temperature difference ($\Delta T_{pp,C}$).

[32] An optimum solution in optimisation problems is the one that is reduced or minimised. If it is necessary to find the largest or maximum solution possible, such as in the case of WHRS power output, then the objective must be multiplied by -1.

8.5.5 Analytic Hierarchy Process

In the case of the Aframax tanker a single solution is required from the whole pareto front. A scoring system is created to find which of the solutions given by MOGA is best suited for the case study. The WHRS design score (*Score*) is found by considering the following equation:

$$Score = w_W * power - w_{size} * size + w_\eta * efficiency \quad [\ 91\ ]$$

Where *power* and *size* variables group together different characteristics of the design such as working fluid mass flow rate or seawater pump power consumption. The values of these variables are normalised, in a scale from 0 to 1, to the extreme values found in the pareto front (i.e. maximum and minimum of each objective looked). The weight factors of *power*, *size* and *efficiency* are w_w, w_{size} and w_n respectively and are determined using an Analytic Hierarchy Process (AHP) [Golden et al. 1989; Saaty 2008] using the authors' preferences between the three variables shown in equation [91].

The AHP method helps the author in selecting the most optimal WHRS by examining as a scale the desirable system's characteristics and performances, creating a decision-making process which is embedded to the code. The AHP requires scaling the characteristics by pairwise preference comparisons finding the WHRS characteristic deemed more important from the vessel point of view. The scale used for this chapter went from one to nine, where one refers to equal importance between preferences and nine refers to a preference being of the highest relevance when compared to a second preference in the comparison. Ratio scales are obtained from the preferences matrix's eigenvector [Saaty 1987]. In the case of equation [91], the preference matrix is 3 by 3 with a diagonal of ones; a comparison of the same characteristic is equal to one. A consistency test to the weight factors is performed in order to detect that the weight factors recorded are aligned to the preferences. In a simple example using three colours – blue, red and green – an inconsistency would be as follows: an individual prefers blue over red and red over green but prefers green over blue. Inconsistencies must be kept to the minimum in order to ensure a coherent decision-making process. The inconsistency threshold in the WHRS code is below 10%, as recommended by Saaty [1987].

Finally, the weight factors values after the AHP process are for w_W 0.73, for w_{size} 0.19 and for w_η 0.08.

8.5.6 Waste Heat Recovery System algorithm

From Figure 86, the WHRS codes start by loading the design condition data for engine and ship per working fluid. The WHRS model uses Matlab® MOGA which selects random values inside the boundaries established in Table 25 – pressure and pinch point temperature difference. In order to enhance the MOGA probabilities of finding an optimum WHRS, a pre-screen process is used where the limits of the search space are tested. Different pressure levels and the extreme values for the pinch point temperatures in both the economiser/heat exchanger and condenser are used inside a simple iterative procedure. The pre-screen process is an evolution from the optimisation process described in 7.5, but in this instance it also changes P_3 and the pinch point temperature per the limits imposed in Table 25.

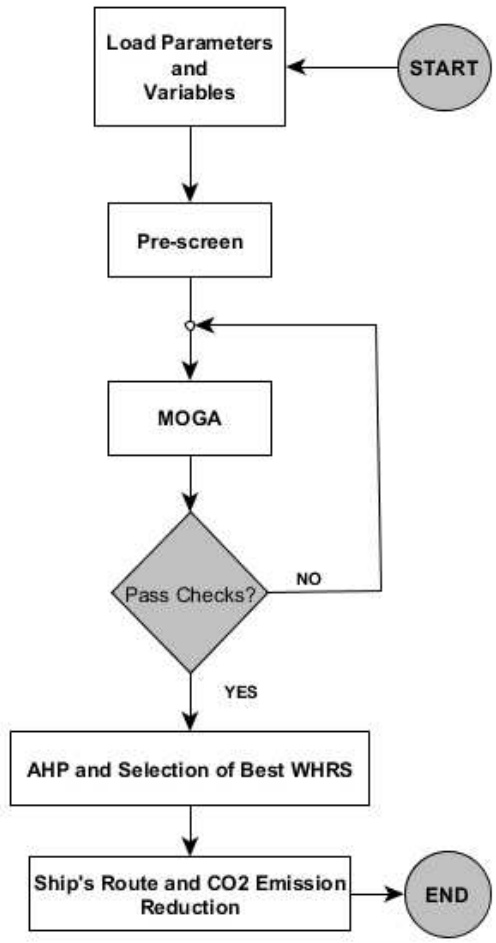

Figure 86: Code structure developed for the analysis of marine WHRS.

But still, MOGA can choose a variable's combination which generates solutions that do not follow physical laws – thermodynamics, fluid flow, heat exchanging, etc. – invalidating the WHRS design.

In order to avoid this situation, the WHRS code could have checks embedded which evaluate the solution behaviour and characteristics, discarding and starting the design process again for that solution. A second option, which was taken by the author, is to constrain further the search space by establishing relationships between the four MOGA variables. These relationships are in the form of inequalities and help MOGA to avoid temperature crossovers inside the different heat exchangers.

However, the relationships also eliminate the possibility of high WHRS power outputs by extracting more waste heat from the source than that the allowed by the exhaust gas temperature (i.e. 132˚C):

$$T_1 \geq T_{sat\ @\ P_1} + \Delta T_{pp,H}$$

Without Thermal Oil $$T_{sat\ @\ P_1} + \Delta T_{pp,H} \geq 132^{\circ}C$$

With Thermal Oil $$T_{sat\ @\ P_1} + \Delta T_{pp,H} \geq 132^{\circ}C - T_{ap,To}$$

$$T_{sat\ @\ P_3} - \Delta T_{pp,C} \geq T_{S,i} + min(\Delta T_{pp,C}) \quad [92]$$

Table 25: Constraints and conditions imposed on the different parts of the WHRS model. These values stay constant unless stated to the contrary.

Equipment	Variable	Value
Expander		
	Inlet temperature, T_1 (˚C)	$T_{WH,i}$ - T_{ap} *(water)or* $T_{To,i}$ - T_{ap} *(organic)*
	η_{exp}	80%
Condenser		
	T_{ap} (˚C)	$\geq$ 5
	$\Delta T_{pp,C}$ (˚C)	5 - 30
	Inlet Sink Temperature, $T_{S,i}$ (˚C)	5
Pump		
	Inlet temperature, T_3 (˚C)	Liquid saturation temperature at low pressure
	Pressure, P_3 (kPa)	10 - 100
	η_p	80%
	η_e	97%
Heat Exchanger/Economiser		
	T_{ap} (˚C)	$\geq$ 5
	$\Delta T_{pp,H}$ (˚C)	5 – 30 [a]
	Pressure, P_1 (kPa)	100 - P_{cr}
	Inlet Source Temperature, $T_{WH,i}$ (˚C)	Per Figure 82
	Minimum exit Source Temperature (˚C)	132
WHRS Generator		
	η_e	97%

[a] For R245fa the high pressure pinch point is set between 15˚C to 40˚C in order to be able to operate under the conditions and constraints set.

An auxiliary check is embedded in the WHRS code in order to eliminate rogue solutions that do not follow the First Law of Thermodynamic due to the variables chosen by MOGA being too close to the boundaries established by equation [92].

In order to ensure that the solutions are repeatable, some MOGA parameters had to be set as shown in Table 26.

Table 26: MOGA setting used to solve the different marine WHRS.

Parameter	***Value***
Population size	1,000
Max. Generations	800
Tolerance	10^{-6}
Crossover percentage (%)	70
Migration percentage (%)	35

After the MOGA, the solutions are assessed and compared using the AHP procedure returning a single optimal WHRS design per working fluid. At the end of this step, the WHRS' characteristics such as the heat exchanger size and performance at design point are given.

In the final step, the WHRS is tested at off-design conditions over the ship's route along a year which will return the annual fuel savings and CO_2 emission reductions per the equations given in section 6.10. The cost analysis is prepared post-process outside Matlab® using the data provided by the WHRS code.

8.6 MODEL VALIDATION

The code was validated against the results presented by Saavedra et al. [2010] who studied a recuperative ORC and simple RC WHRS for a compressor gas plant. Saavedra et al. created a model using the Aspen Hysys® process simulator to find different optimal WHRS by maximising the expander power output. The code used in this paper was adapted to the boundary conditions, T_1 and recuperator efficiency given in Saavedra et al. [2010]. The comparison is made only with heptane since it is the only fluid with conditions at all stages of the process in the work presented by Saavedra and colleagues [ibid.].

Table 27: Some of the important WHRS characteristics for both methodologies, Saavedra et al. [2010] and this work, are shown and compared in order to assess the level of accuracy of the WHRS model.

Properties	Heptane (ORC)		
	[Saavedra et al. 2010]	Author's work	Difference (%)
$\dot{m}_{wf}$ (kg/s)	7.30	7.43	-1.8
$\dot{m}_{to}$ (kg/s)	10.39	10.75	3.5
W_t (kW)	1,083	1,067	-1.5
η_{th} (%)	26.8	26.6	-0.7
P_1 (kPa)	2,594	2,189	-15.6

From Table 27, it can be seen that the results show good correspondence with Saavedra et al. with the exception of the system's high pressure P_1. The main reason for this discrepancy is in the calculation of the thermodynamic properties: Saavedra et al. uses the Peng-Robison Stryek Vera equation, while in this work the data is extracted from NIST Refprop 9.0 [Lemmon et al. 2010]. When using the data points in each stage of the WHRS, there is a reduction of around 1.5% for the expander power output and 3.0% for the heat absorption when using NIST's software. By correcting the data, assuming that all the heat has to be absorbed and relaxing some of Saavedra's restrictions, the heptane's new high pressure would be 2,410 kPa which is down to 7.1%.

Another reason for the discrepancies is that by using MOGA+AHP, the WHRS code considers also the heat transfer area and thermal efficiencies which find designs less powerful than the maximum possible as in the case of the work of Saavedra et al. [2010].

8.7 RESULTS AND DISCUSSION

This section will first show the optimal WHRS design for the six working fluids and then apply it to the vessel's operating profile during a single year. The benefits measured at the end of one year of operation are fuel savings quantified in Sterling Pounds, and CO_2 emissions reduction in metric tonne and its associated EEDI reduction. A third section will present a feasibility study using the concepts of Net Present Value (NPV) and discounted payback period. Finally, a discussion is presented regarding the integration of marine safety systems, regulations and ORC WHRS.

8.7.1 WASTE HEAT RECOVERY SYSTEMS' OPTIMAL DESIGN

Toluene's low high pressure (P_1) and low mass flow rate cannot compensate for the energy drop caused by the thermal oil and it is the WHRS with the lowest power output at 262 kW_e. The largest power output is given by R245fa at 365 kW_e which is around 35% more than the RC system and represents 33% of the power output from the diesel generator. R245fa ORC takes advantage of not needing a thermal oil and with its larger pinch points ($\Delta T_{pp,H}$) manages to operate close to the critical point – P_1 is 3,620 kPa and T_1 is 153.5˚C – increasing the energy entering the expander, thanks to a large mass flow rate and high h_1.

The WHRS returned power at design point to the engine's maximum power installed is between 2.0% and 2.8%. While the values seem low, they are higher than the 1.2% found by Theotokatos and Livanos when making the same comparison between a RC plant and a smaller two-stroke marine diesel engine [Theotokatos & Livanos 2012].

The approach used to calculate the heat transfer area is simple but useful for comparisons between the systems. The RC WHRS offers the most compact design with only 934 m^2 in the heat transfer area. The closest organic system is R245fa with an area of around 1.6 times larger (see Figure 87). The increment in heat transfer area is caused by the inclusion of the recuperator and the intermediate heat exchanger for the thermal oil, excluding R245fa.

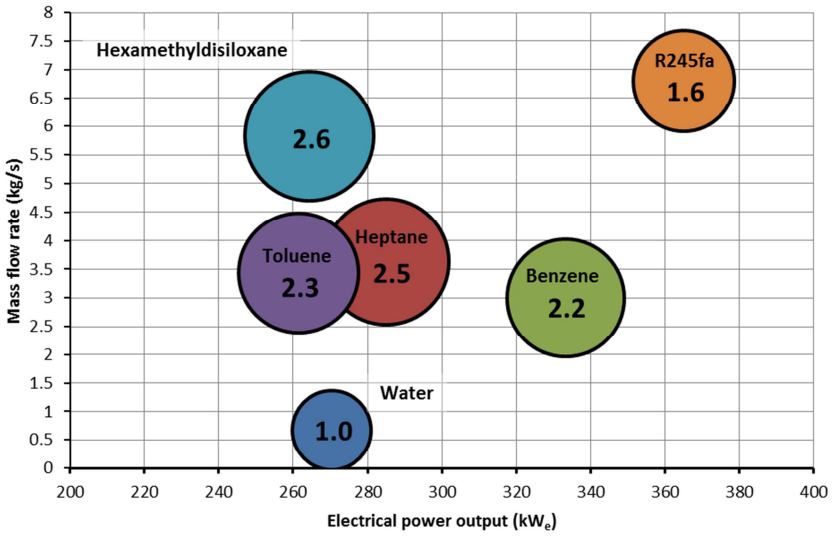

Figure 87: The different WHRS optimal designs per their MOGA objectives at design speed (i.e. at a normalised speed of 88% and a power requirement of 10.0 MW) and fully loaded as seen in Table 23. The bubble diameters represent the heat transfer area and are normalised to the RC system which has an area of 934 m^2.

Water also has by far the smallest mass flow rate at 0.7 kg/s, the closest organic fluid to water is benzene which is 3.5 times greater. R245fa shows the largest mass flow rate at 6.8 kg/s. The increase in mass flow rate is caused by the organic fluid's low evaporative energy and the use of the recuperator forcing larger mass flow rates to absorb the available waste heat [Saavedra et al. 2010].

8.7.2 GREEN TECHNOLOGY: FUEL SAVINGS AND CO_2 EMISSIONS

The fuel savings presented in this section represent only the money saved by not consuming fuel via the use of a marine WHRS, the savings analysis does not consider money saved in taxes or maintenance and operational costs.

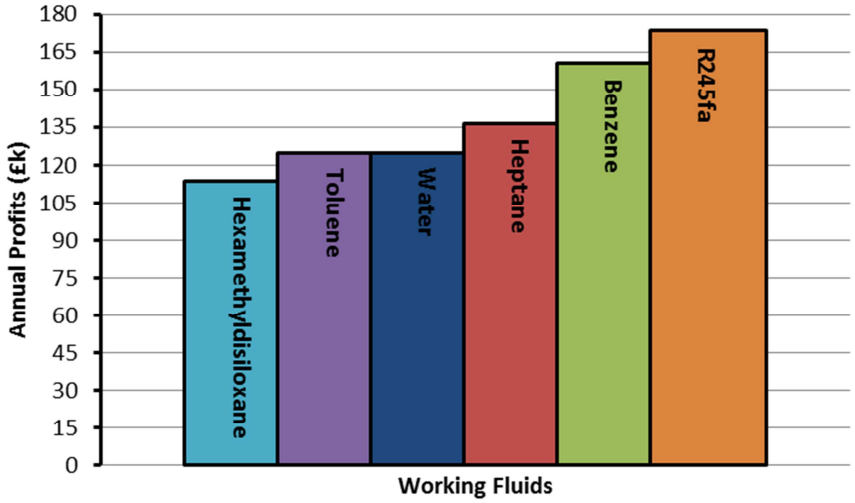

Figure 88: Profit achieved by the different WHRS by reducing fuel consumption during one year of operation on board the Aframax tanker.

Installing a WHRS using the available heat from the vessel's exhaust gas could save at least £144k per year which amounts, after 20 years in operation, to at least £3.3M – not considering the profit depreciation (see Figure 88). The R245fa system has the largest annual savings at approximately £174k. The first flammable fluid is benzene with savings of around £36k more than that achieved by the RC system, representing an increase of around 28%. The ORC fuel savings for the most powerful WHRS are on advantage over a traditional marine RC and cover the initial costs due to larger heat exchangers and more expensive working fluids. Toluene manages to produce the same annual profits than water with an annual profit of £125k, while hexamethyldisiloxane offers the lowest earnings at £114k.

Moving to the emission savings in Figure 89, it is seen that R245fa WHRS delivers the highest emission reductions at 948 t of CO_2 after one year in operation. Next is benzene with around 8% lower emission reductions from R245fa while the RC system is 28% less.

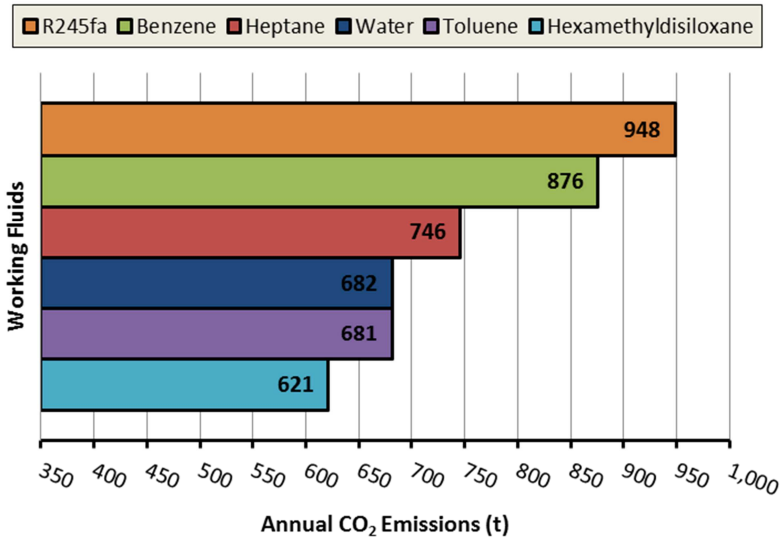

Figure 89: CO_2 emission reductions achieved by the different Aframax's WHRS for a single year of operation.

Interestingly, the extra performance that the RC system – power output – had over toluene at design point is eliminated when operating in a year. All systems at off-design conditions are required to absorb all the available energy; hence the performance increase seen with toluene is given by the organic fluid low evaporative energy forcing larger mass flow rates, thus, more power in comparison to RC. This example shows that ORC WHRS have superior adaptability over a simple RC when facing lower heat availability. On the other hand, hexamethyldisiloxane's larger mass flow rate – almost twice when compared to toluene – is enough to reduce its adaptability at off-design conditions and therefore its CO_2 emissions impact.

The Aframax's EEDI was calculated using BIMCO's EEDI calculator [The Baltic and International Maritime Council 2013], having a score of 3.517 g CO_2/t-nm. When installing a WHRS in the exhaust gas system, the EEDI was reduced by at least 0.103 g CO_2/t-nm which represents a 2.9% drop in the index. The maximum EEDI reduction of 0.143 g CO_2/t-nm is

achieved by the R245fa ORC. The RC WHRS impact on the EEDI is around 3.0% which is similar to that obtained by Theotokatos and Livanos [2012] which achieved a reduction of around 1.8% for a two stroke engine. In another study, Livanos et al. [2014] found the EEDI of a ferry is reduced by 4.6% with a water-based RC using the waste heat from the exhaust gas. The reduction appears small because the WHRS CO_2 reductions are swamped by the amount of CO_2 emitted by the main and auxiliary engines on board the tanker. However, while the EEDI shows only modest improvements with the ORC WHRS, Figures 88 and 89 show considerable fuel savings and CO_2 emissions reductions when using an ORC WHRS throughout a year of operation; this is a better indication of the system's relevance.

8.7.3 WASTE HEAT RECOVERY SYSTEMS FEASIBILITY STUDY

In order to determine whether the use of the technology is feasible on board a commercial vessel, an economic analysis of the different marine WHRS is required. In this analysis only the initial cost and net present value (NPV) for the Aframax tanker are considered. It is also assumed that the fuel savings in Sterling Pounds will remain relatively unchanged throughout the vessel's operational life. A limitation regarding this simple economic analysis is that it does not recognise the differences in equipment (i.e. heat transfer area and expander) and organic fluids, which will further impact the WHRS cost. But it is deemed sufficient by the author for the scope of the chapter where there are other relevant aspects to the case study presented here.

The costs for a RC were found in Cunningham [2002]; the ORC costs are taken from Quoilin et al. [2013]; and the WHRS electrical generator cost was taken from Lian et al. [2010].

Table 28: Initial cost for the different marine WHRS calculated at their design point electrical power output including the cost of the electrical generator [Cunningham 2002; Lian et al. 2010; Quoilin et al. 2013]**.**

Working fluid	Electrical power output (kW_e)	Specific capital cost (10^3 £/kW_e)	Capital cost (10^3 £)	Electric generator cost (10^3 £)	Total cost (10^3 £)
R245fa	365	1.47	538	11	549
Benzene	333	1.51	504	10	514
Heptane	285	1.59	452	8	460
Hexamethyldisiloxane	264	1.62	429	8	437
Toluene	262	1.63	426	8	434
Water	270	1.13	305	8	313

The RC is the cheapest of all the WHRS tested since: a) the specific capital cost for a RC WHRS is approximately at least 30% lower than any ORC WHRS; and b) the WHRS total cost is driven by the electrical power output of the thermodynamic cycles and, as the RC has the third lowest electrical power output, its total cost is lower than any of the ORC.

Using the results shown in Table 28 and Figure 88, it is possible to calculate the different WHRS' discounted payback times and the net present values after 20 years in operation (see Table 29).

The water-based WHRS achieved the fastest payback time in less than three years due again to its low initial cost, while for the fastest ORC to payback the investment is R245fa caused by

its larger annual fuel savings. Superior savings are produced by the R245fa WHRS with an NPV after 20 years of operation, around £373k higher than that achieved by the simple RC, being this difference more than the water-based WHRS initial cost. The low initial cost for the RC manages to bring a similar NPV than heptane which has a better annual profit (see Figure 88). This is important in the case were the ship owner plans to sell the vessel at any point before the end of the ship's operating life, since a water-based RC will give a better net profit at any time than a heptane ORC.

Table 29: Economic performance of the different WHRS where it is shown the time taken to recover the initial investment and the final cash flow after 20 years of operation.

Working Fluid	Discounted payback time (years)	Net present value 20 years (10^3 £)
R245fa	3.53	1,615
Benzene	3.59	1,482
Heptane	3.79	1,240
Hexamethyldisiloxane	4.38	980
Toluene	3.93	1,119
Water	2.75	1,242

While RC WHRS displays a good performance in a short-term period, R245fa and benzene ORC systems deliver a better economic return and higher levels of CO_2 emission reductions for the vessel operator than the other four WHRS.

As mentioned in subsection 6.10.4 the fuel costs are volatile and difficult to predict. In order to understand how the feasibility outcome of this chapter is affected by the fuel cost, a sensitivity analysis will be made to the marine WHRS profit and payback period.

Assuming that the WHRS fuel savings are constant through the ship's 20 years of operation it is seen from Figure 90 that as the fuel's cost reduces the difference in profit reduces between the different WHRS. When the fuel's cost is below £200/t then the profits are better for the water-based RC. This is due to the RC lower initial cost which can be paid back in a shorter period leading to a better profit at the the end of 20 years in operation. From the profit point of view the marine WHRS start to make sense for the Aframax tanker after the fuel costs are above £400/t. For the case of R245fa the profits are above £850k while for the RC is around £750k. For hexamethyldisiloxane the investment would become interesting if the price of the fuel is above £500/t when it is possible to achieve more than £770k in profits after 20 years of operation. On the high fuel price side, the R245fa achieves the largest profits at £3,150k which is around 34% larger than the water-based RC at the end of their operating life.

Regarding the payback times the water-based RC in any fuel cost scenario is the WHRS that pay itself faster mainly due to its lower initial cost as seen in Table 28. The initial cost has an important impact on the WHRS payback time as the fuel price reduces. It is seen in Figure 91 that the difference between the payback times of any ORC WHRS to the water-based RC increases as the fuel cost reduces. If an acceptable payback time is set at four years then the

lowest fuel cost for the water-based RC is at £400/t while for R245fa is around £500/t and hexamethyldisiloxane needs a fuel price of around £600/t. Above a price of £800/t, the payback times are similar between any marine WHRS which are below three years.

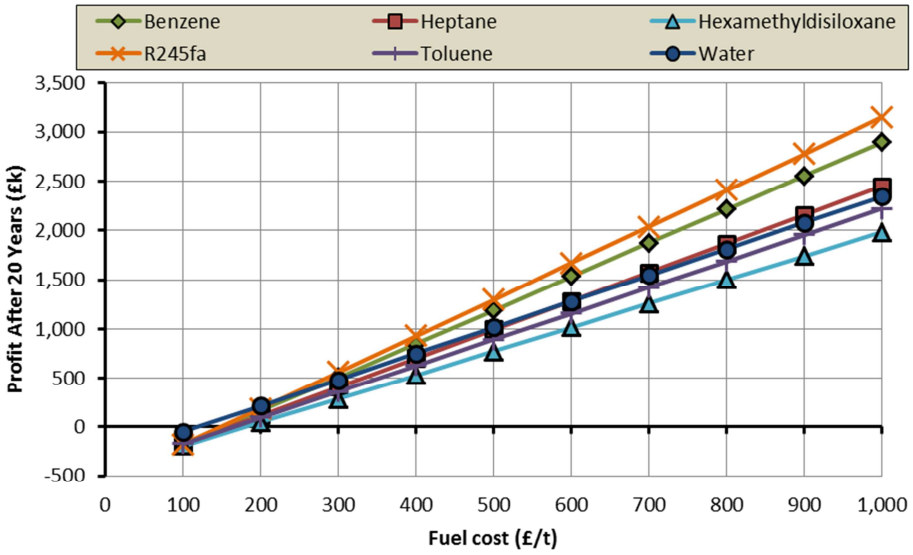

Figure 90: Profits earned by the Aframax tanker at the end of its operating life when installing a marine WHRS over a range of fuel prices per tonne.

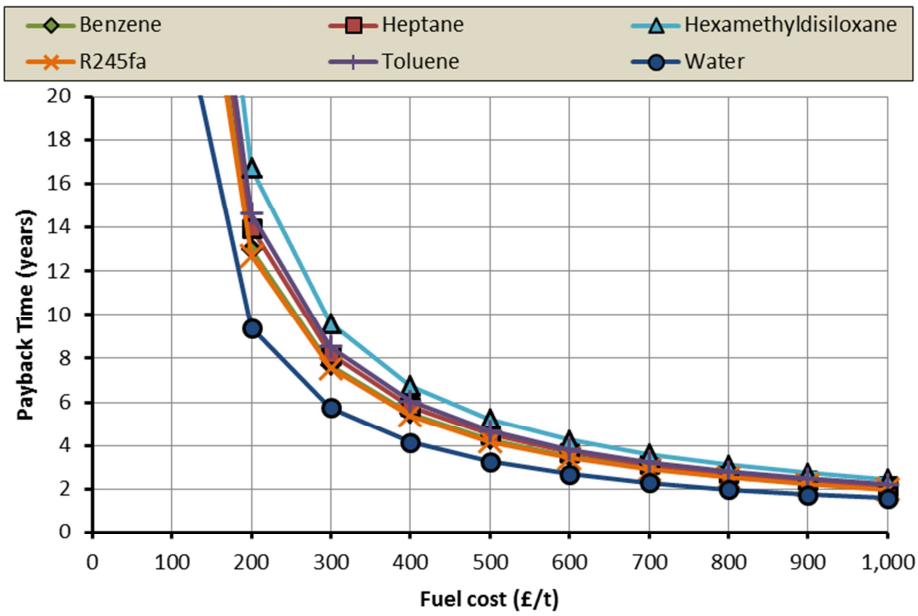

Figure 91: Payback time for the different marine WHRS under a range of fuel cost scenarios.

Depending in the time the ship owner intends to keep the Aframax tanker the optimal payback time for the marine WHRS can be selected which will determine the minimum fuel price to make the investment feasible. For owners that use the ship for less than five years the best option would be the water-based RC due to the low initial cost achieving a fast payback time and starts to generate profits quicker. For longer periods of owenrship and with fuel prices above £300/t the R245fa WHRS is the best option due to a larger profit return.

8.8 SYSTEM INTEGRATION

8.8.1 SAFETY REGULATIONS

The ORC WHRS has clear advantages over the RC, especially when fitted to high efficiency diesel engines. However, current regulations make the use of hydrocarbon-based organic working fluids challenging. Since 1974, IMO SOLAS has considered any fuel having a flash point of less than 60°C to be hazardous and not normally permitted on board ships without specific Administration approval or for certain emergency generators not located inside the engine room [International Maritime Organization 2009b].

Most classification societies base their regulations on IMO SOLAS, however, their situation allows for a more dynamic evolution of the rules, enabling for exemptions such as heating up fuel above its flash point for viscosity purposes, or the Tentative Rules for Low Flashpoint Liquid (LFL) Fuelled Ships released by DNV GL which defines classification requirements for the use of methanol as fuel (12°C flash point). However, LFL include fuels or liquids having a flash point lower than 60°C. [Lloyd's Register 2012d; Det Norske Veritas AS 2013a].

The flash point has historically been considered a major factor in assessing fuel safety. A review of marine accidents showed, however, that the vast majority of incidents relating to fuel were not triggered by the ignition of vapours at a temperature above its flash point but by spilled fuel coming into contact with a surface at a temperature exceeding its auto-ignition temperature, making the latter an important factor when assessing a fluid's safety [Stone 1982]. All hydrocarbons considered for this research except heptane have significantly higher auto-ignition temperatures than MDO (at 250°C [British Petroleum 2011]) as shown in Table 13, making them safer in most hazardous situations encountered in the marine environment [Roberge 2014].

The use of hydrocarbons in ORC systems carries numerous similar hazards as liquefied gas except for the cryogenic state. The International Gas Code regulates liquefied gas fuel carried in bulk, however it prohibits its use as a fuel or in the vicinity of machinery spaces due to its low flash point, which has meant special Administration approval for LNG carriers intending to use LNG boil off as fuel [International Maritime Organization 1993]. The IMO is currently developing the International Code of Safety for Ships using Gases or other Low Flashpoint Fuels (IGF code), a code that has the short-term aim to regulate the use of LNG as fuel for carriers, and later amendments will incorporate other LFL fuels. The IGF is currently being reviewed before implementation [LNG World Shipping 2013]. In the near future ocean going ships fuelled partly or entirely by LNG will be built; plans are already on the drawing board. Ferries fuelled by LNG are already operating successfully in Norwegian coastal waters.

8.8.2 MAKING ORC SAFE

While no current code applies directly to the use of highly flammable fluids in an ORC, a parallel analysis of requirements from the IGF draft code [International Maritime Organization 2014b] and the DNV GL Tentative Regulation for LFL Fuelled Ships [Det Norske Veritas AS 2013a]

allows for an understanding of the necessary measures required to ensure a potential system's compliance with relevant regulations.

When no thermal oil loop is used, the system containing highly flammable fluids is partly housed within the machinery space (exhaust path). The use of thermal oil allows for relocating the working fluid outside the space. The IGF code requires complete separation between the gas and the machinery space. This can be achieved by the use of double walled piping or an enclosure vented to the atmosphere fitted with appropriate gas detection and purging capabilities. There is also a requirement to have an inherently safe space or use an emergency shutdown procedure that will power off all equipment not rated safe should the explosive vapour concentration reach 40% of the Lower Explosion Level (LEL). Double walled separation would not be possible within the boiler in a system not using a thermal loop. While the exhaust gas flow would prevent the accumulation of explosive vapours, an undetected leak could result in a hazardous situation following the shutdown of the plant.

Due to the volatile nature of LFLs, additional leak detection and firefighting systems are required. While a leak of hydrocarbon working fluid causes explosion risks, its higher volatility when compared to diesel fuel oil introduces an additional health hazard for personnel exposed to an undetected leak. A modern platform management and firefighting system with targeted foam and chemical extinguishing agents would ensure that the system meets all the relevant safety requirements of the above codes. Today's platform management systems can monitor thousands of sensors making the incorporation of the additional sensors, and firefighting systems easily feasible [Varela & Soares 2007]. The use of thermal oil would restrict the working fluid to a discrete location, making an enclosure fitted with safety systems ideal to ensure personnel safety.

Fitting an emergency relief and purging system as well as a cooling system in the form of fine water spray to the enclosure would also ensure system protection from other ship-borne emergencies.

8.9 CONCLUSIONS

This paper demonstrates, with the aid of a case study, the advantages of installing a WHRS on board an Aframax tanker navigating in the Baltic and North Seas, achieving yearly fuel savings of at least £114k and CO_2 emission reductions of around 621 t, enabling an EEDI reduction of around 2.9%. It also shows that a marine ORC WHRS, with thermal oil separating the waste heat and the working fluid, can outperform a simple RC by producing up to 63 kW_e more at design point which represents an increase in power output of around 23.0%. In conjunction with the Aframax's operating profile, an R245fa WHRS achieves up to 39.2% savings in both fuel consumption and CO_2 emissions when compared to a typical RC. Furthermore, thanks to the organic fluids' adaptability to lower heat quality and availability, it was seen that during the tanker's operating profile toluene WHRS matches the RC's CO_2 emissions reduction despite having a lower performance at design condition.

This work also shows that the use of a marine WHRS on board recovers the initial investment in less than 4.4 years, regardless of the working fluid selected. While the RC plant has the fastest discounted payback time (i.e. 2.75 years) due to its low initial cost, it is its lower fuel savings that makes it the third highest earner, at £1,242k of the six WHRS tested. On the ORC side, R245fa achieves an NPV after 20 years of operation of £1,615k which represents an increase of 30.0% compared to a traditional RC WHRS. However, it is important to have in mind that the payback period and profit at the end of the ship's operating life is highly dependent on the fuel price. The R245fa WHRS is attractive when the fuel price is above £300/t and the period of ownership is larger than five years, while with low fuel prices and ownership periods of less than five years then the water-based RC is the most convenient waste heat technology.

Organic WHRS will play an important role in the future where regulations will push for tighter emission controls and waste energy availability for electric production on board reductions due to an increase in prime mover efficiency and waste heat utilisation for other processes (e.g. ballast treatment). The ORC technology can be applied to any kind of vessel type and size, keeping in mind that the ORC benefits depend on the waste heat temperature and availability, on board heat requirements and operational profile. It is also important to keep in mind some of the drawbacks of the marine ORC WHRS which requires mass flow rates and heat transfer areas of up to 9.1 times and 1.6 times larger than a RC system respectively. This increase in size has an impact on the initial cost of the ORC system and the space requirement inside the vessel.

The flammability of hydrocarbons as working fluids is also an important aspect of the ORC. While they have the significant advantage of having no ozone depleting potential (ODP) and very low GWP when compared to refrigerants, their flammability introduces additional safety equipment requirements. It was found, however, that the limited amount of fluid carried on board and the compactness of the system allows for this additional risk to be easily mitigated, even in the case of a retrofit to an existing vessel.

Long-standing policies regulating minimum flash point on board ships present a cultural challenge when introducing the technology. The main regulation for flammable fluids dates from 1974 [International Maritime Organization 1974] and was written for ships and technology of that era. Since then, the requirements and priorities of the shipping industry have changed and technology and practices have greatly evolved. Unmanned machinery spaces are now common and sensor and firefighting technology has improved dramatically. In light of this, a regulation revision would be desired so that ships can take full advantage of ORC technology.

It is then considered that a marine WHRS using as working fluid the refrigerant R245fa brings the best environmental, compactness and financial cost benefit for the Aframax tanker. Still, it is important to remember that this refrigerant has a GWP_{100} of 950 years, making it highly important to have monitoring and safety systems on board which can manage and avoid any spillage to the environment.

9

Navigating in the Arctic: Challenges and Opportunities for a Waste Heat Recovery System

In this chapter, the optimisation of marine ORC WHRS and their condensers is undertaken in order to observe their performance, environmental impact and financial benefits. Different stakeholder visions are used to determine the best marine WHRS and cooling approach. Thus, the study of thermodynamic WHRS under extremely cold weather using, as a case study, a container vessel navigating in the Arctic will contribute to the understanding of WHRS in harsh environments.

The work presented in this chapter is a collaborative effort between UCL, Chalmers University and Technical University of Denmark (DTU).

9.1 NAVIGATING IN THE ARCTIC

In the last decades, the ice found in the North Pole has been constantly declining. During the period between 1981 and 2010, an average decline of 4.9% in ice coverage can be observed in each decade [National Snow And Ice Data Center 2013]. This has opened the door for shorter shipping routes via the Arctic [Corbett et al. 2010; Smith & Stephenson 2013; Winther et al. 2014]. For example, the Rotterdam-Yokohama route through the Suez Canal stretches for around 20,600 km, while the same route through the Northern Sea reduces the distance to around 8,500 km [Rodrigue 2013]. Winther et al. [2014] predicted that the shipping activities above the 59˚ north parallel will grow from 133.5 million km in 2012 to 208.7 million km by the year 2050, an increase of more than 55%. The largest increase in the same time frame is for container vessels at around more than 300%, increasing from 6.8 million km to around 28.5 million km.

Travelling in colder waters represents important challenges for the maritime industry. If a ship owner is considering navigating through the north routes, a vessel capable of withstanding the harsh environment found in the Arctic is required [International Maritime Organization 2009c]. Winterisation and Ice classes are concepts that encircle the navigation requirements in extremely cold weather, affecting the ship's architecture and systems. Its core is to safeguard the integrity and operability of the ship, but also to keep the crew safe [International Association of Classification Societies Ltd. 2011]. One of the major modifications that must be made to vessels is an increase in power which is important when facing ice. A comparison of a LNG carrier with the lowest ice class against a regular one, showed that the first required a power increment of around 29.4% more [Lee 2008]. Also, there is a higher heat demand from the vessel due to the larger temperature gradient between the cold environment and the ship. Gymnopoulos [2013] calculated the heating requirements for a 45,000 dwt winterised bulk carrier, finding that there was an increase in auxiliary power of around 64% for the highest winterised level when compared to the base level.

Distance reduction is seen as part of shipping efficiency since it decreases fuel consumption and GHG emissions. However, the predicted increase in the use of Arctic routes will add important environmental pressure into northern areas. Looking into shipping emissions in the Arctic region, Corbett et al. [2010] and Winther et al. [2014], using a business as usual scenario,

predicted that by 2050 there would be at least 24.0 Mt of CO_2[33] which represents an increase of more than 220% from the year 2012. In these cases, it is necessary to develop green and energy efficiency technologies and strategies that can mitigate the negative effects of a future increment in shipping activity on north polar waters such as the WHRS.

As mentioned in previous chapters, the largest engine's heat outlet is found in the exhaust gases, but due to the air's low temperature in the northern region – which could reach - 37°C [Jones et al. 1999; Jones et al. 2012] – and the vessel's heating demand, the use of this heat source to produce power is not feasible [MAN Diesel & Turbo 2014b]. Another source of heat waste is found in the scavenge air after compression which represents around 15% of the fuel energy used [Schmid 2004; Balaji & Yaakob 2012]. The low temperature on the scavenge air, between 130˚C and 150˚C [Shu et al. 2013], is not attractive for power generation using the traditional RC [Yamamoto et al. 2001; Vanslambrouck et al. 2012]. The ORC technology presents a viable option to explore the usage of scavenge air waste heat on board for power generation [Kalikatzarakis & Frangopoulos 2014; Soffiato et al. 2015], but the behaviour of ORC WHRS in Arctic routes has not been studied in the existing literature.

The annual averaged temperatures in the poles are much lower than in other oceans; from a thermodynamic cycle point of view this is an area of opportunity since the WHRS thermal efficiency and power output could increase thanks to: A) a larger expansion of the working fluid [Cengel & Boles 2007] due to a lower saturation temperature; or B) by a reduction in power input at the condenser when holding constant the working fluid saturation temperature. Furthermore, the seawater (SW) can only be found as cold as -2.0˚C [Rayner et al. 2006] while for air, using the annual average, it can be as low as -12.0˚C[34] in navigable waters [Jones et al. 1999; Jones et al. 2012]. The cool air opens an interesting area of research in relation to marine WHRS which is the use of an air condenser instead of the typical SW condenser. In a land-based system some of the strengths of an air-cooled condenser are its low cost and reduction in water need [Salimpour & Bahrami 2010; Moore et al. 2014], while for the vessel's case in the Arctic it is the opportunity to have a lower power demand at the condenser or larger power production at the expander while requiring less corrosion-resistant materials for the heat exchanger. On the other hand, due to air's lower heat transfer coefficient and specific heat, there will be a need for larger heat transfer areas and volumetric flows in order to cope with the condenser's heat rejection, making it an interesting problem to study.

9.2 THE ARCTIC ROUTE

This chapter studies the effects of the Arctic temperature in a marine WHRS on board a container vessel navigating between Reykjavik, Iceland and the port of Ballstad in Norway as indicated in Figure 92. The distance covered by the ship between these two ports is 1,980 km. The route is chosen due to its low temperatures, the fact that it is open for navigation the whole

[33] This is not including the emissions coming from fishing activities which could add at least another 5.7 Mt of CO_2 to the Arctic environment in the year 2050 [Winther et al. 2014].
[34] This is the annual averaged temperature including anomalies for the south of Greenland adjacent to the Denmark Strait.

year, but also to the data availability from commercial shipping which can bring a more realistic scenario. A Japan - Europe route via the Bering Strait could see lower temperatures but this route will be only open in the summer and autumn months when the presence of ice is minimal [Corbett et al. 2010]. On the other hand, during these months the air and seawater temperature are at their highest.

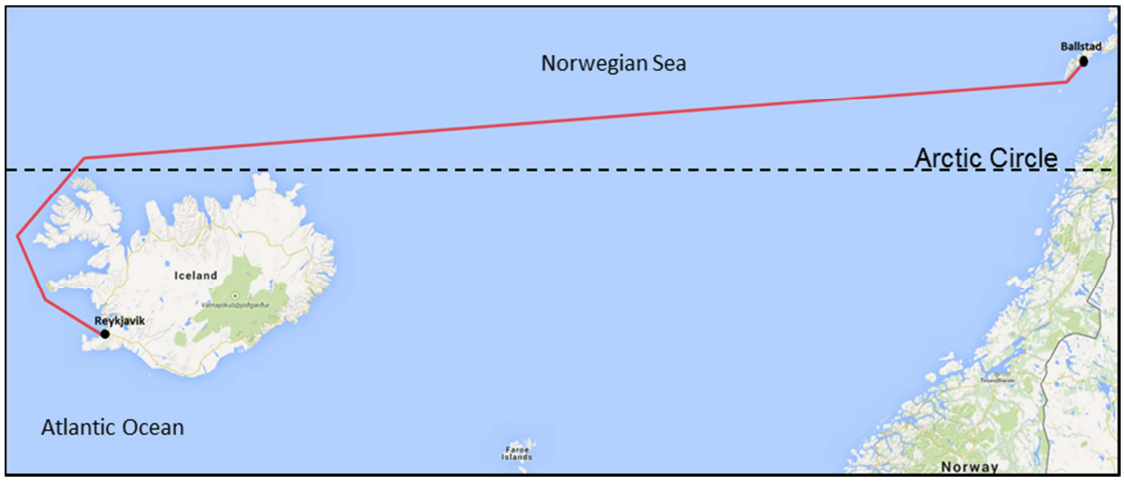

Figure 92: Representation of the route taken by a container ship between Iceland and Norway.

The route temperatures and temperature anomalies for air and SW were taken from CRUTEM4 and HadSST2 data sets [Jones et al. 1999; Rayner et al. 2006; Jones et al. 2012]. The route average temperature difference – without its standard deviation – between air and SW is at its largest between December and March with a maximum of 7.4˚C while its closest is found between May and September where the difference is just above 2.0˚C (see Figures 93 and 94). The air temperature is more susceptible to seasonal change having a large temperature gradient between summer and winter. Seawater temperature, on the other hand, is stable during the winter months and only increases considerably as the spring and summer months go by.

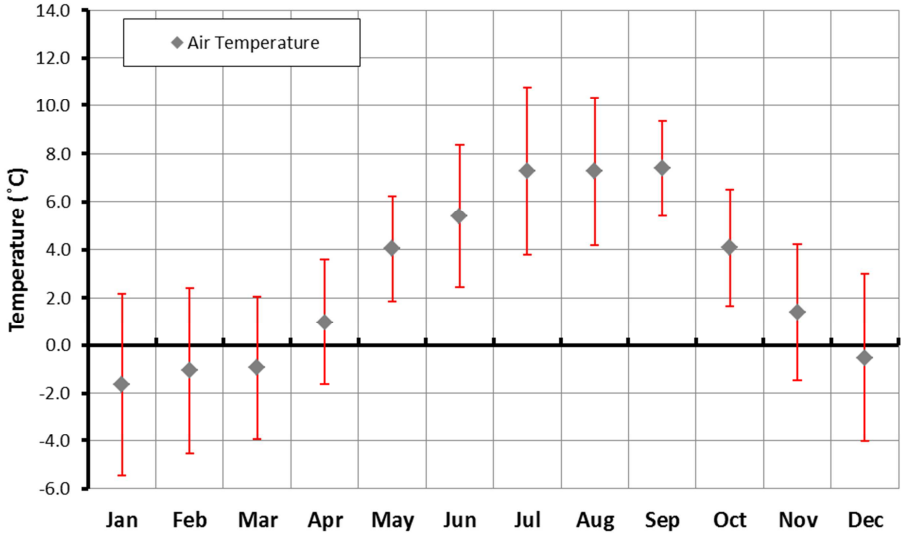

Figure 93: Average temperatures, including anomalies, for air where the container ship will be navigating. The region studied has latitude that goes from 62.5˚N to 67.5˚N and longitude from -22.5˚E to 12.5˚E. The bars on both figures represent the temperatures' standard deviation.

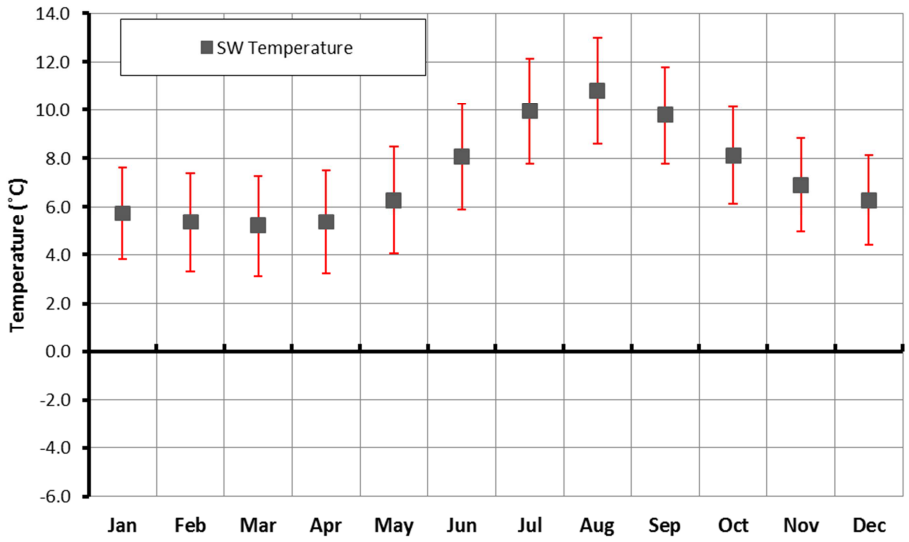

Figure 94: Average temperatures, including anomalies, for SW. The region studied has latitude from 62.5˚N to 67.5˚N and longitude from -22.5˚E to 12.5˚E. SW stands for seawater.

The container ship selected for the case study can carry 4,130 TEU with a design speed of 23.3 kn and a maximum speed of 25.2 kn. The operational profile for the container vessel is shown in Figure 95, where it can be seen that the majority of the time the ship is navigating slower but close to its design speed. The power requirement per vessel's speed was obtained by using the resistance model based on Holtrop and Menenen [1982] and Holtrop [1984] (described in Appendix VI).

Table 30: Container vessel's characteristics used for the case study [Clarkson Research Services Limited 2013; Containership-Info 2014].

Deadweight (t)	*Design Speed (kn)*	*Length (m)*	*Beam (m)*	*Draught (m)*	*Cp*	*Cm*
52,450	23.3	252.0	32.2	12.5	0.981	0.653

From the work of Banks et al. [2013], the container vessel will spend around 66% of the year fully loaded while the rest of the time is spent loading/unloading containers or in maintenance. This means that throughout the year the ship will be able to complete 52 round trips, an average of 4.33 trips per month. It is assumed that the vessel will have an operational life of 20 years.

From the National Ice Centre ice coverage charts, it could be assumed that ice formation would not be present in the route selected during the whole year [National Ice Center 2009]. Still, it is important to consider the possibility of an encounter with drift ice or floes along the route, especially near Iceland due to its vicinity with Greenland. Bearing this in mind, the ship design must consider and assess the hazards of navigating in the presence of ice to maintain the safety standards on board. For this ship, an Ice Class PC 6[35] is recommended which will require hull strengthening for ice and corrosion, engine capabilities for cold starts, and ventilation heat requirements, among others [International Association of Classification Societies Ltd. 2011].

[35] The Ice classification is given by the International Association of Classification Societies which has seven different ice classes [International Association of Classification Societies Ltd. 2011]. The International Maritime Organization adopted in 2014 the Polar code which will take effect at the beginning of 2017 reducing the number of classes to three [International Maritime Organization 2014c].

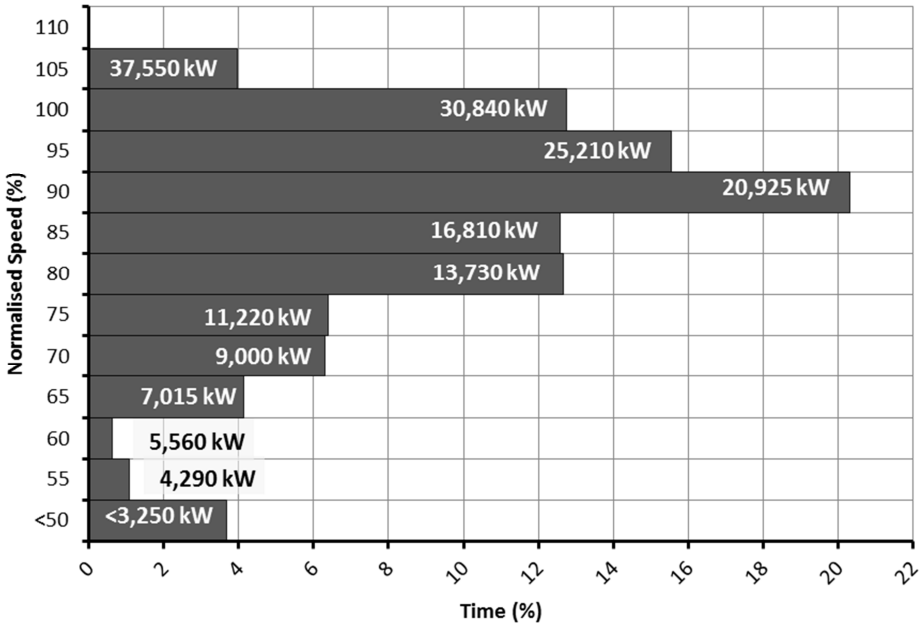

Figure 95: Annual operating profile for a container vessel navigating in the Arctic Circle between the Norwegian Sea and Atlantic Ocean. The speed profile is normalised to the ship's design speed which is 23.3 kn.

Since the ship will be navigating within the limits of the Arctic Circle, where the ambient temperatures are not lower than -15˚C, its winterisation level would be basic per Det Norske Veritas (DNV) AS [2013b].

9.3 DIESEL ENGINE

The vessel is powered by a two-stroke slow speed diesel engine using HFO as fuel [MAN Diesel & Turbo 2015b]. The engine is capable of delivering a maximum of 41,125 kW. The design point – design speed – will be set at 75% MCR with a power output of 30,840 kW. The HFO fuel price is assumed to be the overall price between the July 2013 and July 2015 which is £350 per tonne of HFO [Bunker Index 2015]. This value is assumed to be constant throughout the whole ship life in operation.

As previously mentioned, the vessel's heating requirement is higher in colder weathers. In this chapter, the waste heat availability in the exhaust gas is used for steam generation while the scavenge air waste heat is used for producing power.

The heat availability and quality from the scavenge air increases almost linearly with the change of engine loading (see Figure 96). It is assumed that for different air temperatures, the scavenge air temperature after compression would stay the same. This is caused by a 4 kW/˚C decrease in waste heat availability when the air temperature increases when fixing the engine's loading [MAN Diesel & Turbo 2015b].

The vessel studied in this work achieves, without any green technology on board and considering no auxiliary machinery, an EEDI of 17.753 g CO_2/t-nm. The index is above the maximum EEDI of 17.647 g CO_2/t-nm allowed for its ship type and class.

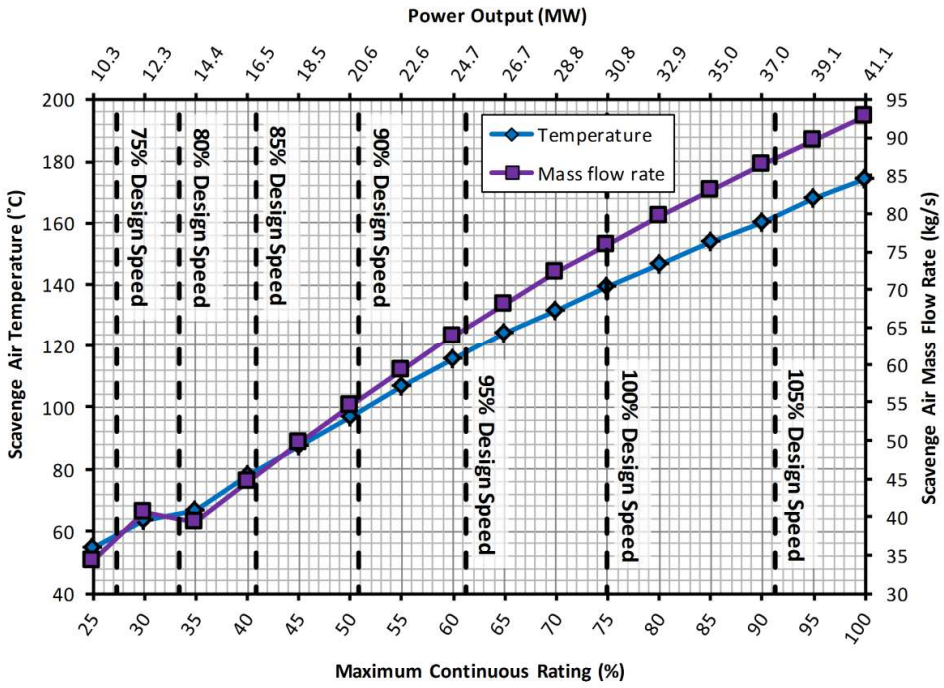

Figure 96: Temperature and mass flow rate after air is compressed. The data shown starts at 25% MCR due to the temperature being too close to the ambient temperature which does not need cooling [MAN Diesel & Turbo 2015b].

9.4 Waste Heat Recovery System

9.4.1 Working fluids

The working fluids studied are R1233zd(E), R236fa, R236ea and R245fa (see Table 13 for their properties) due to their non-flammable nature which permits, as per IMO Safety Of Life At Sea (SOLAS), their presence inside the machinery room [International Maritime Organization 2009b]. This allows for a more compact installation than when using flammable organic fluids on board due to the thermal oil circuit.

9.4.2 General layout

The main engine, ORC and waste heat boiler (WHB) are integrated as shown in Figure 97. Cold air enters the compressor which increases the incoming air pressure but at the same time its temperature which in turn reduces air density. A larger air density guarantees better combustion and fuel economy on board. The air temperature after compression is cooled via the WHRS economiser before it enters the engine. The study of how the combustion process is benefited by colder temperatures, as well as the design and behaviour of the compressor at different engine and air temperatures is outside of the scope of this thesis.

The hot exhaust gas from the turbocharger is used to produce steam inside a WHB as per the conditions given in section 6.6.5 which supports part, or the total, of the heat demand on board.

9.4.3 Organic Rankine cycle internal layout

The ORC uses a simple layout as described in section 2.3.2 and it is shown again in Figure 98. This layout is recommended for low quality heat sources, such as that found in the scavenge air

system, since the impact in thermal efficiency and power output is minimal compared to the investment of an extra heat exchanger on the recuperative layout [Larsen, Pierobon, et al. 2013].

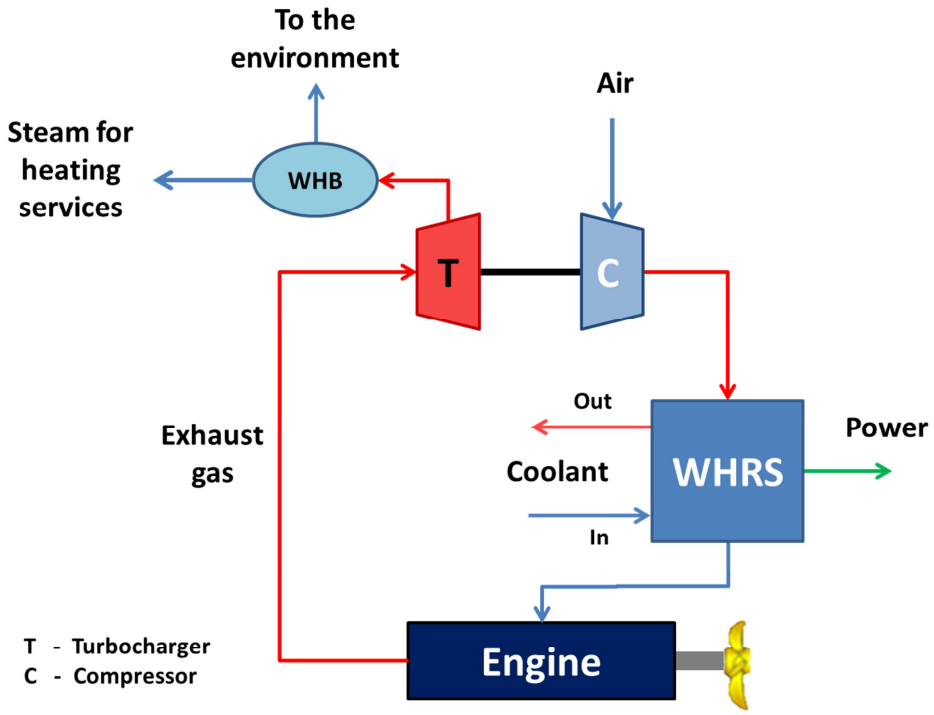

Figure 97: Sketch of the propulsion system layout using a WHRS on the scavenge air side. The layout also considers the use of a WHB on the exhaust gas after the turbochargers to cover the heating requirements when navigating in cold waters. In this chapter, the coolant could be either air or SW.

The saturation temperature at low pressure – point 3 in Figure 98 – is fixed at 25°C. The advantage is that it allows the WHRS to operate even if there are temperature anomalies on the annual voyages or the ship operator wants to switch to a warmer route. Another effect due to a larger saturation temperature is a larger pinch point temperature difference that allows for lower coolant mass flow rates, hence lower power consumption. On the other hand, there is a cost in the expander's work output since it operated at a higher low pressure which reduces the expansion process. From the point of view of the analysis, having a fixed saturation temperature makes the WHRS – not considering the bottom part of the cooler[36] as defined in Figure 98 – immune to weather conditions, only changing due to engine loading. This facilitates the study and understanding of the effect of the bottom section on the overall marine ORC performance.

The power produced by the WHRS is delivered to the main engine's shaft reducing the engine's fuel consumption and CO_2 emissions. When referring to total power output it means the final power delivered to the engine's shaft when considering the cooler's power requirement, as shown in equation [65].

[36] In this chapter, cooler refers to the whole heat exchanger normally known as condenser, and condenser to the two-phase section inside the cooler. This will avoid confusion when explaining the behaviour and characteristics of the cooler's condensing section.

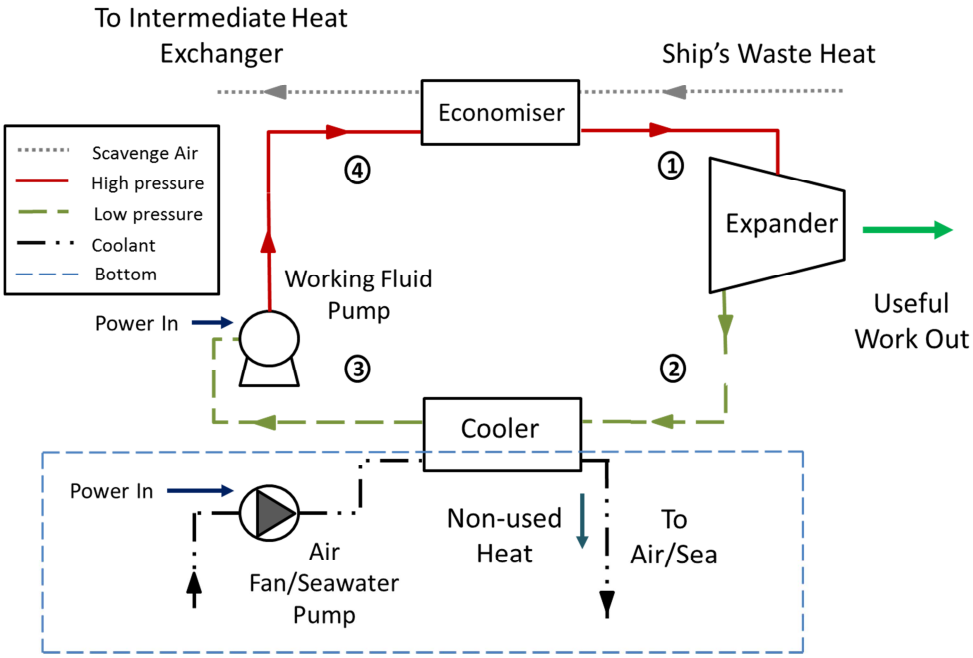

Figure 98: Simple plant layout for a marine ORC using the available waste heat after the air compression in the scavenge air system.

9.4.4 COOLER DESIGNS

The focus of this work is in the WHRS cooler where changes in the environment temperature throughout the year are seen. There are many different options to the construction of the cooler which will have an important impact on power requirement, area footprint and installation.

9.4.4.1 SEAWATER SHELL AND TUBE

This type of heat exchanger is formed by a bundle of round tubes mounted in a cylindrical metallic structure called shell. There are many different layouts for this type of heat exchanger which depend on how many tube and shell passes the fluids – hot and cold – have to do before exiting the heat exchanger.

Flowing inside the tube is recommended for the most corrosive fluids, but is also recommended for liquids. In its most simple layout of a shell and tube heat exchanger, the fluid inside the tube will do one pass inside the shell. In this work, the simplest configuration explored is a double tube pass in the shell in order to have a certain degree of compactness. The tubes in this study are assumed to be rounded and bare (i.e. without any heat transfer enhancers such as fins) for ease of maintenance. The tube layout is assumed to be a rotated square – same pitch between adjacent tubes (see Figure 99) – which gives higher heat transfer rates but with a larger pressure drop from the working fluid side [Sinnott 2005]. Due to the corrosive nature of SW, the cooler would be constructed using stainless steel with a thermal conductivity (κ) of 26 W/m-K and a density of around 7,700 kg/m^3.

The shell volume where the working fluid will flow is formed by the space available between the metallic shell and the tubes. In this region, the working fluid will give the excess heat to the

seawater and condensate until it is a saturated liquid. The shell section will have a series of baffles which modify the flow of the working fluid, increasing the turbulence and hence the heat transfer but raising the pressure drop.

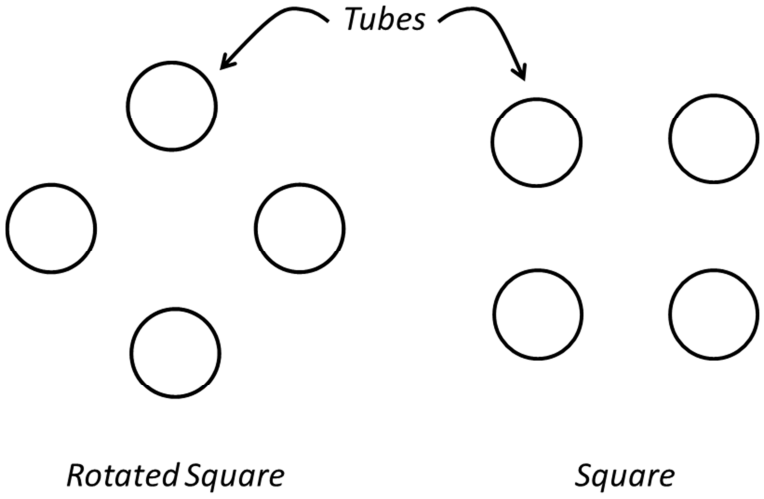

Figure 99: Possible tube's square layouts for a shell and tube cooler.

Shah [1983] considers this type of heat exchanger as not compact (i.e. heat transfer area density above 700 m^2/m^3) since it is not possible to accommodate the heat transfer area required in a small volume. Still, the great flexibility in design and operational conditions, and ease of maintenance makes this type of heat exchanger suitable as the WHRS cooler when using SW as coolant [Sinnott 2005]. The interested reader can access the Tubular Heat Exchangers Manufacturers Association [1999] standard for more information about the layout configurations.

9.4.4.2 AIR FINNED TUBE

The advantages of having a finned tube cooler is that this type of heat exchanger has a better heat transfer area density – could reach values of around 3,300 m^2/m^3 – than the shell and tube heat exchanger which in turn will have an important role in reducing the cooler's mass and volume [Shah & Sekulic 2003]. This is a critical aspect in this work since air's convective heat transfer coefficient (h^*[37]) tends to be low, requiring large heat transfer areas [Palm 2002]. The finned tube cooler is made of aluminium which has a thermal conductivity of 209 W/m-K with a density of 2,700 kg/m^3. It is important to bear in mind that the maintenance on the finned side could become burdensome and it is recommended that the least corrosive fluid with the lowest tendency to foul flows in this section, which in this case is air. This decision also makes sense from the overall heat transfer coefficient (U) point of view since air is flowing in the section of the cooler that offers the largest contact area which is beneficial when having a low h^*.

In order to take full advantage of the tube's fin area, the air flow will be perpendicular to the working fluid's flow which is inside the tubes. Contrary to a shell and tube heat exchanger, the working fluid will be flowing inside the tubes. The shape of the flow inside the tubes – interlaced or face split – is irrelevant to this problem since the working fluid speed inside the tubes is fixed

[37] The "*" is used for differentiation purposes with the specific enthalpy notation.

as an assumption to 15 m/s. A more detailed work with regard to the flow pattern inside the heat exchanger can be found in the work of Kærn et al. [2013].

A design of five finned tube rows with a rotated square layout was selected. This heat exchanger layout is in between the designs tested by Moore et al. [2014] who found that the overall thermodynamic plant efficiency is benefited by a larger number of tube rows. A five tube row layout gives a good trade-off between heat transfer effectiveness, pressure drop on the air side and cost.

The fins used are of circular construction with a small thickness when compared to its diameter and will be of the same material as the tubes. The fins will have an annular layout on the tube (i.e. perpendicular to the tube surface).

9.4.5 STEAM DEMAND

Having lower ambient temperatures translates to larger vessel heat demand in order to maintain the minimum operational temperatures throughout the ship [Lloyd's Register 2012c]. The minimum exhaust gas temperature, when consuming HFO, is 164°C thus the WHB can absorb the available waste heat until this temperature, to then exit to the environment.

Table 31: The table shows the averaged ambient temperature and the steam consumption throughout the operational year.

Month	*Air Temperature (°C)*	*Steam Requirement (kg/h)*
Jan	-1.7	2,430
Feb	-1.1	2,406
Mar	-0.9	2,398
Apr	1.0	2,322
May	4.0	2,202
Jun	5.4	2,146
Jul	7.3	2,070
Aug	7.3	2,070
Sep	7.4	2,066
Oct	4.1	2,198
Nov	1.4	2,306
Dec	-0.5	2,382

Table 31 gives the steam requirement for the ship during the year. The steam demand due to the power installed is assumed to be constant; the variation seen in the following table is caused by the change in the air temperature during the year.

When there is not enough steam coming from the WHB, an auxiliary boiler using HFO will cover the required additional heat supply to the vessel. The design of the WHB, how much of the ship's heating demand is covered by the WHB, and its impact on the CO_2 emissions is out of the scope of this chapter.

9.5 THEORY AND CALCULATIONS

While this work will thermodynamically design the WHRS – points 1 to 4 in Figure 98 – as per the development outlined in section 6.6.2, calculations regarding costs, EEDI and other relevant equations not discussed in this section come from chapter 6.

9.5.1 COOLERS

In order to fully comprehend the implications and differences between the two different cooling fluids, a high detail model for the cooler is required. In this subsection, the basic equations for a shell and tube cooler and a finned tube heat exchanger are shown. The heat rejection occurs in two different steps as shown in Figure 49: desuperheating and condensing.

9.5.1.1 SHELL AND TUBE

The methodology used for the shell and tube heat exchanger is similar to that used in Pierobon, Larsen et al. [2013].

A new term must be added to equation [23] when using a shell and tube heat exchanger, this is known as the temperature correction factor (F_t). It accounts for the deviation of the flow shape inside the cooler from an ideal counter current flow and is calculated as proposed by Fakheri [2003]. In the desuperheating (*ds*) section of the cooler, the heat rejected is found as follows:

$$\dot{Q}_{ds} = U_{ds} A_{ds} F_t \Delta T_{lm,ds} \qquad [\ 93\ ]$$

Since this type of cooler uses bare tubes, the heat transfer area (A_{ds}) is formed only by the tubes' surface area. The overall heat transfer coefficient (U) for this section is found, when seen from the outside of the tubes, as follows:

$$U_{ds} = \frac{1}{\left(\frac{1}{h^*_{ds,o}} + \frac{1}{h^*_{of}}\right) + \frac{d_o}{2\kappa_t} ln\left(\frac{d_o}{d_i}\right) + \frac{d_o}{d_i}\left(\frac{1}{h^*_{ds,i}} + \frac{1}{h^*_{if}}\right)} \qquad [\ 94\ ]$$

Where κ_t is the thermal conductivity of the tube. The fouling convective factors are represented by h^*_{if} and h^*_{of} – inside and outside of the tube – with a value of 5,000 W/m^2-K per Sinnott [2005]. The variables $h^*_{ds,i}$ and $h^*_{ds,o}$ are the convective heat transfer coefficients for the inside and outside of the tube respectively. The internal and external diameters are represented by d_i and d_o respectively (see Figure 100).

To find $h^*_{ds,i}$ the following equation is used [Sinnott 2005]:

$$h^*_{ds,i} = j_{ht,i} \frac{\kappa_{SW}}{d_i} RePr^{0.33} \left(\frac{\mu_t}{\mu_{tw}}\right)^{0.14} \qquad [\ 95\ ]$$

The variable μ_t is the dynamic viscosity at the average tube's temperature between the inlet and outlet, while μ_{tw} is the dynamic viscosity at the wall temperature. The factor $j_{ht,i}$ represents the heat transfer correction factor from the tube side and is evaluated as shown in Sinnott [2005]. The variable κ_{SW} is used for SW thermal conductivity, while *Re* and *Pr* stand for the Reynolds and Prandtl number inside the tubes respectively.

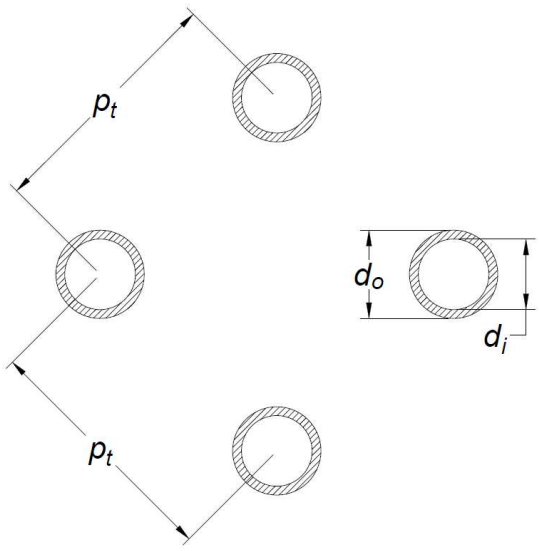

Figure 100: SW cooler tube rotated square pattern inside the shell. The variable p_t represents the tube pitch.

From the shell side, the heat transfer coefficient ($h^*_{ds,o}$) is found with the next equation:

$$h^*_{ds,o} = j_{ht,o} \frac{\kappa_{wf}}{d_s} RePr^{0.33} \left(\frac{\mu_s}{\mu_{sw}}\right)^{0.14} \quad [\ 96\ ]$$

As with $j_{ht,i}$, $j_{ht,o}$ is found for the shell side as described in Sinnott [2005], κ_{wf} is the thermal conductivity of the working fluid, μ_s is the dynamic viscosity at the average shell's temperature between the inlet and outlet, while μ_{ws} is working fluid's dynamic viscosity at the tube's outer wall temperature and d_s is the shell diameter as seen in Figure 101 and is calculated as follows:

$$d_s = d_B + d_{cl} = d_o \left(\frac{N_t}{K}\right)^n + d_{cl} \quad [\ 97\ ]$$

Where d_B is the tube bundle diameter, d_{cl} is the clearance between the shell and the tube bundle as given by Sinnott [2005], N_t is the total number of tubes in the heat exchanger. The constant K and n are used to estimate the shell diameter and are dependent on pitch type, tube pitch (p_t) and number of tube passes. Values of K and n are taken from Sinnott [2005]. The saturation section of the condenser has a different behaviour than a pure gas or liquid since it is a mixture of these two states. The U_{co} for the two-phase working fluid is calculated as in equation [94], with the convective heat transfer ($h_{co,o}$) outside the tube given by:

$$h^*_{co,o} = 0.95\kappa_{wf} \left(\frac{\rho_l(\rho_l - \rho_v) g N_t l_t}{\dot{m}_{wf}}\right)^{0.33} \quad [\ 98\ ]$$

Where ρ_l and ρ_v are the working fluid densities as a saturated liquid and saturated vapour respectively, g is the gravitational acceleration assumed to be 9.81 m/s and l_t stands for the tube's length.

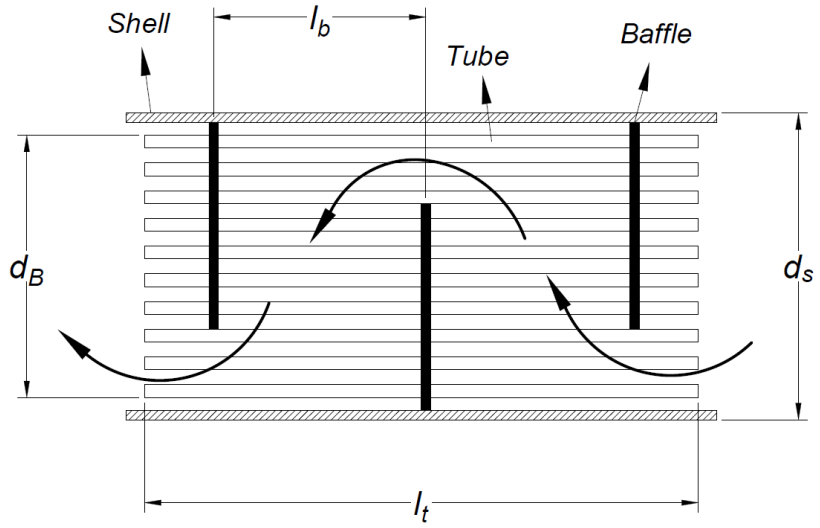

Figure 101: Diagram that shows the important construction dimensions for the SW cooler. Seawater runs inside the tubes while the working fluid flows in a non-ideal counter flow inside the shell. The figure is a simplified construction of a single tube pass inside a shell. The variable l_b stands for the baffle spacing which is controlled by the optimisation process.

For $h^*_{co,i}$, the following expression is used:

$$h^*_{co,i} = \frac{\kappa_{SW} Nu}{d_i} \quad [\ 99\ ]$$

The Nusselt number (*Nu)* is evaluated using the correlations given by Gnielinski [1976]. The pressure drop in the cooling fluid circuit (ΔP_i) is presented [Sinnott 2005]:

$$\Delta P_i = \frac{N_t \rho_i v_i^2}{2}\left[8 j_{f,i}\frac{l_t}{d_i}\left(\frac{\mu_s}{\mu_{sw}}\right)^{-m} + 2.5\right] \quad [\ 100\ ]$$

Where *v* is the speed of the fluid inside the tube, j_{fi} is the correction factor due to friction inside the tube and is found in Sinnott [2005], *m* has a value of 0.25 if the flow inside the tube is laminar (*Re*<2,100) or 0.14 when it is turbulent (*Re*> 2,100). For the pressure drop in the working fluid side (ΔP_o) – shell side – please refer to Sinnott [Ibid.].

An alternative way of finding the power input required by the pressure change device ($\dot{W}_S$) – could be the SW pump but also applies to the air's fan – is used in this chapter:

$$\dot{W}_S = \frac{v_i A_{cf} \Delta P_S}{\eta_S} \quad [\ 101\ ]$$

In the previous equation the change in pressure (ΔP_S) at the SW pump is set to 100 kPa – to overcome the head losses from bringing the SW from the waterline to where the cooler is located on board – plus the ΔP_i given by equation [100]. The SW pump efficiency (η_S) is assumed to be 80% as with the working fluid pump. The cross-sectional area (A_{cf}) where the coolant flows is given by:

$$A_{cf} = \frac{N_t d_i^2}{4} \quad [\ 102\ ]$$

Finally, the cooler's volume (V) is determined by:

$$V = \frac{d_s^2 l_t}{4} \quad [\ 103\ ]$$

9.5.1.2 FINNED TUBE

The finned tube methodology is developed as shown in the work of Kærn et al. [2013] and in this section only the most relevant equations are shown.

Equation [94] must be modified in order to take into consideration the increase area due to fins, hence U_{ds} for finned tube coolers is found as follows:

$$U_{ds} = \frac{1}{\frac{1}{\eta_f A_{T,ds}}\left(\frac{1}{h^*_{ds,o}} + \frac{1}{h^*_{of}}\right) + \frac{d_o}{2\kappa_t} ln\left(\frac{d_o}{d_i}\right) + \frac{1}{A_{t,ds}}\left(\frac{1}{h^*_{ds,i}} + \frac{1}{h^*_{if}}\right)} \quad [\ 104\ ]$$

Where A_T is the total heat transfer area found in the desuperheating section which is built by the total fin's surface area (A_f) plus the tube's total free surface area (A_t) at that section of the heat exchanger, and η_f is the fin's efficiency approximated by Schmidt [1949].

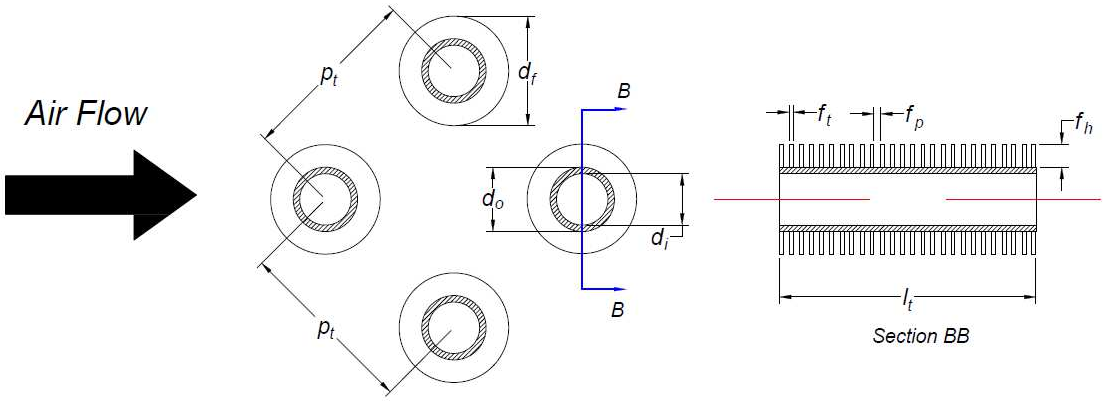

Figure 102: Diagram that represents the tube layout for the marine WHRS cross-flow air cooler. The fin thickness (f_t) is chosen by the optimisation process.

The fin diameter (d_f) is given by d_o plus two times the fin height (f_h) which is a variable controlled by the optimisation process (see Figure 102). So, A_f can be found as follows:

$$A_f = \frac{\pi l_t \left(d_f - d_o\right)^2}{2 f_p} \quad [\ 105\ ]$$

The variable f_p stands for the fin's pitch which, with l_t, gives the total number of fins on a tube (N_f).

Starting from the desuperheating section of the cooler, the convective heat transfer coefficient inside the tubes ($h^*_{ds,i}$) is found as in equation [99], while outside ($h^*_{ds,o}$) is given by:

$$h^*_{ds,o} = 0.38 \frac{\kappa_a}{d_o} Re^{0.6} Pr^{0.33} \left(\frac{A_{T,ds}}{A_{t,ds}}\right)^{-0.15} \quad [\ 106\ ]$$

Where κ_a is the air's thermal conductivity and *Re* is measured for the outside of the finned tubes. For the condensing section, $h^*_{co,o}$ is calculated as given in equation [106] and for $h^*_{co,i}$ is used [Shah 1979]:

$$h^*_{co,i} = 0.02273 \frac{\kappa_{wf} Nu}{d_i} \frac{\left(24.44 P_r^{19/50} + 89.91\right)}{P_r^{19/50}} \quad [\ 107\ ]$$

Where P_r is the reduced pressure – P_3 divided by the working fluid's critical pressure (P_{cr}) – and *Nu* is found by the following expression:

$$Nu = 0.023 Re^{0.8} Pr^{0.4} \quad [\ 108\ ]$$

The pressure drop on the air side (ΔP_o) is found with:

$$\Delta P_o = 2 j_{f,o} \rho_a v_{os}^2 N_{tr} \quad [\ 109\ ]$$

Where v_{os} is the air's speed through the smallest cross-section of the tube bundle, N_{tr} is number of tube rows, and $j_{f,o}$ is the friction factor on the air side found using the Robinson and Briggs correlation for staggered tube bundles [Robinson & Briggs 1966]. For the pressure drop inside the tubes (ΔP_i) – for the working fluid – the correlations from Gnielinski [1976] and Müller-Steinhagen and Heck [1986] are employed.

The fan power can be determined by using equation [101], but in the case of the fan a constant η_S of 60% is used as per Walraven et al. [2015]. The cross-sectional area is found as follows:

$$A_{cs} = l_t p_t N_{tpr} \quad [\ 110\ ]$$

The variable N_{tpr} stands for the number of tubes per row which is fixed at five tubes, while p_t is the transverse pitch between tubes fixed at 0.083 m. As seen in the work of Habl et al. [2012] it can be expected that the air cooler's ΔP_S will impact considerably the fan power input. Hence, ΔP_S is minimised using a single variable optimisation available in Matlab® – fminbnd – with the aim of reducing $\dot{W}_S$ [The MathWorks Inc. 2015a]. The search space for this function is between the atmospheric pressure and 106 kPa which will ensure that the fan will be capable of overcoming the pressure losses and move the air through the cooler.

The total volume of the air cooler is given by:

$$V = p_t^2 l_t N_{tr} N_{tpr} \quad [\ 111\ ]$$

9.5.2 Off-design operation

The previous equations reflect how the model will design the cooler at design point. Heat transfer areas as well as the working fluid's pressure at different engine loadings stay fixed for

the life of the WHRS. As the vessel navigates along its route during the year, there will be instances when it will operate at off-design conditions. To discover how the cooler and its pressure change device will operate under these conditions, it is necessary to calculate how the cooler's overall heat transfer coefficient and SW pump behave[38].

The SW pump power change is related to the increase/decrease of the cooler duty but also to the SW temperature over the months. To cope with these changes the SW pump adapts its mass flow rate which affects its efficiency as given by Veres [1994] and shown in equations [63] and [64]. For the *U* values of both type of cooler, the following expressions were used [Incropera et al. 2007]:

$$U_{ds,off} = U_{ds,d} M^{0.6} \qquad [\ 112\ ]$$

$$U_{co,off} = U_{co,d} M^{0.6} \qquad [\ 113\ ]$$

Where *M* is the working fluid's mass flow rate ratio between the off-design and design condition. This same ratio applies to the other WHRS heat exchangers.

The change in pressure drop in both types of cooler is calculated as shown in the previous subsections and added to $\Delta P_{S,off}$. Finally, to obtain the cooler's power requirement at off-design conditions, equation [101] is used with the off-design values.

9.5.3 Optimisation

The detailed designs of both the WHRS and cooler require a large number of variables to be explored with the aim of reducing the maximum annual CO_2. For the case where the WHRS is cooled by SW, there are 12 different variables while when it is cooled by air, the number of variables is 14 (see Tables 32 and 33). This large dimensional search space requires an efficient optimisation approach which can return reliable data.

Multi-objective optimisations (MO), as that used in the previous chapter, have the advantage of finding optimal results when trading-off between different aims. The MO can have, in general, three approaches to a multidimensional analysis: 1) let the optimisation select random values inside a boundary established by the user, but without nonlinear inequalities or equalities and adding checks inside the objective function in order to guarantee that the physical constraints – thermodynamics, fluid's flow, heat exchanging, etc. – are followed; 2) constrain the problem further by adding nonlinear inequalities or equalities and adding a post-processing quality control to check for abnormal results (i.e. that fall outside of the physical constraints) caused by variables too close to the boundaries imposed; or 3) a hybrid approach between 1) and 2) which eliminates the need of a post-processing quality control.

For the problem analysed in this chapter, case 1) has a low probability of finding an optimal design by choosing random variable values in a 12 dimensional (D) – or 14-D – space which follows the physical constraints. This causes the optimisation process, even with a large number

[38] No literature was found that discussed or experimented with the performance of an air fan on off-design conditions, hence the assumption that its efficiency is constant for any operating conditions.

of data points in an iteration, to take a long time to find a single solution. A first run of the Arctic algorithm using MO took around 23 hours to find a solution being this process too slow. The second approach, while is probably faster in processing time from what was discussed in the previous chapter, has as its main drawback the fact that in order to constrain a large multidimensional space with nonlinear inequalities or equalities; it is necessary to understand the interactions and effects of 12 to 14 different variables. This, if it is possible, is a time consuming task with a high probability of eliminating a critical search space when taking assumptions in the various calculations. In case 3) there are advantages to the previous cases but in general the same critical disadvantage seen in case 2) is found.

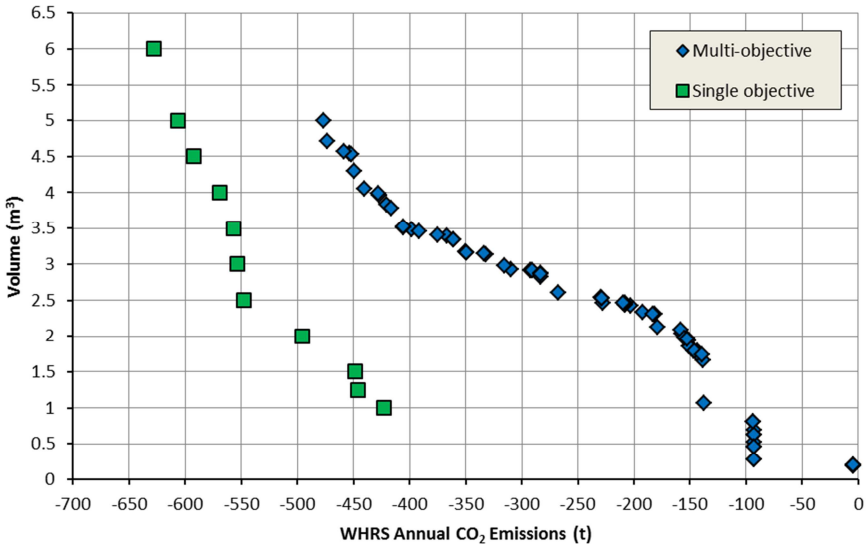

Figure 103: Optimal results from different optimisation approaches which compare the CO_2 emission reduction in a year to the WHRS' SW cooler volume when using as working fluid R236fa.

A single-objective optimisation (SO) trades the ability to compare multiple desired aims for a faster processing time. It is also possible to include a larger population of data points – the author tried up to 25,000 data points per iteration – without requiring a long computational time (i.e. less than one hour). Interestingly, when comparing optimal results between MO and SO, the SO WHRS designs – cooled by SW – returned a larger annual CO_2 emission reduction under the same constraint volume (see Figure 103). This is mainly to do with the amount of data points handled by an SO which enables the optimisation to unstick itself faster from local maxima[39], but also due to the MO trade-off between objectives – CO_2 emission reduction and cooler volume – which inhibits the search of the largest annual CO_2 emission reduction maxima.

The optimisation approach used in this chapter is comprised of a two-step SO conformed by Particle Swarm Optimisation (PSWO) followed by Pattern Search Optimisation (PSO).

9.5.3.1 PARTICLE SWARM

This optimisation technique was first developed by Kennedy and Eberhart [1995] to describe the movements of a bird inside a flock. They assumed that birds, distributed randomly, look for food

[39] Refers to the derivative or gradient being zero which could mean that the solution found could be a minimum or a maximum depending on the criteria used for the optimisation process.

without normally knowing where it is, but they know with each iteration how close they are getting to it. So birds, as social agents, increase their probability of finding food by following the bird that is closer to the food source. In the WHRS algorithm the food is the maximum annual CO_2 emission reduction possible, while the birds – particles – are the different WHRS designs – including the cooler design.

The PSWO is similar to the genetic algorithm (GA) in the sense that it begins with a random distributed population or particles – data points – and looks for the optimum result for each iteration by using gradients or derivatives. But PSWO does not depend on evolution terms such as mutation to increase the solution diversity. This makes PSWO a simpler stochastic approach than GAs. It takes around 30 minutes to find an optimum design using a quad core processor, Matlab® 2015a core parallelisation and 10,000 particles with 10 iterations.

9.5.3.2 PATTERN SEARCH

As previously mentioned, with the large search space there still is a high probability that PSWO is stuck in a local maximum due to the nature of the optimisation to follow the most optimal solution – particle – without finding the global maxima. Pattern search optimisation is a simple derivative-free heuristic method which has the task of finding new directions in the search space to improve the objective (i.e. annual CO_2 emissions). The method does not depend on gradients to find the improved direction since it changes the search size by N-times – when the search was successful – or by 1/N – when the search was unsuccessful – in the different search directions of the optimal reference point [Hooke & Jeeves 1961].

The PSO starts with a reference point in the search space and depends on two different move methods to look for a better WHRS: Exploratory and Pattern. In the Exploratory move, the optimisation searches for an improving direction by creating nodes at fixed distance from the reference point and evaluating the function on those new nodes. Pattern has the task of improving the search time by increasing the distance to the reference point in the successful direction of the Exploratory move. The Pattern move stops when the objective function does not reduce the objective, which in turn restarts the Exploratory move. This process continues until the search size for each variable is considered sufficiently small [Lai & Chan 2007].

One of the most important drawbacks of PSO in large variable spaces is that there is a high probability that it will not find an optimum value since it is only following the reduction of the function without considering the gradient. In order to use this drawback as an advantage, the optimisation process for the marine WHRS uses the optimal result from PSWO and is used as PSO starting point. The Pattern search optimisation direct search approach challenges the PSWO solution and enables the exploring of space near the optimum solution for a better/larger maxima. Matlab® PSO uses an N equal to 2 for the Exploratory and Pattern moves, and examines into two different direction vectors per variable [The MathWorks Inc. 2015b]. For example, for a single variable search the direction vectors will be $\boldsymbol{v}_1 = 1$ and $\boldsymbol{v}_2 = -1$.

In general, running PSO after PSWO for the marine WHRS model manages to increase the annual CO_2 emission reductions found by PSWO by at least 10%.

9.5.4 WASTE HEAT RECOVERY SYSTEM ALGORITHM

The WHRS model is based in Matlab language. The code optimisation procedure is embedded in the WHRS model and has the objective of finding the WHRS design that achieves the maximum CO_2 reduction in a year (see Figure 104). Other important variables for this study such as the EEDI and cost are calculated and stored in memory for later analysis.

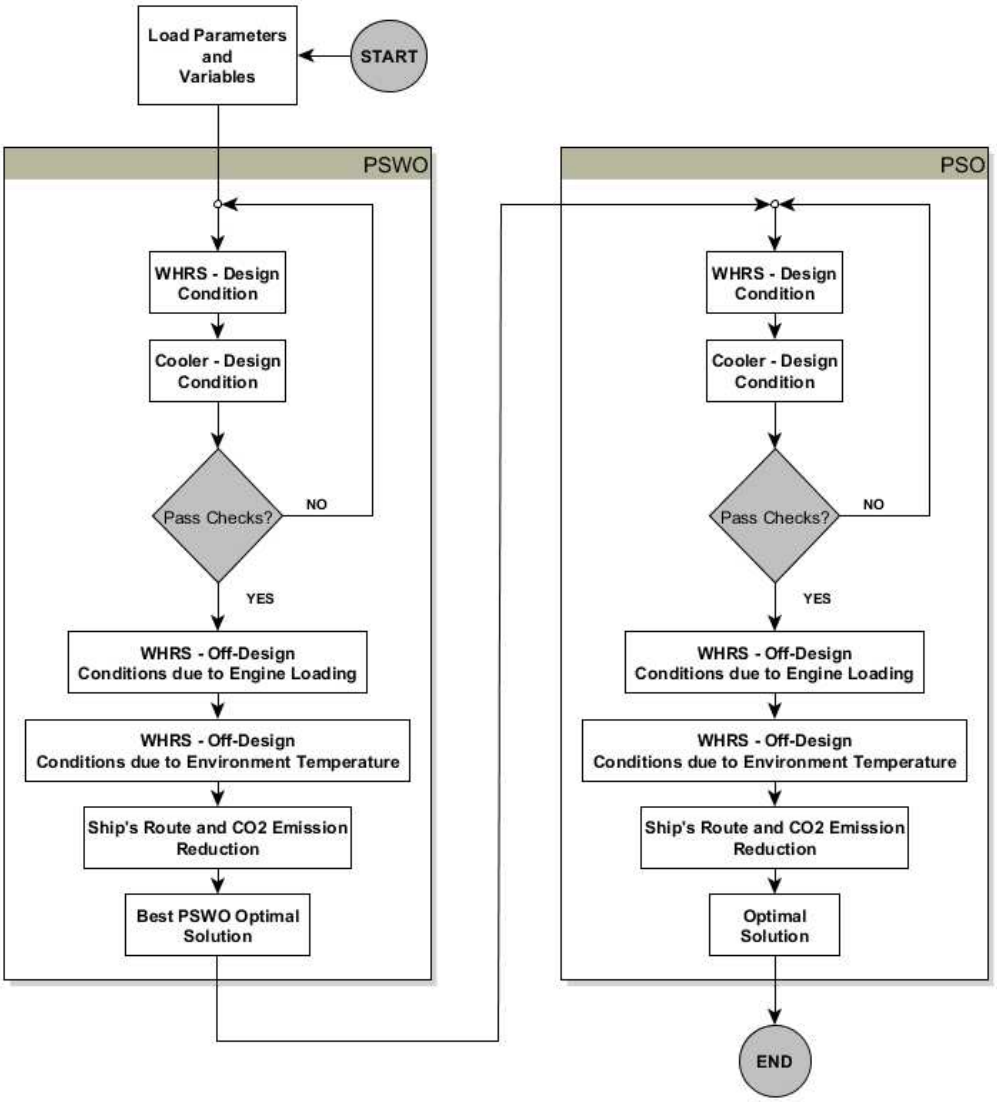

Figure 104: Code structure developed for the analysis of marine WHRS in cold weathers. Inside the optimisation is found the design of the WHRS and cooler integrated to the speed profile and ship's route.

Before starting, it must be manually selected the working fluid, coolant and temperature at which the WHRS will be designed. Only the seven highest vessel speeds per Figure 95 were deemed relevant for this study – due to the waste heat quality and availability – which cover between 27% and 100% of the engine's MCR. The optimisation process begins by choosing the WHRS and condenser design characteristics shown in Tables 32 and 33 which impose the first constraints of the problem.

The process starts with PSWO by designing the WHRS to then move to the cooler design where the equations shown in section 9.5.1 are used. Due to the large search space, a

population of 10,000 particles over 10 iterations is used in PSWO which brings a good trade-off between finding optimal solutions and computational time.

Table 32: Operating characteristic ranges explored by both optimisation techniques which found the best marine WHRS for a container vessel.

Parameter	Cooling Fluid	Range
Scavenge Air Outlet Temperature (˚C)	Air/SW	50 - 120
Scavenge Air Bypass (%)	Air/SW	0 – 75
P_1 (kPa)	Air/SW	300 – 0.95*P_{cr}
Superheating Temperature (˚C)	Air/SW	5 – 100
$\Delta T_{pp,c}$ (˚C)	Air/SW	5 – 25
WHRS Design Point (Ship Speeds)	Air/SW	75% -105% of Design Speed (27% - 91% MCR)

Table 33: Cooler design characteristics with their respective range of values for usage in northern waters.

Parameter	Cooling Fluid	Range
Material	Air	Aluminium
	SW	Stainless Steel
Flow	Air	Cross
	SW	Counter
Fan/pump Design Isentropic Efficiency (%)	Air	60
	SW	80
Tube Internal Diameter (mm)	Air/SW	16 – 100
Tube length (m)	Air/SW	1.83 – 7.32
Transversal Tube Pitch (mm)	Air	93
	SW	1.4 * d_o
Tube Layout	Air/SW	Square Staggered
Fin Height (mm)	Air	2 – 16
Fin Thickness (mm)	Air	$8x10^{-2}$ – 25 $x10^{-2}$
Fin Pitch (mm)	Air	2 – 24
Baffle Spacing (% of Shell Diameter)	SW	50 – 200

Checks are added to the code before entering into off-design conditions which will verify that the solution is following the physical phenomena happening in a thermodynamic cycle. Such checks are, for example, a test of the first law of thermodynamic or acceptable pressure drop level inside the cooler provided by Sinnott [2005]. The cooler design is constrained to a volume similar to a TEU (i.e. 38.5 m^3) which is considered to be enough space on board with low-impact on the cargo capacity. If one of these checks is not passed, the WHRS design is deemed unsuccessful and starts again with a new set of variables selected by the optimisation process.

The first off-design conditions code tests the WHRS under different engine loading conditions and judges, from the net power output point of view, if it is feasible to operate the WHRS at a particular condition. The analysis will be stored in memory for its use in the second off-design stage which allows for a more efficient computational process since it will not be required to calculate the WHRS performance during the months of the year. The second section of the off-design conditions is the analysis of the performance change in the fan/pump due to a change in the coolant temperature. Inside this section, the route information (e.g. temperature and distance) is found and in conjunction with the WHRS and cooler performance it is possible to find the annual CO_2 emissions saved by using a marine ORC. At this stage the vessel EEDI reduction, initial costs and payback time are also quantified.

In the following step, the code selects the most optimal result from PSWO and it is fed into the PSO as the starting point. PSO stops when the distance to the optimal solution is less than $1x10^{-7}$ which is the standard value given in Matlab®. The process in PSO is almost identical to the PSWO except that at the end, PSO returns only a single optimum value.

Due to the large search space – at least 12 variables – the optimisation process is run 240 times – 30 times per working and cooling fluid combination – in order to have a wide range of different optimal WHRS designs which could explain how the operating conditions had an effect on the WHRS design and operation. This also allows for the analysis of different objectives into the results, emulating in a certain degree what an MO does.

9.5.5 SOFTWARE

The Matlab® code generated for this chapter is a collaborative effort between UCL, DTU and Chalmers University. Due to limitations in the range of operating conditions in the SW properties code by Sharqawy et al. [2010] it was decided to use water instead as shown in Bell et al. [2014].

9.6 MODEL VALIDATION

The model developed here is unique in different aspects such as the coupled optimisation process, the number of optimisation variables, the detailed WHRS cooler analysis and the ship's route integrated with the speed profile. This uniqueness makes it difficult to compare it to other works. Still, the WHRS model, both cooler design and routing algorithms have been used successfully in the following works: Larsen, Pierobon et al. [2013], Pierobon, Larsen et al. [2013], Kærn et al. [2013], Pierobon and Haglind [2014], Suárez de la Fuente et al. [2015]. Still,

a validation is made by comparing the results shown in this chapter with those found in related works to the areas of marine WHRS.

9.7 RESULTS AND DISCUSSION

9.7.1 ANNUAL ENVIRONMENTAL IMPACT

In this section, the annual performance of the WHRS at the different ship speeds and environment temperatures are found for each of the cooling and working fluids used. Using equations [71] to [81] and a carbon factor (*CF*) of 3.1144 t CO_2/t HFO (see Table 3), it is quantified the amount of emissions saved thanks to the use on board of a marine WHRS.

In order to understand how the annual emissions savings are achieved, the analysis must be split in two parts: A) the thermodynamic cycle which only varies with the change of engine loading due to the speed profile given in Figure 95; and B) the cooler's bottom section – includes the fan/pump power consumption, heat rejection and physical characteristics – which varies during the year due to cooling fluid changing temperatures.

A. WASTE HEAT RECOVERY SYSTEM POWER PRODUCTION

Firstly, the power output at design speed per working and cooling fluid was compared. Using a one-way analysis of variance (ANOVA) coupled with a Bonferroni test[40] – to correct any probability values for multiple comparisons – only a statistically significant difference was found between the power output at design speed devolved by WHRS using R236fa and R1233zd(E). This is due to the change in enthalpy, where R1233zd(E) shows a larger drop at the expander – 30.62 kJ/kg – than R236fa's 23.55 kJ/kg, caused mainly due to a lower pressure after expansion for the former working fluid.

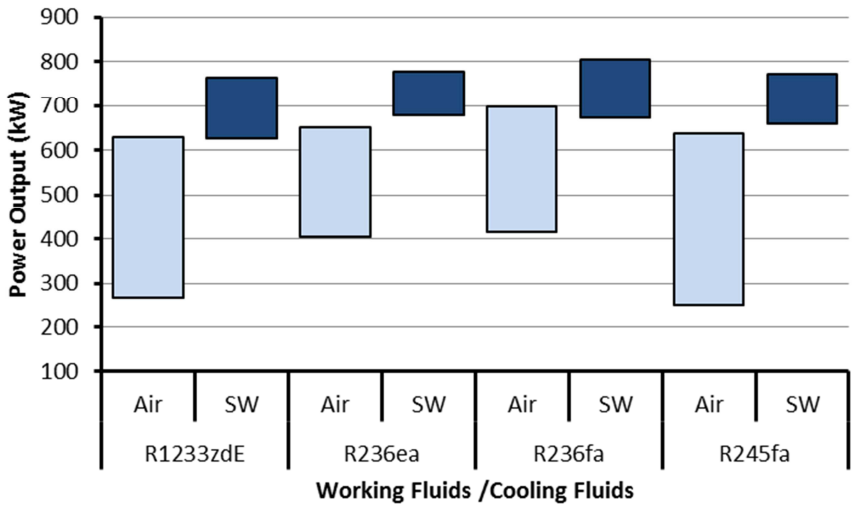

Figure 105: Power output for different ORC WHRS cooled by SW or air at the ship's design speed.

Interestingly, R236fa achieves a larger power output than R1233zd(E) WHRS due to its larger heat absorption. This causes larger mass flow rates (i.e. 28.2 kg/s when using R236fa and

[40] For more about the ANOVA and Bonferroni test please refer to National Institute of Standards and Technology & SEMATECH [2012]

19.4 kg/s for R1233zd(E) systems), which compensate R236fa's low enthalpy change at the expander. Thus, it can be said that R236fa ORC behaves differently than an ORC using R1233zd(E), it is not possible to observe differences between these fluids and the other two refrigerants tested.

However, when analysed the power output by cooling fluid using a t-test with assumed equal variances [Student 1908][41], where important differences between water and air are seen. The SW-cooled cases have a significantly larger mean power output than air cases. Its mean is 727 kW with a standard deviation of 30 kW, while in contrast the air-cooled is around 524 kW with a standard deviation of 82 kW. It is because of this larger difference between cooling fluids that it was decided to continue the main analysis comparing only between cooling fluids (see Figure 106).

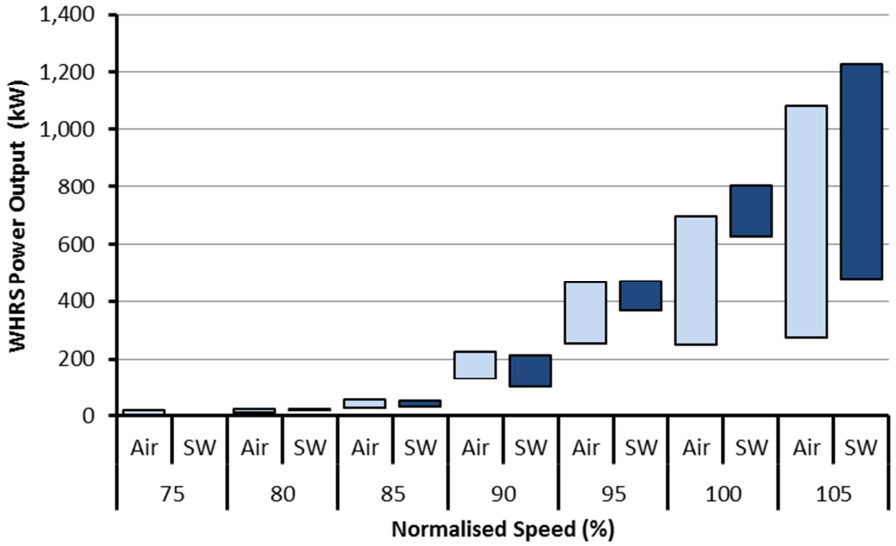

Figure 106: Maximum and minimum power produced by each WHRS – not considering the condenser's power requirement – grouped by cooling fluid at different vessel's speeds.

At the highest speeds – therefore larger engine power output – due to a larger waste heat availability from the scavenge air, the largest WHRS power outputs when cooled by any of the two cooling fluids is achieved. When the WHRS is cooled by SW and the vessel's speed is between 100% and 105% of the design speed, this configuration offers designs that produce higher power outputs than air (see Figure 106). Below these speeds, air-cooled WHRS have exponents that achieve larger power outputs. At the lower end of the speed spectrum for both cooling approaches, it is seen that the power produced is quite insignificant when compared to higher speeds.

At which operating speeds the WHRS is working is another important factor for the annual CO_2 reduction. For example, at the 105% of the design speed the WHRS' largest power output for both cooling fluids is achieved. But this condition only represents 4% of the time the ship is operating which reduces the impact of a larger power output. Along the same lines, another

[41] A t-test is suitable for binary mean comparisons of small groups of data.

interesting finding is that when the WHRS is cooled by air, it will on average operate in 4.7 of the ship's speeds with few designs that can operate over the seven different ship speeds studied (see Figure 107). In the case of SW it operates in 4.3 of the speeds tested with one case which operated under six different speeds.

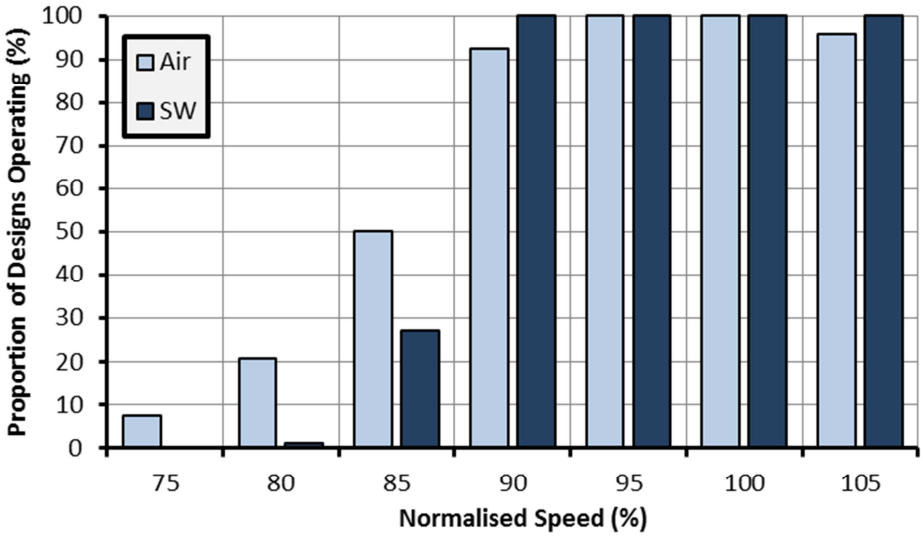

Figure 107: Percentage of the different WHRS studied which operate at the different container ship speeds.

When SW is cooling the WHRS, all designs operate above 90% of the design speed. This means that the ship will see the WHRS operating at least 53% of the time of which is when the most of the waste heat is available. In the case of air, only when the container ship is navigating between 95% and 100% of its design speed is when all designs are operating, this represents around 30% of the operational time. Air cooler designs have exponents that operate at the lower end of the container ship speed spectrum which represents around 32% of the voyage time and will represent a small proportion of the annual CO_2 emission savings due to a low WHRS power output.

B. Cooler: Implication on power consumption

As the ship navigates in northern waters, different engine loadings are requested which will determine the WHRS performance but also the cooler's heat rejection load. These different heat loads define the mass flow rates needed and, coupled with the cooler design, it is possible to define the power requirement from the fan or pump. This analysis will use the data at design speed and at a temperature of 5.4˚C for both cooling fluids – this temperature is seen for air in the month of June and for SW in April.

The heat output and the cooling fluid enthalpy change between the fan's exit and the condenser's pinch point dictate the cooling fluid mass flow rate. These results in the mass flow rate for any air-cooled design being higher than any SW-cooled WHRS (see Figure 108). The minimum mass flow rate for an air case was 144 kg/s while the maximum for the SW case was 115 kg/s.

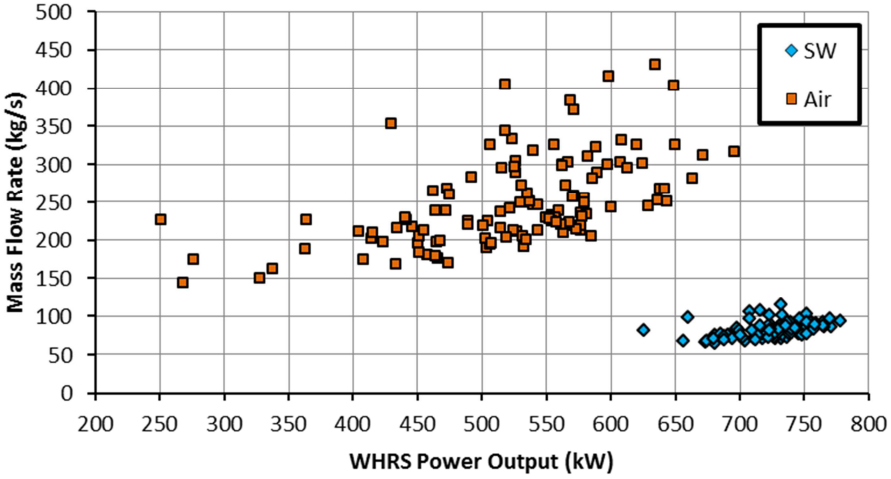

Figure 108: Fan and SW pump mass flow rates when the vessel navigates at design speed. The WHRS shown do not consider the fan/pump power requirement.

For air-cooled designs the heat rejection at the condenser section at design speed goes from 2,080 kW to 4,120 kW; for SW-cooled designs the range moves between 3,960 kW and 5,820 kW. While the increase in heat load at the cooler explains the increment in mass flow rate for each cooling fluid, it does not explain the difference in mass flow rates between cooling fluids. Air-cooled systems have an enthalpy change between the fan's exit and the condenser's pinch point between 7.1 kJ/kg and 25.6 kJ/kg, while for the SW it rises from 44.7 kJ/kg to 61.2 kJ/kg (see Figure 109). The difference between the cooling approaches is due to air's lower heat capacity which produces a faster temperature rise to reach the cooler's pinch point. This limits the heat absorption and requires larger mass flow rates to cover the heat rejection demand.

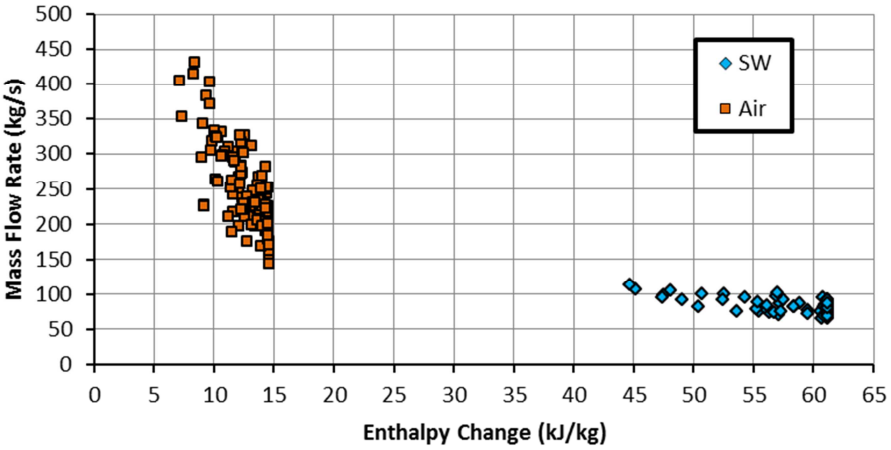

Figure 109: Fan and SW pump mass flow rate compared to the change in enthalpy in the condenser section of the different coolers. The cooling fluid's temperature is set to 5.4°C.

The construction of the cooler will determine the other part of the fan/pump power requirement. Starting with the heat transfer area, air-cooled designs ranged from 7,660 m^2 to 19,530 m^2 while for the SW case, it is from 818 m^2 to 2,630 m^2. This difference has to do with the cooling fluid's overall heat transfer coefficient (U) seen from the cooling fluid side. Seawater-cooled WHRS achieved on average an U_{ds} for the cooler's desuperheating section of 82.9 W/m^2-°C, while for

the condensing section U_{co} was 539 W/m^2-°C. For the air-cooled case, U_{ds} was 8.6 W/m^2-°C and U_{co} of 20.1 W/m^2-°C.

Table 34: Coolers' characteristics for different optimal marine WHRS when using air or SW as cooling fluids.

	Air		SW	
	Min.	**Max.**	**Min.**	**Max.**
d_i (mm)	19	57	16	48
l_t (m)	1.8	7.3	3.3	7.3
p_t (mm)	83.0	83.0	30.8	75.1
N_t	760	3,050	302	3,308
d_s (m)	-	-	1.1	2.4

The SW smaller mass flow rates, plus a lesser heat transfer area requirement allow for the use of smaller tube diameters – which are arranged closer together as per their pitch – producing smaller cooler designs (see Table 34).

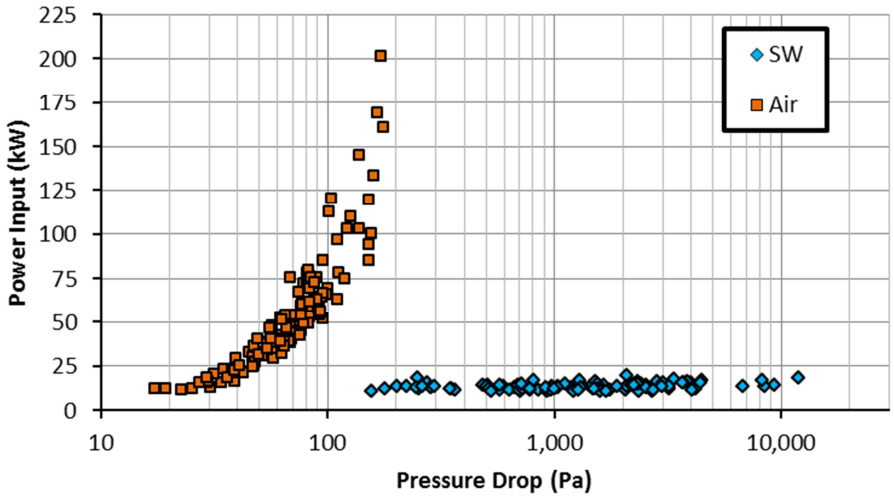

Figure 110: Fan and pump power output demanded at the cooler at the design speed and a temperature of 5.4°C.

For SW designs, the cooler volume could be found from 4.1 m^3 to 25.1 m^3, while when cooling with air the volume goes from 36.8 m^3 to the maximum volume allowed of 38.5 m^3. Air-cooled designs, due to their construction and being a concurrent flow produce cross-sectional areas above 88.90 m^2 with a maximum of 92.77 m^2, while for SW it ranges from 0.12 m^2 to 0.68 m^2. The air cooler's large frontal area plus a high mass flow rate gives a high energetic cost to the pressure change at the fan as per equation [101]. This is also seen and discussed in Habl et al. [2012] which looked into the effects of cooling by air a power land-based plant.

Air's lower density and viscosity, when compared to SW, produced coolers which have a much lower pressure drop than in the case of SW (see Figure 110). But also, SW flowing inside the tubes must cover twice the length of the tube since all cooler designs are double pass inside the shell. So, even though air coolers have smaller pressure drops, their larger power input to pressure change ratio is enough for larger power requirements at the cooler (see Table 35).

Table 35: Power requirements for both fan and pump at different ship speeds. The minimum and maximum values seen for each cooling fluid at each speed are recorded at a temperature of 5.4˚C.

	Fan/Pump Power Input (kW)													
Normalised Speed (%)	75		80		85		90		95		100		105	
Cooling Fluid	*Air*	*SW*	*Air*	*SW*	*Air*	*SW*	*Air*	*SW*	*Air*	*SW*	*Air*	*SW*	*Air*	*SW*
Minimum	2	0	2	3	3	5	4	6	6	8	12	10	10	10
Maximum	5	0	4	3	14	7	39	11	110	14	201	19	383	36

The larger power input to pressure change ratio also explains why in general air-cooled designs prefer WHRS that reject less heat to the cooling fluid than SW designs. At design speed the total heat rejection for air-cooled WHRS goes from 2,290 kW to 6,030 kW, while for SW designs it runs from 4,810 kW to 6,875 kW. Air-cooled designs, in order to minimise the impact of the high fan energy cost on annual CO_2 emissions, sacrifice WHRS power output for a lower heat duty at the cooler (see Figure 111).

Air-cooled WHRS exhibit the most extreme cases of power requirement with a maximum of 383 kW which requires 700 kW in the warmest air month – September. These cases of high fan or pump power input would represent higher initial costs, but also denote a larger burden on the operation and maintenance budget during the vessel life. A good option would be to install designs that have power requirements away from the maximums seen in Table 35 which could have an equal or larger positive environmental impact.

Another option to reduce the high power requirement in air coolers would be to install a recuperator after the expander and working fluid pump. This will effectively reduce the cooler duty and hence the power consumption, but will add an extra heat exchanger in the plant layout. Larsen, Pierobon et al. [2013] found that at low waste heat temperatures, such as is the case of the scavenge air, it is better not to use a recuperator due to the low increase in WHRS thermal efficiency and an increase in initial cost. However, in the previously cited work, the bottom section of WHRS is not studied in detail and the high fan energy cost forces the use of a recuperative WHRS which could reduce enough the heat duty at the cooler to make the heat exchanger cost justifiable.

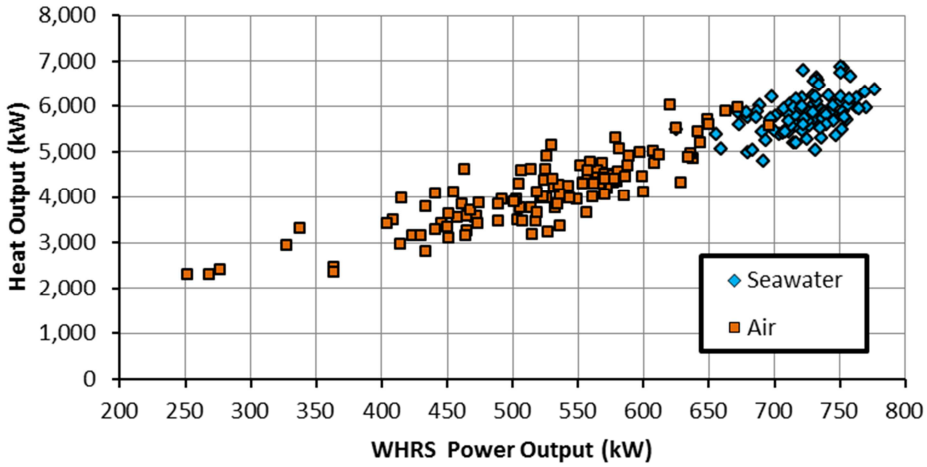

Figure 111: Power output produced by the WHRS and not considering the fan/pump power consumption at design speed compared to the amount of heat rejected at the cooler.

Another interesting idea could be using the natural air flow produced by the moving ship. This idea requires ship design and wind maps, on top of the thermodynamic and heat transfer study which is out of the scope of this thesis but is an interesting road for future research.

9.7.1.1 ANNUAL CO_2 EMISSION REDUCTIONS

The cooling fluid temperature is the other piece of the puzzle that helps the researcher to understand how the vessel's CO_2 emission reductions behave during a year of operation.

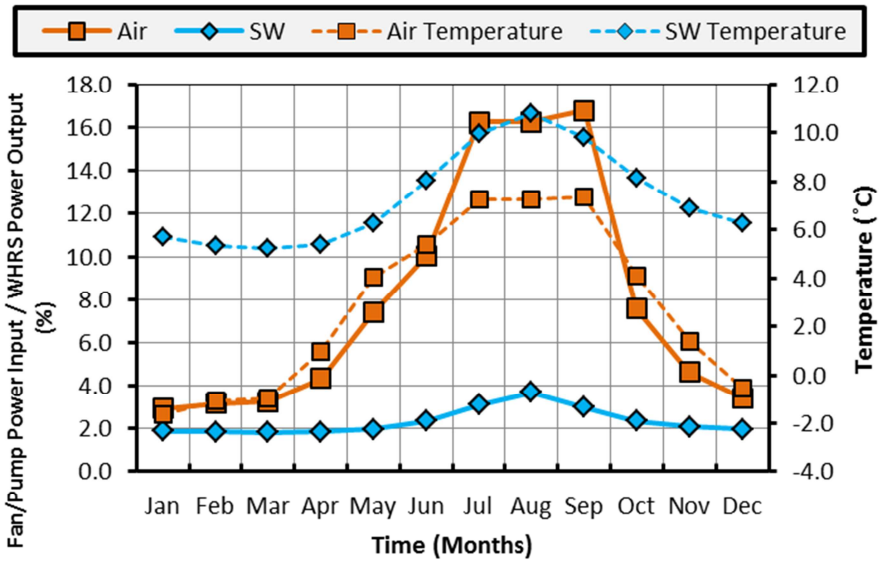

Figure 112: Average change during a year in the proportion of power demanded by the condenser and power output delivered by the optimal WHRS at a speed of 23.3 kn. The plot also shows the monthly change in temperature for both air and SW.

The power input for air-cooled designs represent in any month a larger proportion of what the WHRS is returning to the ship than SW designs. Taking, for example, the month of March in Figure 112, the average power production for SW-cooled designs is 747 kW with a cooler average power demand of 13.7 kW, representing 1.8% of the WHRS power at design speed.

On the other hand, air-cooled designs produce 524 kW with a fan power consumption of 15.8 kW, representing 3.3% of the power output. This has to do with a lower power production (Figure 106), but also to air's larger power demand at the condenser (Table 35).

Since the WHRS power production is fixed, the changes in the net power production during the year are caused solely by the fan/pump power input which changes due to variation in the monthly temperature. This can be corroborated by the shapes in the proportionality curves of both cooling approaches to the shape of the temperature curves for air and SW.

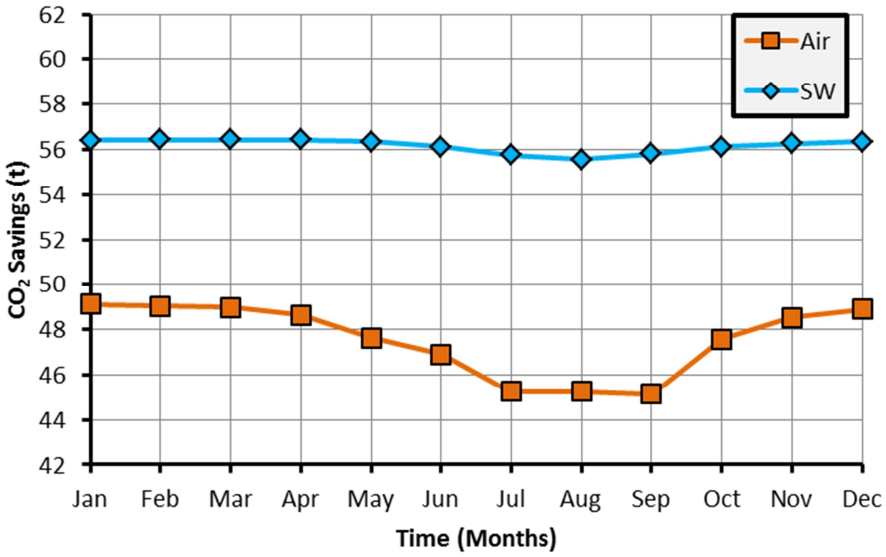

Figure 113: CO_2 emission savings due to the monthly temperature change in air and SW during the year on the route studied. The cases shown are for the WHRS that achieved the highest CO_2 reductions during the year, in both cases the working fluid was R236fa.

The air/SW temperature increase causes a reduction in the cooling fluids' enthalpy change between the fan/pump exit and the condenser's pinch point, requiring a larger mass flow rate to be able to reject the excess heat. In the case of air, the average power requirement goes from 15.4 kW in January to 91.2 kW in September, an increment of 476%. The fan power represents in September around 17% of the average WHRS' power output. In the case of SW in the month of May, the average power consumption at the condenser is around 14.4 kW, while for August it changes to 26.9 kW which represents only 3% of the total power generated. Similar behaviour due to the air temperature changing is seen in the work of Habl et al. [2012]. A drop of 5% was observed in the power generated from winter months to summer months in a power plant located in the south of Spain; this was due to a fan increase in power consumption of around 120% in the same period (i.e. from 1,250 kW to 2,750 kW). The sensitivity of power required at the condenser when the vessel is navigating at 23.3 kn due to a temperature change in an air-cooled design is around 8.13 kW/°C, while for SW is 2.2 kW/°C. With these sensitivities, air-cooled ORC could have a better performance in colder weathers found further north, while SW sensitivity allows the vessel to navigate into warmer waters without losing too much of the WHRS benefit. The high sensitivity for air-cooled designs to the monthly temperature will have

an important impact on annual CO_2 emission reduction, especially in the summer months where the temperature is 9˚C higher than in January (see Figure 113).

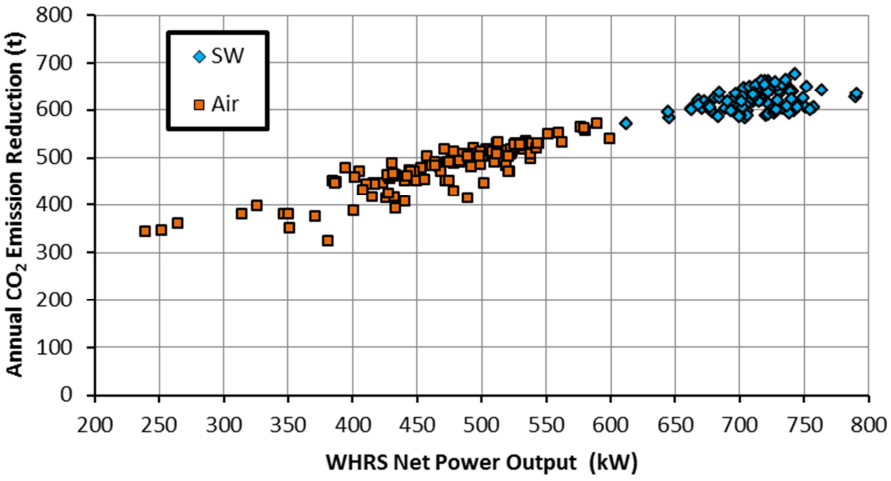

Figure 114: Annual CO_2 emission reduction for different ORC designs compared to the net power output at design speed and when the temperature for both cooling fluids is 5.4˚C.

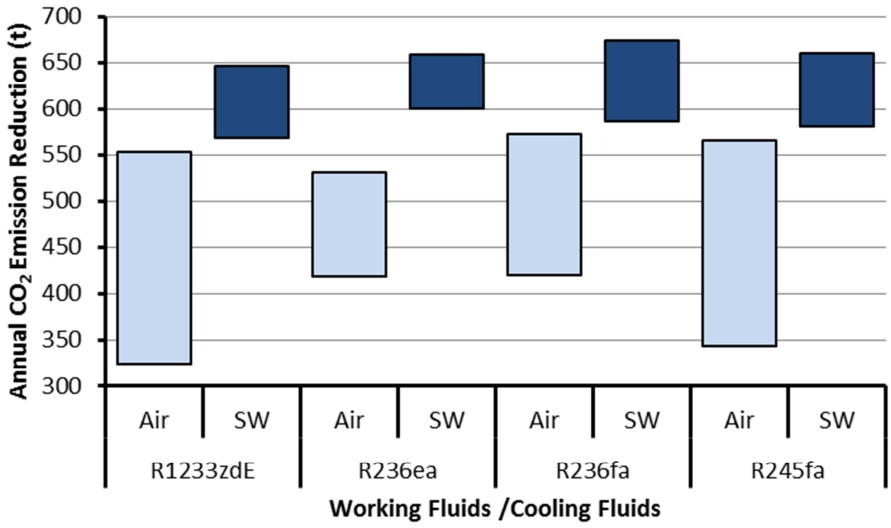

Figure 115: Annual CO_2 emissions when the ship is using an ORC while navigating in northern waters.

The ship operating conditions and air temperature during the year affect differently the WHRS performance in such a way that the most powerful designs are not those which achieve the largest reduction in emissions. For example, SW's most powerful example – with a net power output of 790 kW at design point – achieves a reduction of 632 t CO_2 per year; this is around 6.5% less CO_2 saved than that achieved by the 743 kW SW-cooled WHRS. However, in general it can be said that WHRS that have higher net power outputs at design point are able to reduce larger amounts of CO_2 in a year there. This will mean that SW-cooled systems, which produce more power but simultaneously require less power input at the cooler than their counterpart, are able to reduce more CO_2 emissions annually (see Figure 114).

The refrigerant R236fa achieves the highest CO_2 emission savings when cooled by any of the cooling fluids with 674 t CO_2 using SW and 571 t with air. On the other hand, R1233zd(E) when cooled by SW, achieves the lowest maximum CO_2 emissions during a year with 647 t CO_2; while the maximum savings when cooled by air around 553 t CO_2 – 22 t more in one year than the maximum achieved by R236ea (see Figure 115).

9.7.2 Impact on the Energy Efficiency Design Index

The following subsection analyses how installing an ORC WHRS, depending on its working and cooling fluid, at the container vessel's design stage could have a better EEDI. Using equation [79], the reference attained EEDI without any fuel saving technology is calculated by the CO_2 emissions produced by the engine ($CE_{engine,design}$) when the engine is operating at its 75% MCR (i.e. at design speed) and a temperature for both cooling fluids of 5.4°C. The WHRS CO_2 savings ($CS_{T,design}$) are substracted from $CE_{engine,design}$ in equation [79] to achieve a lower EEDI at design stage.

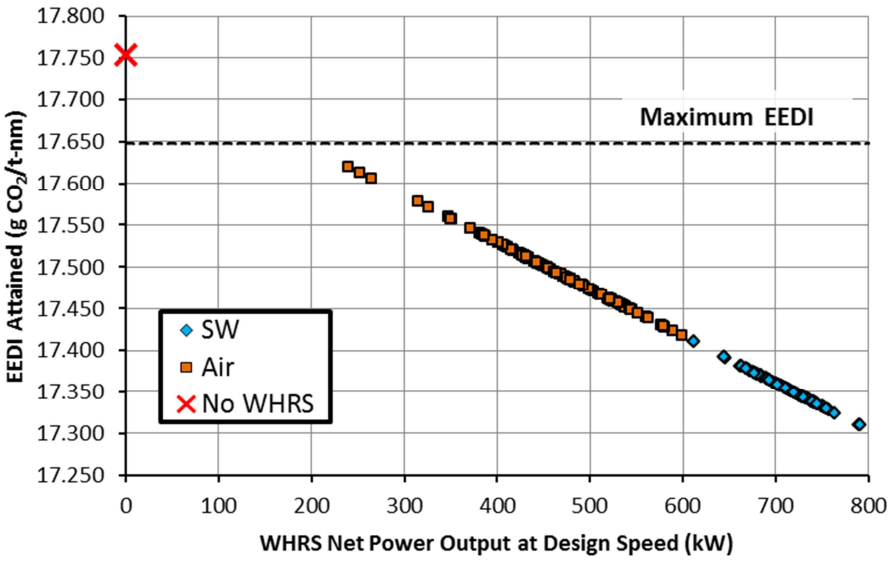

Figure 116: The EEDI achieved when the vessel is designed with a marine ORC WHRS using the waste heat available from the container vessel scavenge air system. The figure also shows the attained container ship EEDI without any fuel saving technology installed on board.

The ORC designs cooled by SW achieve a maximum EEDI reduction of around 2.5% from their original condition while the air-cooled reduces it by around 1.9%. In both cases all the optimal WHRS attained an EEDI below the 2015 reference line of 17.647 g CO_2/t-nm (see Figure 116). Livanos et al. [2014] found that a ferry using HFO could reduce its EEDI by around 4.6% when using a water-based RC extracting the waste heat from the exhaust gas. In other work, Theotokatos and Livanos [2012] found that a WHRS could reduce a bulk carrier EEDI from 5.11 g CO_2/t-nm to 5.02 g CO_2/t-nm, a reduction of around 1.8%. While the type of vessel, engine power, operating conditions and WHRS designs are different in each study, it is possible to say that the results found in this work fall inside what other academic literature has achieved.

As per equations [1], [71] and [79] the larger the WHRS installed power output at design point is, the lower the EEDI will be. In addition, from the results shown in the previous

subsection, it is appreciated that the most powerful designs are those that achieve the largest EEDI reduction – are not the ones that achieve the best CO_2 emissions annually. Furthermore, WHRS are sensitive to temperature changes: in a hypothetical case where the container vessel's EEDI had to be measured at 25˚C, none of the designs shown here will work since the working fluid saturation temperature at low pressures is fixed at the same temperature. Looking from another point of view, if the attained EEDI is measured at an ambient temperature of -1.7˚C, then it would be around 2.1% less than the base EEDI instead of the 1.9% at 5.4˚C. The examples above show the difficulty for the EEDI to predict which on board green technology could represent the best opportunity for the vessel operator whose goal is to have the largest impact on noxious emissions. In the case of marine WHRS, it is the high sensitivity of this system to the ship's speed – engine loading – and weather conditions which increases the degree of uncertainty over the real ship's CO_2 emission reduction. The vessel's operating profile; route and weather conditions during the whole of its operating life – at least 20 years if no accident happens – are important unknowns at the moment of design. In using a generic operating profile from the same operator, plus knowing where the ship will operate, could initially help when deciding which WHRS to use in order to achieve the best emission reductions but also complying with the required EEDI.

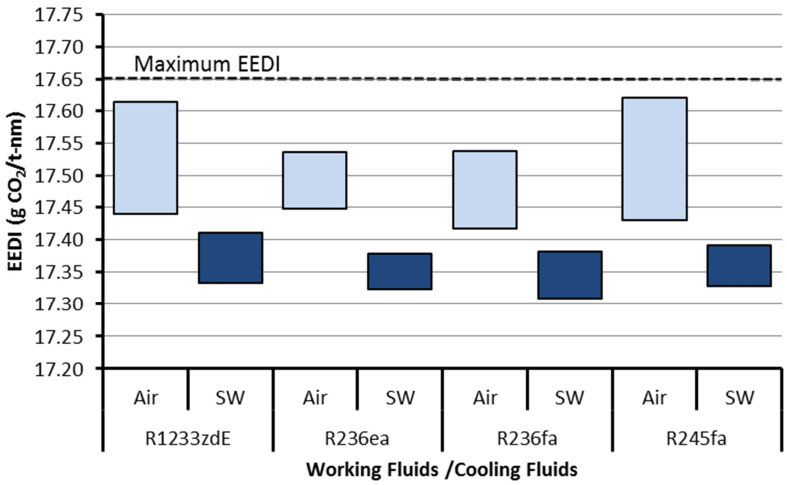

Figure 117: Represents the maximum and minimum EEDI achieved by the different WHRS cooled by either air or SW. The dashed line represents the maximum EEDI possible for the container vessel.

The organic fluid R236fa achieves the lowest attained EEDI for both cooling fluids at 17.310 g CO_2/t-nm for SW and 17.417 g CO_2/t-nm for air. The highest when cooling with SW is achieved by R1233zd(E) with 17.610 g CO_2/t-nm, and for an air-cooled WHRS it is 17.410 g CO_2/t-nm when using R245fa (See Figure 117). This has to do, as mentioned before, with a larger net power output at design conditions.

The environmental impact so far has been defined as how the ORC can reduce the ship's CO_2 emissions, but another important factor is the working fluids' global warming potential. From the refrigerant used in this chapter, R236fa has the largest GWP_{100} at more than 8,000, for R236ea and R245fa is above 900, while for R1233zd(E) it is less than five. In real operating conditions,

it is possible to have leakages from the WHRS releasing the refrigerant into the environment. For the first three mentioned refrigerants, the high GWP_{100} could question if the EEDI benefit is enough to achieve greener shipping. Considering these three working fluids as high environmental risk, the marine WHRS designer could use the guidelines and requirements for highly flammable fuels provided by IMO's [2014] International Code of Safety for Ships using gases or other low flashpoint fuels and the DNV GL [2013] tentative regulation for low flashpoint liquid to ensure that refrigerant leakages and concentrations outside the WHRS are detected in time. From the cost point of view, this extra equipment will have repercussions on the WHRS initial cost and the payback period, which in the case of R1233zd(E) are not necessary.

9.7.3 BEST OPTIMAL DESIGNS PER COOLING FLUID

It was decided then that a fluid with low GWP_{100} would be the most suitable option for the container vessel since in the event of working fluid spillage, the damage to the environment will be minimal. Keeping in mind, this subsection will study only WHRS which use R1233zd(E) as working fluid. It is important then to consider different criteria, in addition to the maximum emission reduction, which could include the stakeholder vision – ship owner, operator, etc. – as well as international organisations that regulate shipping and its environmental impact. In this subsection, different cases are explored using the whole population of R1233zd(E) WHRS which will determine the best designs for the container vessel:

A. Maximum CO_2 emissions reductions.
B. Highest CO_2 emissions reduction per power installed.
C. Just EEDI compliance.
D. EEDI reduction per power installed.

When looking into case A, the ship owner is interested in minimising the impact on the environment due to shipping activity. This could be a probable and relevant scenario in the near future. Smith et al. [2015] state that in order to avoid a global mean temperature rise of 2°C before 2100, the shipping industry needs to half its 2012 operational CO_2 emissions by 2050 and achieve zero emissions or neutrality in the year 2080. The shipping industry, in order to comply with this aggressive aim, is required to install and apply technologies and strategies today that can deliver the highest emission reductions. For case A, the WHRS cooled by SW achieved the largest savings with its maximum exponent at 647 t of CO_2 in one year.

Case B represents the configuration that can reduce CO_2 emissions more efficiently with the power installed. The best design achieves 1.16 t CO_2/kW installed; this WHRS is cooled by air and has a maximum power output of just 327 kW. In the case of water, the highest emission reduction power efficiency reaches a value of 0.91 t CO_2/kW.

Case C could be one of the most common scenarios for a practical ship owner where complying with the regulations is enough. Air designs are the closest to the maximum EEDI allowed for the container vessel (see Figure 118). The design selected has one of the lowest expander power outputs of the whole population of optimal results at 308 kW. The closest SW design to the

compliance EDDI – at 17.410 g CO_2/t-nm – is one that has a maximum power output of 625 kW; more than double what the air-cooled design can deliver.

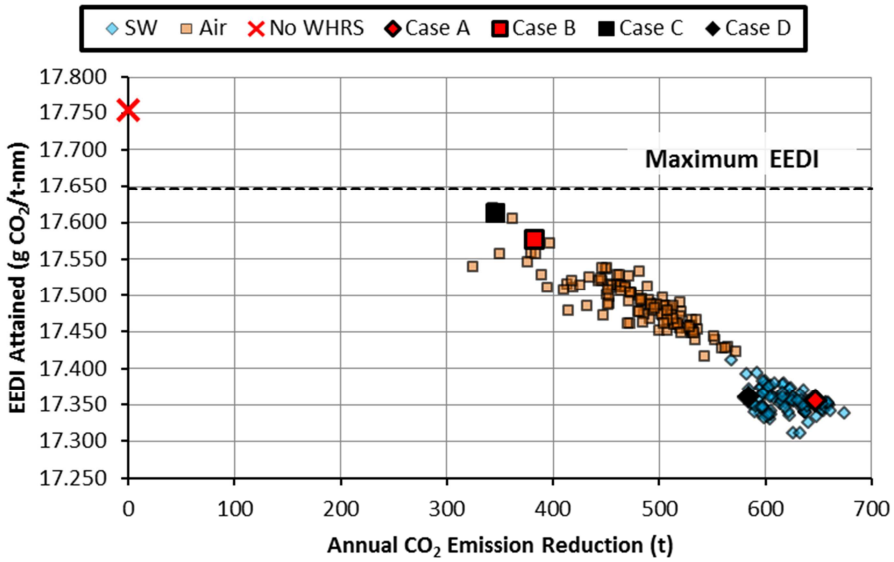

Figure 118: All R1233zd(E) WHRS cooled by air or SW. The figure highlights the "best" optimal designs per case. The container ship's maximum allowed EEDI and EEDI attained without technologies are also shown for reference.

Table 36: Performance and some of the cooler characteristics for the best marine WHRS using as a working fluid R1233zd(E) and dependent on the stakeholders objective. Cells highlighted show the values for which the designs were deemed the best of the whole population of optimal results.

Case	A	B	C	D
Cooling Fluid	SW	Air	Air	SW
WHRS Power Installed (kW)	1,052	327	308	712
WHRS Power @ Design Speed and 5.4˚C (kW)	724	327	268	712
Net WHRS Power @ Design Speed and 5.4˚C (kW)	708	315	252	700
EEDI Attained (g CO_2/t-nm)	17.368	17.577	17.613	17.360
EEDI Reduction Power Efficiency (mg CO_2/t-nm-kW)	0.377	0.536	0.454	0.552
Annual CO_2 Emission Reduction (t)	647	382	346	585
Emission Reduction Power Efficiency (t/kW)	0.62	1.16	1.12	0.82
Heat Transfer Area (m^2)	947	17,876	7,690	1,406
Cross-sectional Area (m^2)	0.21	92.6	88.90	0.24
Volume (m^3)	10.6	38.4	36.9	9.7

In case D, the EEDI reduction achieved by the different marine WHRS is compared to the WHRS' installed power. In this scenario are found stakeholders who want to maximise the

environmental compliance with the waste heat plant power delivered. Seawater designs achieve the highest EEDI reduction per kW installed with plants that can deliver a maximum power output between 625 kW and 720 kW. From Table 36, the EEDI reduction power efficiency for the SW design stands at 0.552 mg CO_2/t-nm-kW while the closest for an air-cooled designs stands at 0.539 mg CO_2/t-nm-kW. As emission regulations tend to reduce the amount of noxious emissions emitted in shipping over time – such as is the case with CO_2 and SO_x – the ship owner could choose a system that has a high efficiency in reducing the ship's emissions in order to comply with future stringent regulations.

As with case B, the efficiency of the systems are the largest seen but are limited to an EEDI and annual CO_2 emission reduction that, when compared to what it is possible to achieve seem small.

9.7.4 COST ANALYSIS

In this subsection, a cost analysis as described in section 6.10.4 is performed to the R1233zd(E) WHRS designs which will give an extra dimension to the decision-making process of different stakeholders. The profits and payback times are analysed only for the marine WHRS.

The installed power output of the different cases will have an important impact on the initial cost as Pierobon et al. [2013] show, the expander's cost represents around 78% of the initial cost of the equipment required in an ORC WHRS. Adding the cost dimension to the cases could in theory offset the results shown in Table 36. A relatively small difference in performance could make the ship owner lean toward less powerful WHRS in search of a more economical but almost equally effective design.

The high installed power output seen in Figure 106 for the majority of the SW-cooled designs causes expensive WHRS. On the other hand, air-cooled WHRS tend to be less powerful and thus more affordable but at the same time they achieve lower annual CO_2 emissions than their counter parts (Figure 119). There are air-cooled designs which have low emission reductions – below 400 t CO_2 per year – with an initial cost of more than £900k. These designs produce a large power output but at the same time, the fan power requirement is high, limiting the net benefit of the WHRS. Interestingly, there is a group of SW designs that can deliver a better annual emission reduction than air at a more affordable cost which has to do with moderate installed power outputs and almost negligible SW pump power consumption when compared to the air-cooled WHRS power requirements.

The initial cost, along with the fuel savings and discount rate, determine the payback period for the different WHRS. The shortest payback time is achieved in 17.9 years by an air-cooled WHRS that has a maximum power output of 328 kW and saves around 381 t CO_2 each year. There are only two SW designs that achieve payback of the initial investment in 19.5 and 19.8 years respectively. These two designs had a maximum power output at around 650 kW and CO_2 emission reductions in the region of 580 t. The long payback periods are caused by the intermittent nature of the vessel's speed profile which has an important impact in the waste

heat quality and WHRS power production. However, it is caused by large maximum power outputs which are only required in small windows of the operating profile, raising the capital investment.

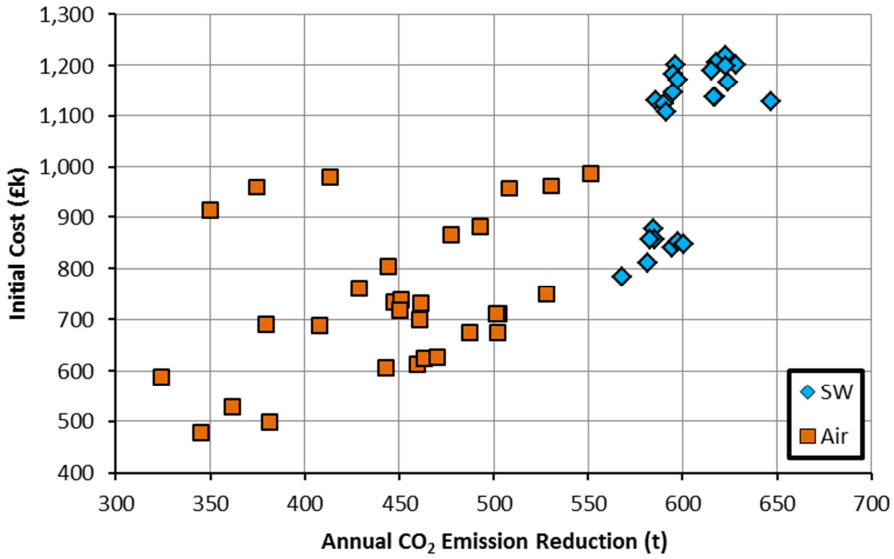

Figure 119: Initial cost for WHRS using as a working fluid R1233zd(E) compared to the annual CO_2 emission reduction achieved on board.

At the end of the container ship's operating life, there are only a handful of WHRS designs which manage to bring a profit to the ship owner (see Figure 120). The highest profit at £36k is provided by the same air-cooled design discussed previously, while for SW-cooled the highest profit is £12k coming from a 625kW WHRS.

With the cost dimension, it is possible to consider different aspects that may occur in the decision-making process. The following cases can be added to the previous ones[42]:

E. Lowest initial cost.
F. Cost of reducing CO_2.
G. Cost of reducing EEDI.

In case E, the ship owner sought the cheapest option available to make the container vessel comply with the EEDI. Under this case, an air-cooled design is the best option since it costs around £480k and delivers an EEDI of 17.635 g CO_2/t-nm. The cheapest SW design cost around £784k, which is around 63% more than the air-cooled design.

In case F, the best cooling approach is again air and is in fact the same WHRS design as that chosen in case B. This makes sense since the cost from Quoilin et al. [2013] is a function of the WHRS power output, and CO_2 emissions are dependent on how the power is produced during the year. This design gives the best trade-off between achieving the maximum CO_2 reduction possible and a low initial cost. Furthermore, this design achieves the fastest payback time and offers the largest profit at the end of the ship's useful life (see Table 37).

[42] The payback time scenario is not studied since the period of time is long and it has been discussed briefly in the previous paragraphs

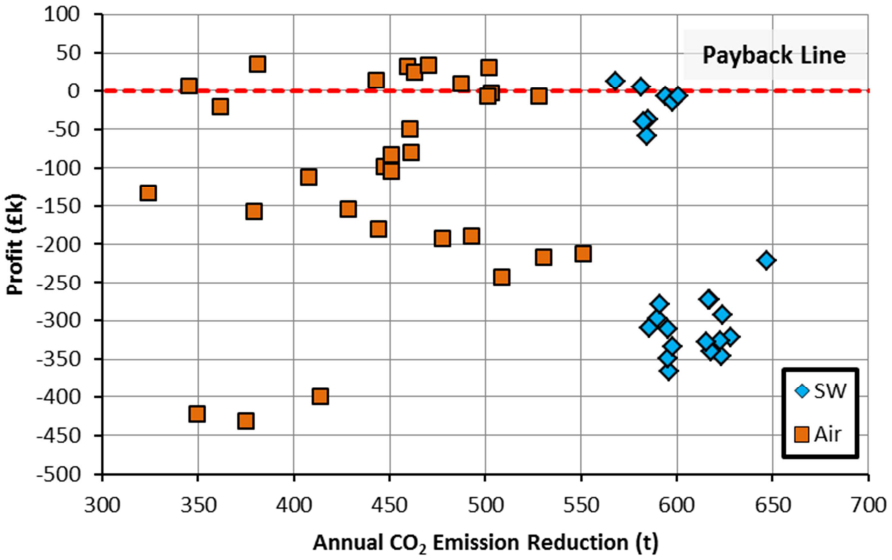

Figure 120: Profit achieved at the end of the container vessel's life by the different marine WHRS. The red dashed line indicates which of the R1233zd(E) WHRS have achieved its initial investment.

Table 37: Cost, payback times and some of the heat exchanger characteristics found for the best marine WHRS for the different cases analysed. Highlighted cells show the values for which the designs were deemed the best from the whole population of optimal results.

Case	E	F	G
Cooling Fluid	Air	Air	SW
WHRS Power Installed (kW)	307	327	712
EEDI Attained (g CO_2/t-nm)	17.635	17.577	17.360
Annual CO_2 Emission Reduction (t)	345	381	585
Initial Cost (£k)	480	499	858
First Year Savings (£k)	38.9	42.9	65.8
CO_2 Reduction Cost (£k/t)	1.38	1.31	1.47
EEDI Reduction Cost (£M t-nm/g CO_2)	3.40	2.84	2.18
Discounted Payback Period (years)	19.5	17.9	21.5
Heat Transfer Area (m^2)	14,386	17,876	1,406
Cross-sectional Area (m^2)	88.9	92.6	1.7
Volume (m^3)	36.9	38.5	9.7

Case G analyses which design offers the lowest cost per g CO_2/t-nm which is relevant for the ship owner when it needs to comply with the EEDI. A SW design offers the best EEDI reduction cost at £2.18M t-nm/g CO_2, around 13% lower than the closest value achieved by an air-cooled WHRS. The drawback of this design is that its payback time is beyond the operational life of the container ship which is not a desirable characteristic. A second best option which offers a better

payback time – below 20 years – and is also cooled by SW-cooled achieves an EEDI cost reduction of £2.24M t-nm/g CO_2.

It is important to remember that the cost analysis does not consider the maintenance and operational cost which will have a considerable impact on the WHRS ship's profits. Better plant layouts, such as the recuperative layout, could reduce the payback time by increasing system efficiency.

9.8 CONCLUSIONS

Looking at different possible stakeholder points of view such as initial cost, payback time or just EEDI reduction, among others, it was difficult to decide which of the cooling approaches brought the optimal result for a container ship navigating in Arctic waters. It was found that air-cooled designs performed better on cases where the stakeholders sought affordable EEDI compliant marine WHRS. The SW-cooled designs achieve the largest CO_2 emission reduction over the course of a year but with a high initial cost, although this cooling approach offers the lowest cost per EEDI reduced.

In the cases where there is a strong need for minimising the shipping activity impact on the Arctic, WHRS cooled by SW manage to be the best due to a reduction of 674 t CO_2 per year. However, the working fluid used is R236fa which has a high GWP_{100} and requires monitoring in order to avoid the refrigerant escaping into the atmosphere where it can have a negative impact on the Arctic environment. Switching to an almost free-GWP working fluid – R1233zd(E) – causes the CO_2 emission reductions in the container vessel to drop to around 27 t. An air-cooled ORC using the same low-GWP working fluid achieved a maximum of 551 t CO_2 per year. The difference in CO_2 emissions between cooling approaches is produced mainly by the fan's high power requirement on the WHRS net power output. This is caused by the air cooler's larger cross-sectional areas and air's low specific heat, requiring larger mass flow rates. The optimisation process when designing air-cooled WHRS chooses systems that absorb less heat allowing for lower fan power consumption. Another important reason is the high sensitivity of air coolers to the air temperature. It was found that the monthly CO_2 emission savings reduced from the air's coolest month to the warmest by 4.0 t, while in the case of SW this amounted to just 0.9 t.

The high power output of SW-cooled WHRS coupled with low SW pump power consumption achieve the lowest EEDI for the 4,100 TEU container ship at 17.310 g CO_2/t-nm, an improvement of 2.5% from the attained EEDI without any fuel-saving technology. The highest EEDI achieved by a SW-cooled R1233zd(E) WHRS is 17.410 g CO_2/t-nm. When stakeholders are looking for just EEDI compliance, the air-cooled WHRS produce designs which require smaller expanders having an important impact on the ORC cost.

The most affordable design stands at £476k by an air-cooled design which has a maximum power output of 307 kW, while the fastest WHRS to payback the initial investment – in

17.9 years – is an air-cooled design that has a power installed of 327 kW. This design also achieves the highest profit at the end of the container ship operational life at £36k.

Air-cooled designs tended to be closer to the maximum volume allowed of 38.5 m^3 while SW designs had a maximum exponent of 25.1 m^3 and a minimum of just 4.1 m^3. While the maximum volume allowed for the WHRS cooler represents around 0.02% of the total cargo capacity of the container vessel, the air's cooler large cross-sectional area – with a minimum of 88.9 m^2 – creates an important challenge for the cooler and vessel design, especially for retrofitting applications. One solution explored is the use of modular heat exchangers which can facilitate the installation and space utilisation on board.

Finally, it can be expected that more stringent emission regulations for the Arctic will be introduced, such as those seen inside ECAs which can ban the use of high sulphur content fuels or other noxious gases. As seen in the previous chapter, when the ship is operated with low-sulphur MDO, this can make the WHRS investment more attractive to the ship owner since MDO and other "greener" fuels cost more than HFO.

.

THESIS CONCLUSIONS AND FUTURE WORK

AN OVERVIEW FOR THE SHIP STAKEHOLDERS

ENERGY ON BOARD

During the past four years, shipping industry has experience drastic changes in regulation, market and fuel prices. Prior to 2012, the Energy Efficiency Design Index (EEDI) was forthcoming and fuel prices where above £600 per tonne of MDO. Under this vision, fuel saving technologies had a fertile ground to evolve and insert into shipping.

The majority of the energy used to move a ship is wasted in its main engine, principally through the exhaust gas and scavenge air systems. Waste heat recovery systems (WHRS) are used to take part of this wasted energy – in its heat form – and produce via a chemical, electrical or mechanical process useful power on board. It is recognised in this thesis that the generation of steam is of vital importance for the ship and therefore before using the wasted energy for any type of power generation first the energy will be used to cover the heating demand. This work focused on the use of the available wasted heat to produce electrical power instead of cooling power due to the many uses a ship has for electricity.

MARINE WASTE HEAT RECOVERY SYSTEMS

From the different types of WHRS two technologies were compared: thermoelectric generators and thermodynamic power cycles (e.g. water-based Rankine cycle). Thermoelectric generators transform heat energy into electricity using the Seebeck effect where the temperature gradient, between the heat source and sink, drives electrons through a circuit, generating a voltage. They offer a silent operation without moving parts, long life and have a direct DC output. However, this technology is still under development, the high thermal efficiency can be achieved only under perfect lab conditions and they are sold in a range from £1,630 to £14,000 per kW_e. On the other hand, thermodynamic power cycles absorb part of the available waste heat via a pressurised working fluid (e.g. water) which is vaporised to then expanded – inside a turbine or other type of expander – to transform part of its energy into mechanical power or, if the turbine's shaft is connected to an electric generator, electrical power. The thermodynamic cycles are able to deliver large power outputs, they are adaptable to any heat source (e.g. exhaust gas) and sink temperature (e.g. sea water) with good thermal efficiency and they are mature technologies which their costs can be found from about £620 per kW_e. Due to these reasons thermodynamic power cycles were selected as the ships' WHRS.

Power thermodynamic WHRS are already installed on board ships using the water-based Rankine cycle (RC). Examples of ships using these plants are the *Emma Mærsk* and the whole fleet of Triple-E container vessels for Mærsk. However, in conjunction with environmental regulations and evolution on marine systems, it could be expected that the waste heat availability and quality will be reduced, making it harder and more expensive for the typical marine WHRS to convert the waste heat to useful power.

Four different types of thermodynamic cycles were assessed qualitatively: RC, organic Rankine cycle (ORC), Kalina cycle (KC) and Stirling cycle (SC). From land-based WHRS evidence it was

detected that ORC could offer to the ship a better performance than the typical water-based RC. The ORC operational flexibility thanks to the large fluid catalogue, high thermal efficiencies for the waste heat temperatures and compactness makes this technology an attractive alternative to the RC. The KC and SC are interesting cycles for the shipping industry but their negative aspects such as size, level of maturity and costs were the reasons of why they were not taken for further analysis.

PERFORMANCE

The operating profile, which is quite different to any non-motorised land-based system, has an important influence over the marine WHRS performance. These systems are sensible to the waste heat source and sink temperatures, ambient temperatures, waste heat availability, fuel's sulphur content and the cycle's own design parameters. Electric power production on board via a WHRS can decrease, due to a reduction in waste heat availability, by at least 16% when changing from MDO to HFO. An ORC WHRS cooled by air installed in a medium size container ship navigating in the Arctic Circle increases its auxiliary power input by more than 400% – from 15 kW to 91 kW – when the air temperature changes from -1.8˚C to 7.4˚C.

In general, it can be said that under the operative condition of three different ships the performance of some of the different ORC WHRS gave a better performance than the water-based RC. For a large container ship using HFO as fuel, a benzene WHRS delivered 1,167 kW_e which represented 13% more electric power than what was achieved by the RC. On an Aframax tanker navigating in the Baltic Sea, an R245fa was able to produce 365 kW_e while the water-based RC produced 270 kW_e. Finally, in a ship navigating in extremely cold weathers, the water-based RC could not operate due to the low temperatures found at the scavenge air system. In this case an R236fa WHRS was capable of producing a maximum of 1,210 kW from a 41,100 kW two-stroke diesel engine.

It is important to have in mind that some of the organic fluids tested did not improve water's performance such as the case of toluene WHRS. Furthermore, due to the ORC WHRS plant layout – more heat exchangers – and the organic fluid short saturated state – requiring larger mass flow rates when compared to water – it was seen that these systems will require more space inside the ship. While this could not be a detrimental for big new-build ships, it could be an issue for small vessels that want to retrofit an ORC WHRS. However, as evidence from land-based systems shows, the most power dense WHRS found was a 10 kW_e ORC module with 0.05 m^3/kW_e while the RC was found to have 0.16 m^3/kW_e.

COSTS

The water-based RC tends to have lower initial costs than ORC WHRS. For the RC the costs are between £688 and £875 per kW_e while for the ORC are between £867 and £5,610 per kW_e. The difference between systems is due to the extra equipment in an ORC – recuperator and thermal oil – and the higher cost of any organic fluid when compared to water. To put costs in perspective, four-stroke diesel engines have an average cost around £100 per kW while for an 87 MW two-stroke engine it was found to be close to £160 per kW. Due to this, WHRS are not

meant to be the ship's main propulsion but more a supportive technology which increases the fuel efficiency.

On the maintenance case cost, the RC and ORC are almost the same at about 0.8p/kW_e-h. It is important to have in mind that the costs refer here come from land-based systems since data regarding marine WHRS are not available in the literature mainly due to its low penetration in the shipping sector. Still, the land-based data can be a good proxy for the marine WHRS costs.

The profitability and payback time sensitivity of marine WHRS were assessed for an Aframax tanker. It was seen that the economic feasibility of this technology is highly dependent on the fuel price. The ORC WHRS is attractive when the fuel price is above £300/t and the period of ownership is larger than five years, while the best WHRS under a scenario of low fuel prices and ownership periods of less than five years is the water-based RC due to its lower initial cost. As the fuel price goes above £300/t the more attractive the ORC technology becomes. It reaches a maximum net profit of more than £3 million after 20 years of operation when the fuel price is £1,000 per tonne, an increase of 34% over the traditional water-based RC achieves.

EMISSION REDUCTIONS

It is important to bear in mind that the environmental benefits – CO_2 and other noxious emissions – are still attractive. For an Aframax tanker, the ORC WHRS caused a maximum CO_2 emission reduction at design point of 4.1% while the typical water-based RC was around 3.0%. The CO_2 reduction is lower for a large container ship – 14,770 TEU – where a benzene WHRS achieved a reduction of 630 kg/h representing a reduction of 1.4%, this is an improvement of 12.5% over the simple RC. The CO_2 emissions are proportionally low due to the fact that the WHRS is absorbing waste heat from an 82.4 MW two-stroke diesel engine with the priority to cover first the heat demand. Furthermore, for ships navigating on extremely cold weathers, such like in the Arctic waters, the heating demand on board is so high that all the waste heat available in the exhaust gas is used for maintaining the ship temperature. For this reason the scavenge air waste heat is used for a WHRS. Organic fluids achieved, at design point, a maximum CO_2 reduction of 2.5% which represents, annually, about 670 t of CO_2 not escaping to the atmosphere.

All marine WHRS help reducing the new-build ships' EEDI, in particular ORC WHRS achieved a larger drop in this index. For the large container ship the best organic WHRS reduces the index by 0.171 g CO_2/t-nm while water achieves a 0.151 g CO_2/t-nm reduction. In the case of the Aframax tanker, the best ORC achieved a reduction of 0.143 g CO_2/t-nm while the RC was around 0.105 g CO_2/t-nm. The maximum reduction on an Arctic container ship was achieved by an R236fa WHRS at 0.441 g CO_2/t-nm when cooled by seawater while when cooled by air the EEDI drop was reduced by 0.335 g CO_2/t-nm.

SAFETY ON BOARD

Some of the organic fluids tested are flammable and under the current Safety Of Life At Sea regulations are not allowed inside the machinery room without specific Administration approval. The flash points of these flammable fluids are below the 60˚C limit requirement but well above

the liquefied natural gas flash point of -164˚C which is allowed inside the machinery room when the fuel system is designed according to the International Code of Safety for Ships using Gases or other Low Flashpoint Fuels. Under this light and with the current monitoring, control, firefighting and leak detection systems plus using an intermediate thermal fluid, it is possible to start a discussion on creating a safety code which could allow the use of flammable organic fluids for its use inside a marine WHRS.

VERDICT

In order to increase the ship fuel consumption efficiency and hence reduce its emissions to the atmosphere it is necessary to move away from the status-quo. This implies to start looking for technologies that are more complex, expensive and sometimes more hazardous which will unlock the extra potential on board. The alternative technologies bring better economic and environmental benefits making them an attractive alternative when the effort is to push for cleaner and more efficient shipping. A regulatory discussion in regards to SOLAS is needed where modern control, monitoring and safety systems and operational procedures are considered and recognised as technologies that can mitigate and control the hazards of flammable fluids on board. In this sense, ORC WHRS operating after a waste heat boiler – to cover the ship's thermal needs – are a viable and mature alternative for the typical RC.

Under the current economic and regulatory scenario the insertion of any type of power WHRS is not feasible. Low fuel price, slow steaming and alternative fuels are covering the ship owner operating needs and environmental regulations. The payback time when fuel prices are below £300 per tonne is too long – at least more than six years – and not attractive, while de-rating the engine manages to make new-built ships to comply with the EEDI.

Fuel prices are difficult to predict hence it is impossible to say when the economic grounds will be apt for WHRS and other green technologies – such as sails and carbon capture. Regulatory measures will be the tools that enable the introduction of WHRS in the medium term, probably via a more stringent EEDI or with a higher carbon tax imposed to fuel consumption. While these regulatory measures are not seen in the near term, it could be expected that discussions on that direction would occur if the environmental goals set by international organisations and countries start to look unattainable.

Increasing the feasibility of WHRS and reducing the impact that fuel price has on them should be a priority for future research and industrial studies. Adaptation of old auxiliary engines and air conditioning systems to produce power based on the organic Rankine cycle could have a large impact on the payback time. The field of alternative marine WHRS is still in its early stages of development and experimenting under real ship operating conditions is difficult and expensive but it is necessary to improve the chances of seeing them on board one day.

THESIS CONCLUSIONS

In the year 2012, Shipping contributed to 2.7% of global CO_2 emissions which could increase in the near future due to shipping's projected growth. In order to avoid a global temperature rise of 2˚C before 2100, it is required from the shipping industry to halve its 2012 CO_2 emissions by 2050 and reach emission neutrality by the year 2080. These reasons and strong objectives place shipping as an important player in the abatement of noxious emissions to the environment and herein, the importance of creating and using technologies and strategies on board which can improve shipping fuel efficiency.

The main area of energy loss on board is found in the engine system which transforms lost energy into heat. The engine's waste heat could represent at least 47% of the fuel's energy, being an important area of opportunity for fuel saving technologies. This thesis has examined technologies that could return mechanical or electrical power to the ship, while recognising the importance of waste heat technologies that support the vessel via heating.

Within the multiple power waste heat recovery systems (WHRS) options available, it was detected that alternative power thermodynamic cycles – such as the organic Rankine cycle (ORC) or Kalina cycle (KC) – and thermoelectric generators were viable options. However, thermoelectric generators being still under development have a large cost to electrical power produced, low thermal efficiencies and power outputs which combine to make it a second best option to challenge the traditional water-based RC on board a ship.

Under the umbrella of power thermodynamic cycles, three different alternative cycles were analysed via a qualitative comparison: ORC, KC and Stirling cycle (SC). The result of the comparison shows that ORC technology can outperform its counterparts due to strengths on compactness, operational flexibility, better thermal efficiencies at low/medium waste heat sources. However, its disadvantages such as initial cost have a low negative impact on the overall results.

Question 1: Can other power waste heat recovery technologies reuse the low/medium quality waste heat available from the ship's prime mover more efficiently than the water-based Rankine cycle?

From the qualitative comparison, the ORC technology score was 2.46 points above the water-based Rankine cycle (RC) – as the reference case, RC score was set to zero – which meant that the ORC could bring, on paper, an improvement on waste heat recovery benefits on board. While this test is not definitive, it gave the author a positive indication to go further with the research and simulations of marine ORC.

From the results in chapter 7, for a container ship at design conditions it was demonstrated that an ORC using benzene offered a better performance where the heat availability and quality were high. This working fluid achieved a maximum power output of 1,167 kW_e, a difference of 13.4% to the water-based RC. When installing a marine WHRS on an Aframax tanker consuming low-sulphur fuel and an ambient temperature of 5°C, the refrigerant R245fa

achieves the highest power output at 365 kW_e which is around 32 kW_e and 95 kW_e more than what it is possible to achieve with the benzene ORC and a water-based RC respectively. When there is lower heat quality (i.e. below 200˚C), such as the case of the scavenge air in the Arctic, the water-based RC and benzene ORC cannot be used, hence the use of low temperature evaporating refrigerants. In this case, R236fa returned to the ship a maximum power output – not considering the condenser power requirement – of around 1,200 kW at the maximum speed of a container ship.

It was seen that most of the organic fluids tested in the empirical chapters outperformed the RC. Toluene ORC in chapters 7 and 8 never delivers better power outputs than water under the same operative conditions and constraints. Furthermore, it is seen that in the absence of a recuperator for the ORC WHRS, water delivers a higher performance than any organic fluid except for benzene which produces 28 kW_e more.

The RC is the preferable marine WHRS due to water's characteristics being non-flammability, is relatively cheap and fast payback time, abundant, and environmentally friendly. On the other hand, organic fluids can be harmful for the environment and, in the case of hydrocarbons, flammable which is one of the most common arguments against ORC WHRS on board ships. However, from the three empirical chapters, it was demonstrated that a marine ORC WHRS could offer a better performance than the water-based RC under a wide range of design and off-design conditions that are commonly seen in shipping. These strengths come from better power production at low/medium quality waste heat, the wide range of organic fluids available which can tailor the WHRS to the heat source and the organic fluids' operational flexibility. Furthermore, the author highlights that the use of organic compounds for marine WHRS is possible using available technology for monitoring and handling flammable fluids which will allow the crew to respond in a safe and quick manner to any spillage or hazard presented. Finally, ORC WHRS will have an important role in the near future when regulations will push for tighter emissions levels, waste heat availability reductions due to an increase in prime movers efficiency and waste heat utilisation increases for other processes on board (e.g. water treatment).

Question 2: How does a waste heat recovery system behave under different WHRS plant layouts, environmental temperatures and the ship's operating conditions?

An important point that the academic marine ORC literature misses is the broader picture of vessel operation. While navigating in different waters and times of the year, the engine's loading, the vessel's steam demand, regulations and fuel type may change which will have an important impact on the waste heat availability and quality. This in turn will have an effect on the WHRS' power production, characteristics and costs. To assess this, the WHRS were subjected to different operative and design conditions seen typically on board.

In chapter 7, under the WHRS design point, different internal and external variables and factors were modified so it was possible to understand how they affected the WHRS' electrical power output. The WHRS high pressure, when the expander's inlet temperature is held constant, is an

important control parameter for a WHRS. The results showed that the maximum electric power output occurs at the lowest operative pressure possible since at this point the majority of the waste heat is absorbed. However, this did not mean that at these low high pressure points, the WHRS was operating at its maximum thermal efficiency.

The use of a recuperator on any ORC increases the electrical power output. The power gains due to the extra heat exchanger must be balanced against an increase in plant size, cost and system complexity. It was shown that a certain degree of superheating is beneficial for all organic fluids since superheating gives ORC more flexibility to match the waste heat source. For a water-based WHRS, the superheating temperature only offers a dryer expansion which reduces the erosion caused by the formation of small droplets inside the expander.

The impact on WHRS performance due to the inclusion and preference for a waste heat boiler is considerable, especially in cold environments. It was shown that the use of the exhaust gas waste heat for producing power is recommended for air temperatures above 8°C. At lower temperatures the heat demand on board is sufficiently large to not only require all the available waste heat from the exhaust gas but also the need for an auxiliary boiler. An alternative option tested in this thesis is to use the scavenge air waste heat to produce power while the exhaust gas is used for steam generation. This option reduces by a maximum of 670 t CO_2 per year – without counting the CO_2 emissions reduced by not using a fired boiler – the carbon emissions of a 4,100 twenty-foot unit navigating in the northern waters.

The study of the bottom section of the WHRS – which includes the condenser power requirement to reject the excess heat not used – was explored. The condenser fan/pump plays an important role in the WHRS net electric power, especially when the working fluid saturation temperature in the low pressure side is close to the sink temperature. This causes large volumes of coolant entering the condenser which in turn require higher power inputs from the fan/pump. A solution explored in this thesis was to increase the low pressure after expansion which had a knock-down effect with the expander's power output. However, in some instances this solution brought a higher net power output from the marine WHRS. The fan/pump power consumption and its impact was further explored in chapter 9 where a detailed model for the condenser was developed to better understand the role of the environment on the WHRS power and CO_2 emission reductions. It was found that the condenser power input could represent on average up to 16% of the power produced by the expander in warm months and at design speed while in the winter months the condenser's power input could represent as little as 1.8% of an average power output of 747 kW.

The temperature profile on northern waters, coupled with a container ship speed profile requires condensers that have volumes between 4.1 m^3 and 25.1 m^3 when cooled with seawater, while for air-cooled designs it was around 38.5 m^3 with a minimum cross-sectional area of 88.9 m^2. This represented an important challenge during on board installation which could be solved by using modular heat exchanger designs. Still, the method of cooling the WHRS on colder weather – air or seawater – depends on what the ship owner preferences are. Air is a strong candidate when the aim is just to comply with the Energy Efficiency Design Index (EEDI) or if

the most affordable WHRS is needed. Seawater cooling, on the other hand, brings the highest annual CO_2 and EEDI reduction possible but comes with a high price tag.

When changing fuels from high-sulphur to low-sulphur, the sulphuric dew point of the exhaust gas changes from 164°C to 132°C. The lower temperature of a low-sulphur fuel allows WHRS to absorb more energy from the waste heat source. Benzene and water took the most out of the extra waste heat by increasing their power output by 57% and 45% respectively.

The costs used in this thesis are estimates, absolute values based on many assumptions over the years and from different sources. However, under the same assumptions, the relative values due when comparing the different WHRS bring a useful financial comparison. Chapters 8 and 9 drew costs, profits and payback time comparisons between different marine WHRS. In chapter 8, the lowest annual profit is seen from a hexamethyldisiloxane ORC while in chapter 9 one of the highest profits seen is for an R1233zd(E) WHRS. Analysing the payback times in chapter 8, it is seen that the water-based RC achieves the fastest payback time in less than 2.8 years thanks to its low specific cost which requires the lowest initial cost. However, several ORC achieved a better profit at the end of the ship's operational life. Another important factor for longer payback times is due to the WHRS power output. In general, a larger expander power output implies larger heat exchangers, but also the pump must work faster to move the working fluid inside the process. In chapter 9, the shortest payback time seen is around 17.9 years with an R1233zd(E) WHRS that produces 327 kW. Using the same working fluid but producing 712 kW requires 21.5 years to return the initial investment. However, as seen in chapter 8 profit and payback time are affected considerably by the fuel price. The economic decision of installing a marine WHRS should be based on the expected fuel price and ownership time giving a better view of which WHRS is the best for a particular ship scenario.

The evidence in this thesis shows that a marine WHRS performance is sensitive to not only the different environmental temperatures and ship speeds – hence engine loading and waste heat availability and quality – but also to the WHRS plant configuration and fuel type. Different working and cooling fluids produce a wide range of optimal solutions whose benefits must be looked at under the light of environmental regulations, overall performance, sizing, safety and costs with a time-frame which benefits the aims of the different shipping stakeholders.

Question 3: How does an alternative waste heat recovery system using the available waste heat from the ship's prime mover compare to a traditional water-based Rankine cycle in terms of the ship's CO_2 emission reductions?

While the aim of this work is not the analysis of the effectiveness of the EEDI, the findings in this thesis regarding the off-design conditions on WHRS show an important shortfall in the CO_2 abatement regulation. The EEDI is dependent on the WHRS – or fuel saving technology – power return to the ship – translated to fuel savings – at the ship's design point and conditions. Including WHRS with large power outputs at the ship's design point will have an important impact on the ship's EEDI compliance. But as demonstrated in this thesis, with the operating profile applied to the WHRS, the apparent optimal system focused on high power output at

design point will not be saving as much in terms of CO_2 emissions – measured on an annual basis – as another WHRS that is focused on maximum emission savings which, in essence, is more in line with EEDI's aim. Furthermore, aiming for more powerful WHRS at design point forces the ship owner to choose high cost WHRS designs that do not return the best profits and payback times possible.

In light of this, the ship's CO_2 emission reductions should be seen from two different moments in the vessel's life. The first one when the ship is new; at this point in time it must comply, under design conditions, with the EEDI. The second stage happens during the operating life of the vessel during which all the off-design and environmental conditions act. As shown in the previous question, the variations of these factors have an important role on the WHRS performance.

For the annual CO_2 emission reductions, it was shown that the organic fluids could return, except for the case of hexamethyldisiloxane, higher CO_2 emissions reductions than the water-based RC when the operational profile was used. The ORC flexibility on saving CO_2 emissions at off-design conditions is highlighted in the comparison between toluene and water. The RC has a 3.0% larger net power output than toluene at design point but at the end of one year of operation, the CO_2 emission reductions are almost identical at around 681 t. When adding the annual route temperature profile in chapter 9, it is appreciated that WHRS with the largest power output installed do not always deliver the highest CO_2 savings. This has to do with how much of the annual operating time the WHRS is working and how much power it returns to the vessel. More flexible WHRS – operationally speaking – with moderate power outputs achieve better annual CO_2 emission reductions.

On a final note regarding CO_2 emissions, the thesis integrated the analysis of a waste heat boiler using part of the waste heat available in the exhaust gas with the intention of supporting the vessel's heat demand. By avoiding the use of a fired boiler to produce steam, it is possible to reduce further the ship's CO_2 emissions showing the importance of combining power generation and heating. Also, the integration of a waste heat boiler delimits the usage of the waste heat on board for a power WHRS, creating a more realistic scenario on board. In chapter 7, the CO_2 savings due to the waste heat boiler represented 55% of the total CO_2 emission reductions on board a container ship.

FINAL CONCLUDING REMARKS

The ORC technology can be applied to any kind of vessel type and size, bearing in mind that the ORC benefits depend on the waste heat temperature and availability, on board heat requirements, fuel type and operational profile. The great catalogue of working fluids and their thermodynamic characteristics manage to create a wide range of ORC WHRS designs which extract more power from the low/medium waste heat sources found on board ships than what is achieved by a typical water-based RC.

Which of the different ORC fluids is better is a question that is dependent on the stakeholders' point of view. As shown in the multi-objective optimisation, the optimal WHRS was chosen by a

combination or trade-off between power output, size and efficiency. This was followed by an analytical hierarchy process which discriminated solutions and contained what the author thought were the desirable characteristics of a marine WHRS. In chapter 9, different angles were used on top of the maximum annual CO_2 emission reductions to evaluate which of the cooling approaches for the ORC WHRS was better. As the preferences changed so did the "best" ORC WHRS, switching from air-cooled to seawater-cooled.

The use of advance optimisation approaches allowed the author to explore the limits of design and the assumptions made with the aim of increasing the accuracy of results via a more realistic model which could consider the different aspects of operating a vessel. The limitations on the design of waste heat boiler, economiser, recuperator, expander and pump, as well as a more detailed cost analysis which considers the operative and maintenance cost can give a better insight into the implications of the different WHRS. Still, the assumptions taken in the WHRS equipment models are sufficient to undertake an unbiased comparison between the different waste heat thermodynamic cycles which give strong indicators of the weaknesses and strengths of each WHRS.

FUTURE WORK

While good quality technical work has been done in the area of marine waste heat recovery system (WHRS), and there are plant configurations ready to be installed on board, this thesis has found areas of opportunity and improvement which are not fully covered yet in the marine and WHRS literature. In this section, a list of recommendations are given to further increase the knowledge of marine engineering, energy efficiency and WHRS.

1. As outlined by Calm [2008], as science in refrigerant design progresses, better organic fluids are available for its use in thermodynamic WHRS. This was the case for R1233zd(E), its thermodynamic properties were not available when the author started to work on the subject of marine WHRS. Now, its properties are publicly available in the work of Bell et al. [2014]. This working fluid is desirable since it does not have the flammability issues of a hydrocarbon, nor the high Global Warming Potential of some other refrigerants. Another recent and important player in the field of refrigerants is DuPont™ R1336mzz-Z (also known as DR-2™) which is claimed to deliver a good performance from low/medium quality waste heat sources but also able to operate as a supercritical fluid at lower pressure levels as those required by CO_2. It is probable that in the near future its thermodynamic behaviour and cost will be part of the public domain. The author has also seen in the organic Rankine cycle (ORC) literature an increase in interest in organic fluid mixtures, such as the WHRS working fluid, emulating the basis of the Kalina cycle. The idea, as discussed in the Kalina cycle section, is to have a better match for the heat source and sink reducing the system's irreversibilities. The researcher who wishes to continue in the field of marine ORC WHRS should look into new and alternative refrigerants or mixtures of refrigerant as working fluids.
2. The use of alternative fuels for shipping is now a reality with several examples of ships powered by liquefied natural gas, and another few by methanol and hydrogen. While these fuels are categorised as more environmentally-friendly – if care is taken – than traditional hydrocarbons, there is still an important area of opportunity in fuel savings which the WHRS could cover. The temperature profile and mass flow rate of the exhaust gas, as well as the compounds found are different from fuel to fuel. The air requirement and characteristics before compression also change from what is required for a traditional heavy fuel oil powered engine. These different characteristics will have an important impact on the WHRS behaviour – design or off-design operation – which must be assessed.
3. As shown in chapter 9, the detailed design of the condenser threw light on the implications of cooling with air or seawater. The study of different heat exchangers is important on board a vessel since this equipment will occupy the largest volume and surface area of the whole WHRS. This detailed heat exchanger modelling will also benefit the study of the waste heat boiler as an important part of a more complete and integral waste heat recovery plant. Compact heat exchangers, apart from the finned tube, could enhance the use of marine WHRS on board since they will require less space. It is recommended that plate and/or printed circuit heat exchangers be studied

for their implementation in marine WHRS since they offer a high heat transfer surface density. On the other hand, it is important to weigh their advantages against their initial and maintenance costs which tend to be higher than a shell and tube heat exchanger.

4. On the same line, expanders – turbine or scroll – should be modelled in detail since their cost is the major force behind the marine WHRS initial investment. Also, a detailed model of the expander will allow the researcher to understand how the ship's operating profile affects its performance, which dictates the WHRS power return. This will also map the expanders' internal operative temperatures and pressures which bring a better understanding as to the expanders' operational flexibility. The same should be completed for the working fluid pumps which play a lesser role in cost, size and performance loss but an important part of the WHRS.
5. One of the biggest arguments against marine WHRS on board is their initial cost and the uncertainty about the payback time of such an investment. This uncertainty is a product of how the system and ship are operated, but is also dependent on fuel prices and global economy making it difficult to add more certainty. Still, the initial cost could be improved by researching materials and geometries, but if large cost reductions are required, the engineer could look into used air conditioning systems which by operating them backwards, could deliver power to the ship at a low cost per CO_2 emitted. The previous case is just an example and the interested reader should look for other technologies that can bring down the WHRS costs which in turn will increase the probability of seeing these systems used inside the ship.
6. From what was first explored by Roberge [2014] and then in chapter 8 of this thesis, the study of flammable organic fluids on board vessels is a new area of research. Normally rejected by manufacturers due to the fluid's low flash point, it is thus underdeveloped for marine applications. There exists equipment such as safety and monitoring systems with improved sensors and automated firefighting capabilities, as well as contingency plans that can support flammable ORC. The design of these systems inspired by what is already in existence for the liquefied natural gas and methanol-powered vessel, plus what can be learned from mining and confined spaces, should be explored as well as the cost implications for the marine ORC WHRS. Also in this field, the researcher may find themselves suddenly investigating aspects more related to the law at sea and the well-being of the crew which highlights the importance of considering every aspect of the ship before installing a new technology.
7. The sensitivity study in chapter 7 lacked an analysis of the quantification of the effect had by that the thermal oil on the performance of WHRS. In addition, the power consumption of the thermal fluid pump, cooling of the oil when the exhaust gas heat is not being totally absorbed by the WHRS, pressure loss, and the thermal oil's total volume required among others are relevant areas of improvement to this work. As a guideline, the work of Delgado-Torres and García-Rodríguez [2012] could be used.
8. The author of this work recommends that the simulation results found in this thesis be taken to the next step which is experimentation. Throughout experimentation several of the assumptions made in this work can be tested and a better understanding of

off-design conditions can be gained. This step is quite expensive since test benches, working fluids and space is required but the researcher can approach other universities which have these facilities and begin a collaborative work project which will benefit the interested parties.

9. Returning to modelling, although this work discarded the use of the Kalina cycle due to its lower performance against the ORC and the water-based Rankine cycle, the Kalina cycle remains a viable marine WHRS option. The Kalina cycle has benefits such as high power output and similar equipment technology to the Rankine cycle which suits its application on board. In recent years, the interest in the Kalina cycle in marine applications has risen with a good example being found in the work of Larsen, Nguyen et al.[2014]. Also, as discussed in terms of the ORC WHRS, exploring how to reduce the initial and operational costs of the Kalina cycle will not only deliver new knowledge to marine and thermal engineering but will also enhance the possibilities of this thermodynamic cycle to be installed and used inside a ship.
10. The impact of using a waste heat boiler on this work was not analysed in-depth since the sizing, cost and performance were out of the scope of this work. An integral model which considers the participation of the waste heat boiler in the total emissions of the ship, as well as its behaviour in off-design conditions is an interesting area of opportunity. Furthermore, it was detected that the fuel consumed by an auxiliary boiler on board is not considered in the Energy Efficiency Design Index (EEDI), but the fuel saved by the waste heat boiler could be added. This unbalance in the EEDI, its implications and whether it should be corrected or not open new lines of study.
11. Following with the EEDI, as discussed in the thesis conclusions, an important area of enhancement for this index is the addition of off-design conditions but also the inclusion of a factor that considers the air and seawater temperature at which the ship is planned to operate. As seen before a winterised ship will be required to burn more fuel just to keep the relevant areas of the ship at operative temperature. This means that the vessel will emit more CO_2 and other noxious emissions than a non-winterised ship.
12. Chapter 9 explored the possibility of cooling the WHRS via air in cold weathers. The case study navigated close to the south limit of the Arctic Circle where the “warmest” temperatures at these latitudes are experienced. As mentioned, ice coverage in the North Pole is reducing every year, opening new and shorter routes at even lower temperatures which can lean the balance for an air-cooled WHRS. Hypothetical routes further north can be tested to understand until what point an air-cooled design is better. One of the biggest drawbacks in the air-cooled design was the large fan power consumption and it was discussed in the same chapter that the use of a recuperative WHRS may enhance the benefits of an air-cooled design since the condenser duty could be much lower, hence a lower power requirement. Furthermore, with an integration of a wind map and ship designed to the operation of marine WHRS in cold weathers, it will be possible to use the ship’s movement to absorb the unused energy eliminating partially or totally the need for fans. This marine WHRS area is unexplored and has great potential.

13. The addition of more waste heat sources on board and their utilisation must be considered so the overall efficiency of the vessel is increased further. A more important question to resolve is how the energy on board is produced, consumed and wasted. The energy map in the propulsive system is clear and well documented, but this is not the case for other ship systems which require energy – produced via fuels, alternative sources or waste heat/energy – and have important interactions and impacts with the whole energy economy on board. The mapping of heating, cooling, mechanical and electrical demands is necessary in order to have an efficient and green operative strategy that not only benefits the environment but also the vessel's stakeholders. Some research questions that should be answered in order to create a full energetic map would be as follows:
    a. ***Auxiliary engines.*** What are the operating profiles for the auxiliary engines? How much electrical power is generated by the auxiliary engines and for what? When are they operational?
    b. ***Heating and steam production.*** How much heating is required in the living areas? For maintaining the fuel viscosity? How much is needed for steam generation? How much of the steam is used for operating the vessel and how much is lost? How much of the heating is provided by the air conditioning system? How does the ship's structure benefit the heating demands on board? How much heat is required to treat the ballast water?
    c. ***Cooling and air conditioning.*** How large are the volumes required for cooling? Are there containers that need to be cooled? How much cooling is provided by the air conditioning system? Is waste heat used to produce cooling power?
    d. **Alternative and external sources of energy supply.** How much of the energy is produced by solar power, wind power etc. Does the alternative energy source produce electricity and heating?
    e. ***Other greenhouse gas emission reduction technologies.*** How do scrubbers affect the performance of a WHRS? Which technologies using waste heat deliver the highest emission reductions? How efficient would it be to couple a power turbine with a marine WHRS? How does an exhaust gas re-circulator affect the waste heat quality and availability?
    f. **Energy storage.** How much of the energy produced, but not used, can be stored? What method of storage is used: batteries? Compressed air? Hydrogen? How much excess energy is dumped into the environment?

    This idea is fairly complex and it is deemed difficult to achieve by a single group of individuals. But this energetic map is an important step forward which must be taken by the shipping industry in order to detect areas of improvement that will unlock a more efficient shipping, delivering a greener future.

(Page left intentionally blank)

GLOSSARY

- **Adiabatic:** It is a thermodynamic process in which there is no heat gain or loss.
- **Bottoming cycle:** A type of generation plant in which rejected heat and partially combusted waste gases from previous processes are used to generate useful work.
- **Bonferroni method:** Controls the simultaneous confidence level for a set of confidence intervals. The probability that at least one of the confidence intervals does not contain the dataset parameter is greater for a group of intervals than for any single interval. This means that in order to maintain the simultaneous confidence interval, the individual confidence interval must increase (e.g. from 95% to 99%).
- **Bubble point:** The temperature at which the first bubble appears when adding heat to a mixture formed by two or more pure components.
- **Coefficient of Performance (*COP*):** Used for measuring the efficiency of cooling or heating. It measures the amount of cooling/heating effects that can be produced by a system with an energy input. It is a number without units, and this number can be bigger than the unit.
- **Cogeneration:** In a process that generates useful work and heating simultaneously from one heat source (i.e. waste heat, combustion or heat collection). Also known as Combined Heat and Power (CHP).
- **Critical Point:** In a pressure versus temperature diagram, the critical point represents the pressure and temperature at which two different states of a fluid coexist. Defined by the critical pressure (P_{cr}) and critical temperature (T_{cr}).
- **Dead Volume:** Term used in Stirling engines and refers to any volume that is not swept by the power or displacement pistons. These volumes are one of the biggest sources of inefficiencies when applying the theoretical Stirling cycle.
- **Deadweight Tonnage (DWT):** The difference in metric tonnes between the light and loaded ship displacement. Its commercial importance is that it represents the total mass that ships can carry, including cargo, fuel, freshwater, crew, etc.
- **Dew point:** Is the temperature at which the first droplet appears when removing heat to a mixture formed by two or more pure components.
- **Dry fluid**: A fluid with a positive slope in its vapour saturation curve when observing a *T-s* diagram.
- **Enthalpy (*H*):** Represents the heat content absorbed or rejected in a system and can be expressed as $H = U + PV$, where P is pressure in Pa and V is volume in m^3. Its unit is J.
- **Entropy (S):** A measure of dissipation in an energy system, commonly seen as a measure of disorder. Its unit are J/K.
- **Evaporator:** A heat exchanger which uses the heat content of its source to change the state of the working fluid from liquid to vapour.
- **Exergy:** A measure of the potential of energy to transform to other forms of energy. Its unit is J.

- **Expander:** Machinery used to generate work. It can be a turbine, any reciprocating machine (i.e. compressors), or a screw expander, among others.
- **Global Warming Potential (GWP):** This coefficient determines the total energy that a GHG absorbs over a period of time compared to CO_2.
- **Gross Tonnage (GT):** A measure function of the moulded volume of the total enclosed spaces. This measurement is dimensionless.
- **Heat:** Energy that is transferred via a temperature difference.
- **Irreversible:** A process which after completion cannot go back to its original state without the input of more work.
- **Isentropic process:** A process in which there is no change of entropy. For this to occur, the process must be reversible and there must be no heat transfer.
- **Isentropic fluid:** A fluid with a large slope (almost infinite) in its vapour saturation curve when observing a *T-s* diagram.
- **Isochoric:** A process which occurs at the same pressure.
- **Liquid saturation curve:** The curve dividing the liquid and the two-phase fluid in a *T-s* diagram, found to the left side of the diagram.
- **Pinch point temperature (T_{pp}):** The source temperature, in a composite *T-H* graph, that gives the smallest temperature difference between working fluid (T_{sat}) and source in a heat exchanger. This point indicates where the ability to transfer heat between the process streams is most constrained.
- **Pinch point temperature difference:** The temperature difference between the heat source and working fluid saturation point (T_{sat}) in a heat exchanger (i.e. evaporators, condensers). Using a *T-ΔH* diagram, both temperatures must be in the same *ΔH* or if using a *T-s* have the same specific entropy (*s*) value.
- **Recuperator:** The heat exchanger used to warm up the fluid by conduction. Also known as preheater or economiser.
- **Regeneration:** The process completed by a heat exchanger where the same fluid is used to heat itself in another section of the process, e.g. bleeding the turbine and using that flow to preheat the fluid coming from the pump and entering the economiser. This process helps to improve the thermodynamic cycle efficiency. There can be two different regeneration processes: one where the hot and cold fluids are mixed together, while the second is where there is no fluid mixture and the heat exchange is completed by conduction.
- **Regenerator:** The heat exchanger used to warm up the fluid by mixing up the hot and cold fluid.
- **Reversible:** A process which can return to its initial state without leaving any trace in the surroundings.
- **Saturated vapour temperature (T_{sat}):** The temperature of the vapour at its saturation point. Since there is no change in temperature from the saturated liquid point to the vapour saturation point, this temperature is the same as the boiling temperature.

- **Saturation curve:** The curve in temperature (*T*) vs. specific entropy (*s*) diagram which defines the two-phase fluid from the individual phases of the fluid.
- **Saturation vapour curve:** The curve dividing the two-phase fluid and its vapour state in a *T-s* diagram, found to the right of the diagram. Depending on the slope of the curve the fluid can be classified as dry, isentropic or wet.
- **Saturation vapour:** "*A vapour whose temperature and pressure are such that any compression of its volume at constant temperature causes condensation at a rate sufficient to maintain a constant pressure*" [Dictionary.com LLC 2012].
- **Sink temperature:** This refers to the temperature of the cooling source before entering the condenser inlet. Also known as the cooling source temperature or rejection temperature.
- **Sink:** Where the heat not used by the system is rejected. Normally this is the coldest point in the system. For a marine WHRS, the most typical sink is seawater.
- **Source temperature:** This refers to the waste heat or hot source temperature before the economiser or boiler inlet. Also known as reservoir temperature.
- **Source:** The point from which the heat comes out. This can be an engine, turbine or fuel cell among others. Normally this is the hottest point in the system.
- **Specific enthalpy (*h*):** The enthalpy (*H*) divided by the mass. Its units are J/kg.
- **Specific entropy (*s*):** The entropy (*S*) divided by the mass. Its units are J/kg-K.
- **Subcritical:** Any thermodynamic process happening below the critical point (i.e. below T_{cr} and P_{cr} simultaneously).
- **Supercritical:** Any thermodynamic process occurring above the critical point (i.e. above T_{cr} and P_{cr} simultaneously).
- **Superheated vapour:** When a vapour starts to increase its temperature after crossing its saturation vapour temperature. The superheat is measured by the increase in the vapour temperature.
- **Thermal efficiency (η_{th}):** The measure of a heat engine's performance, defined as the amount of system heat energy available which is transformed into useful work. Also known as energy efficiency; when used in a thermodynamic system, it can be called cycle efficiency and, finally, as the first law efficiency.
- **Tonne-nautical mile (t-nm):** Measures the activity of the shipping industry and is the amount of cargo shipped multiplied by the average distance that it is transported. This index combines demand, routes, fleet and growth, and can be translated to energy requirements.
- **Transcritical:** Any thermodynamic process which forces the working fluid to operate in both subcritical and supercritical states under a single cycle.
- **Wet fluid:** A fluid with a negative slope in its vapour saturation curve when observing a *T-s* diagram.
- **Work:** Energy form transferred via force acting through a distance.

- **Working fluid:** Operational fluid for a thermal machine which absorbs heat from a source during a cycle. It is because of the fluid's thermodynamic changes that heat and work come in and out of the machine.

WORKS CITED

Aalborg Industries, 2005. VESTA MX Heat Exchanger. , p.2.

Abbas, M., Boumeddane, B., Said, N. & Chikouche, A., 2011. Dish Stirling technology: A 100 MW solar power plant using hydrogen for Algeria. *International Journal of Hydrogen Energy*, 36(7), pp.4305–4314.

Abe, H. & Ebuchi, N., 2014. Evaluation of sea-surface salinity observed by Aquarius. *Journal of Geophysical Research: Oceans*, 119(11), pp.8109–8121.

Afon, Y. & Ervin, D., 2012. An Assessment of Air Emissions from Liquefied Natural Gas Ships Using Different Power Systems and Different Fuels. *Journal of the Air & Waste Management Association*, 58(3), pp.404–411.

Airgas USA LLC, 2015. Safety Data Sheet HFC-236fa. , p.11.

Akbari, M., Mahmoudi, S., Yari, M. & Rosen, M., 2014. Energy and Exergy Analyses of a New Combined Cycle for Producing Electricity and Desalinated Water Using Geothermal Energy. *Sustainability*, 6(4), pp.1796–1820.

Aksoy, F. & Cinar, C., 2013. Thermodynamic analysis of a beta-type Stirling engine with rhombic drive mechanism. *Energy Conversion and Management*, 75, pp.319–324.

Algell, J., Bakosch, A. & Forsman, B., 2012. *Feasibility Study on LNG Fuelled Short Sea and Costal Shipping in the Wider Caribbean Region*, London.

Alibaba.com, 2016. Marine Diesel Engines. *Product Details*, p.1. Available at: http://www.alibaba.com/product-detail/6-cylinder-marine-diesel-engine [Accessed March 22, 2016].

Alliance for Sustainable Energy LLC, 2013. NREL: Concentrating Solar Power Projects - Maricopa Solar Project. , p.1. Available at: http://www.nrel.gov/csp/solarpaces/project_detail.cfm/projectID=58 [Accessed February 18, 2015].

Al-Rabghi, O.M., Beirutty, M., Akyurt, M., Najjar, Y.. & Alp, T., 1993. Review paper. *Heat Recovery Systems and CHP*, 13(5), pp.463–470.

Alvik, S., Eide, M.S., Endresen, Ø., Hoffmann, P. & Longva, T., 2010. *Pathways to low carbon shipping. Abatement potential towards 2030.*, Høvik.

America's Climate Choices, 2010. *Advancing the Science of Climate Change* 1st ed., Washington: The National Academies Press.

American Bureau of Shipping, 2013. Ship Energy Efficiency Measures: Status and Guidance. , p.76.

American Society of Heating Refrigerating and Air-Conditioning Engineers, 2007. ASHRAE STANDARD 34-2007: Designation and Safety Classification of Refrigerants. , p.34.

American Stirling Company, 2012. American Stirling Company | Beautiful Stirling Engines and Kits. *Home*, p.1. Available at: http://www.stirlingengine.com/ [Accessed March 1, 2013].

Anastas, P.T., Wasserscheid, P. & Stark, A., 2009. *Volume 6: Ionic Liquids* P. T. Anastas, ed., John Wiley & Son Limited.

Andersen, W.C. & Bruno, T.J., 2005. Rapid Screening of Fluids for Chemical Stability in Organic Rankine Cycle Applications. *Industrial & Engineering Chemistry Research*, 44(15), pp.5560–5566.

Angelino, G. & Invernizzi, C., 2003. Experimental investigation on the thermal stability of some new zero ODP refrigerants. *International Journal of Refrigeration*, 26(1), pp.51–58.

Appleby, W.G., Avery, W.H. & Meerbott, W.K., 1947. Kinetics and Mechanism of the Thermal Decomposition of n-Heptane. *Journal of the American Chemical Society*, 69(2), pp.2279–2285.

Arsdell, B.H. Van, 2001. *Macmillan Encyclopedia of Energy* 1st ed. H. Bieber et al., eds., New York: Macmillian Reference USA.

Arslan, O., 2010. Exergoeconomic evaluation of electricity generation by the medium temperature geothermal resources, using a Kalina cycle: Simav case study. *International Journal of Thermal Sciences*, 49(9), pp.1866–1873.

Arslan, O., 2011. Power generation from medium temperature geothermal resources: ANN-based optimization of Kalina cycle system-34. *Energy*, 36(5), pp.2528–2534.

ASTM International, 2014a. ASTM E659-14, Standard Test Method for Autoignition Temperature of Liquid Chemicals.

ASTM International, 2014b. ASTM D1310-14, Standard Test Method for Flash Point and Fire Point of Liquids by Tag Open-Cup Apparatus.

ASTM International, 2015. ASTM A106 / A106M-15, Standard Specification for Seamless Carbon Steel Pipe for High-Temperature Service. , p.8.

Astolfi, M., Romano, M.C., Bombarda, P. & Macchi, E., 2014. Binary ORC (Organic Rankine Cycles) power plants for the exploitation of medium–low temperature geothermal sources – Part B: Techno-economic optimization. *Energy*, 66, pp.435–446.

Bachmann, R., Nielsen, H., Warner, J. & Kehlhofer, R., 1999. *Combined-Cycle Gas & Steam Turbine Power Plants* 2nd ed., Tulsa: PennWell Publishing Company.

Bahaa, S., Gerald, K., Martin, W. & Johann, F., 2007. Working fluids for low-temperature organic Rankine cycles. *Energy*, 32, pp.1210–1221.

Bahadori, A., 2011. Estimation of combustion flue gas acid dew point during heat recovery and efficiency gain. *Applied Thermal Engineering*, 31(8-9), pp.1457–1462.

Baines, N., Wygant, K.D. & Dris, A., 2010. The Analysis of Heat Transfer in Automotive Turbochargers. *Journal of Engineering for Gas Turbines and Power*, 132(4), p.042301.

Balaji, R. & Yaakob, O., 2012. An analysis of shipboard waste heat availability for ballast water treatment. *Journal of Marine Engineering and Technology*, 11(2), pp.15–29.

Balmer, R.T., 2011. *Modern engineering thermodynamics* 1st ed., London: Academic Press.

Banks, C., Turan, O., Incecik, A., Theotokatos, G., Izkan, S., Shewell, C. & Tian, X., 2013. Understanding ship operating profiles with an aim to improve energy efficient ship operations. In *Low Carbon Shipping Conference*. London, p. 11.

Bao, J. & Zhao, L., 2013. A review of working fluid and expander selections for organic Rankine cycle. *Renewable and Sustainable Energy Reviews*, 24(null), pp.325–342.

Bazari, Z. & Longva, T., 2011. *Assessment of IMO Mandated Energy Efficiency Measures for International Shipping*, London.

BCS Incorporated, 2008. *Waste Heat Recovery: Technology and Opportunities in U.S. Industry*, Laurel.

Bejan, A., Tsatsaronis, G. & Moran, M., 1995. *Thermal Design and Optimization*, Hoboken: John Wiley & Sons Inc.

Bell, I.H., Wronski, J., Quoilin, S. & Lemort, V., 2014. Pure and Pseudo-pure Fluid Thermophysical Property Evaluation and the Open-Source Thermophysical Property Library CoolProp. *Industrial & engineering chemistry research*, 53(6), pp.2498–2508.

Benvenuto, G., Campora, U. & Trucco, A., 2014. Comparison of ship plants layouts for power propulsion systems with energy recovery. In *12th International Naval Engineering Conference and Exhibition*. Amsterdam: Institute of Marine Engineering, Science and Technology, pp. 329–340.

Benvenuto, G.., Bertetta, D.., Carollo, F.. & Campora, U.., 2011. COGAS plant as possible future alternative to the diesel engine for the propulsion of large ships. In E. Rizzuto & C. G. Soares, eds. *Sustainable Maritime Transportation and Exploitation of Sea Resources*. London: Taylor & Francis Group, pp. 603–613.

Bianchi, M. & De Pascale, a., 2011. Bottoming cycles for electric energy generation: Parametric investigation of available and innovative solutions for the exploitation of low and medium temperature heat sources. *Applied Energy*, 88(5), pp.1500–1509.

Bilgen, E., Ducarroir, M., Foex, M., Sibieude, F. & Trombe, F., 1977. Use of solar energy for direct and two-step water decomposition cycles. *International Journal of Hydrogen Energy*, 2(3), pp.251–257.

Bini, R., Prima, M.D.I. & Guercio, A., 2010. Organic Rankine Cycle (ORC) In Biomass Plants : An Overview On Different Applications. , p.9.

Bliem, C.J., 1988. KALINA CYCLE AND SIMILAR CYCLES FOR GEOTHERMAL POWER PRODUCTION.

Board of Governors of the Federal Reserve System, 2015. Foreign Exchange Rates - H.10. , p.1. Available at: http://www.federalreserve.gov/releases/h10/current/ [Accessed May 23, 2015].

Boatsandoutboards.co.uk, 2016. Doosan Engines. *Inboard Diesel for sale*, p.1. Available at: http://www.boatsandoutboards.co.uk/ [Accessed March 22, 2016].

Bombarda, P., Invernizzi, C.M. & Pietra, C., 2010. Heat recovery from Diesel engines: A thermodynamic comparison between Kalina and ORC cycles. *Applied Thermal Engineering*, 30(2-3), pp.212–219.

Boretti, A., 2012a. Transient operation of internal combustion engines with Rankine waste heat recovery systems. *Applied Thermal Engineering*, 48, pp.18–23.

Boretti, A., 2012b. Recovery of exhaust and coolant heat with R245fa organic Rankine cycles in a hybrid passenger car with a naturally aspirated gasoline engine. *Applied Thermal Engineering*, 36, pp.73–77.

Borgert, J.A.. & Velasquez, J.A., 2004. Exergoeconomic optimisation of a Kalina cycle for power generation. *International Journal of Exergy*, 1(1), p.11.

Bowman, L., 1993. A Technical Introduction to Free-Piston Stirling Cycle Machines: Engines, Coolers, and Heat Pumps. , p.7.

Branchini, L., De Pascale, A. & Peretto, A., 2013. Systematic comparison of ORC configurations by means of comprehensive performance indexes. *Applied Thermal Engineering*, 61(2), pp.129–140.

Brioukov, M.G., Park, J. & Lin, M.C., 1999. Kinetic modeling of benzene decomposition near 1000 K: The effects of toluene impurity. *International Journal of Chemical Kinetics*, 31(8), pp.577–582.

British Electricity International, 1991. *Turbines, Generators and Associated Plant*, Elsevier.

British Petroleum, 2011. *Material Safety Data Sheet Marine Diesel Oil*, Chicago.

Bronicki, L., 2008. Advanced power cycles for enhancing geothermal sustainability 1,000 MW deployed worldwide. In *Power and Energy Society General Meeting - Conversion and Delivery of Electrical Energy in the 21st Century, 2008 IEEE*. Pittsburgh: Ormat, pp. 1–6.

Bronicki, L.Y., 1995. Innovative Geothermal Power Plants Fifteen Years of Experience. In *World Geothermal Conference*. Florence, pp. 2089–2092.

Bronicki, L.Y., 2000. Organic Rankine Cycle Power Plant For Waste Heat Recovery. , p.6.

Bronicki, L.Y., 2007. INTEGRATED ENGINE GENERATOR RANKINE CYCLE POWER SYSTEM. , p.12.

Bronicki, L.Y., 2010. Organic Rankine Cycle Power Plant For Waste Heat. *Ormat Technologies Inc.*, (Figure 1), p.5. Available at: http://www.ormat.com/research/papers/organic-rankine-cycle-power-plant-waste-heat-recovery [Accessed August 23, 2012].

Brown, D.K., 1976. Fouling And Economic Ship Performance. In *Proceedings of the 5th Inter-Naval Corrosion Conference*. Auckland, p. 25.

Browne, C., 2015. Stena Germanica's conversion to methanol power is a world first. *Horizons*, pp.18–21.

Buhaug, Ø., Corbett, J.J., Endresen, Ø., Eyring, V., Faber, J., Hanayama, S., Lee, D.S., Lee, D., Lindstad, H., Markowska, A.Z., Mjelde, A., Nelissen, D., Nilsen, J., Pålsson, C., Winebrake, J.J., Wu, W. & Yoshida, K., 2009. *Second IMO GHG Study 2009*, London.

Bunker Index, 2015. Bunker Index. *Prices*, p.1. Available at: http://www.bunkerindex.com/prices/bixfree.php?priceindex_id=4#Description [Accessed December 5, 2014].

Burel, F., Taccani, R. & Zuliani, N., 2013. Improving sustainability of maritime transport through utilization of Liquefied Natural Gas (LNG) for propulsion. *Energy*, 57, pp.412–420.

Butcher, C.J. & Reddy, B.V., 2007. Second law analysis of a waste heat recovery based power generation system. *International Journal of Heat and Mass Transfer*, 50(11-12), pp.2355–2363.

Calise, F., Capuozzo, C., Carotenuto, A. & Vanoli, L., 2014. Thermoeconomic analysis and off-design performance of an organic Rankine cycle powered by medium-temperature heat sources. *Solar Energy*, 103, pp.595–609.

Calleya, J., Pawling, R. & Greig, A., 2015. Ship impact model for technical assessment and selection of Carbon dioxide Reducing Technologies (CRTs). *Ocean Engineering*, 97, pp.82–89.

Calleya, J.N., 2014. *Ship Design Decision Support for a Carbon Dioxide Constrained Future*. University College London.

Calm, J.M., 2008. The next generation of refrigerants – Historical review, considerations, and outlook. *International Journal of Refrigeration*, 31(7), pp.1123–1133.

Calm, J.M. & Didion, D.A., 1998. Trade-offs in refrigerant selections: past, present, and future. *International Journal of Refrigeration*, 21(4), pp.308–321.

Calm, J.M. & Hourahan, G.C., 2001. Refrigerant Data Summary. *Engineered Systems*, pp.74–88.

Campana, F., Bianchi, M., Branchini, L., De Pascale, A., Peretto, A., Baresi, M., Fermi, A., Rossetti, N. & Vescovo, R., 2013. ORC waste heat recovery in European energy intensive industries: Energy and GHG savings. *Energy Conversion and Management*, 76, pp.244–252.

Carlton, J.S., Smart, R. & Jenkins, V., 2011. The nuclear propulsion of merchant ships: Aspects of engineering, science and technology. *Journal of Marine Engineering & Technology*, 10(2), pp.47–59.

Cengel, Y.A. & Boles, M.A., 2007. *Thermodynamics: An Engineering Approach* 6th ed., Singapore: McGraw-Hill.

Chacartegui, R., Sánchez, D., Muñoz, J.M. & Sánchez, T., 2009. Alternative ORC bottoming cycles FOR combined cycle power plants. *Applied Energy*, 86(10), pp.2162–2170.

Cheang, V.T., Hedderwick, R.A. & McGregor, C., 2015. Benchmarking supercritical carbon dioxide cycles against steam Rankine cycles for Concentrated Solar Power. *Solar Energy*, 113, pp.199–211.

Chen, H., Goswami, D.Y. & Stefanakos, E.K., 2010. A review of thermodynamic cycles and working fluids for the conversion of low-grade heat. *Renewable and Sustainable Energy Reviews*, 14(9), pp.3059–3067.

Chen, W.-L., Wong, K.-L. & Po, L.-W., 2012. A numerical analysis on the performance of a pressurized twin power piston gamma-type Stirling engine. *Energy Conversion and Management*, 62(null), pp.84–92.

Chen, Y., Lundqvist, P., Johansson, A. & Platell, P., 2006. A comparative study of the carbon dioxide transcritical power cycle compared with an organic rankine cycle with R123 as working fluid in waste heat recovery. *Applied Thermal Engineering*, 26(17-18), pp.2142–2147.

Chilcott, R.P., 2011. HPA Compendium of Chemical Hazards - Benzene. , p.33.

Choi, B.C. & Kim, Y.M., 2013. Thermodynamic analysis of a dual loop heat recovery system with trilateral cycle applied to exhaust gases of internal combustion engine for propulsion of the 6800 TEU container ship. *Energy*, 58(null), pp.404–416.

Clarkson Research Services Limited, 2013. Shipping Intelligence Network.

Cleaver-Brooks Inc, 2011a. The technology behind the CBEX: Exploring The Myth of Boiler Heating Square Footage. , p.7.

Cleaver-Brooks Inc, 2011b. Boiler Book CBEX Elite 100-800. , pp.1–74.

Climate Change Division US EPA, 2012. Sea Surface Temperature. *Climate change*, p.1. Available at: http://www.epa.gov/climatechange/science/indicators/oceans/sea-surface-temp.html [Accessed February 13, 2013].

Cohn, A., 1986. *Technology Assessments of Advanced Power Generation Systems II--Kalina Bottoming Cycle*, Palo Alto.

Containership-Info, 2014. JPO LIBRA. , p.1. Available at: http://www.containership-info.com/ [Accessed September 22, 2014].

Cool Energy Inc., 2012. Waste Heat Recovery Applications. , p.1. Available at: http://www.coolenergyinc.com/solar.html [Accessed February 27, 2013].

Corbett, J.J., Lack, D.A., Winebrake, J.J., Harder, S., Silberman, J.A. & Gold, M., 2010. Arctic shipping emissions inventories and future scenarios. *Atmospheric Chemistry and Physics*, 10(19), pp.9689–9704.

Corbett, J.J., Thomson, H. & Winebrake, J.J., 2015. *Methane Emissions from Natural Gas Bunkering Operations in the Marine Sector: A Total Fuel Cycle Approach*,

Coskun, A., Bolatturk, A. & Kanoglu, M., 2014. Thermodynamic and economic analysis and optimization of power cycles for a medium temperature geothermal resource. *Energy Conversion and Management*, 78, pp.39–49.

Council of the European Union & European Parliament, 2009. Directive 2009/30/EC of the European Parliament and of the Council. , pp.L140/88 – L140/113.

Crane, D., LaGrandeur, J., Jovovic, V., Ranalli, M., Adldinger, M., Poliquin, E., Dean, J., Kossakovski, D., Mazar, B. & Maranville, C., 2012. TEG On-Vehicle Performance and Model Validation and What It Means for Further TEG Development. *Journal of Electronic Materials*, 42(7), pp.1582–1591.

Cristiani, P. & Giancola, U., 2000. Prevention of fouling and microbial Corrosion in Power Stations using Seawater as a Coolnat. In H. Müller-Steinhagen, ed. *Heat Exchanger Fouling: Mitigation and Cleaning Technologies*. Essen: Publico Publications, pp. 334–349.

Cunningham, P., 2002. Waste Heat/Cogen Opportunities in the Cement Industry. *Cogeneration & Distributed Generation Journal*, 17(3), pp.31–51.

Daniel, J. & Velders, G., 2006. Halocarbon Scenarios, Ozone Depletion Potentials, and Global Warming Potentials. In *Scientific Assessment of Ozone Depletion: 2006*. Geneva: World Meteorological Organization, pp. 8.1–8.39.

Date, A., Date, A., Dixon, C. & Akbarzadeh, A., 2014. Progress of thermoelectric power generation systems: Prospect for small to medium scale power generation. *Renewable and Sustainable Energy Reviews*, 33, pp.371–381.

Datla, B.V. & Brasz, J., 2014. Comparing R1233zd and R245fa for Low Temperature ORC Applications. In *International Refrigeration and Air Conditioning Conference*. Purdue: Purdue University, p. 7.

Deb, K., 2011. *Multi-objective Evolutionary Optimisation for Product Design and Manufacturing* 1st ed. L. Wang, A. H. C. Ng, & K. Deb, eds., London: Springer London.

Delgado-Torres, A.M. & García-Rodríguez, L., 2012. Design recommendations for solar organic Rankine cycle (ORC)–powered reverse osmosis (RO) desalination. *Renewable and Sustainable Energy Reviews*, 16(1), pp.44–53.

Dentener, F., Derwent, R., Dlugokencky, E., Holland, E., Isaksen, I., Katima, J., Kirchhoff, V., Matson, P., Midgley, P. & Wang, M., 2001. Atmospheric Chemistry and Greenhouse Gases. In M. M. F. Joos, ed. *Climate Change 2001: The Scientific Basis*. Intergovermental Panel on Climate Change, pp. 239–288.

Department of Energy and Climate Change, 2015. *2013 UK greenhouse gas emissions: final figures - statistical release*, London.

Department of Transport, 2015. World fleet registered vessels (FLE05). , p.1.

Det Norske Veritas AS, 2013a. Tentative Rules for Low Flashpoint Liquid Fuelled Ship Installations. , p.37.

Det Norske Veritas AS, 2013b. DNV-OS-A201: Winterization for Cold Climate Operations (Tentative). , (October), p.83.

Dharmalingam, P., Kumar, J.N., Suryanarayanan, R. & Kumar, S.S., 2004. Waste Heat Recovery. In *The National Certification Examination for Energy Managers and Energy Auditors*. New Delhi: Bureau of Energy Efficiency, pp. 1–18.

Dictionary.com LLC, 2012. Saturated Vapor. , p.1.

Dieselenginetrader.com, 2016. Marine Diesel Engines. *Engine Details*, p.1. Available at: http://www.dieselenginetrader.com/search/engine_details.cfm [Accessed March 22, 2016].

Dimopoulos, G.G. & Frangopoulos, C.A., 2008. Optimization of energy systems based on Evolutionary and Social metaphors. *Energy*, 33(2), pp.171–179.

Dimopoulos, G.G., Georgopoulou, C.A. & Kakalis, N.M.P., 2012. The introduction of exergy analysis to the thermo-economic modelling and optimisation of a marine combined cycle system. In U. Desideri, G. Manfrida, & E. Sciubba, eds. *The 25th International Conference on Efficiency, Cost, Optimization, Simulation and Environmental Impact Of energy Systems*. Perugia: Firenze University Press, pp. 221–236.

Dimopoulos, G.G., Georgopoulou, C.A., Stefanatos, I.C., Zymaris, A.S. & Kakalis, N.M.P., 2014. A general-purpose process modelling framework for marine energy systems. *Energy Conversion and Management*, 86, pp.325–339.

Dimopoulos, G.G., Kougioufas, A. V. & Frangopoulos, C.A., 2008. Synthesis, design and operation optimization of a marine energy system. *Energy*, 33(2), pp.180–188.

Dinanno, L.R., Dibella, F.A. & Koplow, M.D., 1983. *An RC-1 Organic Rankine Bottoming Cycle for an Adiabatic Diesel Engine*, Cleveland.

DiPippo, R., 2004. Second Law assessment of binary plants generating power from low-temperature geothermal fluids. *Geothermics*, 33(5), pp.565–586.

DiSalvo, F.J., 1999. Thermoelectric Cooling and Power Generation. *Science*, 285(5428), pp.703–706.

Doble, A., 1917. Steam motor vehicles. *Journal of the Franklin Institute*, 183(2), p.253.

Doerr, R.G., Kohler, J.A., Calm, J.M., Richard, R.G., Kusmierz, A., Rusch, G.M., Didion, D.A., Senediak, J., Troy, E.F., Jepson, G.W., Kennoy, D.H., Knebel, D.E., Kennedy, S.D., Beda, M.F., Hogan, J.F. & Howard, E.P., 2007. ANSI/ASHRAE Standard 34-2004: Designation and Safety Classification of Refrigerants Addenda v and w. , p.12.

Dolz, V., Novella, R., García, A. & Sánchez, J., 2012. HD Diesel engine equipped with a bottoming Rankine cycle as a waste heat recovery system. Part 1: Study and analysis of the waste heat energy. *Applied Thermal Engineering*, 36, pp.269–278.

Domanski, P.., Didion, D.. & Doyle, J.., 1994. Evaluation of suction-line/liquid-line heat exchange in the refrigeration cycle. *International Journal of Refrigeration*, 17(7), pp.487–493.

Domingues, A., Santos, H. & Costa, M., 2013. Analysis of vehicle exhaust waste heat recovery potential using a Rankine cycle. *Energy*, 49(null), pp.71–85.

Douglas, J.D., Braun, J.E., Groll, E.A. & Tree, D.R., 1999. A cost-based method for comparing alternative refrigerants applied to R-22 systems. *International Journal of Refrigeration*, 22(2), pp.107–125.

Endo, T., Kawajiri, S., Kojima, Y., Takahashi, K., Baba, T., Ibaraki, S., Takahashi, T. & Shinohara, M., 2007. *Study on Maximizing Exergy in Automotive Engines*,

Energy Efficiency Guide for Industry in Asia, 2006. Thermal Energy Equipment: Waste Heat Recovery. *Energy Efficiency Guide for Industry in Asia*, pp.1–18. Available at: http://www.energyefficiencyasia.org/docs/ee_modules/Chapter-Waste Heat Recovery.pdf [Accessed October 24, 2012].

Engineers Edge, 2013. Parallel and Counter Flow Designs Heat Exchangers. *Engineers Edge*, p.1. Available at: http://www.engineersedge.com/heat_transfer/parallel_counter_flow_designs.htm [Accessed April 22, 2013].

Environment Agency, 2011. *Technical Guidance Note: Monitoring VOCs in Stack Gas Emissions*, Rotherham.

Environmental Protection Agency, 2012. Causes of Climate Change. , p.1. Available at: http://www.epa.gov/climatechange/science/causes.html [Accessed June 29, 2012].

Environmental Protection Agency, 2013. Global Warming Potentials and Ozone Depletion Potentials of Some Ozone-Depleting Substances and Alternatives Listed by the SNAP Program. *Ozone Layer Protection*, p.1. Available at: http://www.epa.gov/ozone/snap/subsgwps.html [Accessed December 18, 2013].

Epcon Industrial Systems LP, 2010. Heat Exchangers. , p.1. Available at: http://www.epconlp.com/specialty-systems/heat-exchangers.php [Accessed February 21, 2013].

Espinosa, N., Lazard, M., Aixala, L. & Scherrer, H., 2010. Modeling a Thermoelectric Generator Applied to Diesel Automotive Heat Recovery. *Journal of Electronic Materials*, 39(9), pp.1446–1455.

Eto, M. & Kamimura, H., 2011. Comprehensive Semiconductor Science and Technology. In P. Bhattacharya, R. Fornari, & H. Kamimura, eds. *Comprehensive Semiconductor Science and Technology*. Amsterdam: Elsevier, pp. 77–112.

European Central Bank, 2013. Pound sterling (GBP). *Exchange Rates*, p.1. Available at: http://www.ecb.int/stats/exchange/eurofxref/html/eurofxref-graph-gbp.en.html [Accessed June 15, 2015].

European Central Bank, 2015. Euro exchange rates USD. *Exchange Rates*, p.1. Available at: http://www.ecb.europa.eu/stats/exchange/eurofxref/html/eurofxref-graph-usd.en.html [Accessed April 23, 2015].

Eurostat, 2012. Electricity production and supply statistics. *Statistics Explained*, p.1. Available at: http://epp.eurostat.ec.europa.eu/statistics_explained/index.php/Electricity_production_and_supply_statistics [Accessed March 6, 2013].

Eymel, C., Rodríguez, C., Carlos, J., Palacio, E. & Rodríguez, C., 2012. Exergetic and economic analysis of Kalina cycle for low temperature geothermal sources in Brazil. In U. Desideri, G. Manfrida, & E. Sciubba, eds. *Efficiency, Cost, Optimization, Simulation And Environmental Impact Of Energy Systems*. Perugia: Firenze University Press, pp. 1–13.

Fakheri, A., 2003. A General Expression for the Determination of the Log Mean Temperature Correction Factor for Shell and Tube Heat Exchangers. *Journal of Heat Transfer*, 125(3), p.527.

Feng, L., Gao, W., Qin, H. & Xie, B., 2010. Heat Recovery from Internal Combustion Engine with Rankine Cycle. In *2010 Asia-Pacific Power and Energy Engineering Conference*. Chengdu: IEEE, pp. 1–4.

Fernández, F.J., Prieto, M.M. & Suárez, I., 2011. Thermodynamic analysis of high-temperature regenerative organic Rankine cycles using siloxanes as working fluids. *Energy*, 36(8), pp.5239–5249.

Forster, P., Ramaswamy, V., Artaxo, P., Berntsen, T., Betts, R., Fahey, D.W., Haywood, J., Lean, J., Lowe, D.C., Myhre, G., Nganga, J., Prinn, R., Raga, G., Schulz, M. & Dorland, R. Van, 2007. 2007: Changes in Atmospheric Constituents and in Radiative Forcing. In S. Solomon et al., eds. *Climate Change 2007: The Physical Science Basis. Contribution of Working Group I to the Fourth Assessment Report of the Intergovernmental Panel on Climate Change*. Cambridge: Cambridge University Press, pp. 129–234.

Foster, P.R., 2011. Innovative Rotary Displacer Stirling Engine: Sustainable Power Generation for Private and Fleet Vehicle Applications. *The Journal of Technology Studies*, 37(2), pp.95–107.

Frangopoulos, C.A. & Dimopoulos, G.G., 2004. Effect of reliability considerations on the optimal synthesis, design and operation of a cogeneration system. *Energy*, 29(3), pp.309–329.

Fréchette, L.G.., Lee, C.. & Arslan, S., 2004. Development of a MEMS-Based Rankine Cycle Steam Turbine For Power Generation: Project Status. In *The Fourth International Workshop on Micro and Nanotechnology for Power Generation and Energy Conversion Applications*. Kyoto, pp. 92–95.

Freymann, R., Ringler, J., Seifert, M. & Horst, T., 2012. The Second Generation Turbosteamer. *MTZ worldwide*, 73(2), pp.18–23.

Gary, M., 2009. Green Ship Magazine. *Green Ships of the Future*, p.32.

Gilbert, P., 2014. From reductionism to systems thinking: How the shipping sector can address sulphur regulation and tackle climate change. *Marine Policy*, 43, pp.376–378.

Global Geothermal, 2013a. Recover Energy - industrial and binary geothermal. *Applications*, p.1. Available at: http://www.globalgeothermal.com/Applications.aspx [Accessed January 28, 2013].

Global Geothermal, 2013b. Iron & Steel Industry. , p.5.

Global Reports LLC, 2008. *Annual report 2008: Environment volume*, Tokyo.

GmbH, K., 2003. Regenerative Heat Exchangers for Industry and Process Technology. , p.9.

Gnielinski, V., 1976. New Equations for Heat and Mass Transfer in Turbulent Pipe and Channel Flow. *International Journal of Chemical Engineering*, 16, pp.359–368.

Godbole, S.S., 1990. Comparing dynamic responses of recirculating and once-through steam generators for next-generation LWRs. *Transactions of the American Nuclear Society; (USA)*, 62, pp.11–15.

Golden, B.L., Wasil, E.A. & Harker, P.T., 1989. *The Analytic Hierarchy Process: Applications and Studies* 1st ed. B. L. Golden, E. A. Wasil, & P. T. Harker, eds., Berlin, Heidelberg: Springer Berlin Heidelberg.

Google & GeoBasis-De/BKG, 2015. Northern hemisphere 70.3N, 24.4E. *Google Maps*. Available at: https://www.google.co.uk/maps/place/Google/ [Accessed July 6, 2015].

Granryd, E., 2001. Hydrocarbons as refrigerants — an overview. *International Journal of Refrigeration*, 24(1), pp.15–24.

Gu, W., Weng, Y., Wang, Y. & Zheng, B., 2009. Theoretical and experimental investigation of an organic Rankine cycle for a waste heat recovery system. *Proceedings of the Institution of Mechanical Engineers, Part A: Journal of Power and Energy*, 223(5), pp.523–533.

Gymnopoulos, K., 2013. *Shipping in harsh environments*. University College London.

Habl, P., Blanco-Marigorta, A.M. & Erlach, B., 2012. Exergoeconomic comparison of wet and dry cooling technologies for the Rankine cycle of a solar thermal power plant. In U. Desideri, G. Manfrida, & E. Sciubba, eds. *Efficiency, Cost, Optimization, Simulation And Environmental Impact Of Energy Systems*. Perugia: Firenze University Press, pp. 300.1–300.14.

Hards, V., 2005. *Volcanic Contributions to the Global Carbon Cycle*, Keyworth.

Harperscheidt, J., LNG as Fuel - Bunkering, storage and processing. , p.2.

Harvey, F., 2015. Global emissions stall in 2014 following slowdown in China's economy. *The Guardian*, p.1.

Hatchman, J.C., 1991. Steam cycles for waste heat recovery: A case study. *Research and Development Journal*, 7(3), pp.32–38.

He, J., Liu, C., Xu, X., Li, Y., Wu, S. & Xu, J., 2014. Performance research on modified KCS (Kalina cycle system) 11 without throttle valve. *Energy*, 64, pp.389–397.

Heberle, F., Weith, T., Preißinger, M. & Brüggemann, D., 2013. Experimental Investigations of Heat Transfer Characteristics and Thermal Stability of Siloxanes. , p.35.

Hirata, K. & Kawada, M., 2005. Discussion of Marine Stirling Engine Systems. In *Proceedings of*

the 7th International Symposium on Marine Engineering. Tokyo, pp. 1–5.

Hjartarson, H. & Gullev, L., 2003. Húsavík , Iceland – A model of energy efficiency based on geothermal energy. *Hot/Cool*, p.3.

Hnat, G., Patten, J.S.S., Bartone, L.M.M., Cutting, J.C.C. & Hnat, J.G., 1982. Industrial Heat Recovery With Organic Rankine Cycles. In *Proceedings from the Fourth Industrial Energy Technology Conference*. Houston: Energy Systems Laboratory of the Texas A&M University System, pp. 524–532.

Holtrop, J., 1984. A statistical re-analysis of resistance and propulsion data. *International shipbuilding progress*, 31(363), pp.272–276.

Holtrop, J. & Mennen, G.G., 1982. An Approximate Power Prediction Method. *International Shipbuilding Progress*, 29(July), pp.166–170.

Honeywell, 2001. *Genetron 245fa (pressurized), Material Safety Datasheet GTRN-0037*, Morristown.

Honeywell, 2014. Solstice ® 1233zd (E) Safety Data Sheet. , pp.1–14.

Honeywell Refrigerants, 2012. Genetron® 245fa. *Genetron® Refrigerants*, p.6. Available at: http://www.honeywell-refrigerants.com/products/genetron-245fa/ [Accessed December 14, 2012].

Hooke, R. & Jeeves, T.A., 1961. "Direct Search'' Solution of Numerical and Statistical Problems. *Journal of the ACM*, 8(2), pp.212–229.

Horst, T.A., Tegethoff, W., Eilts, P. & Koehler, J., 2014. Prediction of dynamic Rankine Cycle waste heat recovery performance and fuel saving potential in passenger car applications considering interactions with vehicles' energy management. *Energy Conversion and Management*, 78, pp.438–451.

Hossain, S.N. & Bari, S., 2013. Waste heat recovery from the exhaust of a diesel generator using Rankine Cycle. *Energy Conversion and Management*, 75, pp.141–151.

Hsu, S.T., Lin, F.Y. & Chiou, J.S., 2003. Heat-transfer aspects of Stirling power generation using incinerator waste energy. *Renewable Energy*, 28(1), pp.59–69.

Hua, J., Wu, Y.-H. & Jin, P.-F., 2008. Prospects for renewable energy for seaborne transportation—Taiwan example. *Renewable Energy*, 33(5), pp.1056–1063.

Huijbregts, W.M.M. & Leferink, R.G.I., 2004. Latest advances in the understanding of acid dewpoint corrosion: corrosion and stress corrosion cracking in combustion gas condensates. *Anti-Corrosion Methods and Materials*, 51(3), pp.173–188.

Hulse, R.J., Basu, R.S., Singh, R.R. & Thomas, R.H.P., 2012. Physical Properties of HCFO-1233zd(E). *Journal of Chemical & Engineering Data*, 57(12), pp.3581–3586.

Hultqvist, A., 2008. Measures for reducing emissions on Emma Maersk. , (January), p.43.

Hung, T.C., Shai, T.Y. & Wang, S.K., 1997. A Review Of Organic Rankine Cycles (ORCs) For The Recovery Of Low-Grade Waste Heat. *Energy*, 22(7), pp.661–667.

Imran, M., Park, B.S., Kim, H.J., Lee, D.H., Usman, M. & Heo, M., 2014. Thermo-economic optimization of Regenerative Organic Rankine Cycle for waste heat recovery applications. *Energy Conversion and Management*, 87, pp.107–118.

Incropera, F.P., Dewitt, D.P., Bergman, T.L. & Lavine, A.S., 2007. *Fundamentals of Heat and Mass Transfer* 6th ed., Hoboken: John Wiley & Sons, Inc.

Infinity Turbine LLC, 2012. Infinity Turbine ® - Organic Rankine Cycle ORC. , p.1. Available at: http://www.infinityturbine.com/ORC/ORC_Waste_Heat_Turbine.html [Accessed July 15, 2012].

Intergovermental Panel on Climate Change, 2014. *Climate Change 2014: Synthesis Report* 1st ed. Core Writing Team, R. K. Pachauri, & L. A. Meyer, eds., Geneva: Intergovermental Panel on Climate Change.

International Association of Classification Societies Ltd., 2011. *Requirments Concering Polar Class*, London.

International Energy Agency, 2009. *Transport, Energy and CO2*, Paris: International Energy Agency (IEA).

International Energy Agency, 2014. *CO2 Emissions From Fuel Combustion Highlights 2014* 2014th ed., Paris: IEA Statistics.

International Maritime Organization, 1974. International Conference on Safety of Life at Sea. , p.277.

International Maritime Organization, 1993. International Code for the Construction and Equipment of Ships Carrying Liquefied Gas in Bulk. , p.28.

International Maritime Organization, 2009a. *MEPC.1/Circ.681 - Interim Guidelines On The Method Of Calculation Of The Energy Efficiency Design Index For New Ships*, London: International Maritime Organization.

International Maritime Organization, 2009b. *SOLAS, Consolidated Edition 2009* 5th ed., London: IMO Publishing.

International Maritime Organization, 2009c. *Guidelines For Ships Operating In Polar Waters*,

International Maritime Organization, 2010. *MEPC 60/WP.6 - Prevention of Air Pollution From Ships*,

International Maritime Organization, 2011. *Resolution MEPC.203(62) - Amendments to the annex of the protocol of 1997 to amend the international convention for the prevention of pollution from ships, 1973, as modified by the protocol of 1978 relating thereto (Inclusion of regulations on energy effi*, London.

International Maritime Organization, 2012. *Resolution MEPC.212(63) - 2012 Guidelines On The Method Of Calculation Of The Attained Energy Efficiency Design Index (EEDI) For New Ships*,

International Maritime Organization, 2013a. Sulphur oxides (SOx) – Regulation 14. *Air Pollution and GHG Emissions*, p.1. Available at: http://www.imo.org/ourwork/environment/pollutionprevention/airpollution/pages/sulphur-oxides-(sox)-–-regulation-14.aspx [Accessed April 24, 2013].

International Maritime Organization, 2013b. Nitrogen oxides (NOx) – Regulation 13. *Air Pollution and GHG Emissions*, p.1. Available at: http://www.imo.org/ourwork/environment/pollutionprevention/airpollution/pages/nitrogen-oxides-(nox)-–-regulation-13.aspx [Accessed April 24, 2013].

International Maritime Organization, 2014a. Special Areas Under MARPOL. *Pollution Prevention*, p.1. Available at: http://www.imo.org/OurWork/Environment/PollutionPrevention/SpecialAreasUnderMARPOL/Pages/Default.aspx [Accessed October 22, 2014].

International Maritime Organization, 2014b. Draft International Code of Safety for Ships using Gases or other Low flashpoint Fuels (IGF Code).

International Maritime Organization, 2014c. Shipping in polar waters. *Polar Code*, p.1. Available at: http://www.imo.org/MediaCentre/HotTopics/polar/Pages/default.aspx [Accessed February 3, 2015].

International Organization for Standardization, 2002. ISO 2719:2002 Determination of flash point -- Pensky-Martens closed cup method. , p.21.

Invernizzi, C.M., 2010. Stirling engines using working fluids with strong real gas effects. *Applied Thermal Engineering*, 30(13), pp.1703–1710.

Jensen, S.H., 2009. Marine Diesel Engines Improvements on the Efficiency Agenda. , pp.1–24.

Jones, P.D., Lister, D.H., Osborn, T.J., Harpham, C., Salmon, M. & Morice, C.P., 2012. Hemispheric and large-scale land-surface air temperature variations: An extensive revision and an update to 2010. *Journal of Geophysical Research*, 117(D5), p.D05127.

Jones, P.D., New, M., Parker, D.E., Martin, S. & Rigor, I.G., 1999. Surface air temperature and its changes over the past 150 years. *Reviews of Geophysics*, 37(2), p.173.

Jonsson, M. & Yan, J., 2000. Exergy and Pinch Analysis of Diesel Engine Bottoming Cycles

with Ammonia-Water Mixtures as Working Fluid. *International Journal of Thermodynamics*, 3(2), pp.57–71.

Jorgensen, R., 2011. Slow Steaming - The Full Story. , p.10.

Juliussen, L.R., Kryger, M.J. & Andreasen, A., 2011. MAN B&W ME-GI ENGINES. RECENT RESEARCH AND RESULTS. In *Proceedings of the International Symposium on Marine Engineering*. Keyworth, p. 6.

Kærn, M.R., Elmegaard, B. & Larsen, L.F.S., 2013. Comparison of fin-and-tube interlaced and face split evaporators with flow maldistribution and compensation. *International Journal of Refrigeration*, 36(1), pp.203–214.

Kalikatzarakis, M. & Frangopoulos, C.A., 2014. Multi-criteria selection and thermo-economic optimization of Organic Rankine Cycle system for a marine application. In R. Zevenhoven, ed. *International Conference on Efficiency, Cost, Optimization, Simulation and Environmental Impact of Energy Systems*. Turku: Abo Akademi University, p. 15.

Kalina, A.I., 1982. United States Patent 4346561. , p.15.

Kalina, A.I., 1983. Combined cycle and waste heat recovery power systems based on a novel thermodynamic energy cycle utilizing low-temperature heat for power generation. In *Joint power generation conference*. Indianapolis: ASME International, p. 5.

Kalina, A.I., 1984. Combined-Cycle System With Novel Bottoming Cycle. *Journal of Engineering for Gas Turbines and Power*, 106(4), p.6.

Kalina, A.I., 1989. The Kalina Power Cycles, A progress report. In *American Power Conference*. Haywood, p. 16.

Kalina, A.I. & Leibowitz, H.M., 1987. System Design and Experimental Development of the Kalina Cycle Technology. In *The Ninth Annual Industrial Energy Technology Conference*. Houston, p. 6.

Kane, M., Larrain, D., Favrat, D. & Allani, Y., 2003. Small hybrid solar power system. *Energy*, 28, pp.1427–1443.

Kaplan, U., 2007a. Organic Rankine Cycle Configurations. In *European Geothermal Congress 2007*. Unterhaching: Ormat, pp. 1–5.

Kaplan, U., 2007b. ADVANCED ORGANIC RANKINE CYCLES IN BINARY GEOTHERMAL POWER PLANTS. *Ormat Technologies Inc.*, p.8. Available at: http://www.ormat.com/research/papers/papers3.

Karellas, S., Leontaritis, A.-D., Panousis, G., Bellos, E. & Kakaras, E., 2013. Energetic and exergetic analysis of waste heat recovery systems in the cement industry. *Energy*, 58, pp.147–156.

Katsanos, C.O., Hountalas, D.T. & Pariotis, E.G., 2012. Thermodynamic analysis of a Rankine cycle applied on a diesel truck engine using steam and organic medium. *Energy Conversion and Management*, 60(null), pp.68–76.

Kazakov, A., McLinden, M.O. & Frenkel, M., 2012. Computational Design of New Refrigerant Fluids Based on Environmental, Safety, and Thermodynamic Characteristics. *Industrial & Engineering Chemistry Research*, 51(38), p.120917100332001.

Kennedy, J. & Eberhart, R., 1995. Particle swarm optimization. In *Proceedings of ICNN'95 - International Conference on Neural Networks*. Perth: IEEE, pp. 1942–1948.

Khalykov, K.R., 2014. Experimental Plant with Thermoelectric Generator. Program and Technique of Investigation. *Chemical and Petroleum Engineering*, 50(5-6), pp.294–300.

Klell, M., 2010. Storage of Hydrogen in the Pure Form. In M. Hirscher, ed. *Handbook of Hydrogen Storage: New Materials for Future Energy Storage*. Weinheim: Wiley -VCH, pp. 1–36.

Kockums AB, 2009. Kockums Stirling AIP System. , p.3. Available at: http://www.kockums.se/en/products-services/submarines/stirling-aip-system/ [Accessed March 1, 2013].

Kongtragool, B. & Wongwises, S., 2006. Thermodynamic analysis of a Stirling engine including

dead volumes of hot space, cold space and regenerator. *Renewable Energy*, 31(3), pp.345–359.

Kongtragool, B. & Wongwises, S., 2007. Performance of low-temperature differential Stirling engines. *Renewable Energy*, 32(4), pp.547–566.

Kontax Engineering Ltd., 2012. Kontax Stirling & Stove Fan Engines. , p.1. Available at: http://www.stirlingengine.co.uk/ [Accessed March 1, 2013].

Kontomaris, K., 2014. HFO-1336mzz-Z: High Temperature Chemical Stability and Use as A Working Fluid in Organic Rankine Cycles. In *International Refrigeration and Air Conditioning Conference*. Purdue: Purdue University, p. 10.

Kontoulis, P., Kazangas, D. & Kaiktsis, L., 2013. A new model for marine Heavy Fuel Oil thermophysical properties: validation in a constant volume spray chamber. In *25th European Conference on Liquid Atomization and Spray Systems*. Chania, p. 8.

Kosmas, O.T. & Vlachos, D.S., 2012. Simulated annealing for optimal ship routing. *Computers & Operations Research*, 39(3), pp.576–581.

Kristensen, H.O., 2012. *Energy Demand And Exhaust Gas Emissions of Marine Engines*, Copenhagen.

Kristiansen, N.R. & Nielsen, H.K., 2010. Potential for Usage of Thermoelectric Generators on Ships. *Journal of Electronic Materials*, 39(9), pp.1746–1749.

Kristiansen, N.R., Snyder, G.J., Nielsen, H.K. & Rosendahl, L., 2012. Waste Heat Recovery from a Marine Waste Incinerator Using a Thermoelectric Generator. *Journal of Electronic Materials*, 41(6), pp.1024–1029.

Kutscher, C., 2001. Small-Scale Geothermal Power Plant Field Verification Projects: Preprint. In *GRC 2001 Annual Meeting*. San Diego: National Renewable Energy Lab., p. 15.

Ladommatos, N., Adelhalim, S.M., Zhao, H. & Hu, Z., 1998. The effects of carbon dioxide in exhaust gas recirculation on diesel engine emissions. *Proceedings of the Institution of Mechanical Engineers, Part D: Journal of Automobile Engineering*, 212(1), pp.25–42.

Lai, L.L. & Chan, T.F., 2007. The Method of Hooke and Jeeves. In *Distributed Generation: Induction and Permanent Magnet Generators*. Chichester, UK: John Wiley & Sons, Ltd, pp. 227–228.

Larjola, J., 1995. Electricity from industrial waste heat using high-speed organic Rankine cycle (ORC). *International Journal of Production Economics*, 41, pp.227–235.

Larsen, U., Haglind, F. & Oskar, S., 2013. A comparison of advanced heat recovery power cycles in a combined cycle for large ships. In *The 26th International Conference on Efficiency, Cost, Optimization, Simulation and Environmental Impact of Energy Systems*. Guilin: Chinese Society of Engineering Thermophysics, p. 13.

Larsen, U., Nguyen, T.-V., Knudsen, T. & Haglind, F., 2014. System analysis and optimisation of a Kalina split-cycle for waste heat recovery on large marine diesel engines. *Energy*, 64, pp.484–494.

Larsen, U., Pierobon, L., Haglind, F. & Gabrielii, C., 2013. Design and optimisation of organic Rankine cycles for waste heat recovery in marine applications using the principles of natural selection. *Energy*, 55, pp.803–812.

Lecompte, S., Huisseune, H., van den Broek, M. & De Paepe, M., 2015. Methodical thermodynamic analysis and regression models of organic Rankine cycle architectures for waste heat recovery. *Energy*, 87, pp.60–76.

Lee, D. & Lee, H.K., 2013. Optimization of Organic Rankine Cycle to Recover Waste Heat of Marine Diesel Engine. In *ASME ORC 2013*. Rotterdam, p. 1.

Lee, S.-K., 2008. Combining ice class rules with direct calculations for design of artic LNG vessel propulsion. In *The 23rd International Conference & Exhibition for the LNG, LPG and Natural Gas Industries*. Bangkok, p. 23.

Leibowitz, H.M. & Micak, H.A., 1999. Design of a 2MW Kalina cycle binary module for installation in Husavik, Iceland. *Geothermal Resources Council Transactions*, 23, p.6.

Leibowitz, H.M. & Mirolli, M.D., 1997. First Kalina combined-cycle. *Power Engineering*, p.1.

Lemmon, E.W., Huber, M.L. & McLinden, M.O., 2010. NIST Reference Fluid Thermodynamic and Transport Properties Database.

Levander, O., 2009. The Efficient Container Feeder. *Wärtsilä Technical Journal In Detail*, (1), pp.38–41.

Li, Q., Flamant, G., Yuan, X., Neveu, P. & Luo, L., 2011. Compact heat exchangers: A review and future applications for a new generation of high temperature solar receivers. *Renewable and Sustainable Energy Reviews*, 15(9), pp.4855–4875.

Li, S. & Dai, Y., 2014. Thermo-economic comparison of Kalina and CO2 transcritical power cycle for low temperature geothermal sources in China. *Applied Thermal Engineering*, 70(1), pp.139–152.

Lian, Z.T., Chua, K.J. & Chou, S.K., 2010. A thermoeconomic analysis of biomass energy for trigeneration. *Applied Energy*, 87(1), pp.84–95.

Little, A.B. & Garimella, S., 2011. Comparative assessment of alternative cycles for waste heat recovery and upgrade. *Energy*, 36(7), pp.4492–4504.

Liu, B.-T., Chien, K.-H. & Wang, C.-C., 2004. Effect of working fluids on organic Rankine cycle for waste heat recovery. *Energy*, 29(8), pp.1207–1217.

Liu, J.P., Fu, J.Q., Ren, C.Q., Wang, L.J., Xu, Z.X. & Deng, B.L., 2013. Comparison and analysis of engine exhaust gas energy recovery potential through various bottom cycles. *Applied Thermal Engineering*, 50(1), pp.1219–1234.

Liu, W., Jie, Q., Kim, H.S. & Ren, Z., 2015. Current progress and future challenges in thermoelectric power generation: From materials to devices. *Acta Materialia*, 87, pp.357–376.

Livanos, G.A., Theotokatos, G. & Pagonis, D.-N., 2014. Techno-economic investigation of alternative propulsion plants for Ferries and RoRo ships. *Energy Conversion and Management*, 79, pp.640–651.

Lloyd's Register, 2012a. Implementing the Energy Efficiency Design Index (EEDI). , p.22.

Lloyd's Register, 2012b. Understanding exhaust gas treatment systems. , p.55.

Lloyd's Register, 2012c. Provisional Rules for the Winterisation of Ships 2012. , p.104.

Lloyd's Register, 2012d. Rules and Regulations for the Classification of Ships.

LNG World Shipping, 2013. What's new in small-scale LNG. *LNG World Shipping Journal*, 12(5), pp.74–81.

Lockley, P. & Jarabo-Martin, A., 2011. *Ship Efficiency: The Guide* 1st ed. K. Sharma & J. Hill, eds., Windsor: Fathom.

Loctite UK limited, 1998. Technical Data Sheet Product 7031. , p.2.

Lolos, P. a. & Rogdakis, E.D., 2009. A Kalina power cycle driven by renewable energy sources. *Energy*, 34(4), pp.457–464.

Madhawa Hettiarachchi, H.D., Golubovic, M., Worek, W.M. & Ikegami, Y., 2007. The Performance of the Kalina Cycle System 11(KCS-11) With Low-Temperature Heat Sources. *Journal of Energy Resources Technology*, 129(3), p.243.

Mago, P.J., Chamra, L.M. & Somayaji, C., 2007. Performance analysis of different working fluids for use in organic Rankine cycles. *Proceedings of the Institution of Mechanical Engineers, Part A: Journal of Power and Energy*, 221(3), pp.255–263.

Mago, P.J., Chamra, L.M., Srinivasan, K. & Somayaji, C., 2008. An examination of regenerative organic Rankine cycles using dry fluids. *Applied Thermal Engineering*, 28(8-9), pp.998–1007.

Mago, P.J. & Srinivasan, K.K., 2010. Exhaust Waste Heat Recovery From Stationary Engines Using Organic Rankine Cycles. *Knovel*, p.1. Available at: http://www.knovelblogs.com/2010/03/02/ec-exhaust-waste-heat-recovery-from-stationary-

engines-using-organic-rankine-cycles/ [Accessed October 4, 2012].

Maizza, V. & Maizza, A., 1996. Working fluids in non-steady flows for waste energy recovery systems. *Applied Thermal Engineering*, 16(7), pp.579–590.

Majeski, J., 2002. *Stirling Engine Assessment*, Palo Alto.

MAN Diesel & Turbo, 2005. Thermo Efficiency System for Reduction of Fuel Consumption and CO2 Emission. , p.16.

MAN Diesel & Turbo, 2009a. Electronically Controlled Two-stroke Engines. , p.353.

MAN Diesel & Turbo, 2009b. *Soot Deposits and Fires in Exhaust gas Boilers*, Copenhagen.

MAN Diesel & Turbo, 2011. Basic Principles of Ship Propulsion. , p.45.

MAN Diesel & Turbo, 2012a. Tier III Two-Stroke Technology. , p.36.

MAN Diesel & Turbo, 2012b. *Waste Heat Recovery System (WHRS) for Reduction of Fuel Consumption, Emission and EEDI*, Copenhagen.

MAN Diesel & Turbo, 2013a. Ice Classed Ships Main Engines. , p.26.

MAN Diesel & Turbo, 2013b. Engine room and performance data for 14K98ME7.1-TII with 4 x MAN TCA88-21 and part load exhaust gas bypass (EGB) tuning. , p.10.

MAN Diesel & Turbo, 2014a. Engine room and performance data for 12G95ME-C9.5-TII with part load engine control tuning (ECT) tuning. , p.9.

MAN Diesel & Turbo, 2014b. Influence of Ambient Temperature Conditions. , p.17.

MAN Diesel & Turbo, 2015a. Engine room and performance data for 8S90ME-C9.5-TII with low load tuning. , p.10.

MAN Diesel & Turbo, 2015b. Engine room and performance data for 8S90ME-C9.5-TII with high load tuning. , p.10.

MAN Diesel & Turbo, 2015c. Waste Heat Recovery by ORC (Organic Rankine Cycle). *PrimeServ Green*, p.1. Available at: http://primeserv.man.eu/primeserv-green/waste-heat-recovery-by-orc-(organic-rankine-cycle) [Accessed November 9, 2015].

MAN Diesel & Turbo, 2015d. CEAS Engine Calculations. *Marine Engines and Systems*, p.1. Available at: http://marine.man.eu/two-stroke/ceas [Accessed July 15, 2015].

MAN Diesel & Turbo, 2015e. Engine room and performance data for 5S65ME-C8.5. , pp.1–9.

MAN PrimeServ, 2012. *Slow Steaming Practices in the Global Shipping Industry*, Copenhagen.

Mancini, T., Heller, P., Butler, B., Osborn, B., Schiel, W., Goldberg, V., Buck, R., Diver, R., Andraka, C. & Moreno, J., 2003. Dish-Stirling Systems: An Overview of Development and Status. *Journal of Solar Energy Engineering*, 125(2), p.135.

Marechal, F.M.A., 2010. Pinch Analysis. In *Exergy, Energy System Analysis and Optimization, Vol.1*. pp. 166–175.

Marine Engineers Review, 2014. Calentix converts heat to power. *Marine Engineers Review*, p.10.

MarineTraffic.com, 2014. Live Ships Map - AIS - Vessel Traffic and Positions - AIS Marine Traffic. *Live Map*. Available at: https://www.marinetraffic.com/ [Accessed November 26, 2014].

Maritime Knowledge Centre, 2009. International Shipping and World Trade Facts and figures. , p.41.

Maritime Knowledge Centre, 2012. International Shipping Facts and Figures – Information Resources on Trade, Safety, Security, Environment. , p.47.

Martelli, E., Kreutz, T.G., Gatti, M., Chiesa, P. & Consonni, S., 2013. Numerical optimization of steam cycles and steam generators designs for coal to FT plants. *Chemical Engineering Research and Design*, 91(8), pp.1467–1482.

Martin, W.R., 1978. *Stirling engine design manual*, Washington.

McGeorge, H.D., 2002. *Marine auxiliary machinery* 7th ed., Oxford: Butterworth-Heinemann.

Megaloid laboratories limited, 2006. Material Safety Data - Isopentane. , p.4.

Meggitt PLC, 2015. Compact diffusion-bonded heat exchangers. , p.20.

Meijer, M.J., 1970. Prospect of the Stirling Engine for Vehicular Propulsion. *Philips Technical Review*, 31(5), pp.168–185.

Meijer, R.J., 1961. *The Philips stirling thermal engine: analysis of the Rhombic drive mechanism and efficiency measurements*, Eindhoven.

Mezura-Montes, E., Reyes-Sierra, M. & Coello Coello, C.A., 2008. Advances in Differential Evolution. In U. K. Chakraborty, ed. *Advances in Differential Evolution*. Studies in Computational Intelligence. Berlin: Springer Berlin Heidelberg, pp. 173–196.

Mikloski, D., The World's most advanced Green Power Machine. , (8), p.5.

Milles, U., 2001. *Geothermal electricity generation combined with a heating network*, Bonn.

Mirolli, M.D., 2006. The Kalina Cycle for Cement Kiln Waste Heat Recovery Power Plants. *Industry Applications Magazine*, 12(4), pp.60–64.

Mirolli, M.D., 2012. Kalina Cycle power systems in waste heat recovery applications. *Global Cement*, p.1. Available at: http://www.globalcement.com/magazine/articles/721-kalina-cycle-power-systems-in-waste-heat-recovery-applications [Accessed January 17, 2013].

Mlcak, H., Mirolli, M., Hjartarson, H. & Ralph, M., 2002. *Notes from the North: a Report on the Debut Year of the 2 MW Kalina Cycle Geothermal Power Plant in Husavik, Iceland*, Húsavík.

Mlcak, H.A., 2004. An Introduction to the Kalina Cycle. In G. E. Kielasa, L.; Weed, ed. *The International Joint Power Generation Conference*. New York: ASME International, pp. 1–11.

Modi, A. & Haglind, F., 2015. Thermodynamic optimisation and analysis of four Kalina cycle layouts for high temperature applications. *Applied Thermal Engineering*, 76, pp.196–205.

Molés, F., Navarro-Esbrí, J., Peris, B., Mota-Babiloni, A., Barragán-Cervera, Á. & Kontomaris, K. (Kostas), 2014. Low GWP alternatives to HFC-245fa in Organic Rankine Cycles for low temperature heat recovery: HCFO-1233zd-E and HFO-1336mzz-Z. *Applied Thermal Engineering*, 71(1), pp.204–212.

Molland, A., 2008. *The maritime engineering reference book: a guide to ship design, construction and operation* 1st ed. A. F. Molland, ed., Oxford: Butterworth-Heinemann.

Molland, A.F., Turnock, S.R. & Hudson, D.A., 2011. *Ship Resistance and Propulsion* 1st ed., New -York: Cambridge University Press.

Mønster, J., Samuelsson, J., Kjeldsen, P. & Scheutz, C., 2015. Quantification of methane emissions from 15 Danish landfills using the mobile tracer dispersion method. *Waste management (New York, N.Y.)*, 35, pp.177–86.

Moore, J., Grimes, R., Walsh, E. & O'Donovan, A., 2014. Modelling the thermodynamic performance of a concentrated solar power plant with a novel modular air-cooled condenser. *Energy*, 69, pp.378–391.

Morice, C.P., Kennedy, J.J., Rayner, N.A. & Jones, P.D., 2012. Quantifying uncertainties in global and regional temperature change using an ensemble of observational estimates: The HadCRUT4 data set. *Journal of Geophysical Research*, 117(D8), p.D08101.

Morvay, Z. & Gvozdenac, D., 2008. Industrial Electric Power Systems. In *Applied Industrial Energy and Environmental Management*. Chichester: John Wiley & Son Limited, pp. 285–321.

Mounir, I.B.; & Kovach, R.M., 1993. A Kalina Cycle Application for Power Generation. *Energy*, 1(9), pp.961–969.

Müller-Steinhagen, H. & Heck, K., 1986. A simple friction pressure drop correlation for two-phase flow in pipes. *Chemical Engineering and Processing: Process Intensification*, 20(6), pp.297–308.

Myhre, G., Shindell, D., Bréon, F.-M., Collins, W., Fuglestvedt, J., Huang, J., Koch, D., Lamarque, J.-F., Lee, D., Mendoza, B., Nakajima, T., Robock, A., Stephens, G., Takemura, T. & Zhan, H., 2013. 2013: Anthropogenic and Natural Radiative Forcing. In T. F. . Stocker et al., eds. *Climate Change 2013: The Physical Science Basis. Contribution of Working Group I to the Fifth Assessment Report of the Intergovernmental Panel on Climate Change*. Cambridge and New York: Cambridge University Press, pp. 659–740.

Nag, P.G., 2010. *Basic and Applied Thermodynamics* 2nd ed., New Delhi: Tata McGraw-Hill.

Nag, P.K. & Gupta, A.V.S.S.K.S., 1998. Exergy analysis of the Kalina cycle. *Applied Thermal Engineering*, 18(6), pp.427–439.

Nakicenovic, N. & Swart, R., 2000. *Emission Scenarios*, Cambridge.

National Centers for Environmental Information, 2015. Global Surface Temperature Anomalies. *Background Information - FAQ*, p.1. Available at: https://www.ncdc.noaa.gov/monitoring-references/faq/anomalies.php [Accessed July 1, 2015].

National Ice Center, 2009. National Ice Center Arctic Sea Ice Charts and Climatologies in Gridded Format - Weekly Chart Products.

National Institute of Standards and Technology & SEMATECH, 2012. Product and Process Comparisons. In *NIST/SEMATECH e-Handbook of Statistical Methods*. Gaithersburg: U.S. Department of Commerce, p. 144.

National Paint and Coatings Association, 2002. *HMIS " Chemical Ratings Guide Hazardous Materials Identification System* 3rd ed., Neenah: J. J. Keller & Associates, Inc.

National Refrigerants, 2008. Material Safety Data Sheet R-12. , p.7.

National Snow And Ice Data Center, 2013. Sea Ice Index. , p.1. Available at: http://nsidc.org/data/seaice_index/ [Accessed December 12, 2013].

Nguyen, T.-V., Knudsen, T., Larsen, U. & Haglind, F., 2014. Thermodynamic evaluation of the Kalina split-cycle concepts for waste heat recovery applications. *Energy*, 71, pp.277–288.

Nielsen, C.K. & Schack, C., 2012. Vessel Emission Study: Comparison Of Various Abatement Technologies To Meet Emission Levels For Eca's. In *9th annual Green Ship Technology Conference*. Copenhagen: Green Ships of the Future, p. 13.

Nielsen, R.F., Haglind, F. & Larsen, U., 2014. Design and modeling of an advanced marine machinery system including waste heat recovery and removal of sulphur oxides. *Energy Conversion and Management*, pp.687–693.

Nippon Kaiji Kyokai, 2014. Aframax Rio. , p.1.

O´Brien, W.J., 1988. ECONOMICS OF ORGANIC RANKINE CYCLE. In *Industrial Energy Technology Conference*. Toms River: Texas A&M University, pp. 259–263.

Obernberger, I., Bini, R., Neuner, H. & Preveden, Z., 2001. *Biomass Fired CHP Plant Based on an ORC Cycle - Proyect ORC-STIA-Admont*, Admont.

Obieglo, A., Ringler, J., Seifert, M. & Hall, W., 2009. Future Efficient Dynamics with Heat Recovery. , p.30.

Ogriseck, S., 2009. Integration of Kalina cycle in a combined heat and power plant, a case study. *Applied Thermal Engineering*, 29(14-15), p.6.

Öhman, H. & Lundqvist, P., 2013. Comparison and analysis of performance using Low Temperature Power Cycles. *Applied Thermal Engineering*, 52(1), pp.160–169.

Opcon Energy Systems AB, 2012a. Commissioning and testing of first reference installation of Opcon technology for ships. , p.2.

Opcon Energy Systems AB, 2012b. Data Sheet OPB-ORC-750M. , p.11.

Osler, C., 2011. *DIESEL & THERMAL ELECTRICITY GENERATION OPTIONS*, Winnipeg.

Palm, B., 2002. Evaporators. In *Refrigerating Engineering*. Stockholm: Royal Institute of Technology, pp. 8:1 – 8:64.

Pan, X., 2011. *Encyclopedia of Environmental Health*, Elsevier.

Parsons, C.A., 1925. The steam turbine—As a study in applied physics. *Journal of the Franklin Institute*, 199(1), pp.1–12.

Pelc, R. & Fujita, R.M., 2002. Renewable energy from the ocean. *Marine Policy*, 26(6), pp.471–479.

Peng, D.-Y. & Robinson, D.B., 1976. A New Two-Constant Equation of State. *Industrial & Engineering Chemistry Fundamentals*, 15(1), pp.59–64.

Peng, S., Wang, Z., Hong, H., Xu, D. & Jin, H., 2014. Exergy evaluation of a typical 330MW solar-hybrid coal-fired power plant in China. *Energy Conversion and Management*, 85, pp.848–855.

Pierobon, L., Benato, A., Scolari, E., Haglind, F. & Stoppato, A., 2014. Waste heat recovery technologies for offshore platforms. *Applied Energy*, 136, pp.228–241.

Pierobon, L. & Haglind, F., 2014. Design and optimization of air bottoming cycles for waste heat recovery in off-shore platforms. *Applied Energy*, 118, pp.156–165.

Pierobon, L., Larsen, U., Haglind, F., Elmegaard, B. & Nguyen, T.-V., 2013. Multi-objective optimization of organic Rankine cycles for waste heat recovery: Application in an offshore platform. *Energy*, 58, pp.538–549.

Pierobon, L., Rokni, M., Larsen, U. & Haglind, F., 2013. Thermodynamic analysis of an integrated gasification solid oxide fuel cell plant combined with an organic Rankine cycle. *Renewable Energy*, 60, pp.226–234.

Pla Perujo, M., 2004. *Condensation of Water Vapor and Acid Mixtures from Exhaust Gases*. Technischen Universität Berlin.

Podesser, E., 1999. Electricity production in rural villages with a biomass Stirling engine. *Renewable Energy*, 16(1-4), pp.1049–1052.

de Podesta, M., 2013. Ultimate chill: the epic race to reach absolute zero. *New Scientist*, 218(2922), pp.42–45.

Popov, D., 2004. Application of a Gas Turbine with Air Bottoming Cycle in Natural Gas Air Bottoming Cycle in Natural Gas Compressor Stations Compressor Station. In *2nd International Gas Turbine Technology Conference*. Bled: CAME-GT, p. 15.

Pospiech, P., 2014. Is Internal Combustion Engine Methane Slip Harmful to the Environment? *Maritime Reporter & Engineering News*, pp.32–36.

Poullikkas, A., 2005. An overview of current and future sustainable gas turbine technologies. *Renewable and Sustainable Energy Reviews*, 9(5), pp.409–443.

Puech, P. & Tishkova, V., 2011. Thermodynamic analysis of a Stirling engine including regenerator dead volume. *Renewable Energy*, 36(2), pp.872–878.

Quoilin, S., 2008. *An introduction to thermodynamics applied to Organic Rankine Cycles*, Liege.

Quoilin, S., Broek, M. Van Den, Declaye, S., Dewallef, P. & Lemort, V., 2013. Techno-economic survey of Organic Rankine Cycle (ORC) systems. *Renewable and Sustainable Energy Reviews*, 22(null), pp.168–186.

Rankine, W.J.M., 1881. *Miscellaneous Scientific Papers* 1st ed. W. J. Millar, ed., London: Charles Griffin And Company.

Rayner, N.A., 2003. Global analyses of sea surface temperature, sea ice, and night marine air temperature since the late nineteenth century. *Journal of Geophysical Research*, 108(D14), pp.2156 – 2202.

Rayner, N.A., Brohan, P., Parker, D.E., Folland, C.K., Kennedy, J.J., Vanicek, M., Ansell, T.J. & Tett, S.F.B., 2006. Improved analyses of changes and uncertainties in sea surface temperature measured in situ since the mid-nineteenth century: the HadSST2 data set. *Journal of Climate*, 19(3), pp.446–469.

Reid, R., Prausnitz, J. & Poling, B., 2001. *The properties of gases and liquids* 5th ed., London: McGraw-Hill.

Riffat, S.. & Ma, X., 2003. Thermoelectrics: a review of present and potential applications.

Applied Thermal Engineering, 23(8), pp.913–935.

Roberge, D., 2014. *Suitability of Highly Flammable Fluids in ORC On Board Ships.* University College London.

Robinson, K.K. & Briggs, D.E., 1966. Pressure drop of air flowing across triangular pitch banks of finned tubes. *Chemical Engineering Progress Symposium Series*, 62(64), pp.177–184.

Rodrigue, J.-P., 2013. The Geography of Transport Systems. , p.1. Available at: http://people.hofstra.edu/geotrans/eng/ch1en/conc1en/polarroutes.html [Accessed December 12, 2013].

Rodriguez Garcia, J.F., 2010. *Diseño De Un Ciclo Amoniaco-Agua En La Estación (Spanish)*. Escuela Tecnica Superiror de Ingenieros de Minas.

Rovira, A., Sánchez, C., Muñoz, M., Valdés, M. & Durán, M.D., 2011. Thermoeconomic optimisation of heat recovery steam generators of combined cycle gas turbine power plants considering off-design operation. *Energy Conversion and Management*, 52(4), pp.1840–1849.

Royal Academy of Engineering, 2013. *Future Ship Powering Options: Exploring alternative methods of ship propulsion* 1st ed. R. Hill et al., eds., London: Royal Academy of Engineering.

Rui, X., Pan, J. & Wang, Y., 2013. An equation of state for the thermodynamic properties of 1,1,1,2,3,3-hexafluoropropane (R236ea). *Fluid Phase Equilibria*, 341, pp.78–85.

Rusch, G., Bingham, P., Farrar, D., Jepson, G., Libre, J.-M., Malinverno, G., Millischer, R., Sarrif, A., Schmit, B. & Vrijhof, H., 2004. *JACC 044 : 1,1,1,3,3-pentafluoropropane (HFC-245fa) (CAS No. 460-73-1)*, Brussels.

Saaty, R.W., 1987. The analytic hierarchy process—what it is and how it is used. *Mathematical Modelling*, 9(3-5), pp.161–176.

Saaty, T.L., 2008. Decision making with the analytic hierarchy process - International Journal of Services Sciences - Volume 1, Number 1/2008 - Inderscience Publishers. *International Journal of Services Sciences*, 1(1), pp.83–98.

Saavedra, I., Bruno, J.C. & Coronas, A., 2010. Thermodynamic optimization of organic Rankine cycles at several condensing temperatures: case study of waste heat recovery in a natural gas compressor station. *Proceedings of the Institution of Mechanical Engineers, Part A: Journal of Power and Energy*, 224(7), pp.917–930.

Sakalis, G. & Frangopoulos, C.A., 2014. Towards synthesis and design optimization of steam bottoming Rankine cycles with different ship propulsion engines. In R. Zevenhoven, ed. *International Conference on Efficiency, Cost, Optimization, Simulation and Environmental Impact of Energy Systems*. Turku: Abo Akademi University, p. 14.

Sala, F. & Invernizzi, C.M., 2014. Low temperature Stirling engines pressurised with real gas effects. *Energy*, 75, pp.225–236.

Salimpour, M.R. & Bahrami, Z., 2010. Thermodynamic analysis and optimization of air-cooled heat exchangers. *Heat and Mass Transfer*, 47(1), pp.35–44.

Sarbu, I., 2014. A review on substitution strategy of non-ecological refrigerants from vapour compression-based refrigeration, air-conditioning and heat pump systems. *International Journal of Refrigeration*, 46, pp.123–141.

Sarchem Laboratories Inc., 2010. Material Safety Data Sheet: Hexamethyldisiloxane. , p.7.

Sasaki, N., Laapio, J., Fagerstrom, B., Juurmaa, K. & Wilman, G., 2002. Economical and environmental evaluation of double acting tanker. In *17th International Symposium on Okhotsk Sea & Sea Ice*. Monbetsu: : Okhotsk Sea & Cold Ocean Research Association, p. 16.

Schmid, H., 2004. Waste Heat Recovery (WHR): Fuel Savings With Less Emissions. In *Green Ship Technology Conference*. London, p. 10.

Schmidt, T.E., 1949. Heat transfer calculations for extended surfaces. *Refrigerating Engineering*, 4, pp.351–357.

SCI-Pak, 2010. *Waste Heat Recovery Boiler (WHRB) at Nimra Textile Ltd.*, Bremerhaven.

Shah, M.M., 1979. A general correlation for heat transfer during film condensation inside pipes. *International Journal of Heat and Mass Transfer*, 22(4), pp.547–556.

Shah, R.K., 1983. Compact Heat Exchanger Surface Selection, Optimisation and Computer-aided Design. In S. Kakaç, ed. *Low Reynolds Number Flow Heat Exchanger*. Washington DC: Hemisphere, pp. 983–998.

Shah, R.K. & Sekulic, D.P., 2003. *Fundamentals Of Heat Exchanger Design* 1st ed., New Jersey: John Wiley & Sons, Inc.

Shang, R., Zhang, Y., Shi, W., Wang, X. & Zhang, Y., 2014. Fresh Look and Understanding on Carnot Cycle. *Energy Procedia*, 61, pp.2898–2901.

Sharqawy, M.H., Lienhard V, J.H. & Zubair, S.M., 2010. Thermophysical properties of seawater: A review of existing correlations and data. *Desalination and Water Treatment*, 16, pp.354–380.

Shu, G., Liang, Y., Wei, H., Tian, H., Zhao, J. & Liu, L., 2013. A review of waste heat recovery on two-stroke IC engine aboard ships. *Renewable and Sustainable Energy Reviews*, 19, pp.385–401.

Siemens AG, 2013. Siemens - SST-200. *Steam Turbine*, p.1. Available at: http://www.energy.siemens.com/hq/en/fossil-power-generation/steam-turbines/sst-200.htm#content=Package [Accessed March 9, 2013].

Sinnott, R.K., 2005. Heat-transfer Equipment. In *Coulson and Richardson's Chemical Engineering Volume 6 - Chemical Engineering Design*. Oxford: Elsevier, pp. 634–793.

Smil, V., 2010. *Prime Movers of Globalization: The History and Impact of Diesel Engines and Gas Turbines* 1st ed., Cambridge: The MIT Press.

Smith, K. & Thornton, M., 2009. Feasibility of Thermoelectrics for Waste Heat Recovery in Conventional Vehicles Feasibility of Thermoelectrics for Waste Heat Recovery in Conventional Vehicles. In *23rd International Electric Vehicle Symposium*. Anaheim, p. 11.

Smith, L.C. & Stephenson, S.R., 2013. New Trans-Arctic shipping routes navigable by midcentury. *Proceedings of the National Academy of Sciences of the United States of America*, 110(13), pp.E1191–5.

Smith, T.W.., Traut, M., Bows-Larkin, A., K., A., McGlade, C. & Wrobel, P., 2015. *CO2 Targets, Trajectories and Trends for International Shipping*, Manchester.

Smith, T.W.P., Jalkanen, J.P., Anderson, B.A., Corbett, J.J., Faber, J., Hanayama, S.., O'Keeffe, E.., Parker, S.., Johansson, L.., Aldous, L.., Raucci, C.., Traut, M.., Ettinger, S.., Nelissen, D.., Lee, D.S.., Ng, S.., Agrawal, A.., Winebrake, J., J.; Hoen, M.., Chesworth, S.. & Pandey, A., 2014. *Third IMO GHG Study 2014*, London.

Soffiato, M., Frangopoulos, C.A., Manente, G., Rech, S. & Lazzaretto, A., 2015. Design optimization of ORC systems for waste heat recovery on board a LNG carrier. *Energy Conversion and Management*, 92, pp.523–534.

Solutia Inc., 1999. Therminol VP-1: Vapor Phase/Liquid Phase Heat Transfer Fluid. , p.11.

Song, J., Song, Y. & Gu, C., 2015. Thermodynamic analysis and performance optimization of an Organic Rankine Cycle (ORC) waste heat recovery system for marine diesel engines. *Energy*, 82, pp.976–985.

Spear, B., 2008. James Watt: The steam engine and the commercialization of patents. *World Patent Information*, 30(1), pp.53–58.

Sprouse, C. & Depcik, C., 2013. Review of organic Rankine cycles for internal combustion engine exhaust waste heat recovery. *Applied Thermal Engineering*, 51(1-2), pp.711–722.

Stirling Energy Systems Inc., 2015. Power To Perform. , p.1. Available at: http://graphique-us.com/clients/ses/manufacturing.htm [Accessed February 18, 2015].

Stix, G., 2006. A Climate Repair Manual. *Scientific American*, pp.46–49.

Stone, R., 1982. Setting a minimum flash point for shipboard fuels.

Stoppato, A., Mirandola, A., Meneghetti, G. & Lo Casto, E., 2012. On the operation strategy of steam power plants working at variable load: Technical and economic issues. *Energy*, 37(1), pp.228–236.

Strategic Center for Natural Gas, 2004. Natural Gas Facts: Liquefied Natural Gas (LNG). , p.4.

Stroke, E.A., 2003. *Reeds Vol 4: Naval Architecture for Marine Engineers* 4th ed., London: Thomas Reed Publications.

Student, 1908. The Probable Error of a Mean. *Biometrika*, 6(1), pp.1–25.

Suárez de la Fuente, S. & Greig, A., 2013. Making shipping greener: ORC modelling under realistic operative conditions. In *Low Carbon Shipping Conference*. London, p. 18.

Suárez de la Fuente, S. & Greig, A., 2015. Making shipping greener: comparative study between organic fluids and water for Rankine cycle waste heat recovery. *Journal of Marine Engineering & Technology*, 14(2), pp.70–84.

Suárez de la Fuente, S., Roberge, D. & Greig, A.R., 2016. Safety and CO2 emissions: Implications of using organic fluids in a ship's waste heat recovery system. *Marine Policy*, p.21.

Sugden, B. & Drury, T., 2012. Investigation into the viability of replacing internal combustion diesel generators with diesel fired stirling engine generators for remote microwave radio telecommunication applications. In *Intelec 2012*. Scottsdale: IEEE, pp. 1–8.

Sunpower Inc., 2011. Benefits of Sunpower Technology. , p.1. Available at: http://www.sunpower.com/services/technology/benefits.php [Accessed February 28, 2013].

Syamsuddin, M.L., Attamimi, A., Nugraha, A.P., Gibran, S., Afifah, A.Q. & Oriana, N., 2015. OTEC Potential in the Indonesian Seas. *Energy Procedia*, 65, pp.215–222.

Syracuse New York Evening Chronicle, 1853. The Caloric Ship Ericsson. *Syracuse New York Evening Chronicle*, p.1.

Taggart, S., 2008. CSP: dish projects inch forward. *Renewable Energy Focus*, 9(4), pp.52–54.

Tailor, P.R. & Narayankhedkar, K.G., 1988. Thermodynamic analysis of the Stirling cycle. *Cryogenics*, 28(1), pp.36–45.

Tarjanne, R. & Kivistö, A., 2008. *Comparison Of Electricity Generation Costs*, Lappeenranta.

Tartière, T., 2016. Analysis of the Organic Rankine Cycle market. *ORC Market : A World Overview*, p.1. Available at: http://orc-world-map.org/analysis.html [Accessed March 25, 2016].

Taylor, D.A., 1996. *Introduction to marine engineering* 2nd ed., Oxford: Elservier Butterworth-Heinemann.

Tchanche, B.F., Lambrinos, G., Frangoudakis, A. & Papadakis, G., 2011. Low-grade heat conversion into power using organic Rankine cycles – A review of various applications. *Renewable and Sustainable Energy Reviews*, 15(8), pp.3963–3979.

Tchanche, B.F., Papadakis, G., Lambrinos, G. & Frangoudakis, A., 2009. Fluid selection for a low-temperature solar organic Rankine cycle. *Applied Thermal Engineering*, 29(11-12), pp.2468–2476.

Tchanche, B.F., Pétrissans, M. & G. Papadakis, 2014. Heat resources and organic Rankine cycle machines. *Renewable and Sustainable Energy Reviews*, 39, pp.1185–1199.

TECTEG MFR, 2015. Standard TEG Generator Products For Sale. *TEG Thermoelectric Power Generators For Sale*. Available at: http://thermoelectric-generator.com/ [Accessed June 8, 2015].

Terasaki, I., 2011. Thermal Conductivity and Thermoelectric Power of Semiconductors. In P. Bhattacharya, R. Fornari, & H. Kamimura, eds. *Comprehensive Semiconductor Science and Technology*. Amsterdam: Elsevier, pp. 326–358.

The American Society of Mechanical Engineers, 2014. B31.3 - 2014 - Process Piping. , p.536.

The Baltic and International Maritime Council, 2013. Updated BIMCO EEDI Calculator. *Products*. Available at: https://www.bimco.org/en/Products/EEDI.aspx [Accessed October 15, 2014].

The Maritime Executive LLC., 2011. Maersk and the U.S. Navy Collaborate on Biofuel Initiative. *The Maritime Executive*, p.1. Available at: http://www.maritime-executive.com/article/maersk-and-the-u-s-navy-collaborate-on-biofuel-initiative [Accessed November 15, 2015].

The MathWorks Inc., 2015a. Find minimum of single-variable function on fixed interval - MATLAB fminbnd - MathWorks United Kingdom. *Optimization*, p.1. Available at: http://uk.mathworks.com/help/matlab/ref/fminbnd.html?refresh=true [Accessed April 27, 2015].

The MathWorks Inc., 2015b. Pattern Search Terminology. *What Is Direct Search?*, p.1. Available at: http://uk.mathworks.com/help/gads/pattern-search-terminology.html#f7816 [Accessed October 27, 2015].

Theotokatos, G. & Livanos, G., 2012. Techno-economical analysis of single pressure exhaust gas waste heat recovery systems in marine propulsion plants. *Proceedings of the Institution of Mechanical Engineers Part M: Journal of Engineering for the Maritime Environment*, 227(2), pp.83–97.

Thermal & Pressure Engineering, 2013. TPE Fire Tube - Boilers. , p.2.

Thompson, A.T.B.N., 2008. *Guide for the Use of the International System of Units (SI)*, Gaithersburg.

Tien, W.-K., Yeh, R.-H. & Hong, J.-M., 2007. Theoretical analysis of cogeneration system for ships. *Energy Conversion and Management*, 48(7), pp.1965–1974.

Towler, G. & Sinnott, R., 2013. *Chemical Engineering Design* 2nd ed., Oxford: Elsevier.

Tubular Heat Exchangers Manufacturers Association, 1999. Standards of the Tubular Exchangers Manufacturers Association. *Main*, p.294.

U.S. Energy Information Administration, 2010. *Updated Capital Cost Estimates for Electricity Generation Plants*, Washington DC.

Uehara, H., Ikegami, Y. & Nishida, T., 1998. Performance Analysis of OTEC System Using a Cycle with Absorption and Extraction Processes. *Transactions of the Japan Society of Mechanical Engineers Series B*, 64(624), pp.2750–2755.

Uehara, H., Ikegami, Y., Nishida, T., Kikuchi, S. & Tsuboi, K., 1997. OTEC system using Uehara cycle. In *Proceedings of International OTEC/DOWA Association Conference*. Singapore, pp. 29–38.

Ulloa, C., Eguía, P., Miguez, J.L., Porteiro, J., Pousada-Carballo, J.M. & Cacabelos, A., 2013. Feasibility of using a Stirling engine-based micro-CHP to provide heat and electricity to a recreational sailing boat in different European ports. *Applied Thermal Engineering*, 59(1-2), pp.414–424.

UNEP/GRID-Arendal, 2005. *Climate Change Graphics*, Arendal.

United Nations Conference on Trade and Development, 2013. *Review of Maritime Transport 2012* 1st ed., Geneva: United Nations Publications.

United Nations Conference on Trade and Development, 2014. *Review of Maritime Transport 2013* 1st ed., Geneva: United Nations Publications.

United Nations Conference on Trade and Development, 2015. *Review of Maritime Transport 2014* 1st ed., Geneva: United Nations Publications.

Urieli, I. & Berchowitz, D.M., 1984. *Stirling Cycle Engine Analysis* 1st ed., Bristol: Adam Hilger Ltd.

US Department, NOAA of Commerce, Satellite Data and Information, National EnvironmentalService & Office of Satellite and Product Operations, 1998. NOAA's Office of Satellite and Product Operations. , p.12. Available at: http://www.ospo.noaa.gov/Products/ocean/sst/monthly_mean.html [Accessed March 12,

2013].

Usvika, R., Rifaldi, M. & Noor, A., 2009. Energy and exergy analysis of kalina cycle system (KCS) 34 with mass fraction ammonia-water mixture variation. *Journal of Mechanical Science and Technology*, 23(7), pp.1871–1876.

Utlu, Z., 2015. Investigation of the potential for heat recovery at low, medium, and high stages in the Turkish industrial sector (TIS): An application. *Energy*, 81, pp.394–405.

UWE Moch, 2010. Leistungsverzeichnis UWE Moch - Deutschsprachige Version. , p.1. Available at: http://www.uwemoch.de/ [Accessed March 1, 2013].

Valdimarsson, P., 2003. Factors influencing the economics of the Kalina power cycle and situations of superior performance. In ASME, ed. *International Geothermal Conference*. Reykjavík, pp. 32–40.

Vanslambrouck, B., Vankeirsbilck, I., Gusev, S. & Paepe, M. De, 2012. Efficiency comparison between the steam cycle and the organic Rankine cycle for small scale power generation. In *Renewable Energy World Conference and Expo North America*. Long Beach: Howeast, Universiteit Gent, p. 13.

Varela, J.M. & Soares, C.G., 2007. A Virtual Environment for Decision Support in Ship Damage Control. *IEEE Computer Graphics and Applications*, 27(4), pp.58–69.

Vélez, F., Segovia, J.J., Martín, M.C., Antolín, G., Chejne, F. & Quijano, A., 2012. A technical, economical and market review of organic Rankine cycles for the conversion of low-grade heat for power generation. *Renewable and Sustainable Energy Reviews*, 16(6), pp.4175–4189.

Veres, J.P., 1994. *Centrifugal and Axial Pump Design and Off-Design Performance Prediction*, Cleveland.

Vieira da Rosa, A., 2009. Mechanical Heat Engines. In *Fundamentals of Renewable Energy Processes*. Burlington: Academic Press, pp. 116–125.

Walker, G., 1980. *Stirling Engines* 1st ed., Bath: Oxford University Press.

Wall, G., Chuang, C.. & Ishida, M., 1989. Exergy Study of the Kalina Cycle. In E. S. Bajura, R.A.; Spakovsky, M.R.; Geskin, ed. *American Society of Mechanical Engineers (ASME), Winter Annual Meeting (WAM)*. San Francisco, p. 8.

Walraven, D., Laenen, B. & D'haeseleer, W., 2015. Minimizing the levelized cost of electricity production from low-temperature geothermal heat sources with ORCs: Water or air cooled? *Applied Energy*, 142, pp.144–153.

Wang, D., Ling, X. & Peng, H., 2012. Performance analysis of double organic Rankine cycle for discontinuous low temperature waste heat recovery. *Applied Thermal Engineering*, 48, pp.63–71.

Wang, J., Dai, Y. & Gao, L., 2009. Exergy analyses and parametric optimizations for different cogeneration power plants in cement industry. *Applied Energy*, 86(6), pp.941–948.

Wang, J., Yan, Z., Wang, M. & Dai, Y., 2013. Thermodynamic analysis and optimization of an ammonia-water power system with LNG (liquefied natural gas) as its heat sink. *Energy*, 50, pp.513–522.

Wang, J., Yan, Z., Wang, M., Ma, S. & Dai, Y., 2013. Thermodynamic analysis and optimization of an (organic Rankine cycle) ORC using low grade heat source. *Energy*, 49(null), pp.356–365.

Wang, T., Zhang, Y., Peng, Z. & Shu, G., 2011. A review of researches on thermal exhaust heat recovery with Rankine cycle. *Renewable and Sustainable Energy Reviews*, 15(6), pp.2862–2871.

Wärtsilä, 2010. Wärtsilä and Turboden sign agreement to launch Wärtsilä Marine ECC. *Press Releases*, p.1. Available at: http://www.wartsila.com/en/press-releases/agreement-to-launch-Wartsila-Marine-ECC [Accessed March 21, 2015].

Wärtsilä Corporation, 2012. Marine Solutions. , p.196.

Wärtsilä Engines, 2012. Wärtsilä 34DF Product Guide. , p.176.

Wasabi Energy Limited, 2010. Wasabi Energy Corporate Presentation. , p.16.

Wasabi Energy Limited, 2011. *ASX Announcement June 2011*, Melbourne.

Wasabi Energy Limited, 2012. *Annual General Meeting*, Melbourne.

Wasabi Energy Limited, 2015. *Bruschal Geothermal*, Hawthorn.

Wasabi Energy Limited & Global Geothermal Limited, 2010. *ASX Announcement (Shanghai)*, Melbourne.

Weerasinghe, W.M.S.R., Stobart, R.K. & Hounsham, S.M., 2010. Thermal efficiency improvement in high output diesel engines a comparison of a Rankine cycle with turbo-compounding. *Applied Thermal Engineering*, 30(14-15), pp.2253–2256.

Welch, P. & Boyle, P., 2009. New turbines to Enable Efficient Geothermal Power Plants. *Geothermal Resources Council Transactions*, 33, p.8.

Whispergen, 2011. Product Specs. , p.1. Available at: http://www.whispergen-europe.com/productspec_en.php?fm=whispergen&fp=Product Specs [Accessed March 5, 2013].

Whittaker, P., 2009. *Corrosion in the Kalina cycle An investigation into corrosion problems at the Kalina cycle geothermal power plant in Húsavík , Iceland*. University of Iceland, University of Akureyri.

Wiesmann, A., 2010. Slow steaming – a viable long-term option? *In Detail Wärtsilä Technical Journal*, (02), pp.49–55.

Williams, B.W., 2006a. *Principles and Elements of Power Electronics* 2nd ed., Glasgow: McGraw Hill.

Williams, B.W., 2006b. *Principles and Elements of Power Electronics* 2nd ed., Glasgow: McGraw Hill.

Winnes, H. & Fridell, E., 2009. Particle Emissions from Ships: Dependence on Fuel Type. *Journal of the Air & Waste Management Association*, 59(12), pp.1391–1398.

Winther, M., Christensen, J.H., Plejdrup, M.S., Ravn, E.S., Eriksson, Ó.F. & Kristensen, H.O., 2014. Emission inventories for ships in the arctic based on satellite sampled AIS data. *Atmospheric Environment*, 91, pp.1–14.

Wit, C., 1990. Proposal for Low Cost Ocean Weather Routeing. *The Journal of Navigation*, 43(03), pp.428–439.

Woodyard, D., 2009. *Pounder's Marine Diesel Engines and Gas Turbines* 9th ed., Oxford: Butterworth-Heinemann.

World Health Organization, 2010. EXPOSURE TO BENZENE: A MAJOR PUBLIC HEALTH CONCERN. , p.5.

Woud, H.K. & Stapersma, D., 2012. *Design of Propulsion and Electric Power Generation Systems* 1st ed., London: IMarEST.

Wu, F., Chen, L., Wu, C. & Sun, F., 1998. Optimum performance of irreversible stirling engine with imperfect regeneration. *Energy Conversion and Management*, 39(8), pp.727–732.

Wuebbles, D.J., 1983. Chlorocarbon emission scenarios: Potential impact on stratospheric ozone. *Journal of Geophysical Research*, 88(C2), p.1433.

Xu, W., Wang, J., Cai, M. & Shi, Y., 2015. Liquid air fueled open–closed cycle Stirling engine. *Energy Conversion and Management*, 94, pp.210–220.

Yamaguchi, H., Zhang, X.R., Fujima, K., Enomoto, M. & Sawada, N., 2006. Solar energy powered Rankine cycle using supercritical CO2. *Applied Thermal Engineering*, 26(17-18), pp.2345–2354.

Yamamoto, T., Furuhata, T., Arai, N. & Mori, K., 2001. Design and testing of the Organic Rankine Cycle. *Energy*, 26(3), pp.239–251.

Yanagisawa, N., Muraoka, H., Sasaki, M. & Sugita, H., 2012. Starting Field Test of Kalina System using Hot Spring Fluid in Japan. In *Thirty-Seventh Workshop on Geothermal*

Reservoir Engineering. Stanford: Stanford, p. 6.

Yanagisawa, N., Muraoka, H., Sasaki, M., Sugita, H., Ioka, S., Sato, M. & Osato, K., 2012. Production Test of Kalina System Using Hot Spring Fluid at Geopressure Field in Japan. *Geothermal Resources Council Transactions*, 36, pp.1165–1170.

Yang, K., Zhang, H., Song, S., Zhang, J., Wu, Y., Zhang, Y., Wang, H., Chang, Y. & Bei, C., 2014. Performance Analysis of the Vehicle Diesel Engine-ORC Combined System Based on a Screw Expander. *Energies*, 7(5), pp.3400–3419.

Yang, M.-H. & Yeh, R.-H., 2014. Analysis of optimization in an OTEC plant using organic Rankine cycle. *Renewable Energy*, 68, pp.25–34.

Yang, M.-H. & Yeh, R.-H., 2015. Thermo-economic optimization of an organic Rankine cycle system for large marine diesel engine waste heat recovery. *Energy*, 82, pp.256–268.

Yau, P.S., Lee, S.-C. & Ho, K.F., 2012. Speed Profiles for Improvement of Maritime Emission Estimation. *Environmental engineering science*, 29(12), pp.1076–1084.

Yaws, C.L., 1997. *Handbook of Chemical Compounds Data for Process Safety* 1st ed., Houston: Gulf Publishing Company.

Yee, S.K., LeBlanc, S., Goodson, K.E. & Dames, C., 2013. $ per W metrics for thermoelectric power generation: beyond ZT. *Energy Environ. Sci.*, 6(9), pp.2561–2571.

Yildirim, O. & Guo, Z., 2012. A High-Efficiency Micro-Channel Regenerative Heat Exchanger for Fluid Processing. In *Comsol conference*. Boston: COMSOL, p. 3.

Yue, C., Han, D., Pu, W. & He, W., 2015. Comparative analysis of a bottoming transcritical ORC and a Kalina cycle for engine exhaust heat recovery. *Energy Conversion and Management*, 89, pp.764–774.

Yue, G.Q., Dong, S.W., Zheng, Q. & Li, J.R., 2012. Design of Marine Diesel Engine Waste Heat Recovery System with Organic Rankine Cycle G. Chang, ed. *Applied Mechanics and Materials*, 148-149(December), pp.1264–1270.

Zare, V. & Mahmoudi, S.M.S., 2015. A thermodynamic comparison between organic Rankine and Kalina cycles for waste heat recovery from the Gas Turbine-Modular Helium Reactor. *Energy*, 79, pp.398–406.

Zhang, C., Shu, G., Tian, H., Wei, H. & Liang, X., 2015. Comparative study of alternative ORC-based combined power systems to exploit high temperature waste heat. *Energy Conversion and Management*, 89, pp.541–554.

Zhang, X., He, M. & Zhang, Y., 2012. A review of research on the Kalina cycle. *Renewable and Sustainable Energy Reviews*, 16(7), pp.5309–5318.

Zhang, X. & Zhao, L.-D., 2015. Thermoelectric materials: Energy conversion between heat and electricity. *Journal of Materiomics*.

Zhang, Y., He, M., Jia, Z. & Liu, X., 2008. First law-based thermodynamic analysis on Kalina cycle. *Frontiers of Energy and Power Engineering in China*, 2(2), pp.145–151.

Zhao, L.-D., Lo, S.-H., Zhang, Y., Sun, H., Tan, G., Uher, C., Wolverton, C., Dravid, V.P. & Kanatzidis, M.G., 2014. Ultralow thermal conductivity and high thermoelectric figure of merit in SnSe crystals. *Nature*, 508(7496), pp.373–7.

Zheng, X.F., Liu, C.X., Yan, Y.Y. & Wang, Q., 2014. A review of thermoelectrics research – Recent developments and potentials for sustainable and renewable energy applications. *Renewable and Sustainable Energy Reviews*, 32, pp.486–503.

Ziegler, F. & Riesch, P., 1993. Absorption cycles. A review with regard to energetic efficiency. *Heat Recovery Systems and CHP*, 13(2), pp.147–159.

Zmudzki, S., 1999. Feasibility study into Stirling engines application in ship's energy systems. *The Built Environment*, 45, pp.299–304.

(Page left intentionally blank)

(Page left intentionally blank)

APPENDICES

APPENDIX I – ENVIRONMENTAL AND HEALTH CHARACTERISTICS OF A WORKING FLUIDS

This subsection will explain in a more detailed way some of the desirable environmental and health characteristics for a working fluid.

1.1 GLOBAL WARMING POTENTIAL

The Global Warming Potential (GWP) determines the total energy absorbed by a GHG over a period of time compared to CO_2 [Environmental Protection Agency 2012]. Recognising that the compounds have a limited life in the atmosphere means that the impacts effected on the atmosphere change with time. For this reason, the GWP retain different values for different time lengths. This concept helps the researcher to understand the important role and effects that all GHG have in warming Earth. Carbon dioxide is used as the GWP reference – it has a value of 1.0 – because it brings the greatest warming influence on the atmosphere due to its abundance. While CO_2 has a low GWP when compared to other fluids (e.g. R134a has a GWP of 1,600), its abundance in the atmosphere and its emission increment due to the dependence of human activities on fossil fuels makes it the most relevant GHG emission [Calm & Didion 1998].

The GWP measures the effect of a GHG under different timeframes, called time horizons, in order to understand the short, medium and long term effects on the atmosphere [Forster et al. 2007]. As seen in Table 38, not all the fluids reduce their impact on the atmosphere as time passes by, this is probably to do with the fluid's longevity in the atmosphere.

Table 38: Different organic fluids with classification, longevity in the atmosphere and GWP for different time horizons [Forster et al. 2007; Myhre et al. 2013]**.**

Name	Compound	Lifetime (years)	Global Warming Potential		
			GWP_{20} (-)	GWP_{100} (-)	GWP_{500} (-)
Carbon dioxide	Carbon	variable	1	1	1
Methane	Hydrocarbon	12.0	84	30	7.6
R236fa	Hydrofluorocarbon	240.0	6,940	8,060	7,660
R22	Hydrochlorofluorocarbons	12.0	5,280	1,760	549
PFC-14	Fluorinated	$5.0x10^4$	4,880	6,630	11,200
R245fa	Fluorinated Ethers	7.7	2,920	858	-
R143	Fluorinated Ethers	3.5	1,200	320	230

The use of GWP as a tool to assess the global warmth due to GHG emissions has been criticised for the assumptions and simplifications taken. This has motivated researchers to look into alterative methodologies, such as the Global Temperature Potential (GTP) and the introduction of the efficacy of a GHG to warm the atmosphere into the GWP formulation [Forster et al. 2007]. So far as the author is concerned, GWP, in its time horizon of 100 years is the most

common measurement used by refrigerant and organic fluid manufacturers to measure the impact on global warming [e.g. Honeywell Refrigerants 2012].

As explained in Calm [2008], the development of organic fluids is focusing on the creation of refrigerants which have a low GWP without failing to have low ODP, flammability and toxicity. Some examples are R1234yf and R1336mzz-Z (also known as DR-2) [Sarbu 2014; Molés et al. 2014].

The reader is recommended the works of Daniel and Velders [2006] and Forster et al. [2007] for a more detailed analysis and discussion regarding the GWP.

1.2 OZONE DEPLETION POTENTIAL

Ozone (O_3) is considered a GHG, and its creation and destruction due to chemical interactions happens in the lower parts of the atmosphere (i.e. troposphere and stratosphere) [Forster et al. 2007]. The Ozone Depletion Potential (ODP) quantifies the destruction of O_3 by any substance which occurs in the stratosphere [Wuebbles 1983]. Ozone destruction begins to happen when the degradation products from halocarbon (i.e. that contain carbon atoms and any type of halogen atoms: bromine, chlorine, fluorine or iodine) arrive into the stratosphere and react with the O_3 [Daniel & Velders 2006]. Similar to GWP, ODP uses as reference a fluid, in this case R11, to which is assigned a value of one (see Table 39). However, contrary to the GWP, the ODP normally is not considered as time dependant. When ODP is integrated by a certain time horizon, it is seen that compounds that have shorter lifetimes in the atmosphere than R11 tend to reduce their ODP value as the integrated time increases [Ibid.].

Table 39: Different organic fluids are shown with their active presence in the atmosphere and their ODP values [Honeywell 2001; Daniel & Velders 2006; Forster et al. 2007]**.**

Name	Compound	Lifetime (years)	ODP (-)
R11	Chlorofluorocarbon	45	1.0
R12	Chlorofluorocarbon	100	1.0
R123	Fluorinated Ethers	1.3	0.2
R141b	Fluorinated Ethers	9.3	0.1
R245fa	Fluorinated Ethers	7.6	0.0

In the 1980s and 1990s, there was a strong development in new fluids, especially for their application in air conditioning and sprays, that mitigated ozone destruction [Calm 2008]. The use of hydrofluorocarbons (HFC), hydrochlorofluorocarbons (HCFC) and natural refrigerants became common in these two decades. The negative aspect of these types of fluids, excluding the natural refrigerants, as seen in Table 38, is their high GWP.

Please refer to the work of Daniel and Velders [2006] for further reading on ODP.

1.3 FLAMMABILITY AND TOXICITY

These characteristics are of high importance in the vessel environment since they could present, if not correctly assessed, a major risk to the crew and integrity of the vessel.

Flammability is defined as the capability of a substance to ignite and burn. The ease of igniting can be quantified as having different qualitative or quantitative approaches. For example, the Hazardous Materials Identification System (HMIS) uses five levels (i.e. from 0 to 4) which are determined by the material's flash points, auto-ignition temperatures, type of materials, explosiveness, burning speed and boiling points [National Paint and Coatings Association 2002]. The American Society of Heating, Refrigerating and Air-Conditioning Engineers (ASHRAE) uses three different levels (i.e. from 1 to 3) defined by flame propagation, lower flammability limit (LFL), heat of combustion (HoC) and burning speed [Sarbu 2014].

Toxicity is defined as the degree of damage that a substance can inflict on a living organism. To measure this, a dose of the substance is given to the organism via different exposure methods, such as ingestion or inhalation, to then observe and quantify the effects [National Paint and Coatings Association 2002]. As seen in Table 40, the dose size limit is 400 parts per million (ppm); if there is a negative response from the living organism, the substance is defined as toxic.

Table 40: ASHRAE flammability and toxicity classification for substances [American Society of Heating Refrigerating and Air-Conditioning Engineers 2007]**. The Notes column and row explain the limits of each classification.**

Flammability/ Toxicity	**Low**	**High**	***Notes***
High	A3	B3	*LFL $\leq$ 0.10 kg/m^3 or HoC $\geq$ 19,000 kJ/kg*
Low	A2	B2	*LFL > 0.10 kg/m^3 and HoC < 19,000 kJ/kg*
Non-flammable	A1	B1	*No LFL*
Notes	*No toxicity at concentrations $\leq$ 400 ppm by volume*	*Toxicity at concentrations $\leq$ 400 ppm by volume*	

The method to define toxicity by HMIS adds more dimensions such as chronic effects, categorisation of skin and eye reactions and three different types of toxicity measures (i.e. oral, dermal and inhalation). The ASHRAE uses a more simple approach involving a constant dosage which gives, as seen in Table 40, two levels of toxicity – A and B. Table 41 offers a comparison between the two different classification approaches.

Please refer to the following works for more information regarding flammability and toxicity [National Paint and Coatings Association 2002; American Society of Heating Refrigerating and Air-Conditioning Engineers 2007] and ANSI Z129.176.

Table 41: Flammability and toxicity classification from two different sources. N/A refers to data that was not possible to find. [Honeywell 2001; National Paint and Coatings Association 2002; Megaloid laboratories limited 2006; American Society of Heating Refrigerating and Air-Conditioning Engineers 2007; National Refrigerants 2008].

Name	HMIS classification		ASHRAE classification
	Flammability	Toxicity	
R11	N/A	N/A	A1
R12	1	0	A1
R245fa	1	2	B1
Isobutane	4	2	A3
Isopentane	4	1	A3

APPENDIX II – ENERGY EFFICIENCY DESIGN INDEX

The purpose of this appendix is to show in detail the Energy Efficiency Design Index (EEDI) formula. For convenience of the reader the main variables are shown in Table 42. The formula as given by the International Maritime Organization is shown below:

$$EEDI = \frac{\left(\prod_{f=1}^{M} f_f\right)\left(\sum_{i=1}^{nME} \dot{W}_{ME(i)} C_{FME(i)} SFOC_{ME(i)}\right) + \left(\dot{W}_{AE} C_{FAE} SFOC_{AE}\right) + \left(\left(\prod_{j=1}^{n} f_j \sum_{i=1}^{nPTI} \dot{W}_{PTI(i)} - \sum_{i=1}^{neff} f_{eff(i)} \dot{W}_{AEeff(i)}\right) C_{FAE} SFOC_{AE}\right) - \left(\sum_{i=1}^{neff} f_{eff(i)} \dot{W}_{eff(i)} C_{FME} SFOC_{ME}\right)}{f_c f_{reg} f_w v_{ref} Capacity}$$

[114]

Table 42: a) Table that show the main variables in the EEDI formulae; b) shows the subscripts for the different variables in the EEDI formula.

a)

Variable	Name	Unit
C_F	Carbon factor	-
Capacity	Capacity	-
f	Correction factor	-
$\dot{W}$	Power	kW
SFOC	Certified Specific Fuel Oil Consumption	g/kWh
v	Speed	kn

b)

Subscript	Name
AE	Auxiliary engine
c	Cubic capacity
eff	Availability
reg	Technical/regulatory limitation (applies only for correction factors {*f*})
ME	Main engine
PTI	Shaft motor
ref	Reference
w	Weather conditions

For a more detail explanation of how the different parts of the formula works please refer to the following reference: [International Maritime Organization 2012].

APPENDIX III – SOME IMPORTANT CONCEPTS FOR A THERMAL MACHINE

While the purpose of this thesis is not to explain the most basic concept of thermodynamics, it is necessary to introduce the reader to different concepts which are necessary for the understanding of a thermodynamic WHRS as a thermal machine.

If the reader wishes to go into detail about the topics presented in this appendix or cover thermodynamic concepts such as work, heat and energy, the book of Cengel and Boles [2007] is recommended. Also, this thesis includes a Glossary which can help with some of the most basic definitions.

3.1 TOP OR BOTTOM?

Depending on how heat is provided to the thermal machine, it can be classified as a topping cycle or a bottoming cycle.

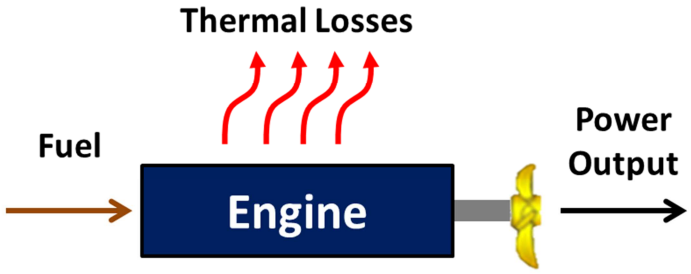

Figure 121: A simplified example of a topping cycle.

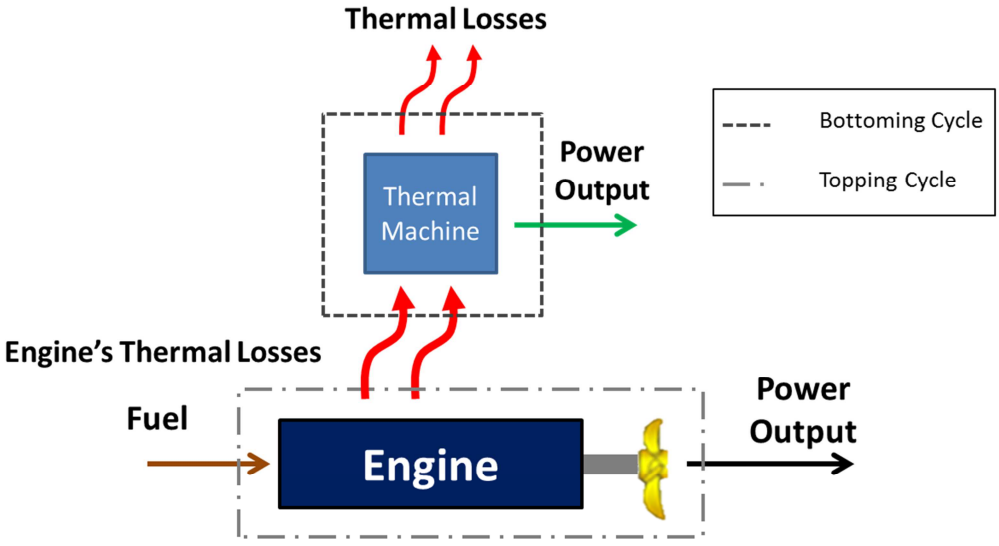

Figure 122: Simplified example of a combined power plant where it is shown the energy map for topping and bottoming cycles.

A topping cycle, also known as direct cycle and seen in Figure 121, extracts energy using available processes from energetic resources in order to produce work [Tien et al. 2007; Liu et al. 2013]. As an example, a diesel engine delivers work by burning fuel with a mixture of air (i.e. combustion). Solar power plants and gas turbines are other examples of topping cycles.

A bottoming cycle, also known as indirect cycle as seen in Figure 122, is that which uses a process waste heat to generate work. The bottoming cycle's source heat has a lower heat quality than that used in the topping cycle. As per this definition, the use of any thermodynamic cycle to produce work from the available heat coming out of a marine engine will be a bottoming cycle.

3.2 GENERATION OR COGENERATION?

A generation plant refers to a process which only produces power, heating or cooling from a single energy source. A generation plant could be as represented in Figure 122 or could also be a fired boiler which produces steam to cover the heating demand in a building.

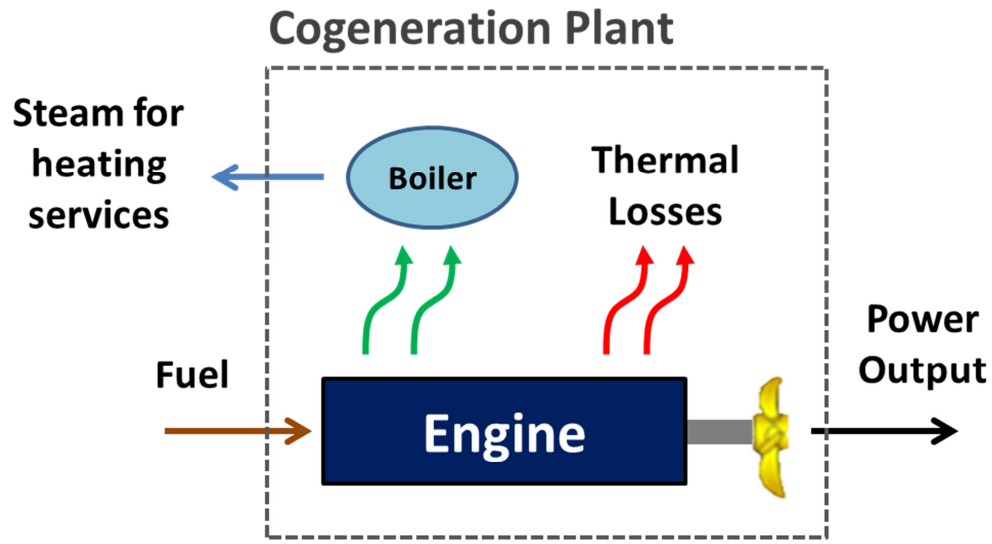

Figure 123: Example of a marine power plant which also produces steam using part of the engine's waste heat.

Cogeneration refers to the production of work and heating from the same energy source (see Figure 123). These kinds of systems have a higher thermal efficiency to a generation system since they use the heat losses when generating power to provide heating, cooling or more power. There would still be heat losses in this type of system due to the cogeneration plant's own inefficiencies. An example of a cogeneration plant would be a marine WHRS which produces mechanical or electrical power but at the same time provides steam for on board heating. Burel et al. [2013] show that a chemical cargo carrier powered by LNG could increase its total efficiency from 56.6% to 68.6% when using the main engine's waste heat to keep warm the cargo and boil the LNG before combustion.

There is also a trigeneration plant which also produces cooling simultanously to power and heating from the same energy source.

3.3 CLOSED OR OPEN?

This refers to the existence, or not, of mass transfer outside the boundaries of the thermal machine.

If a boundary is drawn around the engine presented in Figure 121, it could be appreciated that there is the introduction of mass (i.e. fuel and air) at the beginning of the process while the exhaust gas is the method by which the mass exits the thermal machine. This type of thermal machine is classified as open. In theory, internal combustion engines are a closed thermal machine, but its application, in reality, is open since the mixture of air and fuel do not experience a full cycle before exiting the engine.

On the other hand, a closed machine is any thermal machine that does not have a flux of mass across its border. Examples of this type of machine are the Rankine cycle and Stirling cycle. In real terms, a closed thermal machine is never fully closed due to the presence of leakages along the boundary, but this is considered by the author minimal to have a relevant impact on the performance of thermal machines in one cycle. It is important to mention that heat and work transfer across the thermal machine border would not change the classification of the machine to open.

In special cases with certain modifications in the machine layout, a normally closed thermal machine would become an open machine. This is the case of the modified Stirling engine used by Xu et al. [2015]. This work considers all thermodynamic cycle as closed thermal machines.

3.4 SUBCRITICAL OR SUPERCRITICAL?

To understand these two different thermodynamic processes, it is necessary to define the critical point of a fluid. In a fluid's pressure-temperature diagram, the critical point defines the pressure and temperature at which two different states of a fluid coincide – see Figure 124 [Cengel & Boles 2007]. In this thesis the critical point will refer to the area in a pressure-temperature diagram where the fluid's liquid and vapour forms coexist. The pressure and temperature of the critical point are defined as critical pressure (P_{cr}) and critical temperature (T_{cr}).

If a thermal machine operates below the critical point the process is known as subcritical – marked as 1-2-3-4 in Figure 125 – while if at any point in the process the thermal machine forces the fluid to be above its critical point, it is defined as supercritical – shown as cycle A-B-C-D in Figure 125 [Bahaa et al. 2007; Chen et al. 2010]. The attractiveness of a supercritical cycle is that since it is neither a liquid nor a vapour, it can improve the matching between the heat source and the thermal machine [Chen et al. 2010]. Because of this, the upper supercritical limit would be the fluid's own chemical and thermal stability, and the heat exchanger's material limitation regarding temperature and pressure. Basically, all fluids could operate under supercritical conditions, but the preferable fluid is CO_2 due to its accessibility, is not flammable, cheap, low impact on the environment and requires lower mass flow rates when compared to refrigerants [Chen et al. 2006; Yamaguchi et al. 2006; Chen et al. 2010]. Due to high pressures

supercritical thermal machines need specialised equipment that tends to increase the cost of the thermal machine and requires special risk assessments [Chen et al. 2010]. This drawback can be eliminated by switching from CO_2 to a refrigerant with a lower critical point.

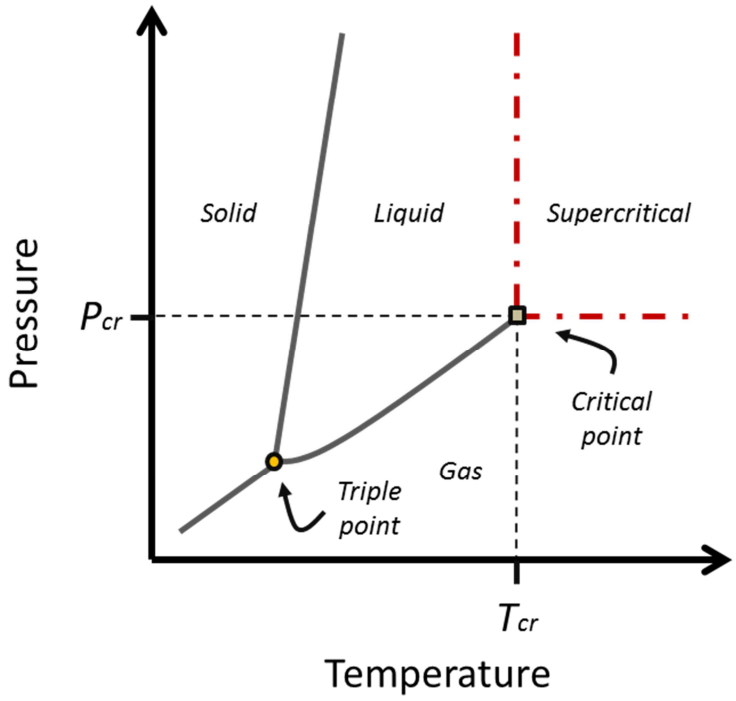

Figure 124: Pressure-temperature diagram of an imaginary fluid where its different phases are shown. The supercritical area is delimited by P_{cr} and T_{cr}. Also the diagram presents the triple point which is the point where the three different phases (i.e. solid, liquid and gas) of a fluid are found [Cengel & Boles 2007].

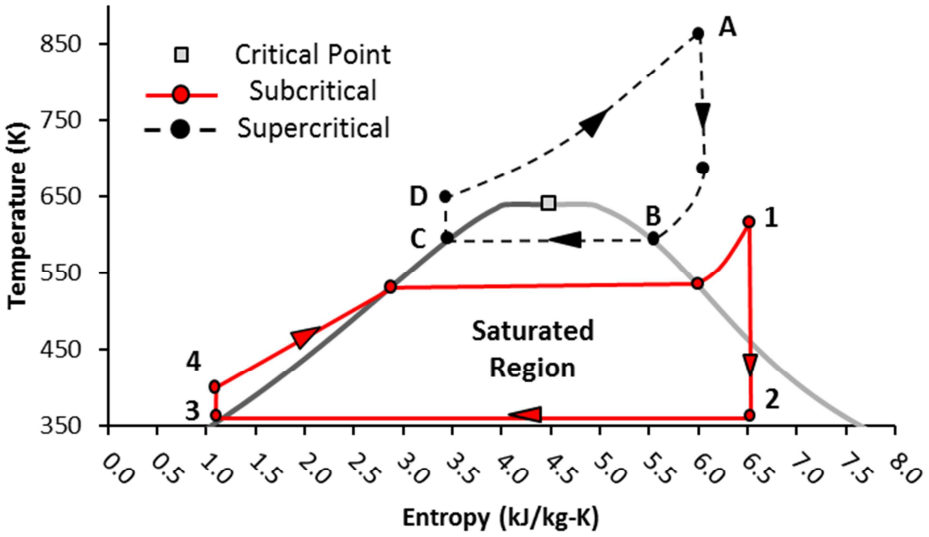

Figure 125: Depiction of a subcritical thermal engine (1-2-3-4) and a supercritical thermal machine (A-B-C-D) using water as the working fluid. Expansion and pumping are assumed to be isentropic.

The thesis focuses only on subcritical thermal machines due to the high pressures seen in supercritical thermal machines which require specialised heat exchangers and difficulties in operations [Chen et al. 2010; Li et al. 2011]. But it is recognise that supercritical machines bring an interesting mixture to alternative waste heat recovery solutions to the typical RC or alternative ORC, as seen in the work of Kalikatzarakis and Frangopoulos [2014].

3.5 CARNOT CYCLE

The Carnot cycle describes a thermal machine that has the highest thermal efficiency possible for a given temperature gradient between the heat source and sink [Balmer 2011]. It was proposed by Sadi Carnot in 1824, and is composed of four reversible processes, as seen in Figure 126 [Cengel & Boles 2007; Nag 2010; Shang et al. 2014]:

1. Isentropic adiabatic expansion (1-2), work is extracted from the thermal machine until it reaches T_C.
2. Isothermal compression (2-3), excess heat not used in the expansion is transferred to the sink.
3. Isentropic adiabatic compression (3-4), external work is required for this step which in turn will increase the working fluid temperature to T_H.
4. Isothermal expansion (4-1), heat is added from the heat source to the working fluid.

From these processes, the Carnot thermal efficiency ($\eta_{th,Carnot}$), also known as reversible thermal efficiency, is given by the following equation:

$$\eta_{th,Carnot} = \frac{W}{Q_i} = \frac{Q_i - Q_o}{Q_i} = 1 - \frac{Q_o}{Q_i} \qquad [\ 115\ ]$$

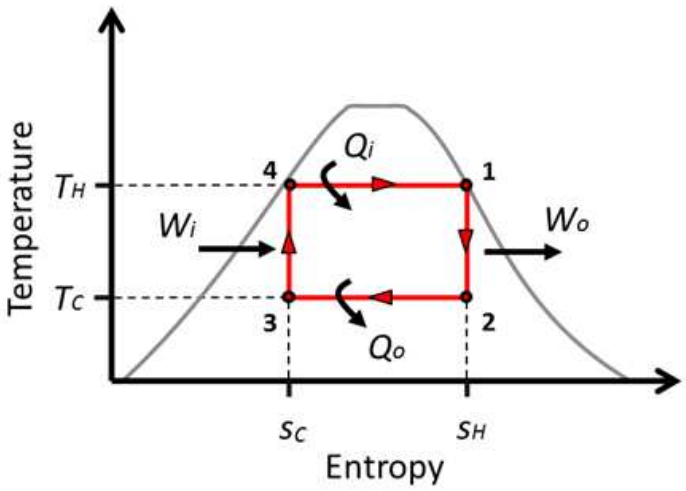

Figure 126: Carnot cycle representation in a *T-s* diagram where all four reversible processes are shown.

From equation [3] some important points can be deducted: a) It does not matter what type of reversible thermal machine and processes are happening in the cycle, the thermal efficiency will

always be the same; b) higher source temperatures will increase the Carnot's thermal efficiency; and c) lower sink temperatures will also increase it (see Figure 9).

The Carnot cycle represents a highly idealised thermal machine which it has not yet been possible to produce due to certain impracticalities [Nag 2010]:

1. The isentropic process expansion (1-2) must deal with the formation of droplets of liquid as it goes from point 1 to 2 since it is inside the saturation curve.
2. The isentropic compression (3-4) must control the quality of the vapour coming from step 3 in order to achieve a saturated liquid at point 4.
3. The compressor must not only handle the pressure increase for a two phase fluid, but also the required compressive work is large.

The list of impracticalities has been solved by other thermal machines but at the cost of system losses, such as condensing totally the working fluid after expansion, which make the thermal machine irreversible.

APPENDIX IV – FURTHER ON THERMODYNAMIC CYCLES

The purpose of this Appendix is to present a more in-depth discussion of some areas of the different thermodynamic cycle. These sections were not added to the main body since it did not add relevant information for the thermodynamic comparison but still it is a piece of work that complements what has been said in chapters 3 and 5.

4.1 KALINA CYCLE

4.1.1 KALINA CYCLE ON A MARINE ENVIRONMENT

At the beginning of this research in 2012, there was a lack of academic and industrial literature regarding KC on board vessels. Back then, there were two probable explanations with different points of view:

1. **Negative.** It is unattractive to investors since the evidence of performance is scarce portraying a technology that is not yet mature, not being a good option for the more conservative owners.
2. **Positive.** Being a novel technology can also mean that it is a big area of opportunity and that with the little evidence of success that there is, it is worth investing in a novel KC for waste recovery within inside a ships.

Nowadays the scientific community has taken a stronger interest in the application of a marine KC, but still it seems that investors are not keen to use this cycle on board, it is probable that one main reason is the high ammonia concentration which is a major hazard. As explained with the flammable fluids in an ORC, the use of a thermal oil and state of the art safety and monitoring systems should reduce the danger for personnel. Another probable reason is that the technology is still patented, not making it easy or cheap for manufacturers to exploit the full advantages of the KC technology in a marine scenario. In the following paragraphs, some of the marine KC papers published will be discussed briefly.

The works of Jonsson and Yan [2000] and Bombarda et al. [2010] seem to be working with large marine diesel engines, however, they did not take into consideration how the vessels' environment affect the marine WHRS performance, such as variable sink temperature and different operating conditions. It is also acknowledged that the study of such marine conditions or the application of the large diesels were not the aims of their papers. Due to these reasons, the works were not considered for a more detailed discussion.

Larsen, Haglind et al. [2013] use an engine model to simulate a 20 MW marine Diesel engine from which a KC WHRS uses the available waste heat from the exhaust gas. The KC WHRS has a similar layout as that used by Bombarda et al. [2010] which has demonstrated its use in the marine environment, but also this study used a thermal fluid in order to increase on board safety. The multi-objective optimisation showed that a suitable KC candidate for the vessel's WHRS is one that has an ammonia concentration of around 76% with a high pressure close to 8.6 MPa. The high pressure levels of the KC system affects negatively its selection when

compared to a typical RC or ORC, high pressure levels imply an increase in the safety and monitoring system impacting the costs. The KC system managed to raise the propulsion system by 0.6 percentual points from its baseline and reduced the fuel consumption by 6 g/kWh. When compared to a RC and an ORC WHRS, the KC power output was the lowest. Overall, Larsen, Haglind et al. concluded that the KC's complexity, ammonia concentration and novelty are important drawbacks when compared to the other mature thermodynamic cycles.

In a more recent study regarding the use of a KC as the ship's WHRS, Larsen et al. [2014] explore again the use of a KC as a marine WHRS, using as source the exhaust gas. This time, they use a different type of KC called the split-cycle which changes the binary working fluid concentration at the evaporative stage, improving even further the heat transfer process. Using a multivariable approach they found out that the split-cycle with reheating had a 23.2% thermal efficiency which is more than two percentual points higher than the typical KC when used with an 18 MW propulsive system. The reasons given in the work of Larsen et al. [2014] is that the split-cycle higher pressures and higher mass flow rate produce a larger power output for the same heat inlet. On the other hand, when quantifying the heat exchanger areas it is seen that the split-cycle requires around 50%-56% more area than the typical KC affecting the cost directly. Interestingly, after applying a typical marine operative time, the split-cycle payback time is not severely affected by the large heat exchanger cost due to its improved performance. The payback time for a KC and a reheated KC is of 2.0 and 2.4 years respectively; while for the split-cycle is 2.15 and 2.6 years.

The KC is a novel thermodynamic solution which, due to its patented nature, has made little progress in real applications. On paper, the performance and cost of this cycle can match any of the more established thermodynamic cycles for low/medium waste heat. Still, the challenges of the cycle to become a viable marine environment are, for the moment, big: complexity, large pressures, heat exchanger surface area and the use of ammonia. All of these cycle characteristics will be solved in time with the aperture of its patent, being a strong challenger to the well-established RC or the simpler ORC.

4.2 STIRLING CYCLE

4.2.1 STIRLING ENGINES IN DETAIL

There are two main families of Stirling engines depending on the drive method [Urieli & Berchowitz 1984; Vieira da Rosa 2009]:

- **Kinematic.** They use mechanisms like crankshafts and flywheels, to move and transmit the work.
- **Free-Piston.** They use the fluid forces to move the reciprocating elements and obtain a work output via a linear alternator or hydraulic pump.

Also the Stirling engines can be classified into three main groups depending on their configuration [Urieli & Berchowitz 1984; Vieira da Rosa 2009]:

- **Alpha configuration:** Has two pistons that work as a power and displacement piston depending on the process in the cycle. The pistons are connected in series by a cooler, regenerator and heater (Figure 127).
- **Beta configuration:** It has a power piston and displacer in the same cylinder (Figure 128).
- **Gamma configuration:** It has a power piston and displacer but in this configuration they are located in different cylinders (Figure 129).

Each family of engines have their own advantages, disadvantages and sub-classifications. The Stirling engines configurations are formed by the combination of the two previously described classifications. For example, the Ford-Philips 4-215 is a kinematic alpha Stirling engine, while the Sunpower M100 is a free-piston beta Stirling engine [Urieli & Berchowitz 1984].

All Stirling configurations will have one or both of the two types of pistons available: power pistons which are in charge of compressing or do work in the expansion process, and displacement pistons which are responsible for the fluid transfer inside the engine [Vieira da Rosa 2009].

4.2.1.1 KINEMATIC STIRLING ENGINES

It was the first drive configuration used to apply the Stirling cycle (SC) and the most common option seen in the market, with more than 60% presence [Majeski 2002]. The kinematic engines are dynamically and thermodynamically simple which helps the analytical calculations and control systems. The performance of the kinematic engines depend basically on the change of the engine's working volumes [Urieli & Berchowitz 1984] which is done by mechanically connecting the hot and cold pistons or displacers. The pistons' mechanical linkage assures a proper reciprocating movement and delivers the power output directly, this part of the engine being a constant area of research and development. Examples include the wobble plate, swashplate, hydralink and rhombic drive [Meijer 1961; Majeski 2002].

Some of its disadvantages are derived from an increase in moving parts increasing friction losses and demands a good level of lubrication in reciprocating parts. There are side loads caused by the rotational movement of the mechanical linkage which will produce wear in the engine. It is necessary to use moving seals in order to separate the working fluid and crankcase, increasing its maintenance [Bowman 1993; Majeski 2002]. Finally, the Stirling engine requires time to warm-up in order to start the working motion and even more time to arrive at its optimal operating conditions.

The kinematic engine has been the option for development and research since its beginning, making the configuration a mature alternative with several options that eliminate several of the inefficiencies of the first Stirling engines. These solutions affect the almost maintenance-free characteristic of the Stirling engine.

4.2.1.2 FREE-PISTON STIRLING ENGINES

This drive configuration was invented and patented by William Beale in 1964 [Walker 1980; Sunpower Inc. 2011]. The engine can produce work due to its fluid forces and mechanical springs that deliver the reciprocating motion required [Urieli & Berchowitz 1984]. The power output is delivered via a linear alternator using a moving coil, a flux-switching plunger or an inertia pump. It is also possible to install a reciprocating shaft seal, but this will increase the points of leakage [Walker 1980].

The free-piston engine only has, in essence, two moving parts (i.e. piston and displacer) concealed in a working volume and with no mechanical linkage, eliminating or reducing several problems found in the kinematic engine such as leakage, maintenance, friction losses, wear, side loads, lubrication and engine vibrations. Some advantages include a fast start-up time, the power output can be easily adapted by only modifying the phase angle between the power piston and displacer, longer periods between maintenance overhauls, cheaper maintenance cost and lower fuel consumption[Walker 1980; Bowman 1993; Majeski 2002; Vieira da Rosa 2009; Sunpower Inc. 2011].

However, it requires a high level of control since the position of the power piston is important for the power output; to have an efficient system, the analytical calculations are complex and complicated; and there is a time response delay when the load changes.

The main applications found for the free-piston engine related to power generation for residential, space and military purposes; pumping and cooling [Walker 1980; Majeski 2002; Sunpower Inc. 2011]. There are few manufacturers of free-piston Stirling engines, one of the most important being Sunpower Inc., owned by the free-piston inventor, which has manufactured Stirling engines capable of generating up to 7.5 kW_e. Through Sunpower licenses other companies have manufactured different free-piston engines which have been able to reduce the cost of such engines [Majeski 2002; Sunpower Inc. 2011].

The free-piston Stirling engine is still a young technology that has proven to be a simple, reliable, silent and vibrationless thermal machine capable of eliminating most of the intrinsic issues found in kinematic engines. Its design complexity may be a detrimental characteristic but this can be a minor issue when taking into account that the engines come with a good control system and that the engine can work properly for longer periods of time than kinematic engines.

4.2.1.3 ALPHA STIRLING ENGINE

It is one of the simplest Stirling configurations and its construction is similar to the ideal engine. The alpha configuration connects in series the cylinders, regenerator and heat exchangers (see Figure 127). The basic alpha engine has two power pistons in two different cylinders which also do the task of sweeping the working fluid. This configuration can be only achieved as a kinematic Stirling engine [Majeski 2002].

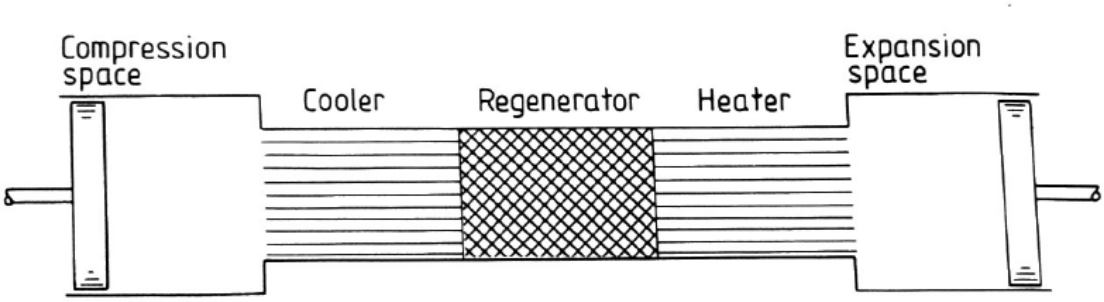

Figure 127: Alpha configuration for a Stirling engine [Urieli & Berchowitz 1984]**.**

The Solar Heart built by Cool energy Inc. uses waste heat or solar energy between 100°C and 300°C to generate electricity [Cool Energy Inc. 2012]. But more interesting is the case of Stirling Biopower Inc. which fabricates four cylinders alpha Stirling engines for a large set of applications from municipal water treatment facilities to biomass plants [Mikloski n.d.]. This engine is interesting in a shipping context because it uses one piston to perform the expansion and compression processes and has a swash-plate, enabling a compact engine design. The manufacturer does not mention any thermal efficiencies or any temperature operability. The working fluids are hydrogen and air. Hydrogen is used when heat sources are between 13.0 MJ/m^3 to 24.4 MJ/m^3 [43], and air when it is less than 13.0 MJ/m^3.

This configuration was used widely in automotive and generating applications by Ford-Philips, General Motors and United Stirling [Urieli & Berchowitz 1984] and an air alpha Stirling engine capable of producing 3 kW_e with the heat available from flue gases in a biomass plant was designed by Podesser [Podesser 1999]. Podesser's design uses a gas entering at a temperature of 1000°C and a sink temperature between 30°C and 70°C. The engine achieved a *COP* of 0.25 which, when compared to an absorption cycle at lower source temperatures [Little & Garimella 2011], reveals itself to be quite low. However, this engine was built with used parts from internal combustion engines and had the purpose of being a simple, economic and maintenance free equipment for a low-resource rural village rather than powerful and efficient equipment.

4.2.1.4 BETA STIRLING ENGINE

The Beta configuration is the classic Stirling engine. Its power piston and displacement piston are located in the same cylinder. The heat exchangers are connected in series, with the regenerator at the middle (see Figure 128). Better efficiencies can be achieved by adding a displacer piston and removing a power piston. Since the displacer piston does not have to be as tightly sealed, this reduces considerably the cylinder friction and seal failure [Foster 2011]. On the other hand, having a displacer piston that is not as tightly sealed can translate to leaks from the compression and expansion volumes. Another advantage of this configuration is that the power and displacement piston swept the same part of the cylinder in one revolution, meaning that this engine efficiently uses the engine space [Walker 1980]. Finally, Beta engines have to add a thermal barrier between the cold and hot space in order to avoid heat escaping the

[43] Measured at standard conditions which mean 20˚C and a pressure of 101.325 kPa.

working space. This happens because the configuration sets the piston as displacer in the same cylinder and sweeps the same volume [Foster 2011].

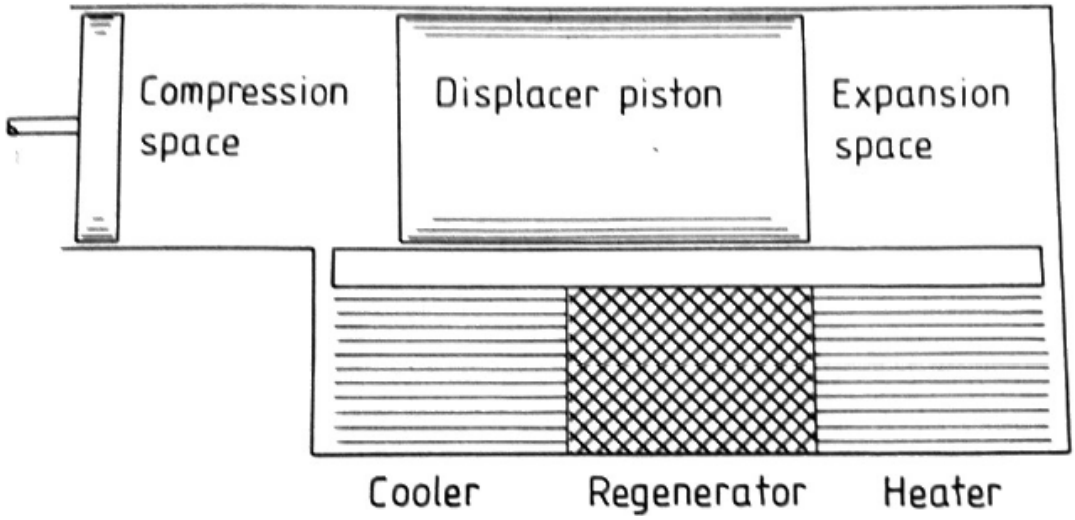

Figure 128: Stirling engine's Beta configuration [Urieli & Berchowitz 1984].

Sunpower Inc. has produced an important catalogue of free-piston beta Stirling engines with the purpose of generating electricity, cooling power or as heat pumps. The engines range from 7.5 kW_e to 35 kW_e with thermal efficiencies that can go up to 40% [Sunpower Inc. 2011].

Philips [Meijer 1961] invented a kinematic beta engine called the rhombic drive mechanism. The mechanism has two crankshafts, one for the power piston and the other for the displacer, these are connected via gears. The advantage of this modification is that enables the cylinder to have high pressures while the crankcase is at atmospheric pressure. This means that a beta engine can have high speeds with high specific work output without having complicated seal systems and bulky crankcases. This benefit is enlarged when used with high displacement engines. Other advantages are that it is vibrationless, since the forces are balanced inside the cylinder and yoke [Urieli & Berchowitz 1984].

4.2.1.5 GAMMA STIRLING ENGINE

The gamma engine also has a power and displacer piston but instead of being located in the same cylinder, as in the beta configuration, it has two cylinders, one for each piston (see Figure 129). These engines are normally used with low/medium heat quality but are also able to run with high quality heat sources [Chen et al. 2012]. Also, since the pistons are in different cylinders, the reciprocating mechanisms are simpler [Foster 2011] and it has the flexibility of having different bore and strokes for the displacement and power pistons.

Gamma engines are often used at low temperature difference between the source and the sink, which it is not possible to do with the other Stirling engine configurations. It has been shown that this type of engine can produce work with temperature differences as low as 0.6°C [Arsdell 2001]. UweMochs specialises in manufacturing Stirling gamma engines; their 500 W engines operate at 650°C and 1.3 MPa with the possibility of working with nitrogen or helium [Majeski 2002; UWE Moch 2010]. The area footprint per kW of the UweMochs Stirling engine is

0.700 m^2/kW whereas the Stirling engine's average area footprint is around 0.065m^2/kW. This could be caused by having two cylinders but since also only one manufacturer was found, it is highly probable that the engine design could be improved in search of more power and less surface area required.

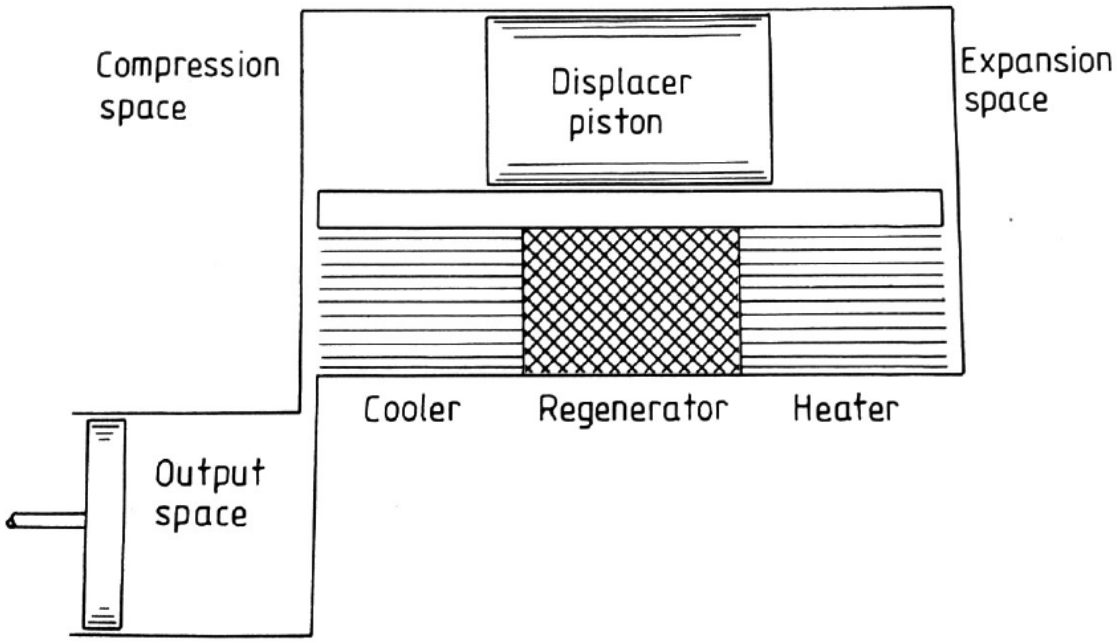

Figure 129: Gamma Stirling engine [Urieli & Berchowitz 1984].

Kongtragool and Wongwises [2007] performed experimental tests to two different gamma kinematic Stirling engines, two and four cylinders, the working fluid was air unpressurised. The main objective was to test the engines using low-medium quality heat to observe how they performed. The maximum power achieved was 11.8 W at a thermal efficiency of 0.5% for the two cylinder engine and 32.7 W at 0.8% for the four cylinder engine.

Other uses for the gamma engines are school demonstration models and gifts [Kontax Engineering Ltd. 2012; American Stirling Company 2012].

4.2.2 Research on marine Stirling Cycle

The first application of Stirling engines in ships was to use them as prime movers. The first record of a Stirling engine installed on a ship dates from 1827 when a 15 kW Stirling engine working with air replaced the *Highland Lad* steam propulsion plant [Syracuse New York Evening Chronicle 1853].

In the middle of the 20th century, Philips – in collaboration with General Motors – used and adapted some of their engine prototypes to be installed in vessels. The first engine was the 1-365 which had only one cylinder and developed 30 kW; it was installed and tested in the yacht *Johan de Witt*. A second prototype, seen in Figure 29, was developed using Philips engine 4-235 Boxer capable of producing 85 kW with a thermal efficiency of around 41%, this engine was never installed [Walker 1980].

United Stirling developed a rhombic drive Stirling engine composed of four cylinders working with helium and a source temperature of 700°C. The power output was rated at 145 kW but the first engines operated at half the design nominal pressure, meaning that the power output was reduced to 75 kW [Walker 1980]. United Stirling became Kockums Maritime Solutions; nowadays it specialises in kinematic Stirling submarine propulsion units where silent operation, low maintenance and high submerged endurance are the most valued characteristics. The engine produces 75 kW_e at a source temperature of 700°C to 750°C by burning liquid oxygen. The working fluid is helium and the reported thermal efficiency is around 39% [Majeski 2002; Kockums AB 2009].

One of the Stirling engine variables that affect most its performance is the source temperature; in the shipping case, the source will be around 250°C which will theoretically drop the thermal efficiency to low levels. Zmudzki [1999] designed a SC WHRS which is required to burn fuel on the Stirling engine's hot side in order to increase its thermal efficiency. By doing this the temperature will rise to 1,300°C. The downside of this idea is that the system becomes complex; there is extra fuel consumption in order to reach the design operating condition so that more heat can be extracted from the main diesel engine; and by burning fuels, there is an increment of GHG emission which the heat waste recovery system is trying to reduce. For the last disadvantage, the author recommends a three way catalyst to bring down the emissions to IMO levels. There is no indication from the author as to what level of efficiency can be expected from this type of heat waste recovery configuration.

Hirata and Kawada [2005] used a Stirling engine as the bottoming cycle of a 40 MW marine diesel engine. They assumed that around 30% of the total diesel engine energy (i.e. 12 MW) was rejected through its exhaust gas at a temperature of 400°C. The Stirling engine sink was set at 40°C and it was assumed that the SC was able to absorb 2.5 MW. The bottoming cycle was able to produce 700 kW, giving a thermal efficiency of around 28%. This power output and thermal efficiency are on similar levels as other plants such as the RC and KC, but the analysis undertaken by Hirata and Kawada does not consider the mechanical losses which are one of the main reasons for low thermal efficiencies in Stirling engines. Furthermore, Hirata and Kawada conclude that the size of the Stirling engine would be too large to become an attractive option for the marine industry. Finally, they recommend that a better option are small Stirling engine generators (i.e. 5 kW) are installed inside the ship with the function of charging batteries via the exhaust gases, so when arriving at port the batteries can supply the electrical demand.

The Stirling engine has been also studied as part of a cogeneration system installed on board a sailing boat. Ulloa et al. [2013] used a compact four cylinders Stirling engine using nitrogen as a working fluid and which was capable of producing around 0.92 kW_e, at an electrical efficiency of around 12%. In addition, the cogenerative system was capable of extracting around 6 kW of thermal power which helped to cover part of the boat's heating demand. They discovered that the Stirling engine covered the total electrical and thermal demand of the sailing boat if it was navigating all the time in the northern region of Europe. If the boat was sailing in the Mediterranean Sea, it would manage to cover around 50% of the electrical demand in the

summer months since all the thermal power recuperated would not be used in its totality due to higher temperatures.

Other applications found for Stirling engines inside vessels are shown by Whisper Tech with its PPS16 DC Stirling engine, used for charging batteries. It is a four cylinder Stirling engine using nitrogen as working fluid. The power output is 1 kW_e at a thermal efficiency of 12% and comes at a cost of around £7,190/kW_e [Majeski 2002; Whispergen 2011].

Due to the cycle nature, it is still required that the engines find a niche where their characteristics offer a big advantage over any disadvantages. In the case of shipping, some of the attractive characteristics are [Walker 1980; Urieli & Berchowitz 1984; Arsdell 2001; Vieira da Rosa 2009]:

1. Low noise and vibration.
2. Reasonable specific power.
3. Mechanical simplicity (e.g. there is no need for valves and turbo machinery).
4. Low and simple maintenance, since there are less mechanical elements moving and the heat input is outside the engine cylinders.
5. Possibility of using light materials when having low grade heat inputs at atmospheric pressures (e.g. plastics).
6. Multiple heat sources.
7. Modularity.

Some of the characteristics of Stirling engines that can have a negative influence during the selection process for marine WHRS are [Meijer 1970; Tailor & Narayankhedkar 1988; Arsdell 2001; Kongtragool & Wongwises 2006; Sugden & Drury 2012]:

1. Long warm-up time. It takes time to reach the optimal operative conditions, this is increased when the engine is large and the heat source is not of high quality. This is a likely scenario within shipping. For example, the water used to cool the main ship engine.
2. Slow adaptability. When the scenarios change, especially when changing the ship's engine load, the Stirling engine will need some time to adapt to new conditions. This characteristic is especially important for ships that require changing their main engine loads constantly.
3. High sensitivity to operating conditions. The power output and efficiency of the system is highly affected by changes in heat source and sink temperature. In the ship scenario, the change of operating conditions is expected, especially in the temperature of the exhaust gas.
4. Low power output. By the amount of power a Stirling engine can produce, bigger or many engines connected together will be required in order to handle the heat waste available from the ship.

5. High initial cost. The cost per kW_e installed can range from around £1,000 to £22,500 which, as previously explained, is due to the engine's low power output and a low demand for this technology.
6. Some of the difficulties of using hydrogen and helium are that their molecules are small, making it difficult to seal the system [Walker 1980]. This also means, in the hydrogen case inside a ship that safety precautions must be taken. For example, it will be necessary to have a well vented space, which will be complicated if the SC system is installed close to the main engine. Also, it is important to have in place a detection system that can warn and react when the concentration of gas becomes dangerous.

APPENDIX V – QUALITATIVE ANALYSIS

The purpose of this appendix is to explain in more detail the scales and values used for the qualitative analysis in chapter 4. At the end of this section there is a list of references (Tables 49 and 50) which were used to obtain the different values for each of the thermodynamic cycles.

5.1 INITIAL COST

The minimum cost was set to zero because there are existing operational strategies that will not cost anything to the ship operator and will reduce CO_2 emissions [Alvik et al. 2010]. The maximum value seen in the literature review was for the Sunpower Inc. Stirling engine at £22,500 per kW_e [Majeski 2002]. Having a higher value than the RC will mean a negative result for the SC.

Table 43: Cost ranges for the qualitative analysis.

Scale value	Range of costs (£/kW_e)
-1	781 - 940
-2	940 – 2,815
-3	2,815 – 5,625
-4	5,625 – 11,250
-5	11,250 - 22,500

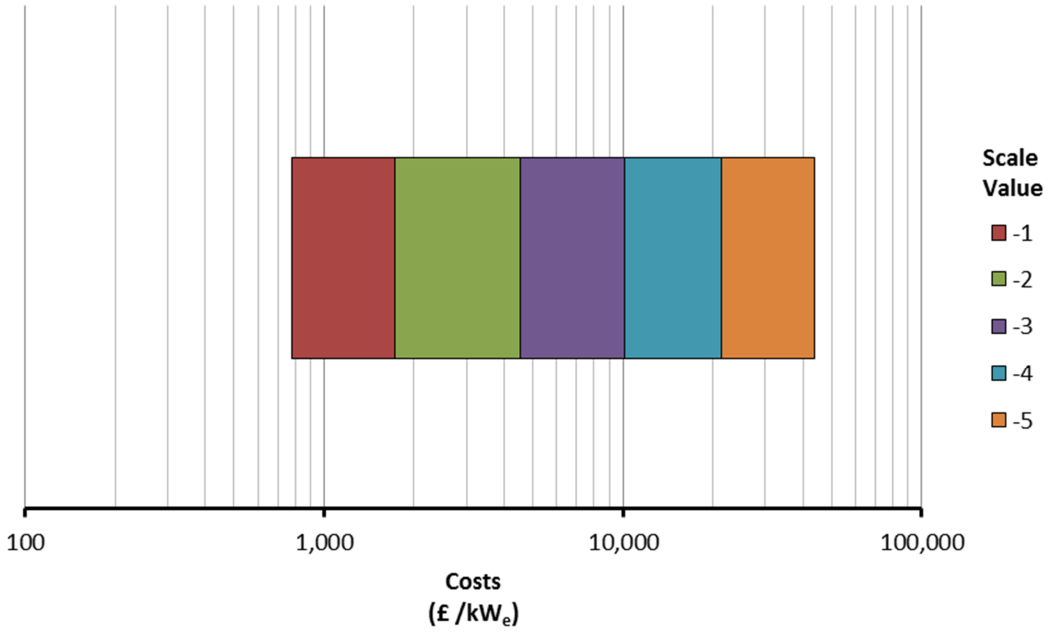

Figure 130: Cost logarithm scale in £/kW_e used for the thermodynamic WHRS comparison.

There is an important issue to address with the initial cost scale; this is related to the range of values seen for the positive and negative side. For the positive side, the range goes from £0/kW_e to £782/kW_e, while for the negative it runs from £782/kW_e to £22,500/kW_e, meaning, a

change of one scale unit in the positive direction requires a change of £156/kW_e in the initial price, while for the negative it is £4,344/kW_e. The consequence of this is that it is more difficult to get negative points for increasing the initial cost, which is not an accurate approximation to reality.

In order to fix this, it is assumed that an increase in the initial price will cause the same response as an equal cost reduction. It is assumed that it is more difficult to reduce costs as to increase them, meaning that a small improvement in cost will have an equally but opposite reaction as a larger cost increase. With these assumptions there is assigned a specific scale value to a range of costs as presented in Table 43 and Figure 130.

This methodology will be used only in the case of the initial cost where the difference between scales is considerable. For the other cases, it will use a simple cross-multiplication to find the data position in the scale.

5.2 OPERATION AND MAINTENANCE COST

The ideal case is that the operational and maintenance cost will be zero; the maximum was set at £8.6x10^{-2}/kW_e-h which is the average cost seen for a diesel generator [Osler 2011].

5.3 AREA AND VOLUME FOOTPRINT PER kW_E

The RC value is given for the area footprint (α_{fp}) and volume footprint (β_{fp}) as 3.4x10^{-2} m^2/kW_e and 1.6x10^{-1} m^3/kW_e respectively [Aalborg Industries 2005; Siemens AG 2013; Thermal & Pressure Engineering 2013]. The minimum value is set to zero; this refers to options to reduce CO_2 emissions that do not require floor or volume from the ship, such as the case of slow steaming. The maximum value was set as double the value of the RC which was observed in the *Emma Mærsk* case [Hultqvist 2008] whose RC WHRS has already a large footprint. Having a higher value than the RC will mean a negative result. If the power outputs available found from the literature are given in kW, it will be assumed that the cycle will be connected to an electrical generator with an efficiency of 90% in order to have the same unit required by α_{fp} and β_{fp}.

5.4 START-UP TIME

The length of the voyage will be a factor when choosing how important this variable is. For container ships that travel from China to the UK, this variable will not be as important as the tourist ship on the Thames.

An ideal case will be the internal combustion engine where as soon as the engine is turned on, it will be able to deliver full power. In the maximum case that will be RC time performance where it can take up to 145 minutes to be able to begin delivering power [Bachmann et al. 1999]. Having a lower value than the RC will mean a positive result.

5.5 APPLICABILITY

The RC has applications in land-based geothermal plants, solar, ships, cars among others. The maximum value, which is assigned to the RC, is three because it attains practical examples in the following areas:

- Marine environments.
- Automotive.
- Portable systems.

For the other thermodynamic cycles one positive point for each application found will be assigned.

5.6 FLEXIBILITY

The characteristics to be examined are:

- Flexibility of the working fluid to adapt.
- Catalogue of working fluids.

Equipment and common operational strategies are not considered. The water-based RC is set at zero since there are no options inside the system that can adapt itself to improve the power output and efficiency depending on the operating conditions. The maximum value is two.

5.7 MAXIMUM POWER OUTPUT

The minimum value will be set to zero. The reference value for the WHRS will be used also as the maximum value. It is set to 2,500 kW which will be a typical value achieved by a single steam turbine in a marine WHRS [MAN Diesel & Turbo 2012b]. From the literature review, the maximum power output achieved by each thermodynamic cycle will be obtained. If the power output is outside the maximum power, it will be assigned the maximum points possible, which are set as the reference.

5.8 THERMAL EFFICIENCY AT LOW/MEDIUM TEMPERATURES

The value set as reference is the average for a double pressure steam turbine reported by MAN Diesel & Turbo [2012] which is 6.5%. Minimum value will be set to zero. The source temperature is set at 260˚C with a sink of 25˚C. Using as a maximum the Carnot efficiency at engine conditions described earlier will put the maximum value (i.e. 44.1%) quite higher than the reference value, reducing the analysis sensitivity. Therefore, the maximum value chosen is triple of the RC which is 19.5%. The information from other cycles will be taken from journals, choosing them with similar temperatures to the RC case.

5.9 FLAMMABILITY AND TOXICITY

The flammability and toxicity classification comes from the ASHRAE [American Society of Heating Refrigerating and Air-Conditioning Engineers 2007] and is complemented by

information from the Hazardous Materials Identification System (HIMS) [National Paint and Coatings Association 2002].

The classification shown in Table 44 was used to generate the scale for this classification. Water, being a non-flammable fluid and having negligible toxicity, falls into the A1 category; this category will be used as reference. Since A1 is the safest category it will have assigned to it the value of zero, while the most flammable and toxic classification, that is B3, will be assigned -5.

Table 44: ASHARE toxicity and flammability classification table with the values assigned for the qualitative comparison [American Society of Heating Refrigerating and Air-Conditioning Engineers 2007]**.**

Flammability/Toxicity	Low	Scale Value	High	Scale Value
No flame propagation	A1	0	B1	-1
Low	A2	-2	B2	-3
High	A3	-4	B3	-5

For the case of the ORC system, the classifications of all the organic fluids presented in the ASHRAE document will be averaged. It is important to keep in mind that not all the organic working fluids available will operate with the ship's waste heat sources as seen in the work of Bao & Zhao [2013].

With the KC, the ammonia ASHARE classification will be used. The reason behind this decision is that the KC has a NH_3-H_2O binary working fluid and the highest power outputs and thermal efficiencies occur at high ammonia concentrations [Kalina & Leibowitz 1987; Nag & Gupta 1998; Borgert & Velasquez 2004; Usvika et al. 2009; Arslan 2011; Eymel et al. 2012].

For the SC, flammability and toxicity classification will be taken for the three most common working fluids for this type of engines: air, hydrogen and helium.

5.10 Results for each thermodynamic Waste Heat Recovery System

The following table presents the results from the ORC:

Table 45: Comparison table between RC and ORC from initial cost to area footprint.

Characteristic	Range	Min. Values	Max. Values	RC Values	ORC Values	Score
Initial cost (£/kW_e)	$\pm$ 5	0.00	22,500	782	2,060 [44]	-2.00
O&M cost (£ x10^{-2}/kW_e-h)	$\pm$ 5	0.00	8.60	0.78	0.80	0.00
α_{fp} (x10^{-2} m^2/kW_e)	$\pm$ 5	0.00	7.20	3.40	5.00	-2.11

[44] Only considered the WHRS cost values from Quoilin et al.[2013], the cost was averaged.

Table 46: Comparison table between RC and ORC from volume footprint to flammability/toxicity.

Characteristic	Range	Min. Values	Max. Values	RC Score	ORC Score	Score
β_{fp} ($x10^{-1}$ m^3/kW_e)	± 5	0.00	3.20	1.60	0.59	3.17
Start-up time (minutes)	0 to 2	0.00	145	145	22.5	1.69
Applicability (-)	-2 to 0	-2.00	0.00	3.00	3.00	0.0
Flexibility (-)	0 to 5	0.00	2.00	0.00	1.00	2.50
Max. Power output (kW)	-2 to 0	0.00	2,500	2,500	<2,500	0.0
Thermal Efficiency (%)	± 5	0.00	19.5	6.50	7.54	0.40
Flammability/Toxicity (-)	-5 to 0	-5	0	0	-1.09	-1.09

In the following table the comparison between the RC and KC is shown:

Table 47: Comparison table between RC and KC.

Characteristic	Range	Min. Values	Max. Values	RC Score	KC Score	Score
Initial cost (£/kW_e)	± 5	0.00	22,500	782	1,650	-2.00
O&M cost (£ $x10^{-2}$/kW_e-h)	± 5	0.00	8.60	0.78	0.57	1.38
α_{fp} ($x10^{-2}$ m^2/kW_e)	± 5	0.00	7.20	3.40	8.20	-5.00
β_{fp} ($x10^{-1}$ m^3/kW_e)	± 5	0.00	3.20	1.60	4.50	-5.00
Start-up time (minutes)	0 to 2	0.00	145	145	22.5 [45]	1.69
Applicability (-)	-2 to 0	-2.00	0.00	3.00	0.00	-2.00
Flexibility (-)	0 to 5	0.00	2.00	0.00	2.00	5.00
Max. Power output (kW)	-2 to 0	0.00	2,500	2,500	<2,500	0.00
Thermal Efficiency (%)	± 5	0.00	19.5	6.50	8.50 [46]	0.75
Flammability/Toxicity (-)	-5 to 0	-5	0	0	-3.00	-3.00

In the following table the comparison between a RC and a SC will be shown:

[45] The reference to the start-up time does not appear as a number, only that was improved from the RC. It will be assumed the same time as the ORC.

[46] There was not any reference that made a good comparison from the literature review at the temperature specified in the methodology section. In this case, it was taken the experience of the author and it was assumed the efficiency of the KC to be around 30% better than the RC in the temperature ranges assumed.

Table 48: Comparison table between RC and SC. It shows values from Initial cost to volume footprint.

Characteristic	Range	Min. Values	Max. Values	RC Score	SC Score	Score
Initial cost (£/kW_e)	± 5	0.00	22,500	782	11,900	-5.00
O&M cost (£ $x10^{-2}$/kW_e-h)	± 5	0.00	8.60	0.78	0.52	1.67
α_{fp} ($x10^{-2}$ m^2/kW_e)	± 5	0.00	7.20	3.40	38.25	-5.00
β_{fp} ($x10^{-1}$ m^3/kW_e)	± 5	0.00	3.20	1.60	1.32	0.88
Start-up time (minutes)	0 to 2	0.00	145	145	22.5[47]	1.69
Applicability (-)	-2 to 0	-2.00	0.00	3.00	3.00	0.00
Flexibility (-)	0 to 5	0.00	2.00	0.00	1.00	2.50
Max. Power output (kW)	-2 to 0	0.00	2,500	2,500	295	-1.76
Thermal Efficiency (%)	± 5	0.00	19.5	6.50	0.35 [48]	-4.73
Flammability/Toxicity (-)	-5 to 0	-5	0	0	-1.33	-1.33

5.11 REFERENCES USED

The following table contains the references used in the qualitative analysis.

Table 49: References used to create the thermodynamic qualitative comparison from Initial cost to area footprint.

Characteristic	RC	ORC	KC	SC
Initial cost (£/kW_e)	[BCS Incorporated 2008]	[Chacartegui et al. 2009; Saavedra et al. 2010; Tchanche et al. 2011; Quoilin et al. 2013; Shu et al. 2013]	[Rodriguez Garcia 2010; Eymel et al. 2012]	[Majeski 2002]
O&M cost (£ $x10^{-2}$/kW_e-h)	[Tarjanne & Kivistö 2008; Morvay & Gvozdenac 2008; U.S. Energy Information Administration 2010; Osler 2011][49]	[Saavedra et al. 2010]	[Kutscher 2001; Mirolli 2006; Wasabi Energy Limited 2010]	[Majeski 2002]
α_{fp} ($x10^{-2}$ m^2/kW_e)	[Aalborg Industries 2005; Siemens AG 2013; Thermal & Pressure Engineering 2013]	[Infinity Turbine LLC 2012]	[Cohn 1986]	[Majeski 2002; UWE Moch 2010]

[47] There are only references to the free piston Stirling engine as a fast start-up time, while the kinematic engines tend to be slow to start up. In lieu of this lack of clarity, again the value of the ORC will be used.

[48] It is reported in the literature higher efficiencies for upper and lower temperature sources that the one shown, but it was taken the decision of using this reference because it was the only one close enough to the RC reference case.

[49] From [U.S. Energy Information Administration 2010] and [Tarjanne & Kivistö 2008] the value was taken by averaging the maintenance costs from nuclear and coal power plants without heat recovery systems.

Table 50: References used to create the thermodynamic qualitative comparison from volume footprint to flammability and toxicity.

Characteristic	RC	ORC	KC	SC
β_{fp} ($x10^{-1}$ m^3/kW_e)	[Aalborg Industries 2005; Siemens AG 2013; Thermal & Pressure Engineering 2013]	[Infinity Turbine LLC 2012]	[Cohn 1986]	[UWE Moch 2010]
Start-up time (minutes)	[Bachmann et al. 1999]	[Bronicki 2007]	[Mlcak et al. 2002]	[Walker 1980; Bowman 1993; Majeski 2002; Vieira da Rosa 2009; Sunpower Inc. 2011]
Applicability (-)	[Doble 1917; Fréchette et al. 2004; Obieglo et al. 2009; Boretti 2012a; MAN Diesel & Turbo 2012b]	[Dinanno et al. 1983; Boretti 2012a; Infinity Turbine LLC 2012; Boretti 2012b; Opcon Energy Systems AB 2012b]	-	[Walker 1980; Zmudzki 1999; Majeski 2002; Sunpower Inc. 2011]
Flexibility (-)	-[50]	[Vanslambrouck et al. 2012]	[Zhang et al. 2012]	[Meijer 1970; Tailor & Narayankhedkar 1988; Invernizzi 2010]
Max. Power output (kW)	[MAN Diesel & Turbo 2012b]	[Bronicki 2010]	[Global Reports LLC 2008; Yanagisawa, Muraoka, Sasaki & Sugita 2012; Global Geothermal 2013b]	[Walker 1980]
Thermal Efficiency (%)	[MAN Diesel & Turbo 2012b]	[Bianchi & De Pascale 2011]	[Mirolli 2006]	[Kongtragool & Wongwises 2007]
Flammability/Toxicity (-)	[National Paint and Coatings Association 2002; American Society of Heating Refrigerating and Air-Conditioning Engineers 2007]	[National Paint and Coatings Association 2002; American Society of Heating Refrigerating and Air-Conditioning Engineers 2007]	[National Paint and Coatings Association 2002; American Society of Heating Refrigerating and Air-Conditioning Engineers 2007]	[National Paint and Coatings Association 2002; American Society of Heating Refrigerating and Air-Conditioning Engineers 2007]

[50] A RC uses water as its working fluid. Also water does not offer an extra degree of freedom like in the KC case due to its modifiable concentration.

APPENDIX VI – RESISTANCE MODEL

While this section does not go into detail about concepts more related to naval architecture, it is necessary to explain in a general way some basic concepts to understand how the resistance model works.

Equation [2] in section 1.3 gives an approximation between the power required and vessel speed, and requires the Admiralty coefficient (A_c) and displacement (Δ) of the ship studied. This approach is good to get a quick approximation of the ship's power requirement without the need of model experiments [Stroke 2003]. The use of the A_c brings some advantage since similar ships share the same A_c, it being only required to know the ship's dimensions or displacement [Woud & Stapersma 2012]. A disadvantage of equation [2] is the speed's power (n), normally assumed a cube relationship (i.e. n = 3) between the ship's speed and power requirement. MAN Diesel & Turbo [2011] recommends for slow vessels an n of 3.2 while for large high speed container vessels n should be equal to 4.0. Figure 131 represents an example of how different the power requirement is for the same handymax container ship when changing the n value. Assuming a design speed of 14 kn, the power requirement when n is equal to 3.0 would be around 5.5 MW; at n equal to 3.2, it is 12.4 MW which is a power requirement increment of 127%. Finally, when n is equal to 3.5 the power goes to 42.4 MW which is more than six times what is required from the first case. The high sensitivity of the vessel's power to the speed's power creates a high degree of uncertainty when taking the decision as to which n value will be used in the simulations. Furthermore, another weaknesses of the Admiralty coefficient approach is that at low vessel speed, the power requirement tends to behave more as the square of the speed (i.e. n = 2) while at higher speeds it goes beyond a cube relationship [Stroke 2003].

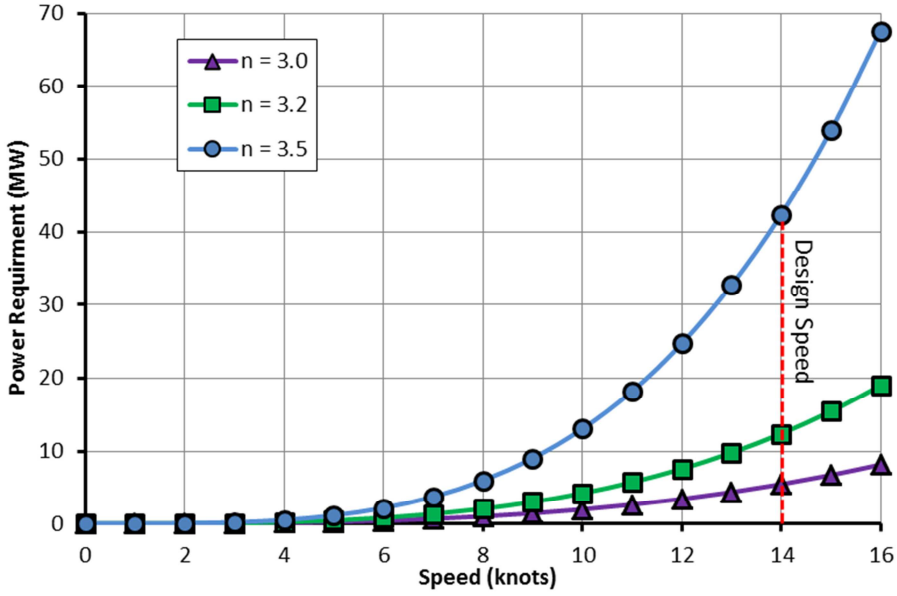

Figure 131: Comparison of power requirement for a handymax container ship when modifying the speed's power in equation [2]. The red line represents the ship's design speed.

Studying the resistance of a vessel at different speeds and loading conditions allows for a better understanding of the power requirement for the vessel's operating profile. When a ship

navigates through water at any given speed, a force is applied onto the wetted surface of the ship's hull. In order for the ship to travel at the desired speed, it must provide a force of equal magnitude. The force against the vessel is known as total resistance (R_T) and that produced by the vessel against the water's resistance is called thrust (T), both given in Newton [Stroke 2003]. When the vessel's resistance is multiplied by the desired speed – in m/s – it is possible to find the power required:

$$\dot{W} = R_T * v \qquad [\ 116\ ]$$

The variable R_T is formed by the frictional resistance (R_{fr}) and residual resistance (R_{rs}). This variable R_{fr} refers to the energy required to overcome the existing friction between the hull and water while the ship moves. The frictional resistance is dependent on the length of the ship, roughness of the hull and speed among others; it can represent up to 75% of R_T. The variable R_{rs} is formed by the water's change of direction due to hull interaction; by abrupt changes in the water's streamline due to the hull's form; and to the formation of waves when the ship moves in the water [Stroke 2003].

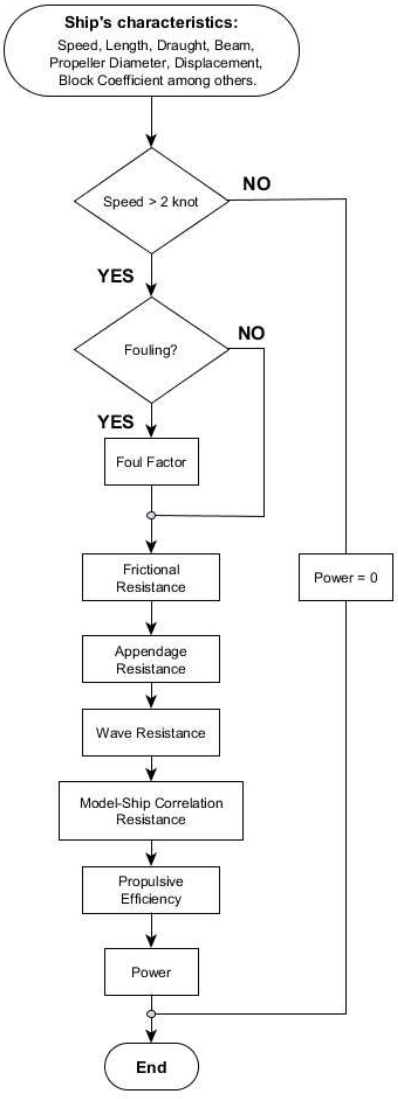

Figure 132: Flow diagram of the Matlab® resistance model created by Calleya [2014] **based on the work of Holtrop and Mennen** [1982] **to predict the ship's power requirement on a single speed.**

The resistance model was developed by Calleya [2014] to be used in Matlab®. The model is based on the papers of Holtrop and Mennen [1982] and Holtrop [1984], which describe the regression analysis and coefficient found from a random set of model experiments and full scale data. It is important to mention that Holtrop and Mennen [1982] group R_T differently from Stroke [2003], dividing it in six different major resistance groups instead of two. These two different classification approaches do not have an influence over the R_T value.

Figure 132 represents in a broad way how the resistance model works for a single vessel speed. The model requires, among others, the ship's waterline length, draught, beam, prismatic coefficient, propeller blades and diameter. These characteristics can be found in databases such as Shipping Intelligence Network [Clarkson Research Services Limited 2013] or web pages similar to MarineTraffic.com [2014]. If the user decides to consider a fouling factor, then the code will add it to the calculation process; this factor is determined by the user. The code calculates the different coefficients described by Holtrop and Mennen [1982] to find the various resistances which forms R_T. At the last step, the power required ($\dot{W}$) is calculated using equation [116]. This process is

done iteratively over the full vessel's speed profile. In the case that the vessel's speed is lower than 2 kn, the model will return a power of zero kW, which is due to a limitation in the Holtrop and Mennen [1982] process and assumptions taken by Calleya [2014]. However, it is assumed that at these low speeds, the power required is low enough to be irrelevant to the WHRS model. Calleya validated the resistance model with experimental data, having a good correlation between them.

The advantages of using this model are that a more realistic power consumption could be found depending on the speed but also allowing for the integration of the cargo condition (i.e. ballast or loaded) into the annual operating profile. The model allows an engine match to the operating profile, which in turn will deliver the relevant conditions to the WHRS models. Furthermore, the regression approximation is fast while keeping a low discrepancy to the experimental models. On the other hand, a drawback found in Holtrop and Mennen [1982] was the accuracy in the wave resistance calculation up to a Froude number equal to 0.5. Holtrop [1984] in order to improve the wave resistance accuracy gave three different wave resistance equations depending in the Froude numbers: A) below 0.4; B) between 0.4 and 0.55; and C) above 0.55. Still, the model has weaknesses in the areas of pressure resistance and additional wave resistance due to a bulb caused by limitations on the methodology of that time. Computational Fluid Dynamics could overcome these difficulties and the regression model limitations but they are computationally and time expensive. The interested reader is recommended to read Holtrop and Mennen [1982] and Holtrop [1984] papers, and Calleya [2014] work in order to understand the process in more detail.